Development of sub-hour on-line comprehensive 2D-LC methods for the analysis of complex samples

Soraya Chapel

N° d'ordre NNT : 2021LYSE1106

THESE de DOCTORAT DE L'UNIVERSITE DE LYON
Opérée au sein de
L'Université Claude Bernard Lyon 1

Ecole Doctorale N° 206
Ecole Doctorale de Chimie de Lyon

Spécialité de doctorat : **Chimie Analytique**

Soutenue publiquement le 29/06/2021, par :
Soraya CHAPEL

Développement de méthodes bidimensionnelles en ligne LC x LC en moins d'une heure pour l'analyse d'échantillons complexes

Devant le jury composé de :

DESMET, Gert	Professeur	Vrije Universiteit Brussel	Rapporteur
VEUTHEY, Jean-Luc	Professeur	Université de Genève	Rapporteur
GRIVEL, Candice	Ingénieure de recherche	Solvay	Examinatrice
SALVADOR, Arnaud	Professeur	Université de Lyon	Examinateur
WEST, Caroline	Professeure	Université d'Orléans	Examinatrice
HEINISCH, Sabine	Ingénieure de recherche	Université de Lyon	Directrice de thèse

UNIVERSITE CLAUDE BERNARD – LYON 1

Administrateur provisoire de l'Université	M. F. FLEURY
Président du Conseil Académique	M. H. BEN HADID
Vice-Président du Conseil d'Administration	M. D. REVEL
Vice-Président du Conseil des Etudes et de la Vie Universitaire	M. P. CHEVALLIER
Vice-Président de la Commission de Recherche	M. J-F. MORNEX
Directeur Général des Services	M. P. ROLLAND

COMPOSANTES SANTE

Département de Formation et Centre de Recherche en Biologie Humaine	Directrice : Mme A-M. SCHOTT
Faculté d'Odontologie	Doyenne : Mme D. SEUX
Faculté de Médecine et Maïeutique Lyon Sud - Charles Mérieux	Doyenne : Mme C. BURILLON
Faculté de Médecine Lyon-Est	Doyen : M. G. RODE
Institut des Sciences et Techniques de la Réadaptation (ISTR)	Directeur : M. X. PERROT
Institut des Sciences Pharmaceutiques et Biologiques (ISBP)	Directrice : Mme C. VINCIGUERRA

COMPOSANTES & DEPARTEMENTS DE SCIENCES & TECHNOLOGIE

Département Génie Electrique et des Procédés (GEP)	Directrice : Mme R. FERRIGNO
Département Informatique	Directeur : M. B. SHARIAT
Département Mécanique	Directeur M. M. BUFFAT
Ecole Supérieure de Chimie, Physique, Electronique (CPE Lyon)	Directeur : G. PIGNAULT
Institut de Science Financière et d'Assurances (ISFA)	Directeur : M. N. LEBOISNE
Institut National du Professorat et de l'Education	Administrateur Provisoire : M. P. CHAREYRON
Institut Universitaire de Technologie de Lyon 1	Directeur : M. C. VITON
Observatoire de Lyon	Directrice : Mme I. DANIEL
Polytechnique Lyon	Directeur : E. PERRIN
UFR Biosciences	Administratrice provisoire : Mme K. GIESELER
UFR des Sciences et Techniques des Activités Physiques et Sportives (STAPS)	Directeur : M. Y. VANPOULLE
UFR Faculté des Sciences	Directeur : M. B. ANDRIOLETTI

Résumé substantiel en Français, requis dans le cas d'une thèse rédigée en anglais :

Le couplage entre la chromatographie en phase liquide et la spectrométrie de masse (LC-MS) est aujourd'hui reconnu comme l'un des outils d'analyse les plus puissants au service des chimistes et biochimistes. Cependant, en dépit de décennies de développement et d'amélioration, les performances de la LC-MS s'avèrent souvent limitées lorsqu'il s'agit d'analyser des mélanges très complexes (échantillons contenant un grand nombre de composés) d'une part, ou des mélanges difficiles à séparer (échantillons contenant un grand nombre d'isomères par exemple) d'autre part. Pour palier ses limitations, grâce à son très haut pouvoir séparatif, la chromatographie liquide bidimensionnelle compréhensive en ligne (LC x LC) a fait l'objet d'un surcroît de développements ces deux dernières décennies. Cependant, du fait de sa complexité par rapport à la chromatographie liquide unidimensionnelle classique (1D-LC), la prolifération de cette technique en dehors des laboratoires de recherche demeure relativement limitée.

L'objectif global de cette thèse, intitulée « Développement de méthodes bidimensionnelles en ligne LC x LC en moins d'une heure pour l'analyse d'échantillons complexes », est de contribuer à l'avancement de la LC x LC en ligne en tant qu'outil puissant pour l'analyse de mélanges complexes. Une tendance en perpétuel essor dans le domaine des sciences séparatives consiste à progresser vers des séparations toujours plus efficaces et plus rapides. Pour cette raison, dans ce travail de thèse, une attention particulière a été portée au développement de méthodes LC x LC en ligne en moins d'une heure. Le domaine d'application cible de ce travail de thèse est l'analyse d'échantillons complexes de protéines et de peptides, tels que ceux retrouvés dans l'industrie biopharmaceutique, ou plus largement, dans la recherche protéomique. Les analyses décrites ici concernent donc la séparation de standard de peptides, de digestion protéiques et de protéines.

Le Chapitre I donne un bref aperçu des principes fondamentaux de la LC x LC en ligne et introduit les principaux défis et difficultés relatifs à cette technique. Un accent particulier est mis sur l'importance de parvenir à maximiser l'orthogonalité des deux systèmes séparatifs combinés, tout en minimisant les effets néfastes qui bien souvent en découlent, sur les performances globales de la méthode. Le chapitre inclut une revue détaillée des problèmes de compatibilité de phases mobile entre dimension, en particulier les différences de forces d'élution. Ces dernières donnent généralement lieu à des déformations de pic, dégradant la qualité de séparation dans la deuxième dimension. Un état de l'art des principales stratégies utilisées dans la littérature pour éviter ces problèmes est présenté. Enfin, le chapitre donne également un aperçu d'applications récentes de méthodes LC x LC en ligne à l'analyse de protéines et de peptides, à travers une revue approfondie axée sur l'analyse des anticorps thérapeutiques. L'accent a été mis sur cette classe particulière de protéines car le domaine des biomolécules est actuellement un vecteur majeur de développement des méthodes bidimensionnelles.

Le chapitre II détaille les conditions expérimentales des différentes études menées dans ce travail, ce qui inclue les phases stationnaires, les phases mobiles et la préparation d'échantillon. Des informations pertinentes sur l'instrumentation, les outils de calcul utilisés et le traitement des données sont également fournies dans cette partie.

Le Chapitre III détaille une étude théorique et expérimentale mettant en évidence les avantages de la LC x LC combinant la chromatographie en phase inverse (RPLC) dans les deux dimensions, par rapport à la chromatographie liquide unidimensionnelle en phase inverse classique (1D-RPLC), pour la séparation de digestions de protéines. La RPLC x RPLC est l'une des approches les plus fréquentes en LC x LC du fait, entre autres avantages, de sa simplicité. Pour les composés ionisables, tels que les peptides, une certaine complémentarité en matière de sélectivité peut être facilement obtenue entre les deux dimensions, en manipulant le pH des phases mobiles. Cette approche permet d'obtenir une orthogonalité suffisante (quoique partielle) pour donner lieu à des capacité de pics très élevées. Outre la capacité de pic, cette étude aborde également la question de la sensibilité de détection, qui est souvent citée comme l'une des limitations de la LC x LC en ligne. Des directives simples pour la maximiser dans le cas de séparations RPLC x RPLC sont décrites.

Dans le chapitre IV, deux approches possibles pour améliorer l'occupation de l'espace de séparation bidimensionnel pour l'analyse de peptides sont explorées. La première approche implique l'utilisation de programmes de gradients variables dans la deuxième dimension, tandis que la deuxième approche repose sur le couplage de deux méthodes différentes et complémentaires, à savoir, la chromatographie liquide à interaction hydrophile (HILIC) et la RPLC. Bien que ces deux approches soient efficaces à cet effet, chacune d'entre elles apporte son lot de difficultés, qui sont discutées en détail ici. La première partie du chapitre décrit le développement d'une méthode RPLC x RPLC en ligne incorporant un programme de gradients variables dans la deuxième dimension. Actuellement, l'approche conventionnelle en LC x LC consiste à utiliser le même gradient d'élution pour chacune des fractions transférées dans la deuxième dimension. Cependant, une pratique de plus en plus répandue consiste à modifier les gradients de deuxième dimension au cours de l'analyse, afin de tenir compte des différences de compositions d'élution dans chaque fraction. Les avantages et inconvénients de l'utilisation de tels programmes pour améliorer la couverture de l'espace de rétention bidimensionnel sont discutés, dans le contexte spécifique de la séparation RPLC x RPLC en ligne de peptides. La deuxième partie du chapitre décrit le développement d'une méthode HILIC x RPLC en ligne pour l'analyse de peptides. Dans le cas de la HILIC x RPLC, la différence de force d'élution entre les phases mobiles des deux dimensions donne généralement lieu à des déformations de pics, qui dégradent la qualité de séparation dans la deuxième dimension. Une stratégie possible pour éviter ces effets est présentée ici. Celle-ci repose sur l'injection de larges volumes de fractions riches en solvant fort dans la seconde dimension, afin de provoquer un phénomène que nous avons nommé le « Total Breakthrough ». Ce phénomène peut être décrit comme un cas limite du phénomène de « breakthrough », au cours duquel un unique pic retenu, parfaitement symétrique et fin, est obtenu lors de l'injection d'un composé,

malgré la présence d'un pic non retenu au temps mort. Dans ce chapitre, le potentiel de cette stratégie est démontré pour la séparation de peptides en HILIC x RPLC.

Le Chapitre V explore plus en détail le problème des différences de force d'élution entre phases mobiles rencontré en HILIC x RPLC. La première partie du chapitre détaille une étude expérimentale de l'impact des conditions d'injection sur la séparation des composés ionisables en chromatographie liquide, avec un accent particulier sur les phénomènes de « breakthrough » en RPLC. La deuxième partie du chapitre présente une étude comparative de quatre stratégies utilisées en HILIC x RPLC pour éviter les effets négatifs liés à des différences de forces d'élution entre dimensions, parmi lesquelles la stratégie alternative introduite dans le Chapitre IV. Les avantages et inconvénients de chacune des stratégies explorées sont mis en exergues, dans le contexte spécifique de l'analyse de peptides. Pour ce faire, les séparations obtenues en HILIC x RPLC avec chacune de ces stratégies sont comparées, en considérant trois descripteurs de qualité principaux incluant la capacité de pic, la forme des pics, et la sensibilité de détection.

Pour finir, dans le Chapitre VI, l'intérêt de la LC x LC couplée à la détection ultraviolet (UV) et à la détection par spectrométrie de masse à haute résolution (HRMS), pour la caractérisation de conjugués d'anticorps-médicaments (ADC), est souligné. Contrairement aux précédents chapitres, pour lesquels les méthodes développées concernent l'analyse de peptides de poids moléculaires en dessous de 7 kDa, ce chapitre met l'accent sur l'analyse de protéines intactes (M > 150 kDa) ou partiellement digérées (25 kDA < M < 100 kDa). Les anticorps conjugués sont des macromolécules structurellement complexes, dont le potentiel thérapeutique pour le traitement des cancers et des maladies auto-immunes n'a cessé de croître ces dernières années. Du fait de leur complexité, diverses techniques analytiques sont généralement nécessaires pour leur caractérisation complète. Ceci explique l'attrait des techniques bidimensionnelles pour l'analyse de ces biomolécules. Ce chapitre détaille le développement d'une méthode LC x LC en ligne couplée à des détections UV et HRMS, combinant la chromatographie à échange de cations (CEX) et la RPLC. La méthode CEX x RPLC-UV-HRMS développée est appliquée à l'analyse des variants de charge d'un anticorps conjugué en cours de développement. Cette combinaison est un parfait exemple de l'apport des approches bidimensionnelles à l'analyse de ce type de composés. La CEX est une méthode de référence pour la séparation des protéines, mais son mécanisme de rétention requiert généralement l'utilisation de concentrations élevées de sels non volatils, ce qui la rend peu compatible avec la détection MS. Outre l'aspect séparatif, le couplage en ligne de la CEX et de la RPLC permet un dessalage en ligne et donc le couplage indirect de la CEX avec la MS.

Development of sub-hour on-line comprehensive 2D-LC methods for the analysis of complex samples

Soraya CHAPEL

2021

TITLE: Development of sub-hour on-line comprehensive 2D-LC methods for the analysis of complex samples

SUMMARY: In response to the increasing demand for ever more efficient and high-throughput separations from most fields of application, a lot of effort is being put into the development of multi-dimensional separation techniques. As a result of its potential to generate high peak capacities in acceptable analysis times, in recent years, on-line comprehensive two-dimensional liquid chromatography (LC x LC) has emerged as a powerful tool for the analysis of highly complex mixtures. Despite its attractiveness, additional complexity and difficulties compared to conventional one-dimensional liquid chromatography (1D-LC) still hamper the proliferation of this technique. One of the most prominent challenges lies in the fact that attempts to maximize the coverage of the 2D separation space often results in counterproductive effects deteriorating the overall performance of the method. Therefore, in this thesis, a particular focus has been put on addressing this issue.

In the present contribution, the value of on-line LC x LC for sub-hour separation of complex protein and peptide samples is demonstrated. First, the advantages of on-line reversed-phase LC x reversed-phase LC (RPLC x RPLC) compared to 1D-reversed-phase LC (1D-RPLC) are highlighted for the separation of a protein tryptic digest, both in terms of peak capacity and detection sensitivity. In a second part, two different approaches to improve the retention space coverage are explored for peptide analysis. The first one involves the use of variable gradients in the second dimension, whereas the second one relies on the use of different and complementary combinations in both dimensions, namely, hydrophilic interaction liquid chromatography (HILIC) and RPLC. It is shown that both approaches are effective for this purpose but also bring about specific constraints, which are discussed in detail here. In on-line HILIC x RPLC, the reversed elution strength of the mobile phases used in both dimensions often causes severe peak shape deformations, which impair the separation performance in the second dimension. A possible strategy to circumvent these deleterious effects is presented. This strategy is then compared to some of the most frequently used approaches in the literature. Their respective strengths and weaknesses are discussed in the specific context of peptide analysis. Finally, in the last part, the applicability of on-line LC x LC methods hyphenated with ultraviolet and high-resolution mass spectrometry detections, to the characterization of antibody-drug conjugates, is demonstrated, using cation-exchange chromatography in the first- and RPLC in the second dimension.

FIELD: Analytical Chemistry

KEYWORDS: Two-dimensional liquid chromatography, 2D-LC, peptides, proteins, reversed-phase liquid chromatography, RPLC, hydrophilic interaction liquid chromatography, HILIC, cation-exchange chromatography, CEX, high-resolution mass spectrometry, HRMS

LABORATORY NAME AND ADRESS: Institut des Sciences Analytiques (ISA), 5 rue de la Doua, 69100, Villeurbanne, France

TITRE : Développement de méthodes bidimensionnelles en ligne LC x LC en moins d'une heure pour l'analyse d'échantillons complexes

RESUME : Grâce à son très haut pouvoir séparatif, la chromatographie liquide bidimensionnelle compréhensive en ligne (LC x LC) s'est imposée comme un outil puissant pour l'analyse d'échantillons complexes ces dernières années. Cependant, du fait de sa complexité par rapport à la chromatographie liquide unidimensionnelle classique (1D-LC), la prolifération de cette technique demeure relativement limitée. L'une des difficultés majeures de cette technique consiste à parvenir à maximiser l'occupation de l'espace de séparation bidimensionnel, tout en minimisant les effets néfastes qui bien souvent en découlent, sur les performances globales de la méthode. Dans cette thèse, une attention particulière a été portée à cette problématique.

Ce manuscrit montre le potentiel de la LC x LC en ligne pour la séparation d'échantillons complexes de protéines et de peptides en moins d'une heure. Tout d'abord, les avantages de la LC x LC combinant la chromatographie en phase inverse (RPLC) dans les deux dimensions, par rapport à la chromatographie liquide unidimensionnelle en phase inverse classique (1D-RPLC), sont mis en évidence, pour la séparation de digestions de protéines. Dans une deuxième partie, deux approches possibles pour améliorer l'occupation de l'espace de séparation bidimensionnel pour l'analyse de peptides sont explorées. La première approche implique l'utilisation de programmes de gradients variables dans la deuxième dimension, tandis que la deuxième approche repose sur le couplage de deux méthodes différentes et complémentaires, à savoir, la chromatographie liquide à interaction hydrophile (HILIC) et la RPLC. Bien que ces deux approches soient efficaces à cet effet, chacune d'entre elles apporte son lot de difficultés, qui sont discutées en détail ici. Dans le cas de la HILIC x RPLC en ligne, la différence de force éluante entre les phases mobiles des deux dimensions, donne généralement lieu à des déformations de pics, qui dégradent la qualité de séparation dans la deuxième dimension. Une stratégie possible pour éviter ces effets est présentée ici. Cette stratégie est ensuite comparée à trois des approches les plus utilisées dans la littérature. Les avantages et inconvénients de chacune des stratégies explorées sont mis en exergues, dans le contexte spécifique de l'analyse de peptides. Pour finir, dans une dernière partie, l'intérêt de la LC x LC couplée à la détection ultraviolet et à la détection par spectrométrie de masse à haute résolution, pour la caractérisation de conjugués d'anticorps-médicaments, est souligné, en utilisant la chromatographie à échange de cations en première dimension et la RPLC en deuxième dimension.

DISCIPLINE : Chimie Analytique

MOTS-CLES : Chromatographie liquide bidimensionnelle, 2D-LC, peptides, protéines, RPLC, HILIC, CEX, spectrométrie de masse haute résolution, HRMS

NOM ET ADRESSE DU LABORATOIRE: Institut des Sciences Analytiques (ISA), 5 rue de la Doua, 69100, Villeurbanne, France

ACKNOWLEDGEMENTS

Undertaking this PhD has been a life-changing experience for me and would not have been possible without the effort and support of several people during all these years. From the bottom of my heart, I would like to thank all those who shared even the slightest part of this long and challenging journey.

First and foremost, I would like to thank my Supervisor, *Sabine Heinisch*, for her guidance and encouragements over the past three and a half years. Thank you Sabine for taking a chance on me when I applied to this project although you barely knew me, for always challenging me, for giving me complete freedom to pursue my ideas, for believing in me even when I did not believe in myself, and for your training in all important aspects of being a good scientist. I will be forever grateful for the opportunity we had to work together.

I am also very grateful to the members of my PhD committee, *Pr. Gert Desmet*, *Pr. Jean-Luc Veuthey*, *Dr Candice Grivel*, *Pr. Arnaud Salvador*, and *Pr. Caroline West* for their willingness to serve on my committee and for their valuable time.

My sincere thanks go to *Sophie Nowak* and *Isabelle Fabing*, who both inspired me and set me on this path so many years ago, and continuously gave me a lot of support to help me get there.

I would also like to acknowledge all my past and present co-workers and fellow labmates at ISA (*Karine*, *Magali*, *Florent*, *Julien*, *Marion I.*, *Marie*, *Fleur*, *Marion B., Noé, Cigdem*…) who have all fostered a wonderful work environment since I have been here. Thank you all for the stimulating discussions we had over coffee (or tea) (or water in my case) and for the lovely and fun time spent together. Thank you *Léa*, *Marion*, and *Marie* for setting such good examples as PhD students, and for sharing your experience and insights with me since day one. I am grateful in more ways than I can express for your support and encouragement over the years, especially you *Marie*. My special thanks go to our assistant engineer, *Florent Rouvière*, for his golden hands, and invaluable help and support throughout this journey. Without you *Florent*, I would probably still be working on some of those awful splits I had so much trouble setting up. Thank you for introducing me to okonomiyaki and takoyaki, and funny strange music videos on YouTube (The weird Russian singer and La poignée de porte being my personal favourites). You have been my very own Samwise Gamgee, until the very end, while strangely reminding me of Gandalf (never late, nor early, but always arriving precisely when you were most needed).

I would also like to express my sincere gratitude to my dear friend *Laura Vidal Benet*, who has been of great support inside and outside of work, and whose wise advice saved me many times during my PhD. Gracias *Laurita* por tu amistad y tu cariño.

I dedicate this thesis to my mother, *Gladys Minfardi*, my father, *Frédéric Chapel*, my older brother, *Nicolas Chapel*, my baby sister, *Naunny Minfardi*, and to you, *Jessy*. Making all of you proud has been and will always be my most driving force.

TABLE OF CONTENTS

GENERAL INTRODUCTION

The coupling of liquid chromatography with mass spectrometry detection (LC-MS) is considered one of the most powerful tools in analytical chemistry. However, despite decades of development and improvement, the performance of LC-MS is often limited when dealing with highly complex mixtures (i.e. samples containing a large number of compounds) on one hand, or difficult-to-resolve mixtures (e.g. isomeric compounds) on the other hand. Because of these limitations, over the last two decades, a great deal of effort has been put into the development of on-line comprehensive two-dimensional liquid chromatography (LC x LC) methods, to provide much more efficient separations for a given analysis time.

The general objective of this thesis, entitled "Development of sub-hour on-line comprehensive 2D-LC methods for the analysis of complex samples", is to make a meaningful contribution to the advancement of on-line comprehensive two-dimensional liquid chromatography as a powerful tool for the analysis of highly complex samples. To this end, this thesis explores ways and means to overcome some of the present challenges and shortcomings pertaining to this technique. The ever-growing trend in separation techniques is to progress towards ever more efficient and faster separations. For this reason, the present contribution focuses on the establishment of sub-hour on-line LC x LC methods. The target application area of this thesis is the analysis of complex protein and peptide samples that can be found in the biopharmaceutical industry or, more broadly, in proteomic research. The analyses described in this thesis thus concern the separation of peptide standards, protein digests, and proteins. The applicability of the developed methods is mainly demonstrated through the analyses of synthetic protein mixtures in Chapter III to Chapter V but are also demonstrated through the analyses of real-life samples consisting of monoclonal antibodies and antibody-drug conjugates in Chapter VI.

Chapter I provides a brief overview of the fundamentals of on-line LC x LC and discusses some of the main challenges and limitations of this separation technique. The importance of separation orthogonality and its most often counter-productive impact on the compatibility of the solvent systems used in both dimensions are especially discussed. The chapter includes a detailed review of the particular issue of solvent strength mismatch between dimensions and the possible solutions to

circumvent this problem in on-line LC x LC. The most promising reported strategies so far are critically compared, and their respective advantages and drawbacks are discussed. Lastly, the chapter also provides an overview of recent applications of on-line LC x LC methods to the analysis of proteins and peptides through an extensive review focusing on the analysis of therapeutic antibodies. The emphasis was put on this specific class of proteins because it currently represents one of the most active and fast-growing areas of development in 2D-LC.

In ***Chapter II***, the experimental conditions used for each study detailed throughout this thesis are described, which include stationary phases, mobile phases, and sample preparation. Relevant information about instrumentation, calculation tools, and data processing are also given.

Chapter III details a theoretical and experimental study highlighting the potential of on-line LC x LC with reversed-phase liquid chromatography (RPLC) in both dimensions for the analysis of a tryptic digest of six proteins. The use of RPLC in both dimensions is by far the most simple and frequently used combination in on-line LC x LC. In the case of ionizable analytes such as peptides, complementary selectivities are easily obtained between dimensions by changing the pH between the two mobile phases. This provides sufficient (albeit partial) orthogonality between dimensions to give rise to quite impressive peak capacities. Besides peak capacity, this study also addresses the issue of detection sensitivity in on-line LC x LC and provides simple guidelines to maximize it in the case of RPLC x RPLC separations. In both cases, the added value of on-line RPLC x RPLC compared to one dimensional-RPLC (1D-RPLC) is demonstrated for the separation of peptides with several sets of conditions.

In ***Chapter IV***, two different approaches to improve the retention space coverage for the on-line LC x LC separation of peptides are explored. The first part of the chapter describes the development of an on-line RPLC x RPLC method incorporating a tailored gradient program in the second dimension. Currently, the conventional approach in on-line LC x LC consists in using the same gradient for each subsequent fraction analysed in the second dimension. However, it has been an increased practice to adjust the second-dimension gradient during the course of the 2D separation to better fit the different elution compositions in each fraction. The rationale behind the implementation of tailored second-dimension gradient programs for combinations with limited orthogonality is explained, and the potential and limitations of using such

programs to improve the retention space coverage in on-line RPLC x RPLC are discussed. The second part of the chapter describes the development of an on-line LC x LC separation method combining hydrophilic interaction liquid chromatography (HILIC) and RPLC in the first- and second dimensions, respectively. The combination of HILIC and RPLC is well-known to provide quite orthogonal conditions in 2D-LC for the separation of peptides. However, this combination also suffers from poor compatibility between the solvent strength used in the first dimension and the second dimension separation, which arises from the reversed elution strength of the mobile phases used in HILIC and RPLC. This issue, commonly referred to as "solvent strength mismatch", is notorious for being quite challenging when combining these two chromatographic modes because it often results in severe peak deformations in the second dimension. The study presented in this work specifically addresses this problem and reports on a possible approach to avoid its detrimental impact on peptide separation in on-line HILIC x RPLC. Lastly, the two approaches for improving the retention space coverage described in this chapter are compared.

Chapter V continues with the problem of solvent strength mismatch in on-line HILIC x RPLC, previously highlighted in Chapter IV. Possible solutions to overcome this incompatibility issue are explored through two detailed studies in the interest of providing guidance to maximize the potential of this orthogonal combination. The first one details an experimental study of the impact of the injection conditions on the separation of ionizable compounds in liquid chromatography, with a particular focus on the breakthrough phenomena in RPLC. The second one describes a comparative study of four currently existing strategies whose purpose is to overcome solvent strength mismatch issues, including the one that we proposed in Chapter IV. A comparison of on-line HILIC x RPLC separations obtained with each strategy for the analysis of a complex tryptic digest sample is made, by considering several quality descriptors, including peak capacity, peak shape, and detection sensitivity. The respective strengths and weaknesses of each of the evaluated strategies are discussed in this specific context.

In ***Chapter VI***, the applicability of on-line LC x LC methods coupled with ultra-violet (UV) and high-resolution mass spectrometry (HRMS) detections is demonstrated for the characterization of therapeutic antibodies. Unlike the previous chapters which focused on the analysis of peptides with molecular weights (MW) below 7 kDa, this chapter focuses on the analysis of proteins at the intact level (MW > 150 kDa) or after

partial digestion leading to large protein subunits (25 kDa < MW < 100 kDa). Therapeutic antibodies are large and structurally complex molecules that require extensive characterization throughout their research and development process. Over the past few years, 2D-LC methods have emerged as attractive tools to address the analytical challenges faced with these complex biomolecules. The work presented in this chapter details the development of on-line LC x LC methods combining cation-exchange chromatography (CEX) and RPLC for the separation of the charge variants of a lysine-linked antibody-drug conjugate. This combination gives an excellent example of the potential benefits of 2D-LC approaches for the analysis of such protein formats. CEX is considered the gold-standard method for the separation of protein charge variants but its retention mechanism usually requires the use of a high concentration of non-volatile salts, which impedes its compatibility with MS detection. In this context, the use of an on-line CEX x RPLC-HRMS approach not only allows on-line desalting and indirect coupling of CEX with HRMS detection but it also provides increased and complementary information within a single analysis.

The chapters in this thesis incorporate materials that have been published or prepared for publication in scientific journals. For this reason, there may be some overlaps throughout this manuscript.

Also of note is the fact that the bibliographic references from the study presented as articles and the rest of the manuscript have been differentiated by using square brackets in the former case ([ref]) and superscript square brackets in the colour blue in the latter case ([ref]), respectively. Cited references are reported directly after the concluding remarks and acknowledgement for the articles, and at the end of each chapter for the rest.

LIST OF PUBLICATIONS

1. **Strategies to circumvent the solvent strength mismatch problem in on-line comprehensive two-dimensional liquid chromatography**
   Soraya and Sabine Heinisch, Journal of Separation Science, **2021**, submitted
   Covered in Chapter I.

2. **Two-dimensional liquid chromatography coupled to high-resolution mass spectrometry for the analysis of ADCs**
   Soraya Chapel, Florent Rouvière, Morgan Sarrut, and Sabine Heinisch, L. Nathan Tumey (Ed.), Antibody-Drug Conjugates: Methods and Protocols, Methods in Molecular Biology, **2020**, vol 2078, pp 163-185, Springer US, New-York, DOI: 10.1007/978-1-4939-9929-3_11
   Covered in Chapter I.

3. **A theoretical and practical approach to manage high peak capacity and low dilution in on-line comprehensive reversed-phase LC x reversed-phase LC: A comparison with 1D-reversed-phase LC**
   Soraya Chapel, Florent Rouvière, and Sabine Heinisch, LC-GC Europe, **2020**, vol 33, number s5, Advances in UHPLC/HPLC, 17-26
   Covered in Chapter III.

4. **Pushing the limits of resolving power and analysis time in on-line comprehensive hydrophilic interaction x reversed phase liquid chromatography for the analysis of complex peptide samples**
   Soraya Chapel, Florent Rouvière, and Sabine Heinisch, Journal of Chromatography A, **2019**, 1615, 460753, DOI: 10.1016/j.chroma.2019.460753
   Covered in Chapter IV.

5. **A comprehensive study on the phenomenon of Total Breakthrough in liquid chromatography**
   Soraya Chapel, Florent Rouvière, Vincent Pepermans, Gert Desmet, and Sabine Heinisch, Journal of Chromatography A, **2021**, Journal of Chromatography A, under review
   Covered in Chapter V.

6. **Detailed numerical study of the peak shapes of neutral analytes injected at high solvent strength in short reversed-phase liquid chromatography columns and comparison with experimental observations**
   Vincent Pepermans, Soraya CHAPEL, Sabine Heinisch, and Gert Desmet, Journal of Chromatography A, **2021**, 1643, 462078, DOI: 10.2016/j.chroma.2021.462078
   Covered in Chapter V.

7. **Comparison of existing strategies for keeping symmetrical peaks in on-line hydrophilic Interaction liquid chromatography x reversed-phase liquid chromatography despite solvent strength mismatch**
   Soraya Chapel, Florent Rouvière, and Sabine Heinisch, Journal of Chromatography A, **2021**, 1642, 462001, DOI: 10.1016/j.chroma.2021.462001
   Covered in Chapter V.

CHAPTER I – CONTEXT

Parts of this Chapter have been published (or submitted to publication) as:

- **Strategies to circumvent the solvent strength mismatch problem in on-line comprehensive two-dimensional liquid chromatography**

  Soraya Chapel and Sabine Heinisch
  Journal of Separation Science, **2021**, submitted

- **Two-dimensional liquid chromatography coupled to high-resolution mass spectrometry for the analysis of ADCs**

  Soraya Chapel, Florent Rouviere, Morgan Sarrut, and Sabine Heinisch
  L. Nathan Tumey (Ed.), Antibody-Drug Conjugates: Methods and Protocols, Methods in Molecular Biology, **2020**, vol 2078, pp 163-185, Springer US, New-York
  DOI: 10.1007/978-1-4939-9929-3_11

A. General overview of on-line LC x LC

Since its introduction in the late 1970s [1], two-dimensional liquid chromatography (2D-LC) has become an important analytical tool for the separation of highly complex and inherently difficult-to-separate samples. In 2D-LC, two individual liquid chromatography separations are combined into one single analysis. Because of this specificity, 2D-LC techniques hold great potential to increase the level of information on a given sample compared to conventional one-dimensional liquid chromatography (1D-LC).

There are two main approaches for 2D-LC [2,3]. They include "heart-cutting" techniques, in which relatively large fractions from the first dimension (^{1}D) chromatogram are transferred to the second dimension (^{2}D); and "comprehensive" ones, in which, conversely, relatively discrete fractions are transferred, so that the peak resolution previously achieved in ^{1}D is essentially maintained during the fraction transfer process. For the comprehensive 2D-LC approach, either selected regions of the ^{1}D-chromatogram or the entire ^{1}D-chromatogram can be considered [4,5]. The former approach is referred to as "selective comprehensive" (sLC x LC) [6], whereas the latter may be referred to as "full comprehensive" when compared to the former, but is mainly known simply as "comprehensive" (LC x LC). Fraction transfer from the first- to the second dimension can be conducted either on-line or off-line [7]. In on-line 2D-LC, the ^{1}D-fractions are collected and transferred into the ^{2}D-column via a valve-based interface, whereas in off-line, the ^{1}D-fractions are collected and stored in vials to be reinjected at a later time into the ^{2}D-column. All the above-mentioned approaches have distinct advantages and limitations, which will be discussed in further detail in Section D of this chapter. In this thesis, we focused on on-line comprehensive two-dimensional liquid chromatography (on-line LC x LC) because of its intrinsic potential to produce impressive peak capacities in relatively affordable analysis times.

As highlighted by Karger et al. [8], then later by Guiochon et al. [9], and Giddings [10], under ideal circumstances, the theoretical peak capacity of an LC x LC system ($n_{2D,\text{theoretical}}$) is equal to the product of the peak capacities in the first and second dimensions (^1n and ^2n, respectively):

$$n_{2D,theoretical} = {}^1n \,.\, {}^2n \qquad \textit{(Eq. I-1)}$$

These "ideal circumstances" include the two following requirements:

(i) The peak capacities generated independently in the first and second dimensions must be maintained.

(ii) The two separation dimensions must provide completely orthogonal conditions so that the entire retention space is accessible for the separation of the sample at hand.

In reality, satisfying simultaneously these two requirements is a very challenging task. First of all, as will be discussed in Section B of this chapter, full orthogonality between dimensions can be difficult to achieve for a given sample [11-13]. Second of all, it is important to understand that it is impossible to deal with the peak capacity in the first and second dimensions separately in on-line LC x LC. This can mostly be ascribed to the interconnection of the two dimensions, which brings many constraints and compromises during method development. Arguably, the most important interaction is that between the ^{1}D-sampling time (and flow rate) and the ^{2}D-analysis time (and injection volume), as will be further explained below.

One of the most critical factors for the success of a given on-line LC x LC method is the rate at which the first dimension is sampled [14]. To maintain the ^{1}D-peak capacity, the ^{1}D-separation must be divided into a sufficient number of fractions so that the chromatographic resolution achieved in ^{1}D is not lost in ^{2}D. The adequate number of fractions will depend on the ^{1}D-peak widths and the sample complexity. If the number of collected fractions is too low, analytes that were well-resolved in the ^{1}D-column are likely to be collected in the same fraction and remixed during the sampling process. This problem is known as undersampling [15].

In on-line LC x LC, fraction collection from ^{1}D and reinjection in ^{2}D is a continuous process that requires that a ^{2}D-run is completed before the next fraction can be transferred. As a consequence, the sampling time is equal to the total analysis time in ^{2}D. Minimizing undersampling imposes a severe time restriction on the second dimension. In practice, a compromise often has to be struck between a decrease in ^{1}D-peak capacity due to large sampling times on one hand, and a decrease in ^{2}D-peak capacity due to short analysis times on the other hand [7]. To essentially maintain the ^{1}D-peak capacity while also ensuring sufficient ^{2}D-peak capacity, it has been

recommended that the sampling rate (i.e. number of fractions collected per 6σ-peak width in ^{1}D) should be between 1.5 and 2.7 [16].

Meanwhile, maintaining the ^{2}D-peak capacity is often hindered by additional band broadening arising from the non-ideal transfer of relatively large sample fractions in the ^{2}D-column [11, 17]. This effect is further aggravated when the search for a high degree of orthogonality between dimensions results in the combination of mobile phase systems that are poorly compatible [14].

The effective peak capacity ($n_{2D,effective}$) of an on-line LC x LC separation must account for all these limitations, which is why it is generally much lower than the simple product rule introduced in Eq. I-1. It can be calculated with the following equation [11,17]:

$$n_{2D,effective} = \alpha \,.\, \beta \,.\, \gamma \,.\, {}^{1}n \,.\, {}^{2}n \qquad \textit{(Eq. I-2)}$$

Where α and β are correction factors taking into account undersampling in ^{1}D and band broadening in ^{2}D due to non-ideal transfer between dimensions, respectively, and γ is the retention space coverage of the 2D separation, which gives a measure of the degree of orthogonality between dimensions. All three factors may range between 0 and 1, and as highlighted above, their optimization is often conflicting. In practice, the contribution of β is included in the determination of the experimental ^{2}D-peak capacity. As will be detailed in Section B, the estimation of γ can be made graphically. As for the correction factor α, it can be estimated using the following equation, as described by Davis et al. [18]:

$$\alpha = \frac{1}{\sqrt{1+\left(t_S / {}^{1}\sigma_{t,total}\right)^{2}}} \qquad \textit{(Eq .I-3)}$$

Where t_S is the sampling time and $^{1}\sigma_{t,total}$ is the total peak standard deviation in time unit in the first dimension.

B. The pursuit of separation orthogonality

In on-line LC x LC, the sample components are subjected to two different separation steps. Evidently, if the two retention mechanisms used in both dimensions provide

similar selectivity, through the use of the same stationary phases and mobile phases, the 2D-LC system will not accomplish much improvement in separation compared to a single separation step. In such a situation, the retention factors in the two dimensions will be strongly correlated, resulting in peaks gathering along a straight diagonal line in the 2D separation space (Fig. I-1a). Conversely, if the two separation dimensions provide completely different and complementary selectivity, in such a way that there is no overlap between the retention times in the two dimensions, the peaks will distribute evenly over the entire separation space (Fig. I-1b) . The ability of a 2D-LC system to spread uniformly the separated peaks throughout the entire retention space is commonly referred to as its "orthogonality", and is one of the most important concepts in 2D-LC [11,13,19]. In the most favourable case in which the 2D-LC system results in full occupation of the separation space (Fig. I-1b), the two separation dimensions are considered to be completely orthogonal [20]. As highlighted by Eq. I-2, separation orthogonality is a crucial factor for maximizing the effective peak capacity in on-line LC x LC. However, in practice, finding completely orthogonal selectivities for the comprehensive separation of a given sample is not a simple process, which is in part due to the fact that many stationary phases share a certain degree of similarity between their mechanisms of interaction. More often than not, a given LC x LC system will only yield a partial coverage of the retention space (Fig. I-1c). This is all the more true for highly complex samples containing compounds with close physio-chemical characteristics.

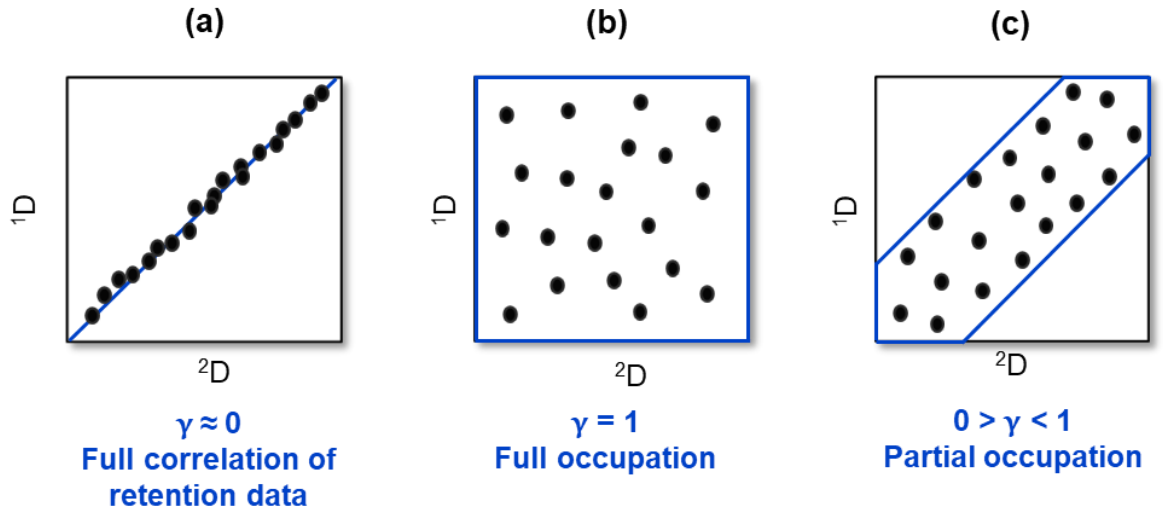

Fig. I-1: Schematic illustration of LC x LC separations with (a) full correlation between retention data in both separation dimensions, (b) full occupation of the separation space (full orthogonality), and (c) partial occupation of the separation space (partial orthogonality).

A variety of metrics and approaches have been developed to quantify the degree of orthogonality of a given LC x LC system. Examples include bin-counting methods [13,21], spreading angles methods among which the convex-hull method [22], the asterisk equations approach [23], the ecological home-range theory approach [24], the nearest-neighbour approach [25,26], as well as more simple correlation coefficient approaches. They can be classified as either mathematical or geometrical approaches, the latter relying on the determination of the proportion of the separation space that can be occupied by chromatographic peaks. The respective strengths and weaknesses of most of these strategies were extensively covered by Bakain et al. [27], Gilar et al. [28], and Schure and Davis [29,30], and discussing them is beyond the scope of this thesis. However, it is important to mention that there is still no consensus on which of these approaches is the best to quantify the degree of orthogonality of a given 2D-LC system.

In pursuit of separation orthogonality, several chromatographic modes have been combined in on-line LC x LC. The most popular of these combinations include reversed-phase liquid chromatography (RPLC) in both dimensions, hydrophilic interaction liquid chromatography (HILIC) and RPLC, ion-exchange chromatography (IEX) and RPLC, normal-phase liquid chromatography (NPLC) and RPLC, size exclusion chromatography (SEC) and RPLC, hydrophobic interaction chromatography (HIC) and RPLC, and supercritical fluid chromatography (SFC) and RPLC [4]. Of course, the capability of a given combination to provide orthogonal conditions for a satisfactory 2D separation will depend on the sample at hand and the targeted analytical goals.

C. Addressing the challenge of mobile phase incompatibility between dimensions

In order to achieve maximal usage of the 2D separation space, markedly different separation methods are usually combined in on-line LC x LC. Such a practice often results in the incompatibility of the first- and second dimension mobile phase systems [31]. These incompatibilities may include problems of miscibility, differences of viscosity, and differences of eluotropic strengths, which may be detrimental to the ^{2}D-separation or even impede the feasibility of certain combinations [14].

1. Main types of solvent incompatibility

1.1. Solvent immiscibility

In the most extreme cases, the two mobile phases used in the two dimensions are so different in nature that they are not even miscible. A well-known example is the combination of NPLC (which uses organic-rich solvents) and RPLC (which uses predominately aqueous-rich solvents). Due to the lack of miscibility between the mobile phases used in these two chromatographic modes, the on-line interfacing of NPLC and RPLC is notorious for being particularly difficult. As a result, despite the potentially high orthogonality of this combination, very few applications involving NPLC and RPLC have been reported in on-line LC x LC [32-37]. Problems arising from the incomplete mixing of the two solvent systems when they meet in the sample loop may include signal interferences, system peaks, pressure instabilities, baseline instabilities, and may have devastating effects on the ^{2}D-separation. All of these limitations were extensively discussed by Francois and co-workers [32] in the context of the on-line NPLC x RPLC separations of both pharmaceutical samples and lemon oil extracts, using mixtures of n-hexane/1-butanol, n-hexane/ethanol or n-hexane/ethyl acetate in ^{1}D-NPLC and water/ACN in ^{2}D-RPLC. The incompatibility issue between NPLC and RPLC is even more important when NPLC is used in the second dimension, as the transfer of aqueous solvent from ^{1}D-RPLC may deactivate the polar adsorbent used in ^{2}D-NPLC and ruin the separation [14,19]. For this reason, all separations involving RPLC in the first dimension and NPLC in the second dimension have been carried out with non-aqueous RPLC (NARP) to avoid this problem [38,39].

Another example is the combination of RPLC and SFC. First of all, it should be mentioned that the use of SFC in the first dimension is not straightforward due to the particular state of carbon dioxide (CO_2) in supercritical conditions [40]. In SFC, the CO2 gas is compressed, heated at its critical point, and then mixed in the mobile phase with low percentages of co-solvent modifiers. During the transfer of fractions from ^{1}D-SFC to ^{2}D-RPLC, CO_2 is exposed to atmospheric pressure through the storage loop connected to the waste, which causes its abrupt decompression. This not only creates a “demixing” effect between the expanded CO_2 and the co-solvent but also strongly increases the risk of both the $C0_2$ and the analytes escaping the loop through the waste. For this reason, on-line SFC x RPLC requires complex setups to be even feasible [33,40-

[42], which mostly involves the use of trapping columns instead of loops to retain the compounds.

These limitations added to the fact that both the low viscosity and high-diffusion coefficients of SFC mobile phases allows fast and efficient separations, make SFC more attractive for the second dimension [40]. With SFC in the second dimension, $C0_2$ decompression can be avoided by injecting sample fractions in full loop. However, this usually results in the injection of relatively large volumes of incompatible RPLC fractions in ^{2}D-SFC. The potential and limitations of on-line RPLC x SFC were investigated by Sarrut et al. [43] for the separation of neutral compounds in bio-oil extracts, and more recently by Sun et al. [44] for the separation of depolymerized lignin samples. Both authors reported a significant pressure increase at the beginning of each ^{2}D-run, which were found to increase with both the injection volume and the percentage of water in the injection solvent. These important pressure spikes can be attributed to the lack of miscibility between the aqueous solvent coming from ^{1}D-RPLC and the apolar SFC mobile phase. Not only this phenomenon restricts the flow rate in the second dimension, but it also produces important baseline fluctuations in the second dimension, thus increasing the background noise and reducing detection sensitivity.

1.2. Solvent strength mismatch

Even when the mobile phases used in the two dimensions are fully miscible, other problems may arise from differences in elution strength between the ^{1}D-fraction solvent and the ^{2}D-mobile phase. In LC, a mismatch of elution strength between injection solvent and mobile phase may impact either positively or negatively the separation, depending on whether the injection solvent is weaker or stronger than the mobile phase. For a short time during the injection process, the sample solvent behaves as if it were the mobile phase. If the retention factor in the injection solvent is high, the analyte plug will move slowly during the injection process, thus creating a band compression effect that will positively impact the separation. Conversely, if the retention factor is very low, the leading front of the band will move faster than its rear part, which may lead to broadening, distortion, and even breakthrough phenomenon. In the latter case, multiple peaks appear on the chromatogram for a single injected analyte, one of which being eluted at the column dead time. The detrimental effects

that can have an inconvenient difference of elution strength between the injection solvent and the mobile phase are well known in 1D–LC [45,46]. In fact, it is considered best practice to use an injection solvent weaker than the mobile phase to avoid poor peak shapes. While this is usually manageable in 1D–LC, in on-line LC x LC the combination of certain chromatographic modes inevitably lead to unfavourable solvent strength mismatch conditions.

A classical example is the combination of HILIC and RPLC. In HILIC, organic-rich mobile phases are typically used, with common proportions ranging from 98% to 50% [47-49], whereas water-rich mobile phases are used in RPLC. Considering that the weaker solvent in HILIC becomes the stronger solvent in RPLC, and vice-versa, the on-line coupling of these two chromatographic modes often results in poor chromatographic performances in the second dimension. For example, Vanhoenacker et al. [50] compared on-line RPLC x RPLC, SCX x RPLC and HILIC x RPLC for the separation of the tryptic digest of a monoclonal antibody. Despite better retention space coverage in HILIC x RPLC, this combination was considered the least attractive due to the occurrence of significant injection problems in the second dimension. Both SCX x RPLC and RPLC x RPLC showed good peak shapes as a result of excellent solvent compatibility between dimensions. However, in HILIC x RPLC, due to the transfer of acetonitrile-rich fractions in ^{2}D-RPLC, peptide breakthrough could not be avoided, even with injection volumes as low as 2% of the column dead volume (V_0), which impacted both the peak shapes and the peak intensities. Cao et al. [51] reported similar results for the on-line HILIC x RPLC analysis of polar phenolic acids in a plant extract. In this case, both band broadening and breakthrough were observed with injection volumes higher than 6% V_0.

As highlighted by D'Attoma and Heinisch [52], similar problems can be expected with HILIC in the second dimension. An example of the extent of the detrimental effects of solvent strength mismatch is illustrated in Fig. I-2 showing a comparison between RPLC x RPLC and RPLC x HILIC for the separation of peptides. In RPLC x RPLC (Fig. I-2a), good peak shapes were obtained despite the large volumes injected in ^{2}D-RPLC (i.e. 21% V_0), whereas in RPLC x HILIC (Fig. I-2b), even relatively small injected volumes (i.e. 7% V_0) resulted in significant peak distortion. As a result, the peak

capacity in RPLC x RPLC exceeded the one in RPLC x HILIC by about 30%, despite a better retention space coverage in the latter case.

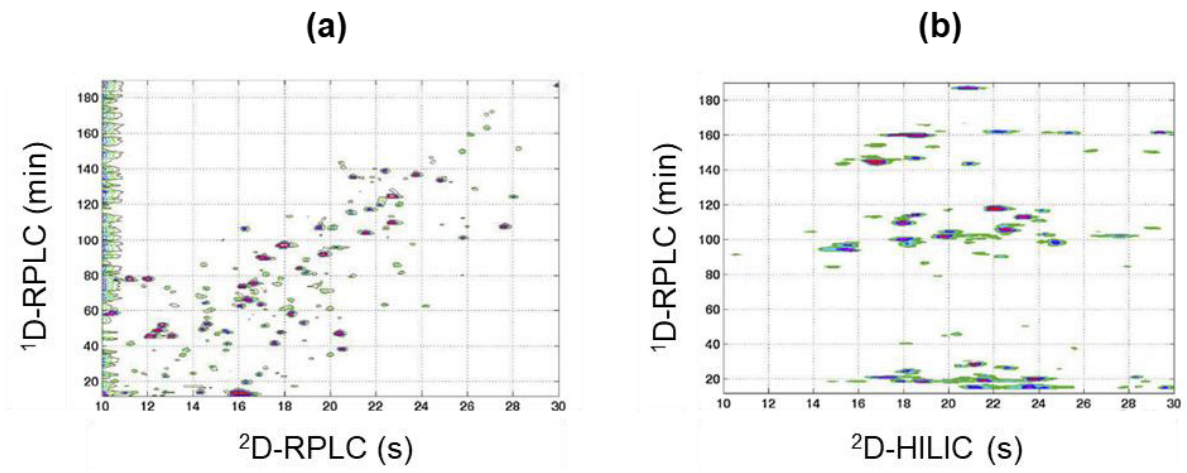

Fig. I-2: Illustration of the detrimental effects of solvent strength mismatch on the separation in RPLC x HILIC through the comparison of (a) on-line RPLC x RPLC and (b) RPLC x HILIC separations of the same protein tryptic digest. Adapted from [52]. Injected volume: (a) 21% V_0 and (b) 7% Vo.

Besides HILIC and RPLC, another combination that is known to cause solvent strength mismatch problems is organic-SEC and RPLC [53-55]. Organic-SEC typically employs low polarity solvents such as tetrahydrofuran (THF), toluene or chloroform, among others. As a result, when coupling organic-SEC in the first dimension with RPLC in the second dimension, injection issues are most likely to occur. For example, significant peak distortions and breakthrough were recorded in on-line organic-SEC x RPLC for the analysis of polymeric compounds [55,56]. With organic-SEC in the second dimension, the transfer of a high concentration of polar solvents from ^{1}D-RPLC solvent has also been demonstrated to result in peak distortion and peak splitting due to analyte adsorption on the stationary phase [53,57]. Other notorious combinations leading to injection problems due to solvent strength mismatch include NPLC x RPLC and RPLC x SFC.

1.3. Viscosity mismatch

In liquid chromatography, it has been demonstrated that differences in viscosity between the sample solvent and the mobile phase could result in significant peak shape deformations. When a fluid pushes another miscible fluid with different

viscosity in a porous medium, the interface between the two may become unstable and create a complex pattern resembling fingers. First observed by Hill in 1952 [58] and named by Saffman and Taylor in 1958 [59], this phenomenon is known as "Viscous Fingering" (VF). So far, VF has received little attention amongst the LC community, and only theoretical papers and few experiments specially designed to illustrate this effect have shown that it could occur in chromatographic columns [60-63]. Viscous fingering may develop on either the frontal part (Fig. I-3b) or the rear part (Fig. I-3c) of the plug, depending on whether the solvent plug is less viscous or more viscous than the mobile phase, respectively. As a result of both finger growth dynamics, band broadening, peak distortion (tailing or fronting depending on the forward or rearward propagation), and even peak splitting have been observed [64]. Comprehensive studies on this phenomenon have permitted to highlight that its severity tends to increase with increasing differences of viscosity between the injection solvent and the mobile phase, injected volumes, flow rates, sample concentrations, and column inner diameters (ID) on one hand, and decreasing analyte retention factors and particle diameters on the other hand [64].

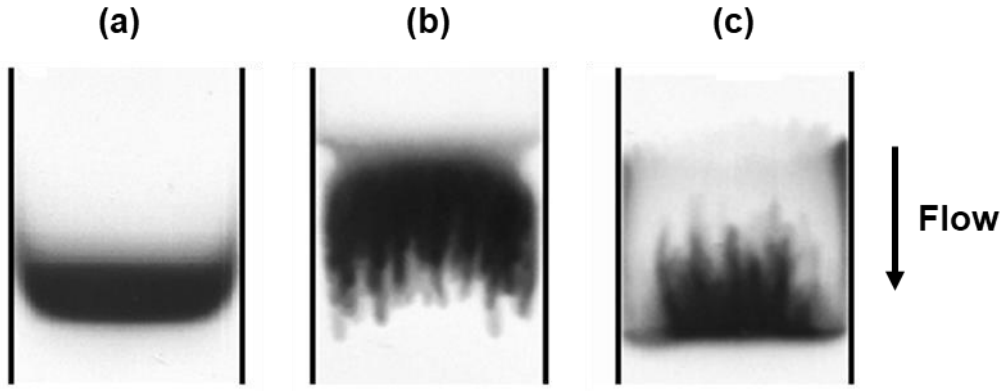

Fig. I-3: On-column photographs showing the two types of band profiles that can be observed during viscous fingering phenomenon. (a) regular band obtained with equal viscosities of solvent plug and mobile phase, (b)solvent plug less viscous than the mobile phase, and (c) solvent plug more viscous than the mobile phase. Direction of the flow indicated by the arrow on the right. Adapted from [63].

Most studies highlighting this phenomenon have been conducted on wide-bore columns (i.e. 17 mm ID) [64], raising doubts on the probability of the occurrence of VF in analytical-scale columns. However, recently, Samuelson et al. [65] provided evidence that viscosity mismatch effects could also be detrimental to the separation in

analytical columns. Although finger-like elution patterns only occurred in the most extreme cases in their study, it was highlighted that a "pre-viscous fingering" state, creating severe band broadening and distortion, could readily occur with small viscosity ratios between the mobile phase and the injection solvent.

Typically, in 1D-LC, the injection solvent is carefully selected to match the mobile phase. For this reason, the occurrence of VF is not very likely. However, as highlighted by Shalliker and Guiochon [64], viscosity mismatch effects seem unavoidable in on-line LC x LC, especially since gradient elution is usually used in both dimensions. This is even more true for combinations leading to the coupling of solvent systems with an important gap of viscosities, such as those encountered with NPLC and RPLC, SFC and RPLC, or even HILIC and RPLC. While considerable attention has been directed toward solvent strength mismatch issues, the destructive potential of viscosity mismatch has mostly been overlooked in on-line LC x LC. However, because both effects are difficult to dissociate in practice, it is reasonable to conceive that they might bear joint responsibility for peak shape deformation. In fact, Rana et al. [66,67] demonstrated with computational simulations that, depending on the situation, both effects might either reinforce each other (sample solvent both stronger and less viscous than the mobile phase) or partially cancel each other (sample solvent both stronger and more viscous than the mobile phase or vice versa).

2. Strategies to circumvent solvent incompatibility

Article 1: Strategies to prevent loss of performance due to solvent strength mismatch in on-line comprehensive two-dimensional liquid chromatography

Abstract

On-line comprehensive two-dimensional liquid chromatography (LC x LC) is a powerful technique for the separation of highly complex samples. Due to the addition of a second dimension of separation, impressive peak capacities can be obtained within a reasonable analysis time compared to one-dimensional liquid chromatography (1D-LC). In on-line LC x LC, the separation power is maximized by selecting two separation dimensions as orthogonal as possible, which most often requires the combination of different mobile phases and stationary phases. The on-line transfer of a different solvent from the first dimension to the second dimension can cause severe injection effect in the second dimension, mostly due to solvent strength mismatch. Those injection effects may include peak broadening, peak distortion, peak splitting or breakthrough phenomenon, and are often found to reduce significantly the peak capacity and the peak intensity. To overcome such effects, arising specifically in on-line LC x LC, different methods have been developed over the years. In this review, we focused on the most recently reported ones. A critical discussion, supported by a theoretical approach, gives an overview of their advantages and drawbacks.

1. Introduction

Increasing the method sensitivity, decreasing the analysis time, and maximizing the separation power are the key objectives in Liquid Chromatography (LC), each of these objectives competing with the others. The associated separation quality descriptors are usually the dilution factor, the gradient time, and the peak capacity. This latter represents the theoretical number of peaks that can be unitarily resolved in a given separation space [1]. In the past few decades, many efforts have been invested in method development and new technology (core-shell, sub-2µm particles, monolithic stationary phases, ultra-high attainable pressure, low instrument dispersion, elevated temperatures…). However, one-dimensional liquid chromatography (1D-LC) seems to have reached a limit in term of separation power with a reported peak capacity value of about 1600 achieved in 40 hours [2]. In the quest for higher peak capacities and shorter analysis times, on-line comprehensive two-dimensional liquid chromatography (on-line LC x LC) has emerged as a viable approach to cope with increasingly complex samples, as highlighted by recent reviews [3–7]. It was also recently shown that peak intensities could be greatly improved in on-line LC x LC compared to 1D-LC [8]. LC x LC is obtained by combining two different separation mechanisms. In the on-line mode, fraction collection in the first dimension (^{1}D) and injection in the second dimension (^{2}D) are conducted in real-time through a switching valve. It is usually admitted that the theoretical peak capacity is the product of the peak capacities in each dimension. In practice, this theoretical value is never achieved due to the combination of three major issues: under-sampling for ^{1}D-peaks, low degree of orthogonality between both dimensions, and non-ideal transfer from ^{1}D to ^{2}D [9]. Improved performance in on-line LC x LC compared to 1D-LC is obtained at the expense of much more complex method development, considering the large number of inter-related parameters [10]. The early stage of method development consists in searching for orthogonal dimensions. In the quest for a very high degree of orthogonality, the selection of two different separation mechanisms, providing markedly different selectivities is attractive. To some extent, the combination of similar chromatographic modes such as RPLC x RPLC can lead to a certain degree of orthogonality if the mobile phase conditions are optimized (different modifiers, pH, temperature…). Usually, the greater the difference between each separation mode, the greater the degree of orthogonality. However, as the degree of orthogonality increases (e.g. from RPLC x RPLC to HILIC x RPLC, RPLC x SFC or even NPLC x RPLC), the on-

line coupling becomes more challenging due to increasing differences between the two mobile phases. Those differences may include solvent immiscibility, solvent strength mismatch, viscosity mismatch or the presence in ^{1}D of salts that are insoluble in ^{2}D. Unlike in 1D-LC, both the injection solvent and the injection volume are difficult to control in on-line LC x LC. Due to the interconnection of the two dimensions, the injection solvent in ^{2}D is the mobile phase at the time the peak fraction is eluted from ^{1}D while the injection volume is the volume of the collected peak fraction. Different modulation interfaces have been proposed to permit better control of the injection solvent and the injection volume. These interfaces were extensively discussed in two recent reviews [11,12].

Solvent strength mismatch is a specific term used in 2D-LC when the ^{1}D-effluent (and thus ^{2}D-injection solvent) and the ^{2}D-mobile phase have different eluotropic strengths. In contrast, solvent strength mismatch represents the main issue when combining HILIC with RPLC but even sometimes RPLC with RPLC. The stronger the injection solvent is, the more likely it is to generate injection effects in the second dimension, such as additional band broadening, peak distortion, and/or breakthrough phenomena, all affecting the separation quality descriptors (peak capacity and dilution factor).

In this review, we discuss the different strategies reported in the literature for reducing the detrimental effects of solvent strength mismatch on peak shapes and hence on both peak capacity and peak intensity in on-line LC x LC. Theoretical aspects are presented in Section 2 to help to better understand these strategies whose main features are listed in Table 1. Their advantages and drawbacks are extensively discussed in Section 3.

2. Theoretical aspects of injection effects

The general problem of solvent strength mismatch is illustrated in Fig. 1. Assuming a rectangular injection plug, the band width inside the column is delimited by the vertical red line (molecules at the front of the plug) and the vertical blue line (molecules at the rear of the plug). X_1 and X_2 are the fractions of the column through which the blue and red molecules have passed, respectively, during the three different stages shown in figs. 1a to 1c. V is the volume of mobile phase that passes through the column. The equations for X_1, X_2, and V are reported on the right of the figure. Fig. 1a

illustrate the injection process right before the injection plug enters the column (i.e. both $X_1 = 0$ and $X_2 = 0$), whereas Fig. 2b portrays the situation once the plug has completely entered the column (i.e. $X_1 = 0$ and $X_2 = V_i/(1 + k_S)V_0$). In Fig. 1c, the injection volume has passed the red molecules. The volume fraction between the two lines (i.e. $X_2 - X_1$) then represents the contribution of the injection process to band broadening. If $X_2 = 1$ (i.e. $V_i = k_s \times V_0$), the red molecules are completely eluted by the injection solvent, while the blue molecules are still retained into the column. This starts a situation of breakthrough in which the red molecules are part of the breakthrough peak, while the blue molecules are part of the retained peak.

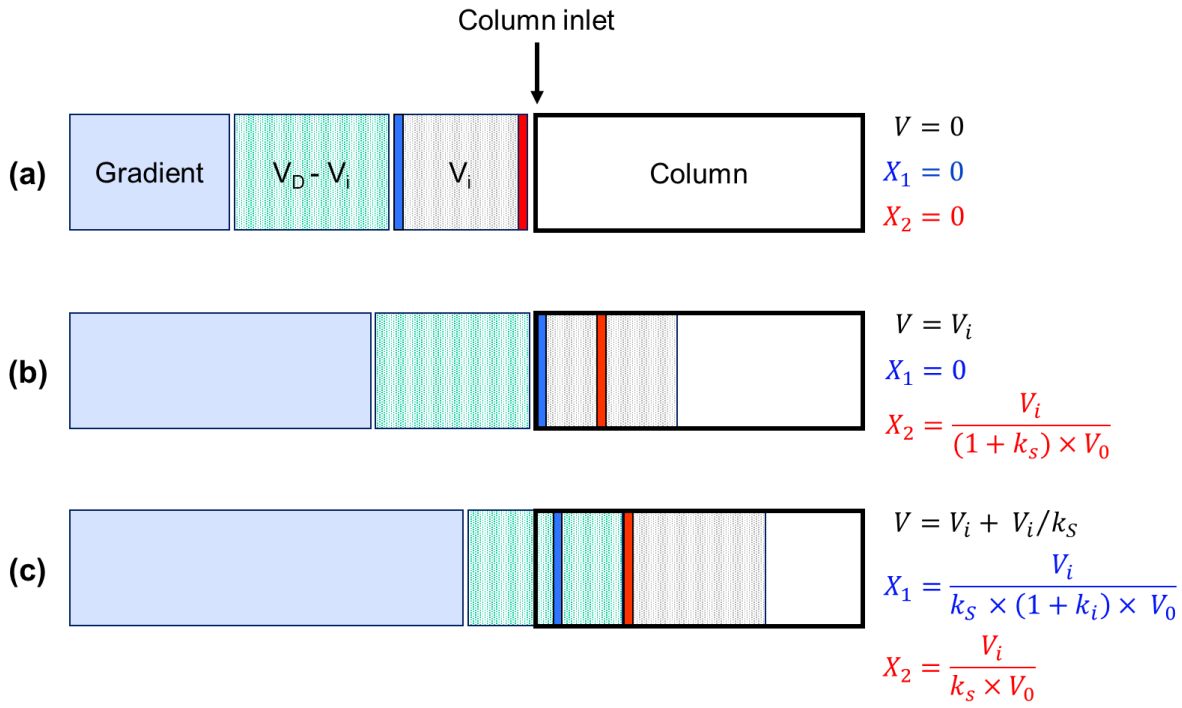

Fig. 1: Schematic representation of the injection solvent effect on the progression of the molecules through the column: (a) just before the injection plug enters the column, (b) once the entire plug has entered the column, and (c) once the plug has passed the last solute molecule. The blue line represents the molecules at the rear of the injection plug. The red line represents those at the front. k_s: retention factor in the injection solvent, k_i: retention factor in the initial composition, V_i: injection volume, V: volume of mobile phase passing through the column, V_D: dwell volume, X_1 and X_2: fractions of the column volume through which the blue and red molecules have passed, respectively.

The breakthrough phenomenon is characterized by the presence of two peaks on the chromatogram, as highlighted in Fig. 2 in the context of the on-line HILIC x RPLC separation of phenolic compounds. The first one is almost not retained while the second one is eluted at the expected retention time. As above stated, this phenomenon is explained by the fact that a significant part of the sample travels through the column

without interacting with the stationary phase. The presence of a breakthrough peak results in a decrease in the retained peak area. When this phenomenon occurs, the retained peak usually presents a severe fronting, as a result of a continuous trail of molecules between the breakthrough peak and the retained peak.

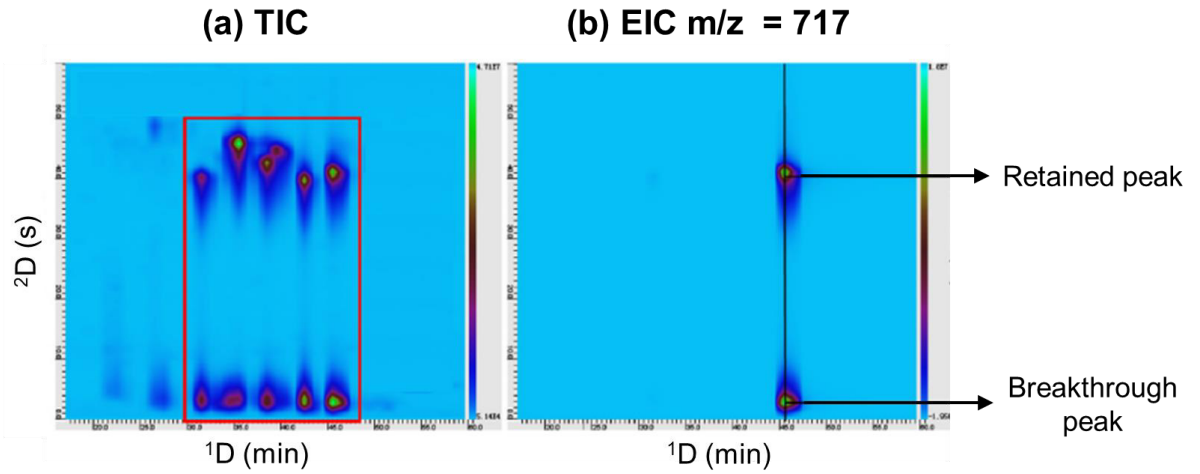

Fig. 2: Illustration of the breakthrough phenomenon on the separation of phenolic acids by on-line HILIC x RPLC: (a) Total ion current (TIC) chromatogram showing the presence of two peaks per detected compounds and (b) extracted ion chromatogram (EIC) of m/z 717 highlighting the breakthrough and retained peaks for this compound. Adapted from [56].

As long as the peak remains approximately symmetrical (i.e. long before the occurrence of breakthrough), the extra-column variance due to the injection process, σ_{inj}^2, can be written as [13]:

$$\sigma_{inj}^2 = \frac{V_i^2}{\delta^2} \times \frac{1}{C_F^2} \qquad (Eq.\ 1)$$

Where V_i is the injection volume, δ^2, a correction factor that depends on the injection process (12 for an ideal injection plug and close to 4 in practice), and C_F, the peak injection compression factor. $C_F > 1$ if the injection plug is reduced due to on-column focusing (injection solvent weaker than the mobile phase), $C_F < 1$ if the injection plug is broadened when travelling through the column (injection solvent stronger than the mobile phase, and $C_F = 1$ if the injection solvent is the mobile phase. The injection compression factor is related to two solute retention factors: k_s, in the injection solvent, and k_e, in the mobile phase at elution. C_F is usually well approximated by the following simple relationship [14]:

$$C_F = \frac{k_S}{k_e} \qquad \textit{(Eq. 2)}$$

The column plate number, N_{col} and peak capacity, n_{col}, are both altered by extra-column solute dispersion, resulting in an effective plate number, N_{eff} and an effective peak capacity, n_{eff}, given by:

$$\mathrm{N}_{eff} = \beta^2 \times \mathrm{N}_{col} \qquad \textit{(Eq. 3a)}$$

And

$$\mathrm{n}_{eff} = \beta \times \mathrm{n}_{col} \qquad \textit{(Eq. 3b)}$$

β is a correction coefficient ranging between 0 and 1 depending on the importance of extra-column dispersion. Ideally, β should be higher than 0.7 ($\beta^2 > 0.5$), otherwise the loss in plates becomes too significant (> 50%), making the assumption of a Gaussian peak shape unrealistic. β^2 is given by:

$$\beta^2 = \frac{1}{1+x^2} \qquad \textit{(Eq. 4)}$$

With x^2, the ratio of the peak variance resulting from extra-column dispersion (σ^2_{ext}), to the peak variance resulting from column dispersion (σ^2_{col}):

$$x^2 = \frac{\sigma^2_{ext}}{\sigma^2_{col}} \qquad \textit{(Eq. 5)}$$

The reduction of any injection effect arising from solvent strength mismatch requires the reduction of β^2 and hence of x.

By combining Eq. 5 with Eq. 1 and assuming that the injection process (σ^2_{inj}) is the main cause for extra-column dispersion in ^{2}D ($\sigma^2_{ext} = \sigma^2_{inj}$), x can be expressed as:

$$x = \frac{1}{{}^2C_F} \times \frac{{}^2V_i}{{}^2\sigma_{col}} \times \frac{1}{\delta} \qquad \textit{(Eq. 6)}$$

Where superscript 2 refers to the second dimension.

To keep β^2 higher than 0.5, x^2 has to be lower than 1 ($\sigma_{inj} < \sigma_{col}$).

The effluent coming from ^{1}D can be split before being sent to ^{2}D (Fig. 5.a), resulting in an injection volume given by:

$$^2V_i = \lambda \times (^1\sigma_{col} \times {}^1z_{split}) \qquad \textit{(Eq. 7)}$$

Where $\lambda(^1\sigma_{col})$ is the volume of the fraction collected in ^{1}D (expressed as a multiple λ of the column standard deviation), $^1z_{split}$ is a split ratio designed to divide the flow rate in ^{1}D before entering the interface.

It can also be diluted with a weaker solvent (Figs. 5b-d). The method consists in adding $(^1z_{dilution} - 1)$ volumes of a weak solvent to the ^{1}D-effluent before injection in ^{2}D, which in turn, increases the injection volume while modifying the composition of the ^{2}D-injection solvent and increasing C_F. Trapping columns can also replace empty loops (Fig. 6a) to reduce the injection volume in ^{2}D. This method is most often associated with solvent dilution.

Accordingly, the general relationship for the injection volume in ^{2}D is:

$$^2V_i = z_{dilution} \times \lambda \times (^1\sigma_{col}) \times {}^1z_{split} \times \frac{1}{C_{F,trap}} \qquad \textit{(Eq. 8)}$$

$^2C_{F,trap}$ is the additional compression factor provided by the trapping column. It is expected to be above 1 with trapping columns while equal to 1 with empty loops.

By combining Eqs. 6 and 8, x can be written in the form of the following global equation:

$$x = \frac{1}{^2C_F} \times \lambda \times \frac{^1\sigma_{col}}{^2\sigma_{col}} \times {}^1z_{split} \times z_{dilution} \times \frac{1}{C_{F,trap}} \times \frac{1}{\delta} \qquad \textit{(Eq. 9)}$$

With $z_{dilution} \geq 1$ (= 1 without dilution)

$^1z_{split} \leq 1$ (= 1 without flow splitting)

$C_{F,trap} \geq 1$(= 1 with empty loops)

Finally, in addition to peak capacity and analysis time (^{1}D-gradient time), the dilution factor in ^{2}D is a key descriptor of the separation quality in on-line LC x LC. The following relationship gives the dilution factor when almost symmetrical peaks are obtained ($\beta > 0.7$):

$$^2D_F = \frac{^2\sigma_{col}\sqrt{2\pi}}{\beta \times (^2V_i)} \qquad \textit{(Eq. 10)}$$

By combining Eqs. 4, 6, and 10, ^2D_F and $^2V_i/\,^2\sigma_{col}$ can be expressed as a function of β and ^2C_F as follows:

$$^2D_F = \frac{\sqrt{2\pi}}{\delta \times\ ^2C_F \times \sqrt{1-\beta^2}} \qquad \textit{(Eq. 11a)}$$

And

$$\frac{^2V_i}{^2\sigma_{col}} = \sqrt{\frac{1-\beta^2}{\beta^2}} \times \delta \times\ ^2C_F \qquad \textit{(Eq. 11b)}$$

Fig.3 shows the variation of ^2D_F (Eq.11a) and $^2V_i/\,^2\sigma_{col}$ (Eq.11b) as a function of β when the injection solvent is the mobile phase ($C_F = 1$).

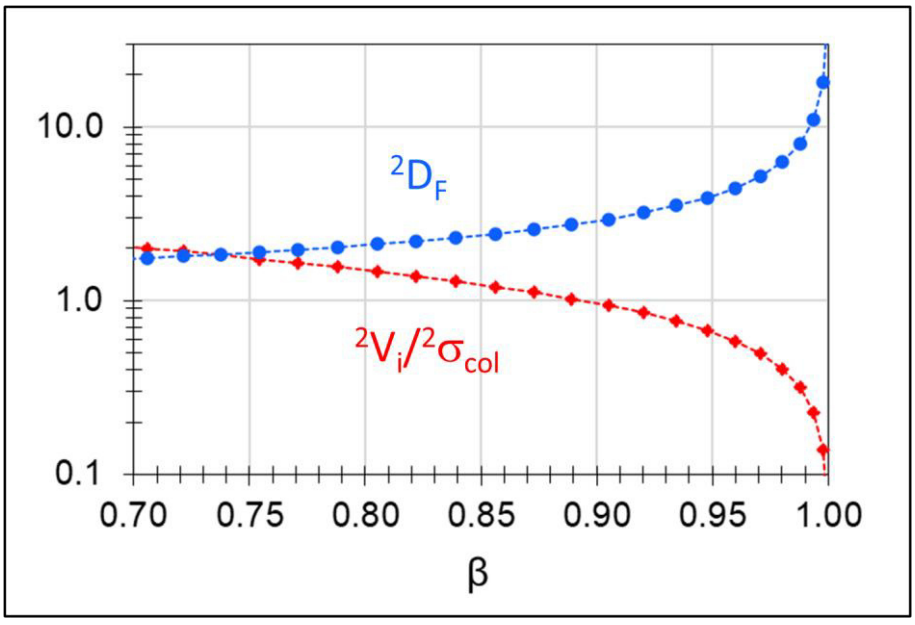

Fig. 3: Evolution of dilution factor ^2D_F (blue circles, Eq. 11a) and $^2V_i/^2\sigma_{col}$ (red diamonds, Eq. 11b) as a function of β.

It is clear that beyond a β value of 0.9, the dilution factor starts to increase exponentially. As said before, below 0.7 the peak distortion becomes significant. This allows us to define an optimized range of β values between 0.7 and 0.9 (i.e. between 30% and 10% peak capacity loss). In this case, the injection volume should be between $^2\sigma_{col}$ and $2 \times\ ^2\sigma_{col}$, and the resulting dilution factor between 1.8 and 2.7. It

should also be noted from Eqs. 11a and 11b that, for a given β value, the injection volume is proportional to C_F whereas the dilution factor is inversely proportional to it. As an example, increasing the compression factor ten times while increasing the injection volume ten times will reduce the dilution factor ten times without changing the peak capacity (β kept constant). This highlights the importance of increasing the compression factor.

3. Strategies to limit injection effects

Different strategies have been designed to reduce the injection effects arising from solvent strength mismatch in on-line LC x LC. Some of them can be combined. Some of them require additional devices for their implementation while others do not. In what follows, Eq. 9 will help to differentiate these strategies and to highlight their possibilities and limitations. Table 1 summarizes the features discussed in this section and gives the associated references.

Table 1: Overview of the most relevant applications in on-line LC x LC highlighting the strategies discussed in this review.

Strategy	Combination	Application	Remarks	Ref.
Increasing ^2C_F	HIC x RPLC	Antibody-drug conjugates		[15]
	HIC x RPLC	Antibody-drug conjugates		[16]
	IEX x RPLC	Proteins		[61]
	IEX x RPLC	Wine and Chinese medicine		[62]
	IEX x RPLC	Monoclonal antibody digests		[63]
	IEX x RPLC	Monoclonal antibodies		[64]
	IEX x RPLC	Monoclonal antibodies		[65]
	Aqueous-SEC x RPLC	Peptides		[66]
	RPLC x RPLC	Peptides		[8]
Decreasing column I.D ratio	HILIC x RPLC	Fatty alcohol derivatives		[67]
	HILIC x RPLC	Phenolics		[68]
	HILIC x RPLC	Procyanidins	Large loop volume	[24]
	HILIC x RPLC	Phenolics		[69]
	HILIC x RPLC	Phenolic and flavonoids		[70]

Table 1 (continued).

Strategy	Combination	Application	Remarks	Ref.
Decreasing column I.D ratio	HILIC x RPLC	Phlorotannins		[71]
	HILIC x RPLC	Surfactants		[72]
	HILIC x RPLC	Phlorotannins		[21]
	HILIC x RPLC	Liquorice metabolites		[22]
	HILIC x RPLC	Red wine sample		[73]
	HILIC x RPLC	Phenolics		[74]
	HILIC x RPLC	Liquorice metabolites	Large loop volume	[25]
	HILIC x RPLC	Phenolics		[75]
	HILIC x RPLC	Lipids		[76]
	HILIC x RPLC	Oligosaccharides	Large loop volume	[93]
	RPLC x HILIC	Peptides		[26]
	Silver ion LC x RPLC	Triacylglycerides		[77]
	NPLC x RPLC	Carotenoids		[78]
	NPLC x RPLC	Lemon oil extract		[87]
	NPLC x RPLC	Carotenoids		[88]
	NPLC x RPLC	triacylglycerols		[89]
	NPLC x RPLC	Aromatic standards		[90]
	NPLC x RPLC	Pharmaceutical standards		[91]
	NPLC x RPLC	Citrus oil extract		[91]
	RPLC x RPLC	Biomass by-products		[28]
	RPLC x RPLC	Bio-oil extract		[27]
	RPLC x RPLC	Phenolics		[74]
	RPLC x RPLC	Hop cone and pellet extracts		[79]
	RPLC x RPLC	Bio-oil extract		[82]
	RPLC x RPLC	Bio-oil extract		[83]
	RPLC x RPLC	Proteins		[84]
	RPLC x RPLC	Phenolics		[85]
	RPLC x RPLC	Plant metabolites		[101]

Table 1 (continued).

Strategy	Combination	Application	Remarks	Ref.
Decreasing column I.D ratio	LC x organic-SEC	Polymers		[86]
	RPLC x SFC	Bio-oil extract		[27]
Decreasing column I.D ratio + Flow splitting	HILIC x RPLC	Phenolics		[32]
	HILIC x RPLC	Procyanidins		[34]
	HILIC x RPLC	Procyanidins		[35]
	HILIC x RPLC	Grape seed tannins		[37]
	HILIC x RPLC	Phenolics		[33]
	HILIC x RPLC	Anthocyanins		[36]
	HILIC x RPLC	Monoclonal antibody digests		[63]
	HILIC x RPLC	Phenolics		[57]
Flow splitting	RPLC x RPLC	Maize extract		[30]
	RPLC x RPLC	Bio-oil extract		[28]
	RPLC x RPLC	Peptides		[10]
	RPLC x RPLC	Peptides		[18]
	RPLC x RPLC	Pharmaceuticals		[80]
	RPLC x RPLC	Pharmaceuticals		[81]
	RPLC x RPLC	Peptides		[92]
Dilution with a weak solvent (empty loops)	RPLC x RPLC	Polycyclic aromatics	Make-up flow	[94]
	RPLC x RPLC	Carboxylic acids	Make-up flow	[95]
	RPLC x RPLC	Pharmaceuticals	Make-up flow	[44]
	RPLC x RPLC	Plant extracts and coffee	Make-up flow	[96]
	HILIC x RPLC	Coffee extract	Make-up flow	[97]
	HILIC x RPLC	Liquorice metabolites	Make-up flow	[25]
	HILIC x RPLC	Rice metabolites	Make-up flow	[38]
	HILIC x RPLC	Phenolic acids	Make-up flow	[56]
	HILIC x RPLC	Phenolics	Make-up flow	[98]
	HILIC x RPLC	Phenolics	Make-up flow	[99]
	HILIC x RPLC	Phenolics	Make-up flow	[100]

Table 1 (continued).

Strategy	Combination	Application	Remarks	Ref.
Dilution with a weak solvent (empty loops)	HILIC x RPLC	Oligosaccharides	Make-up flow	[93]
	HILIC x RPLC	Standard mix	At-column dilution	[39]
	RPLC x HILIC	Red ginseng extract	At-column dilution	[39]
	RPLC x HILIC	Herbal medicine	At-column dilution	[40]
	Organic-SEC x RPLC	Polymers	Active Solvent Modulation	[102]
	Organic-SEC x RPLC	polymers	Active Solvent Modulation	[103]
	RPLC x RPLC	Monoclonal antibody digests	Active Solvent Modulation	[104]
	HILIC x RPLC	Small molecule probes	Active Solvent Modulation	[42]
	HILIC x RPLC	Monoclonal antibodies	Active Solvent Modulation	[43]
Dilution with a weak solvent (trapping columns)	NPLC x RPLC	Polymers		[105]
	SFC x RPLC	Pharmaceuticals		[106]
	SFC x RPLC	Citrus oil extract		[106]
	SFC x RPLC	Fatty acids		[107]
	SFC x RPLC	Triacylglycerols		[108]
	SFC x RPLC	Carotenoids		[109]
	HILIC x RPLC	Oligonucleotides		[52]
	HILIC x RPLC	Surfactants		[53]
	HILIC x RPLC	Phenolics		[57]
	HILIC x RPLC	Liquorice metabolites		[25]
	HILIC x RPLC	Phenolic acids		[56]
	HILIC x RPLC	Phenolics		[110]
	HILIC x RPLC	Lipids		[111]
	HILIC x RPLC	Cocoa bean metabolites		[112]
	HILIC x RPLC	Histone proteoforms		[54]
	HILIC x RPLC	Ginsenosides		[55]
	HILIC x RPLC	Ginsenosides		[113]
	HILIC x RPLC	Oligosaccharides		[93]
	HILIC x RPLC	Microalgae digests		[123]

Table 1 (continued).

Strategy	Combination	Application	Remarks	Ref.
Dilution with a weak solvent (trapping columns)	RPLC x HILIC	Ginseng extract		[114]
	IEX x RPLC	Peptides		[51]
	IEX x RPLC	Dye extracts		[115]
	HDC x RPLC	Nanoparticles		[116]
	RPLC x RPLC	Vacuum gas oil		[117]
	RPLC x RPLC	Flavonoids		[110]
	RPLC x RPLC	Anabolic steroids		[118]
	RPLC x RPLC	Microalgae digests		[123]
	MMG-LC x RPLC	Flavonoids		[110]
Solvent evaporation	NPLC x RPLC	Chinese medicine	Heating-vacuum evaporation	[59]
	NPLC x RPLC	Chinese medicine	Vacuum evaporation	[119]
	NPLC x RPLC	Orange and coal tar extracts	Vacuum evaporation	[120]
	NPLC x RPLC	Bufadienolides	Heating-vacuum evaporation + trapping columns	[121]
	NPLC x RPLC	Bufadienolides	Heating evaporation + trapping columns	[122]
	RPLC x RPLC	Phenolic acids	Heating vacuum evaporation	[60]

3.1. Increase in the injection compression factor

This method is often referred to as "on-column focusing". According to Eq. 2, increasing the injection compression factor can be done by increasing ${}^2k_s$ or by decreasing ${}^2k_e$. When used alone, on-column focusing is the gold standard considering its ease of implementation with no additional device required. However, according to Eq. 9, this method only works in situations where the injection compression factor is high enough. Such situations usually occur when the first dimension uses fully aqueous mobile phases, such as hydrophobic interaction chromatography (HIC), ion-exchange chromatography (IEC) or aqueous size-exclusion chromatography (aqueous SEC), while the second dimension is typically RPLC. The related LC x LC techniques remain very specific, with limited application areas mainly related to polymer or biomolecule analysis (see Table 1). As an illustrative example, on-line HIC x RPLC hyphenated to High-Resolution Mass Spectrometry (HRMS) [15,16] was applied to the

characterization of a cysteine-linked antibody-drug conjugate (ADC). Although HIC is usually considered as the reference technique to separate the different DARs (drug-to-antibody-ratio) of an ADC, its separation mechanism requires the use of a high salt concentration in the aqueous mobile phase, which makes HIC incompatible with MS. The ^{2}D-RPLC dimension was proved to be very attractive, not only to provide on-line desalting before HRMS but also to extend the level of DAR information with separation and identification of subunits. Due to the aqueous mobile phase in HIC, a large column internal diameter could be used in ^{1}D (4.6 mm) while a smaller one in ^{2}D (2.1mm), thereby leading to large injection volumes in ^{2}D (150 µL), and hence high peak intensities (low dilution) in ^{2}D.

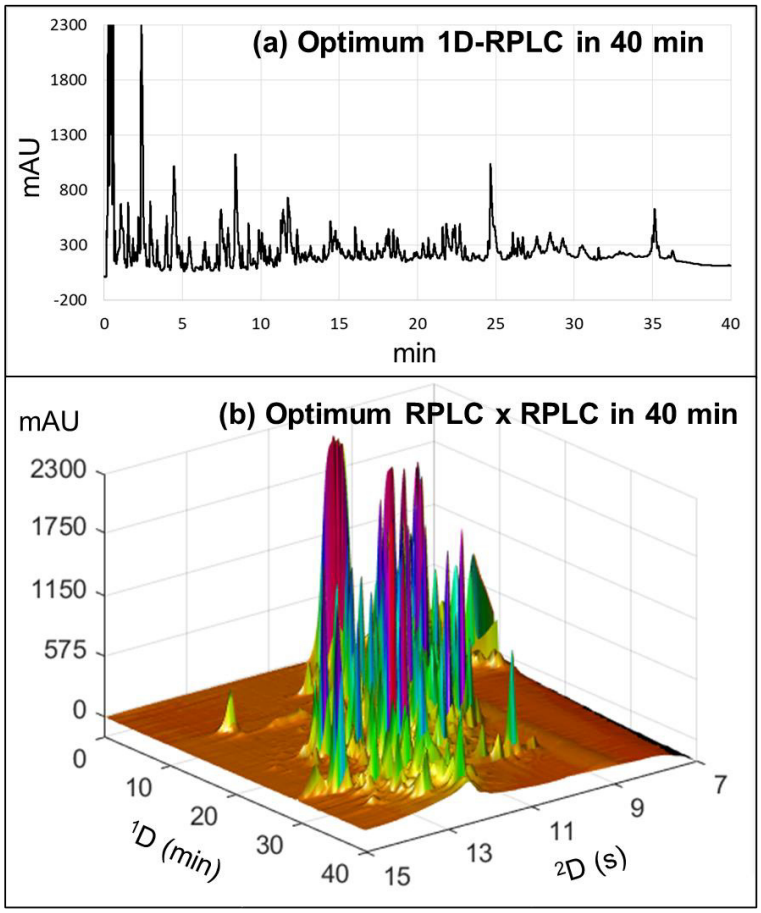

Fig. 4: Comparison of optimized separations of a tryptic digest of proteins illustrating the difference in dilution factor between (a) 1D-RPLC and (b) on-line RPLC x RPLC with UV detection. Adapted from [8].

In RPLC x RPLC, $^{2}k_s$ is most of the time close to $^{1}k_e$ provided that the hydrophobicity of the stationary phases is similar in both dimensions. The mobile phase in ^{1}D is not fully aqueous but the injection compression factor in ^{2}D can be high enough if elution

is very smooth in ^{1}D (high ^1k_e) while very steep in ^{2}D (low ^2k_e). This approach was recently applied to the separation of a tryptic digest of proteins (Fig. 4) [8]. A good trade-off between peak capacity and peak intensity could be obtained for a separation in less than 40 min. Compared to the optimum 1D-RPLC separation, these quality descriptors were increased by a factor of 3 for peak capacity and 5 for peak intensity while using the same column diameter (2.1 mm) in both dimensions.

3.2. Decrease in the collected fraction volume

According to Eq. 9, x can be reduced by increasing the sampling rate, which is the number of fractions collected per 6σ-peak width in ^{1}D (i.e. 6/λ). The sampling rate value must ideally be selected in the range 1.5 to 2.7 [17] (i.e. λ in the range 2.2 to 4) to have a good trade-off between acceptable undersampling in ^{1}D and high peak capacity in ^{2}D. It was recently shown that the optimum value, in terms of effective peak capacity, was strongly dependent on the gradient time in ^{1}D and preferably close to 1 for 2D separations of less than half an hour while higher than 3 for 2D separations of 200 min or more [18].

3.3. Decrease in the column internal diameters ratio

Reducing $\frac{^1\sigma_{col}}{^2\sigma_{col}}$ in Eq. 9 can be done by selecting appropriate column internal diameters (ID) in both dimensions. According to Pirok et al.[19], the column internal diameter in ^{2}D should be, ideally, more than twice the one in ^{1}D (e.g. 1 mm in ^{1}D and 2.1 or 4.6 mm in ^{2}D, or 2.1 mm in ^{1}D and 4.6 mm in ^{2}D). In this case, the gradient pumps have to operate properly considering the resulting very low flow rates in ^{1}D (< 10µL/min with 1-mm ID) or the very high flow rates in ^{2}D (> 5 mL/min with 4.6-mm ID).

Decreasing the ratio of the column internal diameters has often been considered as the method of choice to decrease x (Eq. 9) since this be achieved without using any additional device (flow-splitting and/or solvent dilution). However, it is done at the cost of high dilution due to small peak volumes in ^{1}D (Eqs. 8 and 10). As shown in Table 1, this strategy has been mostly applied to HILIC x RPLC for which injection effects can be dramatic. The peak shapes in ^{2}D indeed worsen rapidly when the injection volumes increases [20]. In addition to peak distortion (especially band fronting), a breakthrough peak is very often observed. A decrease in $^1d_{i,col}/\,^2d_{i,col}$ may limit such injection effects. As an example, one of the studies listed in Table 1 combined a

microbore HILIC column (i.e. 1-mm ID) in ^{1}D and a wide-bore RPLC column in ^{2}D (i.e. 4.6-mm ID) for the separation of phlorotannins [21,22]. Here, the internal diameter in ^{2}D was more than four times higher than in ^{1}D. As explained by the authors, this was necessary to sufficiently reduce the injection volume in ^{2}D ($^{2}V_i$ < 3% V_0) to ensure the absence of injection effects.

Jandera et al. [20] studied the effect of the gradient starting conditions on band broadening for aromatic hydrocarbons in RPLC. They concluded that injection effects were less predominant when lowering the concentration of strong solvent (i.e. acetonitrile in this example) in the initial mobile phase composition. However, this strategy strongly depends on the compounds of interest and is therefore limited in scope. Yang et al. used such a strategy for the separation of polymers in organic-SEC x RPLC [23], which allowed them to combine a 4.6-mm ID column in ^{1}D with a 2.1-mm ID column in ^{2}D. The initial composition in RPLC was set close to 100% water so that the ^{1}D-fraction, rich in organic solvent, could be diluted before injection in ^{2}D (increase in C_F). Similarly, some authors have used large loop volumes to allow the small injection volume to be mixed with the weaker solvent present in the rest of the loop during the injection process [24,25]. However, with this strategy, the resulting increase in injection volume may also negatively impact the peak shapes depending on the C_F increase. Furthermore, larger loop volumes imply larger dwell volume and hence smaller available gradient times in ^{2}D, resulting in lower peak capacity.

The use of RPLC in ^{1}D with a different retention mechanism in ^{2}D is less common [4]. For example, RPLC x HILIC was applied to the separation of peptides [26]. Despite a larger column internal diameter in ^{2}D (2.1 mm) compared to ^{1}D (1 mm), peak broadening was observed due to the high content of water in the ^{2}D-injection solvent. As a result, the peak capacity was smaller than the one obtained in RPLC x RPLC although the separation space coverage was much higher (i.e. 100% vs. 40%). Similarly, RPLC x SFC was applied to the separation of biomass by-products, using the same column diameters as above [27]. Unlike charged compounds, RPLC x RPLC was found to be poorly orthogonal for such neutral compounds. It is worth mentioning that, in RPLC x SFC, the authors underlined additional issues including (i) the CO2 depressurization which prohibits flow splitting and partial loop injection, (ii) the poor miscibility of the mobile phases, (iii) the larger extra-column volumes and gradient dwell volumes with the current SFC instrumentation, and (iv) the sometimes poor wetting of the stationary phase by the water-rich transferred fraction resulting in

significant pressure increase over the course of injections. Despite this, the effective peak capacity, for these neutral compounds was found to be slightly higher in RPLC x SFC than in RPLC x RPLC [27].

3.4. Flow splitting (split ratio < 1)

This method is usually referred to as "post-^{1}D-flow splitting". According to Eqs. 8 and 9, flow splitting between ^{1}D and the interface ($^{1}z_{split} < 1$) allows reducing the injection volume in ^{2}D and hence *x*.

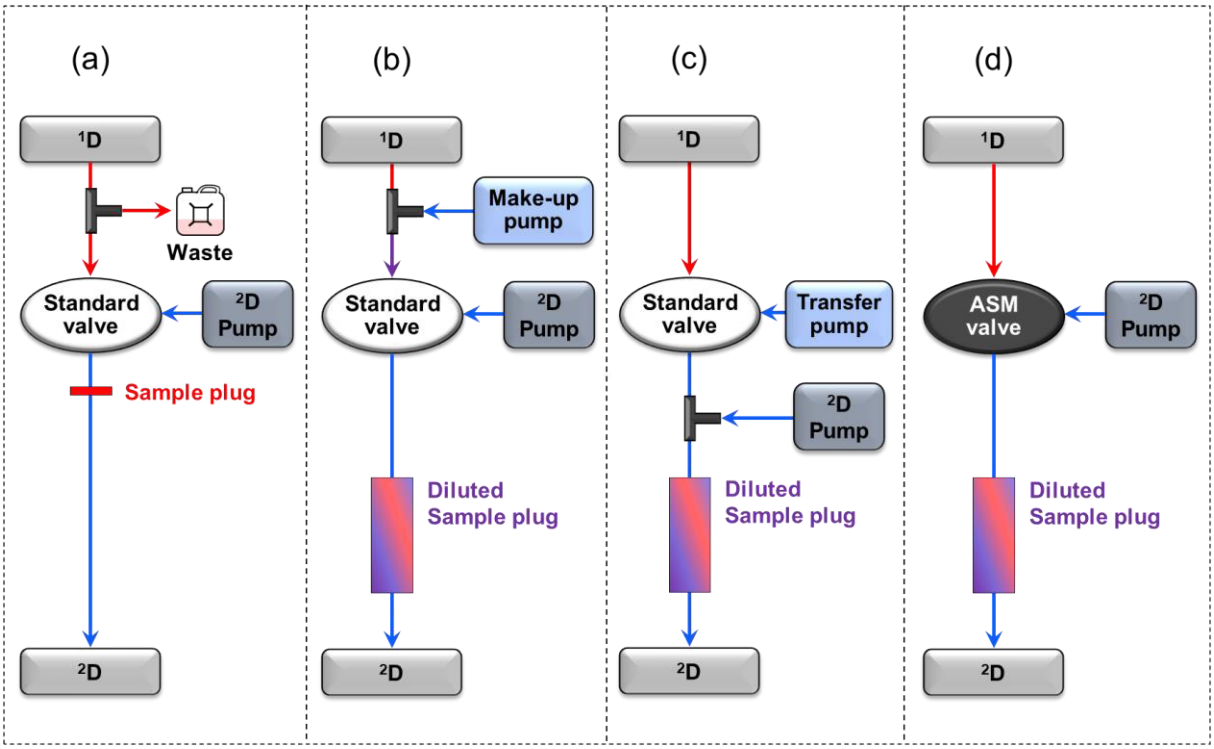

Fig. 5: Schematic representation of the four methods needing additional devices: (a) Flow splitting with a tee-union, on-line solvent dilution with (b) a pump before the valve (make-up flow), (c) a pump after the valve (at-column dilution) or (d) a specific Active Solvent Modulation (ASM) valve. The injected volumes are represented at the bottom of each scheme. Colours stand for the solvent strength (red for strong solvent, blue for weak solvent, purple for diluted solvent). Adapted from [45].

This approach (schematically represented in Fig. 5a) requires a simple device composed of a tee-union and appropriate tubing [10,28,29]. A metering splitting pump or other flow splitter devices can also be used [30]. The main advantage of this method is that it brings a large degree of freedom for selecting column dimensions and flow rates [30]. Flow splitting alone was mainly used in RPLC x RPLC, using similar column diameters in both dimensions (see Table 1). As an example, Sarrut et al. [10] reported

the RPLC x RPLC separation of a tryptic digest of proteins with 2.1-mm ID columns in both dimensions. 2D conditions were optimized to maximize the effective peak capacity while keeping a dilution factor of 1. With a split 1:4, effective peak capacities of 1800, 3400, and 5100 could be achieved in 60 min, 120 min, and 200 min, respectively. Several disadvantages can be stated for post-^{1}D-flow-splitting: (i) maintaining the same split ratio from run-to-run can be challenging and makes this method questionable for quantification, (ii) low split ratios imply high dilution (low ^2V_i in Eq. 10), (iii) significant additional band broadening may occur in case of very low split ratio [31], and (iv) flow splitting alone may not be sufficient to avoid injection effects for fully orthogonal combinations. In the latter case, the additional reduction of $^1d_{i,col}/\,^2d_{i,col}$ may also be necessary. Such a strategy was applied by de Villiers and co-workers [32-37] for the separation of phenolic compounds in HILIC x RPLC. Here, very low split ratios (i.e. $^1z_{split}$ below 0.04) were combined with low $^1d_{i,col}/\,^2d_{i,col}$ (i.e. 1 mm/4.6 mm or 1 mm/2.1 mm), which resulted in very low injection volumes in ^{2}D (i.e. below 0.5% V_0).

3.5. Dilution with a weaker solvent (use of empty loops)

This method consists in diluting ($z_{dilution}$ - 1) times the ^{2}D-injection solvent with a weaker solvent before injection, which leads to a ($z_{dilution}$)-fold increase in V_i (Eq. 8). This should be compensated by a strong decrease in the injection solvent strength (increase in C_F). The objective is to reduce x (Eq.9) by achieving $z_{dilution}/C_F < 1$. Depending on $z_{dilution}$ and on the retention of the solutes, the dilution method may still affect the quality of the separation. As schematically represented in Fig. 5, the dilution can be performed either before (Fig.5b), after (Fig.5c), or within the modulation interface (Fig. 5d). As highlighted in Fig. 5, all three approaches require additional devices, whether it is an additional pump and tee-union for the former two or a specific valve (Active Solvent Modulation valve from Agilent) for the latter one.

In the first approach (Fig.5b), an additional pump, placed before the valve via a tee union, is used to generate what is commonly called a "make-up" flow after the first dimension. The latter is used to introduce a weak solvent into the ^{1}D-effluent to decrease its elution strength. It is important to note that the resulting increase in injection volume requires larger sample loops. This leads to an increase in the dwell time, and thus to a decrease in the available ^{2}D-gradient time, which may result in a

decrease in peak capacity. As shown in Table 1, this approach was extensively used in on-line HILIC x RPLC, with pure water as a make-up solvent to reduce the organic content of the fraction transferred in the ^{2}D-RPLC dimension. This strategy was found to be efficient to avoid injection effects, in particular, breakthrough phenomenon [38].

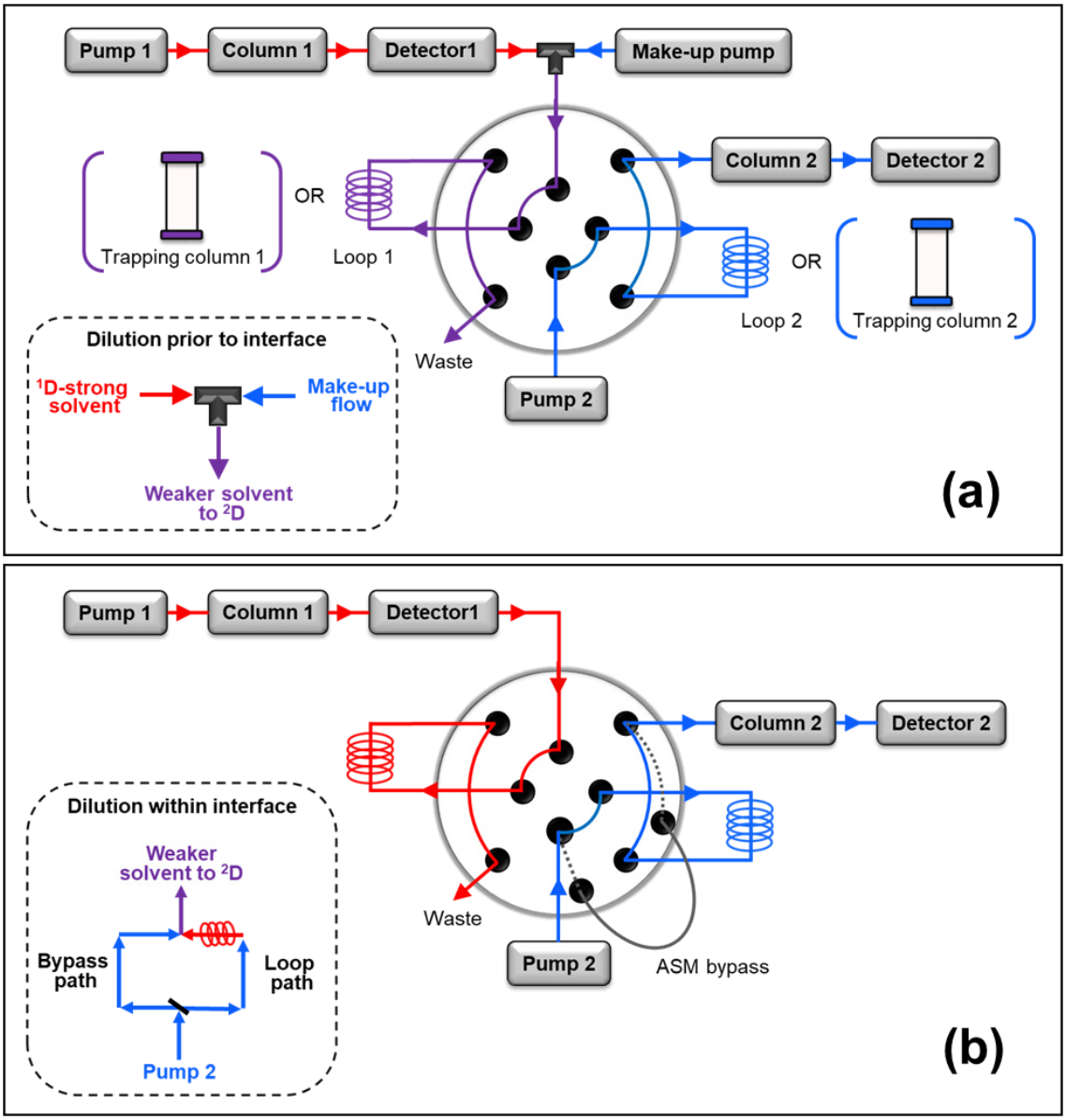

Fig. 6: Schematic representation of an on-line LC x LC set-ups for on-line solvent dilution (a) make-up flow with a 2-position/8-port switching valve equipped with either two sample loops or two trapping columns and (b) ASM valve constituted of a 4-position/10-port switching valve equipped with two sample loops (trademark from Agilent). Dilution operations are detailed in the frames.

Similarly, the second method called "at-column dilution" (Fig.5c) requires a transfer pump, located after the valve and designed to push the sample out of the sample loop. The sample is then diluted by the ^{2}D-pump with a weak initial mobile phase. This

method was used in both RPLC x HILIC and HILIC x RPLC by Chen et al. [39,40] for the analysis of red ginseng extract and herbal medicine.

The third method was introduced by Petersson et al. [41] for multiple heart-cutting 2D-LC and then improved by Stoll et al. [42]. It relies on the use of a modified 4-port/dual-position valve including a bypass flow path, which allows diluting within the modulation interface. The two valves (standard and modified ones) and their operation are shown in Fig. 6. This dilution method is referred to as *Active Solvent Modulation* (*ASM*). It enables the dilution of the collected fraction with a weaker solvent without an additional pump but with a specific valve. The operating principle is based on a difference in capillary restriction between the sample loop and a bypass capillary, which is designed to control the dilution ratio between the transferred fraction and the ^{2}D-mobile phase. To achieve an efficient dilution, the initial composition must be as weak as possible during a sufficiently long time, hence an isocratic hold is needed. It should be pointed out that this is also true for the at-column dilution approach (Fig. 5c). The transferred fraction can be diluted up to a maximum ratio of 5.1, which is the current limit of the process. Since the dilution process takes place at the beginning of each modulation, the use of ASM reduces the available time for the separation. Similarly to the make-up and at-column dilution approaches, the injected volume in the second dimension is multiplied by the dilution ratio, which may result in very large volumes injected in ^{2}D. This may lead to a decrease in the peak capacity for a given sampling time due to the reduction of the available gradient time.

The performance of the ASM approach was recently demonstrated in HILIC x RPLC for the separation of therapeutic antibodies [43]. In this study, peak distortion and breakthrough phenomenon were eliminated with an ASM dilution ratio of 3, leading to 120 µL injected into a 30 x 2.1-mm column after dilution. Compared to a method without dilution, ASM dilution was proved to provide higher peak intensities due to the focusing effect at the column inlet.

Despite on-line dilution, there is a risk of insufficient focusing in the column depending on the analyte retention. The very large volumes usually injected may still lead to peak broadening, which then makes the dilution method counterproductive. Preliminary studies must be conducted to find the proper dilution ratio. For poorly retained analytes, the dilution ratio may be insufficient to provide enough focusing at the column inlet. This problem was highlighted in the context of the RPLC x RPLC separation of pharmaceuticals [37]. The authors concluded that splitting a fraction of

the ^{1}D-effluent before diluting it with water could be beneficial to reduce peak width and enhance peak height. Similarly, broad and distorted peaks were reported for little retained aromatic compounds in HILIC x RPLC [38] despite on-line dilution with a counter-gradient. A recent study on the separation of peptides in HILIC x RPLC [45] showed the occurrence of distorted peaks and breakthrough phenomenon with both the make-up flow and ASM dilution approaches. As shown in Fig. 7, poorly and highly retained peptides were both affected because this effect also depends on their retention in ^{1}D and hence on the percentage of acetonitrile at elution.

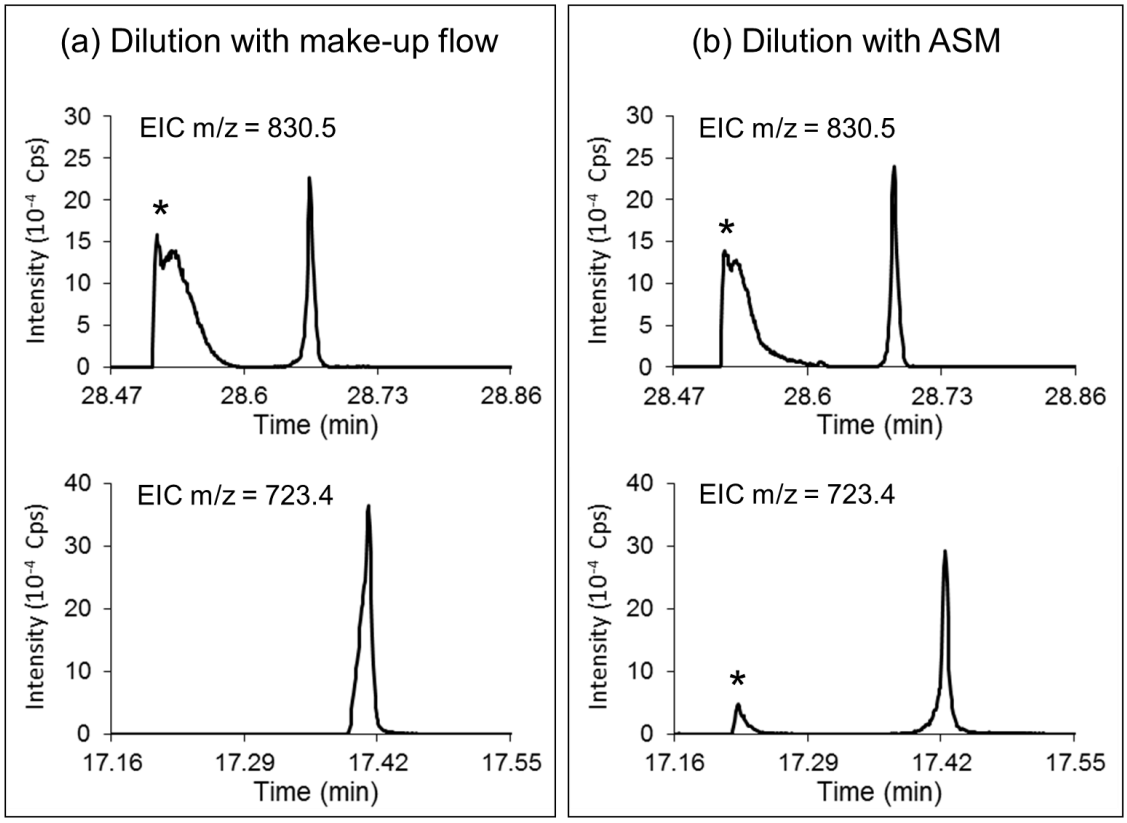

Fig. 7: ^{2}D-separations of two peptides with different retention in on-line HILIC x RPLC-HRMS highlighting the limitations of solvent dilution for both (a) dilution with a make-flow and (b) dilution with ASM with. Dilution ratio of 5 in both conditions leading to the injection of about 100 µL in a (30 x 2.1 mm)-column with an injection solvent containing either 13% ACN (EIC m/z = 830.5) or 17% ACN (EIC m/z = 723.4) after dilution. Breakthrough peak indicated by an asterisk. Adapted from [45].

3.6. Dilution with a weaker solvent (use of trapping columns)

In addition to on-line solvent dilution, trapping columns may be used to substitute the conventional empty loops. This approach is supposed to enable both the removal of the transferred solvent from ^{1}D and the refocusing of the solutes in a weaker solvent

before reinjection in ^{2}D ($C_{F,trap}$ in Eqs. 8 and 9). In this case, the modulation process is the same as when empty loops are used for storage and transfer, except that short packed columns (usually guard columns) are used to trap the analytes eluting from ^{1}D (Fig. 6a). As seen in Table 1, this approach has been used for 2D combinations such as HILIC x RPLC, RPLC x HILIC, RPLC x RPLC, and SCX x RPLC. The choice of the adsorbent is crucial and depends on the properties of the analyte, the mobile phases used in each dimension, and the order in which the columns are coupled. For the trapping to be effective, the trapping columns must be more retentive than the ^{1}D-column but at the same time, not too retentive to be able to desorb the analytes with the ^{2}D-solvent. Typically, the trapping columns are chosen to match the ^{2}D-column selectivity [46]. The sorption solvent must be weak enough to enable the retention on the short trapping column whereas the desorption solvent must be strong enough to rapidly desorb all trapped analytes.

Desmet and co-workers [47-49] studied in detail both the theoretical and experimental aspects of post-column peak refocusing when using trapping columns in 1D-LC to enhance the detection sensitivity. The effects of loading time, trapping column length and inner diameter, elution direction, and retentive properties of the trapping column were assessed. They demonstrated that to achieve an effective post-column refocusing, the retention on the trap should be higher than on the ^{1}D-column. More importantly, they also showed that peak refocusing and thus concentration enhancement strongly depends on the loading time and the elution strength of the desorption solvent. The stronger the desorption solvent and the better the focusing effect. For the trapping process to be effective, the desorption solvent must have the time to overtake and sweep out the analytes before they leave the column. Depending on the trap dimensions, if the timing is not right, the peak might elute in the same solvent as the one used for sorption, which prevents any focusing. To minimize band dispersion, it was concluded that a backward elution of the trap should be preferred. Paradoxically, in the literature, on-line LC x LC methods involving trapping columns have been performed with both backward and forward elution of the trap, with most often little regard for this important parameter.

Due to the instrumental constraints in on-line LC x LC, sorption and desorption solvents are imposed by ^{1}D- and ^{2}D-mobile phases, respectively. For this reason, the development is made complicated with the use of gradient mode in both dimensions, leading to different compositions at elution along the ^{1}D run. Depending on the

conditions, trapping and desorption of the analyte may be less effective throughout the 2D analysis, leading to carry-over between successive fractions. To enhance the trapping process, a make-up flow prior to the valve is generally used to decrease the eluent strength of the ^{1}D-effluent and increase solute retention on the trapping column. However, the fact that the desorption solvent is imposed by the initial mobile phase in ^{2}D makes some of the combinations of similar modes such as RPLC x RPLC less suitable for the use of trapping columns. Moreover, in on-line LC x LC, the requirement for fast separation in ^{2}D can be a limiting factor. Compromises have to be made between trapping efficiency on one hand, and rapid compound desorption and thus fast analysis time in ^{2}D on the other hand [50]. The trapping column dimensions also have to be carefully chosen to find the best trade-off between high loading capability, low flow resistance, and low additional band broadening [51]. In the literature, the use of short trapping columns with length below 10 mm is usually favoured.

Trapping columns have recently gained much interest in HILIC x RPLC (see Table 1). For all set-ups, an apolar stationary phase (usually C18) was chosen while a make-up flow with a high content of water was used before the trapping columns to reduce the ^{1}D-eluent strength and retain the analytes on a short trapping column. For the desorption step, the initial composition in ^{2}D was sometimes composed of a high percentage of organic solvent to achieve fast refocusing of analytes during flushing [52-55]. For example, Gargano et al. [53] used a 2-position/8-port switching valve equipped with two identical short C18 trapping columns (2.1 x 2 mm) for the on-line HILIC x RPLC separation of ethoxylate phosphates. HILIC separation was achieved in gradient elution from 2% to 50% water but a make-up flow dilution with water ($z_{dilution}$ of about 8) allowed diluting the ^{1}D-acetonitrile-rich effluent. For desorption, the initial composition in ^{2}D was rich in organic solvent (35% Methanol) which permitted to achieve trapping and refocusing within a sampling time of 0.35 min without injection effects in ^{2}D. However, starting with an initial composition rich in organic solvent is not always suitable for the least retained compounds. The use of segment gradient [25,26] or shifted gradient [57] in ^{2}D has also been reported. They allow to gradually modify the desorption eluent strength according to the retention of the analytes. Such an approach was applied by Sommella et al. [57] for the on-line HILIC x RPLC separation of phenolic compounds in apple extract shown in Fig. 8b. In their work, C18-guard columns were used as traps after diluting the ^{1}D-effluent 10-fold with

a make-up flow containing water. They reported both higher peak capacity and method sensitivity with this approach compared to a method without dilution nor trapping (Fig. 8a). As highlighted in Fig. 8a vs. 8b, this strategy allowed to eliminate breakthrough in ^{2}D.

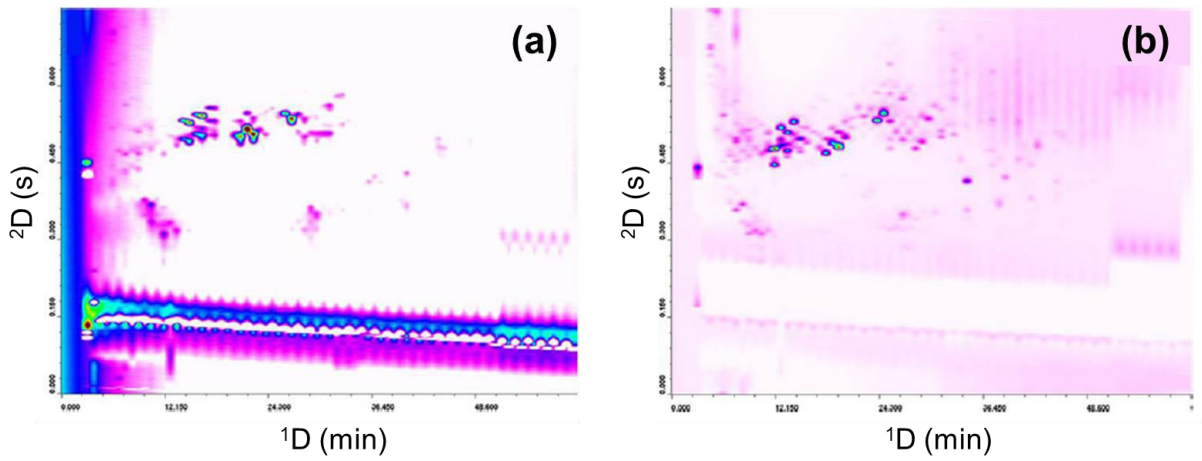

Fig. 8: On-line HILIC x RPLC separations of an apple polyphenolic extract (a) without or (b) with dilution of the ^{1}D-effluent with a make-up flow and trapping columns used at the interface (forward flush). Adapted from [57].

Trapping columns should not be too retentive to avoid carry-over in ^{2}D. For this purpose, short columns must be preferred. Conversely, some solutes may not be sufficiently retained and, therefore, lost. In any case, the conditions of trapping and desorption must be carefully optimized. In most reported studies in on-line LC x LC with trapping columns, trapping conditions were little investigated. Optimized conditions for an effective refocusing of all the analytes present in a complex sample may be hard to find. According to Eq. 9, to reduce x, the objective is $z_{dilution}/\left({}^{2}C_F \times C_{F,trap} \right) < 1$. From our perspective, the contribution of trapping columns to the reduction of injection effects has yet to be proven. If the ^{2}D-initial mobile phase is not strong enough (at least stronger than the sorption solvent), solute refocusing cannot be observed. Besides, in HILIC x RPLC for example, very large dilution ratios (> 10) must be applied to sufficiently reduce the ACN content and allow solute retention on the C18 trapping column.

Van de Ven et al. [58] proposed a novel approach consisting in using cold temperatures during loading to enhance the trapping and hot temperature during flushing to facilitate elution and refocusing. In their study, cooling was achieved through

immersion of the column in a water bath and heating through a column-heating device. The proof of concept was made in 1D-LC on three small aromatic molecules. However, the time necessary to heat and cool the trapping column is likely to be incompatible with a fast ^{2}D separation.

3.7. Solvent evaporation

Given the limitations of active modulation techniques involving dilution and/or trapping columns, some researchers have thought of another strategy to minimize injection effects in ^{2}D. It consists in evaporating the collected fractions before injection in ^{2}D. On-column focusing in ^{2}D is thus achieved by substituting the strong solvent of the collected fraction with a weak solvent. Solvent evaporation in on-line LC x LC can be obtained by heating, vacuum suction or a combination of both. Introduced in 2006 [59], this strategy has been little reported in the context of on-line LC x LC, probably because it requires the in-house development of a special modulation interface.

Fornells et al. [60] recently developed an automated so-called evaporative membrane modulator (EMM) designed to reduce the transfer volume between dimensions. In this work, solvent evaporation was achieved before fraction storage into the loops through a porous hydrophobic membrane constituted of polytetrafluoroethylene (PTFE). The membrane was sandwiched between a liquid and a gas channel and connected to both the inlet of an 8 port valve and a vacuum pump. Vacuum evaporation was supplemented by heating from four infrared LEDs. The benefit of this EMM system was demonstrated for the RPLC x RPLC separation of a standard mixture of phenolic acids. The EMM system allowed a 10-fold decrease in the ^{2}D-injection volume. Unlike in-loop evaporation approaches, the EMM system prevents contamination between fractions.

Although evaporation-based strategies are especially attractive for highly incompatible coupling such as NPLC and RPLC, they can gain interest for fully compatible coupling (e.g. RPLC x RPLC) to increase peak intensity. In addition, reducing the injection volume in ^{2}D can give more freedom in the choice of conditions, and hence could make 2D method development easier. However, both the applicability and efficiency of this technique depends on the volatility of the solvents. Another concern is the risk of precipitation of analytes during the dissolution step which may lead to baseline drifts and pressure increase in ^{2}D.

4. Conclusion

The on-line comprehensive coupling of orthogonal chromatographic modes may cause severe injection effects in the second dimension, deriving from the solvent mismatch between the two systems. These injection effects can seriously ruin the chromatographic performance of on-line LC x LC and must be avoided. Over the years, researchers have been developing strategies to circumvent these effects. Most of the reported strategies have been consisting in modifying the composition and/or the volume of the transferred fraction coming from the first dimension before reinjection into the second dimension column. At first instance, injection effects may be prevented by selecting appropriate column dimensions or by using flow splitting between dimension to decrease the injected volume in the second dimension. However, such strategies come at the price of a decrease in method sensitivity. Other strategies include the use of on-line solvent dilution, trapping columns or solvent evaporation approaches. All of them have proven to be efficient to reduce injection effects to some extent in various applications but also show weaknesses. On-line solvent dilution appears to be the simplest option to circumvent problems related to solvent strength mismatch. However, the dilution of the first dimension effluent may cause a counterproductive decrease in both sensitivity and resolution for poorly retained compounds. The use of trapping columns instead of conventional storage loops may be a solution to improve the sensitivity by allowing solvent switching while promoting focusing and limiting the transferred volume. However, the effective trapping and elution of compounds from the traps strongly depends on the sample at hand and the mobile phase used in each dimension, and can thus be hard to achieve in on-line LC x LC. Solvent evaporation could be the most effective way to eliminate injection effects by allowing the complete solvent exchange of the first dimension transferred fraction. However, this approach is only applicable to low boiling points solvent and high boiling point compounds. Moreover, it seems to be the most difficult approach to implement in routine in on-line LC x LC.

Finally, in the case of combinations leading to significant solvent strength mismatch problems between dimensions (e.g. HILIC and RPLC), a combination between strategies may be necessary. However, more often than not, the side-effect of such an approach is its deleterious impact on method sensitivity.

5. References

[1] J.C. Giddings, Maximum number of components resolvable by gel filtration and other elution chromatographic methods, Anal. Chem. 39 (1967) 1027–1028. https://doi.org/10.1021/ac60252a025.

[2] K. Horie, Y. Sato, T. Kimura, T. Nakamura, Y. Ishihama, Y. Oda, T. Ikegami, N. Tanaka, Estimation and optimization of the peak capacity of one-dimensional gradient high performance liquid chromatography using a long monolithic silica capillary column, J. Chromatogr. A. 1228 (2012) 283–291. https://doi.org/10.1016/j.chroma.2011.12.088.

[3] M. Iguiniz, S. Heinisch, Two-dimensional liquid chromatography in pharmaceutical analysis. Instrumental aspects, trends and applications, J. Pharm. Biomed. Anal. 145 (2017) 482–503. https://doi.org/10.1016/j.jpba.2017.07.009.

[4] B.W.J. Pirok, D.R. Stoll, P.J. Schoenmakers, Recent Developments in Two-Dimensional Liquid Chromatography: Fundamental Improvements for Practical Applications, Anal. Chem. 91 (2019) 240–263. https://doi.org/10.1021/acs.analchem.8b04841.

[5] D.R. Stoll, P.W. Carr, Two-Dimensional Liquid Chromatography: A State of the Art Tutorial, Anal. Chem. 89 (2017) 519–531. https://doi.org/10.1021/acs.analchem.6b03506.

[6] F. Cacciola, F. Rigano, P. Dugo, L. Mondello, Comprehensive two-dimensional liquid chromatography as a powerful tool for the analysis of food and food products, Trac-Trends Anal. Chem. 127 (2020) 115894. https://doi.org/10.1016/j.trac.2020.115894.

[7] S. Ji, S. Wang, H. Xu, Z. Su, D. Tang, X. Qiao, M. Ye, The application of on-line two-dimensional liquid chromatography (2DLC) in the chemical analysis of herbal medicines, J. Pharm. Biomed. Anal. 160 (2018) 301–313. https://doi.org/10.1016/j.jpba.2018.08.014.

[8] S.Chapel, F. Rouvière, S. Heinisch, A Theoretical and Practical Approach to Manage High Peak Capacity and Low Dilution in On-line Comprehensive Reversed-Phase LC × Reversed-Phase LC: A Comparison with 1D-Reversed-Phase LC, LC-GC Europe, 2020, vol 33, number s5, Advances in UHPLC/HPLC, 17-26.

[9] M. Sarrut, G. Crétier, S. Heinisch, Theoretical and practical interest in UHPLC technology for 2D-LC, TrAC Trends Anal. Chem. 63 (2014) 104–112. https://doi.org/10.1016/j.trac.2014.08.005.

[10] M. Sarrut, A. D'Attoma, S. Heinisch, Optimization of conditions in on-line comprehensive two-dimensional reversed phase liquid chromatography.

Experimental comparison with one-dimensional reversed phase liquid chromatography for the separation of peptides, J. Chromatogr. A. 1421 (2015) 48–59. https://doi.org/10.1016/j.chroma.2015.08.052.

[11] P. Česla, J. Křenková, Fraction transfer process in on-line comprehensive two-dimensional liquid-phase separations, J. Sep. Sci. 40 (2017) 109–123. https://doi.org/10.1002/jssc.201600921.

[12] Y. Chen, L. Montero, O.J. Schmitz, Advance in on-line two-dimensional liquid chromatography modulation technology, TrAC Trends Anal. Chem. 120 (2019) 115647. https://doi.org/10.1016/j.trac.2019.115647.

[13] J.C. Sternberg in: J.C. Giddings, R.A. Keller (Eds.), Advances in Chromatography,vol. 2, Dekker, New York, 1966, p. 205, 2 (n.d.) 205.

[14] S.R. Groskreutz, S.G. Weber, Quantitative evaluation of models for solvent-based, on-column focusing in liquid chromatography, J. Chromatogr. A. 1409 (2015) 116–124. https://doi.org/10.1016/j.chroma.2015.07.038.

[15] M. Sarrut, A. Corgier, S. Fekete, D. Guillarme, D. Lascoux, M.-C. Janin-Bussat, A. Beck, S. Heinisch, Analysis of antibody-drug conjugates by comprehensive on-line two-dimensional hydrophobic interaction chromatography x reversed phase liquid chromatography hyphenated to high resolution mass spectrometry. I – Optimization of separation conditions, J. Chromatogr. B. 1032 (2016) 103–111. https://doi.org/10.1016/j.jchromb.2016.06.048.

[16] M. Sarrut, S. Fekete, M.-C. Janin-Bussat, O. Colas, D. Guillarme, A. Beck, S. Heinisch, Analysis of antibody-drug conjugates by comprehensive on-line two-dimensional hydrophobic interaction chromatography x reversed phase liquid chromatography hyphenated to high resolution mass spectrometry. II-Identification of sub-units for the characterization of even and odd load drug species, J. Chromatogr. B. 1032 (2016) 91–102. https://doi.org/10.1016/j.jchromb.2016.06.049.

[17] K. Horie, H. Kimura, T. Ikegami, A. Iwatsuka, N. Saad, O. Fiehn, N. Tanaka, Calculating Optimal Modulation Periods to Maximize the Peak Capacity in Two-Dimensional HPLC, Anal. Chem. 79 (2007) 3764–3770. https://doi.org/10.1021/ac062002t.

[18] M. Sarrut, F. Rouvière, S. Heinisch, Theoretical and experimental comparison of one dimensional versus on-line comprehensive two dimensional liquid chromatography for optimized sub-hour separations of complex peptide samples, J. Chromatogr. A. 1498 (2017) 183–195. https://doi.org/10.1016/j.chroma.2017.01.054.

[19] B.W.J. Pirok, A.F.G. Gargano, P.J. Schoenmakers, Optimizing separations in online comprehensive two-dimensional liquid chromatography, J. Sep. Sci. 41 (2018) 68–98. https://doi.org/10.1002/jssc.201700863.

[20] P. Jandera, T. Hájek, P. Česla, Effects of the gradient profile, sample volume and solvent on the separation in very fast gradients, with special attention to the second-dimension gradient in comprehensive two-dimensional liquid chromatography, J. Chromatogr. A. 1218 (2011) 1995–2006. https://doi.org/10.1016/j.chroma.2010.10.095.

[21] L. Montero, A.P. Sánchez-Camargo, V. García-Cañas, A. Tanniou, V. Stiger-Pouvreau, M. Russo, L. Rastrelli, A. Cifuentes, M. Herrero, E. Ibáñez, Anti-proliferative activity and chemical characterization by comprehensive two-dimensional liquid chromatography coupled to mass spectrometry of phlorotannins from the brown macroalga Sargassum muticum collected on North-Atlantic coasts, J. Chromatogr. A. 1428 (2016) 115–125. https://doi.org/10.1016/j.chroma.2015.07.053.

[22] L. Montero, E. Ibáñez, M. Russo, R. di Sanzo, L. Rastrelli, A.L. Piccinelli, R. Celano, A. Cifuentes, M. Herrero, Metabolite profiling of licorice (Glycyrrhiza glabra) from different locations using comprehensive two-dimensional liquid chromatography coupled to diode array and tandem mass spectrometry detection, Anal. Chim. Acta. 913 (2016) 145–159. https://doi.org/10.1016/j.aca.2016.01.040.

[23] P. Yang, L. Bai, W. Wang, J. Rabasco, Analysis of hydrophobically modified ethylene oxide urethane rheology modifiers by comprehensive two dimensional liquid chromatography, J. Chromatogr. A. 1560 (2018) 55–62. https://doi.org/10.1016/j.chroma.2018.05.033.

[24] L. Montero, M. Herrero, M. Prodanov, E. Ibáñez, A. Cifuentes, Characterization of grape seed procyanidins by comprehensive two-dimensional hydrophilic interaction × reversed phase liquid chromatography coupled to diode array detection and tandem mass spectrometry, Anal. Bioanal. Chem. 405 (2013) 4627–4638. https://doi.org/10.1007/s00216-012-6567-5.

[25] L. Montero, E. Ibáñez, M. Russo, L. Rastrelli, A. Cifuentes, M. Herrero, Focusing and non-focusing modulation strategies for the improvement of on-line two-dimensional hydrophilic interaction chromatography × reversed phase profiling of complex food samples, Anal. Chim. Acta. 985 (2017) 202–212. https://doi.org/10.1016/j.aca.2017.07.013.

[26] A. D'Attoma, S. Heinisch, On-line comprehensive two dimensional separations of charged compounds using reversed-phase high performance liquid chromatography and hydrophilic interaction chromatography. Part II: Application to the separation of peptides, J. Chromatogr. A. 1306 (2013) 27–36. https://doi.org/10.1016/j.chroma.2013.07.048.

[27] M. Sarrut, A. Corgier, G. Crétier, A. Le Masle, S. Dubant, S. Heinisch, Potential and limitations of on-line comprehensive reversed phase liquid chromatography×supercritical fluid chromatography for the separation of

neutral compounds: An approach to separate an aqueous extract of bio-oil, J. Chromatogr. A. 1402 (2015) 124–133. https://doi.org/10.1016/j.chroma.2015.05.005.

[28] A. Le Masle, D. Angot, C. Gouin, A. D'Attoma, J. Ponthus, A. Quignard, S. Heinisch, Development of on-line comprehensive two-dimensional liquid chromatography method for the separation of biomass compounds, J. Chromatogr. A. 1340 (2014) 90–98. https://doi.org/10.1016/j.chroma.2014.03.020.

[29] M. Iguiniz, E. Corbel, N. Roques, S. Heinisch, On-line coupling of achiral Reversed Phase Liquid Chromatography and chiral Supercritical Fluid Chromatography for the analysis of pharmaceutical compounds, J. Pharm. Biomed. Anal. 159 (2018) 237–244. https://doi.org/10.1016/j.jpba.2018.06.058.

[30] M.R. Filgueira, Y. Huang, K. Witt, C. Castells, P.W. Carr, Improving Peak Capacity in Fast Online Comprehensive Two-Dimensional Liquid Chromatography with Post-First-Dimension Flow Splitting, Anal. Chem. 83 (2011) 9531–9539. https://doi.org/10.1021/ac202317m.

[31] M. Bernardin, F. Bessueille-Barbier, A. Le Masle, C.-P. Lienemann, S. Heinisch, Suitable interface for coupling liquid chromatography to inductively coupled plasma-mass spectrometry for the analysis of organic matrices. 1 Theoretical and experimental considerations on solute dispersion, J. Chromatogr. A. 1565 (2018) 68–80. https://doi.org/10.1016/j.chroma.2018.06.024.

[32] T. Beelders, K.M. Kalili, E. Joubert, D. de Beer, A. de Villiers, Comprehensive two-dimensional liquid chromatographic analysis of rooibos (Aspalathus linearis) phenolics, J. Sep. Sci. 35 (2012) 1808–1820. https://doi.org/10.1002/jssc.201200060.

[33] K.M. Kalili, S.D. Smet, T. van Hoeylandt, F. Lynen, A. de Villiers, Comprehensive two-dimensional liquid chromatography coupled to the ABTS radical scavenging assay: a powerful method for the analysis of phenolic antioxidants, Anal. Bioanal. Chem. 406 (2014) 4233–4242. https://doi.org/10.1007/s00216-014-7847-z.

[34] K.M. Kalili, A. de Villiers, Systematic optimisation and evaluation of on-line, off-line and stop-flow comprehensive hydrophilic interaction chromatography×reversed phase liquid chromatographic analysis of procyanidins, Part I: Theoretical considerations, J. Chromatogr. A. 1289 (2013) 58–68. https://doi.org/10.1016/j.chroma.2013.03.008.

[35] K.M. Kalili, A. de Villiers, Systematic optimisation and evaluation of on-line, off-line and stop-flow comprehensive hydrophilic interaction chromatography×reversed phase liquid chromatographic analysis of procyanidins. Part II: Application to cocoa procyanidins, J. Chromatogr. A. 1289 (2013) 69–79. https://doi.org/10.1016/j.chroma.2013.03.009.

[36] C.M. Willemse, M.A. Stander, J. Vestner, A.G.J. Tredoux, A. de Villiers, Comprehensive Two-Dimensional Hydrophilic Interaction Chromatography (HILIC) × Reversed-Phase Liquid Chromatography Coupled to High-Resolution Mass Spectrometry (RP-LC-UV-MS) Analysis of Anthocyanins and Derived Pigments in Red Wine, Anal. Chem. 87 (2015) 12006–12015. https://doi.org/10.1021/acs.analchem.5b03615.

[37] K.M. Kalili, J. Vestner, M.A. Stander, A. de Villiers, Toward Unraveling Grape Tannin Composition: Application of Online Hydrophilic Interaction Chromatography × Reversed-Phase Liquid Chromatography–Time-of-Flight Mass Spectrometry for Grape Seed Analysis, Anal. Chem. 85 (2013) 9107–9115. https://doi.org/10.1021/ac401896r.

[38] M. Navarro-Reig, J. Jaumot, A. Baglai, G. Vivó-Truyols, P.J. Schoenmakers, R. Tauler, Untargeted Comprehensive Two-Dimensional Liquid Chromatography Coupled with High-Resolution Mass Spectrometry Analysis of Rice Metabolome Using Multivariate Curve Resolution, Anal. Chem. 89 (2017) 7675–7683. https://doi.org/10.1021/acs.analchem.7b01648.

[39] Y. Chen, J. Li, O.J. Schmitz, Development of an At-Column Dilution Modulator for Flexible and Precise Control of Dilution Factors to Overcome Mobile Phase Incompatibility in Comprehensive Two-Dimensional Liquid Chromatography, Anal. Chem. 91 (2019) 10251–10257. https://doi.org/10.1021/acs.analchem.9b02391.

[40] Y. Chen, L. Montero, J. Luo, J. Li, O.J. Schmitz, Application of the new at-column dilution (ACD) modulator for the two-dimensional RP×HILIC analysis of Buddleja davidii, Anal. Bioanal. Chem. 412 (2020) 1483–1495. https://doi.org/10.1007/s00216-020-02392-3.

[41] P. Petersson, K. Haselmann, S. Buckenmaier, Multiple heart-cutting two dimensional liquid chromatography mass spectrometry: Towards real time determination of related impurities of bio-pharmaceuticals in salt based separation methods, J. Chromatogr. A. 1468 (2016) 95–101. https://doi.org/10.1016/j.chroma.2016.09.023.

[42] D.R. Stoll, K. Shoykhet, P. Petersson, S. Buckenmaier, Active Solvent Modulation: A Valve-Based Approach To Improve Separation Compatibility in Two-Dimensional Liquid Chromatography, Anal. Chem. 89 (2017) 9260–9267. https://doi.org/10.1021/acs.analchem.7b02046.

[43] D.R. Stoll, D.C. Harmes, G.O. Staples, O.G. Potter, C.T. Dammann, D. Guillarme, A. Beck, Development of Comprehensive Online Two-Dimensional Liquid Chromatography/Mass Spectrometry Using Hydrophilic Interaction and Reversed-Phase Separations for Rapid and Deep Profiling of Therapeutic Antibodies, Anal. Chem. 90 (2018) 5923–5929. https://doi.org/10.1021/acs.analchem.8b00776.

[44] D.R. Stoll, E.S. Talus, D.C. Harmes, K. Zhang, Evaluation of detection sensitivity in comprehensive two-dimensional liquid chromatography separations of an active pharmaceutical ingredient and its degradants, Anal. Bioanal. Chem. 407 (2015) 265–277. https://doi.org/10.1007/s00216-014-8036-9.

[45] S. Chapel, F. Rouvière, S. Heinisch, Comparison of existing strategies for keeping symmetrical peaks in on-line Hydrophilic Interaction Liquid Chromatography x Reversed-Phase Liquid Chromatography despite solvent strength mismatch, J. Chromatogr. A. 1642 (2021) 462001. https://doi.org/10.1016/j.chroma.2021.462001.

[46] M.J. Egeness, M.C. Breadmore, E.F. Hilder, R.A. Shellie, The Modulator in Comprehensive Two-Dimensional Liquid Chromatography, LC-GC Eur. 29 (2016) 268–276.

[47] J. De Vos, G. Desmet, S. Eeltink, A generic approach to post-column refocusing in liquid chromatography, J. Chromatogr. A. 1360 (2014) 164–171. https://doi.org/10.1016/j.chroma.2014.07.072.

[48] J. De Vos, S. Eeltink, G. Desmet, Peak refocusing using subsequent retentive trapping and strong eluent remobilization in liquid chromatography: A theoretical optimization study, J. Chromatogr. A. 1381 (2015) 74–86. https://doi.org/10.1016/j.chroma.2014.12.082.

[49] V. Pepermans, J. De Vos, S. Eeltink, G. Desmet, Peak sharpening limits of solvent-assisted post-column refocusing to enhance detection limits in liquid chromatography, J. Chromatogr. A. 1586 (2019) 52–61. https://doi.org/10.1016/j.chroma.2018.11.078.

[50] C.J. Venkatramani, A. Patel, Towards a comprehensive 2-D-LC–MS separation, J. Sep. Sci. 29 (2006) 510–518. https://doi.org/10.1002/jssc.200500341.

[51] R.J. Vonk, A.F.G. Gargano, E. Davydova, H.L. Dekker, S. Eeltink, L.J. de Koning, P.J. Schoenmakers, Comprehensive Two-Dimensional Liquid Chromatography with Stationary-Phase-Assisted Modulation Coupled to High-Resolution Mass Spectrometry Applied to Proteome Analysis of Saccharomyces cerevisiae, Anal. Chem. 87 (2015) 5387–5394. https://doi.org/10.1021/acs.analchem.5b00708.

[52] Q. Li, F. Lynen, J. Wang, H. Li, G. Xu, P. Sandra, Comprehensive hydrophilic interaction and ion-pair reversed-phase liquid chromatography for analysis of di- to deca-oligonucleotides, J. Chromatogr. A. 1255 (2012) 237–243. https://doi.org/10.1016/j.chroma.2011.11.062.

[53] A.F.G. Gargano, M. Duffin, P. Navarro, P.J. Schoenmakers, Reducing Dilution and Analysis Time in Online Comprehensive Two-Dimensional Liquid Chromatography by Active Modulation, Anal. Chem. 88 (2016) 1785–1793. https://doi.org/10.1021/acs.analchem.5b04051.

[54] A.F.G. Gargano, J.B. Shaw, M. Zhou, C.S. Wilkins, T.L. Fillmore, R.J. Moore, G.W. Somsen, L. Paša-Tolić, Increasing the Separation Capacity of Intact Histone Proteoforms Chromatography Coupling Online Weak Cation Exchange-HILIC to Reversed Phase LC UVPD-HRMS, J. Proteome Res. 17 (2018) 3791–3800. https://doi.org/10.1021/acs.jproteome.8b00458.

[55] H. Zhang, J.-M. Jiang, D. Zheng, M. Yuan, Z.-Y. Wang, H.-M. Zhang, C.-W. Zheng, L.-B. Xiao, H.-X. Xu, A multidimensional analytical approach based on time-decoupled online comprehensive two-dimensional liquid chromatography coupled with ion mobility quadrupole time-of-flight mass spectrometry for the analysis of ginsenosides from white and red ginsengs, J. Pharm. Biomed. Anal. 163 (2019) 24–33. https://doi.org/10.1016/j.jpba.2018.09.036.

[56] J.-L. Cao, S.-S. Wang, H. Hu, C.-W. He, J.-B. Wan, H.-X. Su, Y.-T. Wang, P. Li, Online comprehensive two-dimensional hydrophilic interaction chromatography×reversed-phase liquid chromatography coupled with hybrid linear ion trap Orbitrap mass spectrometry for the analysis of phenolic acids in Salvia miltiorrhiza, J. Chromatogr. A. 1536 (2018) 216–227. https://doi.org/10.1016/j.chroma.2017.09.041.

[57] E. Sommella, O.H. Ismail, F. Pagano, G. Pepe, C. Ostacolo, G. Mazzoccanti, M. Russo, E. Novellino, F. Gasparrini, P. Campiglia, Development of an improved online comprehensive hydrophilic interaction chromatography × reversed-phase ultra-high-pressure liquid chromatography platform for complex multiclass polyphenolic sample analysis, J. Sep. Sci. 40 (2017) 2188–2197. https://doi.org/10.1002/jssc.201700134.

[58] H.C. van de Ven, A.F.G. Gargano, Sj. van der Wal, P.J. Schoenmakers, Switching solvent and enhancing analyte concentrations in small effluent fractions using in-column focusing, J. Chromatogr. A. 1427 (2016) 90–95. https://doi.org/10.1016/j.chroma.2015.11.082.

[59] H. Tian, J. Xu, Y. Xu, Y. Guan, Multidimensional liquid chromatography system with an innovative solvent evaporation interface, J. Chromatogr. A. 1137 (2006) 42–48. https://doi.org/10.1016/j.chroma.2006.10.005.

[60] E. Fornells, B. Barnett, M. Bailey, E.F. Hilder, R.A. Shellie, M.C. Breadmore, Evaporative membrane modulation for comprehensive two-dimensional liquid chromatography, Anal. Chim. Acta. 1000 (2018) 303–309. https://doi.org/10.1016/j.aca.2017.11.053.

[61] D. Li, R. Dück, O.J. Schmitz, The advantage of mixed-mode separation in the first dimension of comprehensive two-dimensional liquid-chromatography, J. Chromatogr. A. 1358 (2014) 128–135. https://doi.org/10.1016/j.chroma.2014.06.086.

[62] G.J. Opiteck, K.C. Lewis, J.W. Jorgenson, R.J. Anderegg, Comprehensive On-Line LC/LC/MS of Proteins, Anal. Chem. 69 (1997) 1518–1524. https://doi.org/10.1021/ac961155l.

[63] G. Vanhoenacker, I. Vandenheede, F. David, P. Sandra, K. Sandra, Comprehensive two-dimensional liquid chromatography of therapeutic monoclonal antibody digests, Anal. Bioanal. Chem. 407 (2015) 355–366. https://doi.org/10.1007/s00216-014-8299-1.

[64] M. Sorensen, D.C. Harmes, D.R. Stoll, G.O. Staples, S. Fekete, D. Guillarme, A. Beck, Comparison of originator and biosimilar therapeutic monoclonal antibodies using comprehensive two-dimensional liquid chromatography coupled with time-of-flight mass spectrometry, MAbs. 8 (2016) 1224–1234. https://doi.org/10.1080/19420862.2016.1203497.

[65] S. Jaag, M. Shirokikh, M. Lämmerhofer, Charge variant analysis of protein-based biopharmaceuticals using two-dimensional liquid chromatography hyphenated to mass spectrometry, J. Chromatogr. A. 1636 (2021) 461786. https://doi.org/10.1016/j.chroma.2020.461786.

[66] G.J. Opiteck, J.W. Jorgenson, R.J. Anderegg, Two-Dimensional SEC/RPLC Coupled to Mass Spectrometry for the Analysis of Peptides, Anal. Chem. 69 (1997) 2283–2291. https://doi.org/10.1021/ac961156d.

[67] V. Elsner, S. Laun, D. Melchior, M. Köhler, O.J. Schmitz, Analysis of fatty alcohol derivatives with comprehensive two-dimensional liquid chromatography coupled with mass spectrometry, J. Chromatogr. A. 1268 (2012) 22–28. https://doi.org/10.1016/j.chroma.2012.09.072.

[68] P. Jandera, T. Hájek, M. Staňková, K. Vyňuchalová, P. Česla, Optimization of comprehensive two-dimensional gradient chromatography coupling in-line hydrophilic interaction and reversed phase liquid chromatography, J. Chromatogr. A. 1268 (2012) 91–101. https://doi.org/10.1016/j.chroma.2012.10.041.

[69] L. Montero, M. Herrero, E. Ibáñez, A. Cifuentes, Profiling of phenolic compounds from different apple varieties using comprehensive two-dimensional liquid chromatography, J. Chromatogr. A. 1313 (2013) 275–283. https://doi.org/10.1016/j.chroma.2013.06.015.

[70] P. Jandera, M. Staňková, T. Hájek, New zwitterionic polymethacrylate monolithic columns for one- and two-dimensional microliquid chromatography, J. Sep. Sci. 36 (2013) 2430–2440. https://doi.org/10.1002/jssc.201300337.

[71] L. Montero, M. Herrero, E. Ibáñez, A. Cifuentes, Separation and characterization of phlorotannins from brown algae Cystoseira abies-marina by comprehensive

two-dimensional liquid chromatography, ELECTROPHORESIS. 35 (2014) 1644–1651. https://doi.org/10.1002/elps.201400133.

[72] V. Elsner, V. Wulf, M. Wirtz, O.J. Schmitz, Reproducibility of retention time and peak area in comprehensive two-dimensional liquid chromatography, Anal. Bioanal. Chem. 407 (2015) 279–284. https://doi.org/10.1007/s00216-014-8090-3.

[73] P. Donato, F. Rigano, F. Cacciola, M. Schure, S. Farnetti, M. Russo, P. Dugo, L. Mondello, Comprehensive two-dimensional liquid chromatography–tandem mass spectrometry for the simultaneous determination of wine polyphenols and target contaminants, J. Chromatogr. A. 1458 (2016) 54–62. https://doi.org/10.1016/j.chroma.2016.06.042.

[74] T. Hájek, P. Jandera, M. Staňková, P. Česla, Automated dual two-dimensional liquid chromatography approach for fast acquisition of three-dimensional data using combinations of zwitterionic polymethacrylate and silica-based monolithic columns, J. Chromatogr. A. 1446 (2016) 91–102. https://doi.org/10.1016/j.chroma.2016.04.007.

[75] L. Montero, V. Sáez, D. von Baer, A. Cifuentes, M. Herrero, Profiling of Vitis vinifera L. canes (poly)phenolic compounds using comprehensive two-dimensional liquid chromatography, J. Chromatogr. A. 1536 (2018) 205–215. https://doi.org/10.1016/j.chroma.2017.06.013.

[76] M. Xu, J. Legradi, P. Leonards, Evaluation of LC-MS and LC×LC-MS in analysis of zebrafish embryo samples for comprehensive lipid profiling, Anal. Bioanal. Chem. (2020). https://doi.org/10.1007/s00216-020-02661-1.

[77] Q. Yang, X. Shi, Q. Gu, S. Zhao, Y. Shan, G. Xu, On-line two dimensional liquid chromatography/mass spectrometry for the analysis of triacylglycerides in peanut oil and mouse tissue, J. Chromatogr. B. 895–896 (2012) 48–55. https://doi.org/10.1016/j.jchromb.2012.03.013.

[78] R. Gallego, K. Arena, P. Dugo, L. Mondello, E. Ibáñez, M. Herrero, Application of compressed fluid–based extraction and purification procedures to obtain astaxanthin-enriched extracts from Haematococcus pluvialis and characterization by comprehensive two-dimensional liquid chromatography coupled to mass spectrometry, Anal. Bioanal. Chem. 412 (2020) 589–599. https://doi.org/10.1007/s00216-019-02287-y.

[79] E. Sommella, F. Pagano, E. Salviati, M. Chieppa, A. Bertamino, M. Manfra, M. Sala, E. Novellino, P. Campiglia, Chemical profiling of bioactive constituents in hop cones and pellets extracts by online comprehensive two-dimensional liquid chromatography with tandem mass spectrometry and direct infusion Fourier transform ion cyclotron resonance mass spectrometry, J. Sep. Sci. 41 (2018) 1548–1557. https://doi.org/10.1002/jssc.201701242.

[80] M. Iguiniz, F. Rouvière, E. Corbel, N. Roques, S. Heinisch, Comprehensive two dimensional liquid chromatography as analytical strategy for pharmaceutical analysis, J. Chromatogr. A. 1536 (2018) 195–204. https://doi.org/10.1016/j.chroma.2017.08.070.

[81] M. Iguiniz, E. Corbel, N. Roques, S. Heinisch, Quantitative aspects in on-line comprehensive two-dimensional liquid chromatography for pharmaceutical applications, Talanta. 195 (2019) 272–280. https://doi.org/10.1016/j.talanta.2018.11.030.

[82] E. Lazzari, K. Arena, E.B. Caramão, M. Herrero, Quantitative analysis of aqueous phases of bio-oils resulting from pyrolysis of different biomasses by two-dimensional comprehensive liquid chromatography, J. Chromatogr. A. 1602 (2019) 359–367. https://doi.org/10.1016/j.chroma.2019.06.016.

[83] E. Lazzari, K. Arena, E.B. Caramão, P. Dugo, L. Mondello, M. Herrero, Comprehensive two-dimensional liquid chromatography-based quali-quantitative screening of aqueous phases from pyrolysis bio-oils, ELECTROPHORESIS. n/a (n.d.). https://doi.org/10.1002/elps.202000119.

[84] Y.Z. Baghdady, K.A. Schug, Online Comprehensive High pH Reversed Phase × Low pH Reversed Phase Approach for Two-Dimensional Separations of Intact Proteins in Top-Down Proteomics, Anal. Chem. 91 (2019) 11085–11091. https://doi.org/10.1021/acs.analchem.9b01665.

[85] M. Russo, F. Cacciola, K. Arena, D. Mangraviti, L. de Gara, P. Dugo, L. Mondello, Characterization of the polyphenolic fraction of pomegranate samples by comprehensive two-dimensional liquid chromatography coupled to mass spectrometry detection, Nat. Prod. Res. 34 (2020) 39–45. https://doi.org/10.1080/14786419.2018.1561690.

[86] A. van der Horst, P.J. Schoenmakers, Comprehensive two-dimensional liquid chromatography of polymers, J. Chromatogr. A. 1000 (2003) 693–709. https://doi.org/10.1016/S0021-9673(03)00495-3.

[87] P. Dugo, O. Favoino, R. Luppino, G. Dugo, L. Mondello, Comprehensive Two-Dimensional Normal-Phase (Adsorption)–Reversed-Phase Liquid Chromatography, Anal. Chem. 76 (2004) 2525–2530. https://doi.org/10.1021/ac0352981.

[88] P. Dugo, V. Škeříková, T. Kumm, A. Trozzi, P. Jandera, L. Mondello, Elucidation of Carotenoid Patterns in Citrus Products by Means of Comprehensive Normal-Phase × Reversed-Phase Liquid Chromatography, Anal. Chem. 78 (2006) 7743–7750. https://doi.org/10.1021/ac061290q.

[89] P. Dugo, T. Kumm, M.L. Crupi, A. Cotroneo, L. Mondello, Comprehensive two-dimensional liquid chromatography combined with mass spectrometric

detection in the analyses of triacylglycerols in natural lipidic matrixes, J. Chromatogr. A. 1112 (2006) 269–275.
https://doi.org/10.1016/j.chroma.2005.10.070.

[90] P. Dugo, T. Kumm, B. Chiofalo, A. Cotroneo, L. Mondello, Separation of triacylglycerols in a complex lipidic matrix by using comprehensive two-dimensional liquid chromatography coupled with atmospheric pressure chemical ionization mass spectrometric detection, J. Sep. Sci. 29 (2006) 1146–1154. https://doi.org/10.1002/jssc.200500476.

[91] I. François, A. de Villiers, P. Sandra, Considerations on the possibilities and limitations of comprehensive normal phase–reversed phase liquid chromatography (NPLC×RPLC), J. Sep. Sci. 29 (2006) 492–498. https://doi.org/10.1002/jssc.200500451.

[92] S. Chapel, F. Rouvière, S. Heinisch, Pushing the limits of resolving power and analysis time in on-line comprehensive hydrophilic interaction x reversed phase liquid chromatography for the analysis of complex peptide samples, J. Chromatogr. A. (2019) 460753. https://doi.org/10.1016/j.chroma.2019.460753.

[93] A. Martín-Ortiz, A.I. Ruiz-Matute, M.L. Sanz, F.J. Moreno, M. Herrero, Separation of di- and trisaccharide mixtures by comprehensive two-dimensional liquid chromatography. Application to prebiotic oligosaccharides, Anal. Chim. Acta. 1060 (2019) 125–132.
https://doi.org/10.1016/j.aca.2019.01.040.

[94] T. Murahashi, Comprehensive two-dimensional high-performance liquid chromatography for the separation of polycyclic aromatic hydrocarbons, Analyst. 128 (2003) 611–615. https://doi.org/10.1039/B212643E.

[95] D.R. Stoll, K. O'Neill, D.C. Harmes, Effects of pH mismatch between the two dimensions of reversed-phase×reversed-phase two-dimensional separations on second dimension separation quality for ionogenic compounds—I. Carboxylic acids, J. Chromatogr. A. 1383 (2015) 25–34.
https://doi.org/10.1016/j.chroma.2014.12.054.

[96] S. Stephan, C. Jakob, J. Hippler, O.J. Schmitz, A novel four-dimensional analytical approach for analysis of complex samples, Anal. Bioanal. Chem. 408 (2016) 3751–3759. https://doi.org/10.1007/s00216-016-9460-9.

[97] P.G. Stevenson, D.N. Bassanese, X.A. Conlan, N.W. Barnett, Improving peak shapes with counter gradients in two-dimensional high performance liquid chromatography, J. Chromatogr. A. 1337 (2014) 147–154. https://doi.org/10.1016/j.chroma.2014.02.051.

[98] P. Venter, M. Muller, J. Vestner, M.A. Stander, A.G.J. Tredoux, H. Pasch, A. de Villiers, Comprehensive Three-Dimensional LC × LC × Ion Mobility Spectrometry Separation Combined with High-Resolution MS for the Analysis

of Complex Samples, Anal. Chem. 90 (2018) 11643–11650. https://doi.org/10.1021/acs.analchem.8b03234.

[99] M. Muller, A.G.J. Tredoux, A. de Villiers, Predictive kinetic optimisation of hydrophilic interaction chromatography × reversed phase liquid chromatography separations: Experimental verification and application to phenolic analysis, J. Chromatogr. A. 1571 (2018) 107–120. https://doi.org/10.1016/j.chroma.2018.08.004.

[100] M. Muller, A.G.J. Tredoux, A. de Villiers, Application of Kinetically Optimised Online HILIC × RP-LC Methods Hyphenated to High Resolution MS for the Analysis of Natural Phenolics, Chromatographia. 82 (2019) 181–196. https://doi.org/10.1007/s10337-018-3662-6.

[101] K. Arena, F. Cacciola, L. Dugo, P. Dugo, L. Mondello, Determination of the Metabolite Content of Brassica juncea Cultivars Using Comprehensive Two-Dimensional Liquid Chromatography Coupled with a Photodiode Array and Mass Spectrometry Detection, Molecules. 25 (2020) 1235. https://doi.org/10.3390/molecules25051235.

[102] M. Pursch, A. Wegener, S. Buckenmaier, Evaluation of active solvent modulation to enhance two-dimensional liquid chromatography for target analysis in polymeric matrices, J. Chromatogr. A. 1562 (2018) 78–86. https://doi.org/10.1016/j.chroma.2018.05.059.

[103] P. Yang, W. Gao, T. Zhang, M. Pursch, J. Luong, W. Sattler, A. Singh, S. Backer, Two-dimensional liquid chromatography with active solvent modulation for studying monomer incorporation in copolymer dispersants, J. Sep. Sci. (2019). https://doi.org/10.1002/jssc.201900283.

[104] D.R. Stoll, H.R. Lhotka, D.C. Harmes, B. Madigan, J.J. Hsiao, G.O. Staples, High resolution two-dimensional liquid chromatography coupled with mass spectrometry for robust and sensitive characterization of therapeutic antibodies at the peptide level, J. Chromatogr. B. 1134–1135 (2019) 121832. https://doi.org/10.1016/j.jchromb.2019.121832.

[105] K. Im, H.-W. Park, Y. Kim, B. Chung, M. Ree, T. Chang, Comprehensive Two-Dimensional Liquid Chromatography Analysis of a Block Copolymer, Anal. Chem. 79 (2007) 1067–1072. https://doi.org/10.1021/ac061738n.

[106] I. François, A. dos Santos Pereira, F. Lynen, P. Sandra, Construction of a new interface for comprehensive supercritical fluid chromatography×reversed phase liquid chromatography (SFC×RPLC), J. Sep. Sci. 31 (2008) 3473–3478. https://doi.org/10.1002/jssc.200800267.

[107] I. François, P. Sandra, Comprehensive supercritical fluid chromatography × reversed phase liquid chromatography for the analysis of the fatty acids in fish oil, J. Chromatogr. A. 1216 (2009) 4005–4012.

https://doi.org/10.1016/j.chroma.2009.02.078.

[108] I. François, A. dos S. Pereira, P. Sandra, Considerations on comprehensive and off-line supercritical fluid chromatography × reversed-phase liquid chromatography for the analysis of triacylglycerols in fish oil, J. Sep. Sci. 33 (2010) 1504–1512. https://doi.org/10.1002/jssc.201000044.

[109] P. Donato, D. Giuffrida, M. Oteri, V. Inferrera, P. Dugo, L. Mondello, Supercritical Fluid Chromatography × Ultra-High Pressure Liquid Chromatography for Red Chilli Pepper Fingerprinting by Photodiode Array, Quadrupole-Time-of-Flight and Ion Mobility Mass Spectrometry (SFC × RP-UHPLC-PDA-Q-ToF MS-IMS), Food Anal. Methods. 11 (2018) 3331–3341. https://doi.org/10.1007/s12161-018-1307-x.

[110] Y.-Q. Wang, X. Tang, J.-F. Li, Y.-L. Wu, Y.-Y. Sun, M.-J. Fang, Z. Wu, X.-M. Wang, Y.-K. Qiu, Development of an on-line mixed-mode gel liquid chromatography×reversed phase liquid chromatography method for separation of water extract from Flos Carthami, J. Chromatogr. A. 1519 (2017) 145–151. https://doi.org/10.1016/j.chroma.2017.08.053.

[111] R. Berkecz, F. Tömösi, T. Körmöczi, V. Szegedi, J. Horváth, T. Janáky, Comprehensive phospholipid and sphingomyelin profiling of different brain regions in mouse model of anxiety disorder using online two-dimensional (HILIC/RP)-LC/MS method, J. Pharm. Biomed. Anal. 149 (2018) 308–317. https://doi.org/10.1016/j.jpba.2017.10.043.

[112] S. Toro-Uribe, L. Montero, L. López-Giraldo, E. Ibáñez, M. Herrero, Characterization of secondary metabolites from green cocoa beans using focusing-modulated comprehensive two-dimensional liquid chromatography coupled to tandem mass spectrometry, Anal. Chim. Acta. 1036 (2018) 204–213. https://doi.org/10.1016/j.aca.2018.06.068.

[113] J.-L. Cao, L.-J. Ma, S.-P. Wang, Y. Deng, Y.-T. Wang, P. Li, J.-B. Wan, Comprehensively qualitative and quantitative analysis of ginsenosides in Panax notoginseng leaves by online two-dimensional liquid chromatography coupled to hybrid linear ion trap Orbitrap mass spectrometry with deeply optimized dilution and modulation system, Anal. Chim. Acta. 1079 (2019) 237–251. https://doi.org/10.1016/j.aca.2019.06.040.

[114] Y. Chen, Y. Wu, X. Liu, B. Li, D. Hu, S. Huang, M. Ma, B. Chen, Pulsed elution modulation for on-line comprehensive two-dimensional liquid chromatography coupling reversed phase liquid chromatography and hydrophilic interaction chromatography, J. Chromatogr. A. 1583 (2019) 98–107. https://doi.org/10.1016/j.chroma.2018.11.023.

[115] B.W.J. Pirok, M.J. den Uijl, G. Moro, S.V.J. Berbers, C.J.M. Croes, M.R. van Bommel, P.J. Schoenmakers, Characterization of Dye Extracts from Historical Cultural-Heritage Objects Using State-of-the-Art Comprehensive Two-

Dimensional Liquid Chromatography and Mass Spectrometry with Active Modulation and Optimized Shifting Gradients, Anal. Chem. 91 (2019) 3062–3069. https://doi.org/10.1021/acs.analchem.8b05469.

[116] B.W.J. Pirok, N. Abdulhussain, T. Aalbers, B. Wouters, R.A.H. Peters, P.J. Schoenmakers, Nanoparticle Analysis by Online Comprehensive Two-Dimensional Liquid Chromatography combining Hydrodynamic Chromatography and Size-Exclusion Chromatography with Intermediate Sample Transformation, Anal. Chem. 89 (2017) 9167–9174. https://doi.org/10.1021/acs.analchem.7b01906.

[117] S.S. Jakobsen, J.H. Christensen, S. Verdier, C.R. Mallet, N.J. Nielsen, Increasing Flexibility in Two-Dimensional Liquid Chromatography by Pulsed Elution of the First Dimension: A Proof of Concept, Anal. Chem. 89 (2017) 8723–8730. https://doi.org/10.1021/acs.analchem.7b00758.

[118] A. Baglai, M.H. Blokland, H.G.J. Mol, A.F.G. Gargano, S. van der Wal, P.J. Schoenmakers, Enhancing detectability of anabolic-steroid residues in bovine urine by actively modulated online comprehensive two-dimensional liquid chromatography – high-resolution mass spectrometry, Anal. Chim. Acta. 1013 (2018) 87–97. https://doi.org/10.1016/j.aca.2017.12.043.

[119] H. Tian, J. Xu, Y. Guan, Comprehensive two-dimensional liquid chromatography (NPLC×RPLC) with vacuum-evaporation interface, J. Sep. Sci. 31 (2008) 1677–1685. https://doi.org/10.1002/jssc.200700559.

[120] K. Ding, Y. Xu, H. Wang, C. Duan, Y. Guan, A vacuum assisted dynamic evaporation interface for two-dimensional normal phase/reverse phase liquid chromatography, J. Chromatogr. A. 1217 (2010) 5477–5483. https://doi.org/10.1016/j.chroma.2010.06.053.

[121] J.-F. Li, H. Fang, X. Yan, F.-R. Chang, Z. Wu, Y.-L. Wu, Y.-K. Qiu, On-line comprehensive two-dimensional normal-phase liquid chromatography × reversed-phase liquid chromatography for preparative isolation of toad venom, J. Chromatogr. A. 1456 (2016) 169–175. https://doi.org/10.1016/j.chroma.2016.06.008.

[122] J.-F. Li, X. Yan, Y.-L. Wu, M.-J. Fang, Z. Wu, Y.-K. Qiu, Comprehensive two-dimensional normal-phase liquid chromatography × reversed-phase liquid chromatography for analysis of toad skin, Anal. Chim. Acta. 962 (2017) 114–120. https://doi.org/10.1016/j.aca.2017.01.038.

[123] E. Sommella, E. Salviati, S. Musella, V. Di Sarno, F. Gasparrini, P. Campiglia, Comparison of Online Comprehensive HILIC × RP and RP × RP with Trapping Modulation Coupled to Mass Spectrometry for Microalgae Peptidomics, Separations. 7 (2020) 25. https://doi.org/10.3390/separations7020025.

D. Protein and peptide analysis in on-line LC x LC

In the last two decades, the development of therapeutic antibodies for the treatment of human diseases has followed a dramatic growth [68]. This accelerated development has driven considerable efforts in the development of 2D-LC methods coupled with MS detection for the comprehensive characterization of these complex biomolecules. In recent years, most work in the area of 2D-LC analysis of protein has been focused on therapeutic antibodies [4]. This section provides a detailed review of recent applications of on-line LC x LC to the analysis of antibody-drug conjugates.

Article 2: Two-dimensional liquid chromatography coupled to high-resolution mass spectrometry for the analysis of ADCs.

Abstract

From a structural point of view, the complete characterization of ADCs is a challenging task due to their high complexity. ADCs combine the heterogeneity of the initial antibody to the variability associated with the conjugation strategy, the manufacturing process, and the storage. Given the inherent complexity of these biomolecules, on-line comprehensive two-dimensional liquid chromatography (LC x LC) is an attractive technique to address the challenges associated with ADC characterization. Compared to conventional one-dimensional liquid chromatography techniques (1D-LC), LC x LC combines two different and complementary separation systems. In the context of ADC analysis, LC x LC has been proven to be a rapid and efficient analytical tool: (1) to provide a higher resolving power by increasing the overall peak capacity and thus allowing to gain more information within a single run and (2) to allow mass spectrometry (MS) coupling with some chromatographic techniques that are not MS-compatible and hence to facilitate the structural elucidation of ADCs. In this chapter, we present the coupling of different chromatographic techniques including hydrophobic interaction chromatography (HIC), reversed phase liquid chromatography (RPLC), size exclusion chromatography (SEC), ion-exchange chromatography (IEX), and hydrophilic liquid chromatography (HILIC). The interest of HIC x SEC, SEC x SEC, HIC x RPLC, IEX x RPLC, RPLC x RPLC, and HILIC x RPLC, all hyphenated to high-resolution mass spectrometry (HRMS), is discussed in the context of the characterization of ADCs.

1. Introduction

Antibody-drug conjugates (ADCs) are one of the most promising classes of human therapeutics [1,2]. Their technology combines the specificity of a monoclonal antibody (mAb) with a potent cytotoxic drug covalently bonded to the mAb via a stable linker. The resulting therapeutic biomolecule is designed to improve treatment efficacy compared to the first generation of mAbs while lowering the side effects encountered with classical chemotherapy. Four ADCs are currently marketed and more than sixty clinical trials are ongoing [3].

The characterization of such formats is of prime importance to study their structure-function relationship by identifying micro-variants, 3D-structures, drug loading, and conjugation sites in order to investigate their influence on antigen-binding, pharmacokinetics, pharmacodynamics, stability [4], and also to prove that ADC manufacturing and stability can be managed in the frame of clinical studies with respect to the critical quality attributes (CQAs), to ensure both treatment efficacy and patient safety.

From a structural point of view, the complete characterization of ADCs is a challenging task due to their high complexity. In addition to the heterogeneity of the initial mAb, the conjugation strategy brings an additional degree of variability [5]. Although several conjugation chemistries exist to bind a cytotoxic drug to a mAb [3,5], in this chapter we will focus on two marketed ADCs, brentuximab vedotin and ado-trastuzumab emtansine, which are respectively cysteine- and lysine-based ADCs. Brentuximab vedotin is made by the chemical conjugation of cytotoxins to mAbs, by reducing the cysteine residues that form interchain disulfide bonds, followed by the conjugation of the resulting free thiols with drugs. This process leads to a heterogeneous population of conjugated products that contain species with various numbers of drugs per antibody, usually an even number (0, 2, 4, 6, 8) [6]. In the case of ado-trastuzumab emtansine, the conjugation takes place on the amino groups of lysine. Since 80–100 lysines are available (vs. only eight interchain cysteines), the lysine conjugation leads to a more heterogeneous mixture of species compared to cysteine conjugation, in spite of a similar overall level of drugs incorporated per antibody (between 0 and 8 with an average of 3–4) [5,7].

To face the complexity of such highly heterogeneous species, numerous analytical techniques are needed [4]. In this context, liquid chromatography (LC) and high-

resolution mass spectrometry (HRMS) are the most used tools since they allow to get orthogonal information in both native and denaturing conditions while using intact, top-down, middle-up (protein level), and bottom-up approaches (peptide level) [8].

As an example, ion-exchange chromatography (IEX), size-exclusion chromatography (SEC), hydrophobic interaction chromatography (HIC), and hydrophilic interaction liquid chromatography (HILIC) can be used to study charge variants, protein aggregation, drug load distribution, and glycoforms, respectively. Reversed-phase liquid chromatography (RPLC) coupled to HRMS is currently the technique of choice to get access to the primary structure of the protein via peptide mapping (bottom-up approach) or to separate and identify large protein fragments obtained after digestion (middle-up approach) [8]. Lastly, ion mobility coupled to MS (IM x MS) has been reported as an interesting tool to characterize conformational changes in the proteins [9].

In spite of this large panel of analytical techniques, some challenges still need to be addressed such as (a) improving the separation power to facilitate both structural elucidation by MS and in-depth comparison between samples, (b) crossing data from different techniques, and/or (c) making the chromatographic techniques using large amounts of salts (HIC, IEX, and SEC) MS-compatible.

In this context, on-line comprehensive two-dimensional liquid chromatography (LC x LC) is an attractive technique to tackle these challenges [10]. It allows, in one single run: (a) to couple two orthogonal techniques, therefore drastically increasing the peak capacity [11], (b) to allow the direct coupling of the first dimension with MS, by means of a second MS-compatible dimension, (c) to avoid off-line sample treatments thereby preventing any sample loss or degradation, and (d) to cross, within one single run, the information provided by two different techniques while reducing sample consumption.

This chapter reports different applications using on-line LC x LC-HRMS for the characterization of ADCs: (a) at the intact level by HIC x SEC-IM x MS and SEC x SEC-IM x MS, allowing structural elucidation of ADCs in native conditions, (b) in denaturing conditions by HIC x RPLC-UV-MS, IEX x RPLC-UV-MS, and HILIC x RPLC-UV-MS to simultaneously obtain information on mAb heterogeneity, drug-to-antibody ratio (DAR) and drug load position, (c) at peptide level with a bottom-up approach by RPLC x RPLC-MS, IEX x RPLC-MS, and HILIC x RPLC-MS.

2. Principles of Two-Dimensional Liquid Chromatography

The main concept in 2D-LC is that one separation obtained in a first dimension is transferred to a second column to undergo a second separation, in which ideally all the unresolved analytes are further separated. To successfully achieve this goal, the two coupled separation dimensions must be complementary by offering different selectivities towards the compounds. Using the nomenclature defined by Marriott et al. [12], the first separation system is referred to as the first dimension and is denoted as ^{1}D and the second separation system is referred to as the second dimension denoted as ^{2}D. In a 2D-LC system, the two dimensions can be coupled either off-line or on-line. In the off-line mode, fractions of the first dimension separation are collected and stored into vials until reinjection at a later time into the second dimension. The same instrument (pump system, sample manager, and detector) can be used for both dimensions by only changing the stationary phase and/or the mobile phase. In the on-line mode, collection, transfer, and reinjection are conducted continuously in real-time. The implementation is therefore more complex and requires two different chromatographic instruments connected via a suitable interface (Fig. 1).

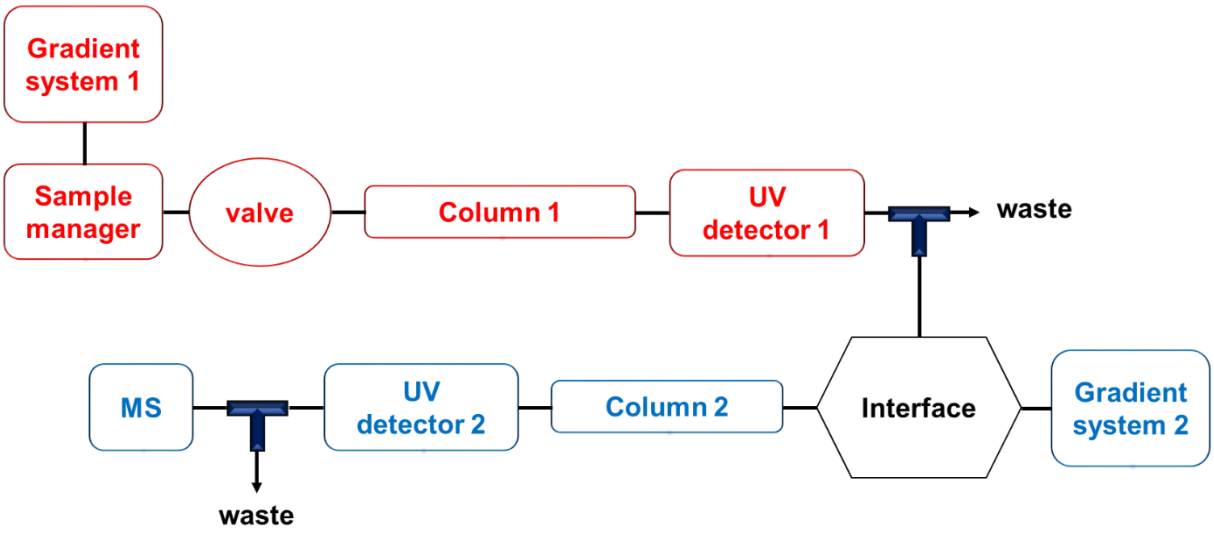

Fig. 1: Generic scheme of online 2D-LC-UV/HRMS instrumentation (see text for explanation).

The interface generally consists of one or several automated two-positions switching-valves with identical sample loops to ensure continuous fractioning of the first dimension eluent before transfer into the second dimension column. While one loop stores the first dimension fraction, the second loop sends the preceding stored fraction in the second dimension and vice versa. Since both dimensions are interconnected,

flow splitting is sometimes required to decrease the flow rate entering the interface and hence to decrease the injection volume in the second dimension. Similarly, a second flow splitter may be necessary to send MS-compatible flow rates into the mass spectrometer. Both on-line and off-line transfer approaches display their own sets of strengths and weaknesses which were extensively highlighted in detailed reviews [13, 14]. Compared to off-line methods, on-line ones are more advantageous, because they avoid the risk of sample loss, sample contamination, and sample degradation. In addition, they are less time-consuming. However, on-line sample handling can lead to serious issues due to the interdependence of the two dimensions, resulting in much more complex implementation. As a consequence, specific method development and optimization are mandatory.

2D-LC methods can be divided into two main modes as illustrated in Fig. 2. The simplest and easiest to be implemented is the heart-cutting mode denoted as LC-LC, in which large volumes of selected portions of ^{1}D are considered. This approach can involve either a single fraction or several fractions along the ^{1}D-chromatogram. In this latter case, it is referred to as multiple heart-cutting denoted as mLC-LC. The heart-cutting approach can be used to increase the resolution of a given unresolved pair of peaks in the first dimension, but it is not designed to increase the overall peak capacity of the 2D-LC method. For this reason, LC-LC or mLC-LC are more commonly used for targeted analysis of a small number of compounds. As an example in the field of ADCs, Li et al. [15] developed a two-dimensional heart-cutting method involving SEC in ^{1}D coupled to RPLC in ^{2}D, to separate unconjugated small molecules drugs and their related impurities in ADC samples. In this approach, SEC was used to separate the small molecules of interest (free drug, linker, and process-related impurities) from ADC and other high molecular weight species (HMWS), whereas in RPLC, all the co-eluting small species were separated from a single collected fraction. A similar approach was reported by Goyon and coworkers [16] in multiple heart-cutting mSEC-RPLC, for the separation of free drugs, linker, and linker-drug from the monomeric ADC in different ADC samples.

In fully comprehensive 2D-LC denoted as LC x LC, the entire sample is subject to a separation in both dimensions with relatively small fractions transferred. Small fractions of ^{1}D are collected to overall maintain the resolution obtained in the first separation. Since the entire sample is subjected to two different separations, impressive peak capacities are expected. The theoretical peak capacity is the product

of the peak capacities in each dimension but the effective peak capacity is usually much lower due to undersampling of first dimension peaks, partial coverage of the retention surface and possible injection effects, particularly in on-line LC x LC. In most applications, the objective of LC x LC is to gain as much information as possible about a highly complex sample.

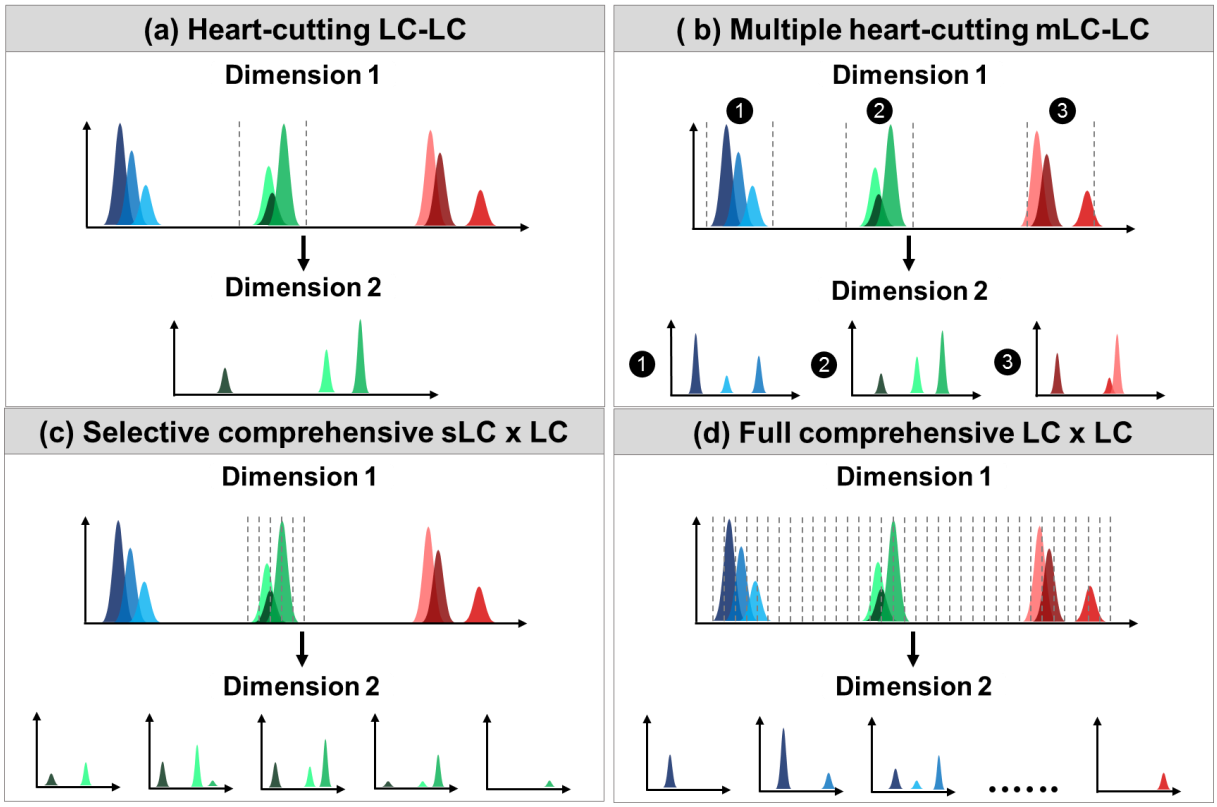

Fig. 2: Illustrative representation of four possible 2D-LC separations: (a) heart-cutting, (b) multiple heart-cutting, (c) selective comprehensive, and (d) full comprehensive (see text for explanation).

Very recently, an intermediate concept between LC-LC and LC x LC called selective comprehensive and denoted as sLC x LC was introduced [17]. In sLC x LC, only selected regions of the ^{1}D-chromatogram are sent to the ^{2}D column. However, unlike mLC-LC where the fractions are quite large, in sLC x LC small fractions are sampled so that the resolution obtained in ^{1}D can be overall maintained in ^{2}D, similarly to full comprehensive LC x LC. Compared to LC-LC or mLC-LC, the major benefit of sLC x LC is to minimize undersampling, thereby providing a higher resolution power in the first dimension and hence in the overall 2D-LC separation. This is a good alternative for LC x LC when the targeted analysis of one or several compounds is needed. In the context of ADC synthesis control, Venkatramani et al. [18] demonstrated the applicability of

sLC x LC with RPLC in both dimensions for qualitative and quantitative studies of the impurity profile of key linker-drug intermediates.

The appropriate selection among these 2D-LC approaches depends on both application scope and sample complexity.

3. Analysis at the intact level (Top-down approach)

The characterization of ADCs at the intact level requires the use of non-denaturing analytical techniques to maintain the structural and conformational form of the protein during the analysis. Denaturing conditions include physical parameters (heat, pH, radiations, etc.) and/or chemical parameters (reducing agents such as dithiothreitol (DTT), strong acid or base, high organic solvent content) which may lead to the dissociation of weak non-covalent binding between ADC subunits and to the loss of the three-dimensional structure of the protein. Various chromatographic techniques are essentially carried out in aqueous solvents and hence, suitable for mAb or ADC analysis at the intact level. Those include HIC, IEX, most often cation exchange (CEX), and SEC. Native MS performed under non-denaturing ionization conditions was also proved to be a valuable tool for the structural characterization of intact mAbs and ADCs, as it allows the direct observation of the protein structure by preserving its intact form [9, 19–24].

3.1. HIC x SEC

The top-down approach, which consists in analysing the protein by starting from its intact form, is a powerful tool to obtain information about ADC sample purity. HIC coupled to ultraviolet (UV) detection (HIC-UV) is the gold-standard analytical technique for separating the different DARs (drug-to-antibody-ratio) of ADCs based on the interchain cysteines. DAR can be defined as the number of cytotoxic drugs conjugated to a specific mAb. For cysteine-linked ADCs, the conjugation process usually results in the formation of DAR species with an even distribution of 0, 2, 4, 6 or 8 drugs incorporated per antibody, due to the presence of four disulfide bridges on the protein (Fig. 3).

In the context of ADC synthesis, it should be noted that DAR 0 is considered as an impurity, since no drugs are linked, whilst DARs with an odd number (DAR 1, DAR 3, DAR 5. . .) are degradation products.

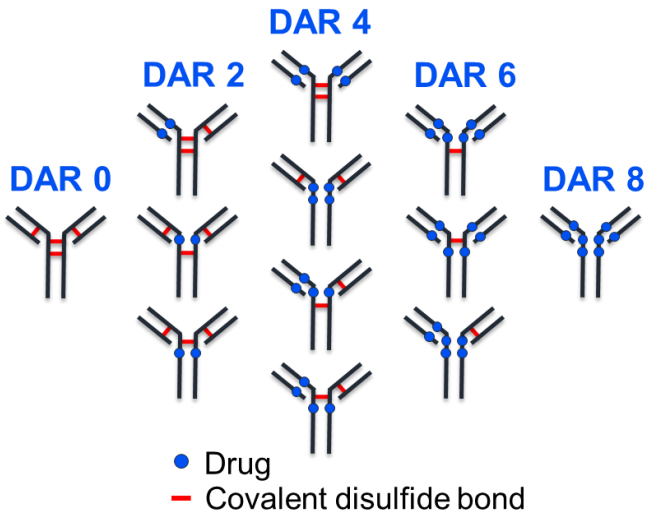

Fig. 3: Schematic representation of the possible positional isomers resulting from the drug conjugation of a cysteine-conjugated ADC.

The precise characterization of the different DAR species present in an ADC sample is of prime importance in quality control because different isoforms may have different toxicological and/or pharmacokinetic properties and hence may affect the overall ADC efficacy and safety. In HIC, the proteins are separated by their hydrophobic interactions with the ligands present on the stationary phase surface. As a result, the retention increases with the protein hydrophobicity. The conjugation of hydrophobic payloads (or drugs) on mAb leads to the creation of species of increasing hydrophobicity compared to the unconjugated mAb (Fig. 3). In HIC, ADCs can thus be separated by increasing conjugation payloads, which leads to the differentiation of the different DARs based on the number of attached drugs and their apparent hydrophobicity. In addition, changes in the protein structure, including post-translational modifications (PTMs) such as deamidation and oxidation, or even glycosylation can be differentiated using HIC, since these changes directly affect the overall hydrophobicity of the molecule [25]. In the context of ADC characterization at the intact level, the coupling of the HIC separation with the structural identification power of MS detection, and especially HRMS may be a powerful tool. Peak overlapping or poor resolution can lead to misleading information when using HIC-UV alone, while the sole use of HRMS does not allow the distinction between different positional isomers (or isoforms) of the same DAR. The on-line coupling of HIC for the separation of DAR species to non-denaturing native MS is therefore of great interest for ADC characterization at the intact level. However, the separation mechanism in HIC

requires the use of a high concentration of non-volatile salts buffers in the mobile phase, which are not compatible with MS detection. The collection of HIC fractions followed by subsequent sample treatment to eliminate the non-volatile salts from the sample, followed by redissolution in a more friendly solvent prior to reinjection in HRMS has been performed [9]. However, such off-line analysis is labour-intensive, time-consuming (sample preparation and multiple injections), and can hardly be automated, which is a major drawback for high-throughput analysis in the context of research and development of ADCs. From this perspective, two-dimensional liquid chromatography is a clever solution to achieve the direct interfacing of HIC with MS, by incorporating a fast on-line desalting step in the second dimension. To have an efficient analytical technique, the second dimension must be compatible with MS detection and must use non-denaturing conditions in order to keep the protein intact. Such a strategy was reported by Ehkirch et al. [26] for the analytical characterization of a marketed cysteine-linked ADC (brentuximab vedotin). HIC and IM x MS were hyphenated by using an on-line LC x LC setup involving HIC in ^{1}D and SEC in ^{2}D (on-line HIC x SEC-IM x MS) resulting in an analytical technique performed under entirely non-denaturing conditions. The schematic representation of the setup is presented in Fig. 4. The on-line LC x LC instrument consisted of two independent LC systems from Waters Corporation (Milford, MA, USA), including an Acquity H-Class in ^{1}D and an Acquity I-Class in ^{2}D, both connected by two 6-port high-pressure two-position valves acting as the interface between the two dimensions.

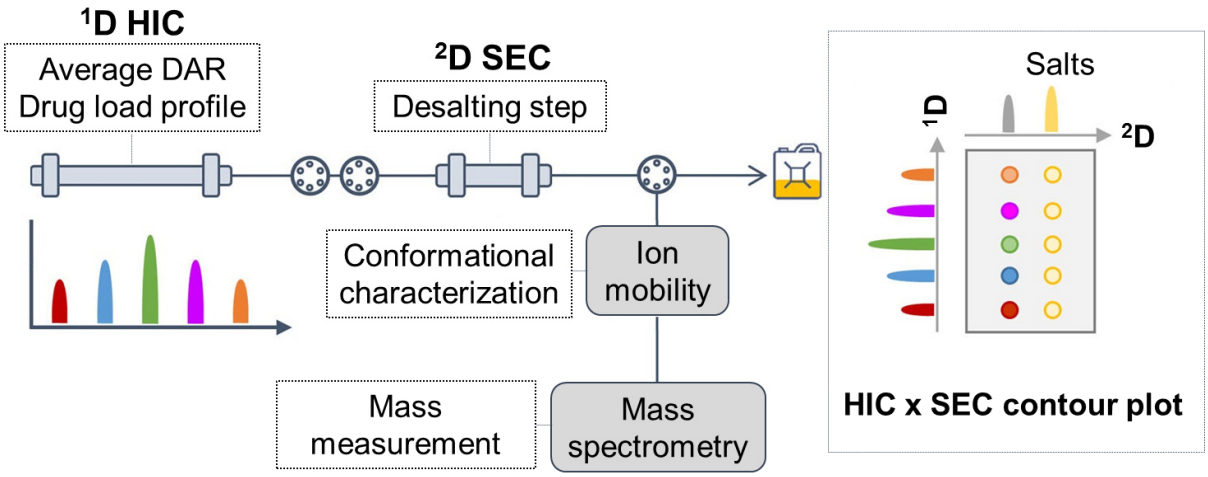

Fig. 4: Schematic representation of the setup for the online HIC x SEC-IM x MS analysis of cysteine-linked ADCs. (Adapted from [26, 27] with permission from ACS Publications).

In the first HIC dimension, a gradient of mobile phase containing 2.5 M of ammonium acetate and 0.1 M of phosphate buffer was used for the separation of the DAR species. Such a high volatile salt concentration, along with the use of a nonvolatile phosphate buffer, makes the direct hyphenation of HIC with MS impossible. In the second dimension, SEC was used as a simple desalting step with a more compatible isocratic mobile phase containing 100 mM of ammonium acetate. In this configuration, SEC, as a size-based separation, was used as a fast on-line desalting step before MS, thereby allowing the differentiation between HIC salts of low molecular weight (MW < 100 Da) and ADC isoforms of high molecular weight (MW > 150 kDa). The first part of the SEC chromatogram, corresponding to the DAR species, was sent to HRMS while the later eluted salts could be directed towards the waste via a 6-port two-position switching-valve. In this analysis, fractions of 150 µL (representing 2–3 fractions per ^{1}D-peak) allowed to maintain the integrity of the ^{1}D-HIC separation by keeping the resolution acquired in the first dimension. All detected peaks in HIC were unambiguously identified as even drug load species from DAR 0 to DAR 8, which led to an average DAR (avDAR) calculation of 4 in agreement with expected values. In addition to the structural peak identification by HRMS, ion mobility spectrometry (IMS) was used to confirm the conformational homogeneity of each individual HIC fraction.

In native HRMS the detection of different positional isomers of identical masses was not possible (Fig. 5a). In 1D-HIC-UV, the unambiguous identification of all peaks, based on their retention only, was not possible (Fig. 5b). Compared to these analytical methods, the on-line HIC x SEC-IM x MS analysis allowed to demonstrate the presence of positional isomers of DAR 4 (Fig. 5c). In addition, the simplification of the ADC matrix entering the ionization source resulted in a significant increase in MS sensitivity, thereby supporting detection and unambiguous identification of minor species such as DAR 0 and DAR 8, much less sensitive in native HRMS (Fig. 5a,c). This on-line LC x LC approach highlights the possibility to have, within a single run, an analytical characterization of ADCs with different information levels. Those include drug profile and average DAR (both in HIC) and accurate identification of the drug load distribution through the mass measurement in HRMS. In addition to the ability to directly hyphenate two analytical techniques (HIC and HRMS), the indisputable advantage of on-line HIC x SEC-HRMS for ADC characterization at the intact level is the substantial improvement of sensitivity in MS, which is essential for the unambiguous identification of all detected species.

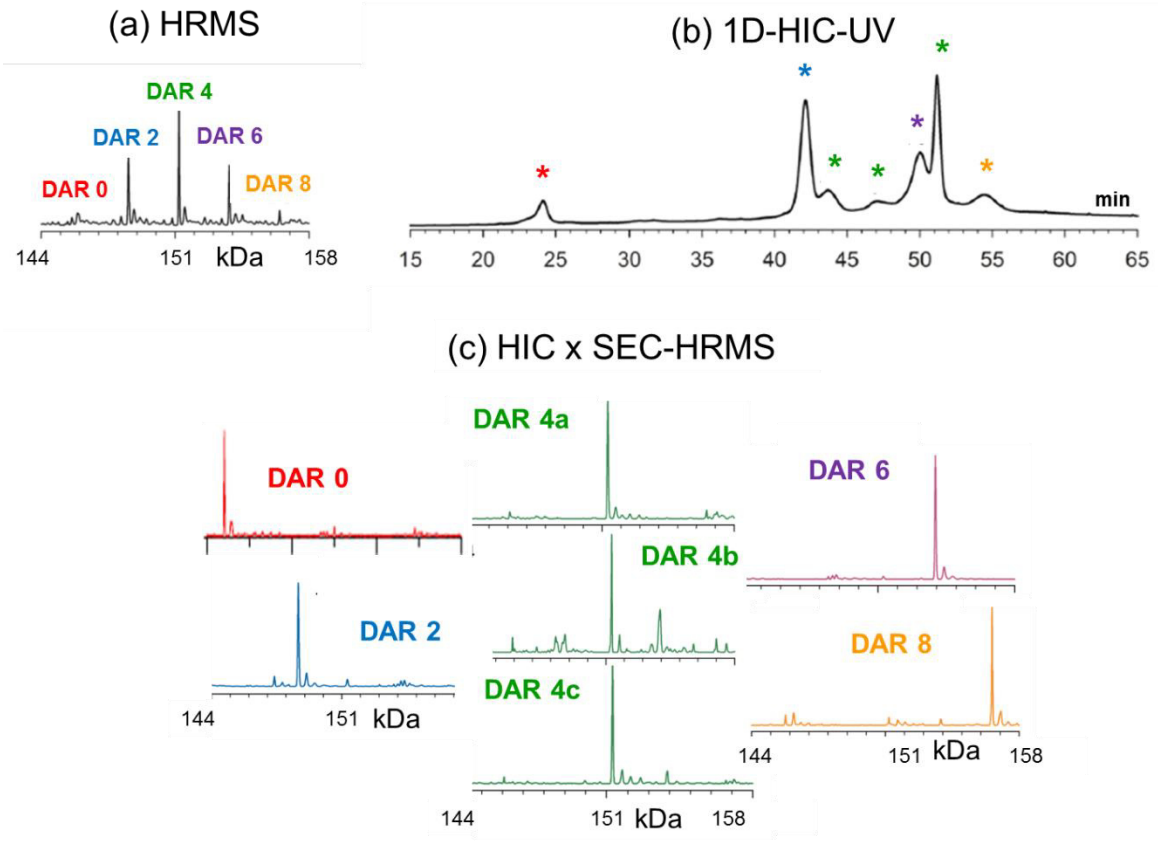

Fig. 5: Illustration of the benefits of online HIC x SEC-MS compared to HIC-UV alone or native MS alone for the characterization of an intact ADC: (a) deconvoluted native HRMS spectrum, (b) HIC-UV profile, and (c) deconvoluted native mass spectra obtained by online HIC x SEC-HRMS. (Adapted from [26] with permission from ACS Publications).

3.2. SEC x SEC

Besides the determination of drug conjugation in ADC samples (average DAR and their drug load distribution), on-line LC x LC may be used in the top-down approach to investigate other critical quality attributes (CQAs) such as size variants. The characterization of the size heterogeneity in mAb or ADC samples mostly relies on SEC and native MS. As opposed to HIC, SEC can be performed with either volatile or non-volatile salts, but lower performance was reported for mAb analysis in SEC with non-denaturing MS-compatible conditions (e.g. with ammonium acetate buffers) compared to more classical non-denaturing conditions using non-volatile phosphate buffers [27]. The limited performance observed in SEC with ammonium acetate buffers can be attributed to the multimodal nature of the elution mechanism (separation not only based on size but also ionic interactions, adsorption, and hydrophobicity) when using a low ionic strength buffer, which results in longer retention times, broader peaks, and

lower sensitivity for basic and/or hydrophobic compounds. To keep optimal performances for mAb or ADC analysis, SEC has therefore to be performed with non-MS-compatible salts, making its direct hyphenation to MS impossible. Similarly to the above HIC x SEC-IM x MS, a second dimension was used as a desalting step to allow the hyphenation of SEC to MS detection. An on-line four-dimensional approach combining two SEC dimensions, ion mobility and HRMS (4D-SEC x SEC-IM x MS) was reported for the structural characterization of a wide range of mAbs [27] (adalimumab, pembrolizumab, and bevacizumab) under non-denaturing conditions. Non-volatile salts (50 mM phosphate buffer and 250 mM potassium chloride) were used in the first SEC dimension for optimum separation of size variants, whereas in the second SEC dimension, a non-volatile buffer composed of 100 mM of ammonium acetate was used to allow the compatibility with MS. The on-line LC x LC instrument was the same as reported above for HIC x SEC and the setup was similar to that presented in Fig. 4, with an SEC column in the first dimension for size separation instead of a HIC column. The benefit of on-line SEC x SEC-IM x MS was proven by the comparison of stressed and unstressed mAb samples. Unexpected species, which could not be correctly identified in SEC-UV alone, were identified. A representative example of this approach is given in Fig. 6.

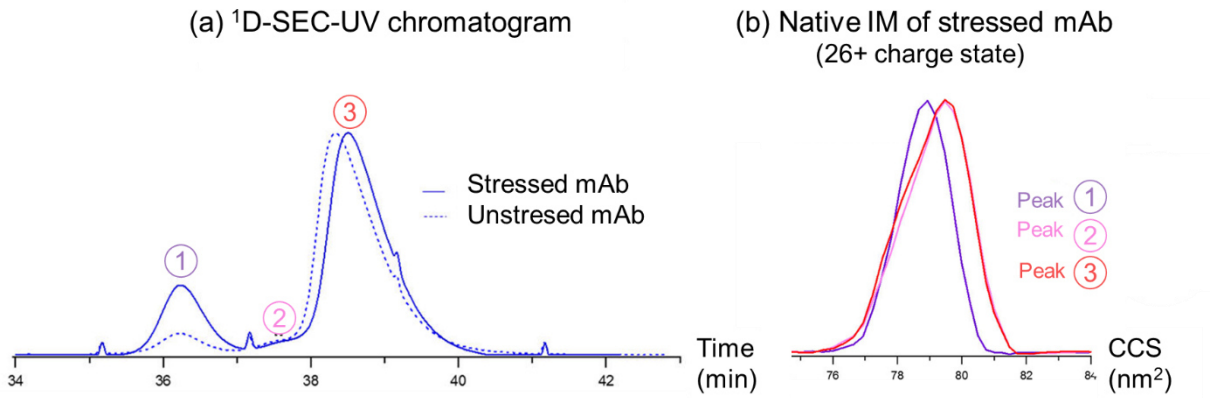

Fig. 6: Online SEC x SEC-IM x MS analysis of pembrolizumab. (a) Overlaid ^{1}D-SEC-UV chromatograms of unstressed (dotted lines) and stressed (solid line) pembrolizumab. (b) Ion mobility collision cross sections (CCSs) of 26+ charge state of the monomeric species detected in ^{1}D-SEC-UV. (Adapted from [27] with permission from ACS Publications).

With the sole use of 1D-SEC-UV (Fig. 6a), peaks #1 and #2, eluted before the most intense peak of monomer (peak #3), would have been attributed to high molecular weight species (HMWS). Surprisingly, similar MS spectra were observed for the three

peaks, suggesting that peaks #1 and #2 correspond to a monomer species instead of dimer or trimer species. Considering this unambiguous identification, it could be stated that the amount of monomer was significantly increased under thermal stress (from 7% to 19.8%). Furthermore, the measurement of the collision cross sections (CCS) (26+ charge state) in IMS (Fig. 6b) not only confirmed the existence of unexpected monomer species but also suggested that the less retained monomer species had a different conformation compared to the other two, considering the slight difference in CCS values (78.9 vs. 79.5 nm^2). By combining the information provided by the SEC separation with the intact mass measurement in native MS and with the CCS values provided by IMS, the on-line SEC x SEC-IM x MS analysis allowed the simultaneous HMWS and low molecular weight species (LMWS) profiling, their accurate relative quantitation, and the unambiguous identification of each size variants. Although this 4D approach was applied to mAbs in this reported study, it should also be very attractive in the case of ADCs.

4. Analysis under denaturing conditions or reducing conditions

The coupling of a non-denaturing separation (e.g. HIC or CEX) maintaining the intact form of the protein in ^{1}D, with a denaturing separation (e.g. RPLC) leading to the generation of protein subunits in ^{2}D designed to obtain more structural information on the formerly separated species, is presented below. The coupling of two orthogonal techniques, HILIC and RPLC, for a middle-up approach is also discussed below.

4.1. HIC x RPLC

Compared to on-line HIC x SEC or on-line SEC x SEC, where ^{2}D-SEC is only a desalting step, the use of RPLC in ^{2}D extends the level of peak information in a top-down approach. In RPLC, denaturing conditions (acidic pH, high organic content, elevated temperature. . .) lead to the dissociation of the weak non-covalent bonds in case of cysteine-linked ADC and hence to the formation of smaller subunits. RPLC in ^{2}D, prior to HRMS and after HIC, SEC or CEX results in more precise structural elucidation of the separated species.

A single heart-cutting HIC-RPLC-UV-HRMS was proposed by Birdsall et al. [28] to identify even DARs in a nontoxic drug mimic. In addition to the fact that the heart-cutting mode requires as many injections as ^{1}D-peaks to analyse and can therefore be

time-consuming, it cannot provide information on the entire HIC separation, hence missing some potential important zones of the chromatogram.

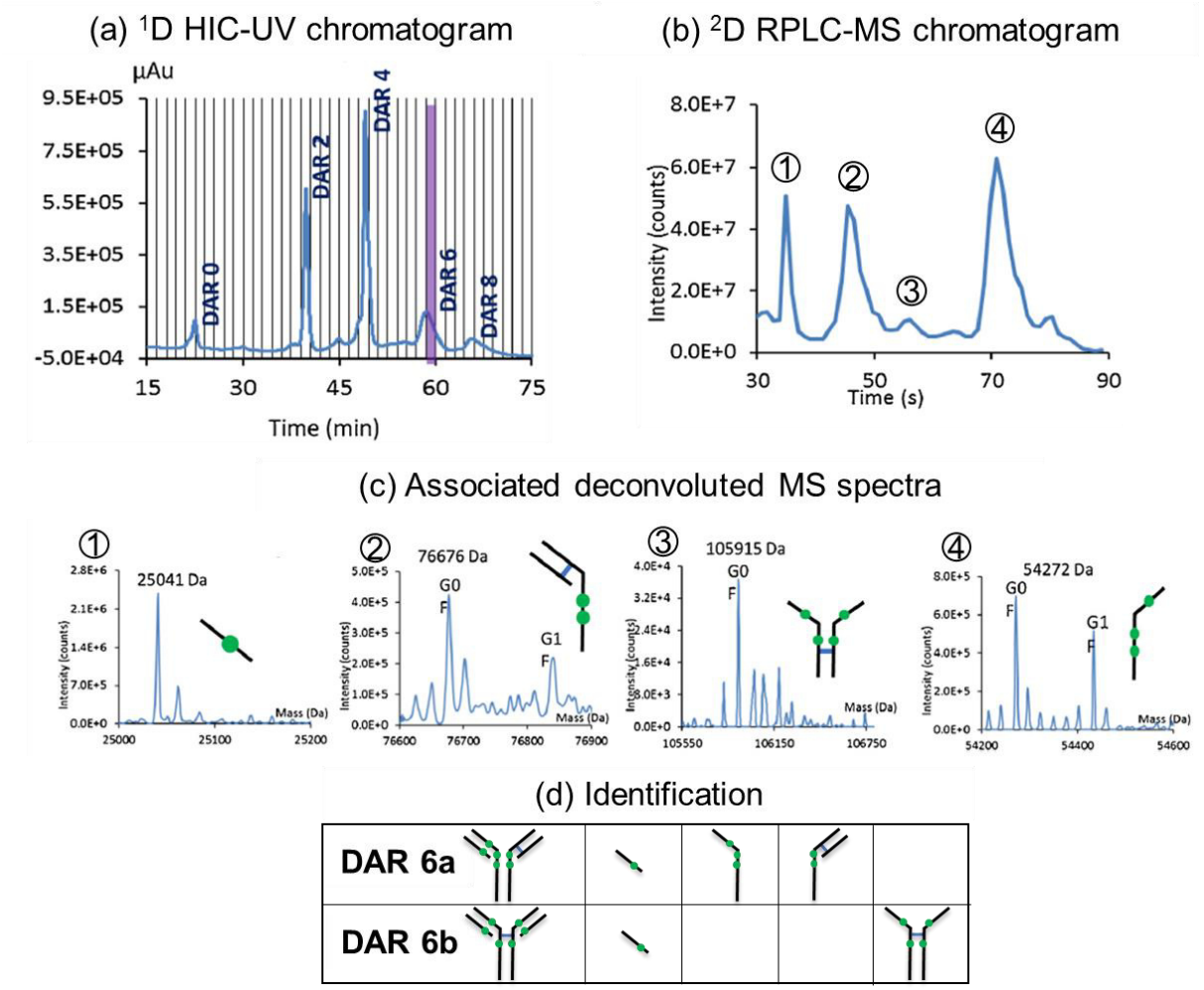

Fig. 7: Illustration of the successive steps for identifying the different DAR species in online HIC x RPLC-UV-HRMS. Example of the identification of DAR 6 and its subunits. (a) First dimension HIC-UV separation (the purple dashed area corresponds to one fraction sent in the second dimension). (b) 2nd dimension RPLC-MS-TIC chromatogram of the preceding fraction. (c) Deconvoluted mass spectra of the four labelled peaks allowing the identification of four subunits. (d) Assignation of the subunits to two different isoforms of DAR 6. (Adapted from [30] with permission from Elsevier).

In two recent studies, Sarrut et al. [29, 30] proposed an on-line HIC x RPLC-UV-HRMS method for the analysis of brentuximab vedotin. The on-line LC x LC instrument consisted of a Waters Acquity 2D-I-Class system (Milford, MA, USA) which includes two high-pressure binary pumps, an auto-sampler, a column manager with two independent column ovens and two 6-port two-position high-pressure valves. The first HIC dimension allowed to separate the different DAR species while maintaining the native form of the proteins. The second RPLC dimension carried out under MS-

compatible conditions (0.05% trifluoroacetic acid +0.1% formic acid in water-acetonitrile mobile phase), allowed the removal of the non-volatile salts used in the first HIC dimension (2.5 M ammonium acetate and 0.1 M phosphate buffer), by redirecting the salt plug to the waste after each ^{2}D-injection, according to the setup presented in Fig. 4.

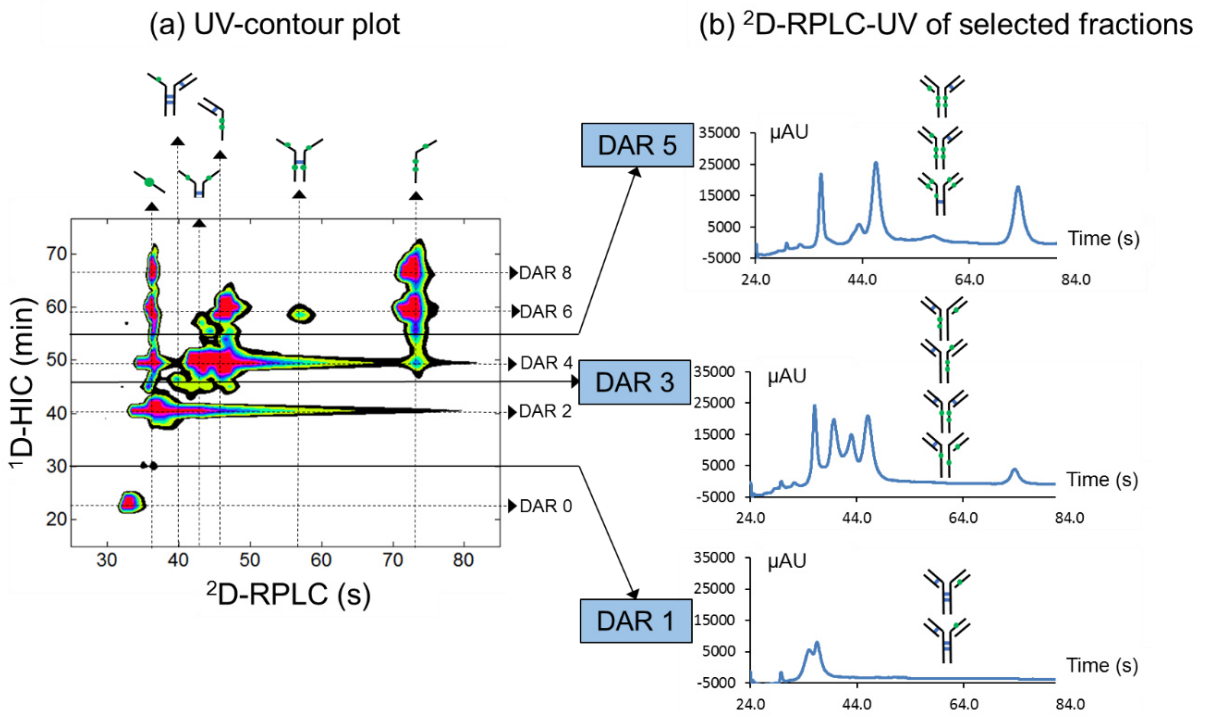

Fig. 8: Structural elucidation of odd DARs of brentuximab vedotin in online HIC x RPLC-HRMS. (a) UV contour plot of the online HIC x RPLC separation. The subunits, separated in RPLC, are indicated on the top of the contour plot; the DAR species, separated in HIC, are indicated on the right side of the contour plot. (b) ^{2}D-RPLC-separations of subunits corresponding to the most concentrated fractions in ^{1}D for subsequent identification of DAR 1, 3 and 5. Identified isoforms are represented for each odd DAR. (Adapted from [30] with permission from Elsevier).

In order to maximize the separation power, several parameters were optimized in both ^{1}D and ^{2}D, including nature of injection solvent, stationary phases, type of salts, salt concentration, and gradient conditions. In particular, significant peak shape improvement was obtained in ^{1}D by adding salt in the aqueous sample solvent to reduce its eluent strength in HIC. It is worth noting that the reduction of possible deleterious injection effects in ^{2}D is a key step in on-line LC x LC method development since non-compatible mobile phases may lead to peak broadening or even peak distortion which in turn leads to a decrease in both overall peak capacity and peak intensity. In this study, the precipitation, in ^{2}D, of the injection plug rich in salts was

avoided by bracketing the gradient elution with two water steps (sandwich injection), designed to minimize the contact of the ^{1}D-HIC salt plug with the ^{2}D-hydro-organic solvent. Unlike other analytical methods used for ADC characterization, this optimized on-line HIC x RPLC-UV-HRMS method was able to unambiguously identify the positional isomers of the different DARs observed in HIC.

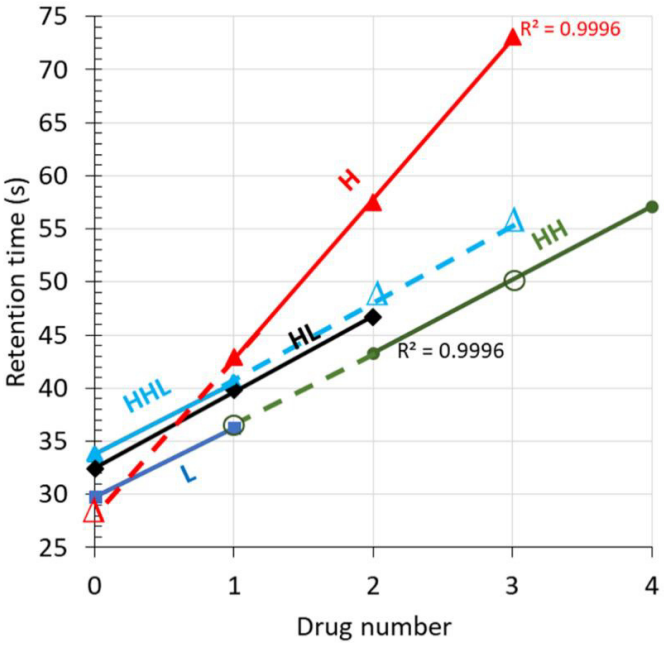

Fig. 9: Illustration of the potential of retention data in RPLC to predict the retention times of non-identified subunits (empty symbols) considering the plot of retention times of identified subunits (full symbols) as a function of drug load number. H and L stand for heavy and light chains respectively. The coefficient of determination is given for HL and H for (with three identified subunits). (Adapted from [30] with permission from Elsevier).

The methodology is presented in Fig. 7, through the illustration of DAR 6 characterization. After the separation of DAR species in the first HIC dimension (Fig. 7a), each fraction was sent in the second RPLC dimension. The denaturing conditions led to the formation of subunits, further separated in RPLC according to their hydrophobicity (Fig. 7b). The separated subunits were then identified after deconvolution of their MS spectra (Fig. 7c). The presence of the four expected subunits of DAR 6 led to the unambiguous identification of the two positional isomers of DAR 6 as shown in Fig. 7. In addition to achieving on-line desalting of the first HIC separation, mandatory for the hyphenation to HRMS, RPLC was also very useful to gain information about the structure of the DAR species separated in HIC. With such an approach, not only even DARs could be identified, but also odd DARs. The contour plot

presented in Fig. 8 summarizes the structural elucidation of both even and odd DARs, with horizontal dotted lines showing the DAR species separated in HIC and dotted vertical lines showing the different subunits separated in RPLC. Using the methodology illustrated in Fig. 7, odd DARs (1, 3 and 5) and most of their related positional isomers could be unambiguously identified. Very large subunits (MW > 100 kDa) were more difficult to ionize and hence to detect in MS. However, subunit identification could be completed by crossing information from both retention and MS data, thereby making the prediction of the retention times of the different subunits possible as shown by the plots of the retention times of identified subunits against the drug load number (Fig. 9).

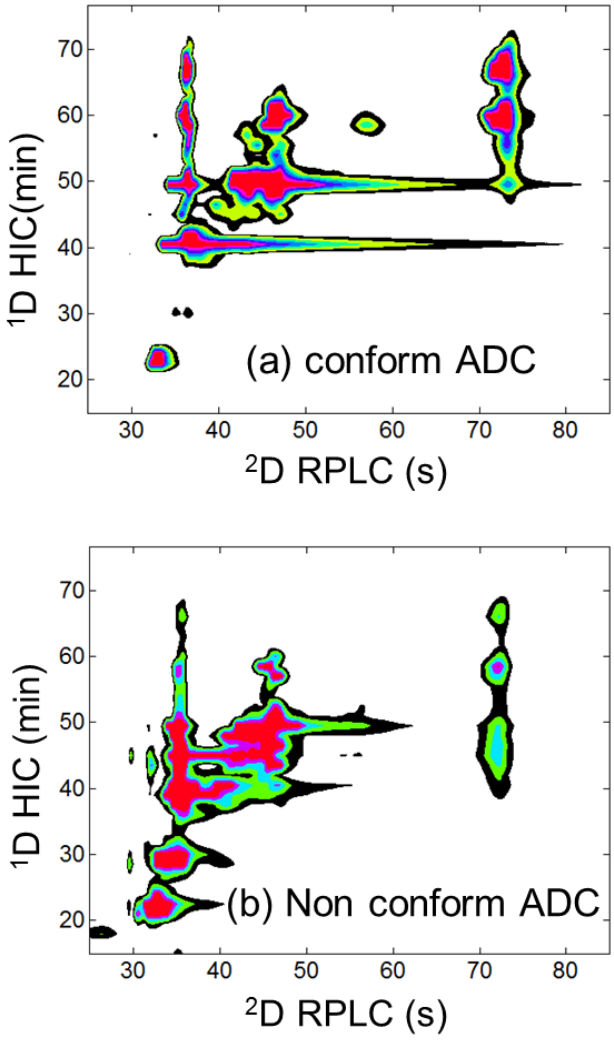

Fig. 10: Contour plots of HIC x RPLC-UV separations of non-stressed (top) and 2-months stressed (bottom) brentuximab vedotin illustrating the possibility of visual assessment of its conformity. (Adapted from [30] with permission from Elsevier).

As pointed out, experimental data were well fitted by straight lines ($R^2 > 0.99$). The good correlation between subunit retention time and conjugated drug number suggests that this latter is the driving force for retention in RPLC. From these different straight lines, it is possible to predict the retention time of any non-identified subunit (empty symbols in Fig. 9) by interpolation or even extrapolation of the fitted straight line. Finally, the excellent repeatability obtained in HIC x RPLC-UV makes the related 2D contour plots very convenient for assessing the conformity of ADCs in their later stage of development as well as in quality control. A visual comparison between non-conform and conform batches can be rapidly performed from 2D UV-contour plots shown in Fig. 10.

On-line HIC x RPLC-UV-HRMS appears to be a powerful technique for fast and extensive characterization of cysteine-linked ADC.

4.2. CEX x RPLC

CEX was also coupled to RPLC in full comprehensive and selective comprehensive for mAbs [31, 32], and in multiple heart-cutting for lysine-conjugated ADCs [7]. CEX, performed with pH gradients, can separate charge variants. The positive charges of the protein interact with the negative charges of the stationary phase, resulting in increased retention with increased protein charge. A positive charge is removed per lysine residue conjugated, which leads to a decrease in retention when the drug conjugation of lysine-linked ADCs increases. Drug conjugation, glycan variants, as well as PTMs (such as deamidation or oxidation) can alter the overall charge, thus changing the retention. In RPLC, the conjugation of hydrophobic drugs shifts the retention towards higher retention times, making the combination of CEX and RPLC, a good option to characterize these ADCs. CEX requires mobile phase salt buffers, usually not compatible with MS. The first role of RPLC is thus to remove salts prior to MS.

Sandra et al. [7] used multiple heart-cutting mCEX-RPLC-UV-HRMS for the characterization of the lysine-conjugated ADC ado-trastuzumab emtansine, commercialized as Kadcyla. The analyses were carried out with a commercially available Agilent 1290 Infinity 2D-LC system (Agilent Technologies, Waldbronn, Germany), with a set of three external valves for the mLC-LC configuration, including a 2-position/4-port duo valve and two “sampling deck” valves ensuring the multiple storage of fractions in mLC-LC. Top-down (protein level) and middle-up (partially

IdeZ-digested protein) approaches were considered in this study. Partial digestion with IdeZ cleaves the protein below the hinge region, leading to two identical Fc/2 fragments and one $F(ab')_2$ fragment. CEX and RPLC were found to be complementary. More conjugated DARs are less retained in CEX while more retained in RPLC. Drug loading distribution from DAR 0 to DAR 8 could be assessed considering both the retention data and the structural information gained from the deconvolution of the MS spectra. Compared to the top-down approach, the analysis of IdeZ-treated samples provided more information such as the presence of linker molecules alone and the distribution of drugs on the protein backbone via lysine linkages. Although this 2D-separation was carried out in multiple heart-cutting, one could easily imagine the additional information that on-line comprehensive CEX x RPLC could provide.

It should be noted that top-down and middle-up approaches were also considered for the characterization of different mAbs (rituximab, trastuzumab, infliximab, and cetuximab) by selective comprehensive (sCEX x RPLC-UV-HRMS) and full comprehensive (CEX x RPLC-UV-HRMS) approaches [31, 32]. In those cases, analyses were performed with a 2D-LC Agilent 1290 Infinity line (Waldbronn, Germany) including a 2-position/4-port duo valve. Two "sampling deck" valves were used for sLC x LC. Using a middle-up approach, mAbs were analysed after partial digestion with IdeS, followed by reduction of disulfide bonds with DTT, leading to small fragments of about 25 kDa. The observed CEX peaks of intact mAb as well as of digested and digested/reduced mAb could be identified by HRMS. Furthermore, the authors drew attention to the increase in peak capacity brought by the second RPLC dimension, particularly relevant when analysing mAb fragments.

4.3. HILIC x RPLC

HILIC involves the use of highly denaturing mobile phases (i.e. high organic content and most often acidic or basic pH). Yet, this technique may be attractive for mAbs or ADCs. In HILIC, the compounds are separated by their increased hydrophilicity, polarity and/or charge. HILIC can therefore be considered as quite complementary to RPLC. Stoll et al. [33] highlighted the potential of on-line comprehensive HILIC x RPLC for the separation of IdeS-digested and IdeS-digested/DTT-reduced mAbs. The benefit of the method was illustrated by analysing three mAbs which differed by their extent of N-glycosylation which could be revealed on the Fc/2 and Fd subunits of each mAb. The glycosylation profile of mAbs and ADCs is part of the CQAs that must be

monitored during process development because it may affect the stability, efficacy, and safety of the protein. The interest of 1D-HILIC had already been shown for the separation of protein glycoforms by differentiating according to glycan size [34–38]. In protein analysis, HILIC usually requires the use of trifluoroacetic acid (TFA) in the mobile phase, acting as an ion-pairing agent to maintain good peak shapes [34]. However, compared to weaker acids such as formic acid, TFA leads to lower protein MS signal. A second RPLC dimension is a clever way to combine the chromatographic resolution of HILIC, with an improved MS signal thanks to formic acid in the mobile phase. Moreover, given the inherent complementarity of these two chromatographic modes, the value of adding RPLC after a first HILIC separation is to gain more information on the separated species by increasing the separation space coverage. Experimentally, the on-line coupling of HILIC and RPLC is challenging because of injection effects resulting from solvent strength mismatch between both mobile phases. In their study, the authors circumvented the deleterious effects on the separation by on-line diluting the first dimension solvent with a weak solvent prior to injection in RPLC. The comparison of on-line CEX x RPLC [31] as discussed earlier, and HILIC x RPLC [33], both performed on an Agilent 2D-LC Infinity line, is given in Fig. 11. HILIC x RPLC was found to be more selective for the separation of the glycoforms of heavily glycosylated species as highlighted by the arrows in Fig. 11.

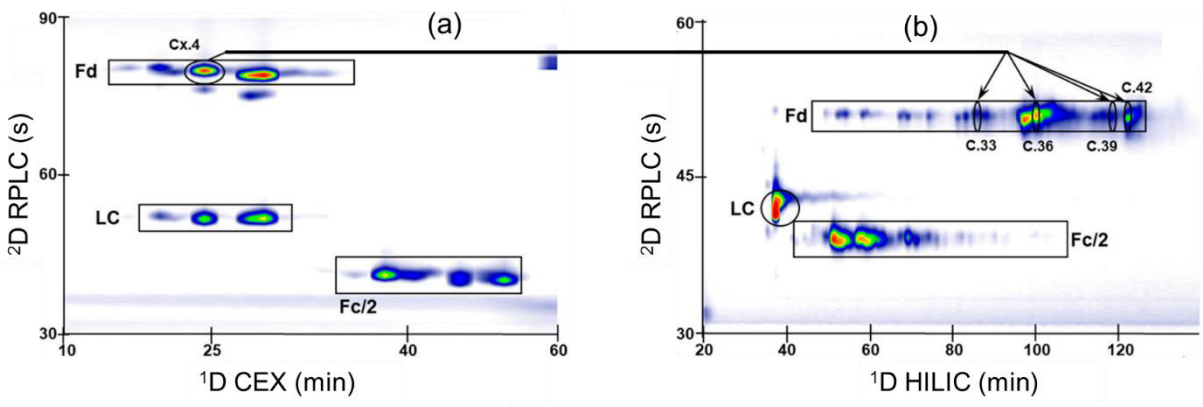

Fig. 11: Comparison of (a) online CEX x RPLC and (b) online HILIC x RPLC for the analysis of rituximab. (Adapted from [33] with permission from ACS Publications).

5. Bottom-up approach

With the bottom-up approach, also known as peptide mapping, the protein undergoes total digestion, typically with trypsin, resulting in small peptide fragments. Unlike

middle-up, bottom-up approach is used to obtain more precise information on the amino-acid sequence and on the specific locations of any post-translational or other modifications in the amino-acid chain of the protein [8]. For very large proteins such as mAbs or ADCs, tryptic digestion leads to a large number of peptides, underlining the interest of on-line LC x LC for peak capacity enhancement. Fig. 12 shows two different on-line LC x LC-UV-HRMS analyses of tryptic digests performed on similar 2D-LC Agilent 1290 Infinity lines as mentioned earlier.

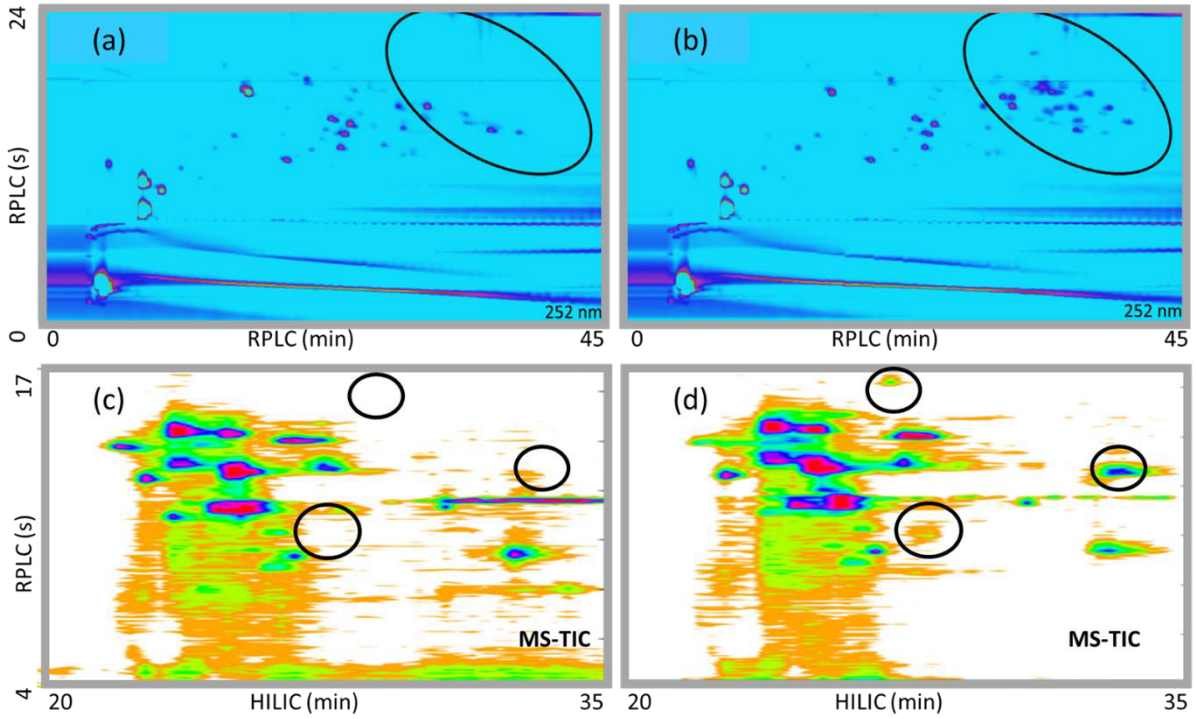

Fig. 12: Peptide maps in RPLC x RPLC-UV of (a) trastuzumab and (b) ado-trastuzumab emtansine, and in HILIC x RPLC-MS-TIC of (c) brentuximab and (d) brentuximab vedotin. Differences between mAb and ADC are circled in black. ((a, b) Adapted from [7] with permission from Elsevier. (c, d) Adapted from [39]).

They were carried out to obtain structural information about the location of the conjugation sites on the proteins. A digest of trastuzumab (Fig. 12a) and a digest of its related lysine-linked ADC (ado-trastuzumab emtansine) (Fig. 12b) were separated in on-line RPLC x RPLC with different mobile phase pHs between ^{1}D and ^{2}D (10 mM NH4-bicarbonate pH 8.2 in ^{1}D and 0.1% formic acid in ^{2}D) [7]. A digest of brentuximab (Fig. 12c) and a digest of its related cysteine-linked ADC (brentuximab vedotin) (Fig. 12d) were separated in HILIC x RPLC with 10 mM ammonium acetate in ^{1}D-HILIC and 0.1% formic acid in ^{2}D-RPLC [39]. In both cases, the direct comparison of the 2D contour plots (Fig. 12) provides valuable insights on sample drug conjugation. In RPLC x RPLC,

a large part of the peptide map is similar for mAb (Fig. 12a) and ADC (Fig. 12b) due to the fact that most peptides are identical. However, some additional spots (circled in black) appear, essentially located on the top of the peptide map. They were most likely attributed to conjugated peptides. Similarly, in HILIC x RPLC, some spots (circled in black) are present for brentuximab vedotin (Fig. 12d) while not present for brentuximab (Fig. 12c). It is interesting to notice the large occupation of the retention space in HILIC x RPLC, which makes this technique very attractive for the separation of biomolecules.

Vanhoenacker et al. [40] compared three combinations for the analysis of trastuzumab, including RPLC x RPLC, HILIC x RPLC and SCX x RPLC with a view to maximize the resolution while minimizing the dilution. The authors found SCX x RPLC was limited by poor efficiency in SCX, resulting in significant band broadening, hence reducing the overall peak capacity despite a large retention space coverage. They found HILIC x RPLC less attractive than RPLC x RPLC, due to the very low volumes transferred from HILIC to RPLC (about 0.5% of the column dead volume) in order to limit the negative impact of the strong injection solvent (high acetonitrile content). However, compared to SCX, HILIC exhibited much better resolution, underlining again the great potential of HILIC x RPLC for the characterization of mAbs or ADCs.

6. Conclusion

Antibody-drug conjugates are large and heterogeneous biomolecules. Their inherent complexity needs multiple complementary analytical approaches to achieve their comprehensive characterization, among which are liquid chromatography and mass spectrometry. Compared to 1D-LC, 2D-LC is a very attractive technique, since it enables to combine two chromatographic separations, hence maximizing the information gained during a single analysis. In the context of ADC analysis, the comprehensive approach is the most efficient way to benefit from extensive information on the complete sample. This chapter gives an overview of the different on-line LC x LC techniques that have been used for ADC analysis. Different orthogonal combinations were proven to be highly valuable for ADC characterization at different levels (intact ADC analysis, top/middle-down, middle-up and bottom-up approaches). Those include on-line HIC x SEC, SEC x SEC, HIC x RPLC, CEX x RPLC, HILIC x RPLC and RPLC x RPLC. In most reported studies, commercially available 2D-LC instruments were used. However, on-line LC x LC can also be carried out by combining two

independent LC instruments, as on-line HIC x SEC or on-line SEC x SEC presented in Subheading 2. At first instance, 2D-LC may be used as a rapid way to enable the on-line coupling of non-compatible chromatographic separations with MS detection by providing a desalting step in the second dimension. This strategy was used with HIC, SEC and CEX in the first dimension. In addition, a second dimension offers more information on the formerly separated species by increasing the chromatographic separation space. Finally, the versatility of on-line LC x LC hyphenated to HRMS and also IMS makes it a powerful analytical tool for extensive characterization of ADCs.

7. References

[1] A. Beck, T. Wurch, C. Bailly, N. Corvaia, Strategies and challenges for the next generation of therapeutic antibodies, Nat. Rev. Immunol. 10 (2010) 345–352. doi:10.1038/nri2747.

[2] A. Beck, J.M. Reichert, Antibody-drug conjugates: present and future, MAbs. 6 (2014) 15–17. doi:10.4161/mabs.27436.

[3] A. Beck, L. Goetsch, C. Dumontet, N. Corvaïa, Strategies and challenges for the next generation of antibody-drug conjugates, Nat Rev Drug Discov. 16 (2017) 315–337. doi:10.1038/nrd.2016.268.

[4] A. Beck, E. Wagner-Rousset, D. Ayoub, A. Van Dorsselaer, S. Sanglier-Cianférani, Characterization of Therapeutic Antibodies and Related Products, Anal. Chem. 85 (2013) 715–736. doi:10.1021/ac3032355.

[5] S. Panowski, S. Bhakta, H. Raab, P. Polakis, J.R. Junutula, Site-specific antibody drug conjugates for cancer therapy, MAbs. 6 (2013) 34–45. doi:10.4161/mabs.27022.

[6] L.N. Le, J.M.R. Moore, J. Ouyang, X. Chen, M.D.H. Nguyen, W.J. Galush, Profiling Antibody Drug Conjugate Positional Isomers: A System-of-Equations Approach, Anal. Chem. 84 (2012) 7479–7486. doi:10.1021/ac301568f.

[7] K. Sandra, G. Vanhoenacker, I. Vandenheede, M. Steenbeke, M. Joseph, P. Sandra, Multiple heart-cutting and comprehensive two-dimensional liquid chromatography hyphenated to mass spectrometry for the characterization of the antibody-drug conjugate ado-trastuzumab emtansine, Journal of Chromatography B. 1032 (2016) 119–130. doi:10.1016/j.jchromb.2016.04.040.

[8] S. Fekete, D. Guillarme, P. Sandra, K. Sandra, Chromatographic, Electrophoretic, and Mass Spectrometric Methods for the Analytical Characterization of Protein Biopharmaceuticals, Anal. Chem. 88 (2016) 480–507. doi:10.1021/acs.analchem.5b04561.

[10] D. Stoll, J. Danforth, K. Zhang, A. Beck, Characterization of therapeutic antibodies and related products by two-dimensional liquid chromatography coupled with UV absorbance and mass spectrometric detection, Journal of Chromatography B. 1032 (2016) 51–60. doi:10.1016/j.jchromb.2016.05.029.

[11] M. Sarrut, F. Rouvière, S. Heinisch, Theoretical and experimental comparison of one dimensional versus on-line comprehensive two-dimensional liquid chromatography for optimized sub-hour separations of complex peptide samples, Journal of Chromatography A. 1498 (2017) 183–195. doi:10.1016/j.chroma.2017.01.054.

[12] P.J. Schoenmakers, P. Mariott, Nomenclature and Conventions in Comprehensive Multidimensional Chromatography – An Update, LCGC Europe 16:335–339

[13] G. Guiochon, N. Marchetti, K. Mriziq, R.A. Shalliker, Implementations of two-dimensional liquid chromatography, Journal of Chromatography A. 1189 (2008) 109–168. doi:10.1016/j.chroma.2008.01.086.

[14] F. Bedani, P.J. Schoenmakers, H.-G. Janssen, Theories to support method development in comprehensive two-dimensional liquid chromatography – A review, J. Sep. Science. 35 (2012) 1697–1711. doi:10.1002/jssc.201200070.

[15] Y. Li, C. Gu, J. Gruenhagen, K. Zhang, P. Yehl, N.P. Chetwyn, C.D. Medley, A size exclusion-reversed phase two dimensional-liquid chromatography methodology for stability and small molecule related species in antibody-drug conjugates, Journal of Chromatography A. 1393 (2015) 81–88. doi:10.1016/j.chroma.2015.03.027.

[16] A. Goyon, L. Sciascera, A. Clarke, D. Guillarme, R. Pell, Extending the limits of size exclusion chromatography: Simultaneous separation of free payloads and related species from antibody-drug conjugates and their aggregates, Journal of Chromatography A. 1539 (2018) 19–29. doi:10.1016/j.chroma.2018.01.039.

[17] S.R. Groskreutz, M.M. Swenson, L.B. Secor, D.R. Stoll, Selective comprehensive multi-dimensional separation for resolution enhancement in high-performance liquid chromatography. Part I: Principles and instrumentation, Journal of Chromatography A. 1228 (2012) 31–40. doi:10.1016/j.chroma.2011.06.035.

[18] C.J. Venkatramani, S.R. Huang, M. Al-Sayah, I. Patel, L. Wigman, High-resolution two-dimensional liquid chromatography analysis of key linker drug intermediate used in antibody drug conjugates, Journal of Chromatography A. 1521 (2017) 63–72. doi:10.1016/j.chroma.2017.09.022.

[19] J. Marcoux, T. Champion, O. Colas, E. Wagner-Rousset, N. Corvaïa, A.V. Dorsselaer, A. Beck, S. Cianférani, Native mass spectrometry and ion mobility characterization of trastuzumab emtansine, a lysine-linked antibody drug conjugate, Protein Science. 24 (2015) 1210–1223. doi:10.1002/pro.2666.

[20] J. Chen, S. Yin, Y. Wu, J. Ouyang, Development of a Native Nanoelectrospray Mass Spectrometry Method for Determination of the Drug-to-Antibody Ratio of Antibody–Drug Conjugates, Anal. Chem. 85 (2013) 1699–1704. doi:10.1021/ac302959p.

[21] S. Rosati, Y. Yang, A. Barendregt, A.J.R. Heck, Detailed mass analysis of structural heterogeneity in monoclonal antibodies using native mass spectrometry, Nature Protocols. 9 (2014) 967–976. doi:10.1038/nprot.2014.057.

[22] S. Rosati, R.J. Rose, N.J. Thompson, E. van Duijn, E. Damoc, E. Denisov, A. Makarov, A.J.R. Heck, Exploring an Orbitrap Analyzer for the Characterization of Intact Antibodies by Native Mass Spectrometry, Angewandte Chemie International Edition. 51 (2012) 12992–12996. doi:10.1002/anie.201206745.

[23] N.J. Thompson, S. Rosati, A.J.R. Heck, Performing native mass spectrometry analysis on therapeutic antibodies, Methods. 65 (2014) 11–17. doi:10.1016/j.ymeth.2013.05.003.

[24] I.D.G. Campuzano, C. Netirojjanakul, M. Nshanian, J.L. Lippens, D.P.A. Kilgour, S. Van Orden, J.A. Loo, Native-MS Analysis of Monoclonal Antibody Conjugates by Fourier Transform Ion Cyclotron Resonance Mass Spectrometry, Anal. Chem. 90 (2018) 745–751. doi:10.1021/acs.analchem.7b03021.

[25] W. Li, J.L. Kerwin, J. Schiel, T. Formolo, D. Davis, A. Mahan, S.A. Benchaar, Structural Elucidation of Post-Translational Modifications in Monoclonal Antibodies, in: State-of-the-Art and Emerging Technologies for Therapeutic Monoclonal Antibody Characterization Volume 2. Biopharmaceutical Characterization: The NISTmAb Case Study, American Chemical Society, 2015: pp. 119–183. doi:10.1021/bk-2015-1201.ch003.

[26] A. Ehkirch, V. D'Atri, F. Rouviere, O. Hernandez-Alba, A. Goyon, O. Colas, M. Sarrut, A. Beck, D. Guillarme, S. Heinisch, S. Cianferani, An Online Four-Dimensional HIC×SEC-IM×MS Methodology for Proof-of-Concept Characterization of Antibody Drug Conjugates, Anal. Chem. 90 (2018) 1578–1586. doi:10.1021/acs.analchem.7b02110.

[27] A. Ehkirch, A. Goyon, O. Hernandez-Alba, F. Rouviere, V. D'Atri, C. Dreyfus, J.-F. Haeuw, H. Diemer, A. Beck, S. Heinisch, D. Guillarme, S. Cianferani, A Novel Online Four-Dimensional SEC×SEC-IM×MS Methodology for Characterization of Monoclonal Antibody Size Variants, Anal. Chem. 90 (2018) 13929–13937. doi:10.1021/acs.analchem.8b03333.

[28] R.E. Birdsall, H. Shion, F.W. Kotch, A. Xu, T.J. Porter, W. Chen, A rapid on-line method for mass spectrometric confirmation of a cysteine-conjugated antibody-drug-conjugate structure using multidimensional chromatography, MAbs. 7 (2015) 1036–1044. doi:10.1080/19420862.2015.1083665.

[29] M. Sarrut, S. Fekete, M.-C. Janin-Bussat, O. Colas, D. Guillarme, A. Beck, S. Heinisch, Analysis of antibody-drug conjugates by comprehensive on-line two-dimensional hydrophobic interaction chromatography x reversed phase liquid chromatography hyphenated to high resolution mass spectrometry. II-Identification of sub-units for the characterization of even and odd load drug species, Journal of Chromatography B. 1032 (2016) 91–102. doi:10.1016/j.jchromb.2016.06.049.

[30] M. Sarrut, A. Corgier, S. Fekete, D. Guillarme, D. Lascoux, M.-C. Janin-Bussat, A. Beck, S. Heinisch, Analysis of antibody-drug conjugates by comprehensive on-line two-dimensional hydrophobic interaction chromatography x reversed phase liquid chromatography hyphenated to high resolution mass spectrometry. I – Optimization of separation conditions, Journal of Chromatography B. 1032 (2016) 103–111. doi:10.1016/j.jchromb.2016.06.048.

[31] M. Sorensen, D.C. Harmes, D.R. Stoll, G.O. Staples, S. Fekete, D. Guillarme, A. Beck, Comparison of originator and biosimilar therapeutic monoclonal antibodies using comprehensive two-dimensional liquid chromatography coupled with time-of-flight mass spectrometry, MAbs. 8 (2016) 1224–1234. doi:10.1080/19420862.2016.1203497.

[32] D.R. Stoll, D.C. Harmes, J. Danforth, E. Wagner, D. Guillarme, S. Fekete, A. Beck, Direct Identification of Rituximab Main Isoforms and Subunit Analysis by Online Selective Comprehensive Two-Dimensional Liquid Chromatography–Mass Spectrometry, Anal. Chem. 87 (2015) 8307–8315. doi:10.1021/acs.analchem.5b01578.

[33] D.R. Stoll, D.C. Harmes, G.O. Staples, O.G. Potter, C.T. Dammann, D. Guillarme, A. Beck, Development of Comprehensive Online Two-Dimensional Liquid Chromatography/Mass Spectrometry Using Hydrophilic Interaction and Reversed-Phase Separations for Rapid and Deep Profiling of Therapeutic Antibodies, Anal. Chem. 90 (2018) 5923–5929. doi:10.1021/acs.analchem.8b00776.

[34] A. Periat, S. Fekete, A. Cusumano, J.-L. Veuthey, A. Beck, M. Lauber, D. Guillarme, Potential of hydrophilic interaction chromatography for the analytical characterization of protein biopharmaceuticals, Journal of Chromatography A. 1448 (2016) 81–92. doi:10.1016/j.chroma.2016.04.056.

[35] V. D'Atri, S. Fekete, A. Beck, M. Lauber, D. Guillarme, Hydrophilic Interaction Chromatography Hyphenated with Mass Spectrometry: A Powerful Analytical Tool for the Comparison of Originator and Biosimilar Therapeutic Monoclonal Antibodies at the Middle-up Level of Analysis, Analytical Chemistry. 89 (2017) 2086–2092. doi:10.1021/acs.analchem.6b04726.

[36] V. D'Atri, E. Dumont, I. Vandenheede, D. Guillarme, P. Sandra, K. Sandra, Hydrophilic Interaction Chromatography for the Characterization of

Therapeutic Monoclonal Antibodies at Protein, Peptide, and Glycan Levels, LCGC Europe 30:424–434.

[37] E. Domínguez-Vega, S. Tengattini, C. Peintner, J. van Angeren, C. Temporini, R. Haselberg, G. Massolini, G.W. Somsen, High-resolution glycoform profiling of intact therapeutic proteins by hydrophilic interaction chromatography-mass spectrometry, Talanta. 184 (2018) 375–381. doi:10.1016/j.talanta.2018.03.015.

[38] V. D'Atri, S. Fekete, D. Stoll, M. Lauber, A. Beck, D. Guillarme, Characterization of an antibody-drug conjugate by hydrophilic interaction chromatography coupled to mass spectrometry, Journal of Chromatography B. 1080 (2018) 37–41. doi:10.1016/j.jchromb.2018.02.026.

[39] S. Chapel, F. Rouvière, S. Heinisch, Unpublished results.

[40] G. Vanhoenacker, I. Vandenheede, F. David, P. Sandra, K. Sandra, Comprehensive two-dimensional liquid chromatography of therapeutic monoclonal antibody digests, Anal Bioanal Chem. 407 (2015) 355–366. doi:10.1007/s00216-014-8299-1.

REFERENCES

[1] F. Erni, R.W. Frei, Two-dimensional column liquid chromatographic technique for resolution of complex mixtures, Journal of Chromatography A. 149 (1978) 561–569. https://doi.org/10.1016/S0021-9673(00)81011-0.

[2] J.C. Giddings, Concepts and comparisons in multidimensional separation, Journal of High Resolution Chromatography. 10 (1987) 319–323. https://doi.org/10.1002/jhrc.1240100517.

[3] P.J. Marriott, P. Schoenmakers, Z. Wu, Nomenclature and Conventions in Comprehensive Multidimensional Chromatography – An Update, LC-GC Europe, 25 (2012) 266.

[4] B.W.J. Pirok, D.R. Stoll, P.J. Schoenmakers, Recent Developments in Two-Dimensional Liquid Chromatography: Fundamental Improvements for Practical Applications, Analytical Chemistry. 91 (2019) 240–263. https://doi.org/10.1021/acs.analchem.8b04841.

[5] D.R. Stoll, P.W. Carr, Two-Dimensional Liquid Chromatography: A State of the Art Tutorial, Anal. Chem. 89 (2017) 519–531. https://doi.org/10.1021/acs.analchem.6b03506.

[6] S.R. Groskreutz, M.M. Swenson, L.B. Secor, D.R. Stoll, Selective comprehensive multi-dimensional separation for resolution enhancement in high performance liquid chromatography. Part I: Principles and instrumentation, Journal of Chromatography A. 1228 (2012) 31–40. https://doi.org/10.1016/j.chroma.2011.06.035.

[7] G. Guiochon, N. Marchetti, K. Mriziq, R.A. Shalliker, Implementations of two-dimensional liquid chromatography, Journal of Chromatography A. 1189 (2008) 109–168. https://doi.org/10.1016/j.chroma.2008.01.086.

[8] L. Karger, L.R. Snyder, C. Horvath, An Introduction to Separation Science, John Wiley and Sons, New York, 1973.

[9] J.C. Giddings, Two-dimensional separations: concept and promise, Anal. Chem. 56 (1984) 1258A-1270A. https://doi.org/10.1021/ac00276a003.

[10] G. Guiochon, L.A. Beaver, M.F. Gonnord, A.M. Siouffi, M. Zakaria, Theoretical investigation of the potentialities of the use of a multidimensional column in chromatography, Journal of Chromatography A. 255 (1983) 415–437. https://doi.org/10.1016/S0021-9673(01)88298-4.

[11] F. Bedani, P.J. Schoenmakers, H.-G. Janssen, Theories to support method development in comprehensive two-dimensional liquid chromatography – A review, J. Sep. Science. 35 (2012) 1697–1711. https://doi.org/10.1002/jssc.201200070.

[12] J.C. Giddings, Sample dimensionality: A predictor of order-disorder in component peak distribution in multidimensional separation, Journal of Chromatography A. 703 (1995) 3–15. https://doi.org/10.1016/0021-9673(95)00249-M.

[13] M. Gilar, P. Olivova, A.E. Daly, J.C. Gebler, Orthogonality of Separation in Two-Dimensional Liquid Chromatography, Anal. Chem. 77 (2005) 6426–6434. https://doi.org/10.1021/ac050923i.

[14] B.W.J. Pirok, A.F.G. Gargano, P.J. Schoenmakers, Optimizing separations in online comprehensive two-dimensional liquid chromatography, J. Sep. Sci. 41 (2018) 68–98. https://doi.org/10.1002/jssc.201700863.

[15] R.E. Murphy, M.R. Schure, J.P. Foley, Effect of Sampling Rate on Resolution in Comprehensive Two-Dimensional Liquid Chromatography, Anal. Chem. 70 (1998) 1585–1594. https://doi.org/10.1021/ac971184b.

[16] K. Horie, H. Kimura, T. Ikegami, A. Iwatsuka, N. Saad, O. Fiehn, N. Tanaka, Calculating Optimal Modulation Periods to Maximize the Peak Capacity in Two-Dimensional HPLC, Anal. Chem. 79 (2007) 3764–3770. https://doi.org/10.1021/ac062002t.

[17] M. Sarrut, G. Crétier, S. Heinisch, Theoretical and practical interest in UHPLC technology for 2D-LC, TrAC Trends in Analytical Chemistry. 63 (2014) 104–112. https://doi.org/10.1016/j.trac.2014.08.005.

[18] J.M. Davis, D.R. Stoll, P.W. Carr, Effect of First-Dimension Undersampling on Effective Peak Capacity in Comprehensive Two-Dimensional Separations, Anal. Chem. 80 (2008) 461–473. https://doi.org/10.1021/ac071504j.

[19] P. Jandera, Column selectivity for two-dimensional liquid chromatography, J. Sep. Science. 29 (2006) 1763–1783. https://doi.org/10.1002/jssc.200600202.

[20] M. Camenzuli The Role of Surface Coverage and Orthogonality Metrics in Two-Dimensional Chromatography, LCGC Europe, 30 (2017), 346–351.

[21] D.R. Stoll, X. Wang, P.W. Carr, Comparison of the Practical Resolving Power of One- and Two-Dimensional High-Performance Liquid Chromatography Analysis of Metabolomic Samples, Anal. Chem. 80 (2008) 268–278. https://doi.org/10.1021/ac701676b.

[22] G. Semard, V. Peulon-Agasse, A. Bruchet, J.-P. Bouillon, P. Cardinaël, Convex hull: A new method to determine the separation space used and to optimize operating conditions for comprehensive two-dimensional gas chromatography, Journal of Chromatography A. 1217 (2010) 5449–5454. https://doi.org/10.1016/j.chroma.2010.06.048.

[23] M. Camenzuli, P.J. Schoenmakers, A new measure of orthogonality for multi-dimensional chromatography, Analytica Chimica Acta. 838 (2014) 93–101. https://doi.org/10.1016/j.aca.2014.05.048.

[24] S.C. Rutan, J.M. Davis, P.W. Carr, Fractional coverage metrics based on ecological home range for calculation of the effective peak capacity in comprehensive two-dimensional separations, Journal of Chromatography A. 1255 (2012) 267–276. https://doi.org/10.1016/j.chroma.2011.12.061.

[25] W. Nowik, S. Héron, M. Bonose, M. Nowik, A. Tchapla, Assessment of Two-Dimensional Separative Systems Using Nearest-Neighbor Distances Approach. Part 1: Orthogonality Aspects, Anal. Chem. 85 (2013) 9449–9458. https://doi.org/10.1021/ac4012705.

[26] W. Nowik, M. Bonose, S. Héron, M. Nowik, A. Tchapla, Assessment of Two-Dimensional Separative Systems Using the Nearest Neighbor Distances Approach. Part 2: Separation Quality Aspects, Anal. Chem. 85 (2013) 9459–9468. https://doi.org/10.1021/ac4012717.

[27] R. Al Bakain, I. Rivals, P. Sassiat, D. Thiébaut, M.-C. Hennion, G. Euvrard, J. Vial, Comparison of different statistical approaches to evaluate the orthogonality of chromatographic separations: Application to reverse phase systems, Journal of Chromatography A. 1218 (2011) 2963–2975. https://doi.org/10.1016/j.chroma.2011.03.031.

[28] M. Gilar, J. Fridrich, M.R. Schure, A. Jaworski, Comparison of Orthogonality Estimation Methods for the Two-Dimensional Separations of Peptides, Anal. Chem. 84 (2012) 8722–8732. https://doi.org/10.1021/ac3020214.

[29] M.R. Schure, J.M. Davis, Orthogonal separations: Comparison of orthogonality metrics by statistical analysis, Journal of Chromatography A. 1414 (2015) 60–76. https://doi.org/10.1016/j.chroma.2015.08.029.

[30] M.R. Schure, J.M. Davis, Orthogonality measurements for multidimensional chromatography in three and higher dimensional separations, Journal of Chromatography A. 1523 (2017) 148–161. https://doi.org/10.1016/j.chroma.2017.06.036.

[31] I. François, K. Sandra, P. Sandra, Comprehensive liquid chromatography: Fundamental aspects and practical considerations—A review, Analytica Chimica Acta. 641 (2009) 14–31. https://doi.org/10.1016/j.aca.2009.03.041.

[32] I. François, A. de Villiers, P. Sandra, Considerations on the possibilities and limitations of comprehensive normal phase–reversed phase liquid chromatography (NPLC×RPLC), J. Sep. Science. 29 (2006) 492–498. https://doi.org/10.1002/jssc.200500451.

[33] I. François, A. dos Santos Pereira, F. Lynen, P. Sandra, Construction of a new interface for comprehensive supercritical fluid chromatography×reversed phase liquid chromatography (SFC×RPLC), J. Sep. Science. 31 (2008) 3473–3478. https://doi.org/10.1002/jssc.200800267.

[34] P. Dugo, M. Fernandez, A. Cotroneo, G. Dugo, L. Mondello, Optimization of a Comprehensive Two-Dimensional Normal-Phase and Reversed-Phase Liquid Chromatography System, Journal of Chromatographic Science. 44 (2006) 561–5. https://doi.org/10.1093/chromsci/44.9.561.

[35] P. Dugo, O. Favoino, R. Luppino, G. Dugo, L. Mondello, Comprehensive Two-Dimensional Normal-Phase (Adsorption)–Reversed-Phase Liquid Chromatography, Anal. Chem. 76 (2004) 2525–2530. https://doi.org/10.1021/ac0352981.

[36] P. Dugo, V. Škeříková, T. Kumm, A. Trozzi, P. Jandera, L. Mondello, Elucidation of Carotenoid Patterns in Citrus Products by Means of Comprehensive Normal-Phase × Reversed-Phase Liquid Chromatography, Anal. Chem. 78 (2006) 7743–7750. https://doi.org/10.1021/ac061290q.

[37] Y. Wei, T. Lan, T. Tang, L. Zhang, F. Wang, T. Li, Y. Du, W. Zhang, A comprehensive two-dimensional normal-phase×reversed-phase liquid chromatography based on the modification of mobile phases, Journal of Chromatography A. 1216 (2009) 7466–7471. https://doi.org/10.1016/j.chroma.2009.08.029.

[38] P. Dugo, T. Kumm, M.L. Crupi, A. Cotroneo, L. Mondello, Comprehensive two-dimensional liquid chromatography combined with mass spectrometric detection in the analyses of triacylglycerols in natural lipidic matrixes, Journal of Chromatography A. 1112 (2006) 269–275. https://doi.org/10.1016/j.chroma.2005.10.070.

[39] P. Dugo, O. Favoino, P.Q. Tranchida, G. Dugo, L. Mondello, Off-line coupling of non-aqueous reversed-phase and silver ion high-performance liquid chromatography–mass spectrometry for the characterization of rice oil triacylglycerol positional isomers, Journal of Chromatography A. 1041 (2004) 135–142. https://doi.org/10.1016/j.chroma.2004.04.063.

[40] A.S. Kaplitz, M.E. Mostafa, S.A. Calvez, J.L. Edwards, J.P. Grinias, Two-dimensional separation techniques using supercritical fluid chromatography,

Journal of Separation Science. 44 (2021) 426–437. https://doi.org/10.1002/jssc.202000823.

[41] I. François, A. dos S. Pereira, P. Sandra, Considerations on comprehensive and off-line supercritical fluid chromatography×reversed-phase liquid chromatography for the analysis of triacylglycerols in fish oil, J. Sep. Science. 33 (2010) 1504–1512. https://doi.org/10.1002/jssc.201000044.

[42] I. François, P. Sandra, Comprehensive supercritical fluid chromatography ×reversed phase liquid chromatography for the analysis of the fatty acids in fish oil, Journal of Chromatography A. 1216 (2009) 4005–4012. https://doi.org/10.1016/j.chroma.2009.02.078.

[43] M. Sarrut, A. Corgier, G. Crétier, A. Le Masle, S. Dubant, S. Heinisch, Potential and limitations of on-line comprehensive reversed phase liquid chromatography×supercritical fluid chromatography for the separation of neutral compounds: An approach to separate an aqueous extract of bio-oil, Journal of Chromatography A. 1402 (2015) 124–133. https://doi.org/10.1016/j.chroma.2015.05.005.

[44] M. Sun, M. Sandahl, C. Turner, Comprehensive on-line two-dimensional liquid chromatography × supercritical fluid chromatography with trapping column-assisted modulation for depolymerised lignin analysis, Journal of Chromatography A. 1541 (2018) 21–30. https://doi.org/10.1016/j.chroma.2018.02.008.

[45] P. Jandera, T. Hájek, P. Česla, Effects of the gradient profile, sample volume and solvent on the separation in very fast gradients, with special attention to the second-dimension gradient in comprehensive two-dimensional liquid chromatography, Journal of Chromatography A. 1218 (2011) 1995–2006. https://doi.org/10.1016/j.chroma.2010.10.095.

[46] M. Mishra, C. Rana, A. De Wit, M. Martin, Influence of a strong sample solvent on analyte dispersion in chromatographic columns, Journal of Chromatography A. 1297 (2013) 46–55. https://doi.org/10.1016/j.chroma.2013.04.025.

[47] B. Buszewski, S. Noga, Hydrophilic interaction liquid chromatography (HILIC)—a powerful separation technique, Anal Bioanal Chem. 402 (2012) 231–247. https://doi.org/10.1007/s00216-011-5308-5.

[48] P. Hemström, K. Irgum, Hydrophilic interaction chromatography, J. Sep. Science. 29 (2006) 1784–1821. https://doi.org/10.1002/jssc.200600199.

[49] P. Jandera, Stationary and mobile phases in hydrophilic interaction chromatography: a review, Analytica Chimica Acta. 692 (2011) 1–25. https://doi.org/10.1016/j.aca.2011.02.047.

[50] G. Vanhoenacker, I. Vandenheede, F. David, P. Sandra, K. Sandra, Comprehensive two-dimensional liquid chromatography of therapeutic monoclonal antibody digests, Anal Bioanal Chem. 407 (2015) 355–366. https://doi.org/10.1007/s00216-014-8299-1.

[51] J.-L. Cao, S.-S. Wang, H. Hu, C.-W. He, J.-B. Wan, H.-X. Su, Y.-T. Wang, P. Li, Online comprehensive two-dimensional hydrophilic interaction chromatography × reversed-phase liquid chromatography coupled with hybrid linear ion trap Orbitrap mass spectrometry for the analysis of phenolic acids in Salvia miltiorrhiza, Journal of Chromatography A. 1536 (2018) 216–227. https://doi.org/10.1016/j.chroma.2017.09.041.

[52] A. D'Attoma, S. Heinisch, On-line comprehensive two dimensional separations of charged compounds using reversed-phase high performance liquid chromatography and hydrophilic interaction chromatography. Part II: Application to the separation of peptides, Journal of Chromatography A. 1306 (2013) 27–36. https://doi.org/10.1016/j.chroma.2013.07.048.

[53] E. Reingruber, J.J. Jansen, W. Buchberger, P. Schoenmakers, Transfer-volume effects in two-dimensional chromatography: Adsorption-phenomena in second-dimension size-exclusion chromatography, Journal of Chromatography A. 1218 (2011) 1147–1152. https://doi.org/10.1016/j.chroma.2010.12.080.

[54] E. Reingruber, F. Bedani, W. Buchberger, P. Schoenmakers, Alternative sample-introduction technique to avoid breakthrough in gradient-elution liquid chromatography of polymers, Journal of Chromatography A. 1217 (2010) 6595–6598. https://doi.org/10.1016/j.chroma.2010.07.073.

[55] P. Yang, L. Bai, W. Wang, J. Rabasco, Analysis of hydrophobically modified ethylene oxide urethane rheology modifiers by comprehensive two dimensional liquid chromatography, Journal of Chromatography A. 1560 (2018) 55–62. https://doi.org/10.1016/j.chroma.2018.05.033.

[56] M. Pursch, A. Wegener, S. Buckenmaier, Evaluation of active solvent modulation to enhance two-dimensional liquid chromatography for target analysis in polymeric matrices, Journal of Chromatography A. 1562 (2018) 78–86. https://doi.org/10.1016/j.chroma.2018.05.059.

[57] A. van der Horst, P.J. Schoenmakers, Comprehensive two-dimensional liquid chromatography of polymers, Journal of Chromatography A. 1000 (2003) 693–709. https://doi.org/10.1016/S0021-9673(03)00495-3.

[58] S. Hill, F.Inst. P, Channeling in packed columns, Chemical Engineering Science. 1 (1952) 247–253. https://doi.org/10.1016/0009-2509(52)87017-4.

[59] P.G. Saffman, G.I. Taylor, The penetration of a fluid into a porous medium or Hele-Shaw cell containing a more viscous liquid, Proc. R. Soc. Lond. A. 245 (1958) 312–329. https://doi.org/10.1098/rspa.1958.0085.

[60] M.L. Dickson, T.T. Norton, E.J. Fernandez, Chemical imaging of multicomponent viscous fingering in chromatography, AIChE Journal. 43 (n.d.) 409–418. https://doi.org/10.1002/aic.690430214.

[61] L.D. Plante, P.M. Romano, E.J. Fernandez, Viscous fingering in chromatography visualized via magnetic resonance imaging, Chemical Engineering Science. 49 (1994) 2229–2241. https://doi.org/10.1016/0009-2509(94)E0046-S.

[62] E.J. Fernandez, C.A. Grotegut, G.W. Braun, K.J. Kirschner, J.R. Staudaher, M.L. Dickson, V.L. Fernandez, The effects of permeability heterogeneity on miscible viscous fingering: A three-dimensional magnetic resonance imaging analysis, Physics of Fluids. 7 (1995) 468–477. https://doi.org/10.1063/1.868645.

[63] R.A. Shalliker, H.J. Catchpoole, G.R. Dennis, G. Guiochon, Visualising viscous fingering in chromatography columns: High viscosity solute plug, Journal of Chromatography A. 1142 (2007) 48–55. https://doi.org/10.1016/j.chroma.2006.09.059.

[64] R.A. Shalliker, G. Guiochon, Solvent viscosity mismatch between the solute plug and the mobile phase: Considerations in the applications of two-dimensional HPLC, Analyst. 135 (2010) 222–229. https://doi.org/10.1039/B908633C.

[65] J. Samuelsson, R.A. Shalliker, T. Fornstedt, Viscosity contrast effects in analytical scale chromatography - Evidence and impact, Microchemical Journal. 130 (2017) 102–107. https://doi.org/10.1016/j.microc.2016.08.007.

[66] C. Rana, A.D. Wit, M. Martin, M. Mishra, Combined influences of viscous fingering and solvent effect on the distribution of adsorbed solutes in porous media, RSC Advances. 4 (2014) 34369–34381. https://doi.org/10.1039/C4RA01965B.

[67] C. Rana, M. Mishra, Effect of Strong Sample Solvent on the Solute Dynamics for More or Less Viscous Sample: A Comparative Study, Procedia IUTAM. 15 (2015) 249–255. https://doi.org/10.1016/j.piutam.2015.04.034.

[68] R.-M. Lu, Y.-C. Hwang, I.-J. Liu, C.-C. Lee, H.-Z. Tsai, H.-J. Li, H.-C. Wu, Development of therapeutic antibodies for the treatment of diseases, Journal of Biomedical Science. 27 (2020) 1. https://doi.org/10.1186/s12929-019-0592-z.

CHAPTER II - EXPERIMENTAL CONDITIONS

INTRODUCTION

This chapter provides a general overview of the experimental materials and equipment used in each of the studies presented in this thesis. More detailed information regarding the analytical methods is given in each chapter.

Section A describes the instruments used for analysis and detection. These include two different one-dimensional liquid chromatography (1D-LC) instruments and one two-dimensional liquid chromatography (2D-LC) system, both hyphenated to ultraviolet (UV) detectors. In addition to UV detection, two different types of mass spectrometers were used for detection: a single-quadrupole instrument and a quadrupole-time-of-flight (Q-TOF) instrument.

Sections B and C compile information about the relevant characteristics of the stationary phases and mobile phases used in each study, respectively.

Section D provides information about the different samples that were analysed in this work, which include various small ionizable molecules (Chapter V), selected peptide standards (Chapters III, IV, and V), a complex peptide sample obtained by tryptic digestion of six model proteins (Chapters III, IV, and V), and monoclonal antibodies and antibody-drug conjugates (Chapters I and VI).

Lastly, ***Section E*** gives details about the calculation tools and methodologies used for method development and/or data processing in 1D-LC and 2D-LC.

A. INSTRUMENTATION

1. Chromatography instruments

1.1. Acquity UPLC and Acquity UPLC I-Class (Waters)

Two different instruments were used to conduct the 1D-LC experiments described in this thesis: an Acquity UPLC system (Chapter VI) and an Acquity UPLC I-Class system (Chapters IV and V), both from Waters Corporation. Each of these two systems includes four modules: a high-pressure binary solvent delivering pump, a thermostated autosampler with a flow-through needle (FTN) injector equipped with a 15-µL loop (UPLC) or a 20-µL loop (I-CLASS), a thermostated column compartment, and a photodiode-array detector (PDA) with a 0.5-µL flow cell and a 10-mm path length. The operating flow rate range for each pump is 0.010 to 2 mL/min. The pressure limits of the two instruments are 1034 bar (UPLC) and 1285 bar (I-Class) up to 1 mL/min. Above 1 mL/min, these pressure limits decrease with the flow rate down to 621 bar (UPLC) and 827 bar (I-Class) depending on the nature and composition of the mobile phase. Both automatic samplers can maintain temperatures between 4°C and 40°C. The injection volume range is 0.1 to 10 µL in the standard configuration for both instruments, but the upper range can be increased by means of optional extension loops. The column compartment temperature ranges are 30°C to 90°C (UPLC) and 20°C to 90°C (I-Class).

The measured dwell volumes and extra-column volumes for these two instruments were, respectively, 120 µL and 15 µL for the UPLC system and 110 µL and 12 µL for the I-Class system.

Instrument control and data acquisition were performed by Waters Empower 2 software (UPLC) and Waters MassLynx v4.1 software (I-Class).

1.2. 1290 Infinity II 2D-LC (Agilent)

The 2D-LC experiments described in this thesis were all performed on the same instrument: a 1290 Infinity 2D-LC system from Agilent Technologies. This system includes the following modules: two high-pressure binary pumps (one for each dimension), a thermostated autosampler with a flow-through needle injection system equipped with a 20-µL loop, two thermostated column compartments (one for each

dimension) with 1-µL ultra-low dispersion pre-heaters, and two diode-array detectors (DAD) with 0.6-µL flow cells and 10-mm path lengths. Three different switching-valve-based systems can be used to connect the two dimensions: the 2-position/4-port duo valve, the multiple heart-cutting valves system, and the Active Solvent Modulation valve system. Each of these systems is detailed in Subsection 2. The operating flow rate range for the two pumps is 0.050 to 5 mL/min. The pumps allow 1200 bar operation up to 2 mL/min, progressively reducing to 800 bar as flow increases to 5 mL/min. The autosampler can be thermostated from 4°C to 40°C. The temperature of both column compartments can be controlled between -15°C and 100°C up to 2.5 mL/min, and -15°C and 80°C up to 5 mL/min.

The measured dwell volumes and extra-column volumes for this instrument were, respectively, 170 µL and 22 µL for the first dimension, and 80 µL and 8.5 µL for the second dimension (storage loop volume excluded).

Instrument control and data acquisition were performed by Agilent OpenLAB CDS Chemstation Edition revision C.01.09.

2. Modulation interfaces

The interface between the first dimension (^{1}D) and the second dimension (^{2}D) is the key element of any on-line comprehensive two-dimensional liquid chromatography (LC x LC) system. Its primary purpose is to ensure the continuous and systematic fractioning and transfer of the ^{1}D-effluent to the ^{2}D-column. This is achieved by means of an electronically controlled switching-valve system often referred to as a modulator. Fraction collection and storage is usually carried out using storage loops, although the use of trapping columns was increasingly reported in the past few years [1,2]. Four different types of 2-position valves are commonly used in on-line LC x LC: the single 4-port duo, 10-port or 12-port valves, and the double 6-port valves [3,4]. Because they have no other function than automatic fraction collection and reinjection into the ^{2}D-column, they can be defined as standard valves, as opposed to the ASM valve which may be considered as a specific valve, as a result of its additional ability to perform on-line fraction dilution [5].

To our knowledge, the only non-valve-based approach that has been reported in the literature is the longitudinal on-column thermal modulation [6]. In brief, this approach

relies on successive switching between low and high temperature to capture and release the analytes eluting from ^{1}D on a modulation column placed between the two dimensions.

In this thesis, the modulator connecting the two dimensions for on-line LC x LC experiments was either a 2-position/4-port duo valve (Fig. II-1) or a 4-position/10-port Active Solvent Modulation (ASM) valve connected to two 14-port/6-position multiple heart-cutting (MHC) valves (Fig. II-2). For the selective comprehensive two-dimensional liquid chromatography (sLC x LC) experiments detailed in Chapter VI, the modulator consisted of a 2-position/4-port duo valve connected to two MHC valves for ^{1}D-fraction parking (Figs. II-3 and II-4).

All these valves are fully symmetrical, which means that the analytes pathways are the same in each set of valve positions (A vs. B for standard valve and decks, A vs. C or B vs. D for ASM). The valves were all operated in back-flush (or counter-current) mode (loop filling and flushing in opposite direction) to minimize extra-column dispersion compared to the forward-flush (or co-current) mode (loop filling and flushing in the same direction).

2.1. Standard valve: 2-position/4-port duo valve (Agilent)

The 2-position/4-port duo valve used for most on-line LC x LC experiments in this thesis is shown in the following Fig. II-1.

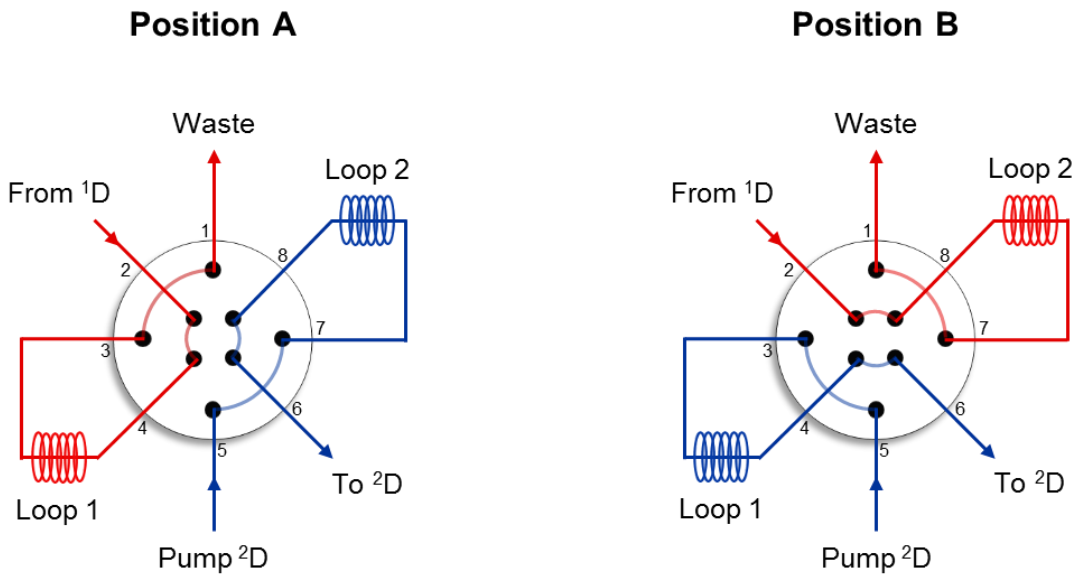

Fig. II-1: Schematic representation of the 2-position/4-port duo valve holding two sample loops.

This valve displays two positions. In position A, loop 1 collects the continuously flowing effluent from ^{1}D (red path) while the previously collected fraction in loop 2 is being injected and analysed in the ^{2}D-column. In position B, loop 2 is the one being filled while loop 1 is being unfilled for analysis in ^{2}D. These co-occurring fraction collection and analysis cycles between loops are controlled by a periodic valve switching determined by the ^{1}D-sampling time (t_S), which also defines the time available for analysis in ^{2}D. For the sake of maintaining the peak resolution already achieved in the ^{1}D-column and avoid the so-called ^{1}D-undersampling, this time slot is usually quite short (i.e. < 0.5 min for sub-hour on-line LC x LC separations) [7,8]. As a result of the ^{1}D-fractions being (almost) immediately transferred and analysed in the ^{2}D-column, the total analysis time in on-line LC x LC can be considered as the ^{1}D-analysis time. However, this interconnection between the two dimensions imposes some practical constraints, which often lead to operating under optimum conditions in both dimensions and entail compromises during method development [9,10].

2.2. Multiple heart-cutting system (Agilent)

The multiple heart-cutting (MHC) system used for sLC x LC experiments in Chapter VI consists of a 2-position/4-port duo valve connected to two MHC valves, customarily referred to as "decks", by means of 1.9-µL transfer capillaries (Fig. II-2). Decks 1 and 2 replace sampling loops 1 and 2 in Fig. II-1, respectively. Each deck holds six sampling loops that enable the temporary storage or "parking" of up to ten consecutive fractions until analysis. It should be pointed out that loops 1 and 6 from decks 1 and 2, respectively, do not act as storage loops but are only here to ensure continuous flowing of the mobile phase. Fraction parking allows breaking the link between sampling time and ^{2}D-analysis time, which among other advantages, enables more flexibility during method development and allows increasing the ^{2}D-analysis time [11]. However, such a gain also comes with the cost of an increased overall 2D analysis time. Besides, given the limited number of sampling loops available for parking, the ^{1}D-separation can only be fractionated "LC x LC-wise" (i.e. with minimal remixing of the analytes formerly separated in ^{1}D) over a selected time range. The consequence of such a limitation is a potential loss of information since parts of the ^{1}D-separation are disregarded.

With this system, the duo valve operates in the same manner as described in Subsection 2.1. Switching of the duo valve alternatively places one deck in position for

storage while the other for ^{2}D-analysis, whereas switching of the 6-position deck valves gives access to each storage loop. As a result, the switching time of the deck valves corresponds to the ^{1}D-sampling time, whereas the one of the duo valve takes place once every loop in one deck has been filled (i.e. ^{1}D-sampling time x 5).

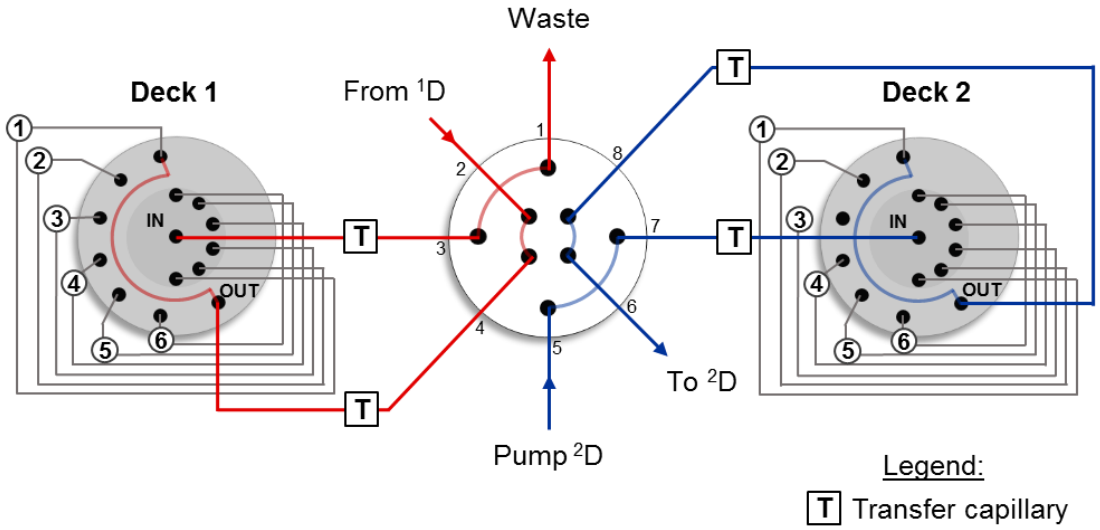

Fig. II-2: Schematic representation of the multiple heart-cutting (MHC) system used for sLC x LC experiments.

2.3. Active Solvent Modulation system (Agilent)

The Active solvent Modulation (ASM) system (Fig. II-3) used for on-line solvent dilution in Chapter V consists of a 4-position/10-port ASM valve connected to two MHC decks in a similar manner as described in Subsection 2.2.

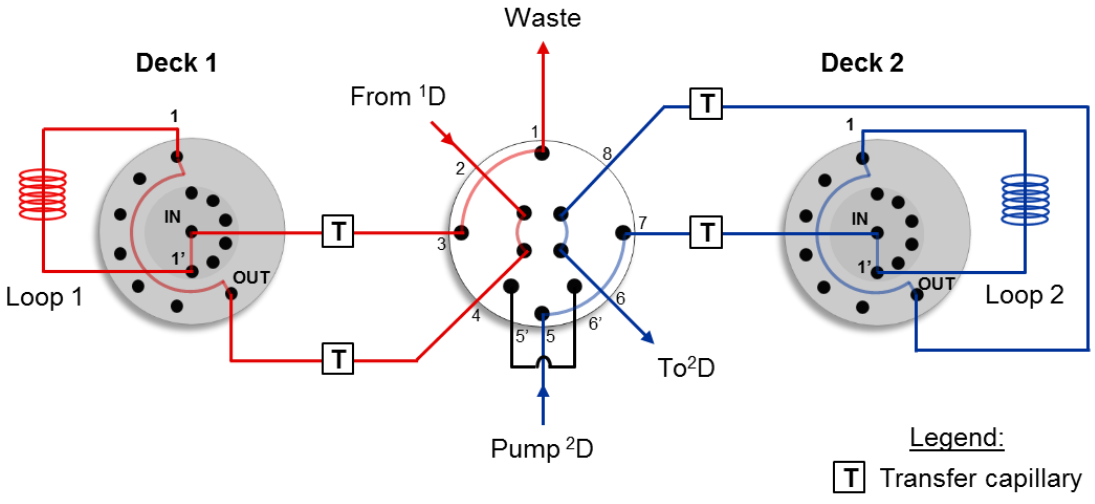

Fig. II-3: Schematic representation of the Active Solvent Modulation (ASM) system

The ASM system was initially designed for sLC x LC and mLC-LC experiments. As a result, not only the ASM valve-ports are incompatible with the sample loop fittings of the standard duo valve, but the system also requires backpressure from specific sample loops and capillaries connected between the ASM valve and the MHC valves to function.

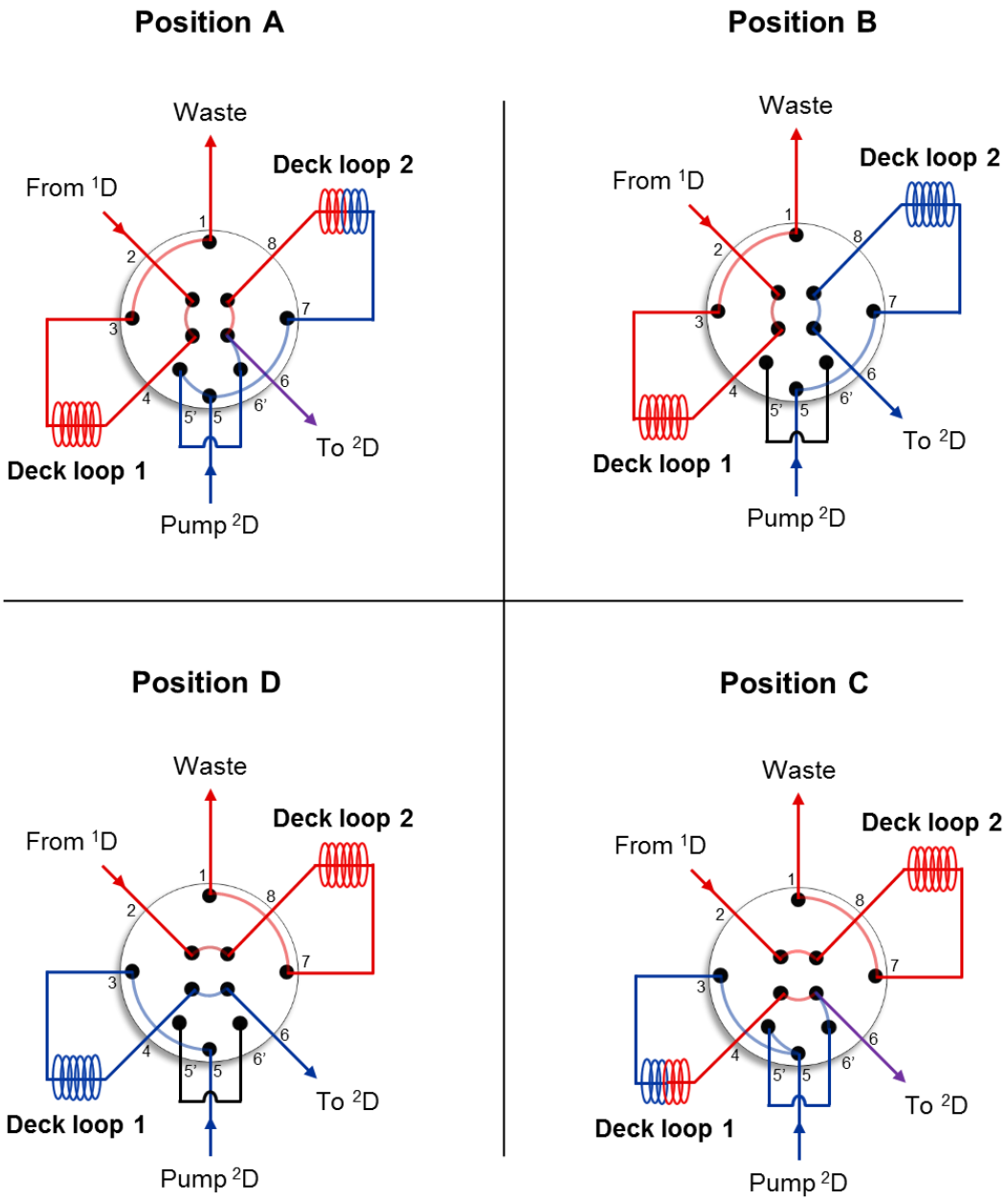

Fig. II-4: Schematic representation of the Active Solvent Modulation (ASM) valve operation.

Compared to the standard valve shown in Fig. 1, the ASM valve displays two additional ports (5' and 6'), which enable two additional valve positions through the use of a bypass capillary (Fig. II-4).

In position A, the ^{2}D-flow is split into two parts. While one part travels through loop 2 to empty its content (port 5 to 7), the other one travels through the bypass capillary (port 5 to 4). With such configuration, the fraction stored in loop 2 undergoes dilution when the two parts of the flow meet in port 6. The achieved dilution ratio depends on the flow restriction in each flow path and is thus determined by the bypass and sample loop capillary dimensions. Different capillary dimensions are commercially available for adjusting the split ratio of the ^{2}D-flow and thus the dilution ratio (up to five-fold).

After dilution of the ^{1}D-fraction, the valve rotates in position B to disable the bypass for analysis in ^{2}D. Finally, the valve switches again position to repeat another cycle of dilution (position C) and analysis (position D).

3. Mass spectrometry instruments

3.1. Acquity QDa detector (Waters)

For the 1D-LC experiments with mass spectrometry (MS) detection described in Chapters IV and V, an Acquity QDa detector from Waters Technology was hyphenated to the Acquity UPLC I-Class instrument described in Section A.

This instrument is equipped with a simple-quadrupole mass analyzer and an electrospray ionization source (ESI) using dry nitrogen (N_2) as nebulizer gas and drying gas. The instrument mass range is 30 Da to 1250 Da. This range was narrowed down to 100-350 Da for the analysis of small ionizable compounds, and 100 or 500-1250 Da for the peptide standards. The ionization source was used in ESI positive mode (ESI+) or ESI negative mode (ESI-) depending on the conditions. Data were simultaneously acquired in full scan mode and selective ion recording mode (SIR) during all analyses, with a sampling rate of 10 Hz. The latter mode was used to precisely monitor targeted ions during analysis. The values that were set for other source parameters are given in the following Table II-1.

Instrument control, data acquisition, and data handling were performed using Waters MassLynx v4.1 software.

Table II-1: Source parameters set on the QDa instrument.

Parameter	Value
Source temperature (°C)	125
Capillary voltages (kV)	0.8
Probe temperature (°C)	600
Cone voltage (V)	15

3.2. G6545B Q-TOF and G6560B IM-Q-TOF (Agilent)

For all experiments performed with the 1290 Infinity 2D-LC system, a 6500 Series Q-TOF instrument from Agilent technologies was used for high-resolution mass spectrometry (HRMS) detection. The instrument was either a G6545B Q-TOF (Chapters IV and V) or a G6560B Ion Mobility (IM)-Q-TOF (Chapters III and VI). Both instruments are mass spectrometers that use a quadrupole analyzer, a hexapole (collision cell), and a time-of-flight analyzer. Compared to the G6545B Q-TOF, the special feature of the G6560 IM-Q-TOF is that it also includes an ion mobility spectrometer connected to the Q-TOF mass spectrometer by a hexapole ion guide. In our studies, this instrument was always used in Q-TOF-only mode. Both instruments include an Agilent JetStream electrospray ionization source (AJS ESI) with nitrogen gas. Acquisitions were performed in MS mode with only the TOF-mass analyzer detecting the ions in scan mode while both the quadrupole and the collision cell worked as ion transmission devices. Specifications for these two instruments in this configuration (MS mode) include:

- Mass ranges from 50 to 10000 Da, 50 to 3200 Da or 50-1700 Da (G6545B), and 100 to 10000 Da, 100 to 3200 Da or 50-1700 Da (G6560B)
- Mass accuracies below 0.9 ppm (G6545B) and 1 ppm (G6560B)
- Mass resolving powers measured at full-width at half-maximum (FWHM) above 45000 (G6545B) and 42000 (G6560B)

The values that were set for the parameters of the two instruments are given in the following Table II-2.

Table II-2: Parameters set on the two Q-TOF instruments.

Parameter	Value (Chapters III to V)	Value (Chapter VI)
Mode	ESI+	ESI+
Masse range (Da)	100-3200 or 100-1700	1200-5000
Acquisition rate (spectra/sec)	20	10
Gaz temperature (°C)	300	325
Drying gaz (L/min)	11	13
Nebulizeur (psig)	40	40
Sheath gaz temperature (°C)	350	350
Sheath gaz flow (L/min)	11	12
Capillary voltage (V)	3500	4000
Nozzle voltage (V)	300	300
Fragmentor voltage (V)	150	185
Skimmer voltage (V)*	20	-
Oct 1 RF Vpp	750	750

*Only for G6545B Q-TOF instrument.

Both Q-TOF instruments were controlled by Agilent MassHunter Acquisition vB.09.00 software. Data handling was performed by Agilent MassHunter Qualitative Analysis vB.10.0.10305.0 software. In Chapter VI, deconvolution of protein mass spectra were performed using Agilent MassHunter Bioconfirm vB.09.00 software.

B. STATIONARY PHASES

All the stationary phases used in this work and their characteristics are listed by chromatographic mode and alphabetic order in the following Table II-3.

Table II-3: Characteristics of the stationary phases used in RPLC, HILIC, and CEX.

	Name	Type	Provider	L (mm)	d_i (mm)	d_p (µm)	d_{pores} (Å)
RPLC	Acquity BEH C4	FP	Waters	50	2.1	1.7	300
	Acquity CSH C18	FP	Waters	150	2.1	1.7	130
	Acquity CSH C18	FP	Waters	50	2.1	1.7	130
	Acquity CSH C18	FP	Waters	30	2.1	1.7	130
	AdvanceBio RP-mAb Diphenyl	FP	Agilent	50	2.1	3.5	450
	Ascentis Express C18	FP	Supelco	50	2.1	2.7	90
	BioResolve RP-mAb Polyphenyl	SP	Waters	50	2.1	2.7	450
	Biozen intact XB-C18	SP	Phenomenex	50	2.1	3.6	200
	Cortecs C18	SP	Waters	30	2.1	2.7	90
	Kinetex C18	SP	Phenomenex	30	2.1	1.3	100
	PLRP-S	NP	Agilent	50	2.1	5	-
	Sunfire C18	SP	Waters	50	1	3.5	100
HILIC	Accucore HILIC	SP	Thermo Fischer Scientific	100	2.1	2.6	80
	Acquity BEH Amide	FP	Waters	50	2.1	1.7	130
	Acquity BEH HILIC	FP	Waters	50	2.1	1.7	130
	Cortecs HILIC	SP	Waters	50	2.1	1.6	90
	Hypersil Gold HILIC	FP	Thermo Fischer Scientific	50	2.1	1.9	175
	Hypersil HILIC	FP	Thermo Fischer Scientific	50	4.6	3	120
	Kinetex HILIC	SP	Phenomenex	50	2.1	1.7	100
	Luna NH_2	FP	Phenomenex	150	2	3	100

Table II-3 (continued)							
	Name	**Type**	**Provider**	**L (mm)**	**d_i (mm)**	**d_p (µm)**	**d_{pores} (Å)**
HILIC	Nucleodur HILIC	FP	Machery-Nagel	60	1	3	110
	Nucleoshell HILIC	SP	Machery-Nagel	100	2	2.7	90
CEX	Bio MAb NP5	NP	Agilent	250	2.1	5	-
	BioResolve SCX mAb	NP	Waters	100	2.1	3	-

FP: Fully porous particles
SP: superficially porous particles
NP: non-porous particles (polymeric)

C. MOBILE PHASES

For all aqueous mobile phases, water was purified and deionized using an Elga (Purelab Classic UV) purification system from Veolia, permitting a resistivity of 18 MΩ.cm at 25°C. Organic mobile phases were prepared with LC-MS grade acetonitrile from sigma Aldrich. Mobile phases were prepared daily to prevent microbial contamination and other suspensions.

Several mobile phase additives were employed in RPLC and HILIC (cf. Table II-4), namely, formic acid (FA), trifluoroacetic acid (TFA), difluorocetic acid (DFA), and ammonium acetate (AA). All those additives were LC-MS grade, except for ammonium acetate (analytical grade). To maintain a constant ionic strength in the mobile phase, those additives were added in both the aqueous and organic mobile phases, apart from ammonium acetate, which is sparingly soluble in organic solvents. When prepared with salts, the aqueous mobile phases were filtered on 0.2-µm mixed cellulose ester membranes using a Millipore filtration assembly before use to eliminate suspensions.

For the separation of monoclonal antibodies and antibody-drug conjugates in CEX, several salts were employed: sodium chloride (NaCl), sodium hydroxide (NaOH), 2-(n-morpholino) ethanesulfonic acid (MES), monosodium phosphate (NaH_2PO_4), and disodium phosphate (Na_2HPO_4), all analytical grade. Several buffer solutions were prepared by dissolving the adequate salts in water before adjusting the pH with NaOH.

Mobile phase A was composed of either 20 mM MES or 10 mM phosphate (Table II-4), whereas mobile phase B contained mobile phase A + 300 mM NaCl.

All these compounds came from Sigma-Aldrich, except for FA (Fischer Scientific), and DFA (graciously provided by Waters).

Table II-4: Composition of the mobile phases used in RPLC, HILIC, and CEX.

Additive	Concentration	$^{w}pH_{25°C}$
Formic acid	0.1% v/v	2.7
Trifluoroacetic acid + formic acid	0.05% v/v + 0.1% v/v	2
Trifluoroacetic acid	0.05% v/v	2
Difluoroacetic acid	0.1% v/v	-
Ammonium acetate	10 mM	6.8
MES	20 mM	6.5 (adjusted with NaOH)
Phosphate	10 mM	6.5 or 7

D. SAMPLES

1. Small ionizable compounds

For the experimental study on the breakthrough phenomenon presented in Chapter V, we investigated several small ionizable compounds, including five acidic compounds and six basic compounds (mostly pharmaceuticals). They were all obtained from Sigma-Aldrich. Their name and most relevant characteristics are given in Table II-5. Most of these compounds were drawn from a list previously established in the thesis of Candice Grivel in 2010 [12]. They were selected to cover a broad range of pKa and hydrophobicity.

For sample preparation, stock solutions of each compound were prepared at a concentration of 200 mg/L in ACN/water (50:50 v/v) for most compounds, except for nadolol, propranolol, and N,N-dimethylaniline (1000 mg/L in 0:100 v/v). Stocks solutions of the acidic compounds were stored at 4°C and replaced monthly. Aliquots of each pharmaceutical compound were stored at -20°C and thawed when needed. Injected samples were prepared with various concentrations and injection solvent compositions by appropriate dilution of each stock solution with water and

acetonitrile. All samples were filtered on 0.22-µm PVDF (polyvinylidene fluoride) membranes before injection.

Table II-5: Characteristics of the seventeen small ionizable compounds studied.

Compound	Molecular weight (MW) (g/mol)	$pKa_{25°C}$	Character	Log P
Salicylic acid	138.12	2.8	Acidic	2.0
Methylparaben	152.15	8.3	Acidic	1.9
Ethylparaben	164.15	8.3	Acidic	2.4
Propylparaben	176.15	8.2	Acidic	3.0
Butylparaben	188.15	8.2	Acidic	3.4
Amitriptyline	277.4	9.2	Basic	6.1
Nadolol	309.4	9.2	Basic	1.3
Propranolol	259.34	9.1	Basic	3.1
Diphenhydramine	255.35	8.8	Basic	3.7
N,N-dimethylaniline	121.18	5.1	Basic	2.3
Caffeine	194.19	1.4	Basic	-0.1

2. Peptide standards

For the studies described in Chapters III to V, we used ten peptide standards. These peptides were drawn from a list previously established in [12]. They were chosen to cover a broad range of molecular weight and isoelectric point, to be as representative as possible of expected peptides from trypsin digestions of proteins.

The physical properties of the ten peptide standards are listed in Table II-6. Apart from WDDHH, custom-synthesized by Genecust, they were all obtained from Merck. Upon reception, stock solutions of each peptide were prepared in water at concentrations of 500 mg/L (influenza hemagglutinin, bombesin, [arg-8]-vasopressin, [ile]-angiotensin, and substance P), 1000 mg/L (bradykinin fragment 1-5), 1500 mg/L (WDDHH), 2000 mg/L (FLAG®), 2500 mg/L (bradykinin), and 5000 mg/L (leucine enkephalin). Aliquots of each peptide were stored at -20°C in polypropylene tubes to prevent peptide adsorption onto glass tubes. The solutions were thawed, diluted at various concentrations with water and acetonitrile, and filtered on 0.22-µm low protein binding PVDF membranes before injection. Polypropylene vials were used instead of

glass vials for the aforementioned reasons. Thawed solutions were kept at 4°C between and during analysis.

Table II-6: Characteristics of the ten peptide standards used in this work.

Peptide	MW (g/mol)	Monoisotopic mass (Da)	Isoelectric point
Influenza hemagglutinin	1102.15	1101.4655	3.5
FLAG® peptide	1012.97	1012.3985	3.9
WDDHH	708.68	708.2615	5.2
Leucine enkephalin	555.62	555.2693	6.0
Bombesin	1619.85	1618.8151	7.6
[arg-8]-vasopressin	1084.23	1083.4379	8.2
[ile]-angiotensin	897.08	896.5232	9.4
Bradykinin fragment 1-5	572.66	572.3071	10.6
Substance P	1347.63	1346.7281	11.7
Bradykinin	1060.21	1059.5614	12.5

3. Tryptic digest of model proteins

Chapter III, Chapter IV, and Chapter V (Section B) describe studies conducted for the analysis of a complex peptide sample. This complex peptide sample was made by trypsin digestion of six model proteins (human serum albumin HSA, bovine serum albumin BSA, β-casein, myoglobin, lysozyme, and cytochrome C) following a standard protocol, first described in [12] and later optimized in [13]. Proteins and trypsin enzyme were all obtained from Sigma-Aldrich. The protocol includes three main steps which are schematically illustrated in Fig. II-5. In the first two steps, the cysteine residues are (1) reduced then (2) alkylated using dithiothreitol (DTT) and iodoacetamide (IA), respectively. Reduction and alkylation help denaturing the proteins and making the proteolytic sites more accessible for proteolysis. In the last step, the trypsin protease cleaves the protein at the carboxy-terminal side of the lysine and arginine amino acid residues (except when either is followed by a proline).

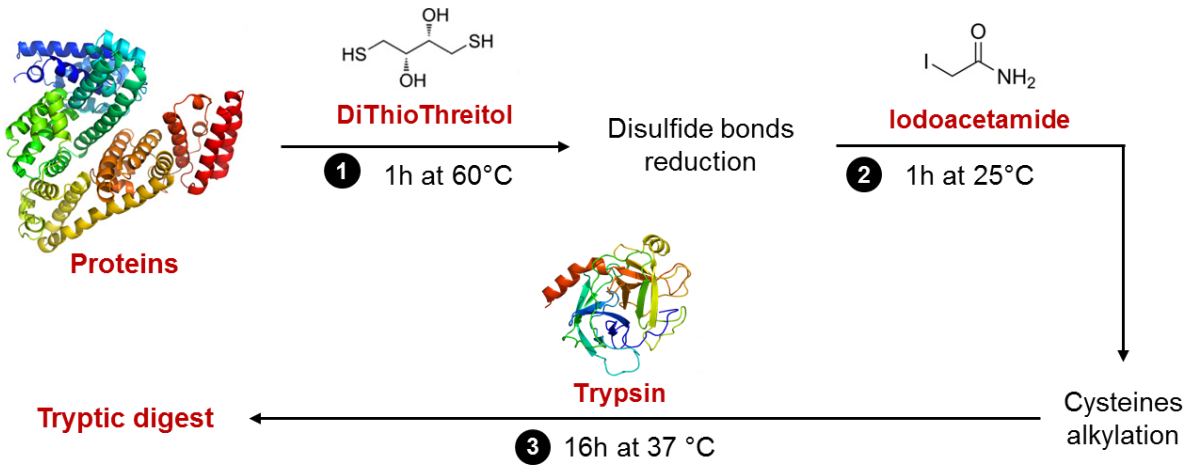

Fig. II-5: Schematic representation of the trypsin digestion protocol.

The experimental protocol used for protein digestion in this work is the following. For the first step, 0.5 mL of DTT (20 mM in water) was added to a polypropylene tube containing 5.8 mg of each protein (35 mg total) and the solution was incubated at 60°C for 1 h. For the second step, 0.5 mL of IA (20 mM in water) was added to the solution and left 1 h at ambient temperature away from light. The final digestion step was carried out by adding 0.5 mL of a solution containing 1mg/mL trypsin (mass-ratio enzyme to substrate of 1/70) solubilized in 20 mM ammonium bicarbonate in water before incubating this solution at 37°C for 16 h. Finally, the proteolytic digestion was stopped by the addition of 1% formic acid into the final solution (v/v). Ammonium bicarbonate (analytical grade) and formic acid (LC-MS grade) were obtained from Fischer Scientific. DTT and IA (both analytical grade) were obtained from Sigma-Aldrich. In steps 1 and 3, the solutions were heated and mixed using an Eppendorf ThermoMixer. The concentration of each protein was about 4000 mg/L and the protocol led to a tryptic digest containing 196 peptides with an average concentration per peptide of 120 mg/L. Aliquots of the tryptic digest were stored at -20°C in polypropylene tubes. The samples were thawed, diluted when needed, and filtered on 0.22-µm PVDF membranes before injection. Thawed solutions were kept at 4°C between and during analysis.

4. Monoclonal Antibodies and Antibody-Drug conjugates

Chapter I (Section D) and Chapter VI discuss results obtained for the analysis of several monoclonal antibodies (mAb) and antibody-drug conjugates (ADC).

Samples of brentuximab B and its associated cysteine-linked ADC brentuximab vedotin (commercialized by Seattle Genetics under the name Adcetris®) were provided graciously by Dr Alain Beck (Centre d'immunologie Pierre Fabre, France). The concentration was 2 mg/mL for both samples.

As part of a collaborative project, one mAB and its associated lysine-linked ADC were analysed in Chapter VI. For confidentiality reasons, the nature and structure of these two samples will not be disclosed in this manuscript. In this work, these two samples will be referred to as mAb-SARD and ADC-SARD. Four samples were provided, namely one mAb-SARD sample, one unstressed ADC-SARD sample, one ADC-SARD sample stressed at 40°C for two weeks, and one ADC-SARD sample stressed at 40°C for four weeks. The sample concentration was 20 mg/mL for the mAb and 5 mg/mL for the ADC.

Aliquots of each sample were stored at -20°C in polypropylene tubes. The samples were thawed, partially digested when needed, and filtered on 0.22-µm PVDF membranes before injection. Thawed solutions were kept at 4°C between and during analysis. Intact mAb and ADC samples were injected at their formulated concentration, without any pre-treatment nor prior dilution. Partially digested ADC samples were obtained using IdeS protease enzyme (commercialized under the name FabRICATOR by Genovis) following the generic protocol in the instruction manual (one unit of enzyme/µg of ADC at 37°C for 30 min).

E. DATA PROCESSING AND CALCULATION TOOLS

1. 2D-LC method optimization

In on-line LC x LC, method development is considerably more complex than in 1D-LC [9,10,14]. This can be ascribed to (i) the increased number of available operational parameters (column dimensions, flow rates, temperatures, gradient elution conditions…) and (ii) the interdependence and conflicting impact on the separation quality of many of these parameters.

A few optimization strategies have been reported to facilitate the process of LC x LC method development [10,14]. In this thesis, LC x LC parameters were optimized using an optimization procedure described by Sarrut et al [9]. The procedure relies on predictive calculations and a Pareto-optimality approach to define optimum sets of conditions

for a given analysis time, considering simultaneously both the effective peak capacity and the dilution factor as quality criteria. All calculations were made using an in-house tool developed on Microsoft Excel software.

2. 1D-LC data processing

1D-LC data were processed on the dedicated instrument's software and Microsoft Excel software after exporting raw data from the instrument's software. Peak integration and measurement of peak parameters, including retention time, peak width, peak intensity, peak area, peak asymmetry factor, and column plate number were performed using Azur software version 5.0.10.0 from Datalys (St Martin d'Hères, France).

3. 2D-LC data processing

LC x LC data were elaborated into two- and three-dimensional representations using an in-house script developed on Matlab.

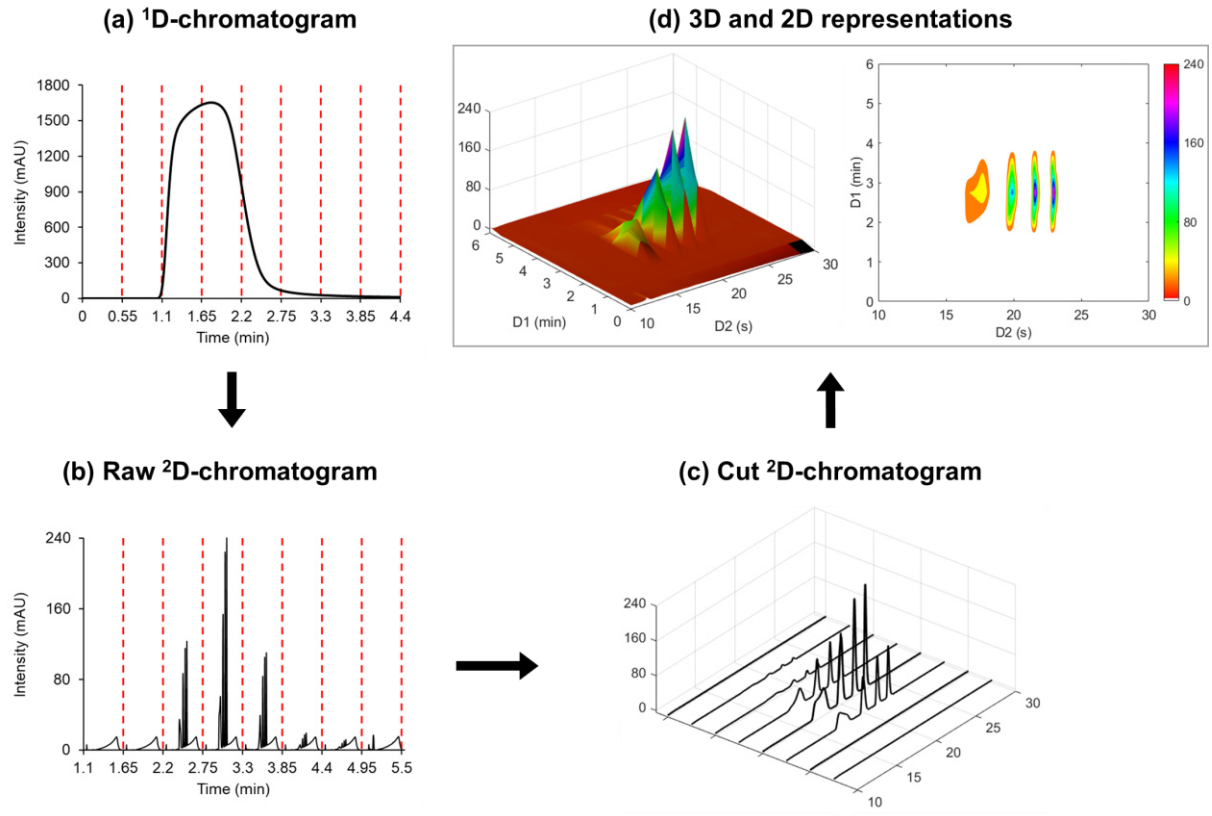

Fig. II-6: Schematic representation of data processing in 2D-LC.

In the second dimension, the successive runs are all acquired in a single chromatogram throughout the 2D-LC analysis (Fig. II-6b). These data are recorded as a two-column matrix, comprising one column for the analysis time and one column for the corresponding signal intensity. The script enables to switch from these raw ^{2}D-data to a representation either in a 3D surface plot (Fig. II-X) or in a 2D contour plot (Fig. II-6). The first step of data processing consists in cutting the raw ^{2}D-data into as many parts as the number of injected fractions in ^{2}D, which is achieved by taking into account the sampling time and the acquisition rate. The resulting matrix of data displays X-, Y-, and Z-coordinates corresponding to the ^{2}D-retention time, the ^{1}D-retention time, and the ^{2}D-peak intensity, respectively (Fig. II-6). This matrix is used to create a 3D surface plot whose edge colours vary linearly with the intensity specified by Z using a standard colourmap on Matlab. Finally, a contour plot is obtained by drawing the contour lines of the Z-values on the X-Y plane using a contour plot function.

REFERENCES

[1] B.W.J. Pirok, D.R. Stoll, P.J. Schoenmakers, Recent Developments in Two-Dimensional Liquid Chromatography: Fundamental Improvements for Practical Applications, Analytical Chemistry. 91 (2019) 240–263. https://doi.org/10.1021/acs.analchem.8b04841.

[2] Y. Chen, L. Montero, O.J. Schmitz, Advance in on-line two-dimensional liquid chromatography modulation technology, TrAC Trends in Analytical Chemistry. 120 (2019) 115647. https://doi.org/10.1016/j.trac.2019.115647.

[3] M.J. Egeness, M.C. Breadmore, E.F. Hilder, R.A. Shellie, The Modulator in Comprehensive Two-Dimensional Liquid Chromatography, LC-GC Europe. 29 (2016) 268–276.

[4] P. Česla, J. Křenková, Fraction transfer process in on-line comprehensive two-dimensional liquid-phase separations, J. Sep. Sci. 40 (2017) 109–123. https://doi.org/10.1002/jssc.201600921.

[5] D.R. Stoll, K. Shoykhet, P. Petersson, S. Buckenmaier, Active Solvent Modulation: A Valve-Based Approach To Improve Separation Compatibility in Two-Dimensional Liquid Chromatography, Anal. Chem. 89 (2017) 9260–9267. https://doi.org/10.1021/acs.analchem.7b02046.

[6] M.E. Creese, M.J. Creese, J.P. Foley, H.J. Cortes, E.F. Hilder, R.A. Shellie, M.C. Breadmore, Longitudinal On-Column Thermal Modulation for Comprehensive Two-Dimensional Liquid Chromatography, Anal. Chem. 89 (2017) 1123–1130. https://doi.org/10.1021/acs.analchem.6b03279.

[7] D.R. Stoll, X. Li, X. Wang, P.W. Carr, S.E.G. Porter, S.C. Rutan, Fast, comprehensive two-dimensional liquid chromatography, Journal of Chromatography A. 1168 (2007) 3–43. https://doi.org/10.1016/j.chroma.2007.08.054.

[8] D.R. Stoll, J.D. Cohen, P.W. Carr, Fast, comprehensive online two-dimensional high performance liquid chromatography through the use of high temperature ultra-fast gradient elution reversed-phase liquid chromatography, Journal of Chromatography A. 1122 (2006) 123–137. https://doi.org/10.1016/j.chroma.2006.04.058.

[9] M. Sarrut, A. D'Attoma, S. Heinisch, Optimization of conditions in on-line comprehensive two-dimensional reversed phase liquid chromatography. Experimental comparison with one-dimensional reversed phase liquid chromatography for the separation of peptides, Journal of Chromatography A. 1421 (2015) 48–59. https://doi.org/10.1016/j.chroma.2015.08.052.

[10] B.W.J. Pirok, A.F.G. Gargano, P.J. Schoenmakers, Optimizing separations in online comprehensive two-dimensional liquid chromatography, J. Sep. Sci. 41 (2018) 68–98. https://doi.org/10.1002/jssc.201700863.

[11] S.R. Groskreutz, M.M. Swenson, L.B. Secor, D.R. Stoll, Selective comprehensive multi-dimensional separation for resolution enhancement in high performance liquid chromatography. Part I: Principles and instrumentation, Journal of Chromatography A. 1228 (2012) 31–40. https://doi.org/10.1016/j.chroma.2011.06.035.

[12] C. Grivel, Développements théoriques et pratiques pour la chromatographie en phase liquide bidimensionnelle (RPLC x RPLC) appliquée à la séparation de composés pharmaceutiques ou biologiques, Doctoral dissertation, Université de Lyon, 2010.

[13] A. D'Attoma, Development of two-dimensional liquid chromatography LCxLC-MS methods for the analysis of charged compounds, Doctoral dissertation, Université de Lyon, 2013.

[14] F. Bedani, P.J. Schoenmakers, H.-G. Janssen, Theories to support method development in comprehensive two-dimensional liquid chromatography – A review, J. Sep. Science. 35 (2012) 1697–1711. https://doi.org/10.1002/jssc.201200070.

CHAPTER III - ADVANTAGES OF ON-LINE RPLC x RPLC COMPARED TO ONE-DIMENSIONAL RPLC

This Chapter has been published as:

- **A theoretical and practical approach to manage high peak capacity and low dilution in on-line comprehensive reversed-phase LC x reversed-phase LC: A comparison with 1D-reversed-phase LC**

  Soraya Chapel, Florent Rouvière, and Sabine Heinisch
  LC-GC Europe, 2020, vol 33, number s5, Advances in UHPLC/HPLC, 17-26

INTRODUCTION

The undisputable advantage of on-line LC x LC methods over 1D-LC is its potential for substantially increasing the resolving power (peak capacity) without increasing the analysis time. As underlined in Chapter I, to achieve the theoretical peak capacity of a 2D-LC system and reach its full potential, the two separation dimensions must be completely orthogonal. When using partially correlated systems in both dimensions, the effective peak capacity will evidently be lower than this targeted theoretical maximum. Nonetheless, impressive peak capacities can be achieved with combinations providing limited coverage of the separation space.

The best example is the combination of RPLC and RPLC. Despite the large array of chromatographic modes at disposal, the use of RPLC in both dimensions remains the most frequently adopted option in the literature [1,2], even if this popularity seems to be on the wane in the last five years, as will be discussed in Chapter IV. The main reasons for this broad use of on-line RPLC x RPLC are (i) the wide availability and applicability of reversed-phase (RP) stationary phases, (ii) the extensive knowledge on RP retention mechanisms, (iii) the high efficiency of this technique allowing to reach large peak capacities in both dimensions, (iv) the good robustness and repeatability of RP separations, especially attractive for the very fast ^{2}D-separations, and (v) the good compatibility of RP mobile phases with MS detection. In fact, it is interesting to point out that very few other applications of separations using similar chromatographic modes in both dimensions have been reported in on-line LC x LC. From our knowledge, these only include the following specific examples, in HILIC x HILIC [3], SEC x SEC [4-8], IEX x IEX [9], and SFC x SFC [10].

Despite the inherent similarity between retention mechanisms in on-line RPLC x RPLC, selectivity can be manipulated with appropriate choice of stationary phases and mobile phases on one hand, and careful optimization of the chromatographic conditions (e.g. column temperatures, flow rates, gradient elution conditions…) on the other. In the case of ionizable compounds, significant differences in selectivity can be observed when changing the pH between the two dimensions. Such an approach has been largely reported in the literature for the analysis of peptides and proteins in on-line RPLC x RPLC [11-16].

Comparisons of performance between on-line RPLC x RPLC and 1D-RPLC have been reported in the past in the literature [12,13,17,18]. All of them highlighted a tremendous gain in peak capacity for a given analysis time and/or in analysis time for a given peak capacity in on-line RPLC x RPLC. For peptide separation, the "cross-over time" above which on-line RPLC x RPLC outperforms 1D-RPLC in terms of resolving power (peak capacity) has been shown to be around five minutes [13].

Although the practical increase in peak capacity seems to be a widely accepted advantage of 2D-LC over 1D-LC, it also appears to be a widely accepted notion that the counteract of this increase should be a decrease in detection sensitivity [19,20]. The main reason behind this is the fact that the second dimension introduces an additional chromatographic separation step at the end of which the already diluted analyte plug is expected to dilute further.

This chapter aims to highlight the potential advantages of on-line RPLC x RPLC compared to 1D-RPLC for the analysis of ionizable compounds such as peptides. In this chapter, we dig deeper into the concept of dilution in gradient elution to propose a systematic approach to compare fairly the dilution factors between on-line RPLC x RPLC and 1D-RPLC. The first part of the chapter is devoted to explaining the premises of this approach from a theoretical standpoint. The second part details the results of an experimental comparison between on-line RPLC x RPLC and 1D-RPLC using the proposed approach for the analysis of a digested six-protein mixture. The two separation methods are compared at a given analysis time using peak capacity (resolving power) and peak intensity (detection sensitivity) as key metrics of performance.

Article 3: A theoretical and practical approach to manage high peak capacity and low dilution in on-line comprehensive reversed-phase LC x reversed-phase LC: A comparison with 1D-reversed-phase LC

Abstract

On-line comprehensive two-dimensional liquid chromatography (on-line LC x LC) provides much higher separation power (higher peak capacity) than one-dimensional liquid chromatography (1D-LC). However, it is also often thought that a larger peak capacity should be obtained at the expense of a higher dilution (lower peak intensity). From a theoretical approach, it is demonstrated that both demands can go hand-in-hand in on-line reversed-phase LC x reversed-phase LC (higher peak capacity and higher peak intensity). Examples involving "sub-hour" separations of a tryptic digest show how this approach can be applied in practice.

1. Introduction

As a result of its huge separation power within relatively short analysis times, comprehensive two-dimensional liquid chromatography (LC x LC) has been used in a wide variety of application fields over the past ten years. The large number of recent books and reviews dealing with 2D-LC applications is an indication of the attractiveness of this separation technique [1–4].

The final goal of LC x LC is to obtain the highest possible separation power (high peak capacity) with the highest possible peak intensity (low dilution), within the shortest possible analysis time. Among these three conflicting goals, the separation power (peak capacity) and the analysis time (the gradient time of the first dimension) are usually considered as the critical quality descriptors, while the dilution is most often disregarded. For the separation of peptides or, more generally, for the separation of ionizable compounds, the use of RPLC in both dimensions allows impressive peak capacities by simply changing the pH between both dimensions to be achieved [5]. For given analysis times, recent studies have compared the peak capacities obtained in 1D-reversed-phase LC against reversed-phase LC x reversed-phase LC. For peptides, it was found that reversed-phase LC x reversed-phase LC outperforms 1D-reversed-phase LC above a total analysis time of 5 min [6]. More recently, a peak capacity of 10 000 was achieved in four hours using an active modulation approach [7].

Compared to conventional one-dimensional liquid chromatography (1D-LC), LC x LC is usually thought to provide limited performance in terms of sensitivity as a result of solute dilution during the separation process. However, a comprehensive and fair comparison of dilution between these two separation techniques has never been investigated so far. In this article, the concept of dilution in gradient elution is revisited to provide efficient tools to compare in a reliable manner the dilution factors between 1D-reversed-phase LC and reversed-phase LC x reversed-phase LC. The validity of the proposed method is assessed through the separations of peptides in 1D-reversed-phase LC and in reversed-phase LC x reversed-phase LC.

2. Theoretical Approach

In gradient elution, the effective peak capacity, n_{eff}, can be estimated by:

$$n_{eff} = \frac{t_G}{4\sigma_{peak}} \qquad \textit{(Eq. 1)}$$

Where t_G is the gradient time and σ_{peak}, the average peak standard deviation in time units, resulting from band broadening into the entire separation system (instrument and column).

In 1D-LC, the sample dilution depends on both the injection volume and the peak width. Assuming a Gaussian peak shape, the dilution factor, D_F, is given by the following relationship:

$$D_F = \frac{\sigma_{col}\sqrt{2\pi}}{\beta \times V_i} \qquad \textit{(Eq. 2)}$$

Where σ_{col} is the column peak standard deviation in volume units, and V_i, the injected volume. β corrects for additional band broadening due to extra-column dispersion ($\beta = \sigma_{col}/\sigma_{peak}$). It may vary from 0 to 1 depending on the importance of extra-column dispersion. Ideally, β should be higher than 0.7 ($\beta^2 > 0.5$) otherwise the loss in plates becomes too significant (> 50%) and, furthermore, the assumption of a Gaussian peak shape becomes unacceptable [6]. According to Eq. 1, β represents the fraction of remaining peak capacity. It is given by:

$$\beta = \frac{1}{\sqrt{1+x^2}} \qquad \textit{(Eq. 3)}$$

With x^2, the ratio of the peak variance, resulting from extra-column dispersion, to the peak variance, resulting from column dispersion (σ^2_{col}):

$$x^2 = \frac{V_i^2}{\sigma_{col}^2} \times \frac{1}{\delta^2} \times \frac{1}{C_F} + \sigma_{ext}^2 \qquad \textit{(Eq. 4)}$$

σ^2_{ext} is the additional extra-column variance due to band broadening in the capillary tubes and in the detector cell, δ^2 is a correction factor which depends on the injection process (12 for an ideal injection plug and close to 4 in practice) [8]. C_F is the peak injection compression factor: $C_F > 1$ if the injection plug is narrowed by on-column focusing (injection solvent weaker than the mobile phase), $C_F < 1$ if the injection plug is broadened when travelling across the column (injection solvent stronger than the mobile phase), and $C_F = 1$ if the injection solvent corresponds to the mobile phase.

In gradient elution, the considered mobile phase is the solvent that accompanies solute elution. Assuming that the injection process is the main cause of extra-column

dispersion, σ^2_{ext} can be considered as close to 0 and then the combination of Eqs. 3 and 4 lead to:

$$V_i = \sigma_{col} \times \delta \times C_F \times \sqrt{\frac{1}{\beta^2} - 1} \qquad \textit{(Eq. 5)}$$

For a given compression factor, Eq. 5 permits the calculation of the injected volume able to keep a given β value (ideally > 0.7 as mentioned previously). For example, in the situation where the injection solvent corresponds to the elution composition of the first eluted solute (i.e. C_F = 1 for this one), the volume that can be injected while keeping 90% or more of the peak capacity for all peaks (exactly 90% for the first eluted one) should be close to the column standard deviation ($V_i = \sigma_{col}$).

If the injection volume is selected from Eq. 5, the dilution factor can then be expressed as:

$$D_F = \frac{\sqrt{2\pi}}{\delta \times C_F \times \sqrt{1-\beta^2}} \qquad \textit{(Eq. 6)}$$

According to Eq. 6, the dilution factor should be 2.9 for the least retained compound in the above example (assuming δ = 2). More generally, if the injected volume is selected as a multiple (λ) of the column standard deviation in such a way that β remains very close to 1 (x close to 0), then the dilution factor is close to $\sqrt{2\pi}/\lambda$ for all peaks in any gradient conditions (Eq. 2). In most reported studies dealing with the comparison of performance between different separation techniques, the injection volume is either fixed [9] or adapted to the column dead volume [6], but never adapted to the gradient conditions and hence to the column standard deviation. However, this latter approach, based on a proper preliminary selection of λ, is much more attractive because, in this case, dilution and, therefore, peak intensity becomes independent of gradient conditions, that is, flow rate, column geometry, gradient time, and column plate number. Of course, that requires a reliable prediction of the column standard deviation, which is given in gradient elution by:

$$\sigma_{col} = G \times \frac{V_0}{\sqrt{N_{col}}} \times (1 + k_e) \qquad \textit{(Eq. 7)}$$

Where V_0 is the column dead volume which can be calculated from both the column dimensions and the total column porosity. N_{col} is the column plate number which can

be estimated from the column length, the particle diameter, Knox curve coefficients, and predicted diffusion coefficients [10], k_e is the retention factor at the time the solute is eluted, and G is the peak compression factor [11] taking into account band compression, especially in the case of very steep gradients. For the rest of this study, G will be assumed to be close to 1 in every gradient conditions.

For Linear Solvent Strength (LSS) gradients [12] such as linear gradients in reversed-phase liquid chromatography (RPLC) and for large retention factors at initial composition, k_e can be expressed as:

$$k_e = \frac{1}{2.3 \times S \times s} \qquad \textit{(Eq. 8)}$$

Where s is the normalized gradient slope ($s = \Delta C \times t_0/t_G$), with ΔC the composition range and t_0, the column dead time) and S, the slope of the relationship between the logarithm of the retention factor and the eluent composition. It should be noted that the calculation of σ_{col} makes it also possible to predict the peak capacity in any gradient conditions according to Eq. 1.

Fig. 1 shows the calculated kinetic curves for different column lengths. Each curve represents the gradient time as a function of the predicted maximum attainable peak capacity. These curves were calculated for peptides (assuming a β value close to 1) according to the procedure described in reference [6]. For a given particle diameter and a given column temperature, each column length (i.e. each curve) is related to the highest possible flow rate considering the maximum allowable pressure (here 1000 bar), thereby leading to the highest column plate number that can be achieved with the resulting column dead time [13–15]. It is widely accepted that reducing the particle size and increasing column temperature allows an increase in the column plate number per time unit [16]. The curves in Fig. 1 were therefore predicted under high-temperature-ultra-high performance liquid chromatography (HT-UHPLC) conditions (sub-2-µm particles, here 1.7 µm were used at a temperature of 80°C which is the highest column temperature that can be applied to current silica-based columns for a long term period). The limit curve (dotted line in Fig. 1) gives the maximum attainable peak capacity for a given gradient time (for example 530 in 30 min) or the shorter gradient time for a given peak capacity (for example 3 days for 1500). It is important to insist on the fact that the limit curve corresponds to the best existing sets of

conditions in 1D-LC, with packed columns, for the separation of peptides. In such HT-UHPLC conditions, the peak capacity seems to tend towards a limit of about 2000. Each circle data points located on the limit curve corresponds to a set of conditions including column length, flow rate, gradient time, and also the injection volume calculated to provide similar peak intensities in all gradient conditions. The arrows in Fig. 1 indicate the column lengths and the injection volumes for a λ value of 1. The required injection volume increases with the gradient time for a given column length.

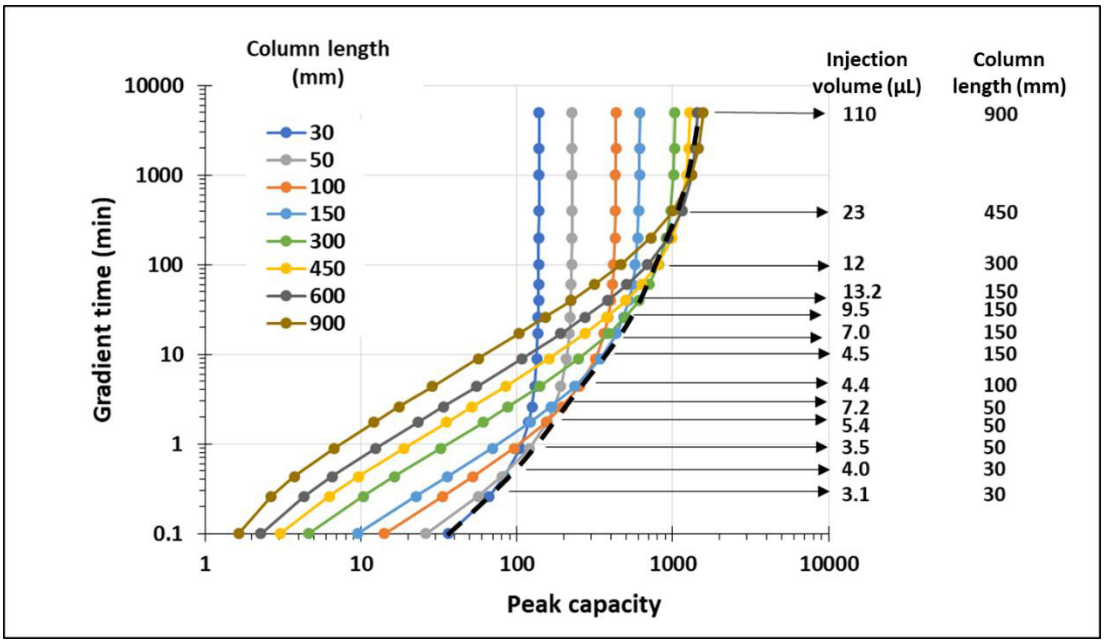

Fig. 1: Gradient time as a function of the predicted maximum attainable peak capacity with different column lengths for HT-UHPLC separation of peptides according to the procedure described in [6]. Conditions: composition range = 35% ACN, T = 80°C, P_{max} = 1000 bar, particle diameter = 1.7 µm, S = 20, D_m = 0.72 x 10^{-9} m^2/s (estimation for a peptide of 1000 Da at 80°C). Flow rates dependent on the column length: 3.5 mL/min (3 cm), 2.1 mL/min (5 cm), 1.05 mL/min (10 cm), 0.7 mL/min (15 cm), 0.35 mL/min (30 cm), 0.23 mL/min (45 cm), 0.175 mL/min (60 cm), and 0.117 mL/min (90 cm). Black arrows indicate the column length and the required injection volume for the points located on the limit curve (dotted line).

In addition to being more attractive due to its ability to standardize the dilution in 1D-LC, the proposed approach is, in our opinion, the only way to provide a relevant comparison in term of dilution between 1D-LC and on-line LC x LC. This is of prime importance in the light of the smooth gradients usually applied in the first dimension (^{1}D) which lead to large peaks and hence high dilution when the injected volume is not properly adapted. Injection volumes in ^{1}D calculated in a similar way than as in 1D-LC (same λ value) should lead to similar peak intensities. The dilution factor in LC x LC is

usually considered as the product of the dilution factors in each dimension ($D_F = {}^1D_F \times {}^2D_F$). Because ${}^1D_F$ should be close to any dilution factor in 1D-LC (provided that λ is kept identical), the comparison of the dilution between 1D-LC and on-line LC x LC thus becomes only dependent on ${}^2D_F$.

Eqs. 1, 2, 3, and 4 can be applied in ^{2}D as well. As discussed above, ${}^2V_i / \sigma^2_{col}$ can be increased and hence ${}^2D_F$ decreased provided that the injection compression factor is high enough to ensure that ${}^2\beta > 0.7$. The injection compression factor is related to two solute retention factors: k_s, obtained with the injection solvent as mobile phase, and k_e, obtained with the mobile phase at elution. C_F is usually well approximated by the following relationship [10,17,18]:

$$C_F = \frac{k_s}{k_e} \qquad \textit{(Eq. 9)}$$

In the particular case of on-line reversed-phase LC x reversed-phase LC, with k_e values expected to be similar in both dimensions ($k_s = {}^1k_e$), the compression factor in ^{2}D can be predicted according to [10]:

$$C_F = \frac{{}^1k_e}{{}^2k_e} \qquad \textit{(Eq. 10)}$$

An optimization procedure has been developed for on-line LC x LC separations, based on predictive calculations tools [10]. As was shown, very steep gradient in ^{2}D (low ${}^2k_e$) along with smooth gradient in ^{1}D (high ${}^1ke$) were able to provide low dilution in ^{2}D due to the resulting high C_F values. The reported procedure allowed to plot the dilution factor as a function of the effective peak capacity for different sets of LC x LC conditions (Pareto plots), considering a given gradient time in the first dimension (given analysis time).

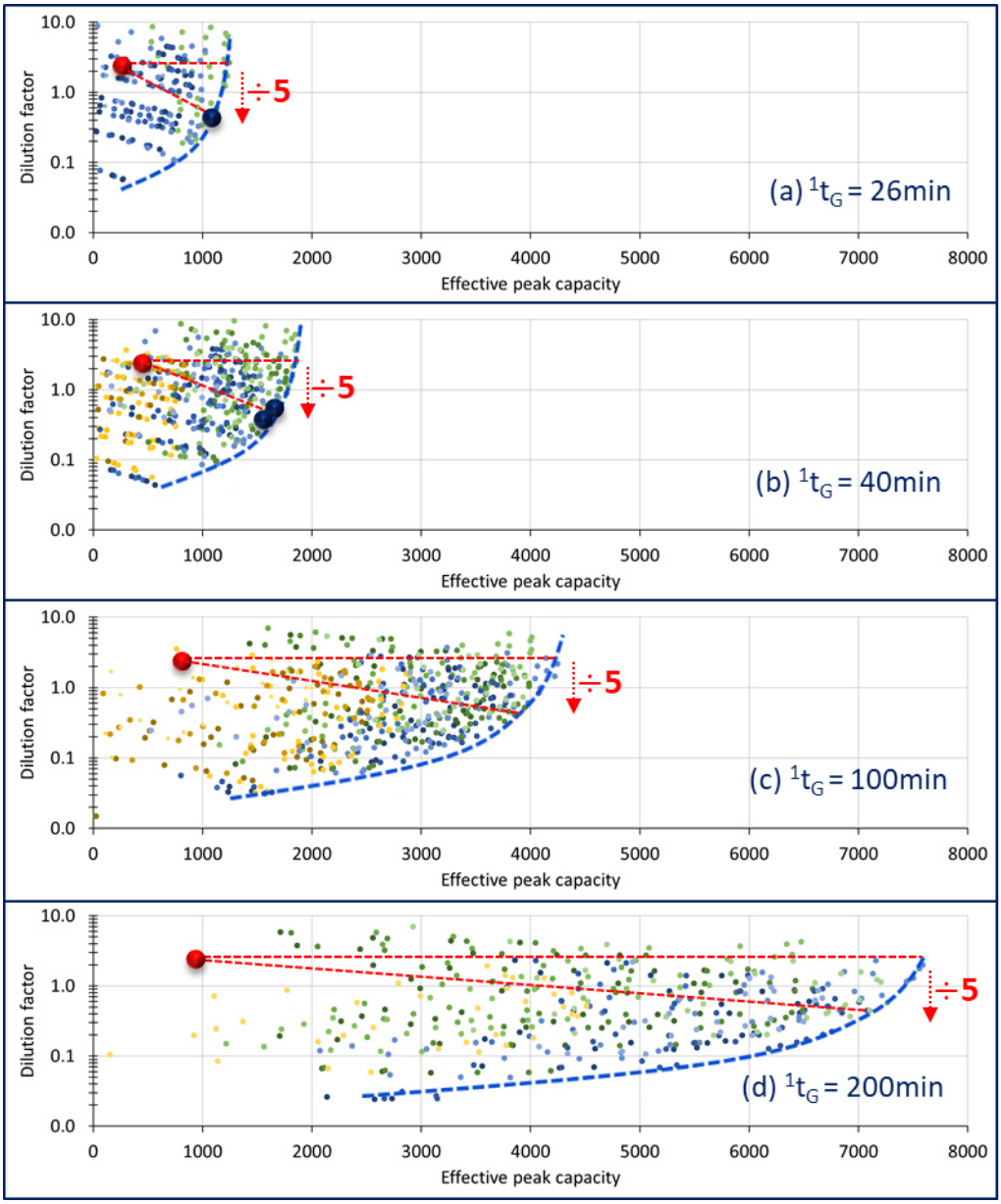

Fig. 2: Predicted dilution factor as a function of the effective peak capacity for different gradient times: (a) 26 min, (b) 40 min, (c) 100 min, (d) 200 min. Each colour is related to a different set of conditions. For a given set, the flow rate in ^{1}D was varied from 20 µL/min to 1000 µL/min, and the sampling rate from 1 to 3 fractions per peak. The different sets result from a screening of conditions including column length (3 cm, 5 cm, and 15 cm in ^{1}D; 3 cm and 5 cm in ^{2}D), internal diameter (1 mm and 2.1 mm in ^{1}D; 2.1 mm in ^{2}D), particle diameter (1.7 µm, 3.5 µm, and 5µm in ^{1}D; 1.7 µm and 2.7 µm in ^{2}D). The flow rate in ^{2}D was adjusted to the highest possible value considering the maximum allowable pressure (1000 bar). **Other conditions**: No flow splitting prior to the interface, composition range = 35% ACN, ^{1}T = 30°C, ^{2}T = 80°C; γ = 0.6, the injection volume in ^{1}D was adjusted to the predicted column standard deviation, 6 µL^2 was considered as additional extra-column variance in ^{2}D. The Pareto-fronts are represented by curved dotted lines. The large red data points correspond to the predicted values in 1D-LC. A reduction of the dilution by a factor 5 is indicated in red. The blue circles correspond to the three different sets of conditions applied to the RPLC x RPLC separations of peptides (conditions listed in Table 2).

Fig. 2 shows the obtained Pareto plots, calculated for four different gradient times (26 min, 40 min, 100 min, and 200 min for a composition range of 35%; all other conditions are given in the figure caption). Each colour is related to a set of conditions (column length, column diameter, and particle size in both dimensions). Each symbol is associated to both a flow rate value in ^{1}D and a sampling rate value. UHPLC instrumentation usually yields low values for σ^2_{ext} (typically < 10 μL^2). However, unlike in ^{1}D and in 1D-LC, its contribution to the total peak variance in ^{2}D may be quite significant (Eq. 4) and was therefore taken into account in our calculations (i.e. 6 μL^2). As in Fig. 1, a λ value of 1 was used for the calculation of injection volumes in ^{1}D, leading to ^1D_F = 2.5 in all studied conditions. Note that the entire fraction, collected at the outlet of ^{1}D, was injected in ^{2}D (no flow splitting), even when the column diameter was the same in both dimensions (i.e. 2.1 mm). The large red data point circles correspond to the best-calculated peak capacities in 1D-LC (limit curve in Fig. 1). For each gradient time, the Pareto-front (blue dotted curve) represents the performance limit in reversed-phase LC x reversed-phase LC with respect to the target objectives, that is, maximizing the peak capacity while minimizing the dilution factor. The large blue circles data points correspond to the three different sets of conditions that were applied to the reversed-phase LC x reversed-phase LC separations of peptides (Table 3) as discussed below. These calculations give rise to some important comments:

(i) The maximum expected peak capacities are 1250, 1850, 4200, and 7600 in 26, 40, 100, and 200 min, respectively. Interestingly, the dilution factors at the maximum peak capacity are very close to the one predicted in 1D-LC, that is, 2.5 (horizontal dotted line). It is important to underline that if post-first-dimension flow splitting was taken into account, Pareto-optimum curves would be shifted towards even more impressive peak capacities but also higher dilution.

(ii) The dilution factors in LC x LC can be decreased by a factor 5 without sacrificing too much of the peak capacity as highlighted by the red dotted lines.

(iii) The dilution factors can be further decreased while keeping fairly good peak capacities. For example, a decrease in the dilution factor by a factor of 25 only leads to a decrease of 40% (26 min), 39% (40 min), 31% (100 min), and 28% (200 min) of the peak capacity.

(iv) Among the various conditions evaluated, those involving a short column in ^{1}D (typically 5 cm) and a very short column packed with sub-2-μm particles in ^{2}D

(typically 3 cm and 1.7 µm) were always located onto or close to the Pareto curve. This is surprising for long analysis times (for example, 200 min) for which longer columns in ^{1}D are usually recommended.

(v) It is noteworthy that dilution factors are not higher when using 1-mm column diameter, rather than 2.1-mm column diameter in ^{1}D. This is confirmed experimentally in the next section.

3. Methods and materials

3.1. Chemicals

Acetonitrile (LC-MS grade) was purchased from Sigma-Aldrich (Steinheim, Germany). An Elga Purelab Classic UV purification system from Veolia water STI (Décines-Charpieu, France) was used for water purification and deionization. Formic acid (LC-MS grade), ammonium acetate, and ammonium bicarbonate (both analytical reagent grade) were obtained from Fischer scientific (Illkirch, France). DL-1,4-dithiothreitol (DTT, 99%) and iodoacetamide (98%) were obtained from Acros Organics (Geel, Belgium). Trypsin, human serum albumin (HSA), bovine serum albumin (BSA), β-casein, myoglobin, lysozyme, and cytochrome C were all obtained from Sigma-Aldrich (Steinheim, Germany). Influenza hemagglutinin (HA), leucine enkephalin, bombesin, [arg8]-vasopressin, [ile]-angiotensin, bradykinin fragment 1-5, substance P, and bradykinin were obtained from Merck (Molsheim, France). The protein digest sample was obtained by tryptic digestion of six proteins (HSA, BSA, β-casein, myoglobin, lysozyme and cytochrome C) following a protocol described elsewhere [10,19]. The ratio enzyme to substrate was 1/70, resulting in a complex sample containing 196 peptides with an average concentration of 120 mg/L.

The standard sample was obtained by diluting eight peptides in pure water at a concentration of 32 mg/L. Their characteristics are listed in Table 1.

Both samples were filtered on a 0.22-µm PVDF (Polyvinylidene fluoride) membrane before injection.

Table 1: Characteristics of the peptide standards (letters are used to locate the peptides in Fig. 3)

#	Peptide name	Molecular weight (g/mol)	Isoelectric point	S (calculated by OSIRIS)
A	Influenza hemagglutinin	1102.15	3.5	19.3
B	Leucine enkephalin	555.62	6	12
C	Bombesin	1619.85	7.6	20.1
D	[arg8]-Vasopressin	1084.23	8.2	23.4
E	[ile]-Angiotensin	897.08	9.4	20.9
F	Bradykinin fragment 1-5	572.66	10.6	22.1
G	Substance P	1347.63	11.7	19.3
H	Bradykinin	1060.21	12.5	20.7

3.2. Instrumentation

2D-LC experiments were performed on a 1290 Infinity series 2D-LC system from Agilent Technologies (Waldbronn, Germany). The system includes two high-pressure binary solvent delivery pumps, an autosampler with a flow-through needle injector, two thermostated column compartments with low-dispersion preheaters, and two diode-array detectors (DAD) with 0.6 µL flow-cells. The interface connecting the two dimensions was a 2-position/4-port duo valve, equipped with two identical 80-µL loops. The loops were emptied in back-flush mode to minimize band dispersion. A pressure release kit was placed between the ^{1}D-outlet and the interface inlet to minimize the pressure downstream coming from the valve switching. The measured dwell volumes and extra-column volumes were respectively 170 µL and 22 µL in ^{1}D, and 80 µL and 8.5 µL in ^{2}D (loop volumes excluded). For 1D-LC experiments, only the first dimension of this system was used. In both cases, the system was hyphenated to a quadrupole-time-of-flight (Q-TOF) high-resolution mass spectrometer (model G6560B) from Agilent Technologies, equipped with a JetStream electrospray ionization (ESI) source. As a result of the very high flow rates operated in ^{2}D, the effluent coming from ^{2}D was split (1:2) before entering the source. Instrument controlling was performed with OpenLab CDS Chemstation software (Agilent) for the 2D-LC-UV system, and MassHunter software (Agilent) for the mass spectrometer. UV data were acquired at 210 nm with an acquisition rate of 40 Hz in 1D-LC, 20 Hz in ^{1}D, and 80 Hz in ^{2}D. HRMS data were acquired in positive ion mode from 100 to 3200 Da, with an acquisition rate of 20 spectra/s. The operational parameters for the Q-TOF instrument were the following: drying gas temperature (300°C), drying gas flow (11

L/min), nebulizer gas pressure (40 psi), sheath gas temperature (350°C), sheath gas flow rate (11 L/min), capillary voltage (3500 V), nozzle voltage (300 V), fragmentor voltage (150 V), Oct 1 RV voltage (750 V). HRMS data were processed with MassHunter qualitative analysis software (Agilent).

In 1D-reversed-phase LC, the separations were performed on two 1.7-µm Acquity CSH C18 columns (Waters). The column dimensions were either 50 mm x 2.1 mm, or 150 mm x 2.1 mm. The mobile phase was composed of water with 0.1% formic acid as solvent A, and ACN with 0.1% formic acid as solvent B (pH = 2.7). The gradient elution was performed from 1% B to 36% B with different gradient times. The gradient time was followed by a quick return to initial eluent composition (one t_0) and a short column equilibration time (five t_0). The several sets of conditions that were used are given in Table 2.

Table 2: Comparison of the peak heights obtained in 1D-LC for four peptide standards in various gradient conditions while keeping the injection volume equal to the expected column standard deviation (λ = 1). Gradient from 1% ACN to 36% ACN, 0.1% formic acid in the mobile phase. UV detection at 210 nm.

Temperature (°C)	**80**									**30**		
Column length (cm)	5					15				5		
Flow rate (mL/min)	2.1					0.7				0.5		
Gradient time (min)	0.4	0.9	1.7	2.6	4.4	9	17	26	40	40		
Injection volume (µL)	2.6	3.5	5.4	7.2	9	4.5	7	9.5	13.2	17		
Peptide	**Peak heights (mAu)**										**Average value**	**RSD (%)**
Bradykinin fragment	195	192	185	195	238	170	175	193	229	169	**194**	**11.3**
[ile]-Angiotensin	189	212	214	207	195	188	172	168	159	158	**186**	**10.8**
Bradykinin	272	235	262	258	257	220	216	213	210	/	**238**	**9.6**
Bombesin	/	286	304	290	214	300	276	259	243	241	**268**	**10.8**

Experimental conditions for the three LC x LC set-ups are given in Table 3.

1D-LC-UV and 2D-LC-UV data were processed using Excel and an in-house script written under MATLAB 7.7. The S values for the eight peptides (listed in Table 2) were determined from a HPLC modelling software (OSIRIS 4.2, Euradif, Grenoble, France) from two gradient data (10 min and 30 min).

Table 3: Experimental conditions for the RPLC x RPLC setups

	Setup #1	Setup #2	Setup #3
First dimension (^{1}D)			
Injection volume (% V_0)	13.1 µL (25.2% V_0)	10.5 µL (44.5% V_0)	10.6 µL (45.0% V_0)
Stationary phase	Cortecs C18	Sunfire C18	Sunfire C18
Column geometry	30 mm x 2.1 mm, 2.7 µm	50 mm x 1 mm, 3.5 µm	50 mm x 1 mm, 3.5 µm
Temperature	30°C	30°C	30°C
Flow rate	0.25 mL/min	0.15 mL/min	0.2 mL/min
Gradient	1-36% B in 40 min	1-36% B in 40 min	1-36% B in 26 min
Split ratio	-	-	-
Sampling time	0.26 min	0.35 min	0.27 min
Second dimension (^{2}D)			
Injection volume (% V_0)	65 µL (104% V_0)	52.5 µL (84.3% V_0)	54 µL (86.7% V_0)
Stationary phase	Acquity CSH C18	Acquity CSH C18	Acquity CSH C18
Column geometry	30 mm x 2.1 mm, 1.7 µm	30 mm x 2.1 mm, 1.7 µm	30 mm x 2.1 mm, 1.7 µm
Temperature	80°C	80°C	80°C
Flow rate	2.6 mL/min	2.6 mL/min	2.6 mL/min
Gradient	1-45% B in 0.12 min	1-45% B in 0.22 min	1-45% B in 0.14 min

4. Experimental validation

The objective of this practical approach was to assess to what extent experimental results are consistent with the calculations above.

A series of ten gradient runs were carried out in 1D-LC with conditions close to those given in Fig. 1 (located onto the limit curve). Ten different sets of gradient conditions (listed in Table 2) were applied to a sample of eight peptide standards and to a tryptic digest of six proteins. UV detection was used to compare the peak heights while HRMS detection was used to identify the different peaks.

Fig. 3 shows the UV-chromatograms obtained with the two samples with four different sets of conditions. As expected, the peak intensities seem to be very similar for a given sample regardless of the gradient conditions. Table 2 lists, for four peptide standards, the measured peak heights obtained with the ten sets of conditions. As highlighted by RSD values, that is, around 10%, the change in gradient conditions has very little

impact on peak heights, thereby demonstrating that injection volumes were properly determined from the predicted peak width. Furthermore, good peak shapes could be obtained for both samples, even for the least retained peptides, suggesting that our preliminary assumption (β values close to 1 for all peaks with $\lambda = {}^1V_i/{}^1\sigma col = 1$) was correct.

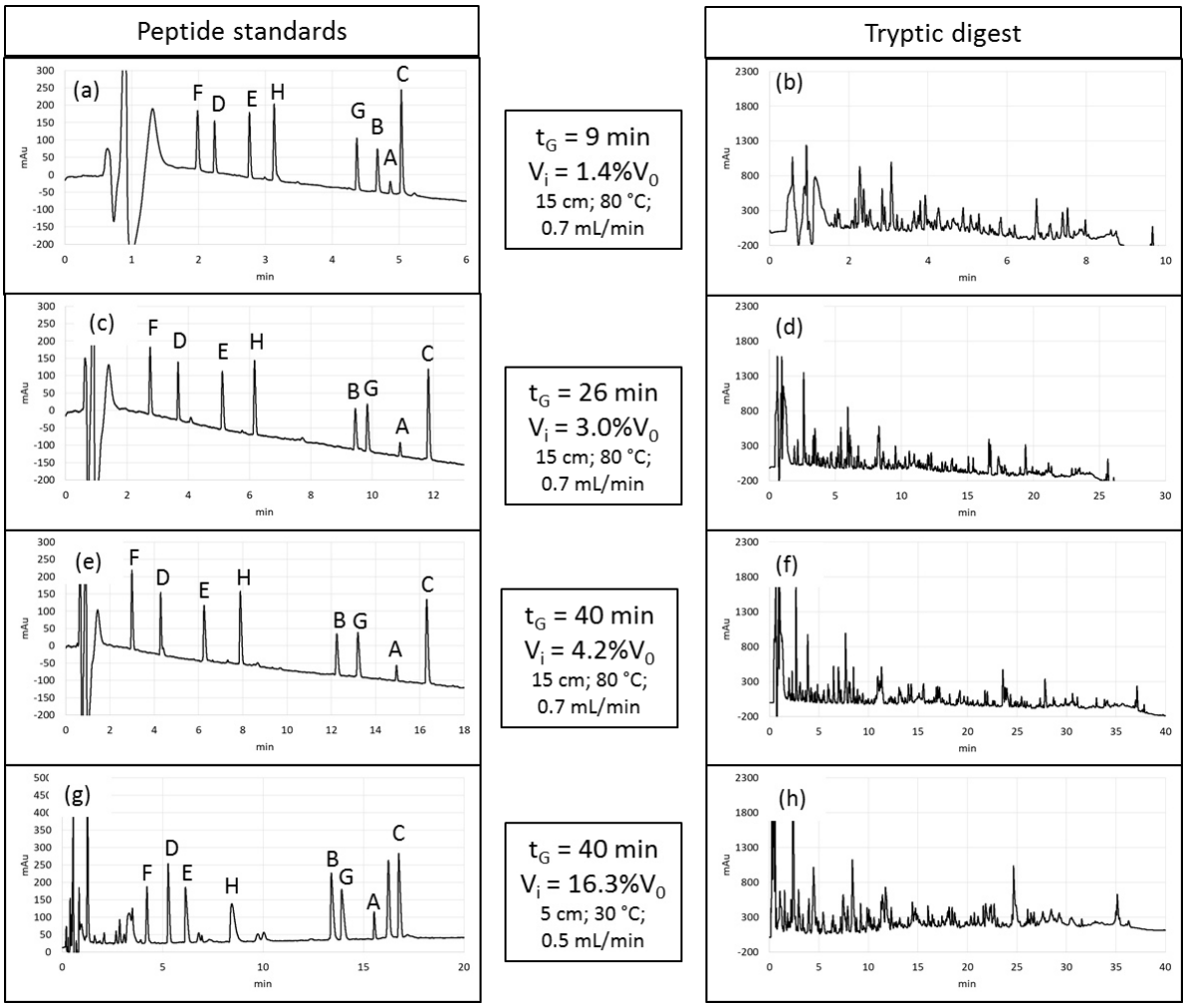

Fig. 3: 1D-RPLC chromatograms for a sample of eight peptide standards (on the left side) and for a tryptic digest of six proteins (on the right side) under different gradient conditions (as indicated in the middle). The injected volumes are specified as a percentage of the column dead volume. The letters correspond to the peptides listed in Table 1. Other conditions given in Table 2.

Particular attention should be paid to the gradient conditions on the right side of Table 2 (see also Figs. 3g and 3h). These conditions are very close to those usually applied to a first dimension in on-line reversed-phase LC x reversed-phase LC. They include a short column (i.e. 5 cm), a long gradient time (i.e. 40 min), a column temperature of 30°C, and a flow rate well below the highest possible one (i.e. 0.5 mL/min vs. 1.2

mL/min). Such conditions imply very large peak widths (high k_e values) and hence large injection volumes (17 µL, which is about 16% V_0). Despite this, peak intensities remain very similar to those obtained in optimum 1D-LC conditions. Our first assumption was that, for any gradient conditions in 1D-reversed-phase LC, it should be possible to keep similar peak heights by injecting the appropriate calculated volume. This assumption seems to be validated by this experimental study.

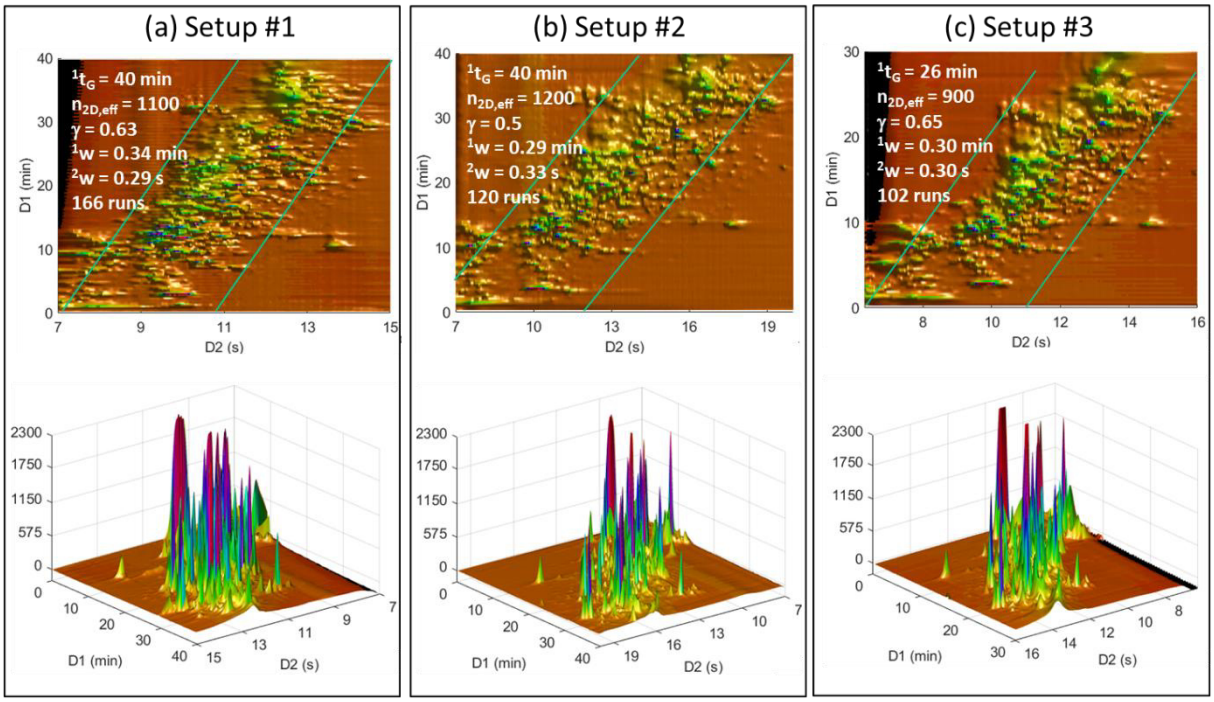

Fig. 4: On-line RPLC x RPLC chromatograms (contour plots and 3D-chromatograms) for a tryptic digest of six proteins using three different setups (conditions given in Table 3). The setups correspond to the large blue data points in Figs. 2a (setup #3 with a gradient time of 26 min) and 2b (setups #1 and #2 with a gradient time of 40 min). The separation quality attributes are given at top right of the contour plots. They include analysis time, obtained effective peak capacity, percentage of surface coverage, peak widths in each dimension, and number of runs in the second dimension. UV detection at 210 nm.

Our second assumption was that the dilution in on-line reversed-phase LC x reversed-phase LC should be greatly reduced compared to 1D-reversed-phase LC. This is demonstrated in Fig. 4, showing on-line reversed-phase LC x reversed-phase LC chromatograms for the tryptic digest of six proteins. Three different setups were selected with conditions listed in Table 3. The predicted performance of these setups can be seen in Figs. 2a (setup #3) and 2b (setups #1 and #2). In Fig. 4, the contour plots (top figure) show the retention space while the 3D-chromatograms (bottom figure) reveal the peak intensities. The separation quality attributes are given in Fig. 4 at top

left of the contour plots. They include analysis time, obtained effective peak capacity, percentage of surface coverage, peak widths in each dimension, and number of runs in the second dimension. As can be seen, the obtained effective peak capacities are very close to (slightly lower than) those predicted in Fig. 2. They were found to be 2.5 times (in 26 min) and 3.5 times (in 40 min) higher than in 1D-RPLC (Figs. 3d and 3f, respectively).

Table 4: Ratio of the peak height in RPLC x RPLC to the peak height in 1D-RPLC (same analysis time) for the sample of peptide standards and for the protein digest with the three different setups (conditions given in Table 2).

	Setup #1 (40 min)	**Setup #2 (40 min)**	**Setup #3 (26 min)**
Sample of 8 peptide standards (average value)	3.4	3.3	4.8
Protein digest (average value for 10 identified peptides)	4.2	4.0	4.5

More important is the increase in peak intensity (reported in Table 4) for both studied samples. Peak intensities were multiplied by an average factor of 3.3 to 4.5 depending on the setup. Such increase is in very good agreement with the predictions shown in Fig. 2 (a predicted factor of 5). It can also be noted that setups #1 and #2 which differ from the column diameter in ^{1}D (that is, 2.1 mm and 1 mm, respectively), lead to quite similar peak capacities (no additional band broadening with 2.1 mm) and quite similar peak intensities (no additional dilution with 1 mm). The number of runs in ^{2}D could be the final quality attribute (120 with 1 mm vs. 166 with 2.1 mm) to define the best set of conditions.

5. Conclusion

From both a theoretical approach and an experimental study on peptides, it has been shown that similar dilution factors and hence similar peak heights can be obtained in any 1D-reversed-phase LC gradient conditions, by injecting the appropriate volume, based on a multiple of the column standard deviation.

This approach, applied to the first dimension of on-line reversed-phase LC x reversed-phase LC, allows an unbiased comparison between the dilution factors obtained in 1D-reversed-phase LC and those in on-line reversed-phase LC x reversed-phase LC. As a result of an important focusing effect in the second dimension (high C_F values), very

large volumes can be injected, thereby significantly reducing the dilution factor in the second dimension and hence the dilution factor in reversed-phase LC x reversed-phase LC, even when the column diameter is smaller in the first dimension (for example, 1mm vs 2.1 mm). According to our calculations, the dilution factor may be reduced by a factor of up to 25 in on-line reversed-phase LC x reversed-phase LC while keeping an impressive peak capacity compared to 1D-reversed-phase LC. This seems to be especially attractive for long analysis times (> one hour).

For sub-hour separations of a protein digest, our experimental results were in perfect agreement with the predicted ones. For an analysis time of 40 min, the peak intensities could be increased by a factor close to 5 in reversed-phase LC x reversed-phase LC while the peak capacity was increased by a factor of 3 compared to the optimum 1D-reversed-phase LC separation.

6. References

[1] S. Chapel, F. Rouvière, M. Sarrut, S. Heinisch, Two-Dimensional Liquid Chromatography Coupled to High-Resolution Mass Spectrometry for the Analysis of ADCs, in: L.N. Tumey (Ed.), Antibody-Drug Conjugates: Methods and Protocols, Springer US, New York, NY, 2020: pp. 163–185. https://doi.org/10.1007/978-1-4939-9929-3_11.

[2] M. Sarrut, G. Crétier, S. Heinisch, Theoretical and practical interest in UHPLC technology for 2D-LC, TrAC Trends in Analytical Chemistry. 63 (2014) 104–112. https://doi.org/10.1016/j.trac.2014.08.005.

[3] B.W.J. Pirok, D.R. Stoll, P.J. Schoenmakers, Recent Developments in Two-Dimensional Liquid Chromatography: Fundamental Improvements for Practical Applications, Analytical Chemistry. 91 (2019) 240–263. https://doi.org/10.1021/acs.analchem.8b04841.

[4] D.R. Stoll, P.W. Carr, Two-Dimensional Liquid Chromatography: A State of the Art Tutorial, Anal. Chem. 89 (2017) 519–531. https://doi.org/10.1021/acs.analchem.6b03506.

[5] A. D'Attoma, C. Grivel, S. Heinisch, On-line comprehensive two-dimensional separations of charged compounds using reversed-phase high performance liquid chromatography and hydrophilic interaction chromatography. Part I: Orthogonality and practical peak capacity considerations, Journal of Chromatography A. 1262 (2012) 148–159. https://doi.org/10.1016/j.chroma.2012.09.028.

[6] M. Sarrut, F. Rouvière, S. Heinisch, Theoretical and experimental comparison of one dimensional versus on-line comprehensive two dimensional liquid

chromatography for optimized sub-hour separations of complex peptide samples, Journal of Chromatography A. 1498 (2017) 183–195. https://doi.org/10.1016/j.chroma.2017.01.054.

[7] D.R. Stoll, H.R. Lhotka, D.C. Harmes, B. Madigan, J.J. Hsiao, G.O. Staples, High resolution two-dimensional liquid chromatography coupled with mass spectrometry for robust and sensitive characterization of therapeutic antibodies at the peptide level, Journal of Chromatography B. 1134–1135 (2019) 121832. https://doi.org/10.1016/j.jchromb.2019.121832.

[8] J.C. Sternberg, in: J.C. Giddings, R.A. Keller (Eds.), Advances in Chromatography, vol. 2, Dekker, New York, 1966, p. 205.

[9] G. Vivó-Truyols, Sj. van der Wal, P.J. Schoenmakers, Comprehensive Study on the Optimization of Online Two-Dimensional Liquid Chromatographic Systems Considering Losses in Theoretical Peak Capacity in First- and Second-Dimensions: A Pareto-Optimality Approach, Anal. Chem. 82 (2010) 8525–8536. https://doi.org/10.1021/ac101420f.

[10] M. Sarrut, A. D'Attoma, S. Heinisch, Optimization of conditions in on-line comprehensive two-dimensional reversed phase liquid chromatography. Experimental comparison with one-dimensional reversed phase liquid chromatography for the separation of peptides, Journal of Chromatography A. 1421 (2015) 48–59. https://doi.org/10.1016/j.chroma.2015.08.052.

[11] L.R. Snyder, D.L. Saunders, Optimized Solvent Programming for Separations of Complex Samples by Liquid-Solid Adsorption Chromatography in Columns, J Chromatogr Sci. 7 (1969) 195–208. https://doi.org/10.1093/chromsci/7.4.195.

[12] L.R. Snyder, J.W. Dolan, J.R. Gant, Gradient elution in high-performance liquid chromatography: I. Theoretical basis for reversed-phase systems, Journal of Chromatography A. 165 (1979) 3–30. https://doi.org/10.1016/S0021-9673(00)85726-X.

[13] H. Poppe, Some reflections on speed and efficiency of modern chromatographic methods, Journal of Chromatography A. 778 (1997) 3–21. https://doi.org/10.1016/S0021-9673(97)00376-2.

[14] J.C. Giddings, Comparison of Theoretical Limit of Separating Speed in Gas and Liquid Chromatography., Anal. Chem. 37 (1965) 60–63. https://doi.org/10.1021/ac60220a012.

[15] G. Desmet, D. Clicq, P. Gzil, Geometry-Independent Plate Height Representation Methods for the Direct Comparison of the Kinetic Performance of LC Supports with a Different Size or Morphology, Anal. Chem. 77 (2005) 4058–4070. https://doi.org/10.1021/ac050160z.

[16] S. Heinisch, J.-L. Rocca, Sense and nonsense of high-temperature liquid chromatography, Journal of Chromatography A. 1216 (2009) 642–658. https://doi.org/10.1016/j.chroma.2008.11.079.

[17] S.R. Groskreutz, S.G. Weber, Quantitative evaluation of models for solvent-based, on-column focusing in liquid chromatography, Journal of Chromatography A. 1409 (2015) 116–124. https://doi.org/10.1016/j.chroma.2015.07.038.

[18] Martin, M. Martin, M. Mishra, A. De Wit, C. Grivel, S. Heinisch, in:28th International Symposium on Chromatography ISC, Valencia, 2010.

[19] S. Chapel, F. Rouvière, S. Heinisch, Pushing the limits of resolving power and analysis time in on-line comprehensive hydrophilic interaction x reversed phase liquid chromatography for the analysis of complex peptide samples, Journal of Chromatography A. (2019) 460753. https://doi.org/10.1016/j.chroma.2019.460753.

CONCLUSIONS

The objective of this chapter was to highlight the advantages of on-line RPLC x RPLC compared to 1D-RPLC for the analysis of ionizable compounds such as peptides.

In on-line LC x LC, method optimization may be oriented toward different (and often conflicting) analytical goals. These include mainly, but not exclusively, maximizing the resolving power and the number of observed peaks on one hand, and minimizing the dilution factor and the analysis time on the other hand. Because of the inherent potential of on-line LC x LC to generate impressive peak capacities, most studies to date have focused on maximizing the resolving power of the method at the expense of the detection sensitivity. Similarly to the peak capacity, the total dilution factor in on-line LC x LC is given by the product of the dilution factors in both dimensions. On that account, poor detection sensitivity has often been described as the weak point of on-line LC x LC.

In this chapter, we showed that it was possible to improve both the resolving power (peak capacity) and the detection sensitivity (peak intensity) in on-line RPLC x RPLC compared to 1D-RPLC by thoughtful optimization of the chromatographic conditions. These conclusions were drawn in the context of the sub-hour analysis of a tryptic digest sample for several sets of conditions. Despite the use of similar chromatographic modes in both dimensions, on-line RPLC x RPLC is still an attractive combination for the separation of ionizable compounds. For peptides, the selectivity can be easily altered by the application of a different pH in each dimension, which ensures satisfactory orthogonality for the separation. In this chapter, we showed that the effective peak capacity in on-line RPLC x RPLC can be significantly greater than in 1D-RPLC for a given analysis time, despite the alikeness of the chromatographic modes. On average, the gain was found to be between 2.5- and 3.5-fold, depending on the conditions. Besides this increase in peak capacity, and contrary to popular belief, our results also showed a clear signal enhancement in on-line RPLC x RPLC in comparison with 1D-RPLC. On average, the peak intensities were found to increase by a factor of 3.3 to 4.5. This increase is mostly the result of significant analyte focusing in the second dimension, allowing the injection of very large volumes of sample with minimal impact on the separation.

In conclusion to this chapter, on-line RPLC x RPLC is undoubtedly a powerful approach allowing to increase the currently achievable peak capacity and detection sensitivity of 1D-RPLC, which makes it very attractive for the analysis of complex samples such as those encountered in the field of proteomics or (bio)pharmaceutical analysis.

REFERENCES

[1] D. Li, C. Jakob, O. Schmitz, Practical considerations in comprehensive two-dimensional liquid chromatography systems (LCxLC) with reversed-phases in both dimensions, Anal Bioanal Chem. 407 (2015) 153–167. https://doi.org/10.1007/s00216-014-8179-8.

[2] B.W.J. Pirok, D.R. Stoll, P.J. Schoenmakers, Recent Developments in Two-Dimensional Liquid Chromatography: Fundamental Improvements for Practical Applications, Analytical Chemistry. 91 (2019) 240–263. https://doi.org/10.1021/acs.analchem.8b04841.

[3] Y. Wang, X. Lu, G. Xu, Simultaneous separation of hydrophilic and hydrophobic compounds by using an online HILIC-RPLC system with two detectors, J. Sep. Science. 31 (2008) 1564–1572. https://doi.org/10.1002/jssc.200700663.

[4] A. Ehkirch, A. Goyon, O. Hernandez-Alba, F. Rouviere, V. D'Atri, C. Dreyfus, J.-F. Haeuw, H. Diemer, A. Beck, S. Heinisch, D. Guillarme, S. Cianferani, A Novel Online Four-Dimensional SEC×SEC-IM×MS Methodology for Characterization of Monoclonal Antibody Size Variants, Anal. Chem. 90 (2018) 13929–13937. https://doi.org/10.1021/acs.analchem.8b03333.

[5] B.W.J. Pirok, N. Abdulhussain, T. Brooijmans, T. Nabuurs, J. de Bont, M.A.J. Schellekens, R.A.H. Peters, P.J. Schoenmakers, Analysis of charged acrylic particles by on-line comprehensive two-dimensional liquid chromatography and automated data-processing, Analytica Chimica Acta. 1054 (2019) 184–192. https://doi.org/10.1016/j.aca.2018.12.059.

[6] B.W.J. Pirok, N. Abdulhussain, T. Aalbers, B. Wouters, R.A.H. Peters, P.J. Schoenmakers, Nanoparticle Analysis by Online Comprehensive Two-Dimensional Liquid Chromatography combining Hydrodynamic Chromatography and Size-Exclusion Chromatography with Intermediate Sample Transformation, Analytical Chemistry. 89 (2017) 9167–9174. https://doi.org/10.1021/acs.analchem.7b01906.

[7] R. Edam, E.P.C. Mes, D.M. Meunier, F.A. Van Damme, P.J. Schoenmakers, Branched polymers characterized by comprehensive two-dimensional separations with fully orthogonal mechanisms: Molecular-topology fractionation×size-exclusion chromatography, Journal of Chromatography A. 1366 (2014) 54–64. https://doi.org/10.1016/j.chroma.2014.09.011.

[8] S.T. Popovici, A. van der Horst, P.J. Schoenmakers, Two-dimensional chromatography as a tool for studying band broadening in size-exclusion chromatography, J. Sep. Science. 28 (2005) 1457–1466. https://doi.org/10.1002/jssc.200400088.

[9] R.A. Shellie, É. Tyrrell, C.A. Pohl, P.R. Haddad, Column selection for comprehensive multidimensional ion chromatography, Journal of Separation Science. 31 (2008) 3287–3296. https://doi.org/10.1002/jssc.200800286.

[10] D. Okamoto, Y. Hirata, Development of Supercritical Fluid Extraction Coupled to Comprehensive Two-dimensional Supercritical Fluid Chromatography (SFE-SFC×SFC), Analytical Sciences. 22 (2006) 1437–1440. https://doi.org/10.2116/analsci.22.1437.

[11] Y.Z. Baghdady, K.A. Schug, Online Comprehensive High pH Reversed Phase × Low pH Reversed Phase Approach for Two-Dimensional Separations of Intact Proteins in Top-Down Proteomics, Anal. Chem. 91 (2019) 11085–11091. https://doi.org/10.1021/acs.analchem.9b01665.

[12] M. Sarrut, A. D'Attoma, S. Heinisch, Optimization of conditions in on-line comprehensive two-dimensional reversed phase liquid chromatography. Experimental comparison with one-dimensional reversed phase liquid chromatography for the separation of peptides, Journal of Chromatography A. 1421 (2015) 48–59. https://doi.org/10.1016/j.chroma.2015.08.052.

[13] M. Sarrut, F. Rouvière, S. Heinisch, Theoretical and experimental comparison of one dimensional versus on-line comprehensive two dimensional liquid chromatography for optimized sub-hour separations of complex peptide samples, Journal of Chromatography A. 1498 (2017) 183–195. https://doi.org/10.1016/j.chroma.2017.01.054.

[14] A. D'Attoma, S. Heinisch, On-line comprehensive two dimensional separations of charged compounds using reversed-phase high performance liquid chromatography and hydrophilic interaction chromatography. Part II: Application to the separation of peptides, Journal of Chromatography A. 1306 (2013) 27–36. https://doi.org/10.1016/j.chroma.2013.07.048.

[15] I. François, D. Cabooter, K. Sandra, F. Lynen, G. Desmet, P. Sandra, Tryptic digest analysis by comprehensive reversed phase×two reversed phase liquid chromatography (RP-LC×2RP-LC) at different pH's, Journal of Separation Science. 32 (2009) 1137–1144. https://doi.org/10.1002/jssc.200800578.

[16] L. Wang, R.K. Marcus, Polypropylene capillary-channeled polymer fiber column as the second dimension in a comprehensive two-dimensional RP × RP analysis of a mixture of intact proteins, Anal Bioanal Chem. 412 (2020) 2963–2979. https://doi.org/10.1007/s00216-020-02539-2.

[17] D.R. Stoll, X. Wang, P.W. Carr, Comparison of the Practical Resolving Power of One- and Two-Dimensional High-Performance Liquid Chromatography Analysis of Metabolomic Samples, Anal. Chem. 80 (2008) 268–278. https://doi.org/10.1021/ac701676b.

[18] L.W. Potts, P.W. Carr, Analysis of the temporal performance of one versus on-line comprehensive two-dimensional liquid chromatography, Journal of Chromatography A. 1310 (2013) 37–44. https://doi.org/10.1016/j.chroma.2013.07.102.

[19] M.R. Schure, Limit of Detection, Dilution Factors, and Technique Compatibility in Multidimensional Separations Utilizing Chromatography, Capillary Electrophoresis, and Field-Flow Fractionation, Anal. Chem. 71 (1999) 1645–1657. https://doi.org/10.1021/ac981128q.

[20] K. Horváth, J.N. Fairchild, G. Guiochon, Detection issues in two-dimensional on-line chromatography, Journal of Chromatography A. 1216 (2009) 7785–7792. https://doi.org/10.1016/j.chroma.2009.09.016.

CHAPTER IV - IMPROVING THE RETENTION SPACE COVERAGE IN ON-LINE LC x LC

Part of this Chapter has been published as:

- **Pushing the limits of resolving power and analysis time in on-line comprehensive hydrophilic interaction x reversed phase liquid chromatography for the analysis of complex peptide samples**

  Soraya Chapel, Florent Rouvière, and Sabine Heinisch
  Journal of Chromatography A, 2019, 1615, 460753
  DOI: 10.1016/j.chroma.2019.460753

INTRODUCTION

One of the main limitations restraining a 2D separation from reaching its full potential is the ability of the 2D system to spread the generated peaks all across the separation space. As previously emphasized in Chapter I, the full theoretical peak capacity in on-line LC x LC can indeed only be realized if the retention space is fully utilized. Working toward this goal for the separation of a given mixture mostly imply either (i) exploiting the differences in selectivity between the two combined systems and/or (ii) dynamically adjusting the gradient in the second dimension throughout the 2D analysis to better fit the elution conditions in each fraction by employing so-called "tailored" second-dimension gradient programs.

In the previous chapter, it was demonstrated that impressive peak capacities could be achieved in on-line RPLC x RPLC for the separation of peptides, despite the use of similar chromatographic modes in both dimensions. In this specific example, the selectivity difference between the two dimensions was mainly achieved by judiciously manipulating the pH of the mobile phase in each dimension. Other strategies to alter the selectivity in RPLC x RPLC may also involve using different RP-stationary phases and/or mobile phases in both dimensions. Yet, regardless of the strategy, the use of partially correlated retention mechanisms in both dimension inevitably leads to a partial occupation of separation space, hence to a lower peak capacity than the theoretical maximum. On that account, there is a large consensus on the fact that, in LC x LC, the combination of chromatographic modes with markedly different retention mechanisms should be the best strategy to maximize the retention space coverage.

In the present chapter, two different approaches to improve the retention space coverage in on-line LC x LC are critically explored and compared for the separation of peptides through two distinct studies. The first study describes the development process of an on-line RPLC x RPLC method incorporating a tailored gradient program in the second dimension. In this work, the logic behind the implementation of such gradient programs for combinations with limited orthogonality is explained and the strengths and weaknesses of such an approach are discussed. The second study describes the development of an on-line LC x LC method combining hydrophilic interaction liquid chromatography (HILIC) in the first dimension and RPLC in the second dimension. This combination is well known to provide quite orthogonal conditions for the separation of peptides, but also to be quite challenging because of

the reversed elution strength of the mobile phases used in these two separation modes. The study presented in this work specifically addresses this problem and reports on a possible approach to avoid its detrimental impact on peptide separation in on-line HILIC x RPLC.

A. Improving the retention space coverage by using tailored gradient programs in the second dimension

*This section has been prepared for publication and is expected to be submitted soon in **Journal of Separation Science**.*

1. Introduction

Despite the wide variety of ways to tweak selectivity in RPLC, the fact that similar separation mechanisms are used in both dimensions for on-line RPLC x RPLC inevitably entails a certain degree of correlation with this combination. As highlighted in the previous chapter, the implementation of on-line RPLC x RPLC will most likely result in peaks concentrated around the diagonal line of the separation space. This can be readily explained by the fact that the analytes have similar retention patterns in both dimensions since compounds eluted early in ^{1}D will also elute early in ^{2}D, and vice versa. As a consequence, the retention space coverage is limited, which in turn reduces the effective peak capacity.

In on-line LC x LC, the most common mode of operation in ^{2}D consists in repeating the same gradient program for each analysed fraction over the course of the 2D analysis (Fig. IV-1a). This mode has been previously referred to as "full-in-fraction" [1] or full gradient mode [2,3]. To ensure complete analyte elution for all fractions, the repeated gradient typically covers a broad range of mobile phase compositions, which usually leads to steep gradient slopes considering the short cycle times required in ^{2}D. The full gradient mode is easy to implement and well-suited in the case of orthogonal combinations. However, it might not be the most suitable mode for partially correlated systems such as RPLC x RPLC, considering the elution pattern of successive fractions in ^{2}D. Because the ranges of composition at elution in ^{2}D progressively shift toward higher values along the 2D analysis, applying the same gradient program inevitably leads to the accumulation of peaks in specific parts of the chromatogram. On that account, a potential solution to improve the retention space coverage in on-line RPLC x RPLC could lie in the development of tailored gradient programs in ^{2}D.

As shown in Fig. IV-1, three other types of ^{2}D-gradient programs have been reported as alternatives to the conventional full gradient mode [3]: the parallel gradient (Fig. IV-1b), the segment-in-gradient or segment gradient (Fig. IV-1c), and the shifted gradient (Fig. IV-1d) modes.

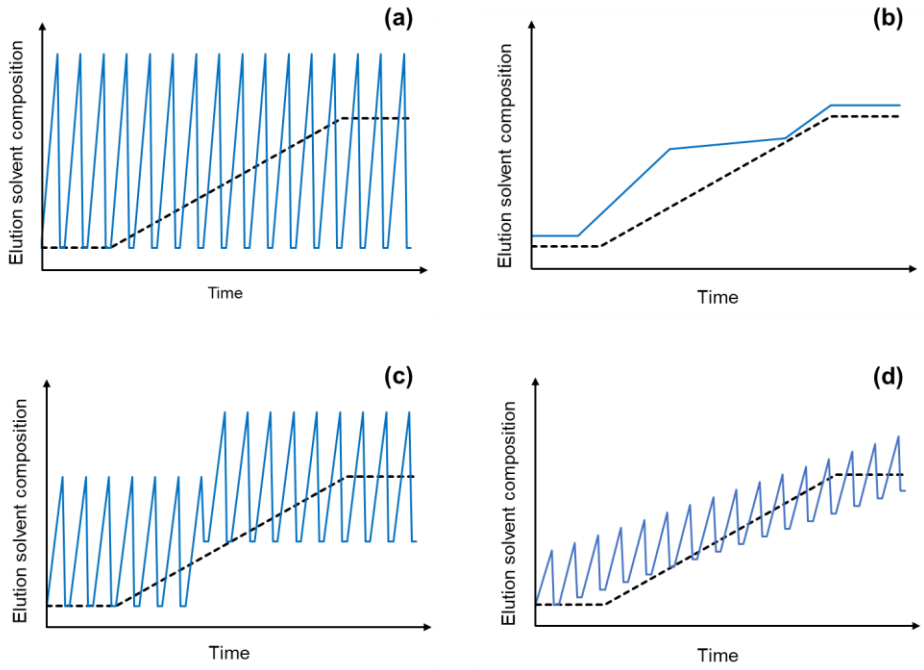

Fig. IV-1: Schematic representation of main gradient programs in on-line LC x LC: (a) full gradient mode, (b) parallel gradient mode, (c) segment gradient mode, and (d) shifted gradient mode. The Black dotted line corresponds to gradient profile in ^{1}D and the blue line corresponds to gradient profile in ^{2}D. Adapted from [2].

In parallel gradient mode (Fig. IV-1b), which has also been referred to as "advancing isocratic elution" mode [4], a single gradient program is carried out in the second dimension over the entire 2D analysis. Although the elution solvent strength increases slightly in each successive run, this approach brings about nearly-isocratic elution in each ^{2}D-separation. This might explain why parallel gradients have been scarcely used in on-line LC x LC, with the exception of several studies conducted by Jandera and co-workers [1,5-7]. Gradient elution is predominantly the preferred elution mode when dealing with highly complex samples, such as those encountered in the field of proteomics, biopharmaceuticals or metabolomics, to cite only a few examples [4,8,9]. In comparison with isocratic elution, gradient elution affords several advantages in on-line LC x LC: (i) It prevents the so-called "wrap-around" effects that might appear between fractions for analytes with large chemical diversity and range in properties, by ensuring their complete elution within the same ^{2}D-run. Wrap-around effects may occur when the eluent composition is too weak to elute all the analytes before the next fraction, which results in compounds eluting at the beginning of the next fraction. (ii) Whereas isocratic elution is expected to produce increasing peak widths with increasing retention times, constant peak widths are expected in gradient elution,

which allows maximizing both peak capacity and detection sensitivity. (iii) As highlighted in Chapter III, using gradient elution with ultra-fast analysis times provides outstanding analyte re-focusing in ^{2}D, which enables the injection of relatively large volumes without band broadening.

It is widely accepted that the peak capacities obtained under isocratic conditions are intrinsically much lower than those obtained under gradient conditions when considering the same analysis time (gradient time equal to isocratic time). In on-line LC x LC, the benefits of using gradient elution in both dimensions instead of isocratic elution have also been demonstrated [10]. In a theoretical study, Vivo-Truyols et al. [10] highlighted a reduction of peak capacity by around 30% when using isocratic elution in at least one dimension, and down to 50% with isocratic elution in both dimensions. However, it is worth emphasizing that these conclusions were drawn without taking into account the column re-equilibration time required between fractions.

The main advantage of using isocratic elution over gradient elution in ^{2}D is the possibility to maximize the time available for elution since no flushing out of the gradient dwell volume nor post-gradient column equilibration is required between each ^{2}D-run. As will be extensively discussed in Chapter V, the re-equilibration process contributes greatly to the reduction of the available gradient time, and thus of the peak capacity, when using gradient elution in ^{2}D. Stoll et al. [4] indeed underlined that this contribution represented at least about 20% of the total analysis time for very short ^{2}D-run time (i.e. sub-minute). From the perspective of maximizing the effective analysis time in ^{2}D, parallel gradients might hold potential in on-line LC x LC. When compared with full gradients in the literature, conflicting results have been reported. In 2010, Jandera et al. [1] demonstrated that parallel gradients could be useful to increase the retention space coverage for partially correlated systems such as RPLC x RPLC, but at the cost of increased band broadening and decreased peak capacity. In 2014, similar observations were made by Leme et al. [11] in the context of the RPLC x RPLC analysis of polyphenolic compounds in sugar cane. Meanwhile, very recently, Aly et al. [12] conversely reported increased retention space coverage and effective peak capacity for the analysis of pharmaceutical compounds in on-line RPLC x RPLC. It should be noted that the latter conclusions were drawn for a relatively simple mixture of standard compounds using a column temperature of 30°C in both dimensions, whereas the importance of using high-temperatures for ultra-fast and

efficient ^{2}D-separations has already been clearly highlighted [13-17]. While parallel gradient might be attractive in specific conditions, it is our view that using isocratic conditions in ^{2}D is not a viable approach for the separation of highly complex mixtures.

In segment gradient mode (Fig. IV-1c), different gradient composition ranges are used in different "segments" of the 2D analysis, which enables less steep gradients compared to the full gradient mode. In theory, numerous time segments with different composition ranges can be adjusted to properly suit sample retention in ^{2}D. Nonetheless, only three segments have been reported at the very most in the literature [1,18-20]. Only a few studies have reported the use of segment gradients in on-line RPLC x RPLC but most of them highlighted an improvement of the retention space coverage compared to full gradients.

Last but not least, in shifted gradient mode (Fig. IV-1d), initial and final ^{2}D-gradient compositions gradually increase during the 2D analysis, which implies that a different gradient is carried out in each ^{2}D-runs. With such a design, the gradient composition span is usually much narrower, and thus less steep than with full gradients or segment gradients. The composition range can either be shifted constantly from a specified time t1 to a specified time t2, which has been referred to as "continuous shifting" [2,21] or using several segments with different change rates, which has been referred to as "multi-segment shifting" [22]. Because they allow full flexibility in terms of gradient optimization in the second dimension, there has been a growing interest for shifted gradient programs in on-line LC x LC, especially with RPLC in both dimensions [23-32]. Several studies have demonstrated increased retention space coverage when using shifted gradients compared to full gradients, but without commenting on any other implications on the separation.

The objective of this study is to explore the potential and limitations of using tailored gradient programs in the second dimension to improve the retention space coverage in on-line RPLC x RPLC. First, we developed an on-line RPLC x RPLC method with a conventional full gradient program in the second dimension for the separation of a tryptic digest of proteins. The separation was conducted using C18 columns in both dimensions with a gradient time of 30 min in the first dimension. Based on the resulting 2D separation, the gradient program in the second dimension was optimized using a combination of segment gradient and shift gradient approaches. The performances of this optimized tailored gradient program were finally compared with the original full gradient program with regard to retention space coverage, effective

peak capacity, method sensitivity, and run-to-run repeatability. Other implications, such as increased complexity of method development and implementation are also discussed.

2. Experimental conditions

For this study, the material and equipment were the same as in Chapter III. All experiments were carried out on a 1290 Infinity II series 2D-LC system from Agilent using 20-µL sample loops for modulation. The two-segment gradient tailored for the second dimension was programmed using a dedicated part of Agilent OpenLab software that enables rapid and easy writing of ^{2}D-gradients with varying composition ranges.

The studied sample was made by tryptic digestion of six model proteins, as described in Chapter III.

In the first dimension, an Ascentis Express C18 column (50 x 2.1 mm, 2.7 µm superficially porous particles) from Sigma-Aldrich was used. The mobile phase consisted of (A) 10 mM ammonium acetate in water and (B) acetonitrile. The gradient conditions were as followed: 1-34-1-1% B in 0-30-32.4-45 min (normalized gradient slope, s, equal to 2.6%).

In the second dimension, an Acquity CSH C18 column (30 x 2.1 mm, 1.7 µm fully porous particles) from Waters Technology was used. The mobile phase consisted of (A) 0.1% formic acid in water and (B) 0.1% formic acid in acetonitrile. The full gradient conditions were: 1-45-1-1% B in 0-0.13-0.16-0.27 min (s = 12.3%). The tailored gradient conditions consisted of two different segments. In the first segment (from 0 to 15 min), the gradient program was: 1-25-1-1% B in 0-0.13-0.16-0.27 min (s = 6.7%). In the second segment (from 15 to 40 min), the ^{2}D-gradients were constantly shifted from 1-25% B at the beginning, to 21-45% at the end (s = 6.7% for each run). The rate of increase of initial and final compositions of solvent B under the course of the shifted gradient program was about 0.22% per modulation cycle.

The graphical representations of the two gradient programs used in this study are shown in Fig. IV-2. The red and blue lines indicate the gradient programmed in the first- and second dimensions, respectively.

The chromatographic conditions used in both dimensions for the two experiments compared in this study are given in the following Table IV-1.

Table IV-1: Experimental conditions for the RPLC x RPLC setups with full gradient program and tailored gradient program in the second dimension.

	RPLC x RPLC with full gradients	**RPLC x RPLC with shifted gradients**
First dimension (^{1}D)		
Injection volume	10 µL	
Sample solvent	0:100 ACN/water (v/v)	
Stationary phase	Ascentis express C18	
Column geometry	(50 mm x 2.1 mm, 2.7 µm)	
Temperature	30°C	
Mobile phase A	10 mM ammonium acetate in water	
Mobile phase B	ACN	
Flow rate	0.04 mL/min	
Gradient	1-34% B in 30 min	
Post-column split	1:2	
Detection	UV absorption at 210 nm, 20 Hz	
Modulation		
Loop volume	20 µL	
Sampling time	0.27 min	
Second dimension (^{2}D)		
Stationary phase	Acquity CSH C18	
Column geometry	(30 mm x 2.1 mm, 1.7 µm)	
Temperature	80°C	
Mobile phase A	0.1% formic acid in water	
Mobile phase B	0.1% formic acid in ACN	
Flow rate	2 mL/min	
Post-column split	1:2	
Detection	UV absorption at 210 nm (80 Hz), Q-TOF HRMS ESI+ (20 Hz)*	
^{2}D- Gradient program	1-45-1-1% B in 0-0.13-0.16-0.27 min	1-25% B in 0.13 min from t = 0 min to t = 15 min shifted to 21-45% B in 0.13 min at t = 40 min

*HRMS detection was used in this study to ensure that the same peaks were compared in Fig. IV-6. The experimental conditions for HRMS detection were the same as in Chapter III.

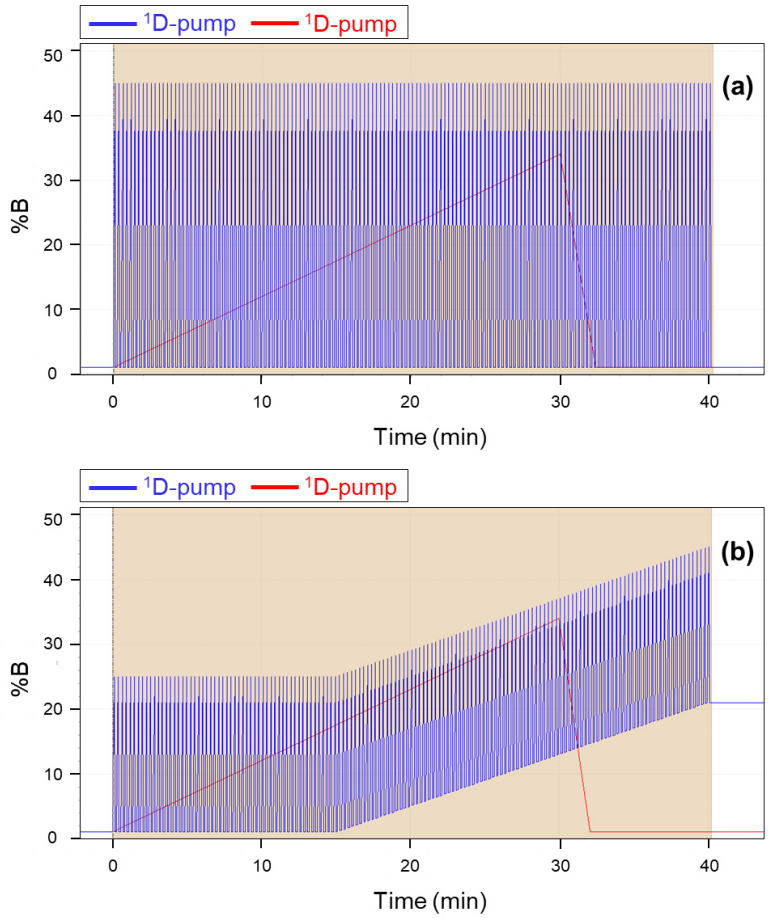

Fig. IV-2: Gradient elution programs used for the two on-line RPLC x RPLC experiments described in this study: (a) full gradient program and (b) tailored gradient program. Adapted from [2].

3. Results and discussion

Fig. IV-3 shows the resulting 2D contour plot obtained for the on-line RPLC x RPLC separation of the tryptic digest sample in full gradient mode. As expected and as previously underlined in Chapter III, the eluted peaks only occupy a limited portion of the separation space. The retention space coverage (γ), evaluated using the approach described by Heinisch's group [13], was estimated to 0.55, as indicated in Table IV-2. In other words, approximately half of the separation space was not used with the full gradient approach. The key metrics that enabled the calculation of the effective peak capacity ($n_{2D,\ effective}$) for the two separations described in this study are listed in Table IV-2. They include under-sampling correction factor (α), retention space coverage (γ), analyte elution time ranges in both dimensions ($^1\Delta t$ and $^2\Delta t$), and average peak widths at 4σ in both dimensions ($^1w_{4\sigma}$ and $^2w_{4\sigma}$). The average peak widths were determined

from a mixture of ten representative peptide standards in the first dimension, and about a hundred peaks eluted all across the chromatogram in the second dimension. The effective peak capacity calculated for the separation in full gradient mode was 880.

Table IV-2: Effective peak capacities ($n_{2D,effective}$) obtained for the on-line RPLC x RPLC separations of a tryptic digest sample with the full gradient program and the tailored gradient program in the second dimension. Intermediate parameters for the calculation of $n_{2D,\ effective}$: under-sampling correction factor (α), retention space coverage (γ), analyte elution time ranges in both dimensions ($^1\Delta t$ and $^2\Delta t$), and average peak widths at 4σ in both dimensions ($^1w_{4\sigma}$ and $^2w_{4\sigma}$).

	α^a	γ^b	$^1\Delta t$ (min)	$^2\Delta t$ (s)	$^1w_{4\sigma}$ (min)	$^2w_{4\sigma}$ (s)	$n_{2D,effective}{}^c$
Full gradient	0.70	0.55	32.6	9.40	0.49	0.29	880
Tailored gradient	0.70	0.82	32.6	9.40	0.49	0.33	1180

[a] Calculated using $\alpha = \frac{1}{\sqrt{1 + 0.21\left(6/\tau\right)^2}}$ according to [33], with τ, the sampling rate (i.e. number of fractions per 6σ–^{1}D-peak widths).

[b] Estimated using the method described by Heinisch's group [13].

[c] Calculated using $n_{2D,eff} = \alpha \times \gamma \times \left(1 + \frac{^1\Delta t}{^1w_{4\sigma}}\right) \times \left(1 + \frac{^2\Delta t}{^2w_{4\sigma}}\right)$.

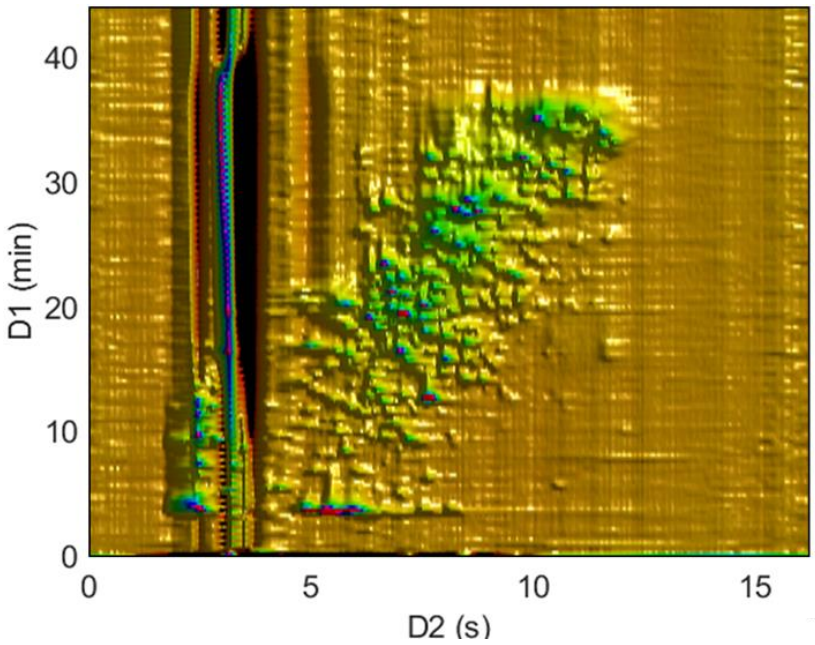

Fig. IV-3: Entire 2D contour plot of on-line RPLC x RPLC separation of tryptic digest sample using full gradients in the second dimension. Chromatographic conditions are given in Table IV-1.

Starting from this first separation, the gradient program in the second dimension was optimized to improve peak spreading across the ^{2}D-retention space. Fig. IV-4 shows the six peaks that were used to optimize the new tailored gradient program, with their respective compositions at elution (C_e). As can be seen in Fig. IV-4a, the ^{2}D-gradient covered a wide range of organic solvent composition from 1% to 45% B (ΔC = 44% B). However, the compositions at elution in ^{2}D ranged from about 1-18% B at the beginning (peaks 1 and 2) to about 15-43% B at the end of the analysis (peaks 5 and 6), as highlighted in Fig. IV-4b. Also, from the beginning of the ^{1}D-analysis to about 15 min (peak 3), many analytes started to elute in ^{2}D at 1% B. To avoid the too-early elution of peaks currently eluting before 5 s in ^{2}D in the first part of the chromatogram (i.e. ^1t < 15 min), two different segments were determined instead of using a constant shift from beginning to end.

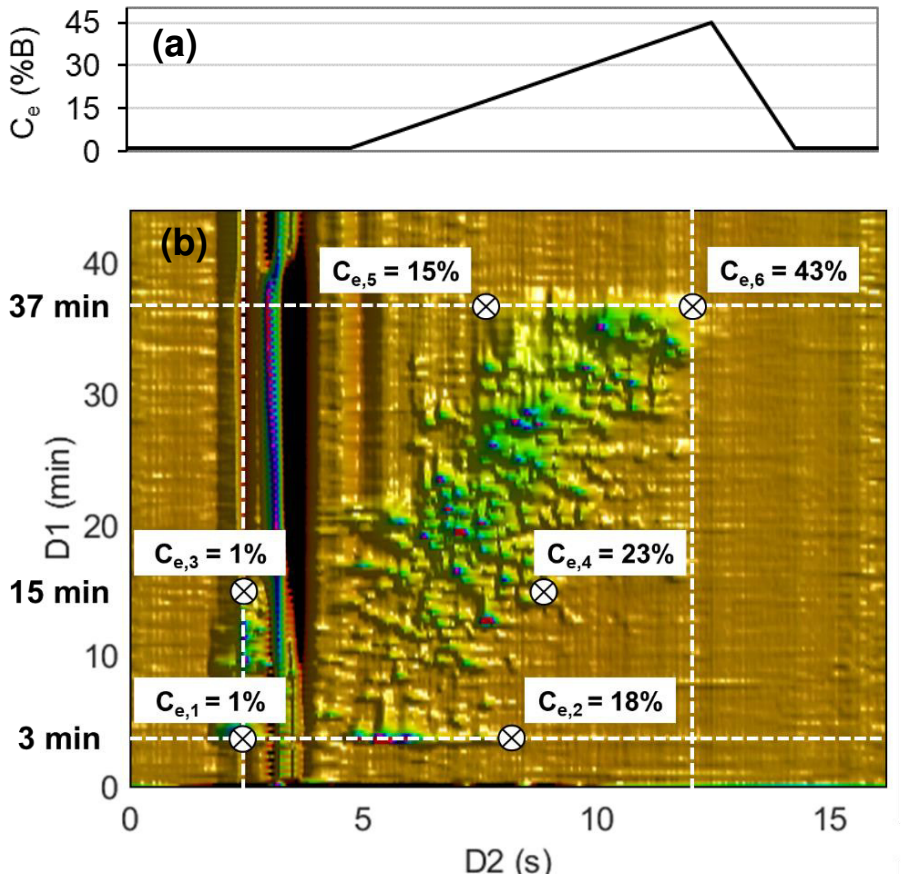

Fig. IV-4: Illustration of the approach used for the optimization of the tailored gradient program. (a) Evolution of the compositions at elution (C_e) at column outlet with analysis time in ^{2}D. (b) Same contour plot as in Fig. IV-3 with most relevant peaks for gradient optimization highlighted.

Considering the compositions at elution of peaks 1 and 3 (i.e. C_e = 1% B) on one hand, and peak 4 on the other hand (i.e. C_e = 23% B), full gradients were used from 1 to 15 min (segment 1), with a gradient ranging from 1% to 25% B (ΔC = 24% B). Then, from 15 to 40 min (segment 2), the gradients were constantly shifted from 1-25% B (at 15 min) to 21-45% B (at 40 min). This led to a gradient composition between 19-43% B at 37 min instead of 15-43% B. It should be noted that this higher starting composition of 19% B was preferred to maintain a constant gradient composition range for all fractions in ^{2}D.

A comparison between the separations obtained with the original full gradient program and the tailored gradient program is shown in Figs. IV-5a and 5b, respectively.

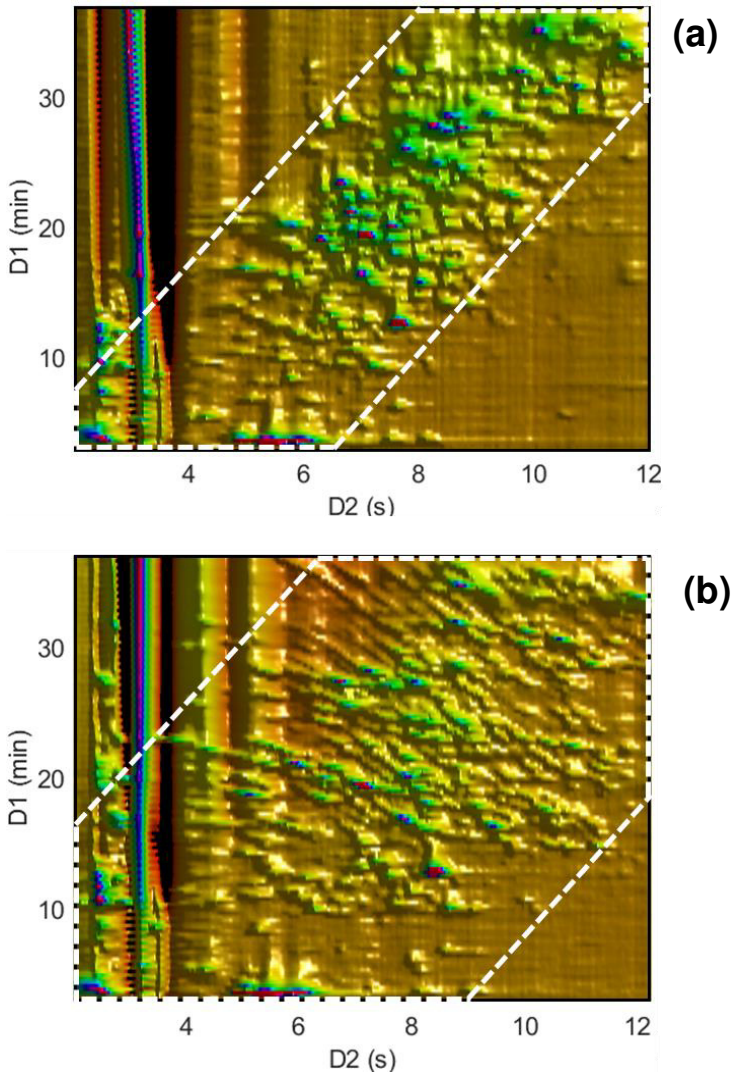

Fig. IV-5: Comparison of on-line RPLC x RPLC separations of tryptic digest sample using either (a) the full gradient program or (b) the tailored gradient program in the second dimension. Chromatographic conditions are given in Table IV-1. The white dotted line highlights the retention space coverage.

It is manifest that the separation obtained with the tailored gradient program (Fig. IV-5b) resulted in greater coverage of the separation space compared to the full gradient program (Fig. IV-5a). In both figures, the retention space coverage is delimited by white dotted lines. Compared to Fig. IV-5a (full gradient program), the peaks in Fig. IV-5b (tailored gradient program) are spread on both sides of the diagonal line of the separation space. As indicated in Table IV-2, the retention space coverage estimated for the separation obtained with the new tailored gradient program was 0.82, which represents an increase of 50% compared to the original full gradient program. The resulting increase in effective peak capacity was not proportional to this increase in retention space coverage as a result of a subsequent increase of 14% in peak width in the second dimension. These larger peak widths can be explained by the reduced analyte focusing in the column that comes along with the use of smoother gradients in ^{2}D (see Chapter III). In the current study, the normalized gradient slope in ^{2}D was about twice as low with the tailored gradient (s = 6.7) as the one with the original gradient (s = 12.3%). Nonetheless, the significant increase in retention space coverage with the tailored gradient mode enabled a notable increase of 35% in effective peak capacity compared to the full gradient mode (i.e. 1180 vs. 880). However, as can be expected, the counteract of the increased band broadening in ^{2}D was a decrease in peak intensity. On average, the peak intensities were found to be 30% lower.

As can be seen in Fig. IV-5, the tailored gradient program clearly gave better separation in the second dimension. Compared to Fig. IV-5a (full gradient), the shallow gradient steepness used in Fig. IV-5b (tailored gradient) enabled fewer coelutions and better peak resolution. This improvement in separation can be best observed from the comparison of selected ^{2}D-chromatograms shown in Fig. IV-6. Examples of chromatograms are given for three relevant parts of the contour plot, going from early elution in ^{1}D (top figure) to late elution in ^{1}D (bottom figure). As highlighted in Fig. IV-6, the tailored gradient program successfully allowed to extend analyte retention time in ^{2}D, (i) toward higher values before 15 min (top chromatograms) and (ii) on both sides of the retention space in the shifted part of the gradient program (middle and bottom chromatograms).

On another note, the comparison of overlaid ^{2}D-chromatograms shown in Fig. IV-6 brought to our attention some retention repeatability issues in the shifted section of the tailored gradient program. These issues can be glimpsed in the bottom

chromatogram in Fig. IV-6b but are better seen in the zoomed view of ^{2}D-chromatograms shown in Fig. IV-7.

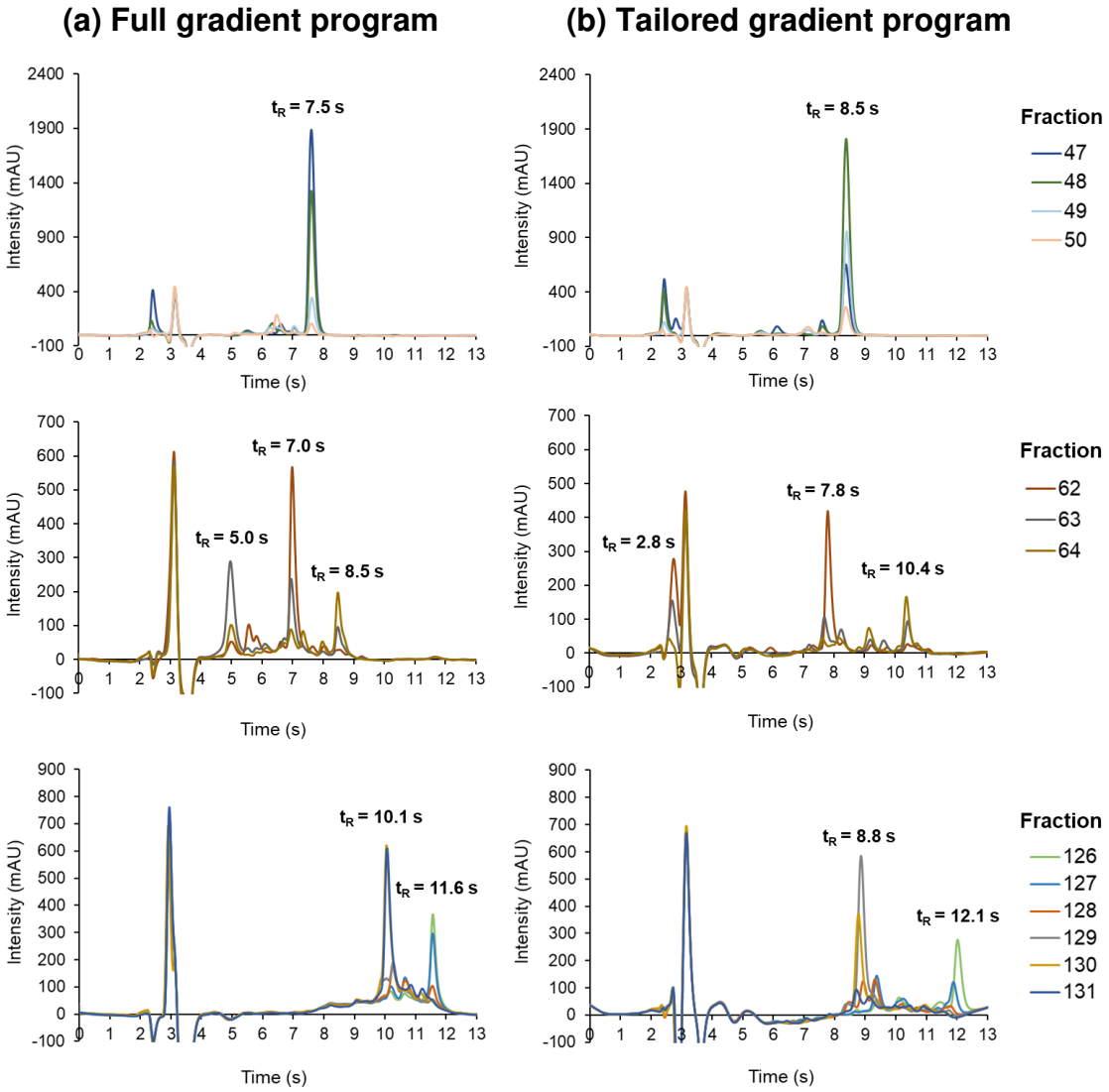

Fig. IV-6: Comparison of overlaid ^{2}D-separations obtained for selected fractions in on-line RPLC x RPLC using either (a) full gradient program in ^{2}D or (b) tailored gradient program in ^{2}D. Chromatographic conditions are given in Table IV-1. The corresponding fraction number is indicated on the right of the figure. The retention time (t_R) of relevant peaks is indicated in each chromatogram.

In on-line LC x LC, the column re-equilibration process contributes to a large extent to the reduction of the gradient time in the second dimension, and especially when using short (< 2.1 mm ID) and narrow-bore columns (< 50 mm length). To maximize the gradient time, the time allocated for column equilibration is usually kept to a minimum in the second dimension. In the literature, it has been demonstrated that excellent run-to-run retention time repeatability could be realized with only about

one column volume of flushing with the initial eluent between each ^{2}D-run [34,35]. In this study, we used a column equilibration time equal to 1.65 times the column dead time (t_0), that is, 0.06 min. As shown in Fig. IV-7a, the repeatability of retention time was excellent with the full gradient program, with a relative standard deviation (RSD) below 0.2% for all integrated peaks. As seen in the top chromatogram in Fig. IV-7b, similar results were obtained with the tailored gradient program in the first segment of the program (i.e. from 0 to 15 min) in which the same gradient was repeated for each run. However, this was not the case in the shifted segment of the program (i.e. from 15 to 40 min), as exemplified in the middle and bottom chromatograms shown in Fig. IV-7b. Retention times were found to shift significantly between successive fractions. On average, the calculated RSD values for the retention times measured between 15 and 40 min were around 1%. These retention time shifts might be explained by (i) the continuous modification of initial and final gradient compositions between successive ^{2}D-runs impeding partial column equilibrium and/or (ii) the continuously increasing concentration of organic solvent throughout the 2D analysis (+0.22% B per modulation cycle in our study). In the matter of retention time repeatability from one run to the next, it has been demonstrated that the most influential parameter was the repeatability of the flushing process, rather than the extent of column re-equilibration [35]. That is quite consistent with the observations made in this study when repeating the same gradient for each ^{2}D-run or not.

In on-line LC x LC, maintaining good run-to-run repeatability in retention time between successive ^{2}D-runs is crucial. Significant variations in retention time between subsequent fractions might hamper the correct reconstruction of the 3D and 2D plots and cause difficulties with identification and quantification. From this perspective, employing the same gradient throughout the 2D analysis is the most reliable approach. It is worth pointing out that similar run-to-run repeatability issues should be expected in parallel gradient mode since the organic composition in the mobile phase increases continuously in the second dimension, as previously underlined by Jandera and co-workers [6].

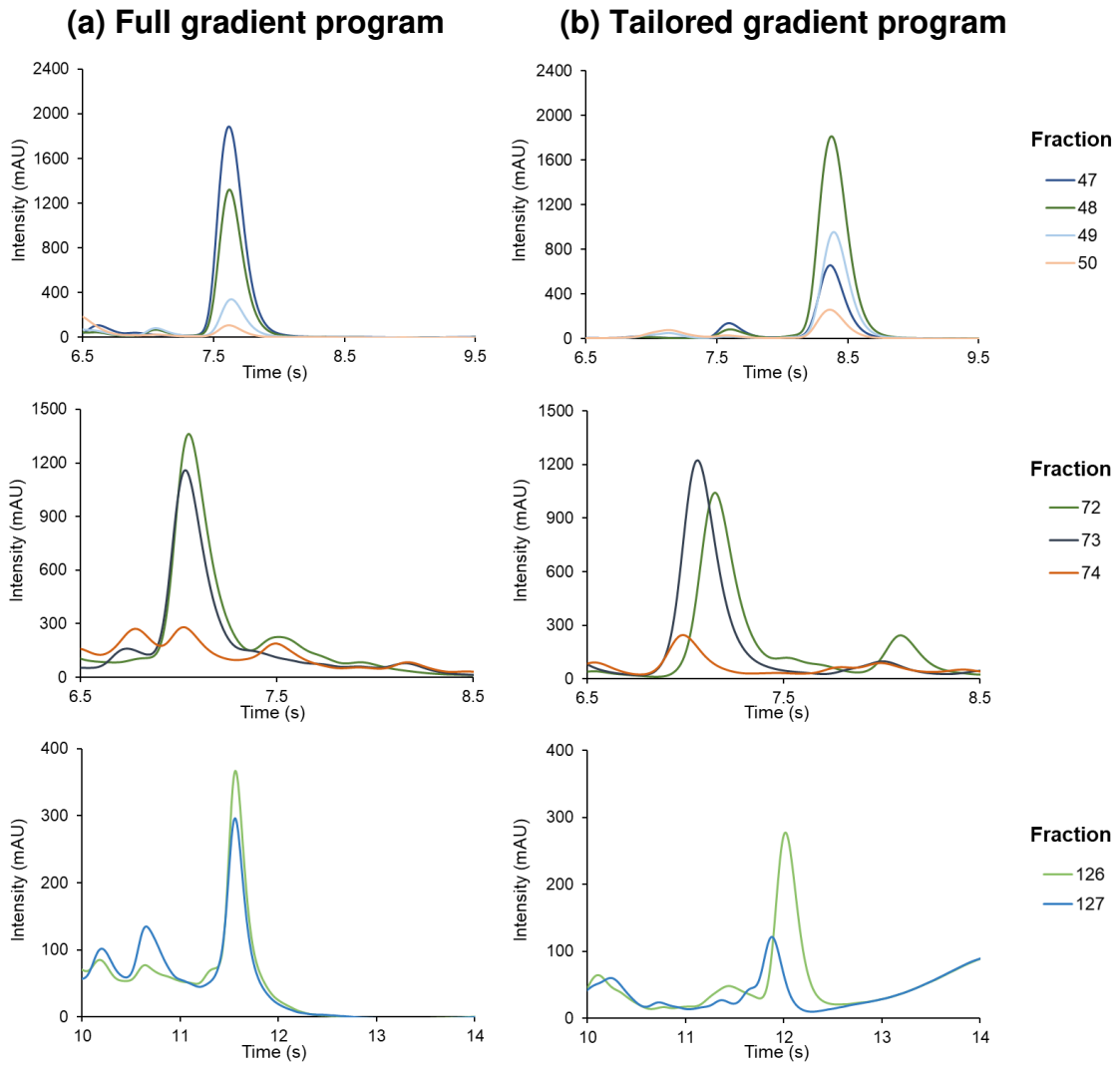

Fig. IV-7: Zoomed views of overlaid ^{2}D-separations obtained for selected fractions in on-line RPLC x RPLC highlighting repeatability issues with the tailored gradient program. (a) full gradient program in ^{2}D or (b) tailored gradient program in ^{2}D. Chromatographic conditions are given in Table IV-1. The corresponding fraction number is indicated on the right of the figure.

4. Concluding remarks

In the current study, we have assessed the advantages and limitations of using tailored gradient programs in the second dimension to improve the retention space coverage in on-line RPLC x RPLC for the analysis of a tryptic digest sample. The optimized gradient program consisted of a mix between the segment gradient mode and the shifted gradient mode. In this study, both the retention space coverage and the peak capacity were significantly increased when compared to a conventional full gradient approach. However, this increase was obtained at the expense of method sensitivity

and run-to-run retention time repeatability. It was found that the use of shifted gradients in the second dimension significantly impacted the precision of the retention time in consecutive ^{2}D-separations, which could most likely be ascribed to the continuous increase in elution strength at the beginning of the gradient throughout the analysis. To the best of our knowledge, this issue of repeatability with shifted gradient programs has never been reported in the literature, even though it definitely might be a critical issue in on-line LC x LC.

On a more practical note, it is worth emphasizing that the implementation of tailored gradient programs such as those integrating shifting gradient assemblies usually require specific software, which is not necessarily available in most laboratories. Without proper software, implementing such programs might be tedious if not impossible. Another aspect that should be taking into consideration is that the design of a tailored gradient program for a given separation will lead to much longer method development times compared to the conventional full gradient approach. In addition, it also introduces additional complexity to the already quite complex method development process in on-line LC x LC.

5. References

[1] P. Jandera, T. Hájek, P. Česla, Comparison of various second-dimension gradient types in comprehensive two-dimensional liquid chromatography, Journal of Separation Science. 33 (2010) 1382–1397. https://doi.org/10.1002/jssc.200900808.

[2] D. Li, O.J. Schmitz, Use of shift gradient in the second dimension to improve the separation space in comprehensive two-dimensional liquid chromatography, Anal Bioanal Chem. 405 (2013) 6511–6517. https://doi.org/10.1007/s00216-013-7089-5.

[3] D. Li, C. Jakob, O. Schmitz, Practical considerations in comprehensive two-dimensional liquid chromatography systems (LCxLC) with reversed-phases in both dimensions, Anal Bioanal Chem. 407 (2015) 153–167. https://doi.org/10.1007/s00216-014-8179-8.

[4] D.R. Stoll, X. Li, X. Wang, P.W. Carr, S.E.G. Porter, S.C. Rutan, Fast, comprehensive two-dimensional liquid chromatography, Journal of Chromatography A. 1168 (2007) 3–43. https://doi.org/10.1016/j.chroma.2007.08.054.

[5] F. Cacciola, P. Jandera, Z. Hajdú, P. Česla, L. Mondello, Comprehensive two-dimensional liquid chromatography with parallel gradients for separation of

phenolic and flavone antioxidants, Journal of Chromatography A. 1149 (2007) 73–87. https://doi.org/10.1016/j.chroma.2007.01.119.

[6] P. Česla, T. Hájek, P. Jandera, Optimization of two-dimensional gradient liquid chromatography separations, Journal of Chromatography A. 1216 (2009) 3443–3457. https://doi.org/10.1016/j.chroma.2008.08.111.

[7] P. Jandera, P. Česla, T. Hájek, G. Vohralík, K. Vyňuchalová, J. Fischer, Optimization of separation in two-dimensional high-performance liquid chromatography by adjusting phase system selectivity and using programmed elution techniques, Journal of Chromatography A. 1189 (2008) 207–220. https://doi.org/10.1016/j.chroma.2007.11.053.

[8] B.W.J. Pirok, A.F.G. Gargano, P.J. Schoenmakers, Optimizing separations in online comprehensive two-dimensional liquid chromatography, J. Sep. Sci. 41 (2018) 68–98. https://doi.org/10.1002/jssc.201700863.

[9] P. Jandera, Programmed elution in comprehensive two-dimensional liquid chromatography, Journal of Chromatography A. 1255 (2012) 112–129. https://doi.org/10.1016/j.chroma.2012.02.071.

[10] G. Vivó-Truyols, Sj. van der Wal, P.J. Schoenmakers, Comprehensive Study on the Optimization of Online Two-Dimensional Liquid Chromatographic Systems Considering Losses in Theoretical Peak Capacity in First- and Second-Dimensions: A Pareto-Optimality Approach, Anal. Chem. 82 (2010) 8525–8536. https://doi.org/10.1021/ac101420f.

[11] G.M. Leme, F. Cacciola, P. Donato, A.J. Cavalheiro, P. Dugo, L. Mondello, Continuous vs. segmented second-dimension system gradients for comprehensive two-dimensional liquid chromatography of sugarcane (Saccharum spp.), Anal Bioanal Chem. 406 (2014) 4315–4324. https://doi.org/10.1007/s00216-014-7786-8.

[12] A.A. Aly, M. Muller, A. de Villiers, B.W.J. Pirok, T. Górecki, Parallel gradients in comprehensive multidimensional liquid chromatography enhance utilization of the separation space and the degree of orthogonality when the separation mechanisms are correlated, Journal of Chromatography A. 1628 (2020) 461452. https://doi.org/10.1016/j.chroma.2020.461452.

[13] A. D'Attoma, C. Grivel, S. Heinisch, On-line comprehensive two-dimensional separations of charged compounds using reversed-phase high performance liquid chromatography and hydrophilic interaction chromatography. Part I: Orthogonality and practical peak capacity considerations, Journal of Chromatography A. 1262 (2012) 148–159. https://doi.org/10.1016/j.chroma.2012.09.028.

[14] S. Heinisch, A. D'Attoma, C. Grivel, Effect of pH additive and column temperature on kinetic performance of two different sub-2μm stationary phases

for ultrafast separation of charged analytes, Journal of Chromatography A. 1228 (2012) 135–147. https://doi.org/10.1016/j.chroma.2011.08.041.

[15] D.R. Stoll, J.D. Cohen, P.W. Carr, Fast, comprehensive online two-dimensional high performance liquid chromatography through the use of high temperature ultra-fast gradient elution reversed-phase liquid chromatography, Journal of Chromatography A. 1122 (2006) 123–137. https://doi.org/10.1016/j.chroma.2006.04.058.

[16] D. Guillarme, J. Ruta, S. Rudaz, J.-L. Veuthey, New trends in fast and high-resolution liquid chromatography: a critical comparison of existing approaches, Anal Bioanal Chem. 397 (2010) 1069–1082. https://doi.org/10.1007/s00216-009-3305-8.

[17] D.T.-T. Nguyen, D. Guillarme, S. Heinisch, M.-P. Barrioulet, J.-L. Rocca, S. Rudaz, J.-L. Veuthey, High throughput liquid chromatography with sub-2μm particles at high pressure and high temperature, Journal of Chromatography A. 1167 (2007) 76–84. https://doi.org/10.1016/j.chroma.2007.08.032.

[18] K. Wicht, M. Baert, A. Kajtazi, S. Schipperges, N. von Doehren, G. Desmet, A. de Villiers, F. Lynen, Pharmaceutical impurity analysis by comprehensive two-dimensional temperature responsive × reversed phase liquid chromatography, Journal of Chromatography A. 1630 (2020) 461561. https://doi.org/10.1016/j.chroma.2020.461561.

[19] K. Arena, F. Cacciola, L. Dugo, P. Dugo, L. Mondello, Determination of the Metabolite Content of Brassica juncea Cultivars Using Comprehensive Two-Dimensional Liquid Chromatography Coupled with a Photodiode Array and Mass Spectrometry Detection, Molecules. 25 (2020) 1235. https://doi.org/10.3390/molecules25051235.

[20] P. Jandera, T. Hájek, P. Česla, Effects of the gradient profile, sample volume and solvent on the separation in very fast gradients, with special attention to the second-dimension gradient in comprehensive two-dimensional liquid chromatography, Journal of Chromatography A. 1218 (2011) 1995–2006. https://doi.org/10.1016/j.chroma.2010.10.095.

[21] F. Bedani, W.Th. Kok, H.-G. Janssen, Optimal gradient operation in comprehensive liquid chromatography×liquid chromatography systems with limited orthogonality, Analytica Chimica Acta. 654 (2009) 77–84. https://doi.org/10.1016/j.aca.2009.06.042.

[22] Y.F. Wong, F. Cacciola, S. Fermas, S. Riga, D. James, V. Manzin, B. Bonnet, P.J. Marriott, P. Dugo, L. Mondello, Untargeted profiling of Glycyrrhiza glabra extract with comprehensive two-dimensional liquid chromatography-mass spectrometry using multi-segmented shift gradients in the second dimension: Expanding the metabolic coverage, ELECTROPHORESIS. 39 (2018) 1993–2000. https://doi.org/10.1002/elps.201700469.

[23] K. Zhu, M. Pursch, S. Eeltink, G. Desmet, Maximizing Two-Dimensional Liquid Chromatography Peak Capacity for the Separation of Complex Industrial Samples, Journal of Chromatography A. (2019) 460457. https://doi.org/10.1016/j.chroma.2019.460457.

[24] L. Wang, R.K. Marcus, Polypropylene capillary-channeled polymer fiber column as the second dimension in a comprehensive two-dimensional RP × RP analysis of a mixture of intact proteins, Anal Bioanal Chem. 412 (2020) 2963–2979. https://doi.org/10.1007/s00216-020-02539-2.

[25] G. Vanhoenacker, I. Vandenheede, F. David, P. Sandra, K. Sandra, Comprehensive two-dimensional liquid chromatography of therapeutic monoclonal antibody digests, Anal Bioanal Chem. 407 (2015) 355–366. https://doi.org/10.1007/s00216-014-8299-1.

[26] D.R. Stoll, H.R. Lhotka, D.C. Harmes, B. Madigan, J.J. Hsiao, G.O. Staples, High resolution two-dimensional liquid chromatography coupled with mass spectrometry for robust and sensitive characterization of therapeutic antibodies at the peptide level, Journal of Chromatography B. 1134–1135 (2019) 121832. https://doi.org/10.1016/j.jchromb.2019.121832.

[27] M. Russo, F. Cacciola, K. Arena, D. Mangraviti, L. de Gara, P. Dugo, L. Mondello, Characterization of the polyphenolic fraction of pomegranate samples by comprehensive two-dimensional liquid chromatography coupled to mass spectrometry detection, Natural Product Research. 34 (2020) 39–45. https://doi.org/10.1080/14786419.2018.1561690.

[28] K. Arena, F. Cacciola, D. Mangraviti, M. Zoccali, F. Rigano, N. Marino, P. Dugo, L. Mondello, Determination of the polyphenolic fraction of Pistacia vera L. kernel extracts by comprehensive two-dimensional liquid chromatography coupled to mass spectrometry detection, Anal Bioanal Chem. 411 (2019) 4819–4829. https://doi.org/10.1007/s00216-019-01649-w.

[29] P. Donato, F. Rigano, F. Cacciola, M. Schure, S. Farnetti, M. Russo, P. Dugo, L. Mondello, Comprehensive two-dimensional liquid chromatography–tandem mass spectrometry for the simultaneous determination of wine polyphenols and target contaminants, Journal of Chromatography A. 1458 (2016) 54–62. https://doi.org/10.1016/j.chroma.2016.06.042.

[30] B.W.J. Pirok, M.J. den Uijl, G. Moro, S.V.J. Berbers, C.J.M. Croes, M.R. van Bommel, P.J. Schoenmakers, Characterization of Dye Extracts from Historical Cultural-Heritage Objects Using State-of-the-Art Comprehensive Two-Dimensional Liquid Chromatography and Mass Spectrometry with Active Modulation and Optimized Shifting Gradients, Anal Chem. 91 (2019) 3062–3069. https://doi.org/10.1021/acs.analchem.8b05469.

[31] E. Sommella, F. Pagano, E. Salviati, M. Chieppa, A. Bertamino, M. Manfra, M. Sala, E. Novellino, P. Campiglia, Chemical profiling of bioactive constituents in

hop cones and pellets extracts by online comprehensive two-dimensional liquid chromatography with tandem mass spectrometry and direct infusion Fourier transform ion cyclotron resonance mass spectrometry, J. Sep. Sci. 41 (2018) 1548–1557. https://doi.org/10.1002/jssc.201701242.

[32] K. Sandra, G. Vanhoenacker, I. Vandenheede, M. Steenbeke, M. Joseph, P. Sandra, Multiple heart-cutting and comprehensive two-dimensional liquid chromatography hyphenated to mass spectrometry for the characterization of the antibody-drug conjugate ado-trastuzumab emtansine, Journal of Chromatography B. 1032 (2016) 119–130. https://doi.org/10.1016/j.jchromb.2016.04.040.

[33] J.M. Davis, D.R. Stoll, P.W. Carr, Effect of First-Dimension Undersampling on Effective Peak Capacity in Comprehensive Two-Dimensional Separations, Anal. Chem. 80 (2008) 461–473. https://doi.org/10.1021/ac071504j.

[34] A.P. Schellinger, D.R. Stoll, P.W. Carr, High speed gradient elution reversed-phase liquid chromatography, Journal of Chromatography A. 1064 (2005) 143–156. https://doi.org/10.1016/j.chroma.2004.12.017.

[35] A.P. Schellinger, D.R. Stoll, P.W. Carr, High-speed gradient elution reversed-phase liquid chromatography of bases in buffered eluents: Part I. Retention repeatability and column re-equilibration, Journal of Chromatography A. 1192 (2008) 41–53. https://doi.org/10.1016/j.chroma.2008.01.062.

B. Improving the retention space coverage by combining two different separations mechanisms

Article 4: Pushing the limits of resolving power and analysis time in on-line comprehensive hydrophilic interaction x reversed-phase liquid chromatography for the analysis of complex peptide samples

Abstract

In the present work, we have investigated the combination of hydrophilic interaction liquid chromatography (HILIC) and reversed-phase liquid chromatography (RPLC) for the separation of peptides in on-line HILIC x RPLC. This combination usually leads to significant solvent strength mismatch, since a weak solvent in HILIC becomes a strong solvent in RPLC. This may result in band broadening, peak distortion, and breakthrough phenomena. Our focus was directed towards the reduction of band broadening and peak distortion. The conditions of the emergence of breakthrough could be investigated with high-resolution mass spectrometry (HRMS) detection. The importance of both the injection volume and the difference in composition between injection and elution solvents was highlighted. Reported strategies to avoid bad peak shapes mostly rely either on flow splitting to limit the injection volume or on on-line dilution. Here, we propose an alternative approach that consists in injecting large volumes in the second dimension. In this case, no flow-splitting nor dilution prior to the second dimension is required. Our results show that above a certain critical injected volume, depending on both the compound and the elution conditions, narrow and symmetrical peaks can be obtained, despite the persistence of breakthrough. As a result, the injected volume in the second dimension must be larger than the largest critical volume. This counter-intuitive approach was applied for the on-line HILIC x RPLC-UV-HRMS analysis of a complex tryptic digest sample. A peak capacity close to 1500 could be achieved in 30 minutes, which is two-fold higher than in RPLC x RPLC within the same analysis time.

1. Introduction

Protein enzymatic digests can contain hundreds of compounds with a wide range of molecular weights, polarity, and hydrophobicity, which makes their complete separation hardly achievable using conventional one-dimensional liquid chromatography (1D-LC). The performance of LC coupled to mass spectrometry (LC-MS) is most often hindered by matrix effects, arising from co-eluting compounds interfering with ionization efficiency. Despite the unarguable selectivity of MS detection, a high separation power is required in LC to simplify the matrix entering MS.

In the quest for higher peak capacities, on-line comprehensive two-dimensional liquid chromatography (LC x LC) has emerged as an attractive technique to overcome the limitations of 1D-LC. The peak capacity in LC x LC is theoretically expected to be the product of the peak capacities in both dimensions [1]. Actually, the effective peak capacity in on-line LC x LC can be much lower due to the combination of three effects: (i) first dimension (^{1}D) under-sampling, (ii) incomplete coverage of the retention space, and (iii) non-ideal fraction transfer between both dimensions [1–4].

Combining two similar retention mechanisms such as reversed-phase liquid chromatography (RPLC x RPLC) has been shown to be attractive for the separation of peptides [5–9], provided that the mobile phase conditions in both dimensions were well selected (i.e. organic modifiers, additives, pHs, flow rates and/or temperatures). One of the benefits of such an approach is that fairly good peak shapes can be obtained in the second dimension (^{2}D) thanks to the compatibility of the ^{1}D-mobile phase with the ^{2}D-separation. However, because the two dimensions are partially correlated, the peaks usually distribute themselves around the diagonal of the 2D separation space, resulting in a retention space coverage rarely exceeding 60% and hence decreasing the effective peak capacity. The highest reported peak capacity in RPLC x RPLC was found to be close to 5000 in 180 min [6]. That is 3-fold higher than the highest value ever attained in 1D-RPLC (about 1600 in 40 h) [10].

Maximizing the retention space coverage can be achieved by selecting two different chromatographic modes, able to change the selectivity for the compounds of interest. The combination of hydrophilic interaction liquid chromatography (HILIC) and RPLC was proved to be very attractive for the separation of peptides with respect to orthogonality [11]. Their respective mobile phases are fully miscible. However, the

weaker solvent in HILIC being the stronger solvent in RPLC and vice-versa, their coupling usually leads to severe injection effects in ^{2}D, including band broadening, peak distortion, and breakthrough phenomena [7,9,12–14]. This latter is the occurrence of two distinct peaks for the same compound: one, not retained, and one, retained, with most often severe peak fronting. This so-called "solvent strength mismatch" is one of the most cited challenges when combining HILIC and RPLC.

Solvent strength mismatch has a strong impact on the chromatographic performance in ^{2}D, resulting in a dramatic loss of peak capacity and peak intensity. For that reason, the coupling of HILIC and RPLC is often performed in the off-line mode [15–17], which allows evaporating the ^{1}D-collected fractions for further injection in ^{2}D in a weaker solvent. Both dimensions being connected in the on-line mode, the ^{2}D-injection solvent composition cannot be easily controlled, resulting in strong injection solvents in ^{2}D. The combination of HILIC and RPLC for on-line LC x LC has been widely used. Among the large variety of applications, surfactants [18–20], saponins [21] phenolics [22–26], lipids [27], and ginsenosides [13,28,29] can be cited. Most of them were performed with HILIC as first dimension separation. As regards peptide analysis, both on-line RPLC x HILIC [7] and HILIC x RPLC [5,9] were used. If the order in which the two chromatographic modes are connected should not impact the degree of orthogonality, it can play a significant role on 2D-LC performance. The potential advantage in RPLC x HILIC for peptide analysis is that a large volume can be injected in ^{1}D-RPLC without affecting column efficiency, considering the aqueous medium of the digest. In similar conditions, ^{1}D-HILIC should lead to severe injection effects, thereby decreasing both peak capacity and peak intensity. The high content of acetonitrile (ACN) in the ^{2}D-mobile phase is also a clear advantage in RPLC x HILIC since it allows faster ^{2}D-separations and better MS signal intensity. However, a major drawback of ^{2}D-HILIC is the need for long equilibration times [30], reducing the available gradient time in ^{2}D and thus the peak capacity. Furthermore, due to their quadratic retention behaviour in HILIC [7], peptides may be not eluted during the gradient time if this latter is short, as required in ^{2}D.

In view of the above, we focused on on-line HILIC x RPLC for the separation of tryptic digests. Several strategies were proposed to limit the negative impact of the ^{1}D-HILIC mobile phase on the ^{2}D-RPLC separation. They mostly rely either on reducing the ^{2}D injection volume [23,24,31–33] or on using active modulation techniques (on-line

dilution with or without trapping column) to decrease the eluent strength of the ^{1}D-mobile phase before entering the ^{2}D-column [13,14,20,22,26–29,34].

The objective of this work was to propose an easy and alternative way to overcome the deleterious impact of solvent strength mismatch in on-line HILIC x RPLC. In each dimension, the impact of injection conditions on peak shapes was deeply investigated. Special emphasis was put on reducing the negative impact of the ^{1}D-mobile phase on the ^{2}D-separation. An alternative strategy relying on the injection of large volumes of fractions in ^{2}D-RPLC is proposed. The applicability and potential of such an approach are illustrated with the separation of a protein tryptic digest and both ultraviolet (UV) and high-resolution mass spectrometry (HRMS) detections.

2. Experimental section

Table 1: Physical properties of the ten peptide standards used in this study.

#	Peptide name	Molecular weight (g/mol)	Isoelectric point
1	Influenza hemagglutinin (HA)	1102.15	3.5
2	FLAG® peptide	1012.97	3.9
3	WDDHH	708.68	5.2
4	Leucine enkephalin	555.62	6
5	Bombesin	1619.85	7.6
6	[arg8]-Vasopressin	1084.23	8.2
7	[ile]-Angiotensin	897.08	9.4
8	Bradykinin fragment 1-5	572.66	10.6
9	Substance P	1347.63	11.7
10	Bradykinin	1060.21	12.5

2.1. Chemicals and reagents

Acetonitrile (LC-MS grade) was obtained from Sigma-Aldrich (Steinheim, Germany). Water was purified and deionized by an Elga Purelab Classic UV purification system (Veolia water STI, Le Plessis Robinson, France). Formic acid (LC/MS grade), ammonium acetate and ammonium bicarbonate (both analytical reagent grade) were obtained from Fischer scientific (Illkirch, France). DL-1,4-dithiothreitol (DTT, 99%) and iodoacetamide (98%) were obtained from Acros Organics (Geel, Belgium). Trypsin, human serum albumin (HSA), bovine serum albumin (BSA), β-casein, myoglobin, lysozyme, and cytochrome C were all obtained from Sigma-Aldrich (Steinheim, Germany). Influenza hemagglutinin (HA), FLAG® peptide, leucine enkephalin,

bombesin, [arg8]-vasopressin, [ile]-angiotensin, bradykinin fragment 1-5, substance P, and bradykinin were obtained from Merck (Molsheim, France). WDDHH was custom-synthesized (Genecust, Luxembourg). The physical properties of the ten peptide standards are listed in Table 1.

2.2. Sample preparation

A peptide sample was obtained from the tryptic digestion of six proteins (HSA, BSA, β-casein, myoglobin, lysozyme, and cytochrome C) according to a protocol described elsewhere [6]. The concentration in each protein was 4000 mg/L and the protocol led to a tryptic digest containing 196 peptides with an average concentration per peptide of 120 mg/L. Aliquots of the tryptic digest were stored at -20 °C in polypropylene tubes. The samples were thawed and filtered on a 0.22-µm low protein binding PVDF (polyvinylidene fluoride) membrane before injection. To study the impact of the sample solvent on peak shapes in HILIC, the tryptic digest was diluted with acetonitrile (ACN) resulting in samples with different sample solvent compositions: 0:100 (no dilution), 50:50 (2-fold dilution), 75:25 (4-fold dilution), or 90:10 ACN/water (10-fold dilution) (v/v). The composition of the sample solvent for the developed 2D method was 50:50 ACN/water (v/v), resulting in an average concentration per peptides of 60 mg/L.

For the study of injection effects in HILIC, the concentrations of the peptide standards were either 42 mg/L with different solvent compositions, including 0:100, 25:75, 50:50, and 75:25 ACN/water (v/v), or 21, 10.5, and 4.2 mg/L with 50:50, 75:25, and 90:10 ACN/water (v/v), respectively.

For the screening of HILIC columns, the sample solvent for the tryptic digest was 50:50 ACN/water (v/v). Peak widths, peak heights, and peak asymmetries were determined from peptide standards at a concentration of 42 mg/L in 75:25 ACN/H2O (v/v).

For the study of overloading effects in RPLC, peptide #4 (see Table 1) was diluted at a concentration of 16, 80 or 160 mg/L in 30:70 water/ACN (v/v). The study of injection effects in RPLC was performed with both peptide #4 and peptide #6 diluted at a concentration of 50 mg/L in 90:10, 70:30, 50:50, 30:70, and 10:90 water/ACN (v/v). For the linearity study in RPLC, peptide #4 was diluted at different concentrations ranging from 5 to 500 mg/L in 30:70 water/ACN (v/v). The peptide standard solutions were all stored at -20 °C and used within a week after thawing.

Table 2: Comparative results and specific operating conditions for the 10 studied stationary phases in HILIC.

#	**Column name** (column dimensions)	Provider (location)	Stationary phase	Flow rate (mL/min)	Gradient time[a] (min)	n_{exp}/n_{th}	Peak asymmetry	Number of peaks[b]	Elution window[c] (% B)	Derringer function
1	**Hypersil HILIC** (50 mm x 4.6 mm, 3.0 µm)	Thermo Fischer Scientific (Cheshire, UK)	Bare silica (P)	1.6	7.2	0.75	1.40	33	38	0.78
2	**Acquity BEH HILIC** (50 mm x 2.1 mm, 1.7 µm)	Waters (Milford, MA, USA)	Bare silica (H, P)	0.6	4	0.62	1.38	46	42	0.93
3	**Acquity BEH Amide** (50 mm x 2.1 mm, 1.7 µm)	Waters (Milford, MA, USA)	Amide (H, P)	0.6	4	0.38	1.74	40	39	0.69
4	**Hypersil gold HILIC** (50 mm x 2.1 mm, 1.9 µm)	Thermo Fischer Scientific (Cheshire, UK)	Bare silica (P)	0.5	4.8	0.37	2.15	26	36	0.46
5	**Nucleodur HILIC** (60 mm x 1.0 mm, 3.0 µm)	Macherey-Nagel (Duren, Germany)	Zwitterionic (P)	0.08	8.2	0.19	3.49	25	30	0.00
6	**Kinetex HILIC** (50 mm x 2.1 mm, 1.7 µm)	Phenomenex (Torrence, CA, USA)	Bare silica (SP)	0.6	2.9	0.37	1.29	38	30	0.61
7	**Nucleoshell HILIC** (100 mm x 2.0 mm, 2.7 µm)	Macherey-Nagel (Duren, Germany)	Zwitterionic (SP)	0.3	10.4	0.32	1.24	34	34	0.59
8	**Accucore HILIC** (100 mm x 2.1 mm, 2.6 µm)	Thermo fischer Scientific (Cheshire, UK)	Bare silica (SP)	0.4	8.6	0.38	1.13	40	30	0.64
9	**Luna NH_2** (150 mm x 2.0 mm, 3.0 µm)	Phenomenex (Torrence, CA, USA)	NH_2 (P)	0.3	22	0.41	1.22	29	33	0.56
10	**Cortecs HILIC** (50 mm x 2.1 mm, 1.6 µm)	Waters (Milford, MA, USA)	Bare silica (SP)	0.6	2.9	0.42	2.01	42	32	0.63

P: Totally porous particles.

SP: Superficially porous particles.

H: hybrid silica.

n_{exp}: experimental peak capacity calculated according to Eq.5 (see Table S1).

n_{th}: theoretical peak capacity calculated according to Eq.6 (See Table S1).

[a] Gradient elution: 2-42% B in 20 t_0, 42% during 5 t_0, 42-2% in 1 t_0, and 2% during 10 t_0.

[b] Number of peaks observed in tryptic digest sample.

[c] Calculated from retention time of last and first eluted compound in tryptic digest sample.

2.3. Columns

The characteristics of the ten columns evaluated in HILIC are summarized in Table 2. Three columns were used in RPLC: Kinetex C18 (30 mm x 2.1 mm, 1.3 µm) from Phenomenex (Torrence, CA, USA), Acquity CSH C18 (30 mm x 2.1 mm, 1.7 µm) from Waters (Milford, MA, USA), and Ascentis express C18 (50 mm x 2.1 mm, 2.7 µm) from Sigma-Aldrich (Saint-Louis, MO, USA).

2.4. Instrumentation

For studies in 1D-LC, experiments were carried out with an Acquity UPLC I-Class liquid chromatography system (Waters, Milford, MA, USA). The instrument includes a high-pressure binary solvent delivery pump, a sample manager with a flow-through needle injector of 15 µL equipped with an additional extension loop of 100 µL, a column manager equipped with a column oven with a maximum temperature of 90°C, and a photodiode-array detector (PDA) equipped with a 0.5-µL flow-cell withstanding pressures up to 70 bar. The dwell volume and extra-column volume for this entire system were measured using a zero-dead volume union connector in place of the column and were respectively 110 µL and 12 µL (without extension loop). The 1D-LC system was hyphenated to a Waters Acquity QDa mass spectrometer, used in scan mode and single ion recording (SIR) mode. A T-connection was placed right after the column to decrease the flow rate entering the mass spectrometer by half (split 1:1) when the flow rate was 1.5 mL/min. Data acquisition and instrument control were performed using Waters MassLynx software.

On-line LC x LC experiments were carried out using an Infinity 1290 2D-LC system (Agilent Technologies, Waldbronn, Germany). The instrument includes two high-pressure binary solvent delivery pumps, an autosampler with a flow-through needle of 20 µL, two thermostated column compartments with a maximum temperature of 100°C equipped with low-dispersion preheaters, and two diode-array detectors (DAD) equipped with 0.6-µL flow-cells. The interface connecting the two dimensions consisted of a 2-position /4-port duo valve, equipped with two identical 20-µL or 40-µL loops, depending on the transferred volume. To minimize dispersion, the valve was configured in back-flush injection mode. A pressure release kit placed between the ^{1}D-outlet and the interface was used to minimize the pressure downstream induced by the switch of the 2D-LC valve to protect the ^{1}DAD flow-cell and to avoid artefacts in the

^{1}DAD signal. The measured dwell volumes and extra-column volumes of this 2D-LC system were respectively 170 µL and 22 µL in ^{1}D, and 80 µL and 8.5 µL in ^{2}D (loop volumes at the interface excluded). The 2D-LC system was hyphenated to an Agilent G6545B Q-TOF mass spectrometer, equipped with a JetStream electrospray ionization (ESI) source. Data acquisition and instrument control were performed using Agilent OpenLab software for 2D-LC and MassHunter software for MS.

MS data processing was performed using Agilent MassHunter qualitative analysis software. LC x LC data were processed using an in-house script developed on Matlab.

2.5. Chromatographic and detection conditions

2.5.1. 1D-HILIC conditions

Optimization of the injection conditions in HILIC was performed on the Acquity BEH Amide column (50 mm x 2.1 mm, 1.7 µm). The mobile phase was composed of ACN as solvent A and water with 10 mM ammonium acetate (pH = 6.8) as solvent B. The aqueous eluent prepared with salts was filtered on a 0.22-µm nylon filter before use. The gradient elution was as follows: from 2% to 60% B in 29 t_0 (with t_0, the column dead time calculated according to Eq.3), from 60% to 2% B in 1 t_0, and 2% B during 10 t_0. The different injection volumes were about 1%, 2%, 5%, and 10% V_0 (with V_0, the column dead volume calculated according to Eq.4).

The comparison of columns in HILIC was performed with the ten columns listed in Table 2 and the following gradient elution: from 2% to 42% B in 20 t_0, 42% during 5 t_0, from 42% to 2% in 1 t_0, and 2% during 10 t_0. The flow rates for column #2 was set at 0.6 mL/min, and other flow rates were calculated according to Eq.1. The column temperature was set to 30°C and the injected volume represented either 0.5% V_0 (for the peptide standards) or 5% V_0 (for the tryptic digest).

UV absorbance data were collected at 210 nm with an acquisition rate of 20 Hz. MS data were acquired from m/z 100 to m/z 1250 in negative electrospray ionization mode (ESI-) at an acquisition rate of 10 Hz. The cone voltage was set to 15 V and the capillary voltage to 0.8 kV. The source and the probe temperature were set at 125°C and 600°C, respectively.

Table 3: Experimental conditions for on-line HILIC x RPLC and RPLC x RPLC separations shown in Fig. 11a and Fig.11b.

	HILIC x RPLC	**RPLC x RPLC**
First dimension (^{1}D)		
Injection volume	6 µL	10 µL
Injection solvent	50/50 ACN/water (v/v)	0:100 ACN/water (v/v)
Stationary phase	Acquity BEH HILIC	Ascentis express C18
Column geometry	(50 mm x 2.1 mm. 1.7 µm)	(50 mm x 2.1 mm. 2.7 µm)
Temperature	30 °C	30 °C
Mobile phase	A: ACN B: 10 mM ammonium acetate in water	A: 10 mM ammonium acetate in water B: ACN
Flow rate	0.05 mL/min	0.04 mL/min
Gradient	2-52% B in 30 min	1-34% B in 30 min
Post-column split	No split for optimized method (1:1 or 1:3 for other methods)	1:2
Modulation		
Loop size	40 µL	20 µL
Sampling time	0.39 min	0.27 min
Second dimension (^{2}D)		
Stationary phase	Acquity CSH C18	Acquity CSH C18
Column geometry	(30 mm x 2.1 mm. 1.7 µm)	(30 mm x 2.1 mm. 1.7 µm)
Temperature	80 °C	80 °C
Mobile phase	A: 0.1% formic acid in water B: 0.1% formic acid in ACN	A: 0.1% formic acid in water B: 0.1% formic acid in ACN
Flow rate	2 mL/min	2 mL/min
Gradient	1-45% B in 0.26 min	1-45% B in 0.13 min
Post-column split	1:2	1:2
HRMS detection		
Ionization mode	ESI positive	
Mass range	100-3200 Da	
Scan rate	20 spectra/s	
Gas temp	300 °C	
Drying gas	11 L/min	
Nebulizer	40 psi	
Sheath gas	350 °C	
Sheath gas flow	11 L/min	
Capillary voltage	3500 V	
Nozzle voltage	300 V	
Fragmentor	150 V	
Skimmer	20 V	
Oct 1 Rf Vpp	750 V	

2.5.2. 1D-RPLC conditions

Kinetex C18 (30 mm x 2.1 mm, 1.3 µm) and Acquity CSH C18 (30 mm x 2.1 mm, 1.3 µm) columns were compared. The mobile phase was composed of water with 0.1% formic acid as solvent A, and ACN with 0.1% formic acid as solvent B (pH = 2.7). The gradient elution was as follows: from 1% to 45% B in either 44 or 5.5 t_0, from 45% to 1% B in 1 t_0, and 1% B during 5 t_0. The flow rate was 1.5 mL/min, and the column temperature was either set to 90°C for the Kinetex column or 80°C for the Acquity CSH column. The different injection volumes were about 1%, 2%, or 6% V_0.

Optimization of the injection conditions in RPLC was performed with the same conditions, but with a gradient ranging from 1% to 45% B in 11.3 t_0. Different volumes ranging from 0.5% to 100% V_0 were injected. UV absorbance data were collected at 210 nm with an acquisition rate of 40 Hz. The effluent from the column was split 1:1 prior to the mass spectrometer using a simple T-connection. MS data acquisition conditions were the same as for 1D-HILIC but in positive electrospray ionization (ESI+) mode. The masses of the standards of peptide #4 and #6 were monitored in selected ion recording (SIR) mode with m/z 556.6 for peptide #4 and m/z 543.1 for peptide #6.

2.5.3. On-line LC x LC conditions

In HILIC x RPLC, ^{1}D was performed using an Acquity BEH HILIC column (50 mm x 2.1 mm, 1.7 µm). The injected volume was 6 µL (5% V_0). The mobile phase was the same as for 1D-HILIC and the gradient was: 0 min (2% B), 30 min (52% B), 32.4 min (2% B), and 50 min (2% B). The flow rate was 0.05 mL/min and the column temperature was 30°C. ^{2}D was performed using an Acquity CSH C18 column (30 mm x 2.1 mm, 1.7 µm). The mobile phase was the same as for 1D-RPLC, and the gradient was: 0 min (1% B), 0.26 min (45% B), 0.29 min (1% B), and 0.39 min (1% B). The flow rate was 2 mL/min and the column temperature was 80°C. The sampling time was 0.39 min, leading to an injection volume of 19.5 µL (27 % V_0) in ^{2}D. In two other comparative 2D experiments, the effluent from ^{1}D was split 1:1 or 1:3 with a T-piece, leading to injection volumes of 9.8 µL (14 % V_0), or 4.9 µL (7% V_0), respectively.

In RPLC x RPLC, ^{1}D was performed using an Ascentis Express C18 column (50 mm x 2.1 mm, 2.7 µm). The injected volume was 10 µL (12% V_0). The mobile phase was the same as for 1D-HILIC and the gradient was: 0 min (1% B), 30 min (34% B), 32.2 min (1% B), and 45 min (1% B). The flow rate was 0.04 mL/min and the column temperature

was 30°C. ^{2}D-conditions were similar as in HILIC x RPLC, with the following gradient: 0 min (1% B), 0.13 min (45% B), 0.16 min (1% B), and 0.27 min (1% B). The sampling time was 0.27 min and a split 1:2 led to an injection volume of 3.6 µL (5 % V_0) in ^{2}D. LC x LC parameters were optimized with an in-house 2D prediction tool based on a Pareto-optimality approach described by Sarrut et al [6].

For both experiments, the effluent from the ^{2}D-column was split between MS and UV (1:2) using a T-connection. UV absorbance data were collected at 210 nm with acquisition rates of 20 Hz and 80 Hz in ^{1}D and ^{2}D, respectively. Q-TOF-HRMS data were acquired in positive ion mode from m/z 100 to m/z 3200 at an acquisition rate of 20 spectra/s. The drying gas temperature and flow rate were 300°C and 11 L/min, respectively. The nebulizer gas pressure was 40 psi. The sheath gas temperature and flow rate were 350°C and 11 L/min, respectively. The capillary, the nozzle, the fragmentor, the skimmer, and the Oct 1 RV voltages were 3500, 300, 150, 20, and 750 V, respectively. The conditions of the 2D separations are recapitulated in Table 3.

2.5.4. Calculations

The flow rate in HILIC for column #2 (see Table 2) was set at 0.6 mL/min. Other flow rates were selected according to the following transfer rule:

$$F_n = F_2 \left(\frac{d_{i,n}}{d_{i,2}}\right)^2 \times \left(\frac{d_{p,2}}{d_{p,n}}\right) \qquad \textit{(Eq. 1)}$$

F_2, $d_{i,2}$, *and* $d_{p,2}$ are the flow rate, the inner diameter, and the particle diameter of column #2, respectively. F_n, $d_{i,n}$, and $d_{p,n}$ are those of a given column #n.

The composition at elution, C_e, was calculated according to:

$$C_e = C_i + \frac{C_f - C_i}{t_G} \times (t_r - t_0 - t_D) \qquad \textit{(Eq. 2)}$$

C_i and C_f are the initial and final composition of strong solvent (%B). t_G, t_r, t_0, and t_d are the gradient time, the retention time of the compound, the column dead time, and the instrument dwell time, respectively.

The column dead time (t_0) was calculated according to:

$$t_0 = \frac{V_0}{F} \qquad \textit{(Eq. 3)}$$

V_0 is the column dead volume, estimated by:

$$V_0 = \frac{\pi L d_i^2 \varepsilon}{4} \quad \textit{(Eq .4)}$$

L, d_i, and ε are respectively the column length, the column inner diameter, and the total column porosity (estimated as 0.5 for superficially porous, and 0.7 for totally porous particles).

Experimental peak capacities for 1D-LC separations and for each dimension in LC x LC were calculated according to:

$$n_{exp} = 1 + \frac{t_n - t_1}{w_{4\sigma}} \quad \textit{(Eq. 5)}$$

t_n and t_1 are the retention times of the last and first eluted compound, respectively, and $w_{4\sigma}$ is the average peak width at 4σ (i.e. 13.4% of peak height).

Theoretical peak capacities in HILIC were predicted according to the Linear Strength solvent (LSS) theory [35] with the following equation:

$$n_{1D,th} = 1 + \frac{2.3S \times \Delta C_e}{2.3b + 1} \times \frac{\sqrt{N}}{4} \quad \textit{(Eq. 6)}$$

N is the column plate number, estimated by:

$$N = \frac{L}{3d_p} \quad \textit{(Eq. 7)}$$

S is the average value of the slope of the relationship between the logarithm of the retention factor k and the solvent composition C *(%)* ($\log(k) = \log(k_0) - S \times C$). An average S value of 0.06 was used for calculations in HILIC based on previous studies [8]. k_0, ΔC_e, b, and L are the retention factor in the weaker solvent, the range of composition at elution, the gradient steepness ($b = S\Delta C t_0 / t_G$, with ΔC, the gradient composition range), and the column length, respectively.

Effective experimental peak capacities in on-line LC x LC were calculated according to:

$$n_{2D,effective} = \alpha \times \gamma \times {}^1n_{exp} \times {}^2n_{exp} \quad \textit{(Eq. 8)}$$

$^1n_{exp}$ and $^2n_{exp}$ are the experimental peak capacities (Eq. 5) in ^{1}D and ^{2}D, respectively. α is a correction factor taking into account under-sampling in ^{1}D and calculated according to [36]:

$$\alpha = \frac{1}{\sqrt{1 + 0.21\left({}^{6}/_{\tau}\right)^2}} \qquad \textit{(Eq. 9)}$$

τ is the sampling rate (i.e. number of fractions per 6σ-^{1}D-peak), and γ is a correction factor that takes into account the retention space coverage of the 2D separation. The evaluation of γ was made using a method described elsewhere [8].

3. Results and discussion

3.1. Preliminary search for optimum conditions in each dimension

A separation in 2D-LC is the combination of two 1D-LC experiments. As part of method development, each separation was first individually optimized. The nature of the stationary phase, the mobile phase conditions, and the injection conditions (i.e. injection solvent and injection volume) were deeply investigated to find the best trade-off between high peak capacity, high peak intensity, and short analysis time. In our context of complex sample analysis, special emphasis was put on improving the kinetic performance of the separation (i.e. peak shape, peak width and peak asymmetry) in both dimensions, to maximize the overall separation power. This first part details the choices that were made in each dimension, with respect to the chromatographic conditions, before developing on-line HILIC x RPLC.

3.1.1. Optimization of injection conditions in HILIC

HILIC mobile phases contain a high percentage of ACN (generally 98 to 50%) and a low percentage of water (2 to 50%). Numerous papers showed the negative impact of an injection solvent too rich in water on HILIC separation [37–39]. It is therefore recommended to minimize as much as possible the amount of water in the injection solvent to maintain proper peak shapes in HILIC. For example, significant band broadening and peak distortion were reported for peptides in the range 1000 to 6000 Da when the water content exceeded 10% (v/v) with injection volumes as low as 1.5% V_0 [39]. The tryptic digest being prepared in water, we investigated the impact of both injection solvent and injection volume on peak shape. The study was carried out in

gradient elution with an Acquity BEH amide column. Injection effects were evaluated from ten representative peptides (see Table 1), individually injected. The injection solvent composition was in the range 0:100 to 75:25 ACN/H2O (v/v) and the injection volumes were in the range 1% to 10% V_0.

Fig. 1 illustrates the impact of the injection solvent on the peak shape of peptide #4 (Fig. 1a) and peptide #8 (Fig. 1b), eluted at two different compositions, 13% and 25% water, respectively. As expected, the peak shape got worse when the percentage of water in the injection solvent increased. For peptide #4, symmetrical peaks were obtained up to 50% water. Peak broadening and peak splitting were observed beyond in spite of an injected volume as low as 1% V_0. Appropriate peak shapes were obtained for a more retained peptide (i.e. #8) with injected volume up to 10% V_0 and 50% water in the injection solvent (Fig. 1b).

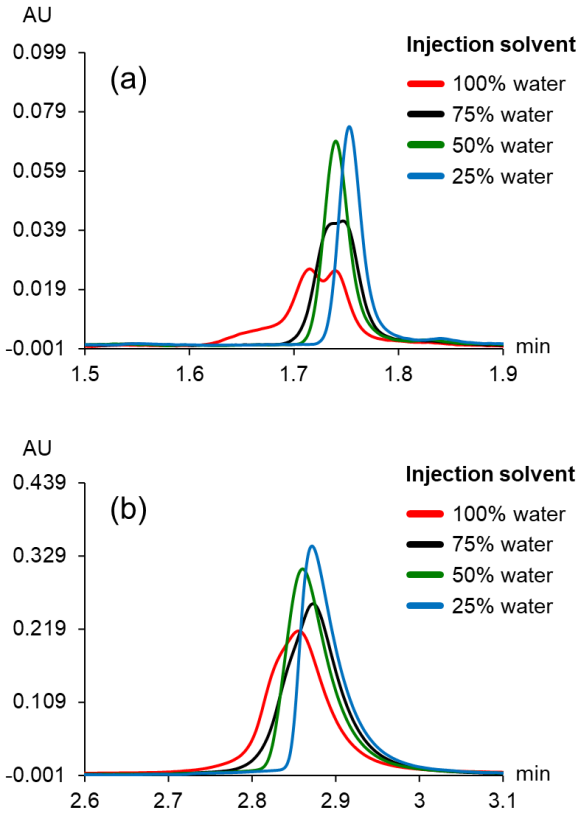

Fig. 1: Influence of the injection solvent on the peak shape of two peptides in HILIC: (a) peptide #4 with 1.2 µL (1% V_0) injected, and (b) peptide #8 with 12 µL (10% V_0) injected, both at a concentration of 42 mg/L. Injection solvent compositions: 0:100 (red), 25:75 (black), 50:50 (green) or 75:25 (blue) ACN/water (v/v). Acquity BEH Amide (50 mm x 2.1 mm, 1.7 µm) column, 30 °C, 0.6 mL/min, A: ACN and B: 10 mM ammonium acetate in water, 2–60% B in 29 t_0. UV detection at 210 nm.

This is in good agreement with a previous study, showing that early eluted compounds are more affected than later eluted ones [39]. It is therefore of prime importance to decrease the water content of the injection solvent. The tryptic digestion being prepared in water, reducing the water content leads to sample dilution. Fig. 2 shows the chromatograms of peptide #4 (Fig. 2a) and peptide #8 (Fig. 2b), obtained with no dilution, 2-fold, 4-fold, and 10-fold dilution with ACN (i.e. 0%, 50%, 75%, and 90% ACN) while maintaining the same amount of peptide by varying the injection volume (1%, 2%, 4%, and 10% V_0).

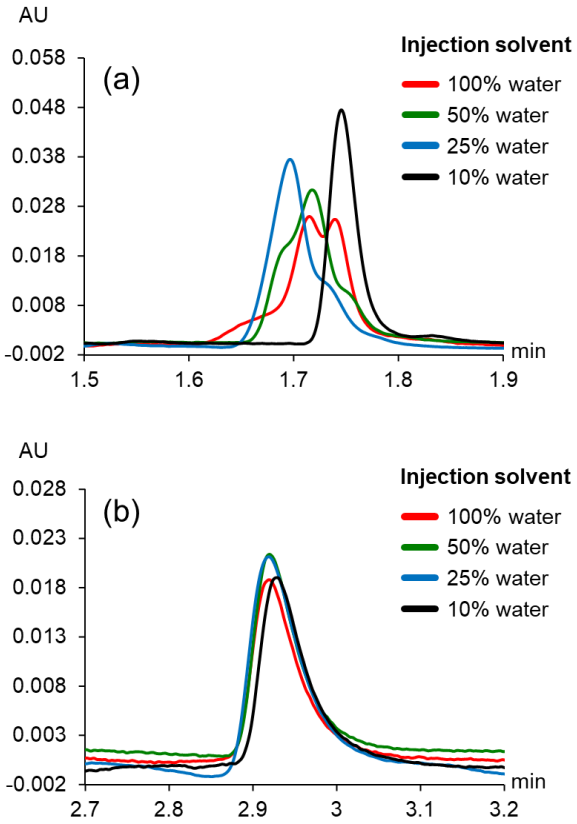

Fig. 2: Comparison of peak shapes of (a) peptide #4 and (b) peptide #8 obtained in HILIC by injecting a constant amount of peptides with different injection volumes and different injection solvents resulting in different dilution with ACN: 1.2 µL (1% V_0) in 0:100 ACN/water (42 mg/L, no dilution) (red), 2.4 µL (2% V_0) in 50:50 ACN/water (21 mg/L, 2-fold dilution) (green), 4.8µL (4% V_0) in 75:25 ACN/water (10.5 mg/L, 4-fold dilution) (blue), and 12µL (10% V_0) in 90:10 ACN/water (4.2 mg/L, 10-fold dilution) (black). Other conditions as in Fig. 1.

As can be observed, the peak shape of the least retained peptide (Fig. 2a) gets better and better by increasing dilution. A symmetrical peak could be obtained up to a 10-fold dilution despite the corresponding large injection volume (10% V_0). However, for the most retained peptide (Fig. 2b), the dilution appears to be useless since the peak

shape is kept identical without and with any dilution. For the ten studied peptides, the peak areas did not vary with dilution, suggesting that they were fully soluble up to 90% ACN (10-fold dilution). However, it was not the case for the tryptic digest (Fig.3). The peak intensities were drastically reduced with 90% ACN which can be ascribed to a decrease in the peptide solubility and hence to partial sample precipitation, as also shown for hydrophilic compounds in ACN-rich solvents [39]. It should be also noted in Fig.3 that peak intensities are lower with no dilution (100% water) than with 2-fold dilution (50% water), which can be explained by the occurrence of a breakthrough phenomenon.

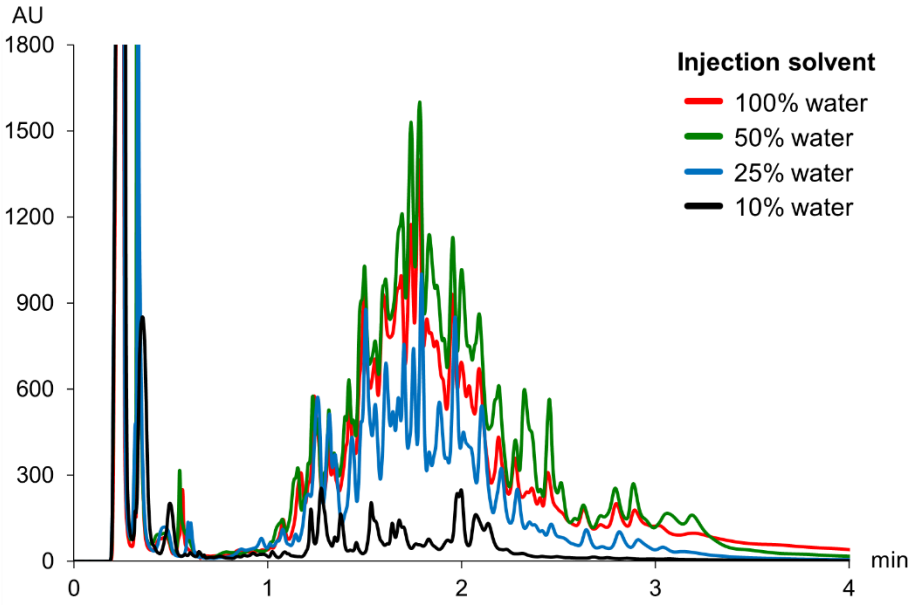

Fig. 3: Overlaid HILIC separations of a constant amount of protein tryptic digest with different injection volumes and different injection solvents resulting in different dilution with ACN: 2 µL (1.7% V_0) in 0:100 ACN/water (no dilution) (red), 4 µL (3.3% V_0) in 50:50 ACN/water (2-fold dilution) (green), 8 µL (6.6% V_0) in 75:25 ACN/water (4-fold dilution) (blue), and 20 µL (16% V_0) in 90:10 ACN/water (10-fold dilution) (black). Column Acquity BEH HILIC (50 mm x 2.1 mm, 1.7 µm), 30 °C, 0.5 mL/min, A: ACN, B: 10 mM ammonium acetate in water, 13–52% B in 9.7 t_0. UV detection at 210 nm.

Alternative solvents such as methanol, ethanol, or isopropanol were also used to dilute the sample as suggested for peak shape improvement [39]. However replacing acetonitrile with these solvents also led to sample precipitation beyond 50% organic solvent. The use of a sandwich injection, as reported for the HILIC separation of very large proteins [14], was also investigated. Various ratios of ACN/sample and ACN/sample/ACN were evaluated. However, no improvement in peak shape could be observed. In light of the above results, a 2-fold sample dilution (50% ACN) with an

injection volume of 6 µL (5% V_0) were selected for the rest of the study. Under such conditions, satisfactory peak shapes could be obtained for most eluted peptides.

Considering the obtained separation (Fig. 3), the elution range for peptides was found to be 13% to 52% water. Still, the initial composition was set at 2% water to promote the dilution of the water-rich injection plug (50%) with the ACN-rich gradient starting conditions (98%). With such an approach, the peak shapes could be significantly improved for early eluted compounds compared to a gradient starting from 13% water (see Fig. S1).

3.1.2. Selection of the stationary phase in HILIC

The mobile phase was composed of ACN as solvent A and ammonium acetate (10 mM dissolved in water) as solvent B, according to previous studies on the separation of peptides in HILIC [7,8]. Ten different stationary phases were evaluated. The related phase chemistries include bare silica, hybrid silica, NH_2-bonded silica, charged silica, and zwitterionic-bonded silica. Their characteristics and specific operating conditions are listed in Table 2. A generic method involving a linear gradient elution from 2% to 42% B in 20 t_0 (followed by an isocratic hold during 5 t_0 to ensure complete elution) was used. Column performance was evaluated by injecting a tryptic digest composed of six proteins diluted in 50:50 ACN/water (5% V_0 injected) and ten individual peptide standards (Table 1) diluted in 75:25 ACN/water (0.5% V_0 injected). Such injection conditions for the peptides aimed at preventing any injection effect according to the above discussion.

The obtained separations for the tryptic digest are shown in Fig. 4. The separations for the peptides are given in Fig. S2. Significant differences can be observed in Fig. 4 between columns with different chemistry (e.g. #1, #3, #5, and #9), but also between bare silica columns coming from different providers (e.g. #2 and #4), or even from the same provider (e.g. #1 and #4). The most striking difference between columns concerns column #4 (bare silica) as opposed to other bare silica columns (#1, #2, #6, #8 or #10). It is also worth noting the marked differences between the zwitterionic columns #5 (bad separation) and #7 (fairly good separation). In contrast, the separations obtained on superficially porous bare silica phases (#6, #8, and #10) are quite similar. Concerning the peptide samples, some significant differences were observed for both the peak shapes and the retention orders between columns (Fig. S2). Four quality descriptors, including peak capacity, peak asymmetry, number of observed peaks, and

elution window (% B) were used to assess the column performances. The first two were measured from the separations of the peptide samples, whereas the last two, from the separations of the tryptic digest (Fig.4). The resulting values are summarized in Table 2.

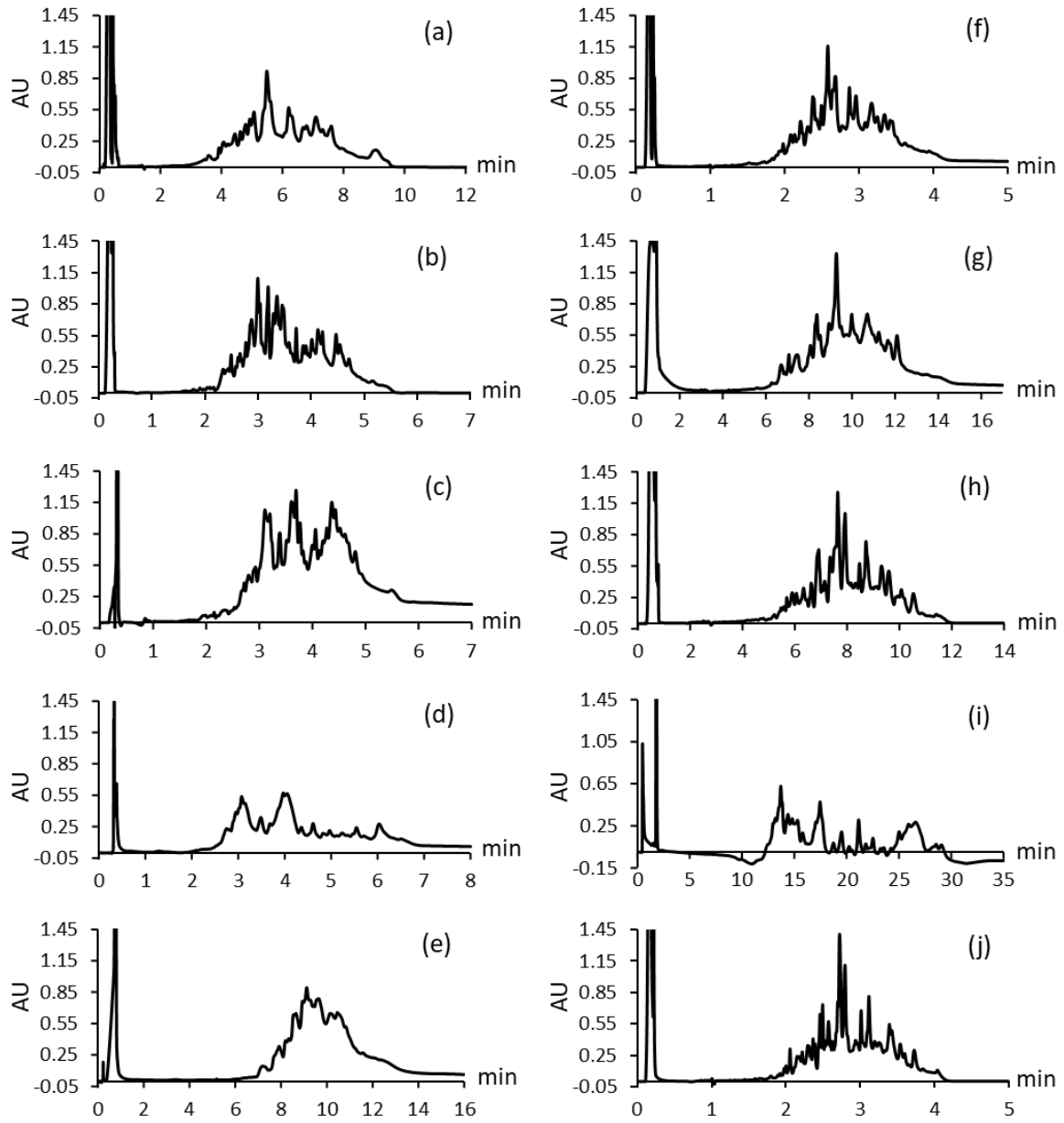

Fig. 4: Separations of a tryptic digest of six proteins in HILIC with ten different stationary phases: (a) Hypersil HILIC (#1 in Table 2), (b) Acquity BEH HILIC (#2), (c) Acquity amide (#3), (d) Hypersil Gold HILIC (#4), (e) Nucleodur HILIC (#5), (f) Kinetex HILIC (#6), (g) Nucleoshell HILIC (#7), (h) Accucore HILIC (#8), (i) Luna NH2 (#9), and (j) Cortecs HILIC (#10). 5% V_0 injected in 50:50 ACN/water (v/v) (2-fold dilution). Column characteristics, associated flow rates, and gradient times are listed in Table 2. Other conditions are given in experimental section.

The peak capacity, which is a key quality descriptor for complex sample analysis, was measured by considering the average 4σ-peak width of three well-distributed peptides (i.e. #1, #4, and #7) and the elution window (Eq.2). For a fair comparison, the peak capacity is here given as the ratio of the experimental (Eq.5) to the theoretical value (Eq.6). The highest values (> 0.6) were found for two bare silica columns (#1 and #2), whereas the lowest ones (< 0.35) for the two zwitterionic columns (#5 and #7). No particular correlation between the phase chemistry and the elution window or the peak asymmetry could be found. The final selection was made by the calculation of a desirability function [40], corresponding to the geometric mean of the four quality descriptors transformed into four functions varying from 0 to 1 (see Table S2 and Fig. S3). According to the resulting values (Table 2), columns #1 and #2 are the most suitable ones for peptides, whereas columns #5 and #6 are the least advantageous ones. The best columns (#1 and #2) are both made of bare silica. With a view to keeping the analysis time as short as possible, the Acquity BEH HILIC column (#2) was selected for ^{1}D-HILIC.

3.1.3. Selection of the stationary phase in RPLC

The choice of water, ACN, and formic acid (0.1%) in RPLC was supported by our previous studies on peptides [7,8]. Due to the need for very fast separations in ^{2}D in on-line LC x LC [2], HT-UHPLC (high-temperature-ultra-high performance liquid chromatography) conditions were selected, with both temperature and flow rate set at the maximum authorized values. For the same reasons, ACN was preferred to methanol due to its lower viscosity. Formic acid was selected for two main reasons: (i) acidic pH is highly recommended at high temperature to prevent column degradation and (ii) this additive is much better than TFA (trifluoroacetic acid) for MS detection, although less attractive from a separation point of view. In fact, due to the resulting low ionic strength of the mobile phase, formic acid (0.1%) may lead to overloading effects with charged compounds [41,42], leading to peak distortion and hence to poor LC x RPLC performance[7].

To achieve ultra-fast separations in ^{2}D, a short column packed with very small particles was first considered. The Kinetex C18 column (30 mm x 2.1 mm, 1.3 μm) was very attractive considering its low particle size (1.3 μm) and its successful use for the separation of peptides in on-line RPLC x RPLC [6]. However, in the present study, we found significant overloading effects under certain conditions. Those are highlighted

in Fig. 5, showing overlaid peaks of peptide #4 obtained with different injection volumes (0.5 to 3 µL corresponding to 1% to 6% V_0) and two different peptide concentrations: 16 mg/L (Fig.5a) and 80 mg/L (Fig.5b). By increasing the peptide concentration and/or the injected volume while keeping the same gradient time (5.5 t_0), the peak distortion increases with the occurrence of a triangular peak shape. The peak distortion further increases with the gradient time (44 t_0) in Fig. 6a, which is in good agreement with previous results [7].

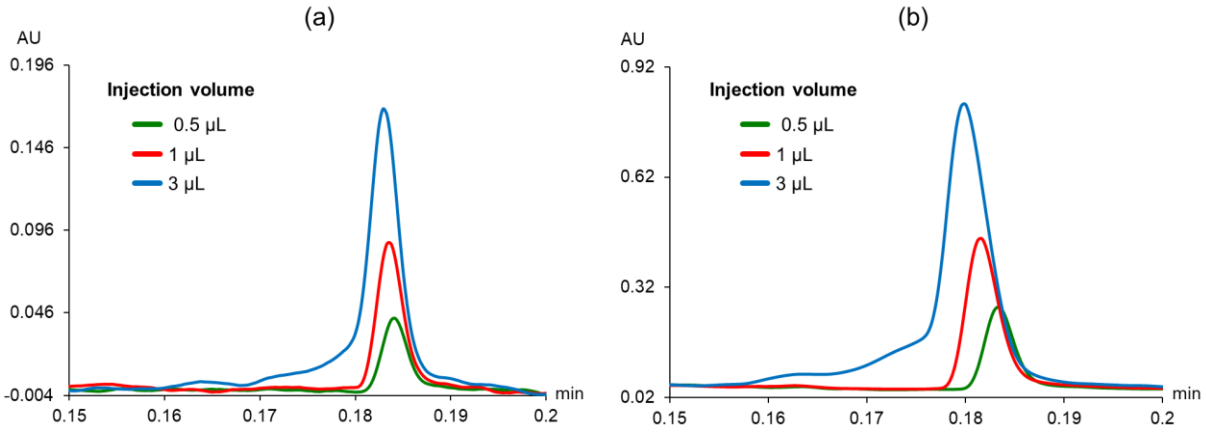

Fig. 5: Overlaid peaks of peptide #4 obtained in RPLC with different injection volumes (0.5, 1, and 3 µL) emphasizing the impact of solute concentration: (a) 16 mg/L vs. (b) 80 mg/L, both in 30:70 water/ACN (v/v). Kinetex C18 (30 mm x 2.1 mm, 1.3 µm) column, A: water with formic acid (0.1%), B: ACN with formic acid (0.1%), 1–45% B in 5.5 t_0. Other conditions given in the experimental section.

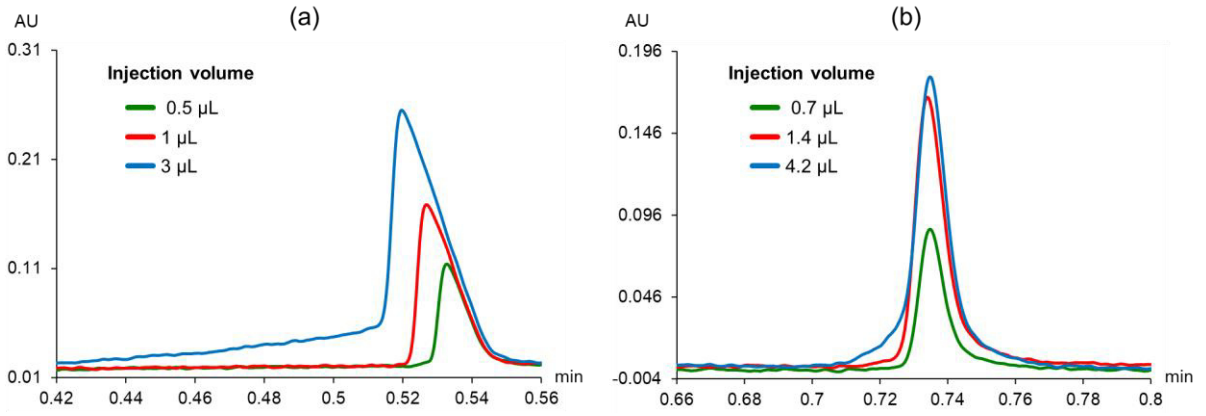

Fig. 6: Overlaid peaks of peptide #4 (80 mg/L in 30:70 water/ACN (v/v)) obtained in RPLC with different injection volumes (1%, 2%, and 6% V_0) emphasizing the impact of the nature of the stationary phase: (a) Kinetex C18 (30 mm x 2.1 mm, 1.3 µm), and (b) Acquity CSH C18 (30 mm x 2.1 mm, 1.7 µm), 1–45% B in 44 t_0. Other conditions as in Fig. 5.

In the present study, the impact of the injection volume in addition to the peptide concentration is also clearly highlighted in Fig. 6a by a gradual shift of the peak apex towards lower retention times. Such overloading effects severely reduce the peak capacity in ^{2}D-RPLC. Furthermore, the retention shift, which depends on the solute concentration and hence on the peak fraction in ^{1}D, makes 2D data very difficult to process [7]. We therefore evaluated an Acquity CSH C18 column (30 x 2.1 mm, 1.7 µm). This stationary phase contains positive charges on the silica surface which are designed to reduce the overloading effects of basic compounds in acidic media. The resulting overlaid peaks are shown in Fig. 6b and can be compared to those in Fig.6a, obtained with the Kinetex C18 column in the same conditions. As can be observed, the peak shapes are markedly improved with the Acquity CSH C18 column. When increasing concentrations up to 160 mg/L and injection volumes up to 18% V_0, the peak was still kept symmetrical (see Fig. S4), making Acquity CSH C18 much more attractive for ^{2}D-RPLC than Kinetex C18 despite larger particles (1.7 µm vs 1.3 µm). The fact that the peak area did not increase between 2% V_0 and 6% V_0 results from a breakthrough phenomenon which will be extensively discussed in the next section.

3.1.4. Optimization of injection conditions in RPLC

As underlined in Section 3.1.1, the nature of the injection solvent and the injected volume are two critical parameters in LC since they may strongly affect the peak shape and thus the chromatographic performances. As a rule, it is usually recommended to match the injection solvent with the initial mobile phase in gradient elution to promote on-column focusing. However, unlike in ^{1}D, the injection solvent cannot be controlled in ^{2}D since both dimensions are connected. For peptides, whereas some combinations such as RPLC x RPLC [6,43] or SCX x RPLC [9] are fairly compatible, others may suffer from solvent strength mismatch between both dimensions. In that way, the injection in ^{2}D-RPLC of an ACN-rich solvent coming from ^{1}D-HILIC can lead to band broadening, peak distortion, and sometimes breakthrough phenomena. That makes the combination of HILIC and RPLC very challenging. Usual strategies to limit injection effects in on-line HILIC x RPLC rely either on the reduction of the injection volumes or on the use of active modulation techniques (i.e. on-line dilution with or without trapping columns). The advantages and limits of these strategies will be discussed in detail in a future study.

In the present work, we conducted a deep investigation on the impact of both the injection solvent and the injection volume on the peak shape of peptides in RPLC. The focus was directed towards finding the easiest and the most efficient way to reduce band broadening and peak distortion in RPLC when injecting very strong solvents such as those coming from ^{1}D-HILIC. Fig. 7 shows the variation of the peak shape of peptide #4 in RPLC with different injection volumes (1.5% to 6.2% V_0) and an injection solvent with moderate strength in RPLC (50:50 water/ACN (v/v)) considering the range of ACN composition (from 98% to 48% ACN) for the separation of peptides in HILIC. As a result, the chromatograms in Fig.7 illustrate the most favourable injection conditions with respect to the peak shape.

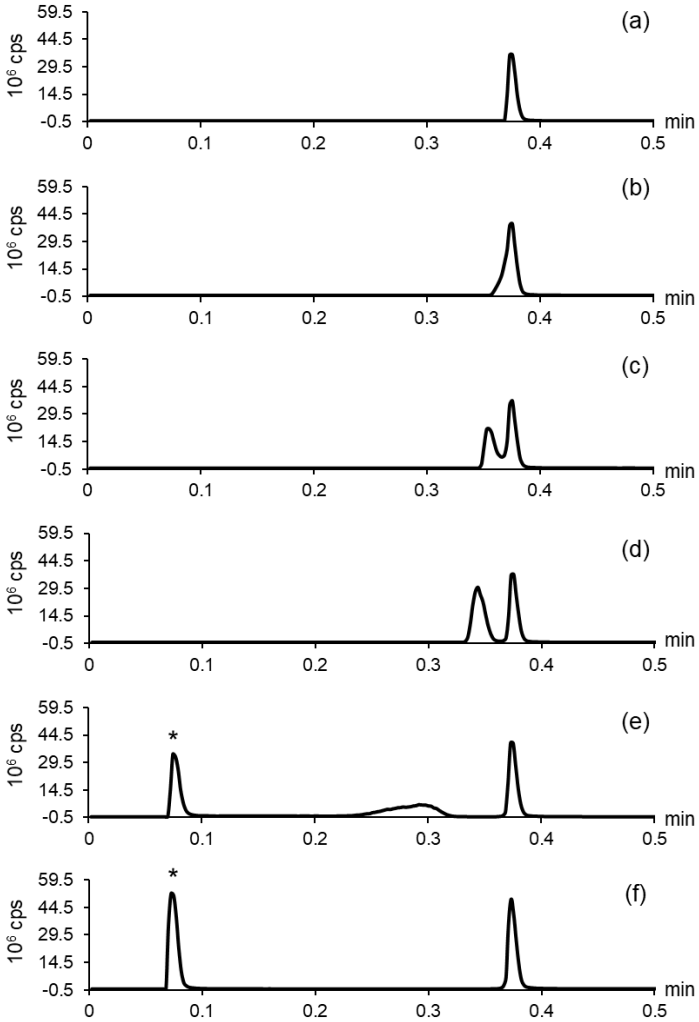

Fig. 7: Evolution of the peak shapes of peptide #4 (50 mg/L in 50:50 water/ACN) with increasing injection volumes: (a) 1 µL (1.5% V_0), (b) 1.5 µL (2.1% V_0), (c) 1.8 µL (2.5% V_0), (d) 2.2 µL (3% V_0), (e) 3.5 µL (4.8% V_0), and (f) 4.5 µL (6.2% V_0). 1–45% B in 11.3 t_0, 80 °C, 1.5 mL/min. MS detection ESI+ (EIC 557.6). Other conditions given in experimental section. The asterisk indicates the breakthrough peak.

When increasing the injected volume from 1 µL (1.5% V_0, Fig. 7a) to 4.5 µL (6.2% V_0, Fig. 7e), the peak evolves from a symmetrical shape to a severe distortion, with furthermore, the occurrence of a breakthrough phenomenon, which results in the presence of an intense non-retained peak (shown in Figs.7e and 7f by an asterisk). Up to 4.8 V_0 injected (Figs.7a to 7e), the peaks can be divided into three groups: (i) the first one (Fig. 7a) without any injection effects (injected volume < 1.5% V_0), (ii) the second one (Figs. 7b to 7d) with more or less distortion (peak splitting and/or distortion) but without any breakthrough, and (iii) the third one (Fig. 7e) with the apparition of three distinct peaks (one unretained breakthrough peak in the dead volume, one retained peak eluted at its expected retention time, and a third broad peak between the two). Consequently, increasing injection volumes in RPLC should severely reduce the chromatographic performance in on-line HILIC x RPLC. The most usual strategy in on-line HILIC x RPLC consists in reducing the injected volume, yet increasing sample dilution in ^{2}D. Our study on a broad range of injection volumes led to surprising observations. When increasing the injection volume above a certain critical value, we found an unexpected fourth group of peaks (as shown in Fig. 7f) where a single retained peak could be obtained despite the persistence of breakthrough. In addition, it is interesting to notice its quite symmetrical shape. The comparison of Fig. 7e and Fig. 7f clearly shows that the additional peak, located between the dead time and the retained peak, has entirely disappeared between 4.8% and 6.2% V_0 injected. We called this specific phenomenon "Total Breakthrough", in contrast to the earlier stage of breakthrough exhibiting strong peak distortion. Those symmetrical retained peaks were observed with injection volumes up to 50% V_0. Above this volume, the retained peak becomes less symmetrical with increased fronting by further increasing the injected volume. The absence of any peak between the non-retained (breakthrough) and the retained peaks was ensured by MS detection.

This thorough study on injection effects in RPLC was conducted with several injection solvent compositions ranging from 0% to 90% ACN and over a broad range of injection volumes ranging from 0.5% V_0 to 100% V_0. The importance of the injection solvent composition, the injection volume, and the difference in composition between injection and elution solvents is highlighted in Fig. 8. This latter shows the variation of the area of the retained peak (peptide #4 eluted with a composition of 16% ACN) with the injection volume (expressed as the ratio of the injected volume to the dead volume) for different injection solvents. The resulting curves underline the different

stages related to the evolution of the peak shapes. No peak distortion nor breakthrough were observed below 10% ACN as an injection solvent, resulting in a straight line for the curve corresponding to 10% ACN (blue curve in Fig. 8). It is worth mentioning that the experimental points beyond an injection volume of 10% V_0 were not represented here because the peak intensity exceeded the UV linearity range.

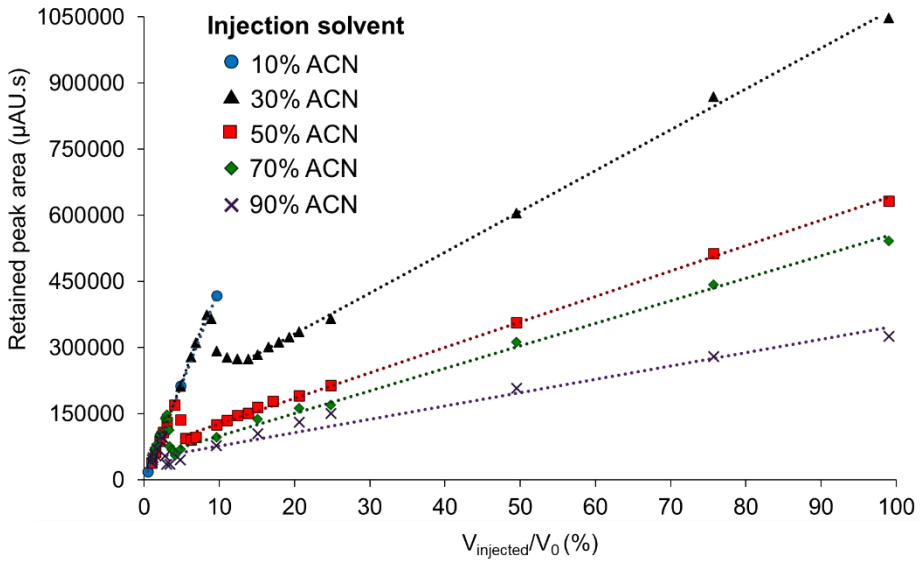

Fig. 8: Variation of the peak area (peptide #4) with the ratio of the injection volume to the column dead volume ($V_{injected}/V_0$). Injection solvent: 10% ACN (blue), 30% ACN (black) 50% ACN (red), 70% ACN (green) or 90% ACN (purple) in water. UV detection at 210 nm. Same other conditions as in Fig. 7.

The range of injected volumes resulting in a linear curve gets smaller as the eluent strength of the injection solvent increases. For instance, the linearity can be maintained up to 8% V_0 injected in 30% ACN (black curve) but only 3% V_0 in 90% ACN (purple curve). A very clear break occurs in the curve beyond a certain injected volume that fully depends on the injection solvent. This loss of linearity is a fair indicator of the emergence of breakthrough phenomena. This broken curve is followed by a transition zone with a downward curve, and again a growing straight line. The starting point of this straight line is the critical injection volume above which Total Breakthrough exists. Part of the sample being lost in the dead volume (breakthrough), the peak area starts to decrease with increasing injection volumes. However, above a certain injection volume, there is a reversed trend, with peak areas increasing again according to a straight line with a gentle slope. The fact that the peak area increases with the injection volume in Total Breakthrough conditions is very attractive because it suggests that larger injection volumes in ^{2}D could lead to better detection sensitivity

despite breakthrough. As shown in Fig. 8, this critical volume depends on the injection solvent. Conditions of Total Breakthrough are reached with lower injection volumes in strong solvents compared to weaker solvents and/or for early eluting peptides. They could be reached with 3% V_0 for peptide #4 (C_e of 16% ACN) in a sample solvent containing 90% ACN but with only 0.5% V_0 for the less retained peptide #6 (Ce of 6% ACN, see Fig. S5).

Overall, this study led to surprising conclusions: (i) the breakthrough phenomena can hardly be avoided in ^{2}D-RPLC since it may appear below 0.5% V_0 injected depending on the compound, (ii) Total Breakthrough could be a good option to maintain good peak shapes in ^{2}D, and (iii) peak area increases linearly with the injected volume beyond the critical injection volume, the slope of the regression line increasing by decreasing the percentage of ACN in the injection solvent. Accordingly, an alternative approach to circumvent the deleterious impact of injection effects on the separation can consist in injecting a sufficiently large volume in ^{2}D to ensure total Breakthrough conditions for all peptides. Such a strategy might seem counter-intuitive, but based on the above observations, it should allow maximizing the peak capacity and the peak intensity in ^{2}D.

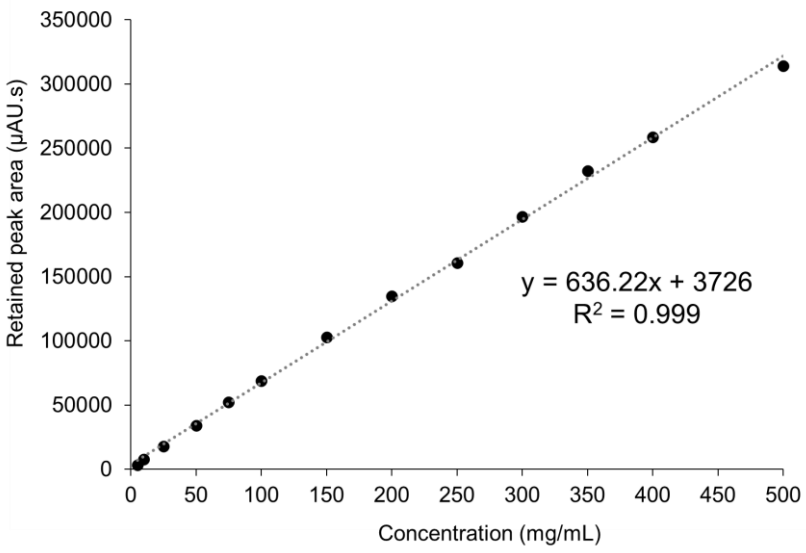

Fig. 9: Variation of the peak area with the concentration (peptide #4) in conditions of « Total Breakthrough ». Injection solvent 30:70 water/ACN (v/v), 3.5 µL (4.8% V_0) injected. UV detection at 210 nm. Other conditions as in Fig. 7.

In order to challenge this new strategy, both repeatability and intermediate precision were evaluated from twelve successive injections and three successive duplicate

injections repeated over five days, respectively. The relative standard deviations calculated for the retention time, the peak intensity, and the peak area for both the breakthrough peak and the retained peak were found to be always below 3%. In addition, the variation of the retained peak area with the peptide concentration (from 5 to 500 mg/L) was quite linear (Fig. 9), with a determination coefficient of 0.999. Furthermore, the relative standard deviations calculated for each concentration on three successive injections was always below 2%. Good linearity is of prime importance in quantitative LC x LC. Our results suggest that the phenomenon of Total breakthrough is not dependent on the solute concentration and hence, that the same proportion of analytes elutes in the dead volume regardless of the analyte concentration. This is important in LC x LC because if injection effects were different depending on the fraction concentration, quantitative analysis would be impossible as well as 2D reconstruction. We therefore found these results very attractive. They confirm that an approach based on Total Breakthrough can be used in HILIC x RPLC. Furthermore, they show that the existence of breakthrough leaves open future perspectives in quantitative analysis.

3.2. Application to on-line HILIC x RPLC-UV-HRMS analysis of a tryptic digest

Once the above conditions selected, the on-line HILIC x RPLC method was optimized according to a previously described procedure [6,7]. This procedure relies on the combined use of predictive calculations and a Pareto-optimality approach to optimize the physical parameters impacting the quality of the 2D separation. The optimized parameters included the ^{1}D-flow rate, the sampling rate, and the split ratio between both dimensions. Our objective was to separate a tryptic digest of six proteins in 30 min, using HRMS detection. In order to test our Total Breakthrough strategy, three different split ratios between ^{1}D and ^{2}D were considered (i.e. no split, split 1:1, and split 1:3), leading to ^{2}D-injected volumes of about 28%, 14%, and 7% V_0, respectively. The operating conditions are given in Table 3.

Fig. 10 shows extracted ion chromatograms (EIC) corresponding to one strongly retained peptide in ^{2}D-RPLC. Three analyses of the tryptic digest were carried out in HILIC x RPLC-UV-HRMS with three different split ratios between both dimensions (no split, 1:1 and 1:3). The peptide was retained in ^{1}D-HILIC with an elution composition, and hence an injection solvent in ^{2}D-RPLC, close to 75 % ACN. Considering the elution

composition of this peptide in ^{2}D-RPLC (40% ACN), it was affected by a breakthrough phenomenon with a breakthrough peak indicated by an asterisk in Figs.10a to 10c. The peak shape is very bad with 1:1 and 1:3 as split ratios (5 and 10 µL injected, respectively) but good with no split (20 µL injected). In this example, the critical injection volume (required to be in conditions of Total Breakthrough) was found to be between 10 and 20 µL. Similarly, 20 µL was found to be above the critical injection volume for all peptides, suggesting that any injected volume higher than 20 µL was suitable.

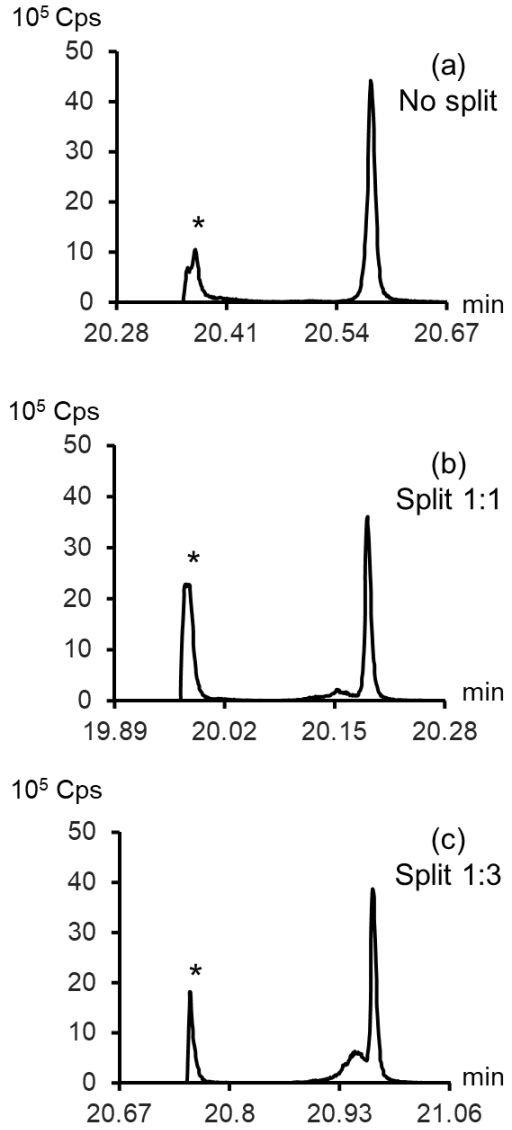

Fig. 10: Extracted ion chromatograms (EIC 742.4536) in ^{2}D of one fraction in HILIC x RPLC–HRMS. Sample: tryptic digest of six proteins. Split between both dimensions: (a) no split (20 µL injected), (b) split 1:1 (10 µL injected), and (c) split 1:3 (5 µL injected). The fraction was injected in nearly 75% ACN. MS detection ESI+. Other conditions are given in Table 3.

Figs.11a shows the 3D-chromatogram of the tryptic digest obtained without split in on-line HILIC x RPLC-UV-HRMS analysis. For the purpose of clarity, only the separation area is represented. The entire 2D contour plot can be seen in Fig. S6.

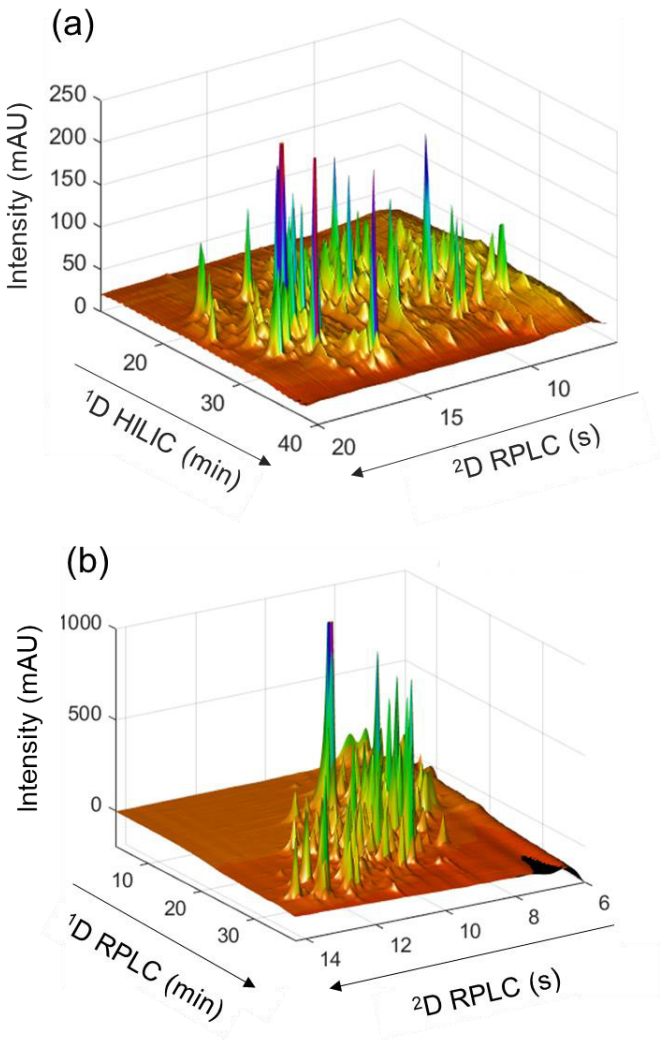

Fig. 11: 3D chromatograms obtained for the separation of a tryptic digest of six proteins in (a) on-line HILIC x RPLC (without split), and (b)) on-line RPLC x RPLC (split 1:2). UV detection at 210 nm. Conditions are given in Table 3.

As can be observed in Fig. 11a, the 2D separation is totally orthogonal, with a calculated retention space coverage (γ) close to 1. Peaks appear to be very narrow and symmetrical. The performance of this optimized on-line HILIC x RPLC separation was evaluated in term of peak capacity by taking into account the retention space coverage, the under-sampling, and the average peak width in each dimension according to Eq.8. All the experimental results are given in Table 4. Due to the matrix complexity, ^{1}D-peak widths were measured from ten representative standards injected in similar

chromatographic conditions. ^{2}D-peak widths were measured from more than a hundred peaks eluted all along the chromatogram. An effective peak capacity of 1500 was found for this separation achieved in 30 min, which is quite impressive compared to what was obtained in RPLC x RPLC within the same time [43].

For more objective comparative purposes, the same sample was analysed in on-line RPLC x RPLC under optimized conditions considering the same gradient time of 30 min. The operating conditions are given in Table 3 and the resulting separation is shown in Fig.11b. The first observation that can be made is that an average 5-fold lower peak height was obtained in HILIC x RPLC (Fig.11a) compared to RPLC x RPLC (Fig.11b). As previously discussed, the benefit of having RPLC in ^{1}D is that large volumes of undiluted aqueous sample could be injected without peak distortion (12% V_0 in RPLC vs. 5% V_0 in HILIC). The lower peak height in HILIC x RPLC compared to RPLC x RPLC is thus both due to the lower injected amount in ^{1}D and to the omnipresence of breakthrough phenomenon in ^{2}D. However, as expected with such a combination, the retention space coverage was incomplete in RPLC x RPLC, with a peak distribution around the diagonal of the separation space. Consequently, the effective peak capacity was found to be 830 despite good peak shapes in ^{2}D. The HILIC x RPLC separation resulted in an increase in peak capacity of about 80% compared to RPLC x RPLC. Such an increase can be ascribed to the full retention space coverage with quite symmetrical peaks.

Table 4: Experimental results for on-line HILIC x RPLC and RPLC x RPLC.

	γ	α	$^{1}w_{4\sigma}$ (min)	$^{2}w_{4\sigma}$ (s)	τ	$n_{2D,\ effective}$
HILIC x RPLC	1	0.67	0.65	0.28	2.5	1500
RPLC x RPLC	0.56	0.70	0.49	0.30	2.7	830

Regarding HILIC x RPLC, It should be emphasized that the presence of only one symmetrical retained peak in ^{2}D despite breakthrough was systematically verified by EIC-HRMS for all expected peptides. Fig. 12a shows the 2D contour plot obtained in HILIC x RPLC-UV. In the latter, nine spots labelled from #1 to #9 and corresponding to nine peptide peaks distributed throughout the 2D separation space are highlighted. Peaks #1 to #3 are strongly retained in HILIC, whereas peaks #7 to #9 are poorly retained. Similarly, peaks #1, #4, and #7 are poorly retained in RPLC, whereas peaks

#3, #6, and #9 are strongly retained. Peak #5 is eluted in the middle of the retention space. The nine corresponding EIC-HRMS are shown in Fig.12b. It is very interesting to note that all the retained peaks are quite symmetrical and that no additional peak appears aside from the non-retained breakthrough peak. As expected, the ratio of peak areas between breakthrough and retained peaks depends on the peptide retention in both ^{1}D and ^{2}D. As above discussed, weakly retained peptides in ^{2}D are more impacted by breakthrough phenomena, especially when they are poorly retained in ^{1}D (strong injection solvent). It is therefore important to note that for good quantitative performance, the internal standard has to be eluted in the same retention conditions as the compound of interest. However, the separations shown in Fig. 12 confirm that an injection volume of 20 µL was sufficient to ensure Total Breakthrough for all peptides and demonstrate the validity of the proposed approach for HILIC x RPLC separations.

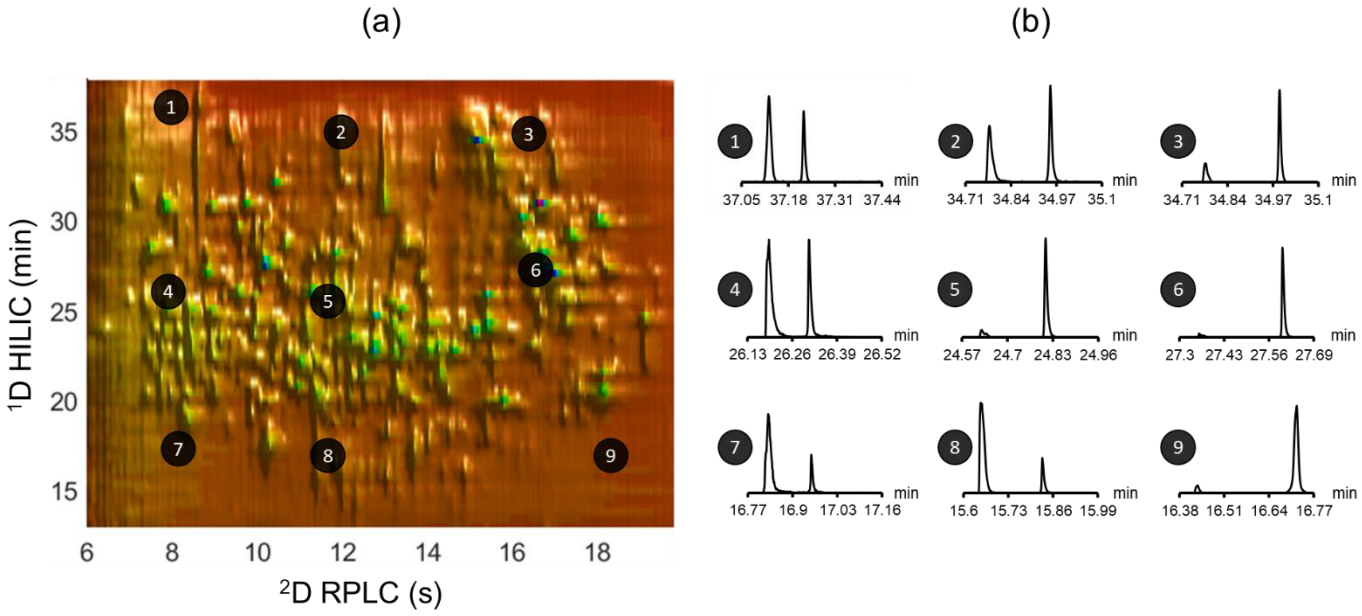

Fig. 12: On-line HILIC x RPLC-UV-HRMS analysis of a tryptic digest of 6 proteins. (a) 2D contour plot with UV detection at 210 nm and (b) RPLC-EIC–HRMS of nine different fractions (#1 to #9) with m/z 803.9648 (#1), 689.9255 (#2), 1585.8743 (#3), (#4), 748.3117 (#5), 1023.5553 (#6), 1557.3651 (#7), 650.3160 (#8), 1013.6004 and 288.2907 (#9). The corresponding retained peaks are indicated by black spots in the 2D contour plot. Conditions are given in Table 3.

4. Conclusion

We have developed an on-line HILIC x RPLC-UV-HRMS method for the comprehensive characterization of a protein digest in 30 min.

In the first dimension, the stationary phase and the injection conditions were deeply studied and carefully selected to find the best trade-off between high peak capacity and low dilution. Bare silicas were found to be the most appropriate stationary phases for the separation of peptides under neutral pH with ammonium acetate as an additive. The use of HILIC in the first dimension raised the issue of finding an adequate sample solvent with respect to both sample solubility and injection effects. It was shown that a minimum of 50% of water was required in the injection solvent for proper peptide dissolution.

The high percentage of acetonitrile in the HILIC mobile phase, and hence in the injection solvent for RPLC may lead to peak broadening, peak distortion, and breakthrough phenomena, resulting in a dramatic loss of peak capacity and peak intensity. The conditions of emergence of peak broadening and peak distortion were deeply investigated. The importance of both the injection volume and the difference in composition between injection and elution solvents were highlighted. Although limiting the injection volume is the most obvious approach to avoid injection effects, we discovered that injecting large volumes offers a powerful alternative approach. Our results proved that above a certain critical injection volume, depending on the elution conditions, narrow and symmetrical peaks can be obtained for peptides, despite the persistence of breakthrough. This counter-intuitive "Total Breakthrough" approach was applied for the on-line HILIC x RPLC-UV-HRMS analysis of a complex tryptic digest sample. Due to both the high retention space coverage and the sharp peaks obtained in the second dimension, a peak capacity close to 1500 could be achieved in 30 minutes. Within the same analysis time of 30 min and under optimized conditions, the obtained peak capacity in RPLC x RPLC was half as high and the average peak intensity was about 5-fold higher. Nonetheless, this work shows the great potential of on-line HILIC x RPLC performed under "Total Breakthrough" conditions for the ultra-fast 2D separation of complex peptide samples.

5. Acknowledgements

The authors warmly thank Agilent Technologies for the loan of the 2D-LC instrument and the Q-TOF-HRMS. They also would like to thank Professor Gert Desmet and Vincent Pepermans from the University of Brussels for stimulating discussions.

6. References

[1] K. Horváth, J.N. Fairchild, G. Guiochon, Generation and Limitations of Peak Capacity in Online Two-Dimensional Liquid Chromatography, Anal. Chem. 81 (2009) 3879–3888. https://doi.org/10.1021/ac802694c.

[2] M. Sarrut, G. Crétier, S. Heinisch, Theoretical and practical interest in UHPLC technology for 2D-LC, TrAC Trends in Analytical Chemistry. 63 (2014) 104–112. https://doi.org/10.1016/j.trac.2014.08.005.

[3] F. Bedani, P.J. Schoenmakers, H.-G. Janssen, Theories to support method development in comprehensive two-dimensional liquid chromatography – A review, J. Sep. Science. 35 (2012) 1697–1711. https://doi.org/10.1002/jssc.201200070.

[4] X. Li, D.R. Stoll, P.W. Carr, Equation for Peak Capacity Estimation in Two-Dimensional Liquid Chromatography, Anal. Chem. 81 (2009) 845–850. https://doi.org/10.1021/ac801772u.

[5] I. François, D. Cabooter, K. Sandra, F. Lynen, G. Desmet, P. Sandra, Tryptic digest analysis by comprehensive reversed phase×two reversed phase liquid chromatography (RP-LC×2RP-LC) at different pH's, J. Sep. Science. 32 (2009) 1137–1144. https://doi.org/10.1002/jssc.200800578.

[6] M. Sarrut, A. D'Attoma, S. Heinisch, Optimization of conditions in on-line comprehensive two-dimensional reversed phase liquid chromatography. Experimental comparison with one-dimensional reversed phase liquid chromatography for the separation of peptides, Journal of Chromatography A. 1421 (2015) 48–59. https://doi.org/10.1016/j.chroma.2015.08.052.

[7] A. D'Attoma, S. Heinisch, On-line comprehensive two dimensional separations of charged compounds using reversed-phase high performance liquid chromatography and hydrophilic interaction chromatography. Part II: Application to the separation of peptides, Journal of Chromatography A. 1306 (2013) 27–36. https://doi.org/10.1016/j.chroma.2013.07.048.

[8] A. D'Attoma, C. Grivel, S. Heinisch, On-line comprehensive two-dimensional separations of charged compounds using reversed-phase high performance liquid chromatography and hydrophilic interaction chromatography. Part I: Orthogonality and practical peak capacity considerations, Journal of Chromatography A. 1262 (2012) 148–159. https://doi.org/10.1016/j.chroma.2012.09.028.

[9] G. Vanhoenacker, I. Vandenheede, F. David, P. Sandra, K. Sandra, Comprehensive two-dimensional liquid chromatography of therapeutic monoclonal antibody digests, Anal Bioanal Chem. 407 (2015) 355–366. https://doi.org/10.1007/s00216-014-8299-1.

[10] K. Horie, Y. Sato, T. Kimura, T. Nakamura, Y. Ishihama, Y. Oda, T. Ikegami, N. Tanaka, Estimation and optimization of the peak capacity of one-dimensional gradient high performance liquid chromatography using a long monolithic silica capillary column, Journal of Chromatography A. 1228 (2012) 283–291. https://doi.org/10.1016/j.chroma.2011.12.088.

[11] M. Gilar, P. Olivova, A.E. Daly, J.C. Gebler, Orthogonality of Separation in Two-Dimensional Liquid Chromatography, Anal. Chem. 77 (2005) 6426–6434. https://doi.org/10.1021/ac050923i.

[12] P.G. Stevenson, D.N. Bassanese, X.A. Conlan, N.W. Barnett, Improving peak shapes with counter gradients in two-dimensional high performance liquid chromatography, Journal of Chromatography A. 1337 (2014) 147–154. https://doi.org/10.1016/j.chroma.2014.02.051.

[13] Y. Chen, J. Li, O.J. Schmitz, Development of an At-Column Dilution Modulator for Flexible and Precise Control of Dilution Factors to Overcome Mobile Phase Incompatibility in Comprehensive Two-Dimensional Liquid Chromatography, Anal.Chem. 91 (2019) 10251–10257. https://doi.org/10.1021/acs.analchem.9b02391.

[14] D.R. Stoll, D.C. Harmes, G.O. Staples, O.G. Potter, C.T. Dammann, D. Guillarme, A. Beck, Development of Comprehensive Online Two-Dimensional Liquid Chromatography/Mass Spectrometry Using Hydrophilic Interaction and Reversed-Phase Separations for Rapid and Deep Profiling of Therapeutic Antibodies, Anal. Chem. 90 (2018) 5923–5929. https://doi.org/10.1021/acs.analchem.8b00776.

[15] L. Montero, M. Herrero, E. Ibáñez, A. Cifuentes, Separation and characterization of phlorotannins from brown algae Cystoseira abies-marina by comprehensive two-dimensional liquid chromatography, ELECTROPHORESIS. 35 (2014) 1644–1651. https://doi.org/10.1002/elps.201400133.

[16] C.M. Willemse, M.A. Stander, A.G.J. Tredoux, A. de Villiers, Comprehensive two-dimensional liquid chromatographic analysis of anthocyanins, Journal of Chromatography A. 1359 (2014) 189–201. https://doi.org/10.1016/j.chroma.2014.07.044.

[17] X.-X. Zheng, Y. Du, B. Xu, T. Wang, Q. Zhong, Z. Li, S. Ji, M. Guo, D. Yang, D. Tang, Off-line two-dimensional liquid chromatography coupled with diode array detection and quadrupole-time of flight mass spectrometry for the biotransformation kinetics of Ginkgo biloba leaves extract by diabetic rat liver microsomes, Journal of Chromatography B. 1109 (2019) 1–9. https://doi.org/10.1016/j.jchromb.2019.01.015.

[18] V. Elsner, V. Wulf, M. Wirtz, O.J. Schmitz, Reproducibility of retention time and peak area in comprehensive two-dimensional liquid chromatography, Anal

Bioanal Chem. 407 (2015) 279–284. https://doi.org/10.1007/s00216-014-8090-3.

[19] S. Abrar, B. Trathnigg, Separation of nonionic surfactants according to functionality by hydrophilic interaction chromatography and comprehensive two-dimensional liquid chromatography, Journal of Chromatography A. 1217 (2010) 8222–8229. https://doi.org/10.1016/j.chroma.2010.10.118.

[20] A.F.G. Gargano, M. Duffin, P. Navarro, P.J. Schoenmakers, Reducing Dilution and Analysis Time in Online Comprehensive Two-Dimensional Liquid Chromatography by Active Modulation, Anal. Chem. 88 (2016) 1785–1793. https://doi.org/10.1021/acs.analchem.5b04051.

[21] L. Montero, E. Ibáñez, M. Russo, R. di Sanzo, L. Rastrelli, A.L. Piccinelli, R. Celano, A. Cifuentes, M. Herrero, Metabolite profiling of licorice (Glycyrrhiza glabra) from different locations using comprehensive two-dimensional liquid chromatography coupled to diode array and tandem mass spectrometry detection, Analytica Chimica Acta. 913 (2016) 145–159. https://doi.org/10.1016/j.aca.2016.01.040.

[22] E. Sommella, O.H. Ismail, F. Pagano, G. Pepe, C. Ostacolo, G. Mazzoccanti, M. Russo, E. Novellino, F. Gasparrini, P. Campiglia, Development of an improved online comprehensive hydrophilic interaction chromatography × reversed-phase ultra-high-pressure liquid chromatography platform for complex multiclass polyphenolic sample analysis, J. Sep. Sci. 40 (2017) 2188–2197. https://doi.org/10.1002/jssc.201700134.

[23] L. Montero, V. Sáez, D. von Baer, A. Cifuentes, M. Herrero, Profiling of Vitis vinifera L. canes (poly)phenolic compounds using comprehensive two-dimensional liquid chromatography, Journal of Chromatography A. 1536 (2018) 205–215. https://doi.org/10.1016/j.chroma.2017.06.013.

[24] P. Donato, F. Rigano, F. Cacciola, M. Schure, S. Farnetti, M. Russo, P. Dugo, L. Mondello, Comprehensive two-dimensional liquid chromatography–tandem mass spectrometry for the simultaneous determination of wine polyphenols and target contaminants, Journal of Chromatography A. 1458 (2016) 54–62. https://doi.org/10.1016/j.chroma.2016.06.042.

[25] P. Jandera, T. Hájek, Z. Šromová, Comprehensive two-dimensional monolithic liquid chromatography of polar compounds, Journal of Separation Science. 42 (2019) 670–677. https://doi.org/10.1002/jssc.201801085.

[26] M. Muller, A.G.J. Tredoux, A. de Villiers, Application of Kinetically Optimised Online HILIC × RP-LC Methods Hyphenated to High Resolution MS for the Analysis of Natural Phenolics, Chromatographia. 82 (2019) 181–196. https://doi.org/10.1007/s10337-018-3662-6.

[27] R. Berkecz, F. Tömösi, T. Körmöczi, V. Szegedi, J. Horváth, T. Janáky, Comprehensive phospholipid and sphingomyelin profiling of different brain regions in mouse model of anxiety disorder using online two-dimensional (HILIC/RP)-LC/MS method, Journal of Pharmaceutical and Biomedical Analysis. 149 (2018) 308–317. https://doi.org/10.1016/j.jpba.2017.10.043.

[28] H. Zhang, J.-M. Jiang, D. Zheng, M. Yuan, Z.-Y. Wang, H.-M. Zhang, C.-W. Zheng, L.-B. Xiao, H.-X. Xu, A multidimensional analytical approach based on time-decoupled online comprehensive two-dimensional liquid chromatography coupled with ion mobility quadrupole time-of-flight mass spectrometry for the analysis of ginsenosides from white and red ginsengs, Journal of Pharmaceutical and Biomedical Analysis. 163 (2019) 24–33. https://doi.org/10.1016/j.jpba.2018.09.036.

[29] J.-L. Cao, L.-J. Ma, S.-P. Wang, Y. Deng, Y.-T. Wang, P. Li, J.-B. Wan, Comprehensively qualitative and quantitative analysis of ginsenosides in Panax notoginseng leaves by online two-dimensional liquid chromatography coupled to hybrid linear ion trap Orbitrap mass spectrometry with deeply optimized dilution and modulation system, Analytica Chimica Acta. 1079 (2019) 237–251. https://doi.org/10.1016/j.aca.2019.06.040.

[30] D.V. McCalley, A study of column equilibration time in hydrophilic interaction chromatography, Journal of Chromatography A. 1554 (2018) 61–70. https://doi.org/10.1016/j.chroma.2018.04.016.

[31] M. Muller, A.G.J. Tredoux, A. de Villiers, Predictive kinetic optimisation of hydrophilic interaction chromatography × reversed phase liquid chromatography separations: Experimental verification and application to phenolic analysis, Journal of Chromatography A. 1571 (2018) 107–120. https://doi.org/10.1016/j.chroma.2018.08.004.

[32] T. Hájek, P. Jandera, M. Staňková, P. Česla, Automated dual two-dimensional liquid chromatography approach for fast acquisition of three-dimensional data using combinations of zwitterionic polymethacrylate and silica-based monolithic columns, Journal of Chromatography A. 1446 (2016) 91–102. https://doi.org/10.1016/j.chroma.2016.04.007.

[33] G. Groeneveld, M.N. Dunkle, M. Rinken, A.F.G. Gargano, A. de Niet, M. Pursch, E.P.C. Mes, P.J. Schoenmakers, Characterization of complex polyether polyols using comprehensive two-dimensional liquid chromatography hyphenated to high-resolution mass spectrometry, Journal of Chromatography A. 1569 (2018) 128–138. https://doi.org/10.1016/j.chroma.2018.07.054.

[34] A. Martín-Ortiz, A.I. Ruiz-Matute, M.L. Sanz, F.J. Moreno, M. Herrero, Separation of di- and trisaccharide mixtures by comprehensive two-dimensional liquid chromatography. Application to prebiotic oligosaccharides, Analytica Chimica Acta. 1060 (2019) 125–132.

https://doi.org/10.1016/j.aca.2019.01.040.

[35] L.R. Snyder, J.W. Dolan, J.R. Gant, Gradient elution in high-performance liquid chromatography: I. Theoretical basis for reversed-phase systems, Journal of Chromatography A. 165 (1979) 3–30. https://doi.org/10.1016/S0021-9673(00)85726-X.

[36] D.R. Stoll, X. Wang, P.W. Carr, Comparison of the Practical Resolving Power of One- and Two-Dimensional High-Performance Liquid Chromatography Analysis of Metabolomic Samples, Anal. Chem. 80 (2008) 268–278. https://doi.org/10.1021/ac701676b.

[37] B. Chauve, D. Guillarme, P. Cléon, J.-L. Veuthey, Evaluation of various HILIC materials for the fast separation of polar compounds, Journal of Separation Science. 33 (2010) 752–764. https://doi.org/10.1002/jssc.200900749.

[38] Y. Yang, R.I. Boysen, M.T.W. Hearn, Hydrophilic interaction chromatography coupled to electrospray mass spectrometry for the separation of peptides and protein digests, Journal of Chromatography A. 1216 (2009) 5518–5524. https://doi.org/10.1016/j.chroma.2009.05.085.

[39] J. Ruta, S. Rudaz, D.V. McCalley, J.-L. Veuthey, D. Guillarme, A systematic investigation of the effect of sample diluent on peak shape in hydrophilic interaction liquid chromatography, Journal of Chromatography A. 1217 (2010) 8230–8240. https://doi.org/10.1016/j.chroma.2010.10.106.

[40] G.C. Derringer, R.L. Markham, A computer-based methodology for matching polymer structures with required properties, Journal of Applied Polymer Science. 30 (1985) 4609–4617. https://doi.org/10.1002/app.1985.070301208.

[41] S. Heinisch, A. D'Attoma, C. Grivel, Effect of pH additive and column temperature on kinetic performance of two different sub-2µm stationary phases for ultrafast separation of charged analytes, Journal of Chromatography A. 1228 (2012) 135–147. https://doi.org/10.1016/j.chroma.2011.08.041.

[42] D.V. McCalley, Overload for Ionized Solutes in Reversed-Phase High-Performance Liquid Chromatography, Analytical Chemistry. 78 (2006) 2532–2538. https://doi.org/10.1021/ac052098b.

[43] M. Sarrut, F. Rouvière, S. Heinisch, Theoretical and experimental comparison of one dimensional versus on-line comprehensive two dimensional liquid chromatography for optimized sub-hour separations of complex peptide samples, Journal of Chromatography A. 1498 (2017) 183–195. https://doi.org/10.1016/j.chroma.2017.01.054.

CONCLUSIONS

In this chapter, two different approaches to improve the retention space coverage for the on-line LC x LC separation of peptides were explored: (i) the use of tailored second-dimension gradient programs and (ii) the combination of different and complementary chromatographic modes (here HILIC x RPLC). The advantages and disadvantages of these two approaches in comparison with a conventional RPLC x RPLC approach with full gradients in the second dimension are listed in the following Table IV-3.

Table IV-3: Advantages and disadvantages of the three on-line LC x LC methods described in this chapter for the analysis of peptides.

Method	Advantages	Disadvantages
RPLC x RPLC (Full gradients)	• Excellent analyte focusing in both D* • No sample dilution required in ^{1}D • Good peak shapes in both D • Excellent method sensitivity • Simplicity and flexibility of method development	• Limited selectivity differences • Limited retention space coverage (60%) • Limited peak capacity (900)
RPLC x RPLC (Tailored gradients)	• Excellent analyte focusing ^{1}D • No sample dilution required in ^{1}D • Fairly good analyte focusing in ^{2}D • Fairly good peak shapes in both D • Good method sensitivity • Increased retention space coverage (80%) • Increased peak capacity (1200)	• Increased peak width • Slightly decreased peak intensity • Poor run-to-run repeatability • Longer and more complex method development • Specific software required
HILIC x RPLC (Total Breakthrough)	• Full retention space coverage (100%) • Good peak shapes under TB** conditions • Greatly increased peak capacity (1500)	• Solvent strength mismatch • Poor analyte focusing in both D • Injection issues in both D • Sample dilution required in ^{1}D • Greatly decreased peak intensity • Longer method development

*D: dimension

**TB: Total Breakthrough

Clearly, the use of tailored gradient programs is an effective approach to improve the retention space coverage for systems employing correlated retention mechanisms such as RPLC x RPLC. It is also worth mentioning that such an approach should be useful for any other LC x LC separations leading to partial retention space coverage, as previously highlighted for peptides in SCX x RPLC [1] or plant metabolites in RPLC

x HILIC [2], among other examples. In this work, it was shown that the retention space coverage could be increased by 50% when using a properly optimized tailored gradient program instead of a full gradient program in the second dimension, which led to a meaningful increase of peak capacity by about 30%. As emphasized in this work, such an increase should however come at the expense of larger peak widths in the second dimension and thus lower detection sensitivity. Probably the greatest disadvantage of using such gradient programs, especially when incorporating shifted gradient assemblies, is the poor run-to-run retention time repeatability, which arises from the constant variations of the gradient conditions in the second dimension. The importance of maintaining good run-to-run repeatability cannot be overstated in on-line LC x LC, so it is our view that this might constitutes an impediment to the routine implementation of such programs, despite their clear benefits on the separation.

As expected, the performance of on-line HILIC x RPLC in terms of orthogonality greatly overlooked that of RPLC x RPLC with either conventional full gradients or tailored gradients in the second dimension. Herein, the increase was found to be close to 80% and 20%, respectively, and came along with a proportional gain in peak capacity. Such a gain was made possible by overcoming the deleterious impact of solvent strength mismatch on peak shapes in the second dimension with an unconventional strategy consisting in triggering a limit case of breakthrough for all compounds, which we called "Total Breakthrough". Under such conditions, the peaks were indeed found to be quite narrow and symmetrical despite the presence of breakthrough. However, the counterpart of this strategy was a significant decrease in peak intensity due to the omnipresence of breakthrough.

REFERENCES

[1] G. Vanhoenacker, I. Vandenheede, F. David, P. Sandra, K. Sandra, Comprehensive two-dimensional liquid chromatography of therapeutic monoclonal antibody digests, Anal Bioanal Chem. 407 (2015) 355–366. https://doi.org/10.1007/s00216-014-8299-1.

[2] Y. Chen, L. Montero, J. Luo, J. Li, O.J. Schmitz, Application of the new at-column dilution (ACD) modulator for the two-dimensional RP×HILIC analysis of Buddleja davidii, Anal Bioanal Chem. 412 (2020) 1483–1495. https://doi.org/10.1007/s00216-020-02392-3.

CHAPTER V - OVERCOMING THE CHALLENGE OF SOLVENT STRENGTH MISMATCH IN ON-LINE HILIC x RPLC

This Chapter has been published as:

- **A comprehensive study on the phenomenon of Total Breakthrough in liquid chromatography**

  Soraya Chapel, Florent Rouvière, Vincent Pepermans, Gert Desmet, and Sabine Heinisch
  Journal of Chromatography A, 2021, under review

- **Comparison of existing strategies for keeping symmetrical peaks in on-line hydrophilic Interaction liquid chromatography x reversed-phase liquid chromatography despite solvent strength mismatch**

  Soraya Chapel, Florent Rouviere, and Sabine Heinisch
  Journal of Chromatography A, 2021, 1642, 462001
  DOI: 10.1016/j.chroma.2021.462001

INTRODUCTION

The combination of different chromatographic modes almost always raises solvent compatibility problems between dimensions [1]. As highlighted in the previous chapter, the mismatch of elution strength between the first- and second dimension mobile phases can be a critical issue in on-line HILIC x RPLC. If not properly addressed, it may cause severe peak deformations and losses of both separation power and detection sensitivity in the second dimension. To circumvent these problems, several strategies have been proposed over the years. Most of them involve the improvement of the modulation interface [2-4]. In the literature, the trend has been to divide these strategies into two broad modulation categories. Different terminologies have been used to express the same idea: non-focusing or focusing [4-6], passive or active [2], simple valve-based or valve-based combined with assistant technology [3]. As for us, we prefer to distinguish strategies based on their goals, which have been mainly so far: (i) reducing the injected volume in the second dimension and/or, (ii) decreasing the elution strength of the ^{1}D-effluent before reinjection into the ^{2}D-column.

In Chapter IV, we introduced a new strategy to address the so-called solvent strength mismatch problem in on-line HILIC x RPLC. While other reported strategies exclusively focus on the complete elimination of injection issues in the second dimension, our approach reversely consists in fully embracing them by deliberately provoking a Total Breakthrough phenomenon for every compound. Therefore, it is a counter-intuitive strategy that relies on the injection of relatively large volumes of fractions in the second dimension.

In the present chapter, several possibilities to alleviate the solvent strength mismatch problem in on-line HILIC x RPLC are explored in the interest of providing guidance to exploit the full potential of this orthogonal combination. The first part of the chapter describes an experimental study focusing on the phenomena of breakthrough and Total Breakthrough, with the aim to clearly define their conditions of occurrence in liquid chromatography. The second part of the chapter describes a comparative study of four strategies to overcome solvent strength mismatch, including the one that we proposed in Chapter IV. The respective advantages and disadvantages of each of the evaluated strategies are discussed in the specific context of the on-line HILIC x RPLC analysis of a complex tryptic digest sample.

A. Article 5: Comprehensive study of the breakthrough phenomena of ionizable analytes in reversed-phase liquid chromatography

Abstract

Differences in elution strength between the sample solvent and the mobile phase usually give rise to undesirable effects on the chromatographic separation, which may range from slight broadening to severe peak deformation or even splitting. In the most extreme case, the retention factor of the analyte at the head of the column is so small at the time of injection that part of it goes through the column with very little interaction with the stationary phase and elutes very close to the column dead time. This phenomenon is known as breakthrough. Usually, during breakthrough, the retained peak displays a wide array of deformations and it is not rare that multiple retained peaks appear for a given injected analyte. However, under certain conditions, it has been demonstrated that these deleterious effects could fully disappear, leaving only one breakthrough peak and one symmetrical peak on the chromatogram. This so-called "Total Breakthrough" phenomenon was recently highlighted in the specific context of the 2D-LC separation of peptides but has yet to be explained. In the present paper, we describe the results of a comprehensive study aiming to better understand and define the conditions of emergence of both breakthrough and Total breakthrough phenomena in liquid chromatography. The effects of a broad range of parameters, including the nature of the solute, the retention mechanism, the injection and elution conditions, the column temperature, and the injected sample concentration on the occurrence of both phenomena were investigated. While breakthrough was found to occur for all studied compounds, it appears that the presence of positive charges on the molecule is a prerequisite for observing a Total Breakthrough phenomenon. Among all the parameters investigated in this work, only the injection conditions and the analyte retention were found to be impactful on the onset of both phenomena. This finding allowed us to suggest one necessary and sufficient condition, relying on the injection of critical volumes to observe each respective phenomenon. These critical volumes only depend on the column dead volume and the retention factor of the analyte in the injection solvent.

1. Introduction

In the quest for ever more sensitive, ever faster separations, and ever higher separation power, comprehensive two-dimensional liquid chromatography (LC x LC) has acquired a place of choice among separation methods [1–3]. One of the most limiting problems in LC x LC is related to injection in the second dimension [4,5]. The injection solvent is often much stronger than the mobile phase while the injection volume is usually much larger than the one in one-dimensional liquid chromatography (1D-LC). This can result in very bad peak shapes including peak broadening, peak distortion, and peak splitting, but also, in some cases, in the occurrence of breakthrough phenomenon. This phenomenon occurs for a given compound when the injection solvent is so strong that part of the molecules elute with the solvent peak while the other part leaves the injection solvent and is normally retained. This leads to the presence of a non-retained peak in the chromatogram in addition to the expected retained one.

The combination of hydrophilic interaction liquid chromatography (HILIC) with reversed-phase liquid chromatography (RPLC) gives a typical example of this situation where the first dimension mobile phase, and thus the injection solvent in the second dimension is very strong compared to the second dimension mobile phase [6–13]. However, such a situation can also be encountered in 1D-LC, either in RPLC with compounds poorly soluble in water-rich solvents or in HILIC with compounds poorly soluble in acetonitrile-rich solvents. The phenomenon of breakthrough was recently investigated for neutral species. Excellent agreement was obtained between computer simulations and experimental results [14] (see Article 6 given in Supplementary Information in page 345 of this manuscript). In particular, the peak distortion which occupied the whole retention space between the breakthrough peak and the retained peak could be well simulated. It was also theoretically demonstrated that breakthrough occurred above a critical injection volume, $V_{crit,B}$, which can be related to the column dead volume, $V_{0,}$ by the following simple relationship:

$$V_{crit,B} = k_s \times V_0 \qquad \textit{(Eq. 1)}$$

Where k_s is the retention factor of the analyte in the injection solvent.

We recently pointed out a new phenomenon [7] which relies on the finding that, injecting a large enough sample volume in RPLC resulted not only in a breakthrough peak but also yielded a symmetrical retained peak (no peak distortion). We called this

phenomenon “Total Breakthrough” in reference to the complete disappearance of the molecules between the breakthrough peak and the retained peak above a critical injection volume, $V_{crit,TB}$, of course, larger than $V_{crit,B}$. This phenomenon was shown to be highly repeatable. The retained peak areas were found to vary linearly with the injected amount, provided that Total Breakthrough conditions were established, which suggests that quantitative analysis is possible under these conditions. In a more recent study, Total Breakthrough conditions were compared to more traditional approaches used in HILIC x RPLC for maximizing peak capacity including post-^{1}D-flow splitting and on-line solvent dilution. It was shown that Total Breakthrough conditions were the only approach that allowed to have symmetrical peaks over the whole 2D separation space [15].

In these two reported studies [7,15], the phenomenon of Total Breakthrough was presented as part of the separation of peptides in RPLC at acidic pH. In the present study, our objective was to know precisely which separation conditions in liquid chromatography and which compounds can lead to this phenomenon. We were also interested in the critical volume ($V_{crit,TB}$) above which the phenomenon of Total Breakthrough appears. Finally, we found it interesting to test and validate Eq. 1 on experimental results.

2. Experimental section

2.1. Chemicals

Deionized water was produced using an Elga Purelab Classic UV purification system from Veolia water STI (Décine-Charpieu, France). LC-MS grade acetonitrile (ACN), clozapine, protriptyline, imipramine, amitriptyline, nadolol, propranolol, diphenhydramine, N,N-dimethylaniline, and salicylic acid were purchased from Sigma-Aldrich (Steinheim, Germany). Analytical reagent grade ammonium acetate (AA) and LC-MS grade formic acid (FA) were purchased from Fischer scientific (Illkirch, France). Influenza hemagglutinin (HA), leucine encephalin, bombesin, [arg8]-Vasopressin, [ile]-angiotensin, bradykinin fragment 1–5, substance P, and bradykinin were obtained from Merck (Molsheim, France). WDDHH was custom synthesized (Genecust, Luxembourg). The physical properties of all the compounds studied are listed in Table 1.

Table 1: Characteristics and Physical properties of the studied compounds.

#	Compound	m/z (Da)	Pi or pKa (25°C)	S_{log}	Log(k_w)
P1	Influenza hemagglutinin (HA)	1103.2	3.5	16.5	3.04
P2	Leucine enkephalin	556.6	6.0	11.4	2.22
P3	[arg8]-Vasopressin	543.1*	8.2	21.1	1.52
P4	[ile]-Angiotensin	898.1	9.4	20.9	1.94
P5	Bradykinin fragment 1-5	573.7	10.6	15.6	1.07
P6	Substance P	674.8*	11.7	20.6	3.25
P7	Bradykinin	531.1*	12.5	20.5	2.22
B1	N,N-dimethylaniline	122.2	5.1	10.5	2.29
B2	diphenhydramine	256.4	8.8	9.7	2.10
B3	propranolol	260.3	9.1	10.7	2.03
B4	amitriptyline	278.4	9.2	9.3	2.64
B5	nadolol	310.4	9.2	23.6	1.64
N1	Caffeine	193.2	1.4	/	/
A1	Salicylic acid	137.1	2.8	/	/

*doubly charged ion

2.2. Sample preparation

For small molecular weight (MW) compounds (MW < 350 Da), stock solutions of each analyte were prepared at a concentration of 200 mg/L in ACN/water (50:50 v/v) for amitriptyline, diphenhydramine, caffeine, and salicylic acid or 1000 mg/L (0:100 v/v) for nadolol, N,N-dimethylaniline, and propranolol. For peptides, the stock solutions of each compound were prepared in pure water at 500 mg/L for influenza hemagglutinin, [arg8]-vasopressin, [ile]-angiotensin, and substance P, 1000 mg/L for bradykinin fragment 1-5, 2500 for bradykinin, and 5000 mg/L for leucine enkephalin. Most injected samples were prepared individually by appropriate dilution of each stock

solution with water and acetonitrile. The final concentration was 50 mg/L for leucine encephalin and 0.5 mg/L for the small MW basic compounds unless stated otherwise. For Fig. S1, the injected samples were prepared by combining stock solutions of all small MW basic compounds (Fig. S1a) or all peptides (Fig. S1b) before adding an appropriate volume of acetonitrile. The final concentrations in these mixtures were 16 mg/L (peptides) and 1 mg/L (small MW basic compounds). The sample solvent composition of each prepared sample is indicated in the figure captions.

2.3. Instrumentation and columns

Chromatographic experiments were performed on two different systems. System 1 was used for the analysis of individually injected compounds, whereas System 2 was used for the injection of mixtures (Fig. S1) and the isocratic experiment. System 1 consisted of the first dimension of a 2D-LC ACQUITY UPLC I-Class instrument from Waters Corporation (Milford, MA, USA). It includes a binary solvent delivering pump (BSM), a sample manager with a flow-through needle (SM-FTN) injector equipped with a 15 µL loop, a thermostated column manager, an ACQUITY photodiode-array detector (PDA) with a 0.5 µL flow cell. For most experiments, an extension loop of 100 µL was added to the injector. For the study of the effect of the isocratic hold at the beginning of the gradient, the experiments were performed without this extension loop. The measured dwell volume (V_D) and extra-column volume (V_{ext}) for this system were 110 µL and 12 µL, respectively (without extension loop). The LC system was hyphenated to an ACQUITY single quadrupole mass spectrometry detector (QDa). A zero dead volume T-piece was placed after the column to reduce the flow entering MS. The T-piece connected the column outlet to the QDa and PDA inlets via PEEK capillary tubings of 100 µm inner diameter. It was designed to send half of the flow to UV and the other half to MS (split 1:1). Instrument control, data acquisition, and data handling were performed by MassLynx v4.1 software (Waters Corporation). System 2 consisted of the first dimension of a 2D-LC 1290 Infinity II instrument from Agilent Technologies (Waldbronn, Germany). It includes a binary pump (G7120A), and autosampler (G7120B) with a flow-through needle injector equipped with a 20 µL-loop, a thermostated column compartment (G7116B), and a diode array detector (DAD) with a 0.6-µL flow cell (G7117A). The measured dwell volume and extra-column volume for this system were 170 µL and 22 µL, respectively. The system was hyphenated with a Q-TOF mass spectrometer (G6560B) equipped with a 35-uL JetStream source (Agilent

Technologies). The LC system was controlled by OpenLAB CDS Chemstation Edition revision C.01.09 and the Q-TOF by MassHunter Acquisition version B.09.00 software (Agilent Technologies). MS data handling was performed by MassHunter Qualitative Analysis version B.10.0.10305.0 software.

An ACQUITY UPLC CSH C18 column (30 x 2.1 mm, 1.7 µm) was used in RPLC and an ACQUITY UPLC BEH Amide column (50 x 2.1 mm, 1.7 µm) in HILIC. Both columns were obtained from Waters Corporation. The measured column void volume (V_0) were 73 µL and 121 µL, respectively (total porosity close to 0.7).

2.4. Chromatographic and detection conditions

For the RPLC experiments, unless otherwise stated, the column temperature was set at 80°C, the flow rate was 1.5 mL/min, and gradient elution was used with 0.1% formic acid in water as solvent A (pH 2.7) and 0.1% formic acid in ACN as solvent B. The solvent gradient was: 1-45-1-1% B in 0-0.54-0.59-1 min (corresponding to a normalized gradient slope of about 4%). As part of this study, the following elution conditions were varied to assess their impact on the separations: the composition of ACN at initial conditions (1, 5 or 10% B), the normalized gradient slope (1, 4, 8 or 12%), the duration of the isocratic hold at the beginning of the gradient (0, 0.13, 0.27 or 0.53 min), the flow rate (0.75 or 1.5 mL/min), and the temperature (30 or 80°C). These specific elution conditions are indicated in the figure captions. Depending on the conditions, the injected volumes varied from 0.35 µL to 72 µL (corresponding to about 0.5% V_0 to 99% V_0).

In isocratic elution, the flow rate was 0.5 mL/min and the mobile phase composition was 0.1% formic acid in water/0.1% formic acid in ACN 90:10 (v/v).

At neutral pH, the column temperature was 30°C, the flow rate was 0.75 mL/min, the mobile phase consisted of 10 mM ammonium acetate in water as solvent A (pH 6.8) and ACN as solvent B, and the solvent gradient was: 1-55-1-1% B in 0-1.33-1.43-3 min.

In HILIC, the column temperature was 30°C, the flow rate was 0.6 mL/min, and the mobile phase consisted of ACN as solvent A and 10 mM ammonium acetate in water as solvent B (pH 6.8). The solvent gradient was 2-60-2-2% B in 0-5.8-6-8 min.

UV chromatograms were recorded at 210 nm with an acquisition rate of 40 Hz. The QDa ionization source was used in the ESI positive mode for most compounds and

negative mode for salicylic acid with Selected Ion Recording (SIR). Data were acquired between 100 and 350 Da for small MW compounds, and 500 and 1250 Da for peptides, with an acquisition rate of 10 Hz. Nitrogen (N_2) was used as a drying gas. The source temperature was maintained at 125°C. The capillary voltage was set at 0.8 kV, the probe temperature at 600°C, and the cone voltage at 15 V.

QTOF-HRMS data were acquired in ESI positive mode between 100 and 1700 Da with an acquisition rate of 20 spectra/s. The drying gas temperature and flow rate were set at 200°C and 11 L/min, respectively. The nebulizer gas pressure was set at 40 psi. The sheath gas temperature and flow rate were set at 350°C and 11 L/min, respectively. The capillary, the nozzle, the fragmentor, the skimmer, and the Oct 1 RV voltages were set at 3500, 300, 150, 20, and 750 V, respectively.

2.5. Calculations

The gradient profile at the column outlet is shown in the different figures (dotted lines with Y-scale on the right). It is related to the composition of the mobile phase at analyte, calculated according to the following relationship:

$$C_{elution} = C_{initial} + \frac{(C_{final} - C_{initial})}{t_G}(t_r - t_D - t_0) \qquad \textit{(Eq. 2)}$$

Where $C_{initial}$ and C_{final} are the initial and final compositions of eluting solvent in the mobile phase, t_r is the retention time, t_D is the total dwell time, and t_0 is the column dead time.

The normalized gradient slope, s, is the product of the gradient slope and the column dead time:

$$s = \frac{\Delta C}{t_G} \times t_0 \qquad \textit{(Eq. 3)}$$

Where ΔC and t_G are the gradient composition range and the gradient time, respectively.

The intercept, *log(kw)*, and the slope, S_{log}, of the relationship between the logarithm of the retention factor and the volume fraction of the strong solvent were calculated from two gradient runs using OSIRIS software (V 4.2, Euradif, Grenoble, France) with an Acquity CSH C18 (150 x 2.1 mm, 1.7 µm) column at 80°C (A: water + 0.1% FA, B: ACN

+ 0.1% FA; 1% B to 41% B in 10 min and 30 min; 0.7mL/min). The values are given in Table 1.

3. Results and discussion

3.1. Determination of the compounds concerned by Total Breakthrough

As stated above, Total Breakthrough (TB) has been defined in circumstances where there are two distinct peaks for a given solute, the first one non-retained (breakthrough peak) and the second one, retained and quite symmetrical [7]. Thus, the conditions required, for a given compound, to recognize a Total Breakthrough situation are: (i) the presence of a breakthrough peak, (ii) the presence of a retained peak, which should be quite symmetrical, (iii) the absence of compound molecules detected between the breakthrough peak and the retained peak (i.e. no middle peak and no peak fronting should be observed).

It was found for peptides that TB occurred when the injection volume was higher than a critical one. For smaller volumes, between the critical breakthrough volume ($V_{crit,B}$) and the critical TB volume ($V_{crit,TB}$), a transition step was pointed out, in which breakthrough occurred while the retained peak was distorted and sometimes split. In this section, the phenomenon of breakthrough is studied for different solutes (neutral, acid, basic, peptides) in different chromatographic conditions including RPLC at acidic pH, RPLC at neutral pH, and HILIC, with the objective of identifying the conditions required for the emergence of Total Breakthrough.

3.1.1. In RPLC at acidic pH

The occurrence of breakthrough and sometimes Total Breakthrough in RPLC at acidic pH is highlighted in Fig.1. Various volumes were injected for four different compounds. These include caffeine (neutral at this pH), leucine enkephalin (multi-charged compound with pI = 6.0), propranolol (weak base with pKa = 9.4), and salicylic acid (weak acid with pKa = 3.0). Their separations were obtained in RPLC under acidic conditions (pH 2.7). The injection solvent strength was rather high (50:50 water/ACN), thus leading to a significant difference between the injection solvent and the composition of the mobile phase at peak elution (of the order of 35% ACN). In these acidic conditions, both leucine enkephalin and propranolol were expected to be mainly positively charged, whereas salicylic acid was expected to be mainly in its acid form

(uncharged). The same gradient conditions were applied to all solutes. The ratio of the injection volume to the column dead volume (V_i/V_0) was increased (from the top of Fig. 1 to the bottom) in order to study its impact on the separation. The dotted lines represent the evolution of the composition at elution with the analysis time.

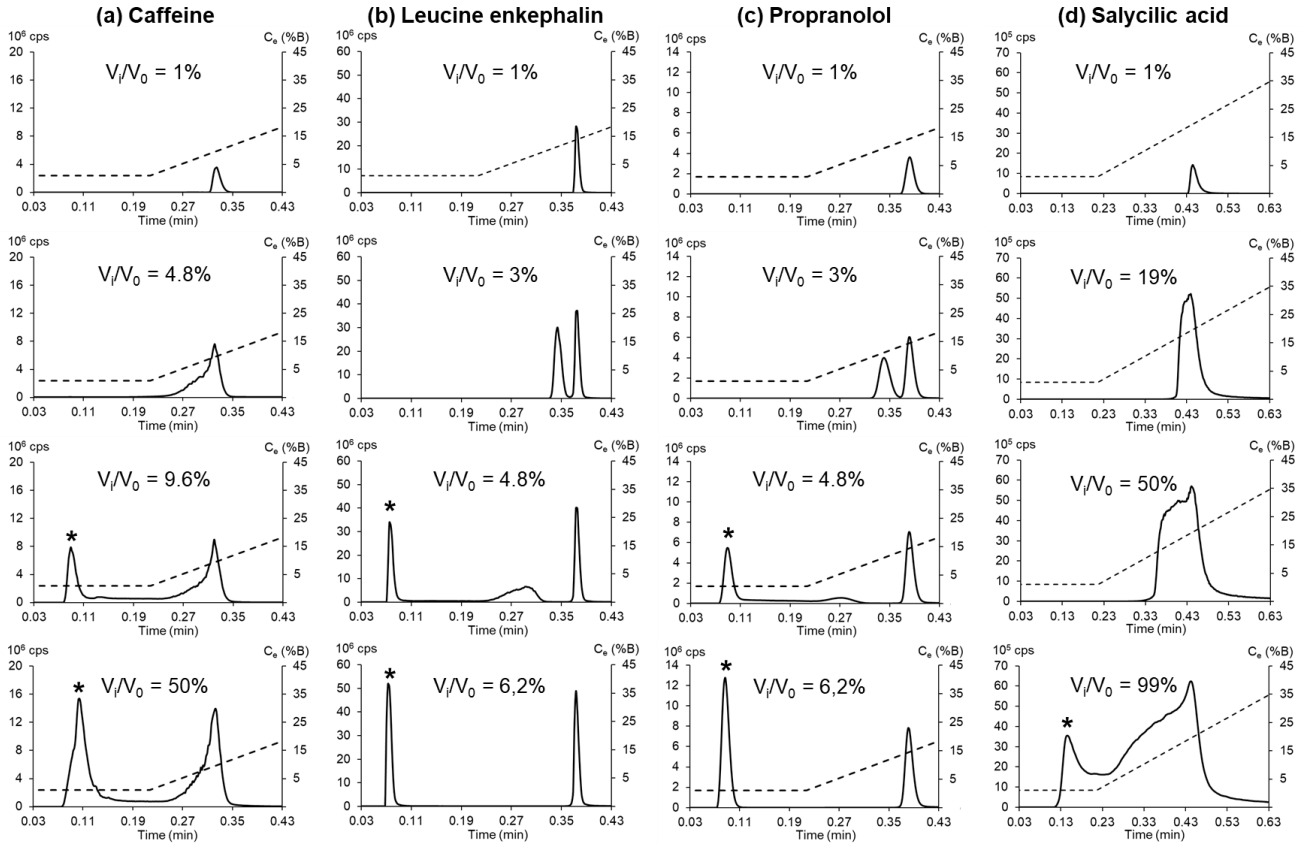

Fig. 1: Occurrence of breakthrough and Total Breakthrough in gradient elution at acidic pH for (a) caffein (2 mg/L), (b) leucine enkephalin (50 mg/L), (c) propranolol (0.5 mg/L), and (d) salicylic acid (25 mg/L). Injection solvent: 50% ACN. Increased injection volumes (V_i/V_0) from top to bottom. Acquity CSH C18 column (30 x 2.1 mm, 1.7 µm); 1.5 mL/min; 80°C; Mobile phase : A: water + 0.1% FA, B: ACN + 0.1% FA; 1-45-1-1% B in 0-0.54-0.59-1 min (normalized gradient slope of 4%). The gradient profile at the column outlet is given in dotted line with the composition scale on the right. The asterisk indicates the non-retained breakthrough peak. ESI-MS detection.

As can be observed, when the injection volume is low enough (i.e. V_i/V_0 = 1% here), there is only one retained peak, nearly symmetrical whatever the solute. As the injected volume increases (2nd row of chromatograms), the peaks of caffeine (Fig.1a) and salicylic acid (Fig.1d) are broadened and even distorted, while those of leucine enkephalin (Fig.1b) and propranolol (Fig.1c) are split, resulting in the latter case in the appearance of a second peak with smaller retention.

For large enough injection volumes, a breakthrough peak (marked with an asterisk) appears for all solutes. As can be observed in Fig.1, $V_{crit,B}$ was between 5% and 10% V_0 for caffeine, 3% and 4.8% V_0 for both leucine enkephalin and propranolol, and larger than 50% V_0 for salicylic acid. In the case of caffeine and salicylic acid, the breakthrough peak and the retained peak are always connected by a bridge of molecules, even well beyond $V_{crit,B}$. Furthermore, from the moment the retained peak starts to broaden, peak distortion consistently increases as the injection volume increases. Unlike these two compounds for which TB could therefore not be attained whatever the volume injected (up to 140% V_0 in this study), TB can be observed for both leucine enkephalin and propranolol (bottom chromatogram in Fig. 1b and Fig. 1c, respectively). For both compounds, $V_{crit,TB}$ was between 4.8% and 6.2% V_0, hence slightly larger than $V_{crit,B}$. It is important to note that, between $V_{crit,B}$ and $V_{crit,TB}$, three distinct peaks are present on the chromatogram. In the rest of this study, we will refer to each of these three peaks as "breakthrough peak", "middle peak", and "retained peak", respectively.

The fact that the trend for leucine enkephalin and propranolol was exactly the same can be related to the similarity of their retention model coefficients (k_w and S_{log} given in Table 1), thereby leading to very close retention times. Since the main difference between these two compounds is their size, this suggests that this phenomenon is independent of diffusion. Similar results were obtained with different peptides and different weak bases exhibiting various retention times (various coefficients as shown in Table 1) under the same chromatographic conditions. The resulting separations of these compounds are shown in Fig. S1. In all cases, the retained peak was narrow and rather symmetrical as long as the injected volume was above a specific $V_{crit,TB}$ value.

From these preliminary results, two important conclusions can be drawn: (i) under acidic conditions, while breakthrough can be achieved with any compound as long as it exceeds the critical volume ($V_{crit,B}$), Total Breakthrough appears to be achievable only with positively charged compounds such as peptides or weak bases, (ii) the advantages of TB conditions, in terms of peak shape, previously highlighted for peptides [7] should apply to weak bases as well.

All the above-discussed results were obtained in gradient elution. It is interesting to note that the trend was somewhat different in isocratic elution. As exemplified for leucine enkephalin in RPLC at acidic pH (Fig. 2), the shape of the retained peak at an

early stage of breakthrough (V_i/V_0 = 3.4%) seems to be similar to the one obtained with neutral compounds in gradient elution (Figs. 1a and 1d), with a continuous bridge of molecules between the breakthrough and the retained peaks. However, unlike neutral compounds, the bridge height decreases almost down to the baseline above a critical injection volume ($V_{crit,TB}$ value of about 6.9% V_0) which reminds a Total Breakthrough situation. However, unlike gradient elution, the retained peak is not quite symmetrical but exhibits low fronting regardless of the injection volume above $V_{crit,TB}$.

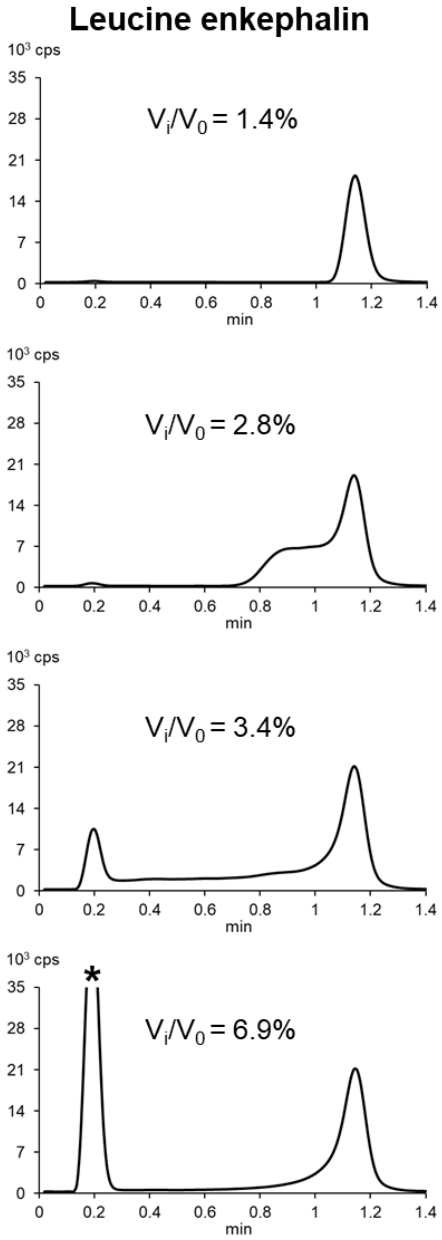

Fig.2: Occurrence of breakthrough and Total Breakthrough in isocratic elution at acidic pH for leucine enkephalin (0.5 mg/L). Injection solvent: 50% ACN. Increased injection volumes (V_i/V_0) from top to bottom. 0.5 mL/min; mobile phase A: water + 0.1% FA, B: ACN + 0.1% FA (90:10 A/B). Same other conditions as in Fig. 1. The asterisk indicates the non-retained breakthrough peak.

3.1.2. In RPLC at neutral pH

The first question that naturally arises from the preceding results is whether or not the charge of the molecule plays a part in the occurrence of Total Breakthrough. To answer this question, we performed the same study as in Fig. 1, but under neutral conditions (pH 6.8). Propranolol (very strongly retained in such conditions) was replaced by N,N-dimethylaniline (pKa of 5.1). The main stages of the separation according to the injection volume, are shown in Fig. 3 for the peptide (Fig. 3a), the weak base (Fig.3b), and the weak acid (Fig. 3c).

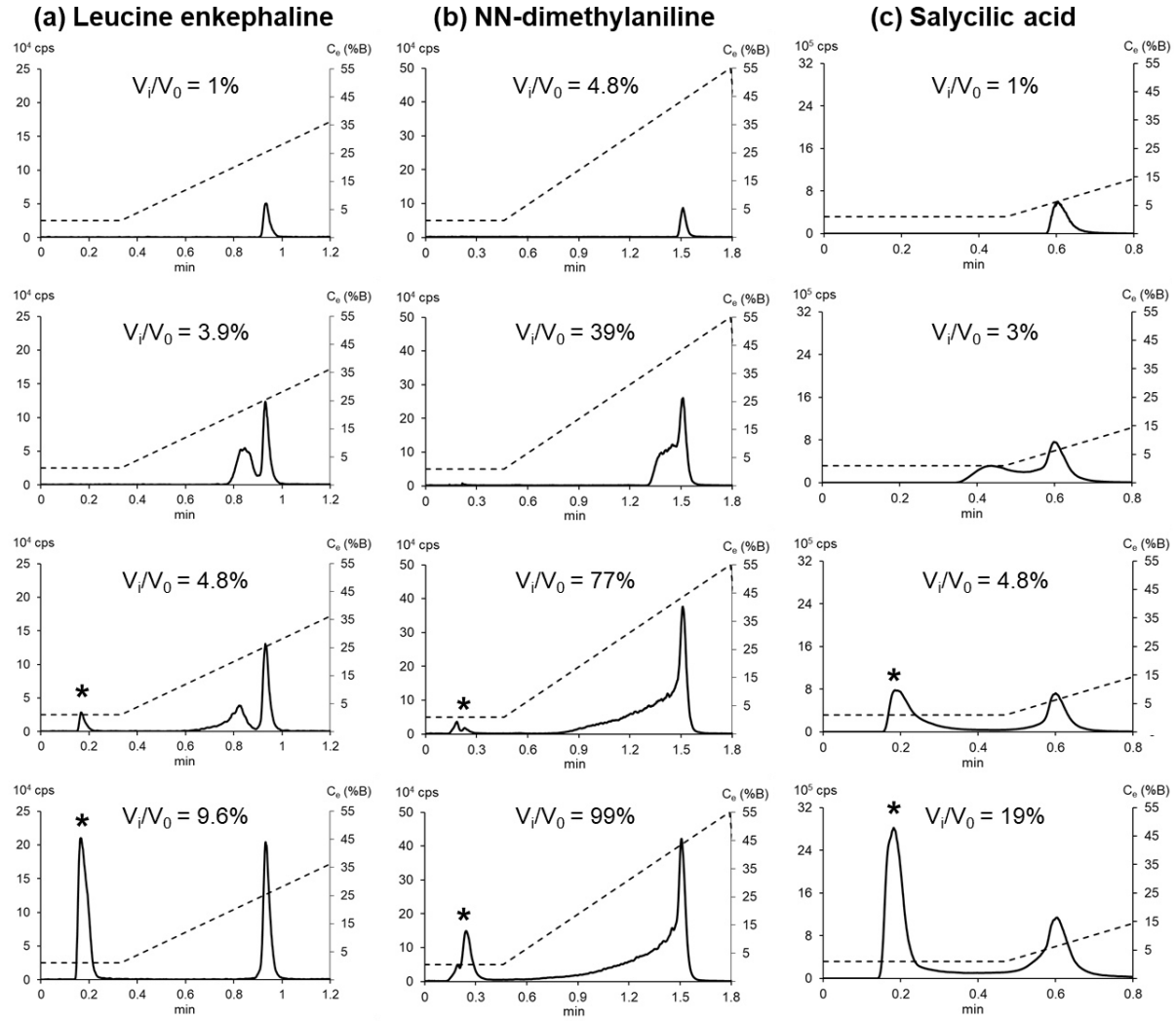

Fig.3: Occurrence of Breakthrough and Total Breakthrough in gradient elution at neutral pH for (a) leucine enkephalin (5 mg/L), (b) NN-dimethylaniline (0.05 mg/L), and (d) salicylic acid (25 mg/L). Injection solvent: 70% ACN (a, b) or 50% ACN (c). Increased injection volumes (V_i/V_0) from top to bottom. Acquity CSH C18 column (30 x 2.1 mm, 1.7 µm); 0.75 mL/min; 30°C; mobile phase : A: water + ammonium acetate 10 mM, B: ACN; 1-55-1-1% B in 0-1.33-1.43-3 min (normalized gradient slope of 4%). The gradient profile at the column outlet is given in dotted line with the composition scale on the right. The asterisk indicates the non-retained breakthrough peak. ESI-MS detection.

The sample solvent consisted of a mixture of water/ACN (30:70 or 50:50, v/v). Under these pH conditions, N,N-dimethylaniline was expected to be mainly neutral, salicylic acid to be negatively charged, while the dominant form of leucine should be the zwitterion (N-terminus protonated, uncharged chain, and C-terminus deprotonated).

As shown in Fig. 3a, the trend for leucine enkephalin at neutral pH is quite the same as at acidic pH (see Fig. 1b) despite the presence of as many negative charges as positive charges on the molecule. By increasing the injected volume, the separation goes through a single symmetrical peak (1% V_0) to the occurrence of breakthrough (4.8% V_0) and then Total Breakthrough (9.6% V_0). A middle peak with intermediate retention is observed, without (3.9% V_0) or with (4.8% V_0) breakthrough. The same trend was also observed for more acidic peptides (lower pI) as well as for more basic peptides (higher pI) as exemplified in Fig. S2 for influenza hemagglutinin and bradykinin fragment 1-5, respectively. For N,N-dimethylaniline (Fig. 3b), the trend at neutral pH is similar to the one observed for any neutral compound regardless of pH [14]. $V_{crit,B}$ is high and close to 77% V_0. By further increasing the injected volume, the retained peak exhibits an increasing fronting, which persists even with very large injected volumes (> 99% V_0). For salicylic acid (Fig. 3c), the trend is different. The retained peak exhibits a fronting shoulder with injection volumes as low as 2.8% V_0. By increasing the injection volume, a middle peak appears (3.4% V_0) and then a breakthrough peak ($V_{crit,B}$ between 3.4% V_0 and 4.8% V_0). However, unlike positively charged compounds, a complete baseline resolution was never achieved between the breakthrough peak and the retained peak. Both remained connected by a continuous bridge of molecules, the height of which increased with the injected volume. In other words, Total Breakthrough was never observed for this negatively charged analyte.

To summarize, we only observed a Total Breakthrough phenomenon with positively charged compounds (here peptides and small pharmaceuticals). With neutral or anionic compounds, the shape of the retained peak got worse and worse as the injection volume increased. These results suggest that only the presence of positive charges on the molecule leads to the occurrence of Total Breakthrough. In this specific case, an unexplained phenomenon appears during the injection process, which divides the molecules into different populations (two or three depending on whether there is a middle peak or not) that will travel through the column at different linear velocities during the separation process. The resulting separation and the resulting peak shapes cannot be accurately predicted with the previously developed approach [14] which has

been shown to work well with neutral compounds. The different behaviour between neutral/negatively charged and positively charged analytes is certainly difficult to explain. The first explanation that comes to mind is that this phenomenon is related to the mixed retention mechanism (on both alkyl chains and ionized silanols) that exists in RPLC with protonated compounds on silica-based columns. These two mechanisms have different kinetic interactions (fast for hydrophobic interaction while low for electrostatic interaction), which might support the existence of different populations. However, solute retention is a thermodynamic process that makes the solutes continuously adsorb and desorb during their travel through the column. Furthermore, against an explanation based on a mixed retention mechanism, Total Breakthrough was observed for positively charged compounds at low pH (i.e. 2.7) where there are supposedly very few ionized silanols. We are, therefore, still working on finding a possible explanation.

3.1.3. In HILIC

The phenomenon of Total Breakthrough was also observed for peptides in HILIC. An example is given in Fig. 4, showing the evolution of elution profiles of leucine enkephalin with the injected volume after dissolution in a strong solvent (i.e. pure water). Below 10% V_0 injected, the peaks were split into two (1% V_0) or multiple distinct peaks (2% V_0), until the occurrence of breakthrough with the presence of a broad middle peak (5% V_0). Interestingly, the presence of multiple distinct peaks before the emergence of breakthrough was never observed in RPLC. Above 10% V_0 injected, the middle peak completely disappeared, leaving only two peaks on the chromatogram, the breakthrough peak and a narrow and symmetrical retained peak. The retention mechanism in HILIC is known to be multimodal [16,17]. For ionized compounds such as peptides, it might involve partitioning between the organic-rich mobile phase and the water-enriched layer partially immobilized on the stationary phase, electrostatic interaction (attractive or repulsive) between the charged analyte and the residual silanols, and hydrogen bonding with the stationary phase. From our perspective, the fact that the peptide behaviour seems to be similar in HILIC and RPLC might also be related to the existence of secondary interactions. However, as in RPLC, it is quite difficult to explain the reasons for which distinct peaks are present, and above all, why Total Breakthrough emerged with positively charged compounds only.

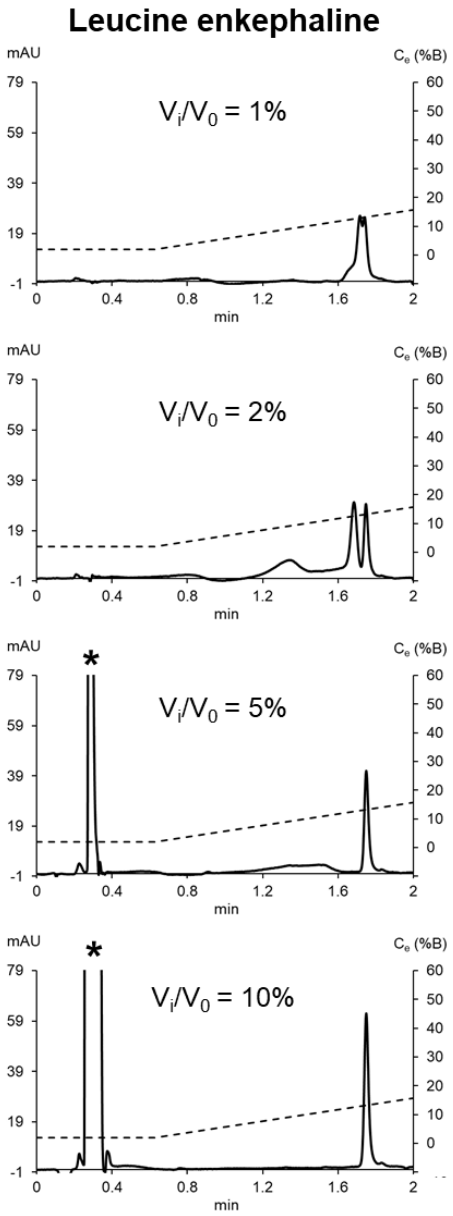

Fig.4: Occurrence of breakthrough and Total Breakthrough in HILIC for leucine enkephalin (32 mg/L). Injection solvent: 100% water. Increased injection volumes (V_i/V_0) from top to bottom. Acquity BEH Amide column (50 x 2.1 mm, 1.7 µm); 0.6 mL/min; 30°C; mobile phase : A: ACN and B: water + ammonium acetate 10 mM (pH 6.8); 2-60-2-2% B in 0-5.8-6-8 min (normalized gradient slope of 2%). UV detection at 210 nm. The gradient profile at the column outlet is given in dotted line with the composition scale on the right. The asterisk indicates the non-retained breakthrough peak.

3.2. Identification of the relevant factors affecting breakthrough and Total Breakthrough

In this part of the work, we evaluated the effect of various parameters on the emergence of breakthrough and Total Breakthrough. The study was carried out in RPLC with positively charged analytes eluted in gradient elution at acidic pH. The

investigated parameters included the eluent strength of the injection solvent, the gradient conditions, the column temperature, and the concentration of the analyte. The goal of this study was to make progress in the understanding of the phenomenon of Total Breakthrough.

3.2.1. Effect of the injection solvent composition

Fig. 5 illustrates the effect of the injection solvent composition on the elution profiles of leucine enkephalin. Figs. 5a to 5d show the results obtained with an organic solvent content ranging from 30% ACN to 90% ACN in the injection solvent, respectively.

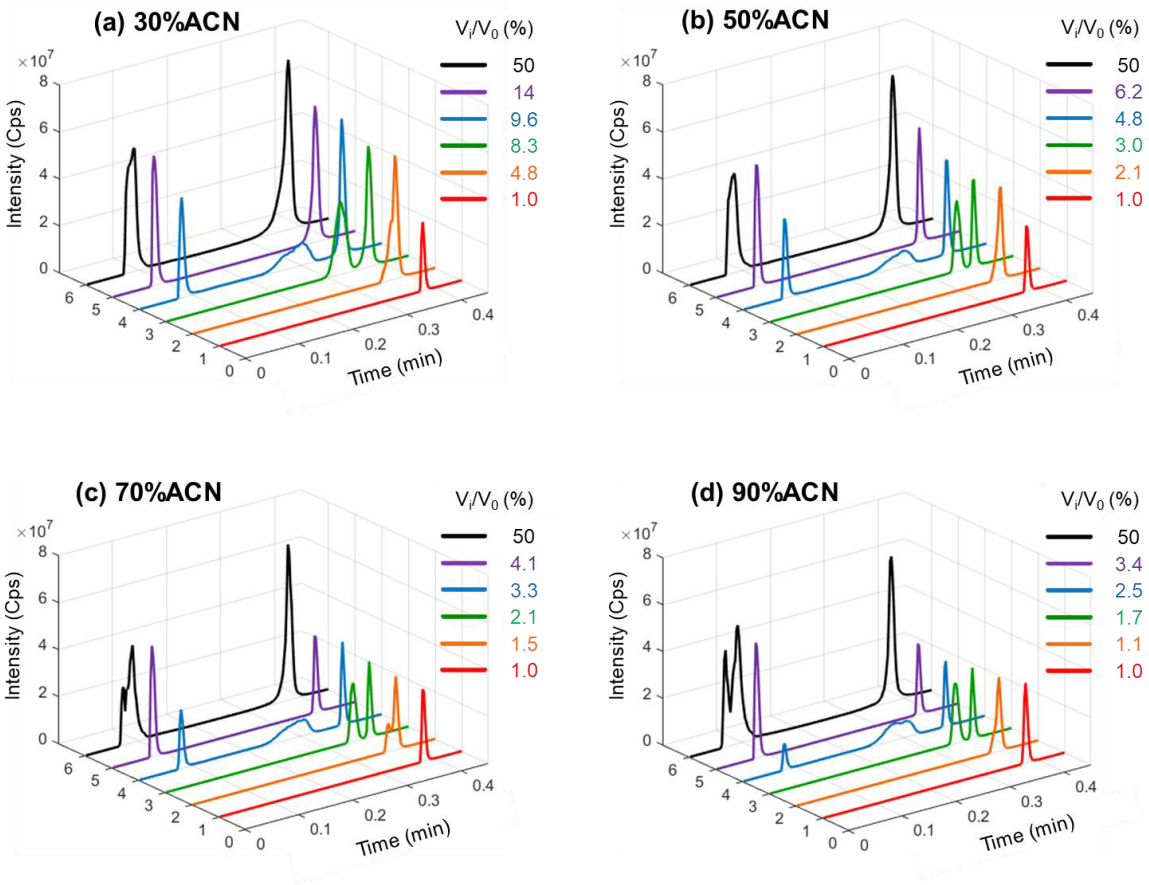

Fig.5: Effect of the injection solvent composition on the separation: (a) 30% ACN, (b) 50% ACN, (c) 70% ACN, and (d) 90% ACN. V_i/V_0 was varied from 1% to 50% ACN. Solute: leucine enkephalin (50 mg/L). Same other conditions as in Fig. 1.

In each figure, a given colour is related to a given peak shape in order to highlight the similarities between the four injection solvents. For example, the red curves reflect conditions for which a single symmetrical peak is observed on the chromatogram,

whereas the purple curves capture the onset of Total Breakthrough. The first observation that can be made when comparing Figs. 5a-d is that the evolution of the elution profile with the injection volume is the same regardless of the eluent strength of the injection solvent. For the four conditions of injection solvent depicted in Fig.5, the separation goes through the same stages: (i) no injection issues (red curve), (ii) peak broadening (orange curve), (iii) appearance of a middle peak (green curve), (iv) emergence of breakthrough with persistence of this middle peak (blue curve), and (v) occurrence of Total Breakthrough (purple curve). The only difference is that injection issues start with smaller injection volumes when the injection solvent is stronger (i.e. with a larger content of acetonitrile). Whereas $V_{crit,TB}$ represents about 13.8% V_0 with 30% ACN in the sample solvent (Fig. 5a), it is close to 3.4% V_0 with 90% ACN (Fig. 5d). Similar observations can be made for the emergence of breakthrough, which appears with injection volumes of about 9.6% and 2.5% V_0 with 30% ACN (Fig. 5a)and 90% ACN (Fig. 5d), respectively. It is interesting to point out that $V_{crit,TB}$ seems to be slightly higher than $V_{crit,B}$ (about 40 % higher) regardless of the injection solvent composition (i.e. $V_{crit,TB} = 1.4\ V_{crit,B}$). Considering Eq. 1, this means that the following relationship could be used to estimate $V_{crit,TB}$ in the current conditions of the study:

$$V_{crit,TB} = 1.4 \times k_s \times V_0 \qquad \textit{(Eq. 4)}$$

In the case of leucine enkephalin, this implied that very small differences in injection volume (e.g. < 0.7 µL in Fig. 5d) were sufficient to go from one phenomenon (i.e. breakthrough) to the other (i.e. Total Breakthrough).

The comparison of both the width and the shape of the retained peak, once the middle peak has appeared (blue curve), is interesting. With 30% ACN (Fig. 5a), the peak is larger than with 90% ACN (Fig. 5d) and exhibits a slight fronting. This trend is maintained under Total Breakthrough conditions (purple and black curves). The fact that better peak shapes were obtained with stronger sample solvents is counter-intuitive. Furthermore, with the same injected volume of 50 % V_0 (black curves in Fig.5), both the width and the shape of the retained peak are clearly improved when the percentage of acetonitrile in the injection solvent increases. Nevertheless, black and purple curves show that rather good peak shapes were obtained with very large injection volumes once Total Breakthrough conditions have been attained. Another effect occurring for very large injected volumes was the broadening and, in some cases,

the splitting of the breakthrough peak. As expected, for a given injection volume (e.g. 50% V_0), its shape is more affected by stronger sample solvents. On the other hand, with stronger injection solvents, the shape of the retained peak improves but its area decreases. For example, with 50% V_0 (black curve), the retained peak area was about three times larger with 30% ACN (Fig. 5a) than with 90% ACN (Fig. 5d). This is in agreement with the fact that a larger number of molecules are retained when the injection solvent is weaker.

An interesting point to discuss is the evolution of the separation of the middle peak with the injection volume, which is exemplified in Fig. S3 with 70% ACN as injection solvent. The trend was found to be the same regardless of the injection solvent. In Fig. S3, the asterisk and the diamond indicate the breakthrough and the retained peaks, respectively. The middle peak is located between them. As seen, both its retention and its height progressively decreases with the injection volume. The peak height is maximum when the middle peak is fully resolved from the retained peak (purple curve). Then, it progressively decreases as the injection volume increases, while the peak width increases. Once breakthrough has emerged (yellow curve), the retention and the width are no longer evolving. At this point, the beginning of the middle peak is close to the onset of the gradient (about 0.2 min). As the injection volume further increases, the peak height of the middle peak decreases until the peak completely disappears when Total Breakthrough occurs (red curve). During all these stages, the height and the area of the retained peak (diamond) remained approximately the same. As highlighted in our previous work [7] and shown in Fig. 5 (purple curve vs. black curve), both the height and the area of the retained peak start to increase again with the injected volume once Total Breakthrough has emerged. The appearance and the evolution of this middle peak are very surprising and totally unexplained so far. The understanding of the different separation stages preceding Total Breakthrough will be necessary to be able to predict and simulate the separations under Total Breakthrough conditions.

3.2.2. Effect of gradient conditions

- **Initial mobile phase composition**

Fig. 6 shows the effect of the initial composition of the mobile phase on the peak profile of leucine enkephalin. Three initial percentages of acetonitrile (strong solvent B) were studied: 1% (Fig. 6a), 5% (Fig. 6b), and 10% (Fig. 6c). The gradient elution was

carried out from the indicated initial composition to the same final composition of 45% B while keeping the normalized gradient slope constant by adjusting the gradient time. Consequently, the compositions at elution were similar. The same volume (2.5% V_0) was injected in the same solvent (50% ACN).

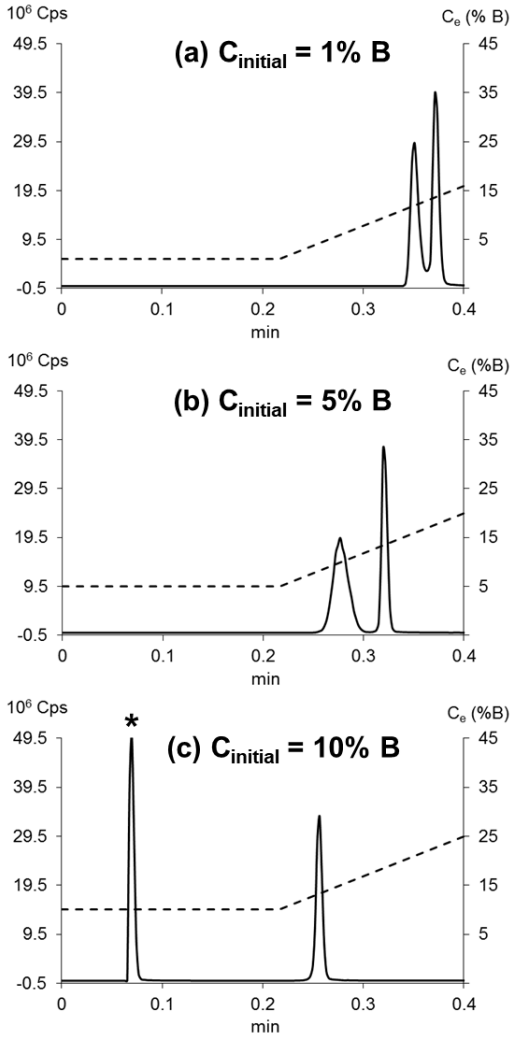

Fig.6: Effect of the initial composition ($C_{initial}$) on the separation: (a) 1% ACN, (b) 5% ACN, and (c) 10% ACN. The normalized gradient slope was maintained at 4% by changing the gradient time : (a) 0.54 min, (b) 0.49 min, (c) 0.43 min. Injection volume (V_i/V_0) = 2.5%. Solute: leucine enkephalin (50 mg/L). Same other conditions as in Fig. 1. The asterisk indicates the non-retained breakthrough peak.

As observed in Fig.6, injection issues are more critical when the initial percentage of acetonitrile is higher. With 1% ACN (Fig. 6a), the retained peak is split with no breakthrough. With 5% ACN (Fig. 6b), the middle peak is fully resolved from the retained peak and still, no breakthrough has appeared. With 10% ACN (Fig. 6c), a Total Breakthrough can be observed. This progression is comparable to what was observed

when increasing the injected volume for a given injection solvent strength (Fig. S3) or the injection solvent strength for a given injected volume (Fig. 5). Our hypothesis to explain this effect is that the injection plug is partly diluted in the initial mobile phase before entering the column, making the actual injection solvent weaker (i.e. k_s higher) with 1% ACN as initial composition than with 10% ACN.

- **Gradient time**

Fig. 7 shows the effect of the gradient time on the separation of leucine enkephalin. The separations were obtained with four different gradient times corresponding to $44t_0$ (Fig. 7a), $11t_0$ (Fig. 7b), $5.5t_0$ (Fig. 7c), and $3.7t_0$ (Fig. 7d), thus leading to four different normalized gradient slopes (i.e. 1%, 4%, 8%, and 12%, respectively). The four injection volumes show all the stages of the separation, i.e., from a single symmetrical retained peak (black curve) to Total Breakthrough (orange curve).

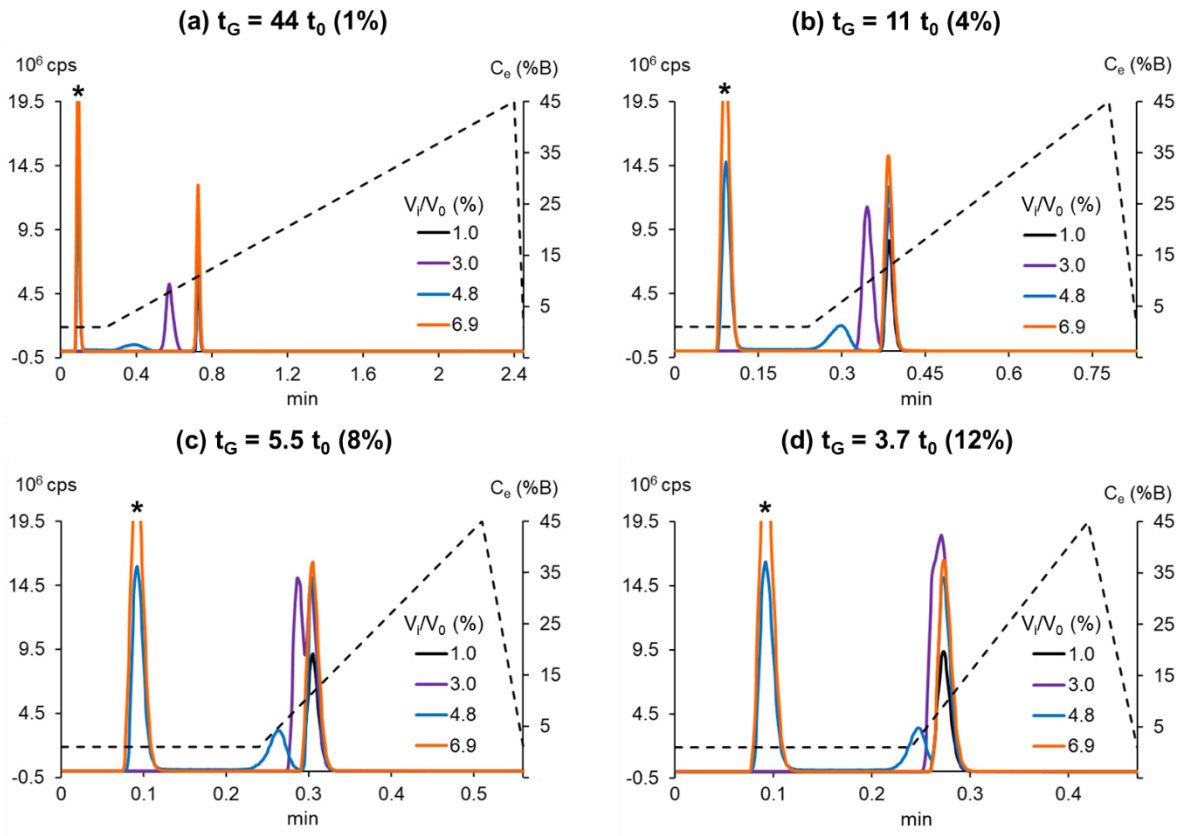

Fig.7: Effect of the gradient time on the separation. The gradient time is expressed as a multiple of the column dead time (t_0): (a) $44t_0$, (b) $11t_0$, (c) $5.5t_0$, and (d) $3.7t_0$, (t_0 = 0.049min). The resulting normalized gradient slope is given in brackets. V_i/V_0 was varied from 1% to 6.9%. Solute: leucine enkephalin (50 mg/L). Same other conditions as in Fig. 1.

The first observation that can be made is that, for a given injection volume (given colour in Fig. 7), the separations appear very similar, suggesting that the gradient time does not play a part in the onset of the different separation stages and, in particular, in the emergence of Total Breakthrough. The same set of separation stages is observed regardless of the gradient time: (i) one peak without breakthrough (black curve, 1% V_0), (ii) two peaks without breakthrough (purple curve, 3.0% V_0), (ii) three peaks including the breakthrough peak (blue curve, 4.8% V_0), and (iv) Total Breakthrough (orange curve, 6.9% V_0). For a given separation stage, the resolution between the middle and retained peaks decreases with the gradient time, which can be related to the decrease in peak capacity. Similar observations were made for two other peptides (bombesin and [ile]-angiotensin) and two small pharmaceuticals (nadolol and propranolol) (data not shown). The fact that both breakthrough and Total Breakthrough appear with the same injected volume regardless of the gradient time is in good agreement with the fact that both $V_{crit,B}$ and $V_{crit,TB}$ are only dependent on k_S, and hence totally independent of the gradient time.

- **Initial isocratic hold duration**

The same observations were made when changing the isocratic hold duration as shown in Fig. 8 for two compounds ([ile]-angiotensin and nadolol) with similar retentions but markedly different molecular weights (see Table 1). Both the gradient time (i.e. 1.08 min) and initial composition (i.e. 1%) were unchanged while the initial hold duration was varied from 0 min (Fig. 8a) to 0.53 min (Fig. 8c), leading to a total delay time (including the instrument dwell time) between 0.15 min and 0.68 min. The overlaid separations correspond to three injection volumes (1%, 1.2%, and 1.5% V_0). The two analytes were weakly retained in such conditions and eluted at the very beginning of the gradient elution (composition at elution close to 5% ACN) as shown by the gradient profile (dotted lines). This explains why injection issues could already be observed with very small injected volumes (<1% V_0) and why very small variations (i.e. ± 0.2% V_0) significantly modified the separations. For both analytes, injecting 1.0% V_0 (black curves) resulted in the appearance of two peaks without breakthrough, whereas 1.2% V_0 (purple curves), and 1.5% V_0 (blue curves) were sufficient to trigger breakthrough and Total Breakthrough, respectively. Similarly to the effect of the gradient time, different observations are noteworthy in Fig. 8: (i) the different stages of the separation and in particular $V_{crit,B}$ (close to 1.2% V_0) and $V_{crit,TB}$ (close to 1.5% V_0) are

quite the same regardless of the duration of the isocratic hold and the analyte, (ii) the ratio between those values are once again close to 1.4 (to the nearest measurement of uncertainty), (iii) the only difference in behaviour between the two analytes is the width and the shape of the middle peak of nadolol which is broader and less retained than that of [ile]-angiotensin, and (iv) the initial hold does not seem to affect the different stages of the separation but it does impact the shape and the position of the middle peak. In the case of [ile]-angiotensin, with 1.2% V_0 injected (purple curves in Figs. 8c), the middle peak flattens out so much that it seems to completely disappear. However, as shown by the zoomed figures (Fig. S4a), it is still present, suggesting that the situation of total breakthrough has not yet been achieved.

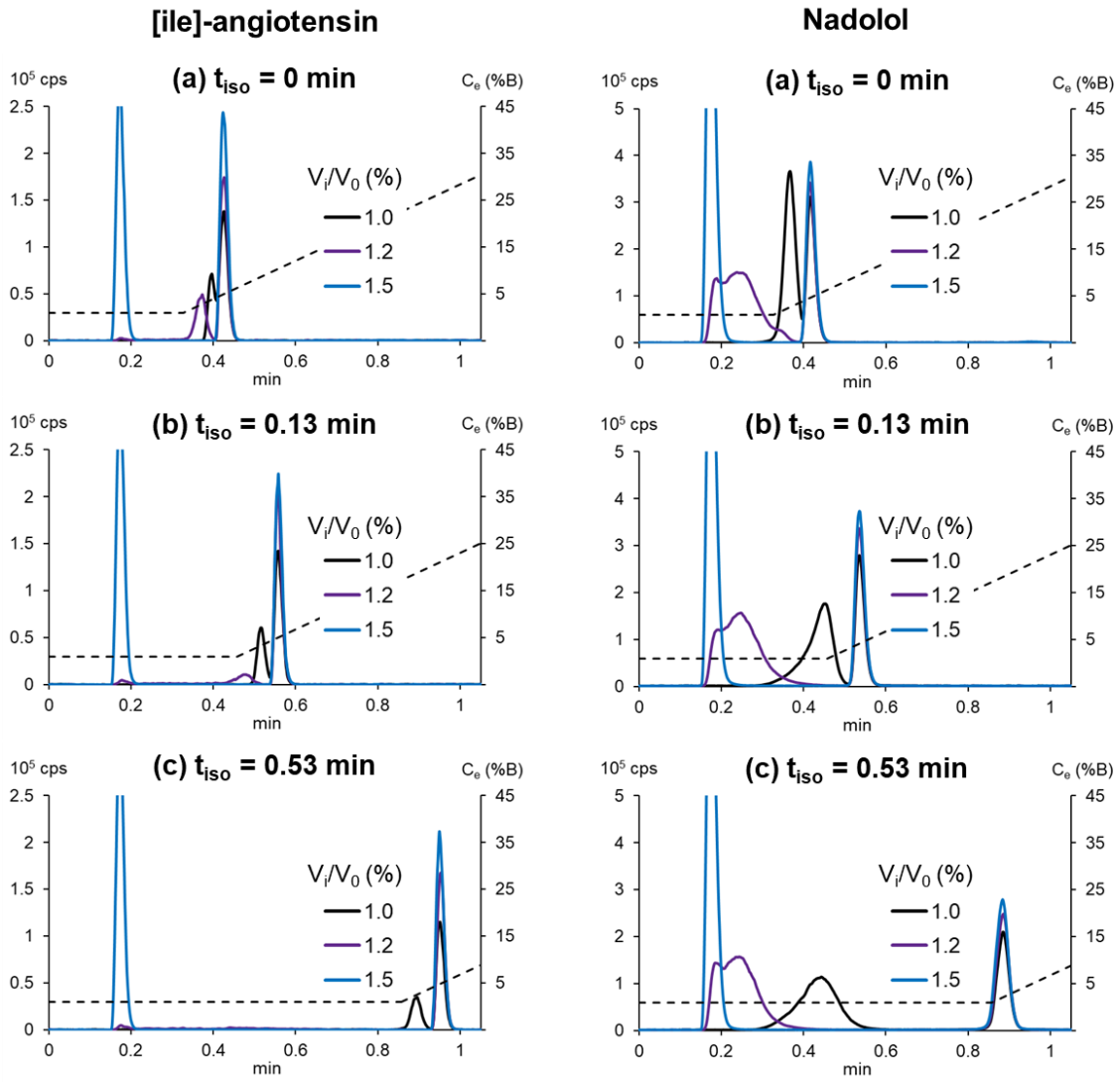

Fig.8: Effect of the initial isocratic hold duration on the separation: (a) 0 min, (b) 0.13 min, and (c) 0.53 min. Gradient time : 1.08 min (normalized gradient slope of 4%). V_i/V_0 was varied from 1% to 1.5%. Solutes: [ile]-angiotensin (100 mg/L) and (D-F) nadolol (0.5 mg/L). Flow rate: 0.75 mL/min. Same other conditions as in Fig. 1.

- **Flow rate**

The effect of the flow rate is shown in Fig. 9 for [ile]-angiotensin (Figs. 9a/b on the left) and nadolol (Figs. 9c/d on the right). The study was performed at 1.5 mL/min (Figs. 9a/c on the top) and 0.75 mL/min (Figs. 9b/d on the bottom). The normalized gradient slope was kept constant (i.e. s=4%) by changing the gradient time. As previously observed, for both compounds, there is no major difference on the separation between the two flow rates except a less good separation at 1.5 mL/min between the retained and the middle peak of [ile]-angiotensin which seems to results in a slightly larger injection volume for the emergence of Total Breakthrough (>1.2% V_0 at 1.5 mL/min vs. < 1.2% V_0 at 0.75 mL/min). For nadolol, the trend at both flow rates is exactly the same. As shown in Fig. S5, the same conclusions could be drawn for amitriptyline, a more retained base (C_e = 23% ACN), for which the similarity of the separations between the two flow rates is remarkable.

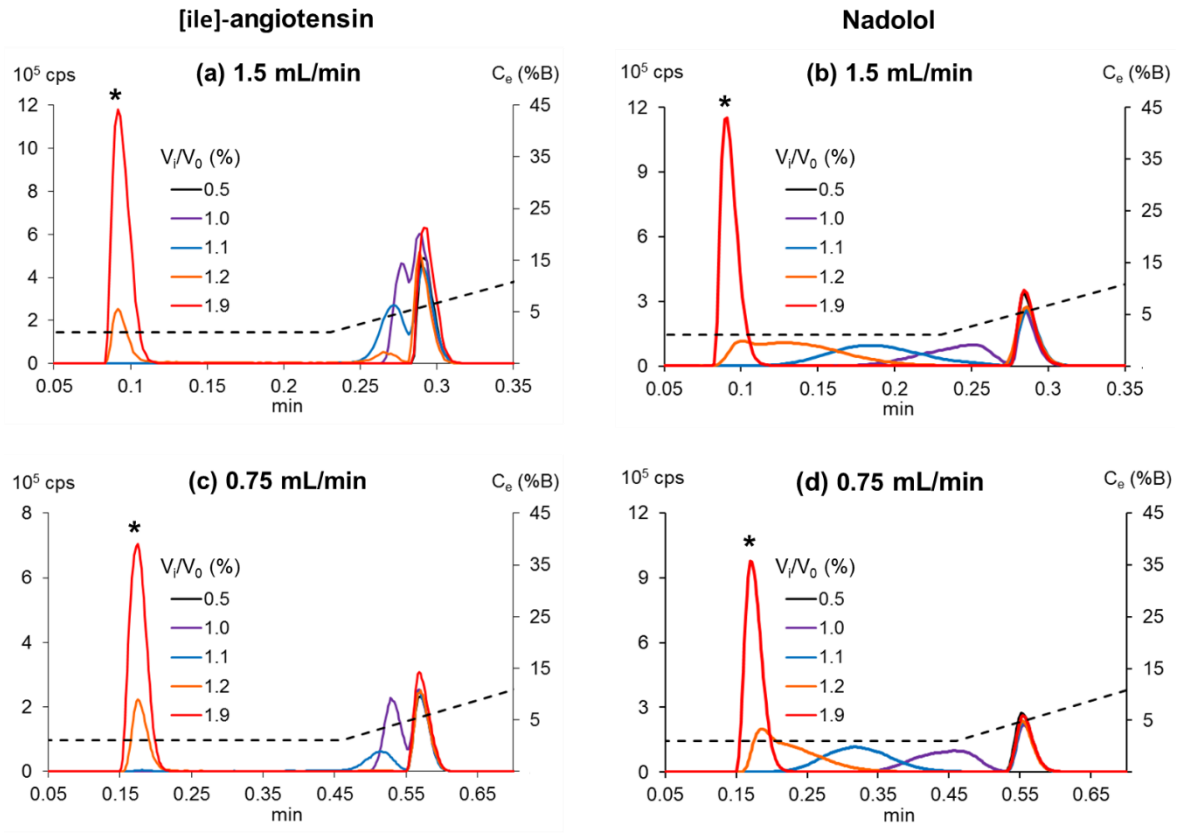

Fig.9: Effect of the flow rate on the separation: (a, b): 1.5 mL/min with a gradient time of 0.54 min and (c, d) 0.75 mL/min with a gradient time of 1.08 min. 80°C; Solute: (a, c) [ile]-angiotensin (250 mg/L) and (b, d) nadolol (0.5 mg/L). V_i/V_0 was varied from 1% to 1.9%. Same other conditions as in Fig. 1.

As also previously underlined, the middle peak is larger and more distorted for nadolol than for the peptide. Also, for nadolol, the retention shift of the middle peak is progressive when increasing the injected volume until co-elution with the breakthrough peak. That was not the case for peptides, [ile]-angiotensin (Figs. 9a/d) or leucine enkephalin (Fig. S3) although a similar trend was sometimes noticed for little retained peptides as exemplified in Fig. S6. It is interesting to note that, since nadolol and [ile]-angiotensin have a similar retention model (see Table 1), a possible relevant difference between them is their molecular weight, which might suggest an effect of molecular diffusion on the middle peak behaviour.

3.2.3. Effect of the column temperature

To highlight a possible effect of molecular diffusion, the column temperature was decreased from 80°C to 30°C, with a flow rate of 0.75mL/min. The obtained separations at 30°C for [ile]-angiotensin (Fig.10a) and nadolol (Fig.10b) can be compared to those at 80°C shown in Figs. 9c and 9d, respectively.

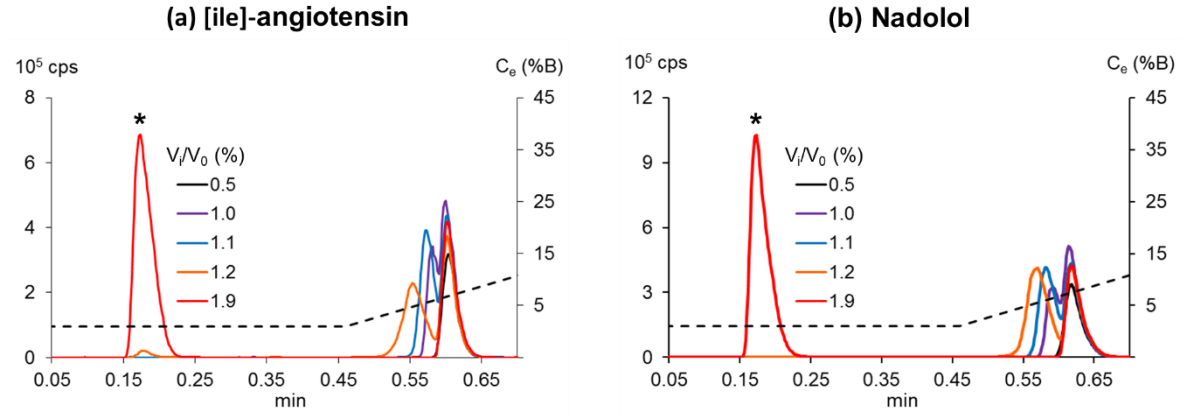

Fig.10: Effect of a decrease in column temperature (30°C) on the separation of (a) [ile]-angiotensin (250 mg/L) and (b) nadolol (0.5 mg/L). Same other conditions as in Figs. 9c and 9d.

At a lower temperature, the retention increases while the diffusion coefficient decreases. As can be observed, Total Breakthrough appears with a slightly injected volume at 30°C, suggesting that decreasing the temperature has the same effect (in terms of the emergence of Total Breakthrough) as increasing the flow rate. Apart from this difference, the separations evolve in a similar way at the two studied temperatures. As shown in Fig. S7, similar conclusions could be drawn for amitriptyline (more retained basic compound). Yet, it is interesting to point out the

significant difference in both the shape and the retention of the middle peak for nadolol between 30°C (Figs. 10b) and 80°C (Fig. 9d). The middle peak is indeed thinner and more retained at 30°C, resulting in a behaviour similar to that of the peptide, unlike at 80°C.

3.2.4. Effect of the sample concentration

Fig. 11 shows the separations obtained for [ile]-angiotensin (Fig. 11a) and nadolol (Fig. 11b) by dividing the sample concentration by a factor of 25 and 100, respectively compared to those in Figs. 9c and 9d, respectively.

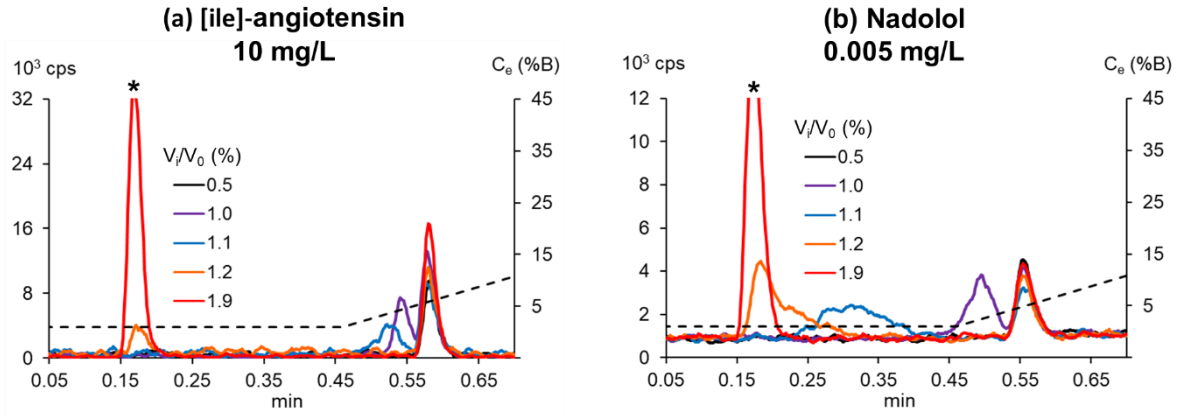

Fig.11: Effect of a decrease in sample concentration on the separation of (a) [ile]-angiotensin (10 mg/L) and (b) nadolol (0.005 mg/L). Same other conditions as in Figs. 9c and 9d.

Once again, for both solutes, the similarity in the way the separation evolves with the injected volume is absolutely remarkable. It is interesting to note that, in the case of nadolol, the middle peak seems to have the same evolution when decreasing the sample concentration as when decreasing the column temperature (Fig. 10b). As may be seen when comparing the purple curves (V_i/V_0 = 1%) in Figs. 11b an 9d, the middle peak is narrower and more retained by decreasing the sample concentration. We measured the ratio of the retained peak area to the total area (breakthrough peak and retained peak) for both concentrations under Total Breakthrough conditions (1.9% V_0, red curves in Fig. 11). For both compounds, this ratio was found to be independent of the concentration (about 0.30 for [ile]-angiotensin and 0.25 for nadolol). Similar observations could be drawn for amitriptyline (Fig. S8). Those results are quite consistent with our previous study [7] in which we found excellent linearity between

the retained peak area and the analyte concentration once Total Breakthrough conditions were attained.

4. Conclusions

In this work, we have conducted an extensive study on the phenomena of breakthrough and Total Breakthrough in liquid chromatography. Total Breakthrough can be described as a critical case of breakthrough with two distinct peaks for a given solute: an unretained breakthrough peak and a well retained symmetrical peak eluted at the expected retention time. The main objective of this work was to gain some insight into this particular phenomenon and to better define the conditions under which it occurs. To this end, the effect of numerous parameters, including the nature of the solute, the retention mechanism, the injection solvent composition, the injection volume, the gradient elution conditions, the column temperature, and the injected sample concentration, was investigated. Special attention was paid to the impact of these parameters on the emergence of both breakthrough and Total Breakthrough phenomena. The most important findings from our results are reported below:

(i) It was previously theoretically established that the injection volume required for breakthrough for a given analyte could be given by a very simple relationship (i.e. $V_{crit,B} = k_S \times V_0$) [14]. In the present experimental study, it was found that the injection volume required for Total Breakthrough was about 1.4 times larger ($V_{crit,TB} = 1.4 \times k_S \times V_0$).

(ii) Whereas breakthrough might be observed for any compounds as long as the previous relationship is satisfied, the occurrence of Total Breakthrough seems to be limited to positively charged compounds only. Experimentally, this was confirmed for several weak bases and peptides. Meanwhile, Total Breakthrough was never reached for negatively charged or neutral compounds whatever the conditions.

(iii) Considering the importance of the presence of positive charges on the molecule and given that this phenomenon was also observed in HILIC, we believe that the Total Breakthrough phenomenon could be explained by the circumstances of a mixed retention mechanism. Yet, further investigation should be conducted to confirm this theory and demystify this singular phenomenon.

(iv) Among all the studied parameters, the injection solvent composition (k_s) and the injection volume (V_i/V_0) for a given analyte were found to be the only ones to have an impact on the onset of breakthrough and Total Breakthrough. Both phenomena turned out to appear at the same injected volumes regardless of other analytical conditions. This supports the premise that the critical volumes required for breakthrough ($V_{crit,B}$) and Total Breakthrough ($V_{crit,TB}$) are only dependant on the retention factor of the analyte in the injection solvent (k_S) and the column volume (V_0).

(v) All the studied parameters seem to act on the retention and shape of the middle peak in contrast to the other peaks (breakthrough and retained peaks).

(vi) Considering the previously established relationship for $V_{crit,B}$ [14] and based on the above-mentioned conclusions regarding $V_{crit,TB}$, it becomes clear that the only two options to avoid breakthrough, and by extension Total Breakthrough, for a given analyte, is to reduce the injected volume and/or reduce the eluent strength of the injection solvent. On the other hand, if the goal is to reach Total Breakthrough, the injection volume should be set so that $V_{crit,TB}$ exceeds $V_{crit,B}$ by a specific factor that was found to be close to 1.4 in the current study. While theoretically, such conditions should be accessible for all compounds as long as they are positively charged, it is worth pointing out that in practice, the required volumes might be very large, hence difficult, if not impossible to reach experimentally in the case of strongly retained compounds injected in weak solvents.

5. References

[1] D.R. Stoll, P.W. Carr, Two-Dimensional Liquid Chromatography: A State of the Art Tutorial, Anal. Chem. 89 (2017) 519–531. https://doi.org/10.1021/acs.analchem.6b03506.

[2] B.W.J. Pirok, A.F.G. Gargano, P.J. Schoenmakers, Optimizing separations in online comprehensive two-dimensional liquid chromatography, J. Sep. Sci. 41 (2018) 68–98. https://doi.org/10.1002/jssc.201700863.

[3] B.W.J. Pirok, D.R. Stoll, P.J. Schoenmakers, Recent Developments in Two-Dimensional Liquid Chromatography: Fundamental Improvements for Practical Applications, Analytical Chemistry. 91 (2019) 240–263.

https://doi.org/10.1021/acs.analchem.8b04841.

[4] P. Česla, J. Křenková, Fraction transfer process in on-line comprehensive two-dimensional liquid-phase separations, J. Sep. Sci. 40 (2017) 109–123. https://doi.org/10.1002/jssc.201600921.

[5] Y. Chen, L. Montero, O.J. Schmitz, Advance in on-line two-dimensional liquid chromatography modulation technology, TrAC Trends in Analytical Chemistry. 120 (2019) 115647. https://doi.org/10.1016/j.trac.2019.115647.

[6] G. Vanhoenacker, I. Vandenheede, F. David, P. Sandra, K. Sandra, Comprehensive two-dimensional liquid chromatography of therapeutic monoclonal antibody digests, Anal Bioanal Chem. 407 (2015) 355–366. https://doi.org/10.1007/s00216-014-8299-1.

[7] S. Chapel, F. Rouvière, S. Heinisch, Pushing the limits of resolving power and analysis time in on-line comprehensive hydrophilic interaction x reversed phase liquid chromatography for the analysis of complex peptide samples, Journal of Chromatography A. (2019) 460753. https://doi.org/10.1016/j.chroma.2019.460753.

[8] A. D'Attoma, S. Heinisch, On-line comprehensive two dimensional separations of charged compounds using reversed-phase high performance liquid chromatography and hydrophilic interaction chromatography. Part II: Application to the separation of peptides, Journal of Chromatography A. 1306 (2013) 27–36. https://doi.org/10.1016/j.chroma.2013.07.048.

[9] E. Sommella, O.H. Ismail, F. Pagano, G. Pepe, C. Ostacolo, G. Mazzoccanti, M. Russo, E. Novellino, F. Gasparrini, P. Campiglia, Development of an improved online comprehensive hydrophilic interaction chromatography × reversed-phase ultra-high-pressure liquid chromatography platform for complex multiclass polyphenolic sample analysis, J. Sep. Sci. 40 (2017) 2188–2197. https://doi.org/10.1002/jssc.201700134.

[10] J.-L. Cao, S.-S. Wang, H. Hu, C.-W. He, J.-B. Wan, H.-X. Su, Y.-T. Wang, P. Li, Online comprehensive two-dimensional hydrophilic interaction chromatography×reversed-phase liquid chromatography coupled with hybrid linear ion trap Orbitrap mass spectrometry for the analysis of phenolic acids in

Salvia miltiorrhiza, Journal of Chromatography A. 1536 (2018) 216–227. https://doi.org/10.1016/j.chroma.2017.09.041.

[11] D.R. Stoll, D.C. Harmes, G.O. Staples, O.G. Potter, C.T. Dammann, D. Guillarme, A. Beck, Development of Comprehensive Online Two-Dimensional Liquid Chromatography/Mass Spectrometry Using Hydrophilic Interaction and Reversed-Phase Separations for Rapid and Deep Profiling of Therapeutic Antibodies, Anal. Chem. 90 (2018) 5923–5929. https://doi.org/10.1021/acs.analchem.8b00776.

[12] S. Toro-Uribe, L. Montero, L. López-Giraldo, E. Ibáñez, M. Herrero, Characterization of secondary metabolites from green cocoa beans using focusing-modulated comprehensive two-dimensional liquid chromatography coupled to tandem mass spectrometry, Analytica Chimica Acta. 1036 (2018) 204–213. https://doi.org/10.1016/j.aca.2018.06.068.

[13] Q. Li, F. Lynen, J. Wang, H. Li, G. Xu, P. Sandra, Comprehensive hydrophilic interaction and ion-pair reversed-phase liquid chromatography for analysis of di- to deca-oligonucleotides, Journal of Chromatography A. 1255 (2012) 237–243. https://doi.org/10.1016/j.chroma.2011.11.062.

[14] V. Pepermans, S. Chapel, S. Heinisch, G. Desmet, Detailed numerical study of the peak shapes of neutral analytes injected at high solvent strength in short Reversed-Phase liquid chromatography columns and comparison with experimental observations, Journal of Chromatography A. (2021) 462078. https://doi.org/10.1016/j.chroma.2021.462078.

[15] S. Chapel, F. Rouvière, S. Heinisch, Comparison of existing strategies for keeping symmetrical peaks in on-line Hydrophilic Interaction Liquid Chromatography x Reversed-Phase Liquid Chromatography despite solvent strength mismatch, Journal of Chromatography A. 1642 (2021) 462001. https://doi.org/10.1016/j.chroma.2021.462001.

[16] B. Buszewski, S. Noga, Hydrophilic interaction liquid chromatography (HILIC)—a powerful separation technique, Anal Bioanal Chem. 402 (2012) 231–247. https://doi.org/10.1007/s00216-011-5308-5.

[17] D.V. McCalley, Understanding and manipulating the separation in hydrophilic interaction liquid chromatography, Journal of Chromatography A. 1523 (2017) 49–71. https://doi.org/10.1016/j.chroma.2017.06.026.

B. Article 7: Comparison of existing strategies for keeping symmetrical peaks in on-line Hydrophilic Interaction Liquid Chromatography x Reversed-Phase Liquid Chromatography despite solvent strength mismatch

Abstract

In two-dimensional liquid chromatography, the combination of hydrophilic interaction liquid chromatography (HILIC) and reversed-phase liquid chromatography (RPLC) is very attractive due to the complementarity of their separation mechanisms. On-line comprehensive HILIC x RPLC is well-known to give rise to a large retention space coverage when dealing with ionizable compounds. However, method development in on-line HILIC x RPLC is challenging due to the reversed solvent strength between both dimensions, which can greatly affect the peak shapes in the second RPLC dimension, and thus the separation quality and the method sensitivity. In the present contribution, we compared four strategies designed to avoid this problem: (i) flow splitting, which consists in reducing the injection volume in the second dimension (^{2}D), (ii) on-line dilution with a make-up flow and (iii) on-line dilution with Active Solvent Modulation (ASM), which both consist in reducing the solvent strength of the injected fractions, and (iv) Total Breakthrough Strategy, which we recently proposed. Unlike the three preceding strategies, this latter one consists in injecting large volumes of strong solvent in ^{2}D. The performance of each strategy was evaluated for sub-hour separations of a tryptic digest in on-line HILIC x RPLC. In this work, we considered the critical case for which the same column internal diameters (i.e. 2.1 mm here) are used in both dimensions. Peak capacity, peak shapes and peak intensities were considered for this evaluation. The highest peak capacity could be achieved with Total Breakthrough Strategy while the lowest one with on-line dilution using ASM. Peak intensities were usually higher with on-line dilution approaches (make-up flow and ASM). However, despite the presence of breakthrough, peak intensities were approximately 7-fold higher with Total Breakthrough Strategy than with flow splitting.

1. Introduction

On-line comprehensive two-dimensional liquid chromatography (LC x LC) is a powerful tool to deal with highly complex samples. The potential of this technique has been highlighted in various application areas, including, among the most recent ones, proteomics [1], metabolomics [2], natural product research [3], polymer analysis [4], and pharmaceutical analysis [5]. The basic principle of two-dimensional liquid chromatography (2D-LC) is the combination of two chromatographic systems, referred to as dimensions, to expand the level of information on a given sample. To be effective, the two dimensions must provide different selectivities. This is usually achieved by selecting two chromatographic modes with different retention mechanisms. In on-line comprehensive 2D-LC (on-line LC x LC), the entire effluent from the first dimension (^{1}D) is fractionated and continuously transferred to the second dimension (^{2}D) through a switching-valve, often referred to as a modulator. Compared to conventional one-dimensional liquid chromatography (1D-LC), a drastic improvement of the resolving power is expected. In theory, the peak capacity should be the product of the peak capacities in the two dimensions. In practice, this is true if the ^{1}D-separation is preserved and if the available ^{2}D separation space is fully occupied by peaks (i.e. if the two separation dimensions are fully orthogonal). Apart from a few lucky combinations, such as HIC x RPLC [6], HIC x SEC [7] or IEX x RPLC [8], for which the mobile phase in ^{1}D becomes a weak injection solvent in ^{2}D, the quest for a higher degree of orthogonality between the two dimensions often leads to a decreased compatibility between the mobile phase in ^{1}D and the separation in ^{2}D.

A typical example of this duality is the combination of hydrophilic interaction liquid chromatography (HILIC) and reversed-phase liquid chromatography (RPLC). In the past decade, HILIC x RPLC has received a substantial increase in interest for the on-line LC x LC separation of polar and ionizable compounds [9–12]. This growing popularity is driven by the complementarity of the two separation mechanisms, which gives rise to high coverage of the two-dimensional retention space [2,13]. However, due to the opposite eluent strengths of the two mobile phases, on-line HILIC x RPLC is not guaranteed to succeed. The mobile phase in HILIC typically contains a high percentage of acetonitrile (i.e. > 50%), which is a strong eluent in RPLC. The transfer of acetonitrile-rich fractions from ^{1}D-HILIC usually greatly impacts the peak shapes in ^{2}D-RPLC, the solute band being not or partly retained in the ^{2}D-column. This may lead to band broadening, peak distortion, and/or analyte breakthrough. Breakthrough is a

phenomenon that occurs when part of the sample migrates through the column without any retention and elute with the solvent peak, whereas the other part undergoes normal retention, which results in the presence of an unretained peak in addition to the expected retained peak. The shape of the retained peak depends on (i) the solute retention in the injection solvent, (ii) the solute retention in the mobile phase, and (iii) the injection volume. These injection effects negatively impact the separation in 2D by decreasing both the peak capacity and the peak intensity.

Solvent strength mismatch is by far the most critical reported issue in on-line HILIC x RPLC [2,3,14–16]. To overcome its deleterious impact on the separation, a few strategies were proposed over the years. They fall into two broad categories: (i) reducing the injection volume or (ii) reducing the eluent strength of the injection solvent by on-line dilution with a weak solvent. Reducing the volume injected in ^{2}D can be achieved either by selecting appropriate column internal diameters in each dimension [9] (usually at least twice as large in ^{2}D) or more commonly by splitting the flow coming from ^{1}D with a tee-piece and appropriate tubing [17]. Both approaches inevitably result in increased dilution. On-line solvent dilution consists in diluting the ^{1}D-organic-rich fractions with water before injection in ^{2}D. Three different methods were reported. The most widespread one makes use of a make-up pump between the ^{1}D-column and the interface valve [18]. The flow rate delivered by the pump can be varied depending on the desired dilution. In 2017, a new valve permitting to achieve dilution inside the valve using restriction capillaries was introduced. It was referred to as "Active Solvent Modulation" (ASM) [19,20]. More recently, the so-called "At-Column Dilution" (ACD) was proposed. In this case, dilution is carried out between the valve and the ^{2}D-column by using an additional pump to empty the sample loop while the ^{2}D-pump dilutes the transferred fractions [21,22]. Regardless of the method, very large volumes, which are proportional to the desired dilution ratio, are injected in ^{2}D. Nevertheless, improvements in both peak shape and peak intensity can be expected from the substantial decrease in eluent strength, which promotes band focusing at the ^{2}D-column inlet. It should be noted that despite the decrease in solvent strength, very large injection volumes can still have a detrimental effect on peak shapes, especially for less retained compounds. This was highlighted in the context of the separation of pharmaceuticals in 1D-LC [23]. The combination of both on-line dilution and flow splitting was suggested to lessen this problem [11,23] but this approach was not compared to on-line dilution alone. Similarly, the use of short trap columns instead of

conventional empty loops after on-line dilution with a make-up flow was subjected to numerous developments in recent years [24]. Trap columns are supposed to reduce the injection volume after on-line dilution by trapping the analytes before being sent to the ^{2}D-column. Despite the increased popularity of trap columns in on-line HILIC x RPLC [10,12,25,26], their added value in combination with on-line dilution has still to be demonstrated. Furthermore, the use of 2D methods with trap columns is questionable for routine analysis since it is more difficult to develop and less rugged considering the risk of sample loss and incomplete recovery.

In a previous work [13], we presented an alternative approach for the separation of peptides in on-line HILIC x RPLC that we called "Total Breakthrough Strategy" (TBS). This approach relies on the injection of relatively large volumes of strong solvent without flow-splitting and on-line dilution. Unlike the above strategies, for which breakthrough is unwelcome, our approach is supported by the existence of breakthrough. For large enough injection volumes, it was shown that quite symmetrical peaks could be obtained in ^{2}D-RPLC. It was also proved that the peak retention time exactly matches the one obtained by injecting a small analyte volume in a weak solvent. Furthermore, despite the presence of breakthrough, quantitative analysis on the retained peak was proved to be quite reliable. Such conclusions could be drawn provided that the injected volume was above a specific critical volume which depends on the analyte, its retention, and its injection solvent [13]. In this case, the area of the retained peak varies linearly with the injected amount, which is not the case at an earlier stage of breakthrough (i.e. below the critical volume). The validity of this approach in on-line HILIC x RPLC was demonstrated under a broad range of conditions in the context of peptide analysis.

The aim of the present study was to compare four of the above-cited strategies, designed to overcome solvent strength mismatch in on-line HILIC x RPLC. In this work, we have considered the critical case for which the same column internal diameter (here 2.1 mm) is used in both dimensions. The compared strategies include (i) the Total Breakthrough strategy (TBS) [13], (ii) the flow splitting strategy (FSS), (iii) the make-up flow strategy (MFS), and (iv) the active solvent modulation strategy (ASMS). Their strengths and weaknesses are identified in the context of an optimized sub-hour separation of a tryptic digest in on-line HILIC x RPLC with a view to select the most appropriate one.

2. Experimental section

2.1. Chemical and reagents

Acetonitrile (ACN, LC-MS grade) was obtained from Sigma-Aldrich (Steinheim, Germany). Water was purified and deionized in-house using an Elga Purelab Classic UV purification system from Veolia water STI (Décines-Charpieu, France). Formic acid (FA, LC-MS grade), ammonium acetate, and ammonium bicarbonate (both analytical reagent grade) were obtained from Fischer scientific (Illkirch, France). DL-1,4-dithiothreitol (DTT, 99%) and iodoacetamide (98%) were obtained from Acros Organics (Geel, Belgium). Trypsin, human serum albumin (HSA), bovine serum albumin (BSA), β-casein, myoglobin, lysozyme, and cytochrome C were all obtained from Sigma-Aldrich (Steinheim, Germany).

2.2. Sample preparation

A model sample was obtained by tryptic digestion of six proteins (HSA, BSA, β-casein, myoglobin, lysozyme, and cytochrome C) following a protocol described elsewhere [13,17].

The aqueous digests were 2-fold diluted with ACN and filtered on 0.22 μm PVDF (polyvinylidene fluoride) membranes before injection in ^{1}D-HILIC.

2.3. Instrumentation

2D-LC experiments were carried out on a 1290 Infinity series 2D-LC system from Agilent Technologies (Waldbronn, Germany). The system includes two high-pressure binary pumps, a thermostated autosampler with a flow-through needle injector, two thermostated column compartments with low-dispersion preheaters, and two diode-array UV absorbance detectors (DAD) with 0.6 μL flow-cells. The switching-valve connecting the two dimensions was either a 2-position /4-port duo valve (Fig. S1) or a 4-position/10-port Active Solvent Modulation (ASM) valve (Fig. S2), both configured in backflush mode to minimize extra-column dispersion. In this paper, the first one will be referred to as a standard valve, the second one as the ASM valve. Depending on the transferred fraction volume, the valves were equipped with two identical sample loops of either 20 μL (0.2 mm ID), 40 μL (0.25 mm ID for the standard valve, and 0.35 mm ID for the ASM valve) or 180 μL (0.35 mm ID). For on-line dilution, the sample loops were connected to the valve through two parking decks (valves used for multiple

heart-cutting 2D-LC) using two transfer capillaries of 1.9 µL (0.35 mm ID). A schematic representation of this configuration is shown in Fig. S3. For the make-up flow approach, this setup was used to circumvent the incompatibility of the commercialized 180 µL loops fitting with the standard valve ports. In the case of ASM, not only the comprehensive 2D-LC sample loops are not compatible with the ports of the ASM valve, but this technique also requires backpressure from capillaries between the ASM valve and the multiple heart-cutting valves to function. A pressure release kit was installed between the ^{1}D-outlet and the modulation valve inlet to minimize baseline disturbances coming from 2D-LC valve switching. The dwell volumes and extra-column volumes were respectively 170 µL and 22 µL in ^{1}D, and 80 µL and 8.5 µL in ^{2}D (loop volume excluded). For the make-up flow strategy, an additional high-pressure binary pump from an Acquity UPLC I-Class liquid chromatography system from Waters (Milford, MA, USA) was used. The schematic representations of the four different setups used in this work are given in Fig. 1.

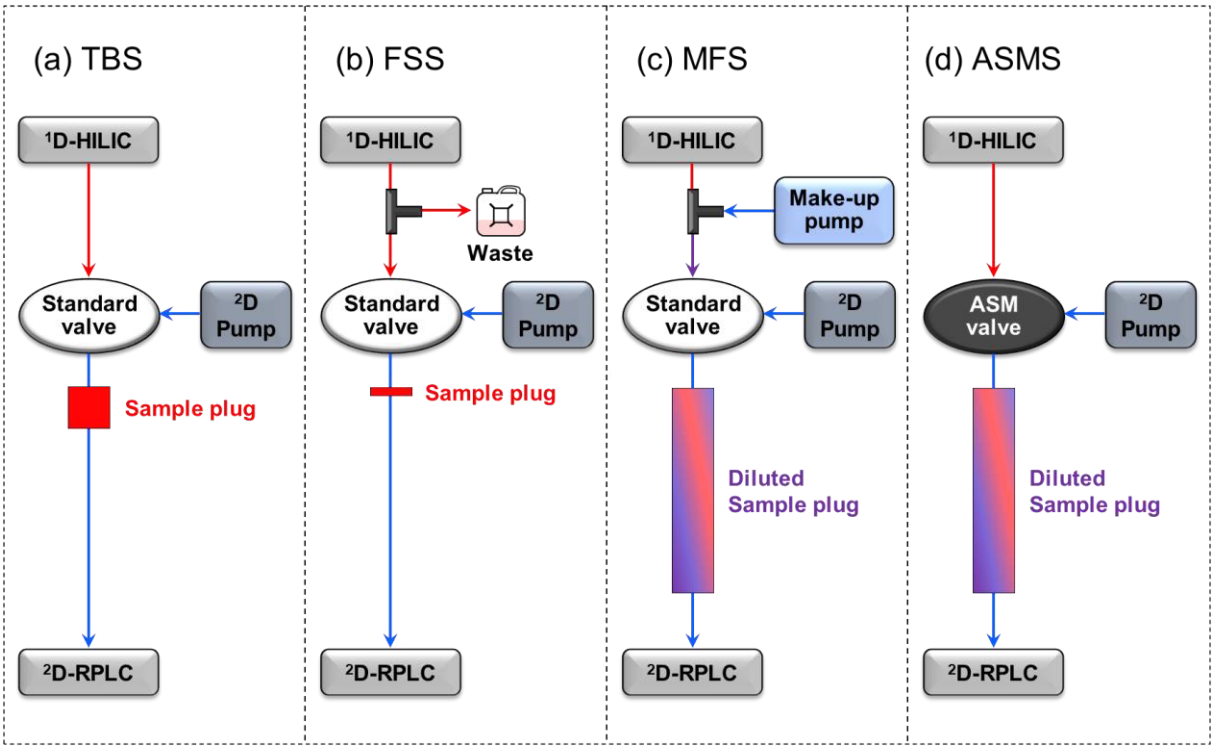

Fig.1: Schematic representation of the four interfaces for the four studied strategies: (a) Total Breakthrough strategy (TBS), (b) Flow splitting strategy (FSS), (c) Make-up flow strategy (MFS) and Active solvent modulation strategy (ASMS). The injected volumes are represented at the bottom of each scheme. Colours stand for the solvent strength (red for strong solvent, blue for weak solvent, purple for diluted solvent).

The 2D-LC system was hyphenated to an Agilent Q-TOF mass spectrometer (model G6545B) equipped with a JetStream electrospray ionization (ESI) source. The 2D-LC-UV system and the additional high-pressure pump were controlled using Agilent OpenLab software and Waters MassLynx software, respectively. The mass spectrometer was controlled using Agilent MassHunter software. HRMS data were processed using Agilent MassHunter qualitative analysis software. 2D data were processed with Matlab (V7.12.0635).

2.4. Chromatographic and detection conditions

For a fair comparison, similar conditions were used for the four presented strategies. The conditions were optimized in a previous study dealing with the on-line HILIC x RPLC separation of peptides in 30 min [13]. The ^{1}D-HILIC separation was performed using an Acquity BEH HILIC column (50 × 2.1 mm; 1.7 µm particles) from Waters (Milford, MA, USA). The column temperature was set at 30 °C and the flow rate was 0.05 mL/min. The injected volume was 6 µL. A gradient elution with ACN as solvent A and 10 mM ammonium acetate in water as solvent B (pH of 6.8 in the aqueous phase) was carried out as follows: 0 min (2% B), 30 min (52% B), 32.4 min (2% B), and 50 min (2% B). UV chromatograms were recorded at 210 nm with an acquisition rate of 20 Hz. The sampling time was 0.39 min. Depending on the studied strategy, the transferred fractions were modified or not before injection in ^{2}D, as discussed in the next section. The ^{2}D-RPLC separation was performed using an Acquity CSH C18 column (30 × 2.1 mm; 1.7 µm particles) from Waters (Milford, MA, USA). The column temperature was set at 80°C and the flow rate was 2 mL/min. Water was used as solvent A and ACN as solvent B, both with 0.1% formic acid (pH = 2.7). Initial and final compositions were 1% B and 45% B. The gradient times and the interface conditions were dependent on the studied strategies, as discussed in the next section. Their values are summarized in Table 1.

The effluent from ^{2}D was split using a zero dead volume tee-piece (split 1:2; MS:UV). UV chromatograms were recorded at 210 nm with an acquisition rate of 80 Hz in ^{2}D. Q-TOF-HRMS data were acquired in positive ion mode from 100 to 3200 m/z with an acquisition rate of 20 spectra/s. The drying gas temperature and flow rate were 300°C and 11 L/min, respectively. The nebulizer gas pressure was 40 psi. The sheath gas temperature and flow rate were 350°C and 11 L/min, respectively. The capillary, the

nozzle, the fragmentor, the skimmer, and the Oct 1 RV voltages were 3500, 300, 150, 20, and 750 V, respectively.

Table 1: Experimental interface conditions for the four compared strategies: Total Breakthrough strategy (TBS), flow splitting strategy (FSS), make-up flow strategy (MFS), and Active solvent modulation strategy (ASMS). The different terms refer to Eqs. 3 to 9. ^{2}F = 2000 µL/min; sampling time = 0.39 min. The graphical representation of the time repartition is presented in Fig. 2.

	$^{1}V_{fraction}$ (µL)	$^{1}z_{split}$	$^{1}z_{dilution}$	V_{loop} (µL)	$^{2}V_{injection}$ (µL)	$^{2}t_{loop}$ (min)	$^{2}t_{D,instru}$ (min)	$^{2}t_{iso}$ (min)	$^{2}t_{G}$ (min)	$^{2}t_{post}$ (min)	$^{2}t_{eq}$ (min)
TBS	19.5	1	1	40	19.5	0.02	0.04	0	0.26	0.03	0.04
FSS	1.95	10	1	20	1.95	0.01	0.04	0	0.27	0.03	0.04
MFS	97.5	1	5	180	97.5	0.09	0.04	0	0.19	0.03	0.04
ASMS	19.5	1	1	40	97.5	0.02	0.04	0.1	0.16	0.03	0.04

2.5. Calculations

The effective peak capacities, $n_{2D,eff}$, were calculated from the following relationship:

$$n_{2D,eff} = \alpha \times \gamma \times \left(1 + \frac{^{1}\Delta t}{^{1}w_{4\sigma}}\right) \times \left(1 + \frac{^{2}\Delta t}{^{2}w_{4\sigma}}\right) \quad \textit{(Eq. 1)}$$

Δt is the whole range of elution times, $w_{4\sigma}$, the average peak width at 4σ (i.e. 13.4% of peak height). α corrects for undersampling in ^{1}D [27] and γ corrects for partial retention space coverage [28]. In all present 2D separations, their values were found to be 0.67 for α and 1 for γ (100% coverage), respectively.

The composition of acetonitrile at elution was calculated according to:

$$C_{elution} = C_{initial} + \frac{(C_{final} - C_{initial})}{t_G}(t_r - t_D - t_0) \text{ in RPLC}$$

Or

$$C_{elution} = 100 - \left[C_{initial} + \frac{(C_{final} - C_{initial})}{t_G}(t_r - t_D - t_0)\right] \text{ in HILIC} \quad \textit{(Eq. 2)}$$

Where $C_{initial}$ and C_{final} are the initial and final compositions of acetonitrile in the mobile phase, t_r is the retention time, t_D is the total dwell time, and t_0 is the column dead time.

The following asymmetry factor, A_f was considered to assess the peak asymmetry:

$$A_f = \frac{a+b}{2a} \qquad \textit{(Eq. 3)}$$

With a and b the left and the right half peak width respectively, both measured at 5% of the peak height.

3. Results and discussion

The objective of this study was to compare four strategies that are currently proposed to reduce broad and distorted peaks and hence to improve the separation in the second dimension of on-line HILIC x RPLC. We considered the peak shape, the peak width, and the peak capacity as the main quality descriptors. The peak intensity, and hence the extent to which the analytes were diluted was also compared between the four strategies. Broad and distorted peaks mainly arise from a difference in solvent strength between the organic-rich fraction coming from HILIC and the water-rich mobile phase in RPLC. The four studied strategies included: (i) the Total Breakthrough strategy (TBS), which consists in injecting the entire fractions coming from ^{1}D so that a situation of Total Breakthrough occurs in ^{2}D for all peaks [13], (ii) The flow splitting strategy (FSS), which consists in splitting the flow prior to the valve, and hence in injecting small volumes of undiluted fractions, and (iii) the make-up flow strategy (MFS) and (iv) the active solvent modulation strategy (ASMS). Both latter strategies result in injecting large volumes of fractions previously diluted with a weak solvent (usually water). This is carried out with a make-up pump in the first case and the ASM-valve (marketed by Agilent) in the second case. It should be noted that dilution after the switching-valve was also recently reported under the name "at-column dilution" [21,22]. In this study, we considered the critical case in which the same column internal diameters (i.e. here 2.1 mm) are used in both dimensions. However, it should be noted that FSS with a split ratio of 1/10 should give similar results as those obtained with a ratio of 3 between the internal diameters (e.g. 1 mm in ^{1}D and 3 mm in ^{2}D). The studied sample was a tryptic digest of six proteins. Some conditions were specific to the studied strategy, including the gradient time in ^{2}D and other specific interface conditions. The other conditions, optimized in a previous study [13], are given in the experimental section.

3.1. Preliminary considerations and operating conditions for the four strategies

In on-line LC x LC, the continuous transfer of fractions from ^{1}D to ^{2}D is achieved by a switching-valve equipped with two sample loops. The interfaces for the four studied strategies are schematically represented in Fig. 1. While a fraction is stored in the first loop, the fraction previously stored in the second loop is injected and analysed in ^{2}D. The sampling time (i.e. the storage time) represents the total analysis time in ^{2}D (^{2}t). To essentially maintain the resolution obtained in ^{1}D while ensuring a sufficient peak capacity in ^{2}D, the ratio of the sampling time to the ^{1}D-peak standard deviation ($^{1}\sigma$) must be at least 2 [29,30] and sometimes up to 6 in case of sub-hour separations [31]. The sampling time and hence the analysis time in ^{2}D must be short (typically $^{2}t < 0.5$ min for sub-hour separations). It includes different times. Their repartition is schematically represented in Fig. 2 for the four different strategies.

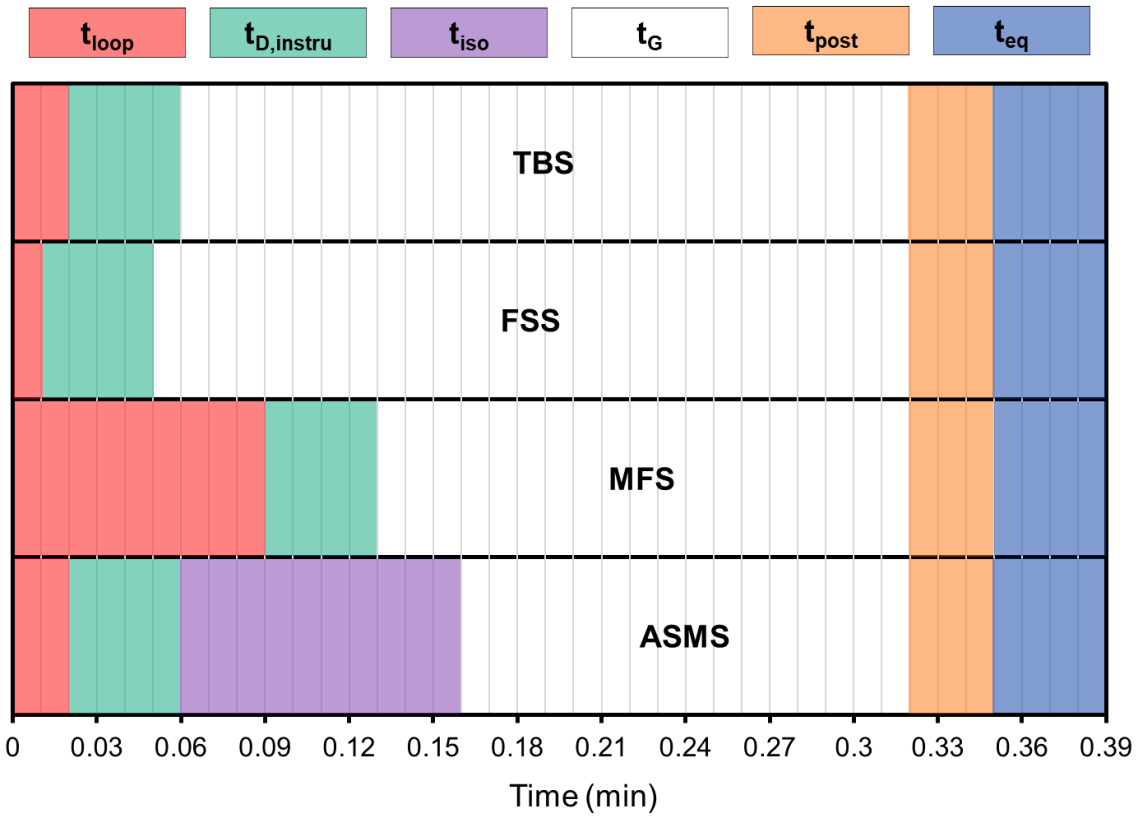

Fig. 2: Schematic representation of the time repartition in ^{2}D with the four compared strategies (sampling time = 0.39 min): Total Breakthrough strategy (TBS), flow splitting strategy (FSS), make-up flow strategy (MFS), and Active solvent modulation strategy (ASMS). t_{loop}, $t_{D,instru}$, t_{iso}, t_G, t_{post}, t_{eq} (Eqs. 3 and 9) are represented by different colours. Experimental values are given in Table 1.

With TBS, FSS, and MFS, the available gradient time in ^{2}D is related to these different times according to:

$$^2t_G = {}^2t - \left({}^2t_{loop} + {}^2t_{D,instrum} + {}^2t_{post} + {}^2t_{eq} \right) \quad \textit{(Eq. 4)}$$

$^2t_{loop}$ is the time required for the ^{2}D-mobile phase to travel across the sample loop ($^2t_{loop} = {}^2V_{loop} / {}^2F$, *with* $^2V_{loop}$ the loop volume and ^2F , the flow rate in ^{2}D). $^2t_{D,instrum}$ is the instrument dwell time without considering the sample loop ($^2t_D = {}^2t_{loop} + {}^2t_{D,instrum}$). $^2t_{post}$ is the short time required for going back to the initial composition and $^2t_{eq}$, the column equilibration time. Both $^2t_{post}$ and $^2t_{eq}$ can be expressed as multiple of the column dead time ($^2t_0$), typically one $^2t_0$ and two $^2t_0$, respectively [32].

Whereas $^2t_{D,instrum}$, $^2t_{post}$ and $^2t_{eq}$ cannot be further modified once properly selected, $^2t_{loop}$ will depend on the loop volume and hence on the selected strategy. Thus, according to Eq. 4, the maximum gradient time that can be used will also depend on the selected strategy.

With FSS (Fig. 1b), the flow rate coming from ^{1}D (^1F), is split with a desired split ratio ($z_{split} < 1$) using a tee-piece placed between the ^{1}D-column outlet and the valve inlet.

With MFS (Fig. 1c), the dilution of the fractions is achieved by continuously mixing the mobile phase coming from ^{1}D with a weak solvent delivered by an additional pump. Its flow rate is given by:

$$F_{pump} = (z_{dilution} - 1) \times {}^1F \quad \textit{(Eq. 5)}$$

Where ^1F is the flow rate in ^{1}D and $z_{dilution}$ is the desired dilution ratio (> 1).

With ASMS (Fig. 1d), dilution of ^{1}D-fractions is achieved with a specific four-position switching-valve equipped with restriction capillaries [19]. Different capillaries are available for adjusting the split ratio, and thus the dilution. The interface and the way it operates are schematically represented in Figs. S2 and S3 of Supplementary Information. Compared to the standard valve (Fig. S1), the ASM valve displays two additional positions (A and C) and two additional ports (5' and 6'), all involved in the dilution process. The basic principle of ASMS is to make use of the initial ^{2}D-mobile phase for diluting the fraction volume. It is achieved by using a bypass capillary between ports 5' and 6' (Figs. S2 and S3b). In position A, the flow coming from the ^{2}D-

pump is divided into two distinct paths. In one path (port 5 to 7), the mobile phase goes through the loop to empty its content, whereas, in the other path (port 5 to 4), it goes through the bypass capillary. Depending on the selected bypass capillary, the content of the sample loop is more or less diluted by the ^{2}D-mobile phase when the two paths meet in port 6. After the dilution step, the ASM valve is switched back to the regular flow path (position B) for analysis. The desired dilution factor ($z_{dilution}$) is determined by the capillary dimensions.

Regardless of the strategy, the injection volume in ^{2}D ($^2V_{injection}$) and the composition of the injection solvent ($C_{injection}$) can be expressed as:

$$^2V_{injection} = {}^1F \times {}^2t \times z_{dilution} \times {}^1z_{split} \qquad \textit{(Eq. 6)}$$

And

$$C_{injection} = \frac{^1C_e + C_{dilution} \times (z_{dilution} - 1)}{z_{dilution}} \qquad \textit{(Eq. 7)}$$

With $C_{dilution,}$ the composition of strong solvent in the diluting solvent.

$z_{dilution} > 1$ with MFS or ASMS; =1 otherwise

$z_{split} < 1$ with FSS; =1 otherwise

It was often shown that the peak injection compression factor, C_F, which expresses how much the injection plug is reduced ($C_F > 1$) or broadened ($C_F < 1$) into the column, is directly related to the ratio of the retention factor in the injection solvent (k_s) to the retention factor in the mobile phase at elution (k_e) [17,33,34]:

$$C_F = \frac{k_s}{k_e} \qquad \textit{(Eq. 8)}$$

For this reason, the difference, ΔC, between the composition of the injection solvent and the composition at peak elution, can be considered as a measure of the solvent strength mismatch:

$$\Delta C = {}^2C_{injection} - {}^2C_e \qquad \textit{(Eq. 9)}$$

Solvent strength mismatch is favourable when $\Delta C < 1$. It is all the more critical as ΔC is much higher than 1.

With ASM, the duration of the dilution step, and hence the required dilution volume must be specified. This latter must be at least equal to ${}^2V_{injection}$. However, a larger volume expressed as a multiple, $\lambda_{injection}$, of ${}^2V_{injection}$ (with $\lambda_{injection} > 1$) is recommended to ensure the complete dilution of the fraction stored in the loop. It should be noted that the settable parameter required by the software is the number of loop volumes (λ_{loop}) in place of the number of injection volumes ($\lambda_{injection}$). It can be derived from the desired $\lambda_{injection}$ by:

$$\lambda_{loop} = \lambda_{injection} \times \frac{{}^1F \times {}^2t}{V_{loop}} \qquad \textit{(Eq. 10)}$$

A value of 3 is recommended for λ_{loop} by Agilent. However, this value is most often too high considering the very short cycle times needed in sub-hour on-line LC x LC. To dilute the injection plug with the initial mobile phase, an initial isocratic hold has to be included in the pump program so that the gradient starts after the dilution step. Its duration, ${}^2t_{iso}$, is recommended to be the same as that of the dilution step, and hence given by:

$${}^2t_{iso} = \frac{\lambda_{injection} \times {}^2V_{injection}}{{}^2F} \qquad \textit{(Eq. 11)}$$

The analysis time in ^{2}D using ASMS includes this initial hold, and consequently, the available gradient time is decreased compared to Eq.4 according to:

$${}^2t_G = {}^2t - \left({}^2t_{loop} + {}^2t_{D,instrum} + {}^2t_{iso} + {}^2t_{post} + {}^2t_{eq} \right) \qquad \textit{(Eq. 12)}$$

As a rule of thumb, the volume occupied by the fraction in the loop, $V_{fraction}$, should not exceed two-thirds of the loop volume ($V_{loop} \geq 1.5 \times V_{fraction}$) to take into account the molecular dispersion due to the parabolic flow. With ASMS, because the dilution is achieved after the sample loop, $V_{fraction}$ is the same as with TBS (*i.e.* ${}^1F \times {}^2t$), whereas with FSS and MFS, it corresponds to the injection volume (Eq. 6). Whereas small loop volumes can be used with FSS ($z_{split} < 1$) or even with TBS or ASMS, larger ones are required with MFS ($z_{dilution} > 1$). Accordingly, the available time for the gradient is shorter (Fig. 2). Of greater practical consequence is the fact that the peak capacity is expected to be lower since the peak capacity decreases with the gradient time.

The interface conditions for the four different strategies and the remaining gradient times are listed in Table 1. For a fair comparison, the chromatographic conditions were basically the same and quite close to those previously applied to the on-line HILIC x RPLC analysis of a tryptic digest [13]. The gradient time in ^{1}D (assumed to be the analysis time) was 30 min. The analysis time in ^{2}D (i.e. the sampling time) was 0.39 min. The flow rate in ^{2}D (i.e. 2 mL/min) was fixed in such a way that the maximum allowable pressure (i.e. 1000 bar) could be reached. The sample loop volumes were selected among commercially available loops so that the injection volume did not exceed two-thirds of the loop volume. As shown in Fig. 2, some times during the run in ^{2}D were maintained identical for the four studied strategies. Those include $^2t_{D,instrum}$, $^2t_{post}$, and $^2t_{eq}$, equal to 0.04, 0.03 and 0.04 min, respectively. Accordingly, interface conditions being different, the gradient times in ^{2}D (Table 1) were also different depending on the strategy (see Eqs. 4 and 10).

With TBS (Figs. 1a and 2), no additional device is required, making this strategy very easy to operate. The whole fraction coming from ^{1}D was injected in ^{2}D. That resulted in relatively large volumes of strong solvent injected in ^{2}D. For the separation of peptides, the percentage of ACN in the HILIC fractions was between 98% and 48% depending on the solute retention in HILIC. A conventional 2-position/4-port duo-valve was used in the backflush mode (Fig. S1). Considering the flow rate in ^{1}D (i.e. 50 µL/min) and the sampling time of 0.39 min, the volume of each transferred fraction, and hence the volume injected in ^{2}D, was exactly 19.5 µL. That represented about 27% $^2V_0$ ($^2V_0$ being the ^{2}D-column dead volume). Considering commercially available loop sizes and with respect to a filling percentage of no more than 66%, the selected sample loop volume was 40 µL. Accordingly, $^2t_{loop}$ was 0.02 min, resulting in a gradient time of 0.26 min (Eq. 4).

With FSS (Figs. 1b and 2), restriction capillaries were mounted to provide a split 1:9 (z_{split} = 0.1), thus allowing sending nine-tenths of the flow to the waste while one-tenth to the sample loop. As said above, a split ratio of 1/10 with similar inner diameters (ID) in both dimensions (e.g.. 2.1 mm) mimics a situation in which the column ID ratio would be close to 3 (e.g. 1 mm in ^{1}D and 3 mm in ^{2}D). Under these conditions, the injected volume in the second dimension was exactly 1.95 µL. That represents about 2.7% V_0. By reducing the loop volume down to the lowest available standardized loop volume (i.e. 20 µL), the gain in time was rather small (of the order of 0.01 min) but allowed for a very small increase in the gradient time (0.27 min).

With both MFS and ASMS, a dilution ratio of 5 (maximum dilution ratio with ASMS) was selected. This one was recommended in case of strong solvent strength mismatch [19]. A lower dilution ratio would reduce the transfer volume (Eq. 6) but also increase the injection solvent strength (Eq. 7).

With MFS (Figs. 1c and 2) and a dilution ratio of five, F_{pump} was 200 µL/min (Eq.2). The diluting solvent composition was the same as for the starting composition of the ^{2}D-mobile phase (i.e. 1% ACN + 0.1% FA and 99% water + 0.1% FA). In these conditions, the percentage of ACN in the injection solvent was decreased from 98% to 20.4% in ^{1}D-initial conditions and from 52% to 11.2% in ^{1}D-final conditions (Eq. 7). The fraction volume entering the valve was multiplied by 5 (i.e. 97.5 µL), thus requiring a larger loop volume than previously (i.e. 180 µL). As a consequence, $^{2}t_{loop}$, and thus $^{2}t_{G}$ became 0.09 min and 0.19 min, respectively. The available gradient time with this approach was about 27% smaller than with the two preceding ones (0.19 min vs. 0.26 or 0.27 min).

With ASMS (Figs. 1d and 2), dilution is carried out without an additional pump. A specific ASM valve allows diluting the collected fractions inside the valve itself. As a result, the fraction volume entering the valve was the same as with TBS (i.e. 19.5 µL), needing the same loop volume of 40 µL. Considering the sample loop volume, twice as large as the fraction volume, only one sample loop volume (λ_{loop} = 1 and $\lambda_{injection}$ close to 2) was used to flush the loop. As a result and according to Eq. 11, a dilution step and hence an isocratic hold ($^{2}t_{iso}$) of 0.1 min was required for complete sample dilution which, according to Eq. 12, reduced the available gradient time by about 16% compared to MFS (0.16 min vs. 0.19 min).

3.2. On-line HILIC x RPLC with TBS or FSS

The main difference between FSS and TBS is the use of restriction capillaries with FSS, which divides the flow before entering the valve. This results in lower injection volumes (here ten-fold lower than with TBS). With TBS, as discussed above, the injection volumes in ^{2}D are large enough to attain a situation of Total Breakthrough for all peptides. As previously defined [13], Total Breakthrough exists when there are only two distinct peaks for a given solute, the first one unretained (breakthrough) and the second one retained and quite symmetrical. It was found for peptides that Total Breakthrough occurs when the injection volume is higher than a critical one. For

smaller volumes, a transition step was pointed out, in which breakthrough occurs while the retained peak is distorted and sometimes split.

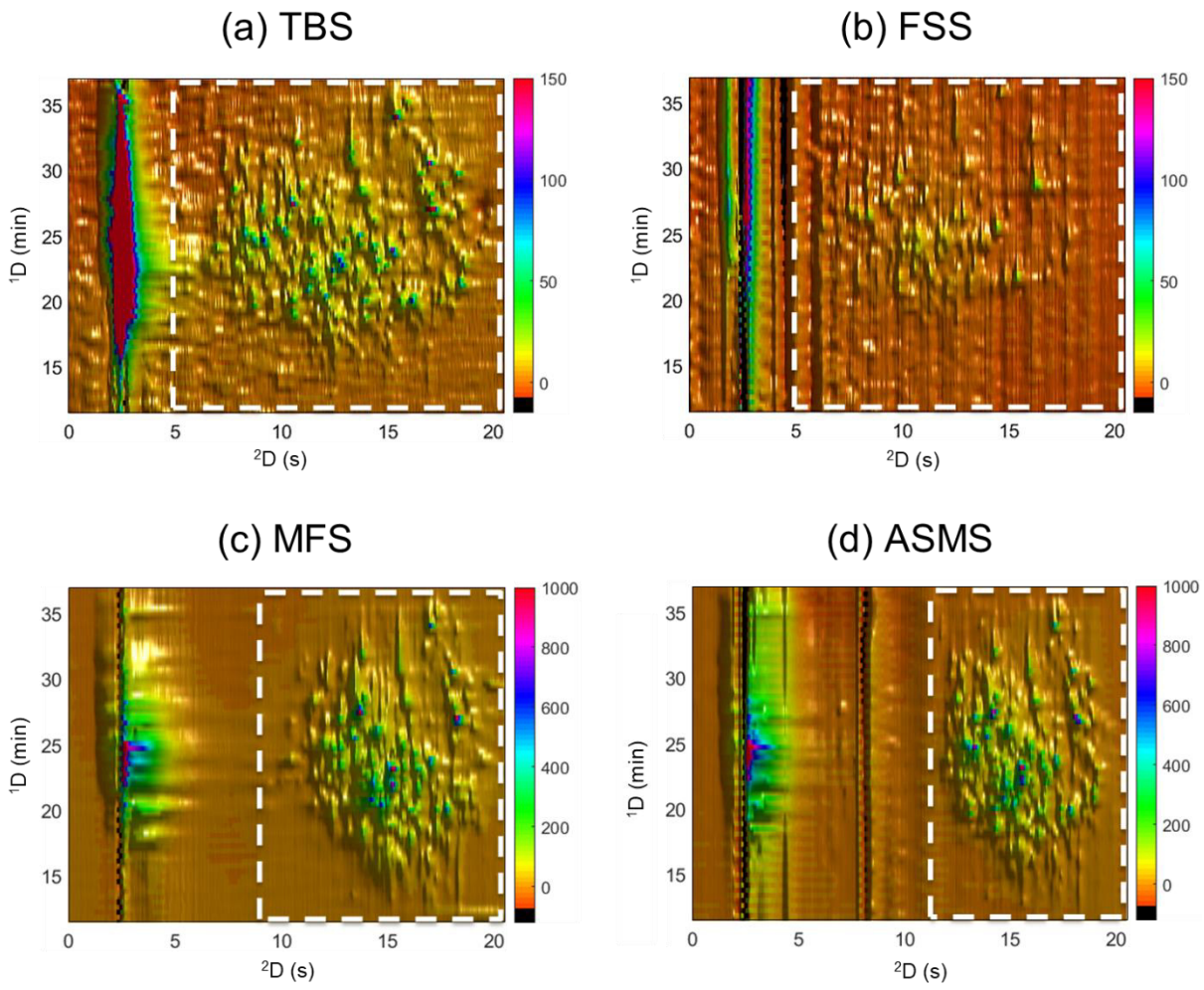

Fig. 3: On-line HILIC x RPLC separations (2D contour plots) of a tryptic digest of six proteins with (a) Total Breakthrough strategy (TBS), (b) flow splitting strategy (FSS), (c) make-up flow strategy (MFS), and (d) Active solvent modulation strategy (ASMS). The white dotted lines delimit the separation space. UV detection at 210 nm. Other conditions given in experimental section and in Table 1.

Fig. 3 shows the 2D contour plots obtained for the separations of the tryptic digest with TBS (Figs. 3a) and FSS (Figs. 3b), with a view centred on the useful separation space. The entire 2D contour plots are shown in Fig. S4. The 3D plots are given in Fig. S5 to compare the peak intensities of the two separations. With TBS, an intense and large band appears between 2 and 3 s. It corresponds to the expected ^{2}D-column dead time (about 2.2 s) and is therefore composed of peaks of breakthrough as also confirmed by HRMS. Those are omnipresent in ^{2}D during the entire ^{1}D-separation. As can be observed, they do not enter the separation space delimited by dotted lines. With

FSS, despite a much lower injection volume (1.95 µL vs. 19.5 µL), some peaks of breakthrough are still present, although less intense than with TBS (Fig. 3b vs. Fig.3a). This is not surprising since breakthrough has been observed for peptides in on-line HILIC x RPLC with injection volumes as low as 2% V_0 [8]. Breakthrough could have been mitigated provided that lower volumes had been injected in ^{2}D. In our case, this could have been done by means of larger split ratios between the two dimensions (e.g. 1/26 for Vi = 1% V_0). Nevertheless, we do not believe that breakthrough could have been eliminated given that its occurrence was reported with injected volumes as low as 0.5% V_0 under similar chromatographic conditions [13]. Furthermore, such a decrease in injection volume would have significantly impacted the method sensitivity, as will be underlined in the subsequent section.

Table 2: Effective peak capacities ($n_{2D,eff}$) and number of peptides identified compared to the expected number of peptides with the four compared strategies: Total Breakthrough strategy (TBS), flow splitting strategy (FSS), make-up flow strategy (MFS), and Active solvent modulation strategy (ASMS). Intermediate parameters for the peak capacity calculation (Eq. 1): ranges of elution times (Δt) and average 4σ peak widths ($w_{4\sigma}$) measured with UV detection (210 nm). Other values required in Eq.1: α = 0.673 and γ = 1.

	^{1}D		^{2}D		$n_{2D,eff}$ (UV)	Number of peptides identified (%)
	$^1\Delta T$ (min)	$^1w_{4\sigma,UV}$ (min)	$^2\Delta T$ (s)	$^2w_{4\sigma,UV}$ (s)		
TBS	26	0.65	15.0	0.39	1100	99
FSS			15.6	0.46	970	86
MFS			11.0	0.41	770	99
ASMS			9.0	0.38	680	99

As shown by dotted lines in Fig. 3, the entire separation space is occupied by peaks in HILIC x RPLC (i.e. γ = 1 in Eq.1). Key values for the effective peak capacity calculation (Eq. 1) are listed in Table 2. The average peak widths in ^{1}D and ^{2}D (UV detection) were assessed from about fifty single symmetrical peaks. The conditions in ^{1}D being the same with the four strategies, $^1\Delta t$ and $^1w_{4\sigma}$ values are the same. $^2\Delta t$ is slightly larger with FSS, but the main difference comes from average $^2w_{4\sigma}$ values (0.39 s with TBS vs. 0.46 s with FSS), resulting in a higher peak capacity (i.e. 1100 with TBS vs. 970 with FSS). As discussed before, TBS ensures a situation of Total Breakthrough due to an injection volume well above the critical one for all peptides. With FSS, the injection volume is most time too low for Total Breakthrough, but not low enough to avoid

broadening, distortion or breakthrough, as will be further discussed. In addition to the effect of injection solvent strength, low split ratios (here z_{split} = 0.1) can also significantly broaden the peaks [35]. It is important to note that peak widths could only be measured on symmetrical peaks, which makes the peak capacity of 970 very optimistic.

The 3D-chromatograms bring attention to the significant difference in peak intensity between TBS (Fig. S5a) and FSS (Fig. S5b). This difference can also be assessed with the overlaid ^{2}D-chromatograms shown in Fig. S6. With a view to even better assess the difference in peak intensity between the studied strategies, 39 different single peaks, identified by HRMS, were selected. Those peaks had to be well distributed among the whole retention space with a signal-to-noise ratio higher than five (UV detection) for accurate measurements. Their peak height ratios between TBS and FSS are listed in Table 3. The largest peak height ratios concerned the most retained peaks in ^{2}D. Their intensities were less affected since the intensity of the breakthrough peak decreased as the peptide retention increased as earlier discussed [13]. On average, the peak intensity was found to be about 8-fold higher with TBS, ranging from 3- to 22-fold. As seen in Table 2, about 99% of the expected peptides from the trypsin digestion (i.e. 237/238, including known post-translational modifications) were identified with HRMS detection for TBS. In comparison, only 86% (i.e. 205/238) could be unambiguously identified for FSS due to low detection sensitivity. These results underline the high dilution caused by FSS conditions.

Finally, considering both peak capacity (Table 2) and peak intensity (Table 3), TBS was proved to be a much better choice than FSS to reduce undesirable effects of strong injection solvents in the ^{2}D-RPLC.

Table 3: Peak height ratios between different strategies for 39 relevant peaks well-spread among the 2D retention space. UV detection at 210 nm.

Peak #	^1t_r	m/z	Peak height ratio			
			TBS/FSS	MFS/TBS	ASMS/TBS	MFS/ASMS
1	21.1	1156.9329	22	1.1	3.5	0.3
2	21.4	1368.221	20	1.2	3.3	0.4
3	19.9	742.4514	4.1	6.0	5.8	1.0
4	26.9	1557.3634	9.6	3.1	2.6	1.2
5	30.4	1622.2051	21	3.7	3.3	1.1
6	19.9	1300.6981	5.3	6.8	6.8	1.0
7	23.8	864.9531	4.7	4.2	4.0	1.1
8	33.9	1057.5826	21	3.4	2.8	1.2
9	19.9	1231.5983	8.4	5.8	3.3	1.7
10	23.0	908.9567	6.1	6.9	6.4	1.1
11	26.1	680.9209	9.0	3.1	3.3	0.9
12	28.5	761.3974	7.6	4.8	6.2	0.8
13	30.8	460.2878	6.9	4.0	4.5	0.9
14	24.2	682.7068	6.6	3.5	4.5	0.8
15	25.0	748.3533	4.2	5.6	7.1	0.8
16	20.3	478.2555	6.3	7.1	5.6	1.3
17	22.6	482.772	8.0	13	13	1
18	23.0	692.4062	8.3	9.1	8.3	1.1
19	23.4	461.9383	7.4	4.8	4.1	1.2
20	26.1	756.4278	6.8	7.9	8.1	1.0
21	18.7	650.317	3.9	4.3	6.1	0.7
22	20.7	390.2289	5.8	8.5	7.4	1.1
23	19.9	890.3897	3.8	3.9	9.6	0.4
24	22.2	374.7234	4.0	7.1	6.0	1.2
25	23.4	500.8064	3.5	6.4	5.0	1.3
26	25.4	536.2919	6.7	7.2	7.1	1.0
27	26.1	488.287	7.7	2.7	2.3	1.2
28	27.3	584.817	7.5	6.9	5.6	1.2
29	28.5	627.982	12	5.7	5.4	1.1
30	32.0	547.319	15	5.7	5.4	1.1
31	19.5	513.2828	5.8	2.6	6.4	0.4
32	20.3	497.2036	7.9	1.6	3.8	0.4
33	24.6	424.5606	4.7	3.3	7.7	0.4
34	26.9	780.5013	8.8	4.5	6.8	0.7
35	24.6	636.3365	6.3	5.2	7.4	0.7
36	25.0	604.3474	5.3	3.0	3.1	1.0
37	32.0	415.7313	9.0	2.9	4.3	0.7
38	24.2	678.3842	3.9	2.0	2.6	0.8
39	18.7	1013.6022	8.4	5.4	4.8	1.1
Average values			**8.3**	**5.0**	**5.5**	**0.9**

TBS: Total breakthrough strategy; FSS: Flow splitting strategy; MFS: Make-up flow strategy, ASMS: Active Solvent Modulation strategy; m/z: mass-to-charge ratio; ^1t_r: retention time in the first dimension.

3.3. On-line HILIC x RPLC with MFS or ASMS

Both strategies consist in diluting the injection plug with a weak solvent (here 1% ACN in water with 0.1% FA). The eluent strength of the ^{1}D-effluent is therefore decreased before entering the ^{2}D-column to promote on-column focusing. On-line dilution was achieved before the switching-valve (MFS) or inside the switching-valve (ASMS). The 2D contour plots and the 3D-chromatograms for both MFS and ASMS are shown in Fig. 3 and Fig. S5, respectively. The similarity between the two separations is noteworthy. As a consequence of the large isocratic hold before the gradient enters the column, a large empty space with MFS (Fig. 3c) and even larger with ASMS (Fig. 3d) is clearly observed. Since the sampling time was identical for all strategies, the available gradient time (Fig. 2) and hence the separation space (i.e. $^{2}\Delta t$ in Table 2) was inevitably much smaller compared to TBS or FSS (27% and 40% smaller with MFS and ASMS, respectively). As could be expected, a smaller average peak width was obtained with both MFS and ASMS compared to FSS (Table 2). The average peak width was yet close to that with TBS. Due to the shorter $^{2}\Delta t$ with both dilution approaches, peak capacities were much smaller with MFS (770) and ASMS (680) than with TBS (1100) or even FSS (970). Furthermore, despite on-line dilution, intense peaks of breakthrough were still observed with MFS as well as with ASMS (Fig. 3), especially for moderately retained compounds in ^{1}D.

As seen in Fig. S5 and confirmed in Table 3, the peak heights of the retained peaks are similar between MFS and ASMS. On average, they were about five times higher than with TBS. The presence of breakthrough did not seem to impair much the peak intensity. As seen in Table 2, the percentage of expected peptides identified with both strategies was the same as for TBS.

In the next section, the comparison of the peak shapes from HRMS detection will complete the evaluation of the four strategies.

3.4. Comparison of peak shapes in on-line HILIC x RPLC with the four studied strategies

To provide an objective comparison of the peak shapes depending on the studied strategies, extracted ion chromatograms (EICs) of five relevant peptides are shown in Figs. 4 to 8. Each separation displays the most intense fraction among the two or three ^{1}D-peak fractions. The figures are ranged from the most retained peptide in ^{2}D (Fig. 4)

to the least retained one (Fig. 8). The location of each peak is indicated on the 2D maps in Fig. S4. Useful information, listed in Table 4, includes m/z values, retention times in both dimensions, compositions at elution in both dimensions (Eq. 2), compositions of the injection solvent in ^{2}D (Eq. 7), measured effective peak capacities (Eq. 1), observed type of separation (Total Breakthrough, single symmetrical peak, peak distortion, split peak, transition step accompanied by both peak distortion and breakthrough), and peak asymmetry factors (Eq. 3). Note that the effective peak capacities, as well as the asymmetry factors, could not be measured when the peak distortion was significant or when the peak intensity was too low. It should be pointed out that the effective peak capacities were calculated from MS-peak widths in Table 4 but from UV-peak widths in Table 2. The resulting lower values in Table 4 are due to significant additional solute dispersion between the UV-instrument and the Q-TOF-MS connected in parallel with a tee-piece.

Finally, as previously said, ΔC (Eq. 9) can be considered as a measure of the solvent strength mismatch and was therefore also reported in Table 4 as an additional relevant characteristic.

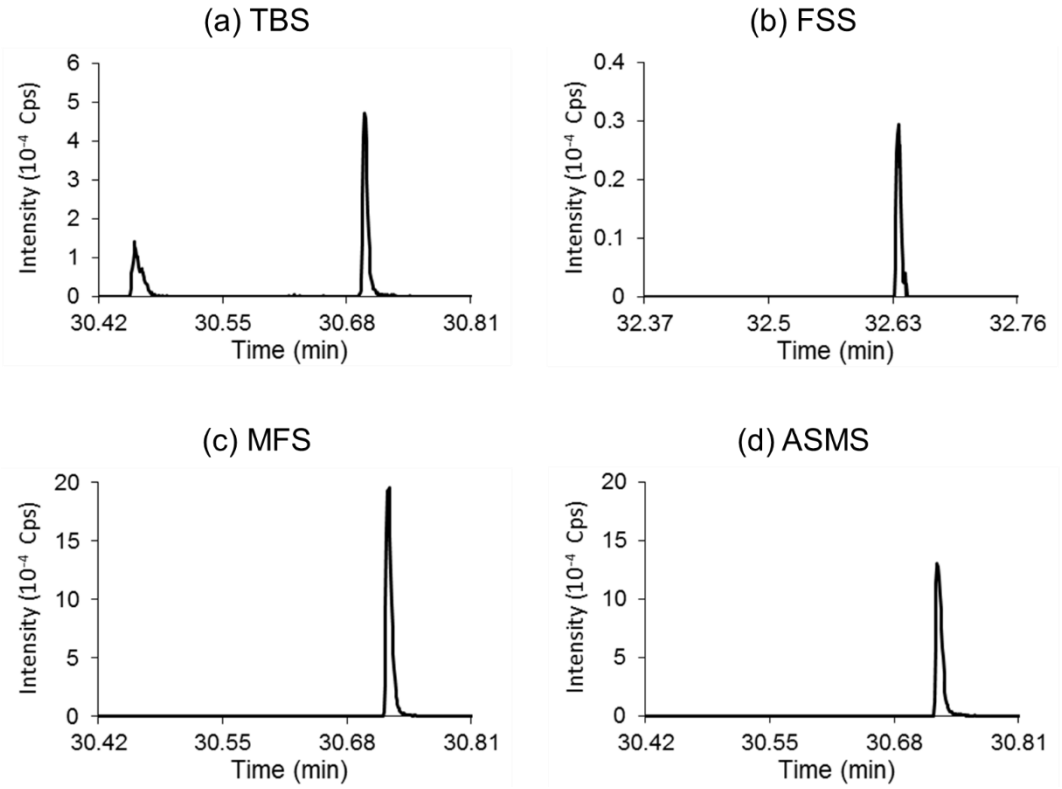

Fig. 4: ^{2}D-separation of a strongly retained peptide (EIC 1622.5389) with the four studied strategies used in on-line HILIC x RPLC: (a) Total Breakthrough strategy (TBS), (b) flow splitting strategy (FSS), (c) make-up flow strategy (MFS), and (d) Active solvent modulation strategy (ASMS). The characteristics of the retained peak are given in Table 4.

The peptide in Fig. 4 is strongly retained in both dimensions. As a result, the injection solvent strength is moderate (57% and 54% ACN with TBS and FSS respectively) and more importantly, ΔC is low with both TBS and FSS (i.e. 25%) and negative with both MFS and ASMS (i.e. -20%). As expected, a small breakthrough peak appears with TBS. In such conditions, the retained peak is kept rather symmetrical with all strategies (i.e. $1 \leq As \leq 1.6$, except for ASMS). However, for the reasons already given above, the effective peak capacities are much lower with MFS and ASMS.

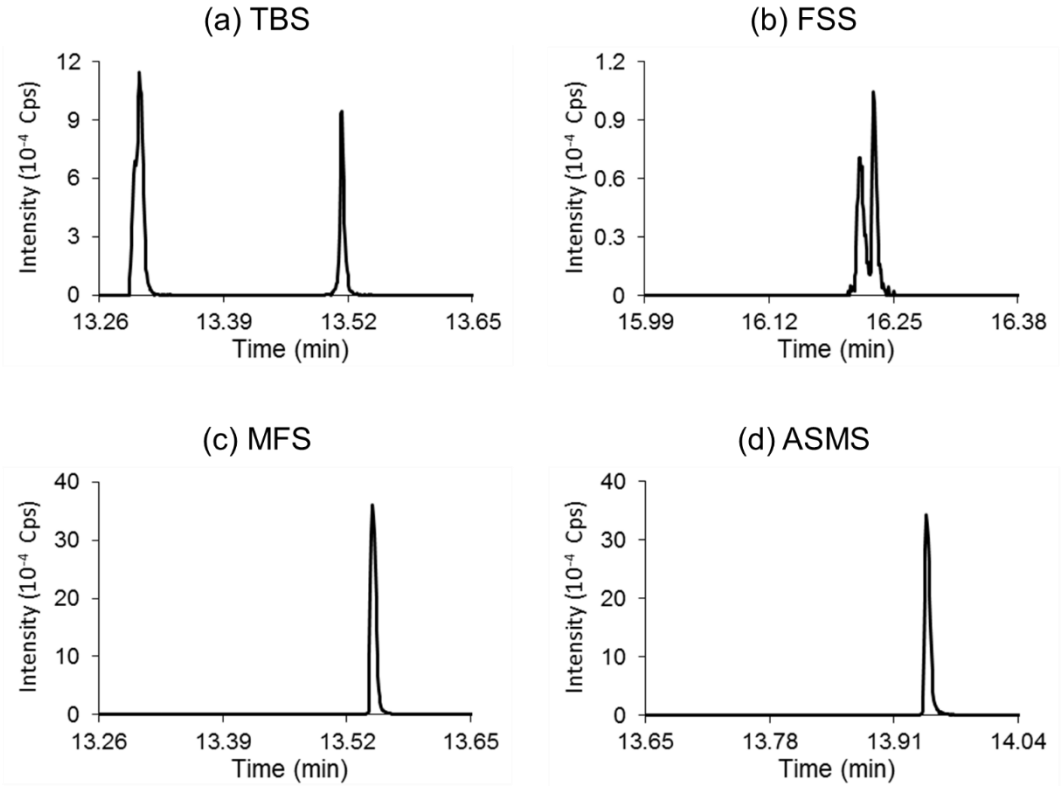

Fig. 5: ^{2}D-separation of a moderately retained peptide (EIC 588.3769) with the four studied strategies used in on-line HILIC x RPLC: (a) Total Breakthrough strategy (TBS), (b) flow splitting strategy (FSS), (c) make-up flow strategy (MFS), and (d) Active solvent modulation strategy (ASMS). The characteristics of the retained peak are given in Table 4.

In Figs. 5 to 7, the peptides are poorly retained in ^{1}D ($^{1}C_{elution}$ from 86% to 71%ACN) while moderately retained in ^{2}D ($^{2}C_{elution}$ from 29% to 15% ACN), which results in high ΔC values with TBS and FSS (about 60% ACN). With FSS, despite a very small injection volume, the peaks are split in Figs. 5b and 6b, while Total Breakthrough similar to what is always observed with TBS can be observed in Fig. 7b. Regarding MFS and ASMS, the ΔC values remain negative for the peptide in Fig. 5 (i.e. close to -10%), thus allowing

a fairly symmetrical retained peak. However, ΔC values seem to be too high for the peptides in Figs. 6 and 7, taking also into account the very large injection volume resulting from these strategies (i.e. 97.5 µL). Peak fronting can be observed with MFS in Fig. 6c and a breakthrough peak appears with ASMS in Fig. 6d, suggesting a transition step before a further situation of Total Breakthrough. The earlier emergence of breakthrough in the case of ASMS can be readily explained by the slight difference in ΔC between the two strategies. In Fig. 7, the peaks are distorted with both MFS (Fig. 7c) and ASMS (Fig. 7d). In addition to the very bad peak shapes, a breakthrough peak is present in both cases. This suggests that on-line dilution is not sufficient to circumvent the deleterious impact of solvent strength mismatch, and thus to ensure symmetrical peaks. This bad separation can be related to the ΔC values (here close to 0%), higher than for the peptide in Fig. 6 and much higher than for the peptide in Fig. 5.

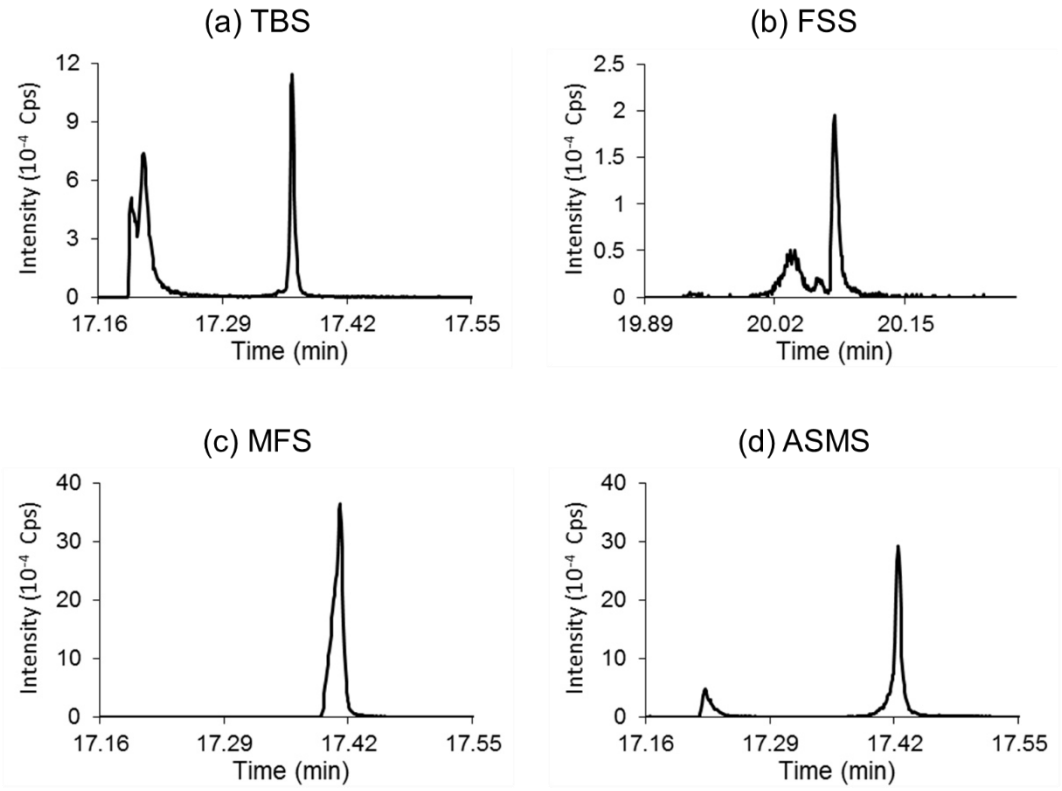

Fig. 6: [2]D-separation of a moderately retained peptide (EIC 723.3568) with the four studied strategies used in on-line HILIC x RPLC: (a) Total Breakthrough strategy (TBS), (b) flow splitting strategy (FSS), (c) make-up flow Strategy (MFS), and (d) Active solvent modulation strategy (ASMS). The characteristics of the retained peak are given in Table 4.

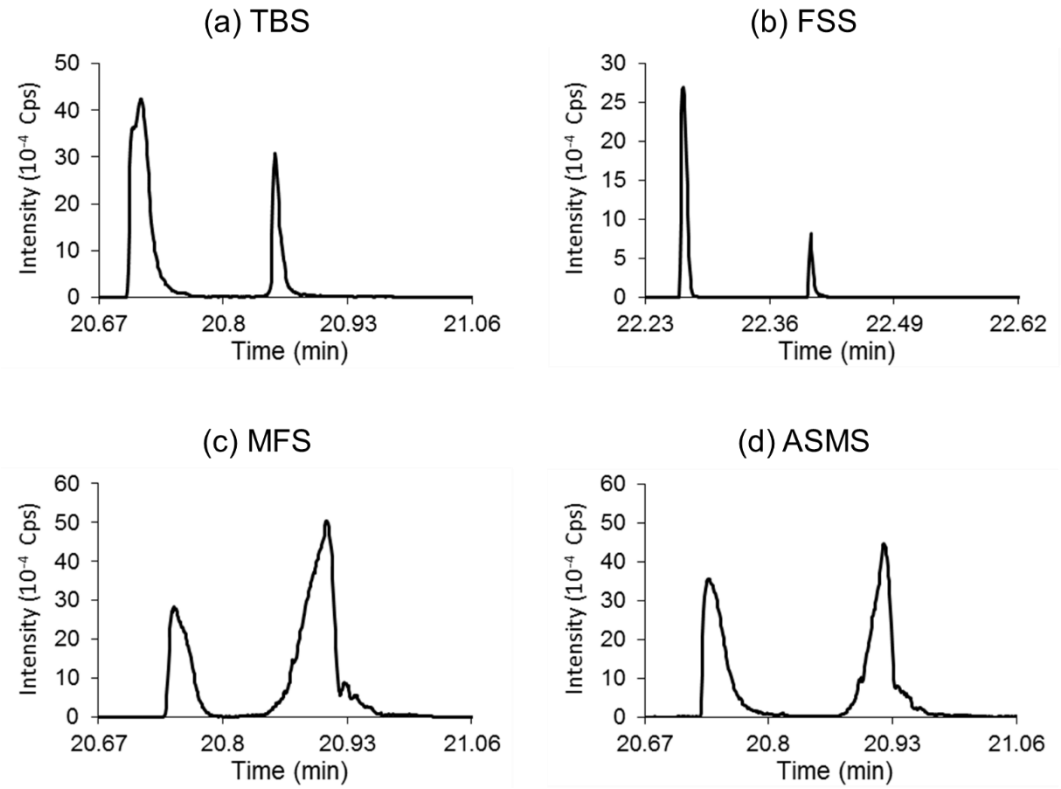

Fig. 7: [2]D-separation of a moderately retained peptide (EIC 779.4492) with the four studied strategies used in on-line HILIC x RPLC: (a) Total Breakthrough strategy (TBS), (b) flow splitting strategy (FSS), (c) make-up flow strategy (MFS), and (d) Active solvent modulation strategy (ASMS). The characteristics of the retained peak are given in Table 4.

Three approaches could be considered to reduce the transferred volume while maintaining the same dilution ratio (same ΔC): (i) splitting the flow rate prior to the valve, (ii) sending part of the fraction to the waste by using loop volumes smaller than the fraction volume or (iii) using trapping columns. The first approach involves the combination of two strategies (FSS and on-line dilution). The second one cannot strictly be referred to as comprehensive 2D-LC, and furthermore cannot be considered for quantitative analysis since the percentage of component sent in the second dimension may vary from run-to-run. Furthermore, these two approaches should result in a reduction of the peak heights (lower sensitivity). Regarding the use of trapping columns in combination with on-line dilution (MFS only), its benefit in terms of transferred volume reduction has never been clearly proved as above highlighted.

The last proposed example (Fig. 8) is interesting. In this case, the peptide is strongly retained in [1]D like the peptide in Fig. 6 ($^{1}C_{elution}$ close to 60% ACN) but poorly retained in [2]D ($^{2}C_{elution}$ close to 6% ACN). With both TBS and FSS (Figs. 8a and 8b), the situation

of Total Breakthrough is attained. With MFS and ASMS (Figs. 8c and 8d), a transition step close to a situation of Total Breakthrough, but with a low fronting between the breakthrough peak and the retained peak, can be observed. Once again, these results can be correlated to the high ΔC values (here positive values close to 7% ACN). It is interesting to point out that the breakthrough peak is much larger with MFS (Fig. 8c) and ASMS (Fig.8d) than with TBS (Fig. 8a). It is the thinnest with FSS (8b). That is not surprising considering that the width of the non-retained breakthrough peak is expected to vary linearly with the injected volume.

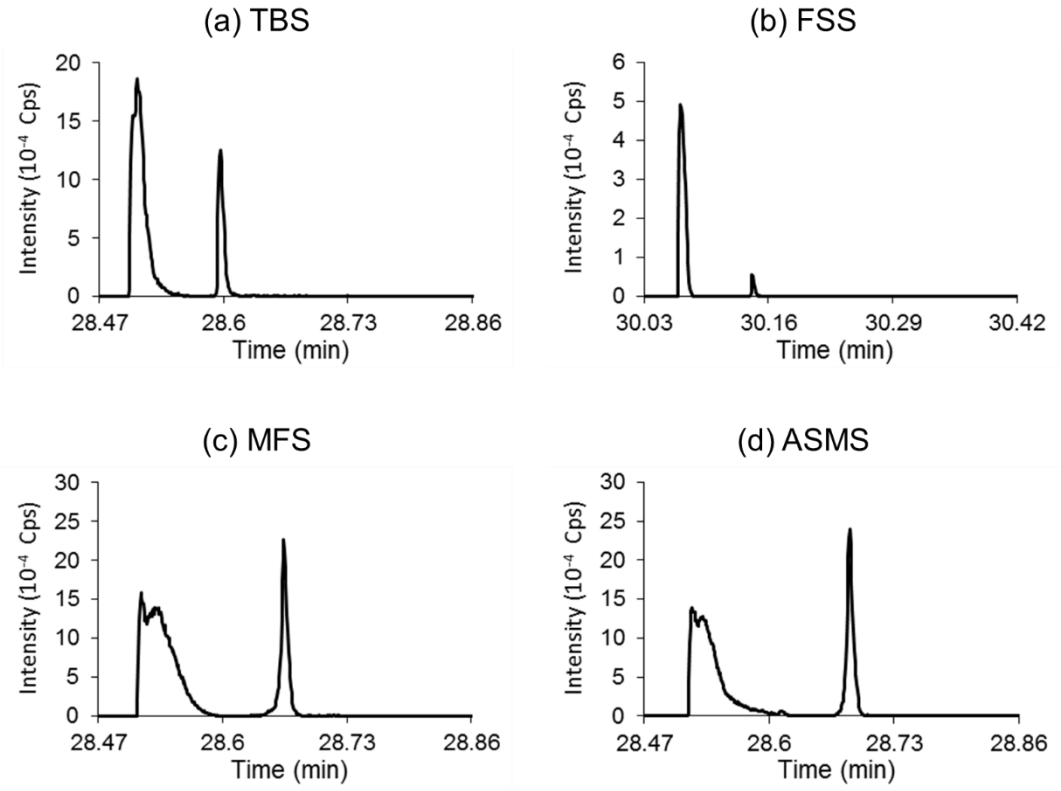

Fig. 8: ^{2}D separation of a poorly retained peptide (EIC 830.4534) with the four studied strategies used in on-line HILIC x RPLC: (a) Total Breakthrough strategy (TBS), (b) flow splitting strategy (FSS), (c) make-up flow strategy (MFS), and (d) Active solvent modulation strategy (ASMS). The characteristics of the retained peak are given in Table 4.

Apart from obvious consequences on separation and sensitivity, the occurrence of breakthrough in each of these strategies raises the question of quantitative analysis. In our previous study [13], we observed a linear variation of the retained peak area with the amount of peptide injected, as soon as the situation of Total Breakthrough was attained. However, the variation was no more linear when the peak was eluted under the conditions of a transition step (i.e. after the emergence of breakthrough but before

Total Breakthrough). This suggests that quantitative analysis should be quite reliable with TBS while problematic with the three other strategies (transition step with FSS in Figs. 6b, with MFS in Fig. 7c or with ASMS in Fig. 7d).

Table 4: Main characteristics of EICs shown in Figs.4 to 8 depending on the strategy used (TBS, FSS, MFS or ASMS).

Fig.	m/z	Strategy	^{1}tr (min)	$^1C_{elution}$ (%) (Eq.2)	$^2C_{injection}$ (%) (Eq.7)	^{2}tr (min)	$^2C_{elution}$ (%) (Eq.2)	ΔC (%) (Eq.9)	$n_{2D,eff}$ (Eq.1)	Peak state(1)	A_f (Eq.3)
4	1622.539	TBS	30.75	57	57	0.280	32	25	830	TB	1.6
		FSS	32.68	54	54	0.266	30	24	-	S	1.5
		MFS	30.77	57	12	0.302	32	-20	500	S	1.6
		ASMS	30.77	57	12	0.306	31	-19	400	S	2.1
5	588.377	TBS	13.56	86	86	0.253	28	58	750	TB	1.0
		FSS	16.28	81	81	0.240	26	55	-	D	1.5
		MFS	13.60	86	18	0.287	29	-11	550	S	1.4
		ASMS	13.99	85	18	0.293	28	-10	420	S	1.5
6	723.357	TBS	17.41	79	79	0.203	19	60	740	TB	1.1
		FSS	20.13	75	75	0.190	18	57	-	TS	-
		MFS	17.46	79	17	0.252	21	-4.2	260	D	0.8
		ASMS	17.47	79	17	0.263	19	-2.7	250	TS	0.8
7	779.449	TBS	20.90	73	73	0.184	16	57	570	TB	1.6
		FSS	22.45	71	71	0.173	15	56	720	TB	1.8
		MFS	20.96	73	15	0.240	18	-2.6	-	TS	-
		ASMS	20.97	73	15	0.252	16	-0.9	-	TS	-
8	830.453	TBS	28.65	60	60	0.127	6	54	590	TB	1.3
		FSS	30.19	58	58	0.113	5	52	-	TB	1.5
		MFS	28.71	60	13	0.193	7	5.7	370	TS	0.9
		ASMS	28.73	60	13	0.214	6	7.0	320	TS	1.1

(1) Peak state: TB: Total Breakthrough; S: single symmetrical retained peak; D: distortion and/or peak splitting; TS: transition step before Total Breakthrough; A_f: Asymmetry factor

In summary, the following conclusions can be drawn from the separations shown in Figs. 4 to 8: (i) TBS was the only strategy ensuring fairly symmetrical peaks ($1 \leq As \leq 1.6$) for all peptides in on-line HILIC x RPLC, (ii) the success of the three other strategies (FSS, MFS, and ASMS), for a given peptide, strongly depended on ΔC values which had to be low enough to avoid injection issues, (iii) considering that it was not possible to ensure sufficiently low ΔC values for all peptides given the broad range of

elution in both dimensions, the peak capacity and hence the quality of the separation was inevitably more or less affected with MFS and ASMS, and (iv) MFS and ASMS yielded quite similar results with the same dilution ratio.

In this study, TBS was used for the separation of peptides. We are currently studying the occurrence of Total Breakthrough over a wider range of solutes (acidic and basic, multi-charged or not) and a wider range of chromatographic conditions (different stationary phases, different mobile phases, pHs, temperatures, gradient conditions). Our obtained results allow asserting that Total Breakthrough can also be attained with small monocharged molecules in RPLC. An example is given in Fig. S7 for propranolol. We hope to be able soon to publish a complete overview of the circumstances leading to the phenomenon of Total Breakthrough.

4. Concluding remarks

In this study, we compared four strategies designed to reduce undesirable effects of strong injection solvents on peak shapes in the second dimension of on-line HILIC x RPLC for the separation of peptides: (i) the Total Breakthrough strategy (TBS) with the injection of large volumes of raw fractions, (ii) the flow splitting strategy (FSS) with the injection of low volumes of raw fractions, and two on-line dilution strategies with the injection of very large volumes of diluted fractions, either (iii) with a make-up flow (MFS) or (iv) with an ASM-valve (ASMS). The quality of the separation was assessed on the basis of peak shapes, peak capacity, and peak intensity. The comparison was made in the context of a separation of a complex peptide sample performed in 30 min by considering the most critical case where similar column inner diameters are used in both dimensions (i.e. 2.1 mm).

The best results in term of peak shapes and peak capacity were obtained with TBS. A feature of this strategy is that it deliberately copes with breakthrough, unlike the three other ones where breakthrough is highly critical. No additional device is required with TBS, making this strategy very easy to operate. A peak capacity of 1100 could be achieved within just half an hour. Due to both peak broadening and a reduction of the separation space in ^{2}D, the obtained peak capacity was more than 40% lower with the on-line dilution strategies. Unlike TBS, it was shown that neither a split ratio of 1/10 (FSS) nor a dilution ratio of 5 (MFS and ASMS) were sufficient to provide symmetrical peaks across the entire 2D separation space and hence to avoid excessive band broadening, fronting, split peaks, and breakthrough.

The difference in composition between the injection solvent and the mobile phase at peak elution (ΔC) in combination with the injection volume was found to be related to the extent to which peaks are distorted and also to the occurrence of breakthrough. Above a critical ΔC value depending on the injection volume, a situation of Total Breakthrough takes place. Due to low ΔC values, this situation was rarely attained with MFS or with ASMS.

On average the peak intensity was five times higher with the on-line dilution strategies than with TBS. However, TBS led to much better results than FSS, with an eight-fold increase in peak intensity. This highlights the poor sensitivity involved by FSS while this strategy is still the most reported one in on-line HILIC x RPLC.

ASMS and MFS gave very similar results. Both techniques need an additional device, either an ASM valve or an isocratic pump (MFS). This latter solution benefits from easy implementation. Furthermore, the present study shows that the current limitation for the dilution ratio (not higher than 5) in the case of the ASM valve can be a critical issue for the quality of the separation in on-line HILIC x RPLC.

Finally, there are many ways to compare the different strategies for given 2D conditions. The quality descriptors are multiple (peak height, peak width, peak capacity, peak asymmetry…). Depending on the objectives, one of the descriptors may prevail over another. However, peak heights, peak widths and hence peak capacity cannot be assessed if the peaks are distorted. The first objective of the analyst should therefore be to obtain only quasi-symmetrical peaks. The main conclusion of this study on HILIC x RPLC is that this objective can only be achieved with TBS.

5. Acknowledgements

The authors gratefully acknowledge Agilent technologies for the loan of the 2D-LC instrument and the Active Solvent Modulation 2D-LC valve.

6. References

[1] Y.Z. Baghdady, K.A. Schug, Online Comprehensive High pH Reversed Phase × Low pH Reversed Phase Approach for Two-Dimensional Separations of Intact Proteins in Top-Down Proteomics, Anal. Chem. 91 (2019) 11085–11091. https://doi.org/10.1021/acs.analchem.9b01665.

[2] M. Muller, A.G.J. Tredoux, A. de Villiers, Predictive kinetic optimisation of hydrophilic interaction chromatography × reversed phase liquid chromatography separations: Experimental verification and application to phenolic analysis, Journal of Chromatography A. 1571 (2018) 107–120. https://doi.org/10.1016/j.chroma.2018.08.004.

[3] M. Muller, A.G.J. Tredoux, A. de Villiers, Application of Kinetically Optimised Online HILIC × RP-LC Methods Hyphenated to High Resolution MS for the Analysis of Natural Phenolics, Chromatographia. 82 (2019) 181–196. https://doi.org/10.1007/s10337-018-3662-6.

[4] B.W.J. Pirok, N. Abdulhussain, T. Brooijmans, T. Nabuurs, J. de Bont, M.A.J. Schellekens, R.A.H. Peters, P.J. Schoenmakers, Analysis of charged acrylic particles by on-line comprehensive two-dimensional liquid chromatography and automated data-processing, Analytica Chimica Acta. 1054 (2019) 184–192. https://doi.org/10.1016/j.aca.2018.12.059.

[5] M. Iguiniz, E. Corbel, N. Roques, S. Heinisch, Quantitative aspects in on-line comprehensive two-dimensional liquid chromatography for pharmaceutical applications, Talanta. 195 (2019) 272–280. https://doi.org/10.1016/j.talanta.2018.11.030.

[6] M. Sarrut, A. Corgier, S. Fekete, D. Guillarme, D. Lascoux, M.-C. Janin-Bussat, A. Beck, S. Heinisch, Analysis of antibody-drug conjugates by comprehensive on-line two-dimensional hydrophobic interaction chromatography x reversed phase liquid chromatography hyphenated to high resolution mass spectrometry. I – Optimization of separation conditions, Journal of Chromatography B. 1032 (2016) 103–111. https://doi.org/10.1016/j.jchromb.2016.06.048.

[7] A. Ehkirch, V. D'Atri, F. Rouviere, O. Hernandez-Alba, A. Goyon, O. Colas, M. Sarrut, A. Beck, D. Guillarme, S. Heinisch, S. Cianferani, An Online Four-Dimensional HIC×SEC-IM×MS Methodology for Proof-of-Concept Characterization of Antibody Drug Conjugates, Anal. Chem. 90 (2018) 1578–1586. https://doi.org/10.1021/acs.analchem.7b02110.

[8] G. Vanhoenacker, I. Vandenheede, F. David, P. Sandra, K. Sandra, Comprehensive two-dimensional liquid chromatography of therapeutic monoclonal antibody digests, Anal Bioanal Chem. 407 (2015) 355–366. https://doi.org/10.1007/s00216-014-8299-1.

[9] L. Montero, V. Sáez, D. von Baer, A. Cifuentes, M. Herrero, Profiling of Vitis vinifera L. canes (poly)phenolic compounds using comprehensive two-dimensional liquid chromatography, Journal of Chromatography A. 1536 (2018) 205–215. https://doi.org/10.1016/j.chroma.2017.06.013.

[10] H. Zhang, J.-M. Jiang, D. Zheng, M. Yuan, Z.-Y. Wang, H.-M. Zhang, C.-W. Zheng, L.-B. Xiao, H.-X. Xu, A multidimensional analytical approach based on

time-decoupled online comprehensive two-dimensional liquid chromatography coupled with ion mobility quadrupole time-of-flight mass spectrometry for the analysis of ginsenosides from white and red ginsengs, Journal of Pharmaceutical and Biomedical Analysis. 163 (2019) 24–33. https://doi.org/10.1016/j.jpba.2018.09.036.

[11] J.-L. Cao, S.-S. Wang, H. Hu, C.-W. He, J.-B. Wan, H.-X. Su, Y.-T. Wang, P. Li, Online comprehensive two-dimensional hydrophilic interaction chromatography×reversed-phase liquid chromatography coupled with hybrid linear ion trap Orbitrap mass spectrometry for the analysis of phenolic acids in Salvia miltiorrhiza, Journal of Chromatography A. 1536 (2018) 216–227. https://doi.org/10.1016/j.chroma.2017.09.041.

[12] A. Martín-Ortiz, A.I. Ruiz-Matute, M.L. Sanz, F.J. Moreno, M. Herrero, Separation of di- and trisaccharide mixtures by comprehensive two-dimensional liquid chromatography. Application to prebiotic oligosaccharides, Analytica Chimica Acta. 1060 (2019) 125–132. https://doi.org/10.1016/j.aca.2019.01.040.

[13] S. Chapel, F. Rouvière, S. Heinisch, Pushing the limits of resolving power and analysis time in on-line comprehensive hydrophilic interaction x reversed phase liquid chromatography for the analysis of complex peptide samples, Journal of Chromatography A. (2019) 460753. https://doi.org/10.1016/j.chroma.2019.460753.

[14] S. Toro-Uribe, L. Montero, L. López-Giraldo, E. Ibáñez, M. Herrero, Characterization of secondary metabolites from green cocoa beans using focusing-modulated comprehensive two-dimensional liquid chromatography coupled to tandem mass spectrometry, Analytica Chimica Acta. 1036 (2018) 204–213. https://doi.org/10.1016/j.aca.2018.06.068.

[15] L. Montero, E. Ibáñez, M. Russo, L. Rastrelli, A. Cifuentes, M. Herrero, Focusing and non-focusing modulation strategies for the improvement of on-line two-dimensional hydrophilic interaction chromatography × reversed phase profiling of complex food samples, Analytica Chimica Acta. 985 (2017) 202–212. https://doi.org/10.1016/j.aca.2017.07.013.

[16] E. Sommella, O.H. Ismail, F. Pagano, G. Pepe, C. Ostacolo, G. Mazzoccanti, M. Russo, E. Novellino, F. Gasparrini, P. Campiglia, Development of an improved online comprehensive hydrophilic interaction chromatography × reversed-phase ultra-high-pressure liquid chromatography platform for complex multiclass polyphenolic sample analysis, J. Sep. Sci. 40 (2017) 2188–2197. https://doi.org/10.1002/jssc.201700134.

[17] M. Sarrut, A. D'Attoma, S. Heinisch, Optimization of conditions in on-line comprehensive two-dimensional reversed phase liquid chromatography. Experimental comparison with one-dimensional reversed phase liquid

chromatography for the separation of peptides, Journal of Chromatography A. 1421 (2015) 48–59. https://doi.org/10.1016/j.chroma.2015.08.052.

[18] P. Venter, M. Muller, J. Vestner, M.A. Stander, A.G.J. Tredoux, H. Pasch, A. de Villiers, Comprehensive Three-Dimensional LC × LC × Ion Mobility Spectrometry Separation Combined with High-Resolution MS for the Analysis of Complex Samples, Anal. Chem. 90 (2018) 11643–11650. https://doi.org/10.1021/acs.analchem.8b03234.

[19] D.R. Stoll, K. Shoykhet, P. Petersson, S. Buckenmaier, Active Solvent Modulation: A Valve-Based Approach To Improve Separation Compatibility in Two-Dimensional Liquid Chromatography, Anal. Chem. 89 (2017) 9260–9267. https://doi.org/10.1021/acs.analchem.7b02046.

[20] D.R. Stoll, D.C. Harmes, G.O. Staples, O.G. Potter, C.T. Dammann, D. Guillarme, A. Beck, Development of Comprehensive Online Two-Dimensional Liquid Chromatography/Mass Spectrometry Using Hydrophilic Interaction and Reversed-Phase Separations for Rapid and Deep Profiling of Therapeutic Antibodies, Anal. Chem. 90 (2018) 5923–5929. https://doi.org/10.1021/acs.analchem.8b00776.

[21] Y. Chen, J. Li, O.J. Schmitz, Development of an At-Column Dilution Modulator for Flexible and Precise Control of Dilution Factors to Overcome Mobile Phase Incompatibility in Comprehensive Two-Dimensional Liquid Chromatography, Anal. Chem. 91 (2019) 10251–10257. https://doi.org/10.1021/acs.analchem.9b02391.

[22] Y. Chen, L. Montero, J. Luo, J. Li, O.J. Schmitz, Application of the new at-column dilution (ACD) modulator for the two-dimensional RP×HILIC analysis of Buddleja davidii, Anal Bioanal Chem. 412 (2020) 1483–1495. https://doi.org/10.1007/s00216-020-02392-3.

[23] D.R. Stoll, E.S. Talus, D.C. Harmes, K. Zhang, Evaluation of detection sensitivity in comprehensive two-dimensional liquid chromatography separations of an active pharmaceutical ingredient and its degradants, Anal Bioanal Chem. 407 (2015) 265–277. https://doi.org/10.1007/s00216-014-8036-9.

[24] B.W.J. Pirok, D.R. Stoll, P.J. Schoenmakers, Recent Developments in Two-Dimensional Liquid Chromatography: Fundamental Improvements for Practical Applications, Analytical Chemistry. 91 (2019) 240–263. https://doi.org/10.1021/acs.analchem.8b04841.

[25] A.F.G. Gargano, M. Duffin, P. Navarro, P.J. Schoenmakers, Reducing Dilution and Analysis Time in Online Comprehensive Two-Dimensional Liquid Chromatography by Active Modulation, Anal. Chem. 88 (2016) 1785–1793. https://doi.org/10.1021/acs.analchem.5b04051.

[26] E. Sommella, E. Salviati, S. Musella, V. Di Sarno, F. Gasparrini, P. Campiglia, Comparison of Online Comprehensive HILIC × RP and RP × RP with Trapping Modulation Coupled to Mass Spectrometry for Microalgae Peptidomics, Separations. 7 (2020) 25. https://doi.org/10.3390/separations7020025.

[27] J.M. Davis, D.R. Stoll, P.W. Carr, Effect of First-Dimension Undersampling on Effective Peak Capacity in Comprehensive Two-Dimensional Separations, Anal. Chem. 80 (2008) 461–473. https://doi.org/10.1021/ac071504j.

[28] A. D'Attoma, C. Grivel, S. Heinisch, On-line comprehensive two-dimensional separations of charged compounds using reversed-phase high performance liquid chromatography and hydrophilic interaction chromatography. Part I: Orthogonality and practical peak capacity considerations, Journal of Chromatography A. 1262 (2012) 148–159. https://doi.org/10.1016/j.chroma.2012.09.028.

[29] R.E. Murphy, M.R. Schure, J.P. Foley, Effect of Sampling Rate on Resolution in Comprehensive Two-Dimensional Liquid Chromatography, Anal. Chem. 70 (1998) 1585–1594. https://doi.org/10.1021/ac971184b.

[30] K. Horie, H. Kimura, T. Ikegami, A. Iwatsuka, N. Saad, O. Fiehn, N. Tanaka, Calculating Optimal Modulation Periods to Maximize the Peak Capacity in Two-Dimensional HPLC, Anal. Chem. 79 (2007) 3764–3770. https://doi.org/10.1021/ac062002t.

[31] M. Sarrut, F. Rouvière, S. Heinisch, Theoretical and experimental comparison of one dimensional versus on-line comprehensive two dimensional liquid chromatography for optimized sub-hour separations of complex peptide samples, Journal of Chromatography A. 1498 (2017) 183–195. https://doi.org/10.1016/j.chroma.2017.01.054.

[32] C. Grivel, J.-L. Rocca, D. Guillarme, J.-L. Veuthey, S. Heinisch, Selection of suitable operating conditions to minimize the gradient equilibration time in the separation of drugs by Ultra-High-Pressure Liquid Chromatography with volatile (mass spectrometry-compatible) buffers, Journal of Chromatography A. 1217 (2010) 459–472. https://doi.org/10.1016/j.chroma.2009.11.059.

[33] S.Chapel, S. Heinisch, F. Rouvière, A Theoretical and Practical Approach to Manage High Peak Capacity and Low Dilution in On-line Comprehensive Reversed-Phase LC × Reversed-Phase LC: A Comparison with 1D-Reversed-Phase LC, LC-GC Europe (2020), vol 33, number s5, Advances in UHPLC/HPLC, 17-26.

[34] S.R. Groskreutz, S.G. Weber, Quantitative evaluation of models for solvent-based, on-column focusing in liquid chromatography, Journal of Chromatography A. 1409 (2015) 116–124. https://doi.org/10.1016/j.chroma.2015.07.038.

[35] M. Bernardin, F. Bessueille-Barbier, A. Le Masle, C.-P. Lienemann, S. Heinisch, Suitable interface for coupling liquid chromatography to inductively coupled plasma-mass spectrometry for the analysis of organic matrices. 1 Theoretical and experimental considerations on solute dispersion, Journal of Chromatography A. 1565 (2018) 68–80. https://doi.org/10.1016/j.chroma.2018.06.024.

CONCLUSIONS

The main objective of this chapter was to provide useful guidelines to address the challenge of solvent strength mismatch in on-line HILIC x RPLC.

In the last decade, several strategies have been developed in an effort to improve the compatibility of these two highly orthogonal chromatographic modes. Four of these strategies were compared in this chapter: (i) the Total Breakthrough strategy, which we introduced in Chapter IV, (ii) the flow splitting strategy, which has been historically the most frequently used approach in on-line LC x LC, and (iii) two on-line solvent dilution approaches that have been increasingly popular in recent years, namely the make-up flow strategy and the Active Solvent Modulation strategy. The performances of each of these strategies were evaluated and compared for the separation of a complex tryptic digest sample. As highlighted in the following Table V-1, each of the studied strategies showed its own strengths and limitations.

Table V-1: Strengths and limitations of the three types of strategies compared in this chapter for the on-line HILIC x RPLC separation of peptides.

Strategy	Strengths	Limitations
Total Breakthrough	• Easy implementation • Fraction volume no more a limiting factor • Good peak shapes for all compounds • Peak capacity maximized	• Analyte breakthrough • Decreased peak intensity • Limited applicability
Flow splitting	• Reduction of injection volume in ^{2}D • Solvent incompatibility alleviated	• More complex implementation • High split ratio might be required • High dilution • Poor detection sensitivity • Additional devices required
On-line dilution	• Reduction of ^{1}D-effluent elution strength • Solvent incompatibility alleviated • Detection sensitivity improved	• More complex implementation • Dilution process is a limiting factor • High dilution ratio might be required • Very large injected volume in ^{2}D • Reduced gradient time • Reduced peak capacity • Additional devices required

For both the flow splitting and the on-line dilution approaches, it was found that injection problems could be very difficult to avoid in the second dimension without impacting severely either the detection sensitivity (in the former case) or the peak

capacity (in the latter case). In that regard, it appears that a combination of these two strategies may be an attractive option. Despite unavoidable losses in peak intensity in the second dimension, our results highlighted the great potential of the Total Breakthrough strategy for providing good peak shapes and maximizing the peak capacity in on-line HILIC x RPLC. Moreover, in this chapter, both the reliability and validity of the Total Breakthrough approach were confirmed for a broad range of analytical conditions, which emphasizes the viability of this unusual strategy in on-line LC x LC. However, it was also demonstrated that this approach had limited applicability since it requires the presence of positive charges on the studied compounds.

In conclusion to this chapter, overcoming solvent strength mismatch is not an easy task in on-line HILIC x RPLC. The different strategies investigated in this work all have, to some extent, proven effective to alleviate the deleterious impact of the ^{1}D-solvent eluotropic strength on the ^{2}D-separation. However, each of them came with specific strengths and weaknesses, and being aware of them is essential to make the right choices during method development.

REFERENCES

[1] B.W.J. Pirok, A.F.G. Gargano, P.J. Schoenmakers, Optimizing separations in online comprehensive two-dimensional liquid chromatography, J. Sep. Sci. 41 (2018) 68–98. https://doi.org/10.1002/jssc.201700863.

[2] B.W.J. Pirok, D.R. Stoll, P.J. Schoenmakers, Recent Developments in Two-Dimensional Liquid Chromatography: Fundamental Improvements for Practical Applications, Analytical Chemistry. 91 (2019) 240–263. https://doi.org/10.1021/acs.analchem.8b04841.

[3] Y. Chen, L. Montero, O.J. Schmitz, Advance in on-line two-dimensional liquid chromatography modulation technology, TrAC Trends in Analytical Chemistry. 120 (2019) 115647. https://doi.org/10.1016/j.trac.2019.115647.

[4] P. Česla, J. Křenková, Fraction transfer process in on-line comprehensive two-dimensional liquid-phase separations, J. Sep. Sci. 40 (2017) 109–123. https://doi.org/10.1002/jssc.201600921.

[5] L. Montero, E. Ibáñez, M. Russo, L. Rastrelli, A. Cifuentes, M. Herrero, Focusing and non-focusing modulation strategies for the improvement of on-line two-dimensional hydrophilic interaction chromatography × reversed phase profiling of complex food samples, Analytica Chimica Acta. 985 (2017) 202–212. https://doi.org/10.1016/j.aca.2017.07.013.

[6] M.J. Egeness, M.C. Breadmore, E.F. Hilder, R.A. Shellie, The Modulator in Comprehensive Two-Dimensional Liquid Chromatography, LC-GC Europe. 29 (2016) 268–276.

CHAPTER VI - APPLICATION OF ON-LINE LC x LC HYPHENATED TO MASS SPECTROMETRY TO THE CHARACTERIZATION OF ANTIBODY-DRUG CONJUGATES

This chapter has been prepared for publication and is expected to be submitted soon in ***Talanta.***

INTRODUCTION

In the three previous chapters, the studies that were described exclusively involved on-line LC x LC approaches applied to the analysis of protein after enzymatic digestion leading to complex mixtures of peptides. In this chapter, the focus is put on the analysis of protein either at the intact level or after cleavage into large subunits following limited proteolysis.

Herein, the investigated molecules are antibody-drug conjugates (ADCs). As outlined in Chapter I, antibody-drug conjugates belong to a new and fast-growing class of highly potent biotherapeutic drugs targeted for the treatment of cancer, autoimmune, and inflammatory diseases [1]. Structurally speaking, an ADC is composed of a monoclonal antibody (mAb) covalently linked to small molecule drugs via a chemical linker. Monoclonal antibodies are highly complex "Y-shaped" tetrameric glycoproteins with molecular weights near 150 kDa that are composed of two identical heavy chains and two identical light chains held together by disulfide bonds [2,3]. Product heterogeneity, introduced during manufacturing or storage, is very common for these compounds but can influence biological activity and product safety [4,5]. For this reason, a comprehensive characterization of mAbs and ADCs is mandatory before they can become drug candidates. The analytical characterization of mAbs and ADCs requires the investigation and monitoring of numerous critical quality attributes (CQAs), among which drug distribution, average drug-to-antibody ratio, amount of unconjugated mAb, site occupancy, glycosylation patterns, protein aggregation, size variants, and charge variants [6]. In practice, such a thorough characterization often involves multiple complementary methods based on electrophoresis, liquid chromatography, and mass spectrometry [6-11]. Therefore, it is not surprising that two-dimensional liquid chromatography techniques coupled with mass spectrometry detection (2D-LC-MS) have emerged as attractive analytical approaches to address the challenges associated with the characterization of these complex molecules [12-14].

The objective of this chapter is to highlight the potential benefits of using 2D-LC techniques for the analysis of therapeutic antibodies at both the intact and subunit levels. The chapter describes the development of on-line 2D-LC methods combining cation-exchange chromatography (CEX) in the first dimension and RPLC in the second dimension for the characterization of the charge variants of a lysine-linked antibody-

drug conjugate. In this work, both the selective comprehensive mode (sLC x LC) and the full comprehensive mode (LC x LC) were investigated.

1. Introduction

The characterization of antibody-drug conjugates (ADCs) is a challenging task due to their high complexity, which arises both from their size and their structure heterogeneity. Given the inherent complexity of these biomolecules, two-dimensional liquid chromatography (2D-LC) is an attractive technique to address the challenges associated with ADC characterization. It has been proven to be a rapid and efficient analytical tool: (i) to provide a very high resolving power by increasing the overall peak capacity compared to conventional one-dimensional liquid chromatography (1D-LC) and (ii) to allow mass spectrometry (MS) coupling with chromatographic techniques that are not MS-compatible to facilitate structural elucidation. The characterization of ADCs can be achieved from three different and complementary approaches: top-down (analysis of intact protein), middle-up (analysis after protein cleavage into large subunits between 25 and 100 kDa) or bottom-up (analysis after protein cleavage into peptides < 7 kDa), each of them giving specific information on the protein.

Because of their potential influence on biological activity and stability, charge variants are considered as critical quality attributes of ADCs. Cation-exchange chromatography (CEX) is the gold-standard technique to separate protein charge variants in liquid chromatography but it requires a large amount of salt which makes it incompatible with MS detection. For in-depth characterization of mAbs and ADCs with MS detection, the use of reversed-phase liquid chromatography (RPLC) as a desalting step after a first dimension (^{1}D) CEX has been successfully reported in the literature in top-down [1,2], middle-up [1–3], and bottom-up [4], both in multiple heart-cutting (mCEX-RPLC) and comprehensive (CEX x RPLC). Thanks to MS-friendly solvents and added selectivity brought by RPLC, this combination not only allows direct assignment of the ^{1}D-CEX peaks with MS detection but also extends the level of peak information in one single analysis.

The objective of the current project was to develop an on-line 2D-LC method combining CEX and RPLC for the characterization of the charge variants of a lysine-linked antibody-drug conjugate. For confidentiality reasons, the name, the structure, and any other information relevant to identify the investigated molecule will not be disclosed. In this work, we will refer to it as ADC-S01.

The analyses of ADC-S01 and its parent mAb (mAb-S01) were performed using top-down and middle-up approaches. The first part of this study was devoted to the choice

of stationary phases and the optimization of chromatographic conditions in both dimensions. Based on the results obtained in 1D-CEX with ultraviolet detection (UV) and 1D-RPLC with UV and high-resolution mass spectrometry (HRMS) detections, the 2D-LC conditions were optimized in both selective comprehensive (sCEX x RPLC) and fully comprehensive (CEX x RPLC) modes. The last part of this study consisted in the identification of the separated species using HRMS detection and in the comparison of three ADC samples exposed to different durations of thermal stress.

2. Experimental section

2.1. Chemical and reagents

Acetonitrile (ACN, LC-MS grade) was obtained from Sigma-Aldrich (Steinheim, Germany). Water was purified and deionized by an Elga Purelab Classic UV purification system (Veolia water STI, Le Plessis Robinson, France). Formic acid (FA, LC/MS grade), trifluoroacetic acid (TFA, LC/MS grade), sodium chloride (NaCl), 2-(N-morpholino) ethanesulfonic acid (MES), sodium hydroxide (NaOH), monosodium phosphate (NaH_2PO_4), and disodium phosphate (Na_2HPO_4), all analytical grade, were obtained from Fischer scientific (Illkirch, France). IonHance™ Difluoroacetic Acid (DFA, LC/MS grade) was provided graciously by Waters (Milford, MA, USA). IdeS protease enzyme (FabRICATOR) was obtained from Genovis (Lund, Sweden).

The samples of mAb-S01 and ADC-S01 were formulated at 20 mg/mL and 5 mg/mL, respectively. For the stability study presented in Subsection 3.2.3, two additional thermally-stressed ADC samples were used. They were obtained by exposing ADC-S01 to elevated temperature (40°C) for either two weeks or four weeks. In Subsection 3.2.3, unstressed (t = 0), stressed for two weeks (t = 2), and stressed for four weeks (t = 4) samples will be referred to as ADC-t0, ADC-t2, and ADC-t4, respectively.

2.2. Sample preparation

Intact mAb and ADC samples were injected at their formulated concentration, without any pre-treatment nor prior dilution. Partially digested ADC samples were obtained using IdeS protease enzyme (FabRICATOR) following the generic protocol in the instruction manual provided by Genovis (1 unit of enzyme/µg of ADC at 37°C for 30 min). Partial digestion with IdeS cleaves the protein below the hinge region of the

heavy chain, which leads to the formation of two Fc/2 subunits and one F(ab')2 subunit.

2.3. Columns

Two columns were evaluated for the first dimension CEX: BioResolve SCX (100 x 2.1 mm, 3 µm) from Waters (Milford, MA, USA) and Bio MAb NP5 (250 x 2.1 mm, 5 µm) from Agilent Technologies (Waldbronn, Germany).

Five columns were evaluated for the second dimension RPLC: BioResolve RP mAb polyphenyl (50 x 2.1 mm, 2.7 µm) and Acquity BEH C4 (50 x 2.1 mm, 1.7 µm) from Waters (Milford, MA, USA), Biozen intact XB-C8 (50 x 2.1, 3.6 µm) from Phenomenex (Torrence, CA, USA), PLRP-S (50 x 2.1mm, 5 µm) and AdvanceBio RP-mAb diphenyl (50 x 2.1mm, 3.5 µm) from Agilent Technologies (Waldbronn, Germany).

2.4. Instrumentation

Most 1D-LC experiments were carried out using an Acquity UPLC liquid chromatography system from Waters (Milford, MA, USA). The instrument includes a high-pressure binary solvent delivery pump, a sample manager with a 20-µL loop, a column manager equipped with a column oven with a maximum temperature of 90°C, and a photodiode array detector (PDA) equipped with a 0.5-µL flow-cell withstanding pressure up to 70 bar. The dwell volume and extra-column volume for this entire system were measured using a zero-dead volume union connector in place of the column and were respectively 110 µL and 12 µL.

1D-LC-UV-HRMS experiments were carried out using the first dimension of a 1290 Infinity series 2D-LC system (see description of the instrument below).

On-line LC x LC experiments were carried out using a 1290 Infinity series 2D-LC system from Agilent Technologies (Waldbronn, Germany). The instrument includes two high-pressure binary solvent delivery pumps, an autosampler with a flow-through needle of 20 µL equipped with a 160-µL extension loop when needed, two thermostated column compartments with a maximum temperature of 100°C equipped with low-dispersion preheaters, and two diode-array detectors (DAD) equipped with 0.6-µL flow-cells.

The interface connecting the two dimensions consisted of a 2-position/4-port duo valve, equipped with two identical 80-µL loops in comprehensive LC x LC. In selective comprehensive LC x LC, a multiple heart-cutting 2D-LC interface consisting of a 2-position/4-port duo valve connected to two 6-position/14-port deck valves mounted with six identical 180-µL loops was used. To minimize dispersion, the valve was configured in back-flush injection mode. A pressure release kit placed between the ^{1}D-outlet and the interface was used to minimize the pressure downstream induced by the switch of the 2D-LC valve to protect the ^{1}DAD flow-cell and avoid artefacts in the ^{1}DAD signal. The measured dwell volumes and extra-column volumes of this 2D-LC system were respectively 170 µL and 22 µL in ^{1}D, and 80 µL and 8.5 µL in ^{2}D (loop volumes at the interface excluded).

The 2D-LC system was hyphenated to an Agilent G6560B Q-TOF mass spectrometer, equipped with a JetStream electrospray ionization (ESI) source. In some cases (see Table VI-1), a diverter valve was placed between the 2D-LC and MS instruments to redirect part of the ^{2}D-effluent to the waste following each injection and prevent contamination of the MS source with NaCl.

Data acquisition and instrument control were performed using Agilent OpenLab software for 2D-LC and MassHunter software for MS. MS data processing was performed using Agilent MassHunter qualitative analysis software for MS data and Agilent BioConfirm software for deconvolution of the MS spectra. LC x LC data were processed using an in-house script developed on Matlab.

2.5. Chromatographic and detection conditions

The conditions used in 1D-CEX and 1D-RPLC for developing and optimizing the 2D-LC methods are indicated in the figure captions and in the text.

The conditions for the two optimized sCEX x RPLC and CEX x RPLC methods are given in the following Table VI-1.

Table VI-1: Experimental conditions for the two optimized CEX x RPLC (fully comprehensive) and sCEX x RPLC (selective comprehensive) methods.

	CEX x RPLC	sCEX x RPLC
First dimension (^{1}D)		
Injection volume	40 µL	10 µL
Injection solvent	Water	Water
Stationary phase	Bioresolve SCX	Bioresolve SCX
Column geometry	(100 x 2.1 mm, 3 µm)	(100 x 2.1 mm, 3 µm)
Temperature	30°C	30°C
Mobile phase	A: water + 20 mM MES pH = 6.5 B: A + 300 mM NaCl	A: water + 20 mM MES pH = 6.5 B: A + 300 mM NaCl
Flow rate	75 µL/min	200 µL/min
Gradient	1-17-1-1% B in 0-20-22.77-31.3 min	1-40-1-1% B in 0-20.28-21.32-63.73 min
Post-column split	None	None
Modulation		
Loop size	80 µL	180 µL
Sampling time	0.78 min Starting from 5 min (t0-IdeS and t2-IdeS) or 4 min	0.5 min (from 1.5 min to 6.5 min)
Second dimension (^{2}D)		
Stationary phase	Bioresolve RPmAb pk	Bioresolve RPmAb pk
Column geometry	(50 x 2.1 mm, 2.7 µm)	(50 x 2.1 mm, 2.7 µm)
Temperature	80°C	80°C
Mobile phase	A: 0.1% FA + 0.05% TFA in water B: 0.1% FA + 0.05% TFA in ACN	A: 0.1% FA + 0.05% TFA in water B: 0.1% FA + 0.05% TFA in ACN
Flow rate	1700 µL/min	1200 µL/min
Gradient	30-50-30-30% B in 0-0.49-0.55-0.78 min	20-35-95-20-20% B in 0-3-4.4-4.48-5.43 min
Post-column split	1:1.5	None
Diverter valve	Flow to the waste from 0 to 0.1 min Flow to MS at 0.1 min	/
UV detection	280 nm (40 Hz in ^{1}D and 80 Hz in ^{2}D)	
HRMS detection		
Ionization mode	ESI+	
Mass range (Da)	1200-5000	
Scan rate (spectra/s)	10	
Gas temp (°C)	325	
Drying gas (L/min)	13	
Nebulizer (psi)	40	
Sheath gas (°C)	350	
Sheath gas flow (L/min)	12	
Capillary voltage (V)	4000	
Nozzle voltage (V)	300	
Fragmentor (V)	185	
Oct 1 Rf Vpp (V)	750	
Quad AMU (V)	600	

3. Results and discussion

3.1. Development and optimization of 2D-LC conditions

A 2D-LC separation is the combination of two 1D-LC experiments. As part of method development, each dimension (i.e. CEX on one hand and RPLC on the other hand) was individually optimized with a view to maximize the separation power. The investigated parameters were: the nature of the stationary phase, the nature and the composition of the mobile phase, the gradient conditions, and the injection conditions.

3.1.1. Choice of stationary phase and mobile phase buffer in 1D-CEX

The first step of this study was to develop a suitable CEX method for the separation of charge variants in the first dimension. For this purpose, we evaluated several stationary phases and mobile phase buffers. In the literature, the Agilent Bio MAb NP5 column has been exclusively used in ^{1}D-CEX for the 2D-LC separation of mAbs and related products [1–3], with either MES [1,2], phosphate [1] or ammonium acetate [3] as mobile phase buffers.

In this work, we evaluated two columns from different manufacturers: the Bio MAb NP5 column from Agilent and the BioResolve SCX column from Waters. Both columns consist of non-porous polymeric-based particles and are specifically designed for the separation of charge isoforms of biotherapeutic proteins. Non-porous polymeric particles are usually preferred for protein analysis in CEX. They enable to work across a wide range of mobile phase pH and provide better chromatographic performances by limiting trans-particle mass transfer resistance [5], which can be a critical issue for large proteins. The Bio MAb column features a weak cation-exchange (WCX) phase, whereas the BioResolve column features a strong cation-exchange (SCX) one. Because SCX phases employ strong acids, the number of charges on their surface is expected to remain constant over a broad pH range, which makes them attractive in CEX. In contrast, WCX phases employ weak acids that gradually lose their ionization when the pH decreases below pH 5 [6]. It is important to be aware of such limitations during method development. However, it should be pointed out that in our study, the conditions were operated over a small pH range between 6.5 and 7.6, in which both columns are expected to deliver optimal performance.

In CEX, protein elution may be performed with either salt gradients, pH gradients or salt-mediated pH gradients (combined salt/pH gradients) [6–8]. In this work, we used

a classical salt gradient for the separation, as this is the most frequently used mode for the separation of protein charge variants [6]. Sodium chloride (NaCl) was used for the salt gradient while two different mobile phase buffers were evaluated for the separation (MES and phosphate). In CEX, the separation mechanism relies on the binding of positively charged analytes on a negatively charged stationary phase. Because a positive charge is removed when a lysine is conjugated with a drug, increasing drug conjugation is expected to lead to decreasing retention. For this reason, the influence of the mobile phase pH on the separation was also investigated. Analyte retention was found to be insufficient above pH 7.6 and the best separation was achieved with pH 6.5 (data not shown).

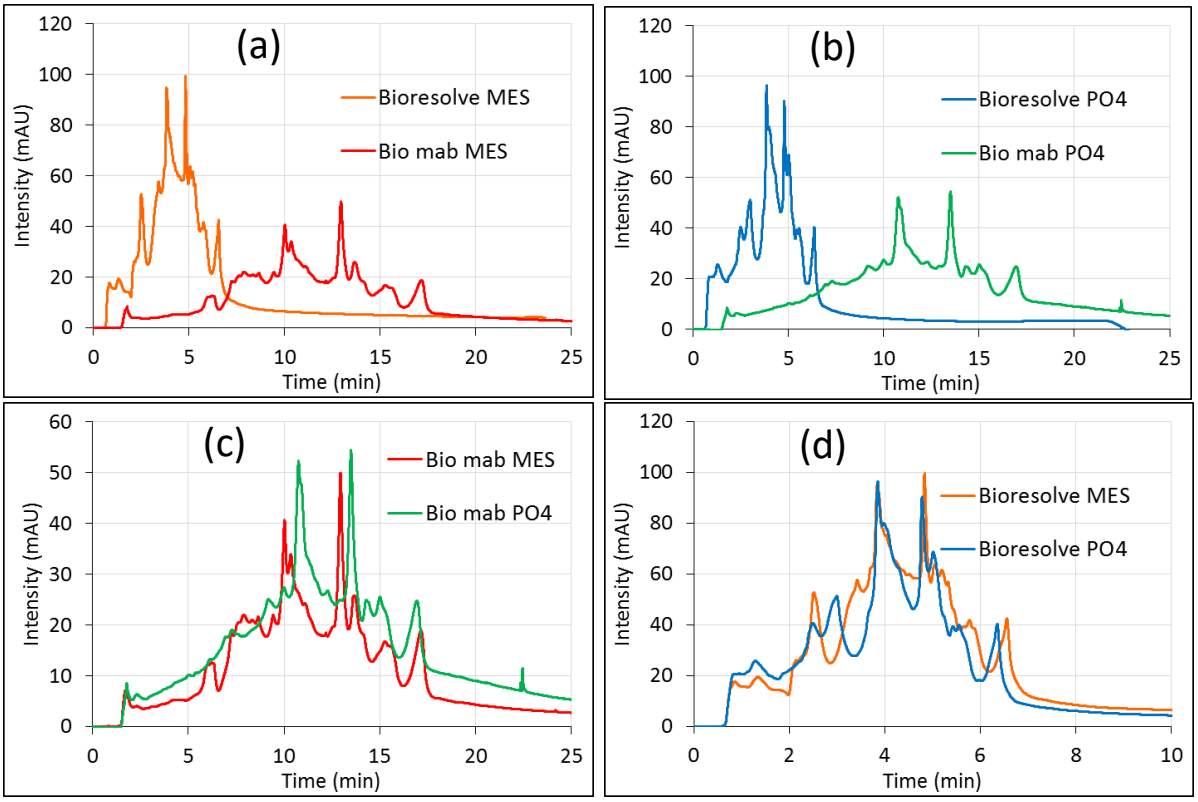

Fig. VI-1: 1D-CEX-UV (280 nm) analyses of IdeS-treated ADC-S01 using water + 20 mM MES at pH 6.5 (red and orange lines) or water + 10 mM PO_4 at pH = 6.5 (green and blue lines) as solvent A using either BioResolve SCX (100 x 2.1 mm, 3 µm) column (orange and blue lines) or Bio MAb NP5 (250 x 2.1 mm, 5 µm) column (red and green lines). Conditions: solvent A + 300 mM NaCl as solvent B, gradient 1% to 40% B in 20.28 min (BioResolve SCX) or 50.7 min (Bio MAb NP5), flow rate = 0.2 mL/min, temperature = 30 °C, injected volume = 5 µL.

Evaluation of the two sets of stationary phase and mobile phase buffers was performed on IdeS-treated ADC-S01 sample at pH 6.5. The results obtained for this comparison are shown in Fig. VI-1.

Figs. VI-1a and 1b allow comparing the two columns for a given buffer (MES in Fig. VI-1a and phosphate in Fig. VI-1b), whereas Figs. VI-1c and 1d draw attention to the effect of the buffer for a given column (Bio MAb in Fig. VI-1c and BioResolve in Fig. VI-1d). As can be seen when comparing Fig. VI-1c with Fig. VI-1d, overall, the separations were quite similar with the two columns. Although the Bio Mab column gave slightly better peak separation and resolution than the BioResolve column, no significant differences were found between the two columns. Therefore, we made a decision based on column dimensions and selected the BioResolve SCX column to keep the analysis time as short as possible in 2D-LC (shorter column length allowing shorter gradient time in ^{1}D). As shown in Fig. VI-1d, the MES buffer (orange line) gave slightly better separation than the PO_4 buffer (blue line) and was thus selected for the ^{1}D-CEX.

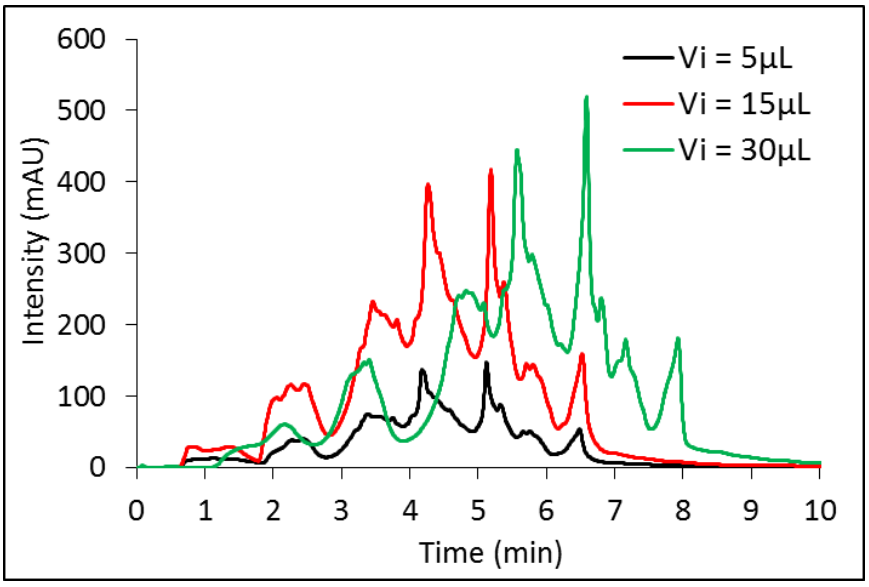

Fig. VI-2: Effect of the injected volume (Vi) on 1D-CEX-UV (280 nm) separation of IdeS-treated ADC-S01. Injected volumes: 5 µL (blue), 15 µL (red), and 30 µL (green). Column: BioResolve SCX (100 x 2.1 mm, 3 µm). Conditions: water + 20 mM MES (pH = 6.5) as solvent A and solvent A + 300mM NaCl as solvent B, gradient 1% to 40% B in 20.28 min, flow rate = 0.2 mL/min, ambient temperature. Injection of 30 µL was achieved using a 160-µL extension loop.

With a view to minimize the dilution factor in ^{1}D, a brief study of the effect of the injected volume on the separation was conducted. Fig. VI-2 shows the 1D-CEX-UV separations of IdeS-treated ADC-S01 with injected volumes ranging from 5 µL to 30 µL. As highlighted, no deterioration of the chromatographic performances was observed up to 30 µL injected. It should be mentioned that the retention shift observed with 30 µL compared to the other two volumes is merely the result of the increased

dwell time when using a 160-µL extension loop. As will be demonstrated in the following sections, we managed to increase the injected volume up to 80 µL without impacting the chromatographic separation. This is mainly due to the excellent focusing at the head of the column when injecting a sample diluted in water in CEX.

3.1.2. Choice of stationary phase and mobile phase additive in 1D-RPLC

For the analysis of mAbs and ADCs in top-down and/or middle-up, the use of RPLC in ^{2}D after a ^{1}D-CEX separation provides two benefits: (i) it allows the indirect on-line coupling of CEX with MS detection and (ii) it potentially brings an additional and complementary separation to the ^{1}D-CEX.

Because the cytotoxic drugs are hydrophobic, the process of drug conjugation increases the hydrophobicity of the molecule. A separation by increasing drug load or drug-to-antibody (DAR) can be thus be expected in RPLC. The RPLC conditions were optimized in this work keeping two main objectives in mind: (i) maximizing peak separation and (ii) allowing sufficient mass spectrometric sensitivity for peak identification.

In RPLC-MS analysis of proteins, the selection of the mobile phase additive is a key parameter during method development. Due to its strong hydrophobic, acidic, and ion-pairing characters, TFA is well-known to provide the best chromatographic results for the separation of proteins in RPLC [9–11]. Its use allows solving many of the problems faced when analysing proteins in RPLC, including adsorption on the stationary phase, peak tailing, and peak broadening. However, TFA is also well-known to provide a dramatic decrease in MS detection sensitivity due to analyte ionization suppression and spray instability arising from higher conductivity and surface tension of the eluent. In the literature, decreasing the concentration of TFA in the mobile phase has been demonstrated to be an effective strategy to preserve the chromatographic separation while maintaining enough MS sensitivity [12]. In this work, the influence of the concentration of TFA in the mobile phase on the separation was investigated on intact and IdeS-treated ADC-S01 samples. Fig. VI-3 shows 1D-RPLC-UV separations of both samples using 0.1% TFA (Fig. VI-3a) or 0.05% TFA + 0.1% FA (Fig. VI-3b) in the mobile phase. Decreasing the concentration of TFA in the mobile phase from 0.1% to 0.05% had no significant impact on chromatographic performance. However, it has

been demonstrated that reducing too much the amount of TFA in the mobile phase could lead to a substantial decrease in recovery for intact proteins as a result of adsorption on the stationary phase [13]. For this reason, we chose to maintain a concentration of at least 0.05% TFA in the mobile phase for the rest of this study.

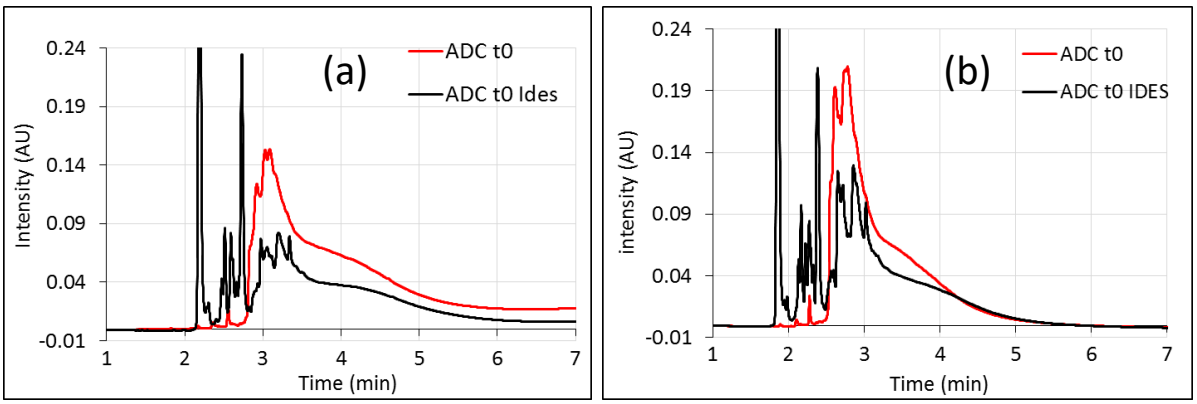

Fig. VI-3: 1D-RPLC-UV (280 nm) analyses of intact (red) and IdeS-treated ADC-S01 (black) using (a) 0.1% TFA or (b) 0.05% TFA + 0.1% FA as additive in the mobile phase. Column: BioResolve RP mAb polyphenyl (50 x 2.1 mm, 2.7 µm). Conditions: water + additive as solvent A and ACN + additive as solvent B, gradient 20% to 80% B in 7 min, flow rate = 0.3 mL/min, temperature = 80°C, injected volume = 8 µL.

Several stationary phases were investigated for the second dimension. Except for the non-porous polymeric-based PLRP-S column, all columns contained silica-based particles with C4 alkyl- (Acquity BEH C4), C8 alkyl- (Biozen intact XB-C8), diphenyl- (AdvanceBio RP-Mab diphenyl) or polyphenyl ligands (BioResolve RP mab Polyphenyl) on superficially porous particles. Non-porous and superficially porous particles are usually preferred for the analysis of protein in RPLC for the aforementioned reasons (i.e. reduced mass transfer resistance) [14].

Fig. VI-4 shows a comparison of RPLC-UV separations of intact and IdeS-treated ADC-S01 samples obtained with each of these stationary phases. From a chromatographic standpoint, the best results were obtained with the Bioresolve RP mAb column (Fig. VI-4a). The Agilent PLRP-S column (Fig. VI-4b) also showed good performance and could have been attractive to prevent high temperature-related silica bleeding in ^{2}D as it is a polymeric-based column. However, the very low pressure limit of this column (P_{max} < 200 bar) makes it incompatible with the relatively high flow rates usually required in ^{2}D. The Acquity BEH C4 column was also evaluated but showed poorer

performance than the BioResolve RP mAb column. The comparison between these two columns can be found in Fig. VI-S1.

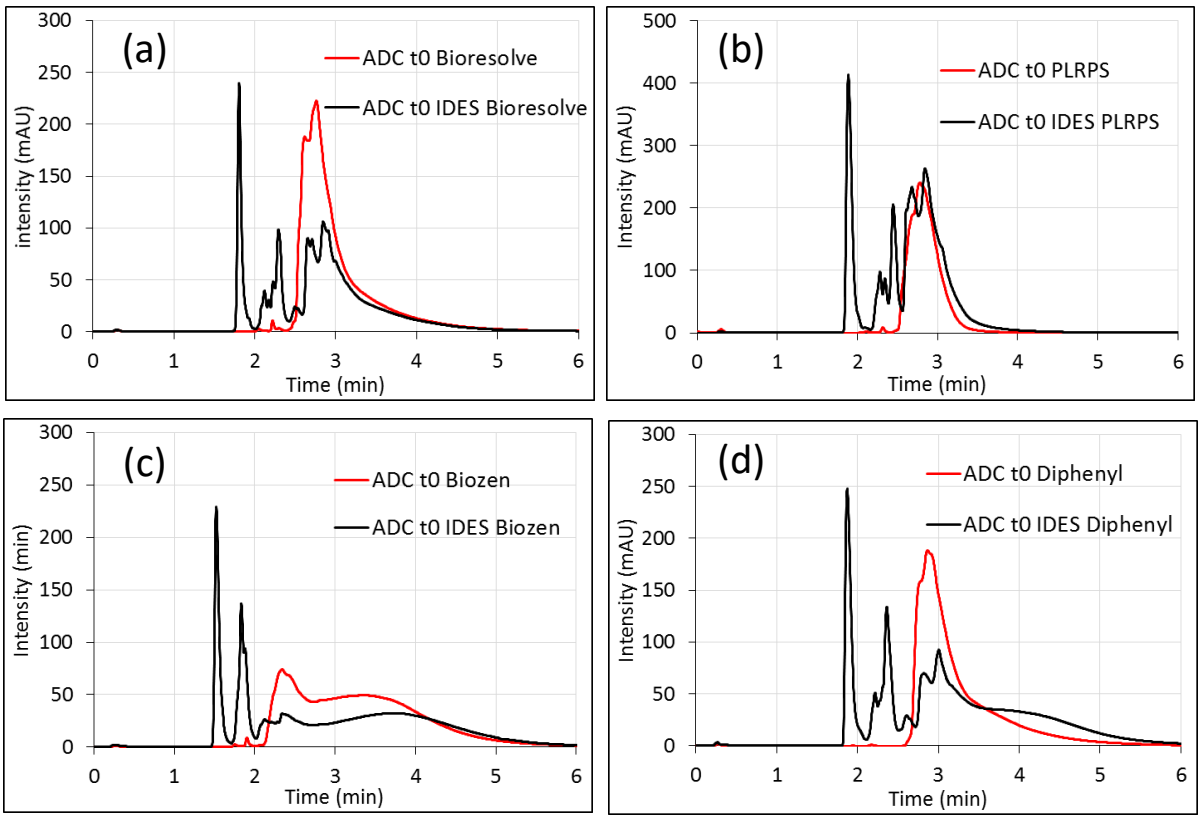

Fig. VI-4: 1D-RPLC-UV (280 nm) analyses of intact and IdeS-treated ADC-S01 with (a) BioResolve RP mAb polyphenyl (50 x 2.1 mm, 2.7 µm), (b) PLRP-S (50 x 2.1 mm, 5 µm), (C) Biozen intact XB-C8 (50 x 2.1 mm, 3.6 µm) and (D) AdvanceBio RP-mAb diphenyl (50 x 2.1 mm, 3.5 µm) columns. Conditions: water + 0.05% TFA + 0.1% FA as solvent A and ACN + 0.05% TFA + 0.1% FA as solvent B, gradient 20% to 95% B in 8.8 min or 7 min (PLRP-S), flow rate = 0.6 mL/min. Same other conditions as in Fig. VI-3.

3.1.3. Determination of the useful separation space in RPLC

To better optimize the second RPLC dimension, intact mAb-S01, intact ADC-S01, and IdeS-treated ADC-S01 samples were all analysed in 1D-RPLC using both UV and HRMS detections. Here, we will discuss only the results obtained for the IdeS-treated ADC sample as this sample provides more peaks for the separation.

As shown in Fig. VI-5a (UV) and Fig. VI-5b (MS), the area of interest in the chromatogram (i.e. the time range during which the species of interest elute) was found to be very small relative to the entire separation space. The useful separation space ranged from about 2.5 min to 4.4 min with a gradient elution ranging from 20% to 95% B in 8.8 min. This area of interest was delimited after identifying the separated

peaks based on their exact masses using HRMS detection. The peaks of interest are labelled from 1 to 7 in Fig. VI-5b and the corresponding assignments are given in Table VI-2. Assignments were made by comparing experimentally measured masses with expected theoretical masses. For confidentiality reasons, theoretical and experimental masses, as well as deconvoluted mass spectra used for peak identification will not be given in this study. Species corresponding to Fc/2 subunits with 1 or 2 drugs were identified in the first part of the area of interest, whereas F(ab')2 subunits with drug loads from 0 to 5 were found in the second part. Several peaks with very close masses but different retention times were observed (e.g. peak #3, #4, #5, and #6a), suggesting the presence of isomeric compounds. The presence of distinct subunits with identical drug load in RPLC could be explained by drug conjugation at different lysine residues. Similar results have been reported for the analysis of the commercialized lysine-linked ADC trastuzumab emtansine in mCEX-RPLC [1].

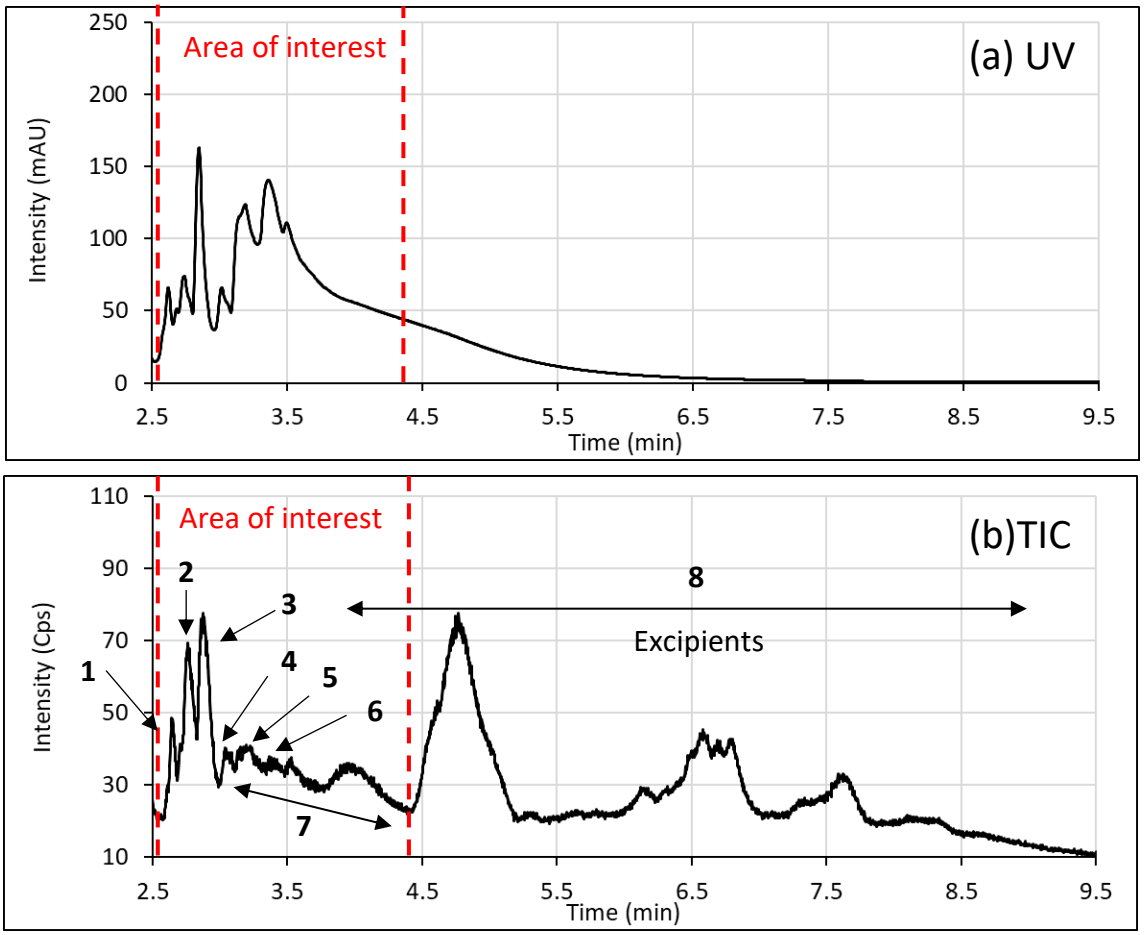

Fig. VI-5: (a) 1D-RPLC-UV (280 nm) and (b) 1D-RPLC-HRMS (TIC, ESI+) analyses of IdeS-treated ADC-S01 with BioResolve RP mAb polyphenyl (50 x 2.1 mm, 2.7 µm) column. The two dotted horizontal red lines delimit the area of interest of the separation. Numbers 1 to 8 indicate the identified species in Table VI-2. Conditions: flow rate = 0.3 mL/min. Same other conditions as in Fig. VI-4.

In the three samples that were analysed (i.e. intact mAb, intact ADC, and IdeS-treated ADC), the presence of numerous interfering peaks that could correspond to various excipients was highlighted in the second half of the chromatogram (label #8 in Fig. VI-5b). Excipients are substances that are added to biotherapeutic protein formulations to improve their stability and manufacturability. In our study, those compounds were found to be quite retained in RPLC. Most of them were more retained than the species of interest. However, some of the earlier eluted excipients were found to coelute with the later eluted species of interest and appeared to create significant ion suppressions.

Table VI-2: Proposed species for the peaks labelled in Fig. VI-5b after comparison between experimental and theoretical masses.

#	Difference between theoretical and experimental masses (Da)	Proposed specie
1	-1	Fc/2 + 1 drug
2	-1	Fc/2 + 1 drug
3	-1	Fc/2 + 1 drug
4a	-1	Fc/2 + 1 drug
4b	-2	Fc/2 + 2 drugs
5a	+2	(Fab')2 + 0 drug
5b	+2	(Fab')2 + 1 drug
5c	+2	(Fab')2 + 2 drugs
6a	+2	(Fab')2 + 1 drug
6b	+1	(Fab')2 + 2 drugs
6c	0	(Fab')2 + 3 drugs
6d	+1	(Fab')2 + 4 drugs
7a	+3	(Fab')2 + 0 drug
7b	+2	(Fab')2 + 1 drug
7c	+54	(Fab')2 + 2 drugs
7d	0	(Fab')2 + 3 drugs
7e	-1	(Fab')2 + 4 drugs
7f	-1	(Fab')2 + 5 drugs

3.1.4. Optimization of gradient conditions in on-line sCEX x RPLC and CEX x RPLC

In the context of top-down and/or middle-up analysis of mAb and ADC, both on-line multiple heart-cutting mCEX-RPLC (for ADC) [1] and full comprehensive CEX x RPLC (for mAb) [2,3] have been reported in the literature. In this study, the limited useful separation space in RPLC and the presence of excipients creating MS signal suppressions both raised questions about the relevance of performing fully

comprehensive 2D-LC, since this analytical technique requires very fast separations in ^{2}D. From this perspective, selective comprehensive 2D-LC was considered at first glance because it allows longer gradient times in ^{2}D, and, therefore, potentially, better separations.

Before conceding on the 2D-LC strategy to use, we performed an on-line CEX x RPLC analysis to study the retention of the excipients in CEX and determine whether or not these compounds could be eliminated in ^{1}D. Fig. VI-6 shows the contour plot obtained for the analysis of the IdeS-treated ADC (t0) using MS detection. Most of the excipients eluted before the delimited area of interest in ^{1}D-CEX (i.e. before 5 min) whereas only a small part of them (highlighted by a black circle) coeluted with the species of interest. It should be pointed out that, contrary to the observations made in 1D-RPLC-HRMS (Fig. VI-5b), the different excipients elute all along the RPLC separation. Because of this, MS signal intensity was too low to unambiguously identify F(ab')2 species in RPLC. As pointed out before, the retention space of interest is quite small which is discouraging for on-line LC x LC.

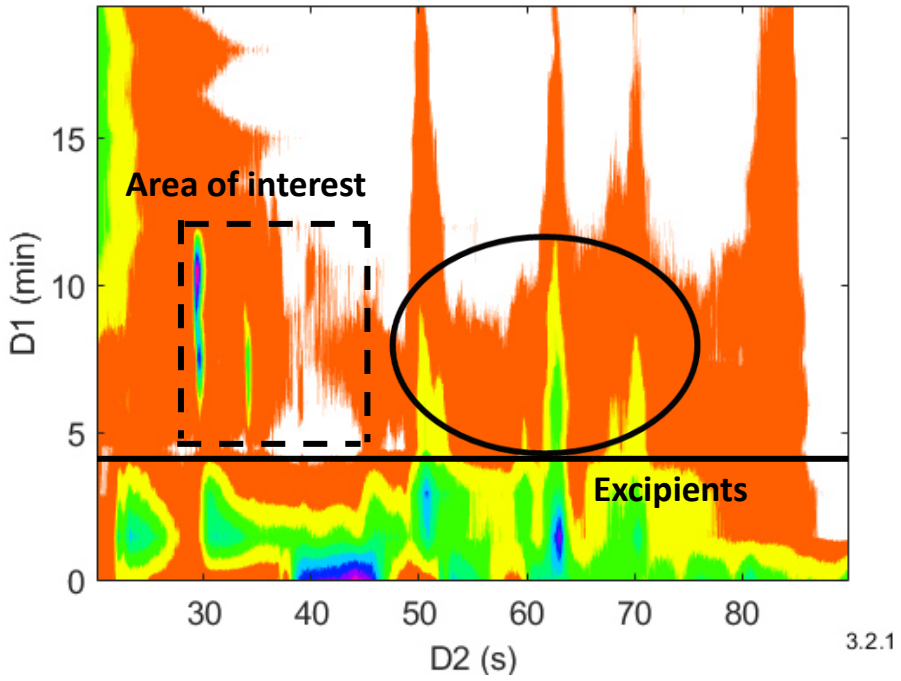

Fig. VI-6: Contour plot (TIC, ESI+) of the on-line CEX x RPLC analysis of IdeS-treated ADC-S01 used for method development. Conditions in ^{1}D: flow rate = 0.1 mL/min, gradient 1-40% B in 40.56 min, V_i = 5 µL. Conditions in ^{2}D: flow rate = 1.2 mL/min, gradient 20-95% B in 1.1 min, sampling time = 1.5 min (loop volume = 180 µL). Same other conditions as for optimized CEX x RPLC in Table VI-1. The dotted square indicates the area of interest, the straight line indicates the time below which most of the excipients are eluted in ^{1}D-CEX and the circle shows the excipients coeluting with the species of interest in ^{1}D-CEX.

Based on those results, we first developed and optimized a selective comprehensive method to maximize the separation power as much as possible in ^{2}D. Ten fractions were collected in ^{1}D between 1.5 min and 6.5 min every 0.5-min interval. Fig. VI-7 shows the first dimension separation of the IdeS-treated ADC sample. As can be seen, only part of the chromatogram could be sampled due to the limited number of possible fractions in sLC x LC (≤ 10). The total analysis time for this sCEX x RPLC method was 64 min with a run time of 5.43 min for each fraction in ^{2}D.

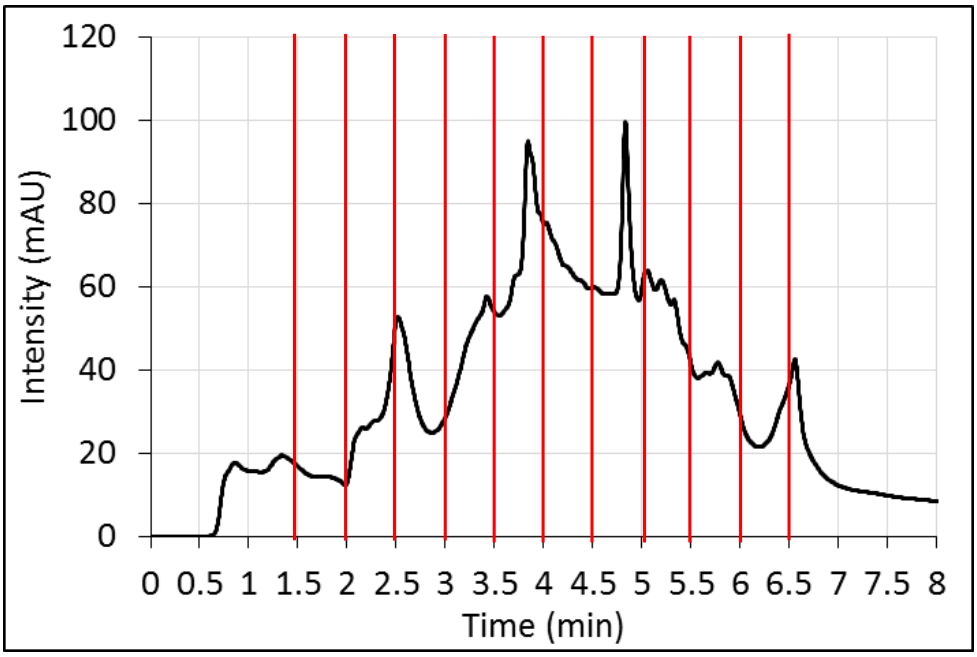

Fig. VI-7: ^{1}D-CEX-UV (280 nm) analyses of IdeS-treated ADC-S01 in on-line sCEX x RPLC. See conditions in Table VI-1. The horizontal red lines show the ten fractions sent to ^{2}D.

Contrary to the selective comprehensive mode, fully comprehensive methods impose no restrictions on the number of fractions that can be transferred from the first dimension. On that account, an on-line LC x LC method could bring more information compared to sLC x LC.

Conditions were thus further optimized in full comprehensive mode, keeping three main objectives in mind: (i) removing interfering excipients as much as possible, (ii) finding sub-hour conditions, and (iii) maximizing MS-detection sensitivity. Given the limited elution range in CEX, the gradient time was set at 20 min with gradient compositions ranging from 1% to 17% B (total analysis time = 31.3 min). The sampling time and hence the analysis time in ^{2}D was set at 0.78 min to maintain 2 to 3 fractions

per ^{1}D-peak. The strategy used to avoid MS signal suppression arising from coelutions with excipient species was to take advantage of their low retention in ^{1}D-CEX and remove them as much as possible before starting to send the fractions to ^{2}D-RPLC.

Fig. VI-8 shows a comparison of 1D-RPLC-UV separations of IdeS-treated ADC-S01 sample with a composition range between 30-50% B (black line) or 30-95% B (red line). As highlighted, reducing the gradient composition range while keeping the same gradient time allows to significantly improve the chromatographic separation. The resulting optimized conditions for the two 2D-LC methods (selective and fully comprehensive) are given in Table VI-1.

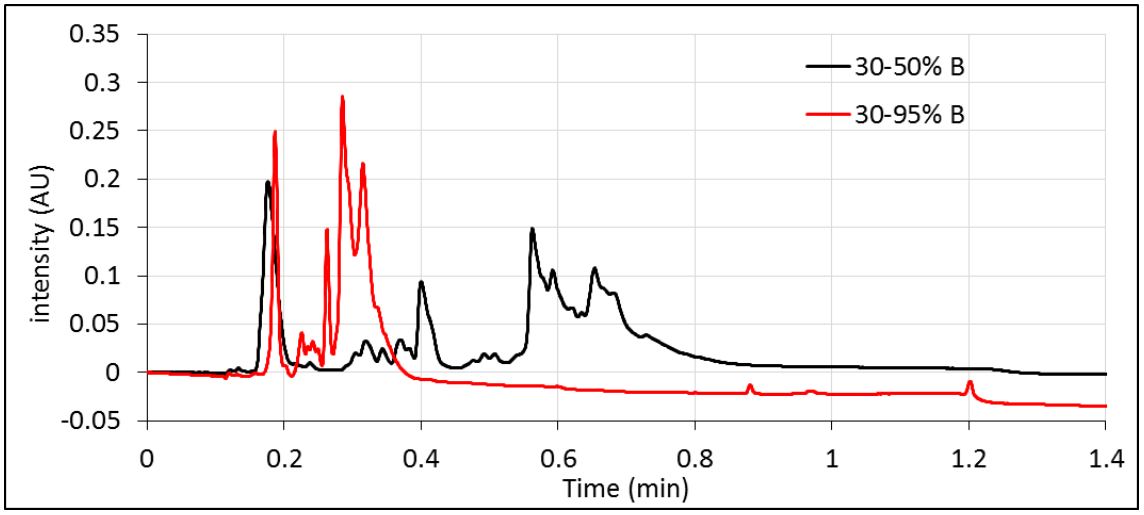

Fig. VI-8: 1D-RPLC-UV (280 nm) analyses of IdeS-treated ADC-S01 with Bioresolve RPmAb (50 x 2.1 mm, 2.7 µm) column. Conditions: flow rate = 1.2 mL/min, gradient 30-50% B in 1.1 min (black line) or 30-95% B in 1 min (red line), V_i = 5 µL. Same other conditions as in Fig. VI-4.

3.2. Result exploitation

3.2.1. On-line sCEX x RPLC analysis of IdeS-digested ADC-S01

Fig. VI-9 shows the resulting on-line sCEX x RPLC-HRMS separations of IdeS-treated ADC-S01 sample. Fig. VI-9a shows a wide view of the separation space, while Figs. VI-9b and 9c show zoomed windows on Fc/2 and F(ab')2 species, respectively. The associated contour plot obtained in UV is shown in Fig. VI-S2.

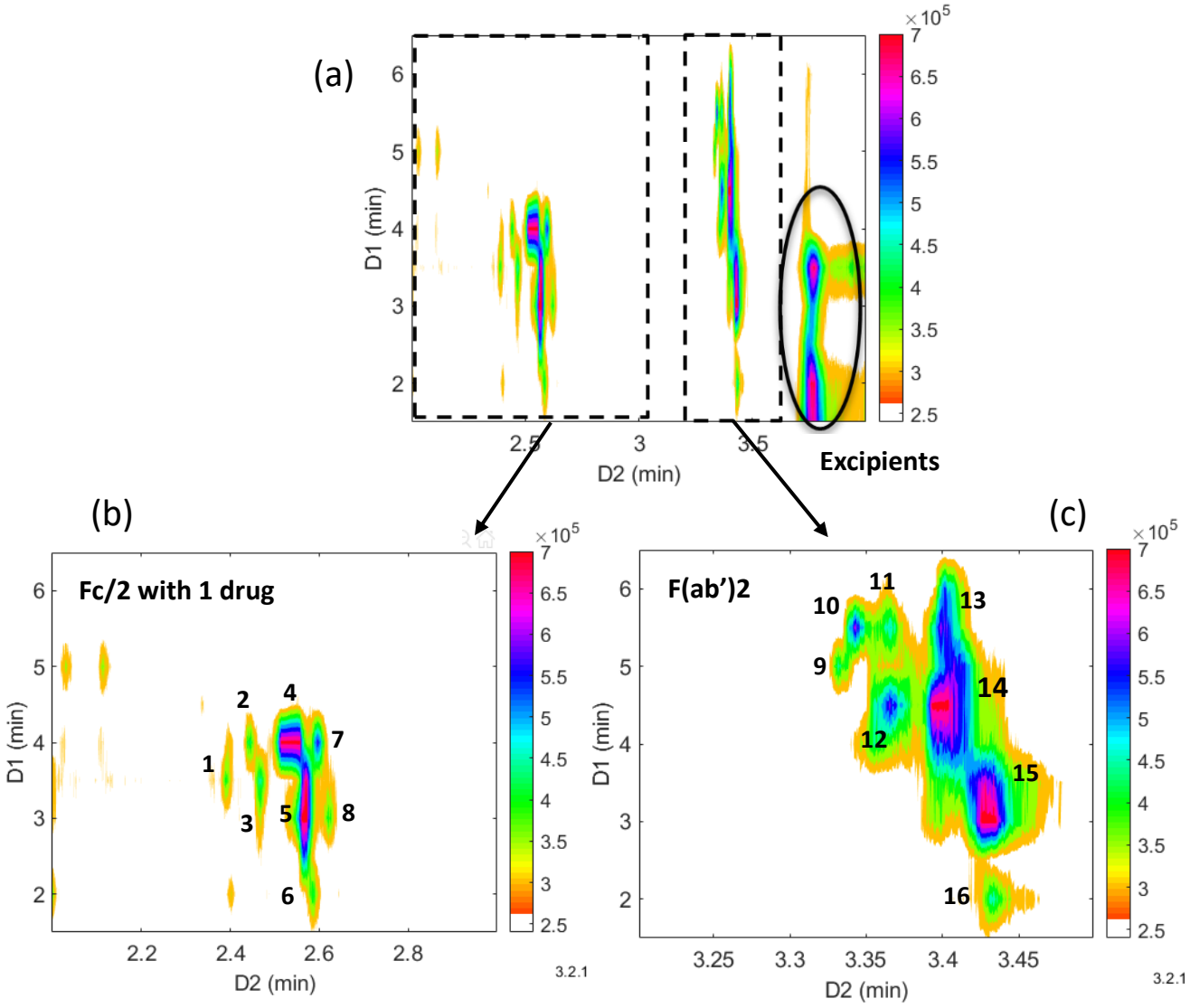

Fig. VI-9: Contour plot (TIC, ESI+) of on-line sCEX x RPLC analysis of IdeS-treated ADC-S01 sample. (a) Large view of the separation space, (b) zoom on Fc/2 species, and (c) zoom on F(ab')2 species. See conditions in Table VI-1. Numbers from 1 to 16 indicate the species identified in Table VI-3.

As seen in Fig. VI-9, this selective comprehensive method led to a good separation of Fc/2 and F(ab')2 species in both dimensions. It is interesting to point out the good complementarity of the two chromatographic techniques for the separation of these species. Multiple peaks are observed on the contour plot, some of which being well separated in CEX but not in RPLC, and vice-versa. For example, in Fig. VI-9b, peaks #3 and #5 have very similar retention times in ^{1}D which means that these two compounds would have coeluted in a single 1D-CEX separation. The two peaks are, on the other hand, easily separated in ^{2}D. Similarly, peaks #4 and #5 mainly coelute in ^{2}D but are well separated in ^{1}D. This underlines that different and complementary selectivities are provided by the two dimensions.

Several peaks are observed on the contour plot, which indicates a large number of isoforms in the analysed sample. We used numbers from 1 to 16 to label the separated peaks shown in Fig. VI-9. The proposed assignments for each of these peaks are given in Table VI-3. Distinct species with the same measured mass that were identified as Fc/2 subunits with the one drug were found to be separated in one or both dimensions (e.g. peaks #1 to #8 highlighted in Fig. VI-9b). In addition, F(ab')2 fragments with drug loads from 1 to 5 could be identified in the second part of the contour plot (Fig. VI-9c). Similarly to the Fc/2 species, a few isobars identified as F(ab')2 with the same number of drugs were separated in sCEX x RPLC (i.e. peaks #10 and #11, and peaks #12 and #13). As pointed out before, some of these species could correspond to subunits with the same number of drugs but conjugated at different lysine residues.

Table VI-3: Proposed species for the peaks labelled in Fig. VI-9.

#	Difference between theoretical and experimental masses (Da)	Proposed specie
1	-1	Fc/2 + 1 drug
2	-1	Fc/2 + 1 drug
3	-1	Fc/2 + 1 drug
4	-1	Fc/2 + 1 drug
5	-1	Fc/2 + 1 drug
6	-1	Fc/2 + 1 drug
7	-1	Fc/2 + 1 drug
8	-1	Fc/2 + 1 drug
9	/	/
10	+3	(Fab')2 + 1 drug
11	+3	(Fab')2 + 1 drug
12	+1	(Fab')2 + 2 drugs
13	+3	(Fab')2 + 2 drugs
14	0	(Fab')2 + 3 drugs
15	-3	(Fab')2 + 4 drugs
16	+6	(Fab')2 + 5 drugs

Differences in conjugated sites could explain differences in retention in RPLC for subunits displaying the same drug load (e.g. peaks #3, #5, and #8). However, such an explanation does not work for species separated in ^{1}D-CEX since such differences should not impact the net charge of the molecule (e.g. peaks #4, #5, and #6). For those compounds, the different peaks exhibiting the same mass that we observe could be the result of post-translational modifications (PTMs) that would change the charge and/or

hydrophobicity of the molecule while creating very small mass differences (barely detectable in MS), such as deamidation, isomerization or racemization among others [3,15].

As highlighted in Fig. VI-9a (black circle), the presence of some excipients was still noted in the contour plot. These compounds were observed in the first four ^{1}D-CEX fractions (i.e. from 0 to 3.5 min). If they clearly coeluted with the early eluted species of interest in ^{1}D-CEX, they were efficiently separated from the later eluted ones in ^{2}D-RPLC. The separation of Fc/2 species was quite satisfactory in ^{2}D. However, F(ab')2 species eluted in a much narrower range. As previously underlined, the separation space was quite small in ^{1}D-CEX. All compounds eluted before 7 min with a gradient elution ranging from 1% to 40% B in 20 min. Considering the reduced elution range in ^{1}D, the conditions in CEX could be further optimized by decreasing the upper composition range to decrease the gradient slope (e.g. 1-15% in 20 min) and hence improve the separation.

3.2.2. On-line CEX x RPLC analysis of IdeS-digested ADC-S01

Fig. VI-10 shows the resulting on-line CEX x RPLC separations of IdeS-treated ADC-S01 sample using MS detection (Fig. VI-10a) and UV detection (Fig. VI-10b). The separated peaks are labelled from 1 to 21 and the proposed assignments for each peak are given in Table VI-4.

As explained in Subsection 2.1.4, the 2D-LC conditions were optimized in each dimension to maximize the peak capacity and eliminate the excipient species that were found to impact MS sensitivity. The composition range was reduced in both dimensions to fit the elution range of the species of interest regardless of the excipients. These species could be removed from the separation space of interest by taking advantage of their low retention in ^{1}D-CEX and starting to send the fractions in ^{2}D from 4 min or 5 min depending on the conditions (see Table VI-1). To further improve method sensitivity, the injected volume in ^{1}D-CEX was four times larger than the one injected in sCEX x RPLC (i.e. 40 µL).

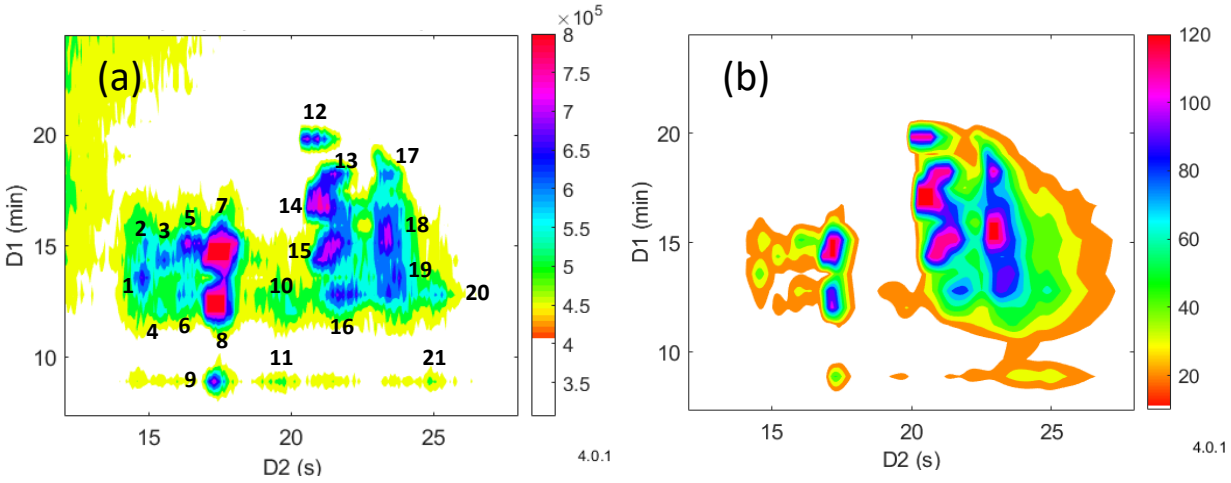

Fig. VI-10: Contour plots of optimized on-line CEX x RPLC analysis of IdeS-treated ADC-S01 sample: (a) MS detection (TIC, ESI+) and (b) UV detection (280 nm). See conditions in Table VI-1. Numbers from 1 to 21 labelled in (a) indicate the species identified in Table VI-4.

Table VI-4: Proposed species for the peaks labelled in Fig. VI-10a and Fig. VI-15.

#	Difference between theoretical and experimental masses (Da)	Proposed specie
1	-3	Fc/2 + 1 drug
2	-3	Fc/2 + 1 drug
3	-3	Fc/2 + 1 drug
4	-1	Fc/2 + 1 drug
5	-3	Fc/2 + 1 drug
6	-2	Fc/2 + 1 drug
7	-3	Fc/2 + 1 drug
8	-3	Fc/2 + 1 drug
9	-3	Fc/2 + 1 drug
10	-4	Fc/2 + 2 drugs
11	-1	Fc/2 + 2 drugs
12	-7	(Fab')2 + 0 drug
13	-4	(Fab')2 + 1 drug
14	-9	(Fab')2 + 1 drug
15	+3	(Fab')2 + 2 drugs
16	+405	(Fab')2 + 3 drugs*
17	+198	(Fab')2 + 1 drug*
18	+11	(Fab')2 + 2 drugs
19	+7	(Fab')2 + 3 drugs
20	/	/
21	/	/
22	/	/

*Given the large mass difference between theoretical and experimental deconvoluted masses, these two assignments were made based on the relative positions of peaks on the contour plot.

The resulting separation of Fc/2 and F(ab')2 species was very satisfactory and quite close to the one obtained in sCEX x RPLC (Fig. VI-9). As indicated in Table VI-4, Fc/2 subunits with 1 and 2 drugs, as well as F(ab')2 subunits with 0, 1, 2, and 3 drugs could be unambiguously identified using HRMS detection. As highlighted before, numerous peaks exhibiting the same mass were identified on the chromatogram (e.g. peaks #1 to #9, all identified as Fc/2 subunits with 1 drug).

Contrary to sCEX x RPLC, F(ab')2 subunits with 4 and 5 drugs could not be identified in CEX x RPLC due to the limited MS signal obtained for these large fragments. Based on its retention time in both dimensions (least retained peak in CEX but most retained one in RPLC), we suspected peak #21 to be an F(ab)2 fragment with a drug load of 4. However, the signal was too low for proper MS spectrum deconvolution. Considering the retention time of peak #21, it is most likely that any F(ab')2 fragments with a drug load of 5 eluted before the first analysed ^{1}D-fraction (i.e. before 5 min), which explains their absence on the chromatogram.

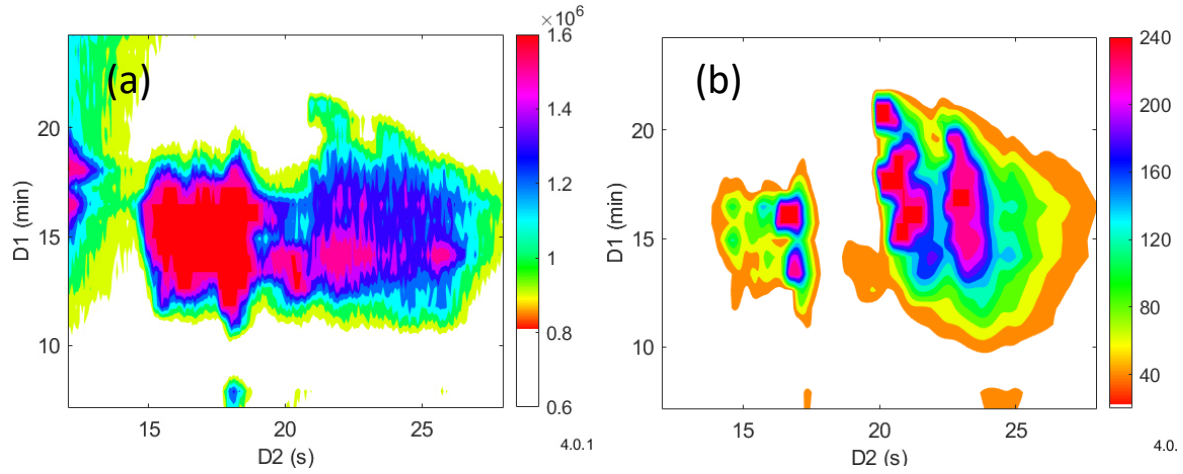

Fig. VI-11: Contour plots of on-line CEX x RPLC analysis of IdeS-treated ADC-S01 with 80 µL injected in ^{1}D: (a) MS detection (TIC, ESI+) and (b) UV detection 280 nm. See conditions in Table VI-1 (2D starting from 4 min).

Intending to increase MS sensitivity, we further increased the injected volume in ^{1}D-CEX (from 40 µL to 80 µL). The resulting MS and UV contour plots are shown in Figs. VI-11a and 11b, respectively. As expected, increasing the injected volume from 40 µL (Fig. VI-10b) to 80 µL (Fig. VI-11b) resulted in a 2-fold increase in peak intensity in UV without affecting the separation. This observation can be better appreciated when comparing Figs. VI-S3b and S3d, showing the overlaid ^{2}D-chromatograms obtained

with both injected volumes. However, as seen in Fig. VI-11a and Figs. VI-S3a vs. S3b, poorer results were obtained in MS detection due to a significant increase of background noise that counteracted the expected increase of signal-to-noise (S/N) ratio. This increase in background noise when doubling the injected volume is probably the result of increased matrix effects. In any case, increasing the injected volume in ^{1}D did not facilitate MS identification as expected but rather made it more difficult.

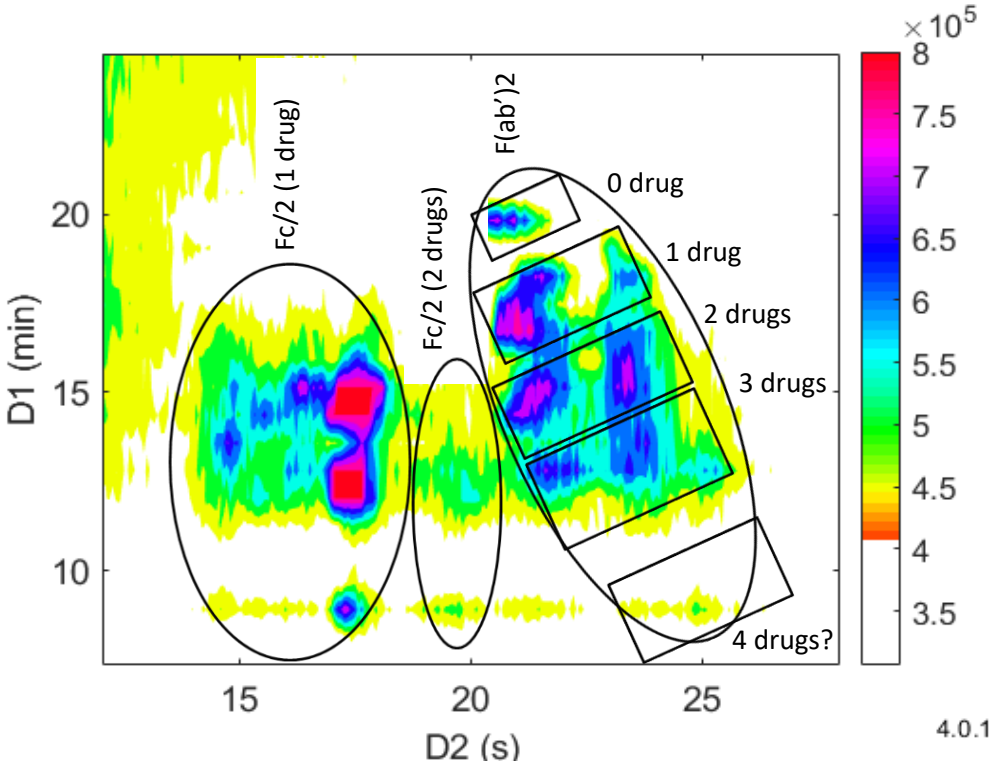

Fig. VI-12: Same contour plot as in Fig. VI-10a highlighting the different separated zones.

Fig VI-12 shows a summary view of the species that were identified in the IdeS-digested ADC-S01 sample in on-line CEX x RPLC. As can be expected, ^{2}D-RPLC allowed separating Fc/2 species from F(ab')2 species on one hand, and Fc/2 subunits according to their drug load on the other hand. F(ab')2 subunits with different drug load were poorly separated in RPLC while curiously, well separated in ^{1}D-CEX. As can be expected, the most retained F(ab')2 fragment in CEX was the one with the lowest drug load (0 in this case). Conversely, RPLC was very useful to discriminate F(ab')2 fragments exhibiting a close mass, whereas Fc/2 fragments exhibiting a close mass were better separated in CEX. Each black rectangle in Fig. VI-12 includes one or several

peaks identified as F(ab')2 fragments with the same drug load. Interestingly, the more retained isoform in CEX was also the more retained one in RPLC, although the shift in retention was very subtle in CEX. This suggests that those additional variants might be the result of PTMs that would simultaneously increase the net negative charge and the hydrophobicity of the protein.

3.2.3. Comparison of non-stressed, 2-week-stressed, and 4-week-stressed samples

The stability of biotherapeutic antibodies is a critical quality attribute that is essential to assess to support formulation development, understand degradation pathways, and evaluate product shelf life, among other objectives [16]. Applicability of the developed 2D-LC method to stability studies was investigated by analysing three types of samples:

- a non-stressed sample (ADC-t0)

- a sample stressed at 40°C for two weeks (ADC-t2)

- a sample stressed at 40°C for four weeks (ADC-t4)

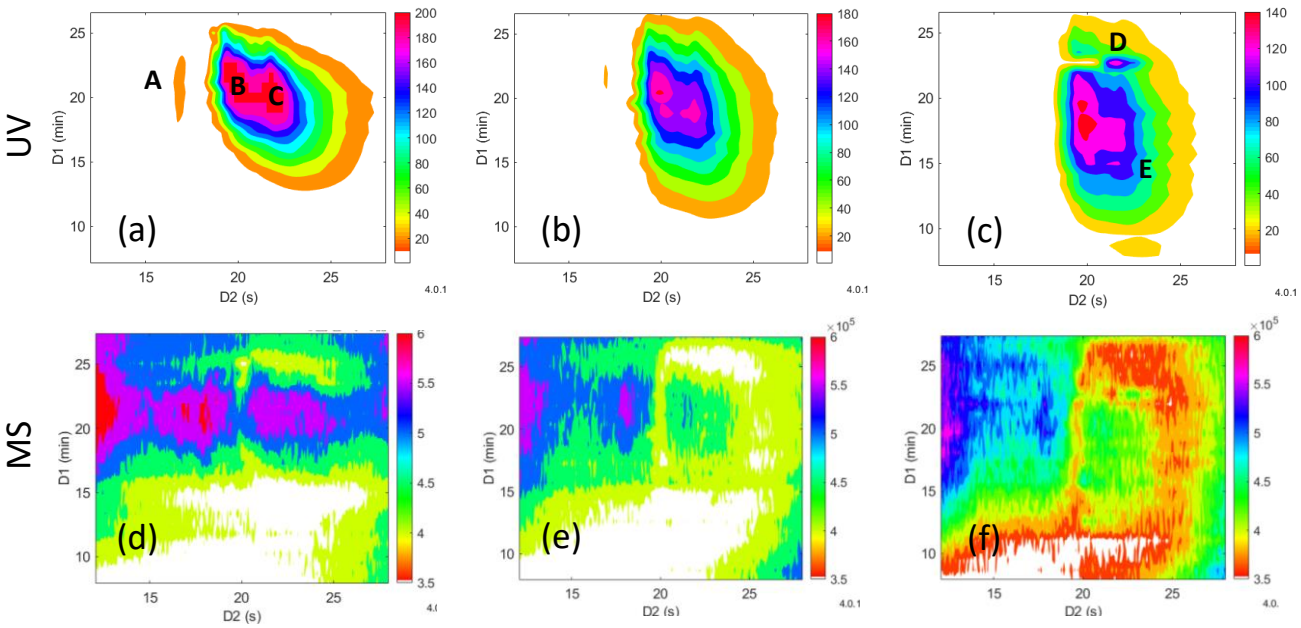

Fig. VI-13: Comparison of on-line CEX x RPLC separations of intact ADC samples with different levels of stress: (a, d) non-stressed sample, (b, e) sample stressed for two weeks, and (c, f) sample stressed for four weeks. (a, b, c) UV detection (280 nm) and (d, e, f) MS detection (TIC, ESI+). Conditions are given in Table VI-1.

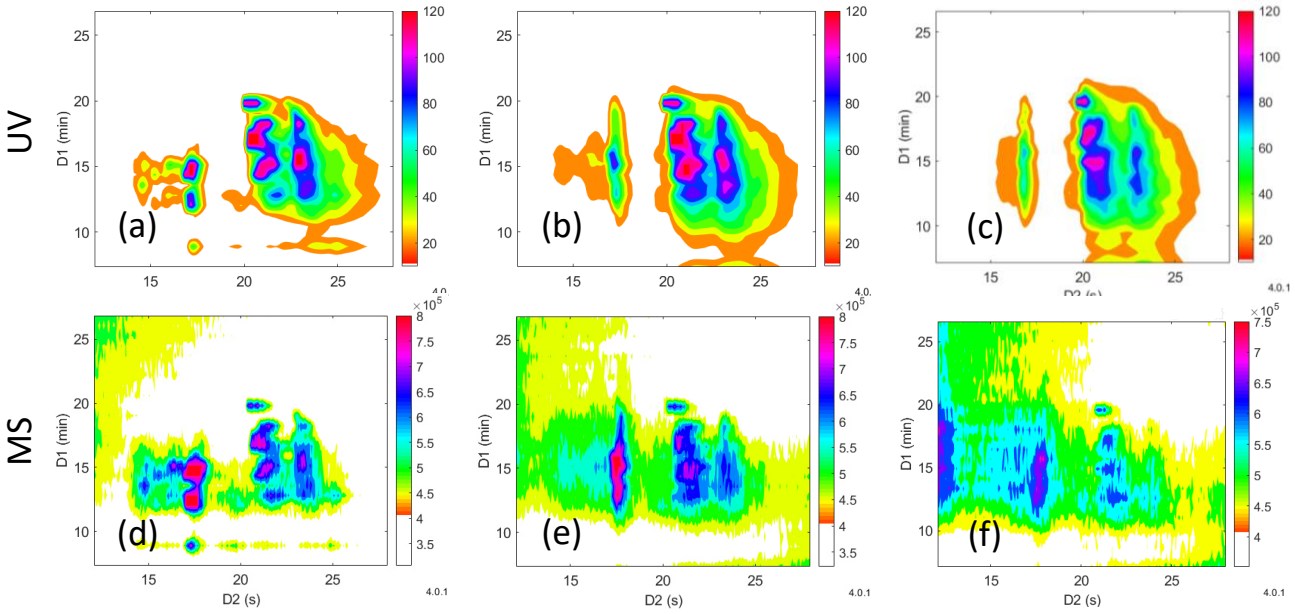

Fig. VI-14: Comparison of on-line CEX x RPLC separations of IdeS-treated ADC samples with different levels of stress: (a, d) non-stressed sample, (b, e) sample stressed for two weeks, and (c, f) sample stressed for four weeks. (a, b, c) UV detection (280 nm) and (d, e, f) MS detection (TIC, ESI+). Conditions are given in Table VI-1.

In this work, these three samples were analysed, both at the intact form and after IdeS digestion, using the previously optimized on-line CEX x RPLC-UV-HRMS method. Fig. VI-13 shows the contour plots obtained in UV and MS detections for intact samples, whereas Fig. VI-14 shows the results for IdeS-digested samples. For the purpose of clarity, the main differences found by visual comparison of the 2D maps shown in Figs. VI-14a-d are highlighted in the separate Fig. VI-15.

First of all, the 2D method was found to be highly repeatable between analyses (in terms of retention times), which allowed easy and fast comparison of the 2D maps. As mentioned before, the two dimensions were very complementary for the separation of these species. As shown in Figs. VI-13a-c, this good complementarity allowed to highlight the presence of two distinct species (i.e. #B and #C) in intact ADC samples. When comparing intact samples ADC-t0 (Fig. VI-13a), ADC-t2 (Fig. VI-13b), and ADC-t4 (Fig. VI-13c), it appears clear that intensities of peaks #A, #B, and #C gradually decrease from t0 to t4. On the contrary, peaks #D and #E, both missing in ADC-t0, appear in ADC-t4. Unfortunately, none of these four highlighted peaks could be identified as a result of multi-charged mass spectra with a low signal intensity which made the deconvolution impossible.

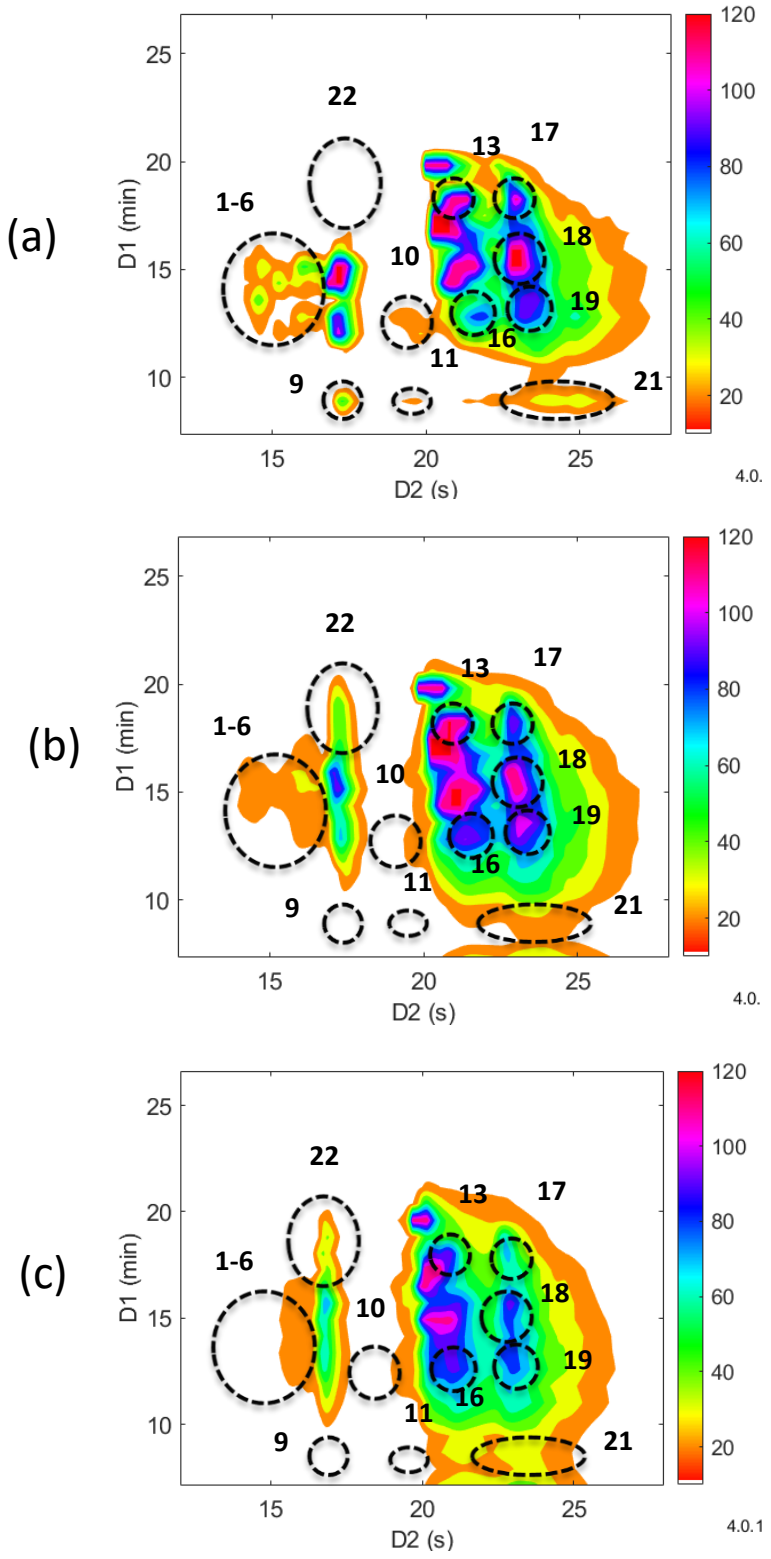

Fig. VI-15: Same contour plots as in Figs. VI-16a-c with the main differences between samples highlighted by black dotted circles.

As shown in Fig. VI-15, the direct visual comparison of the 2D maps showed marked differences between the three IdeS-digested samples. The most striking differences are indicated by black dotted circles (see Table VI-4 for corresponding identifications). For the large majority of peaks, intensities decrease from t0-IdeS to t4-IdeS (i.e. #1-6, 9, 10, 11, 13, and 17), until even completely disappearing for some peaks (e.g. #9, 10, and 11). These peaks correspond to Fc/2 with 1 drug (#1-6 and 9), Fc/2 with 2 drugs (#10 and 11), F(ab')2 with 1 drug (#18 and 19), and F(ab')2 with 2 drugs (#13 and 17). Other peaks, initially absent in t0-IdeS, progressively appear in the chromatogram (i.e. #22, which could not be identified). Lastly, for other species (i.e. # 16, 18, 19, and 21), the peak intensity increases from t0-IdeS to t2-IdeS but decreases from t2-IdeS to t4-IdeS.

Those results emphasize the great potential of using on-line LC x LC for stability studies during mAb and ADC research and development.

3.2.4. Conclusions

In this study, we developed an on-line CEX x RPLC method allowing to efficiently separate the charge variants of the lysine-conjugated ADC-S01 in less than 30 min. The two dimensions were found to be very complementary for the separation of these molecules, which allowed to highlight the presence of multiple peaks corresponding to variants of Fc/2 and F(ab')2 fragments in the partially-digested samples analysed.

This complementarity permitted a good separation between (i) Fc/2 and F(ab')2 species, (ii) subunits with a different number of drugs, and (iii) numerous species with very close masses that were attributed to subunits with the same drug load.

The matrix effects arising from the presence of excipients in the samples could be mostly solved by eluting these species in ^{1}D-CEX before sending the fractions in ^{2}D-RPLC.

This led to the identification of Fc/2 subunits with 1 and 2 drugs, and F(ab')2 subunits with drug loads from 0 to 3. The presence of F(ab')2 subunits with 4 and 5 drugs was suspected in the analysed samples. F(ab')2 subunits with 4 drugs could not be unambiguously identified due to a very low MS signal. F(ab')2 sub-units with 5 drugs eluted too early in ^{1}D-CEX and were thus eliminated prior to ^{2}D. The good complementarity of the two separation dimensions also allowed to highlight the presence of several species with very close masses that were identified as subunits with

the same drug load. Such compounds could result from drug conjugations on different lysine residues or from post-translational modifications.

3.3. First tests on the replacement of TFA by DFA in ^{2}D

Recently, some studies highlighted the potential of using difluoroacetic acid (DFA) in the mobile phase as an alternative modifier for protein and peptide analysis [17]. The molecular structure of DFA is shown in Fig. VI-S4. DFA is less acidic and less hydrophobic than TFA and also creates lower surface tension of droplets during electrospray ionization. For this reason, it is expected to increase MS sensitivity compared to TFA while maintaining similar chromatographic performances.

Because MS-detection sensitivity was one of the weak points of our method, we investigated the potential of using DFA as an acidic additive in ^{2}D-RPLC.

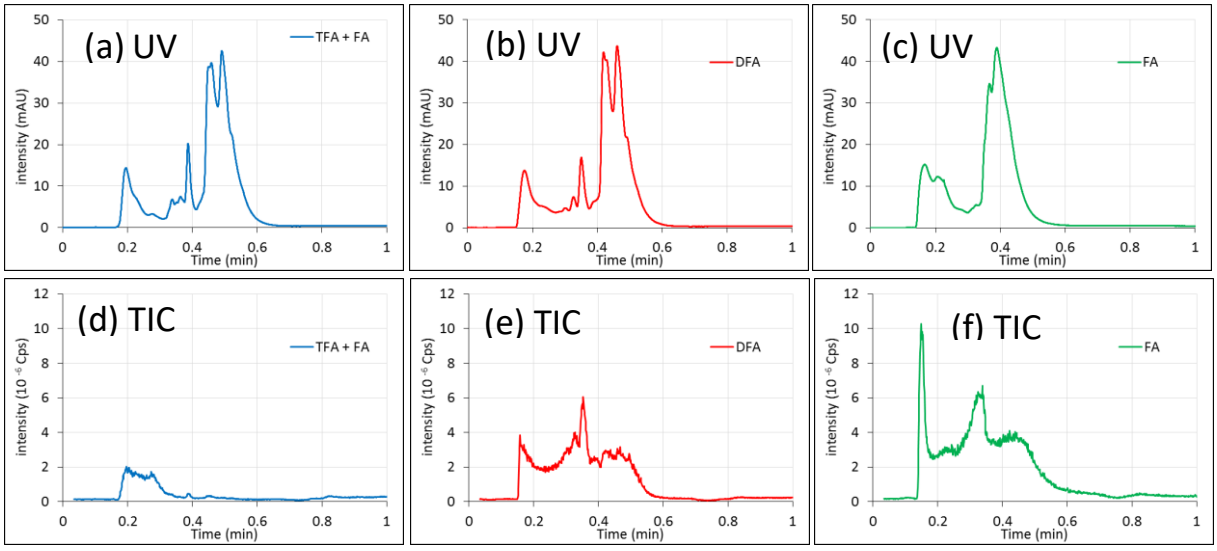

Fig. VI-16: 1D-RPLC analyses of IdeS-treated ADC sample using (a) 0.05% TFA + 0.1% FA, (b) 0.1% DFA, and (c) 0.1% FA as additive in the mobile phase. (a, b, c) UV detection (280 nm) and (d, e, f) MS detection (TIC, ESI+). Column: Bioresolve RPmAb pk (50 x 2.1 mm, 2.7 µm). Conditions: water + additive as solvent A and ACN + additive as solvent B, gradient 30% to 95% B in 1.59 min, flow rate = 1.7 mL/min, temperature = 80°C, injected volume = 1 µL, split 1:1 prior to MS detector.

Figs. VI-16a-c and 16d-f show comparisons of IdeS-treated ADC-S01 separations in RPLC-UV and RPLC-MS, respectively, using either a combination of TFA and FA (blue line), DFA (red line) or FA (green line) in the mobile phase. It should be reminded that a comparison between TFA only and TFA/FA was already performed in Subsection 3.1.2 (Fig. VI-3). Both conditions gave quite similar results in terms of separation. As seen

in Figs. VI-16a-c, the worst separation was obtained when using only FA in the mobile phase. A dramatic loss of peak resolution can be witnessed when comparing the chromatogram obtained with FA (Fig. VI-16c) to the ones obtained with the TFA/FA combination (Fig. VI-16a) or with DFA (Fig. VI-16b). Interestingly, TFA /FA and DFA gave quite similar results in terms of chromatographic separation. Regarding MS detection, DFA (Fig. VI-16e) gave slightly lower peak intensities compared to FA (Fig. VI-16f), especially for early eluted species. However, a clear gain in peak intensity was obtained compared to TFA/FA (Fig. VI-16d).

To improve MS detection sensitivity for the previously developed on-line CEX x RPLC-UV-HRMS method, we tested conditions with DFA instead of TFA/FA in the ^{2}D-mobile phase. Figs. VI-17a-b and 17c-d show the comparisons of contour plots obtained for the separations of IdeS-digested ADC using either DFA or TFA/FA in the mobile phase, respectively. The same labels were used for the two contour plots to better compare the results. Additional peaks observed with DFA were labelled with letters from A to D. As seen in Fig. VI-17, the separation was quite similar with the two additives, although most peaks were found to be slightly broader with DFA and thus less intense with UV detection. As expected, the MS signal was much higher with DFA (Fig. VI-17a) compared to TFA/FA (Fig. VI-17c). Most peaks identified with TFA/FA could also be identified with DFA, except for peaks #4, #5, #6, #16, and #17. It is likely that these peaks could not be found in the contour plot as a result of coelutions in ^{2}D-RPLC.

Due to better MS sensitivity, a few peaks that could not be identified with TFA/FA could be unambiguously identified with DFA (i.e. peaks #20 and 21, both identified as (Fab')2 + 4 drugs) as indicated in Table VI-5. A few additional peaks were observed and identified with DFA (i.e. peaks #A, #B, and #D) They were identified as Fc/2 with 1 drug, (Fab')2 with 2 drugs, and (Fab')2 with 1 drug, respectively.

Table VI-5: Proposed species for the additional peaks labelled in Fig. VI-17a.

#	Difference between theoretical and experimental masses (Da)	Proposed specie
A	0	Fc/2 + 1 drug
B	+11	(Fab')2 + 2 drugs
C	/	n.d
D	-1	(Fab')2 + 1 drug
20	+4	(Fab')2 + 4 drugs
21	+27	(Fab')2 + 4 drugs

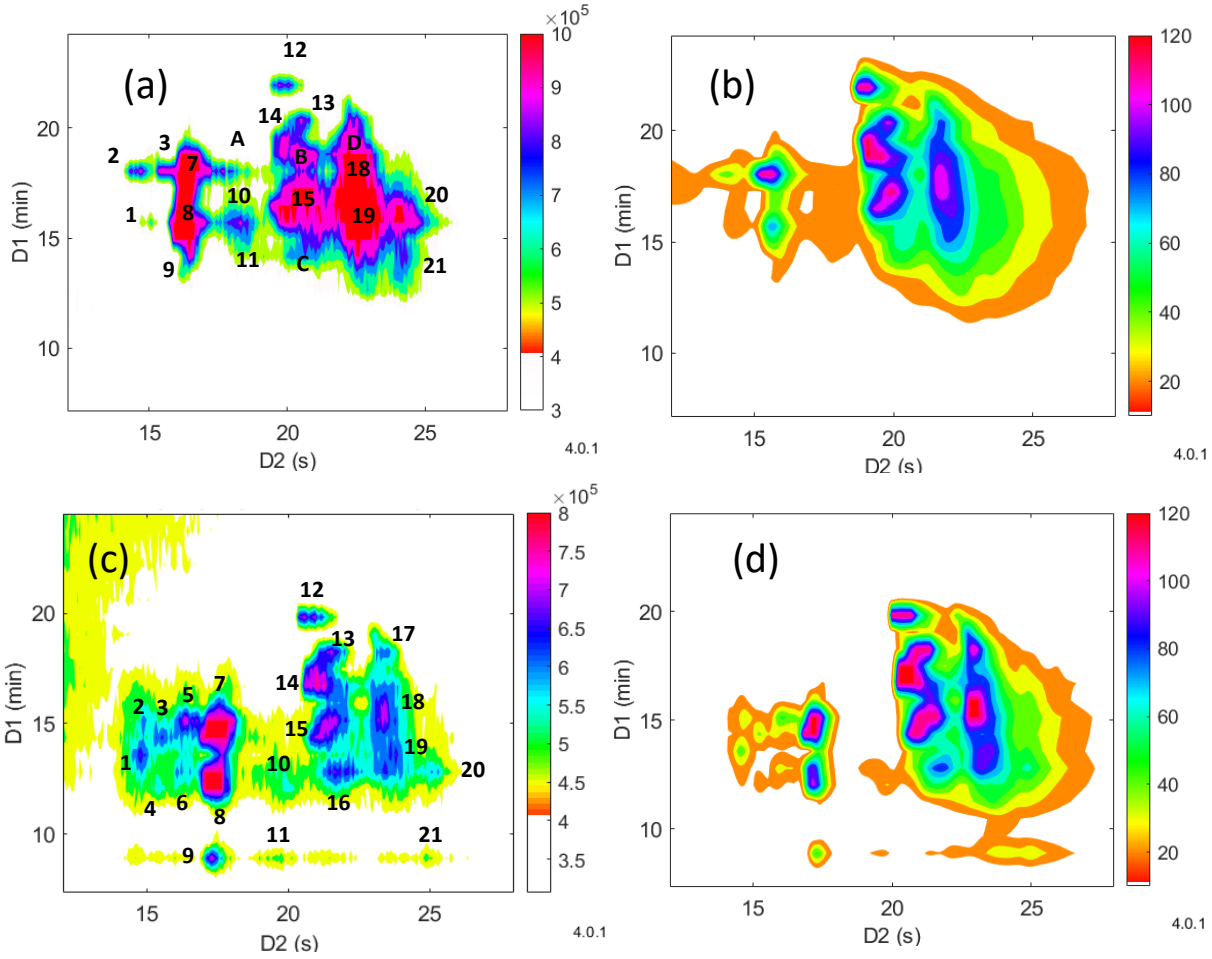

Fig. VI-17: (a, c) Contour plot UV (280nm) and (b, d) MS (TIC, ESI+) of on-line CEX x RPLC analysis of IdeS-treated ADC-S01 sample using (a, b) 0.1% DFA or (c, d) 0.05% TFA + 0.1% FA as additive in ^{2}D. Same conditions as in Table VI-1 but with 2D starting from 4 min instead of 5 min (to make sure no compounds eluted between 4 and 5 min) and V_i = 30 µL for the separation with DFA.

4. Conclusion and prospects

This work has led to the development of on-line 2D-LC-UV-HRMS methods for the characterization of the charge variants of the lysine-linked antibody-drug conjugate ADC-S01. Promising results in terms of peak capacity and peak intensity were obtained in sCEX x RPLC-UV-HRMS. However, the total analysis time was twice as long as that in full comprehensive mode. Besides, the low number of permitted fractions with this approach (i.e. 10) could not provide sufficient information on the entire sample.

The conditions for an on-line CEX x RPLC-UV-HRMS analysis in less than 30 min were optimized. The samples were analysed using both the top-down and middle-up approaches to cross-link information. The good complementarity between the two dimensions provided much insight into the different isoforms present in this sample

and highlighted the existence of numerous species with very similar masses, possibly resulting from drug conjugations on different lysine residues or post-translational modifications. Fc/2 sub-units with 1 and 2 drugs on one hand, and F(ab')2 sub-units with drug loads from 0 to 5 drugs could be identified in the IdeS-digested sample. The direct comparison of the 2D maps obtained for samples subjected to temperature-induced stress provided valuable insight into the possible modifications arising from sample degradation.

One of the major issue encountered in this work was the limited MS detection sensitivity, which impeded deconvolution of some MS spectra, and thus peak identification. This limited sensitivity can be ascribed to (i) the formation of highly multi-charged ions reducing peak intensity, (ii) the use of TFA in the mobile phase creating ion suppression, (iii) the omnipresence of excipients creating ion suppression, and (iv) the high-salt content coming from ^{1}D-CEX, which might impact ionization efficiency despite the use of a diverted valve before MS (as suggested by the large amount of white deposits observed on the source cone at the end of each analysis). Possible solutions to alleviate the latter issue might consist in using more volatile ingredients as CEX buffer. Several buffer combinations have been successfully reported in the literature for the analysis of mAb in 1D-CEX-MS [18–21] and on-line CEX x RPLC-MS [3].

In this work, we explored two options to improve MS detection sensitivity: (i) increasing the injected volume in ^{1}D (which mostly resulted in increased background noise and thus decreased signal-to-noise ratio) and (ii) replacing TFA with the newly introduced modifier DFA (which gave promising results). Besides an extensive optimization of the ESI-MS ionization conditions, other options to improve MS sensitivity might involve (i) further reduction of the flow entering MS employing larger flow splitting ratios [22], (ii) introduction of a make-up flow prior to MS to decrease TFA concentration without impacting the chromatographic separation [22,23] or (iii) evaluation of other alternative mobile phase additives [24]. These three options were extensively discussed by d'Atri et al. [14] in a recent review focusing on current trends for the analysis of therapeutic proteins in RPLC.

To further improve separation and detection sensitivity, the potential of other chromatographic combinations such as on-line HILIC x RPLC could be investigated. The interest of this combination has previously been demonstrated for the separation of mAbs [25]. HILIC requires less MS-incompatible salts for the separation compared

to CEX, which could be attractive for reducing ion suppression. However, this combination is also known to be very challenging for the separation of peptides and proteins due to injection issues arising from solvent strength mismatch in both dimensions [25,26]. Finally, the separation power might be improved by increasing the gradient time in ^{1}D. However, this could only be done at the expense of the analysis time. Besides, such an approach would require much more amount of sample to maintain similar sensitivity.

5. References

[1] K. Sandra, G. Vanhoenacker, I. Vandenheede, M. Steenbeke, M. Joseph, P. Sandra, Multiple heart-cutting and comprehensive two-dimensional liquid chromatography hyphenated to mass spectrometry for the characterization of the antibody-drug conjugate ado-trastuzumab emtansine, Journal of Chromatography B. 1032 (2016) 119–130. https://doi.org/10.1016/j.jchromb.2016.04.040.

[2] D.R. Stoll, D.C. Harmes, J. Danforth, E. Wagner, D. Guillarme, S. Fekete, A. Beck, Direct Identification of Rituximab Main Isoforms and Subunit Analysis by Online Selective Comprehensive Two-Dimensional Liquid Chromatography–Mass Spectrometry, Anal. Chem. 87 (2015) 8307–8315. https://doi.org/10.1021/acs.analchem.5b01578.

[3] M. Sorensen, D.C. Harmes, D.R. Stoll, G.O. Staples, S. Fekete, D. Guillarme, A. Beck, Comparison of originator and biosimilar therapeutic monoclonal antibodies using comprehensive two-dimensional liquid chromatography coupled with time-of-flight mass spectrometry, MAbs. 8 (2016) 1224–1234. https://doi.org/10.1080/19420862.2016.1203497.

[4] G. Vanhoenacker, I. Vandenheede, F. David, P. Sandra, K. Sandra, Comprehensive two-dimensional liquid chromatography of therapeutic monoclonal antibody digests, Anal Bioanal Chem. 407 (2015) 355–366. https://doi.org/10.1007/s00216-014-8299-1.

[5] S. Fekete, A. Beck, J.-L. Veuthey, D. Guillarme, Ion-exchange chromatography for the characterization of biopharmaceuticals, Journal of Pharmaceutical and Biomedical Analysis. 113 (2015) 43–55. https://doi.org/10.1016/j.jpba.2015.02.037.

[6] E. Farsang, D. Guillarme, J.-L. Veuthey, A. Beck, M. Lauber, A. Schmudlach, S. Fekete, Coupling non-denaturing chromatography to mass spectrometry for the characterization of monoclonal antibodies and related products, Journal of Pharmaceutical and Biomedical Analysis. 185 (2020) 113207. https://doi.org/10.1016/j.jpba.2020.113207.

[7] E. Farsang, A. Murisier, K. Horváth, A. Beck, R. Kormány, D. Guillarme, S. Fekete, Tuning selectivity in cation-exchange chromatography applied for monoclonal antibody separations, part 1: Alternative mobile phases and fine tuning of the separation, Journal of Pharmaceutical and Biomedical Analysis. 168 (2019) 138–147. https://doi.org/10.1016/j.jpba.2019.02.024.

[8] A. Murisier, E. Farsang, K. Horváth, M. Lauber, A. Beck, D. Guillarme, S. Fekete, Tuning selectivity in cation-exchange chromatography applied for monoclonal antibody separations, part 2: Evaluation of recent stationary phases, Journal of Pharmaceutical and Biomedical Analysis. 172 (2019) 320–328. https://doi.org/10.1016/j.jpba.2019.05.011.

[9] D.V. McCalley, D. Guillarme, Evaluation of additives on reversed-phase chromatography of monoclonal antibodies using a 1000 Å stationary phase, Journal of Chromatography A. 1610 (2020) 460562. https://doi.org/10.1016/j.chroma.2019.460562.

[10] B. Bobály, A. Beck, J. Fekete, D. Guillarme, S. Fekete, Systematic evaluation of mobile phase additives for the LC–MS characterization of therapeutic proteins, Talanta. 136 (2015) 60–67. https://doi.org/10.1016/j.talanta.2014.12.006.

[11] M.C. García, The effect of the mobile phase additives on sensitivity in the analysis of peptides and proteins by high-performance liquid chromatography–electrospray mass spectrometry, Journal of Chromatography B. 825 (2005) 111–123. https://doi.org/10.1016/j.jchromb.2005.03.041.

[12] B. Bobály, E. Tóth, L. Drahos, F. Zsila, J. Visy, J. Fekete, K. Vékey, Influence of acid-induced conformational variability on protein separation in reversed phase high performance liquid chromatography, Journal of Chromatography A. 1325 (2014) 155–162. https://doi.org/10.1016/j.chroma.2013.12.022.

[13] B. Bobály, V. D'Atri, M. Lauber, A. Beck, D. Guillarme, S. Fekete, Characterizing various monoclonal antibodies with milder reversed phase chromatography conditions, Journal of Chromatography B. 1096 (2018) 1–10. https://doi.org/10.1016/j.jchromb.2018.07.039.

[14] V. D'Atri, A. Murisier, S. Fekete, J.-L. Veuthey, D. Guillarme, Current and future trends in reversed-phase liquid chromatography-mass spectrometry of therapeutic proteins, TrAC Trends in Analytical Chemistry. 130 (2020) 115962. https://doi.org/10.1016/j.trac.2020.115962.

[15] A. Beck, E. Wagner-Rousset, D. Ayoub, A. Van Dorsselaer, S. Sanglier-Cianférani, Characterization of Therapeutic Antibodies and Related Products, Anal. Chem. 85 (2013) 715–736. https://doi.org/10.1021/ac3032355.

[16] C. Nowak, J.K. Cheung, S.M. Dellatore, A. Katiyar, R. Bhat, J. Sun, G. Ponniah, A. Neill, B. Mason, A. Beck, H. Liu, Forced degradation of recombinant

monoclonal antibodies: A practical guide, MAbs. 9 (2017) 1217–1230. https://doi.org/10.1080/19420862.2017.1368602.

[17] J.M. Nguyen, J. Smith, S. Rzewuski, C. Legido-Quigley, M.A. Lauber, High sensitivity LC-MS profiling of antibody-drug conjugates with difluoroacetic acid ion pairing, MAbs. 11 (2019) 1358–1366. https://doi.org/10.1080/19420862.2019.1658492.

[18] Y. Leblanc, C. Ramon, N. Bihoreau, G. Chevreux, Charge variants characterization of a monoclonal antibody by ion exchange chromatography coupled on-line to native mass spectrometry: Case study after a long-term storage at +5°C, J Chromatogr B Analyt Technol Biomed Life Sci. 1048 (2017) 130–139. https://doi.org/10.1016/j.jchromb.2017.02.017.

[19] A.O. Bailey, G. Han, W. Phung, P. Gazis, J. Sutton, J.L. Josephs, W. Sandoval, Charge variant native mass spectrometry benefits mass precision and dynamic range of monoclonal antibody intact mass analysis, MAbs. 10 (2018) 1214–1225. https://doi.org/10.1080/19420862.2018.1521131.

[20] Y. Yan, A.P. Liu, S. Wang, T.J. Daly, N. Li, Ultrasensitive Characterization of Charge Heterogeneity of Therapeutic Monoclonal Antibodies Using Strong Cation Exchange Chromatography Coupled to Native Mass Spectrometry, Anal Chem. 90 (2018) 13013–13020. https://doi.org/10.1021/acs.analchem.8b03773.

[21] F. Füssl, A. Trappe, K. Cook, K. Scheffler, O. Fitzgerald, J. Bones, Comprehensive characterisation of the heterogeneity of adalimumab via charge variant analysis hyphenated on-line to native high resolution Orbitrap mass spectrometry, MAbs. 11 (2018) 116–128. https://doi.org/10.1080/19420862.2018.1531664.

[22] J. Liigand, R. de Vries, F. Cuyckens, Optimization of flow splitting and make-up flow conditions in liquid chromatography/electrospray ionization mass spectrometry, Rapid Communications in Mass Spectrometry. 33 (2019) 314–322. https://doi.org/10.1002/rcm.8352.

[23] A. Apffel, S. Fischer, G. Goldberg, P.C. Goodley, F.E. Kuhlmann, Enhanced sensitivity for peptide mapping with electrospray liquid chromatography-mass spectrometry in the presence of signal suppression due to trifluoroacetic acid-containing mobile phases, J Chromatogr A. 712 (1995) 177–190. https://doi.org/10.1016/0021-9673(95)00175-m.

[24] B. Bobály, V. D'Atri, M. Lauber, A. Beck, D. Guillarme, S. Fekete, Characterizing various monoclonal antibodies with milder reversed phase chromatography conditions, Journal of Chromatography B. 1096 (2018) 1–10. https://doi.org/10.1016/j.jchromb.2018.07.039.

[25] D.R. Stoll, D.C. Harmes, G.O. Staples, O.G. Potter, C.T. Dammann, D. Guillarme, A. Beck, Development of Comprehensive Online Two-Dimensional Liquid Chromatography/Mass Spectrometry Using Hydrophilic Interaction and

Reversed-Phase Separations for Rapid and Deep Profiling of Therapeutic Antibodies, Anal. Chem. 90 (2018) 5923–5929. https://doi.org/10.1021/acs.analchem.8b00776.

[26] S. Chapel, F. Rouvière, S. Heinisch, Pushing the limits of resolving power and analysis time in on-line comprehensive hydrophilic interaction x reversed phase liquid chromatography for the analysis of complex peptide samples, Journal of Chromatography A. (2019) 460753. https://doi.org/10.1016/j.chroma.2019.460753.

CONCLUSIONS

The objective of this chapter was to underline the potential benefits of using 2D-LC-UV-HRMS platforms for the analysis of therapeutic antibody samples.

In this chapter, the applicability of such an approach was demonstrated for the specific case study of the development of on-line 2D-LC methods using CEX as the first dimension and RPLC as the second dimension for the charge variant analysis of a lysine-linked antibody-drug conjugate. This combination gives a typical example of the added value of a second separation dimension to the analysis of large protein formats because it addresses the challenge of the on-line coupling of non-MS-compatible chromatographic modes to MS detection.

The successful hyphenation of the two highly orthogonal chromatographic modes, CEX and RPLC, was demonstrated on protein samples analysed at the intact and subunit levels, both in the selective comprehensive and the full comprehensive modes. In this work, the full comprehensive approach was found to be more attractive since it allowed a complete overview of the sample. The developed on-line CEX x RPLC-UV-HRMS approach permitted to gain useful and complementary information on the analysed samples within one single run with a total analysis time of only 30 min.

Based upon this work, it is clear that on-line LC x LC-MS methodologies hold great potential to facilitate and improve the study of large molecules such as ADCs by (i) enabling on-line desalting and indirect interfacing of chromatographic modes using non-volatile salts with MS detection and (ii) providing increased and complementary information within a single analysis.

REFERENCES

[1] R.-M. Lu, Y.-C. Hwang, I.-J. Liu, C.-C. Lee, H.-Z. Tsai, H.-J. Li, H.-C. Wu, Development of therapeutic antibodies for the treatment of diseases, Journal of Biomedical Science. 27 (2020) 1. https://doi.org/10.1186/s12929-019-0592-z.

[2] A. Beck, T. Wurch, C. Bailly, N. Corvaia, Strategies and challenges for the next generation of therapeutic antibodies, Nat. Rev. Immunol. 10 (2010) 345–352. https://doi.org/10.1038/nri2747.

[3] A. Beck, L. Goetsch, C. Dumontet, N. Corvaïa, Strategies and challenges for the next generation of antibody-drug conjugates, Nat Rev Drug Discov. 16 (2017) 315–337. https://doi.org/10.1038/nrd.2016.268.

[4] S. Panowski, S. Bhakta, H. Raab, P. Polakis, J.R. Junutula, Site-specific antibody drug conjugates for cancer therapy, MAbs. 6 (2013) 34–45. https://doi.org/10.4161/mabs.27022.

[5] P.L. Ross, J.L. Wolfe, Physical and Chemical Stability of Antibody Drug Conjugates: Current Status, JPharmSci. 105 (2016) 391–397. https://doi.org/10.1016/j.xphs.2015.11.037.

[6] A. Wagh, H. Song, M. Zeng, L. Tao, T.K. Das, Challenges and new frontiers in analytical characterization of antibody-drug conjugates, MAbs. 10 (2018) 222–243. https://doi.org/10.1080/19420862.2017.1412025.

[7] S. Fekete, A.-L. Gassner, S. Rudaz, J. Schappler, D. Guillarme, Analytical strategies for the characterization of therapeutic monoclonal antibodies, TrAC Trends in Analytical Chemistry. 42 (2013) 74–83. https://doi.org/10.1016/j.trac.2012.09.012.

[8] S. Fekete, D. Guillarme, P. Sandra, K. Sandra, Chromatographic, Electrophoretic, and Mass Spectrometric Methods for the Analytical Characterization of Protein Biopharmaceuticals, Anal. Chem. 88 (2016) 480–507. https://doi.org/10.1021/acs.analchem.5b04561.

[9] B. Bobály, S. Fleury-Souverain, A. Beck, J.-L. Veuthey, D. Guillarme, S. Fekete, Current possibilities of liquid chromatography for the characterization of antibody-drug conjugates, Journal of Pharmaceutical and Biomedical Analysis. 147 (2018) 493–505. https://doi.org/10.1016/j.jpba.2017.06.022.

[10] A. Beck, E. Wagner-Rousset, D. Ayoub, A. Van Dorsselaer, S. Sanglier-Cianférani, Characterization of Therapeutic Antibodies and Related Products, Anal. Chem. 85 (2013) 715–736. https://doi.org/10.1021/ac3032355.

[11] A. Beck, V. D'Atri, A. Ehkirch, S. Fekete, O. Hernandez-Alba, R. Gahoual, E. Leize-Wagner, Y. Francois, D. Guillarme, S. Cianférani, Cutting-edge multi-level analytical and structural characterization of antibody-drug conjugates: present and future, Expert Review of Proteomics. 16 (2019) 337–362. https://doi.org/10.1080/14789450.2019.1578215.

[12] J. Camperi, A. Goyon, D. Guillarme, K. Zhang, C. Stella, Multi-dimensional LC-MS: the next generation characterization of antibody-based therapeutics by unified online bottom-up, middle-up and intact approaches, Analyst. 146 (2021) 747–769. https://doi.org/10.1039/D0AN01963A.

[13] B.W.J. Pirok, D.R. Stoll, P.J. Schoenmakers, Recent Developments in Two-Dimensional Liquid Chromatography: Fundamental Improvements for Practical Applications, Analytical Chemistry. 91 (2019) 240–263. https://doi.org/10.1021/acs.analchem.8b04841.

[14] D. Stoll, J. Danforth, K. Zhang, A. Beck, Characterization of therapeutic antibodies and related products by two-dimensional liquid chromatography coupled with UV absorbance and mass spectrometric detection, Journal of Chromatography B. 1032 (2016) 51–60. https://doi.org/10.1016/j.jchromb.2016.05.029.

GENERAL CONCLUSION AND FUTURE PROSPECTS

The research presented in this thesis falls in line with years of ongoing research activity of the "Chromatography & Hyphenated Techniques" Group at the "Institute of Analytical Sciences" (ISA) on the development of multi-dimensional workflows for the analysis of complex samples. The main objective of this thesis was to contribute to furthering the advancement of on-line comprehensive 2D-LC as a powerful tool for the analysis of highly complex mixtures. To achieve this goal, a major focus was laid on the development of fast (sub-hour) separation methods hyphenated with high-resolution mass spectrometry detection. The main application area of this thesis was protein and peptide analysis, but most of the work covered in this manuscript may be more broadly extended to the analysis of ionizable compounds.

First of all, the advantages of on-line RPLC x RPLC over 1D-RPLC for the separation of peptides were demonstrated. The performances of several RPLC x RPLC and 1D-RPLC systems were compared, both theoretically and experimentally, for given analysis times. One of the main factors limiting the progress of on-line LC x LC is the fact that this technique is usually thought to yield poor performance in terms of detection sensitivity, on account of additional solute dilution expected during the separation process. In this thesis, it was shown that, with properly optimized conditions, RPLC x RPLC could not only offer higher separation power but also higher detection sensitivity compared to 1D-RPLC. For all studied conditions, the increase in peak capacity and peak intensity was, at the very least, 2.5- and 3.3-fold, respectively, for gradient times below 40 min. However, it was theoretically highlighted that much larger gains should be expected for gradient times above 200 min. Such improvements can be expected for combinations providing (i) sufficient orthogonality for the chromatographic peaks to occupy a satisfactory part of the 2D retention space, and (ii) excellent analyte focusing in the second dimension allowing to inject large sample volumes without compromising the separation quality.

The use of RPLC in both dimensions is usually the most used combination in on-line LC x LC. In the case of ionizable compounds such as peptides, selectivity can easily be tuned between dimensions to spread out the chromatographic peaks over the separation space to some extent. Yet, this combination may be of limited usefulness for the separation of highly complex mixtures, since partial correlation between

dimensions ineluctably entails partial occupation of the separation space, and thus limited effective peak capacity. Dynamic adjustments of the second-dimension gradients, tailored to the elution range in each fraction, can improve the performance of RPLC x RPLC in terms of occupation space coverage and effective peak capacity. However, as highlighted in this work, such an approach should also impair detection sensitivity on one hand, and retention time run-to-run repeatability on the other hand. From our standpoint, the latter shortcoming strongly reduces the attractiveness of this kind of approach in on-line LC x LC, especially in the case of fast second-dimension separations.

Combining different and complementary chromatographic modes can also improve the retention space coverage compared to RPLC x RPLC. In this thesis, the combination of HILIC and RPLC was explored for peptide analysis. Despite being attractive in terms of retention space coverage, this combination is not straightforward, due to major solvent incompatibility problems between dimensions. In the case of peptides, differences of elution strength between sample solvent and mobile phase in both dimensions usually engender severe peak issues, including broadening, distortion, and breakthrough phenomena. Those are often found to impact severely both the peak capacity and the detection sensitivity of the method. To avoid such deleterious effects and make the best use of this orthogonal combination, two main groups of strategies, relying on minimizing either the volume or the solvent strength of the sample injected into the ^{2}D-column, or both, have been reported in the literature. Quite conversely, in this thesis, an alternative strategy consisting in injecting relatively large volumes of strong solvent in RPLC, to provoke the onset of a phenomenon that we called "Total Breakthrough", was proposed. This phenomenon can be defined as a limit-case of breakthrough for which a narrow and symmetrical retained peak is obtained for a given analyte despite the occurrence of breakthrough. In this work, such conditions were highlighted for positively charged compounds when the injected volume exceeded a critical value, which was found to depend on both the column dead volume and the analyte retention factor in the injection solvent. To the best of our knowledge, this is the first time that such a phenomenon is described. Although rather unusual and counter-intuitive, this "Total Breakthrough" strategy was proven to be very reliable, and quite competitive for peptide separation in on-line HILIC x RPLC when compared to other frequently used strategies, such as post-^{1}D-flow splitting and on-line solvent dilution. By and large, on-line HILIC x RPLC was shown

to be very attractive for the separation of peptides. Compared to RPLC x RPLC, the developed HILIC x RPLC method enabled to increase both the retention space coverage and the peak capacity, but at the great expense of detection sensitivity.

Finally, the applicability of on-line LC x LC-UV-HRMS methodologies to the characterization of complex real-life protein samples was demonstrated. An on-line CEX x RPLC method was developed for the separation of the charge variants of a lysine-linked antibody-drug conjugate currently under development. Owing to (i) the excellent complementarity of these two chromatographic modes for these compounds and (ii) the on-line desalting provided by the second dimension before HRMS detection, the developed approach enabled to gain valuable insights on the analysed samples in less than 30 min. Also, the potential of exploiting visual comparisons of 2D contour plots for stability studies or even batch-to-batch comparability studies was highlighted.

The research described in this thesis allowed to highlight the potential of on-line LC x LC for fast and efficient separation of highly complex samples. Despite the progress made in this work, some challenges and constraints remained. Key areas for improvements are listed below:

(i) In this work, a lot of effort has been devoted to understanding the Total Breakthrough phenomenon, which was highlighted for peptides in on-line HILIC x RPLC. The conditions of occurrence and limits of this phenomenon were clearly defined in RPLC, and both its validity and reliability were demonstrated under a fairly broad range of conditions. However, although our findings led us to suspect that Total Breakthrough could be explained by the circumstances of a mixed retention mechanism, the intricacies of this singular phenomenon remains a mystery. As for now, neither the difference in behaviour between neutral/negatively charged analytes and positively charged ones, nor the surprising binary presence/absence of a fully resolved "middle peak" between breakthrough and retained peaks are explained. In the future, further investigation should be conducted to demystify this phenomenon. First of all, most of our conclusions were drawn in RPLC, and for a relatively narrow range of compounds. Extending the study to other families of compounds, such as carbohydrates and lipids for example, could help strengthening our conclusions. It was demonstrated that this phenomenon also occurred in HILIC. Perhaps

investigating this phenomenon more extensively in HILIC as well as in other chromatographic modes could shed new lights on its mechanism of occurrence.

(ii) The past five to ten years have seen a dramatic rise in the development of techniques involving the dilution of the ^{1}D-effluent before transfer into the ^{2}D-column to improve the performance of on-line LC x LC in terms of peak capacity and detection sensitivity. However, as demonstrated in this work, the resulting volume transferred from ^{1}D to ^{2}D can be a limiting factor with these approaches since it has a direct impact on the available time for the separation. This is especially true for fast on-line LC x LC separations (i.e. sub-hour), which usually require short analysis times in ^{2}D (i.e. < 0.5 min). In these cases, the process of on-line dilution may leave very little room for the separation, especially when large dilution ratio are required. Flow splitting may be used to reduce the transferred volume and circumvent this problem, but not without impacting detection sensitivity. Another possible solution could be to use low-volume trapping columns instead of empty loop since this approach holds the promise of removing most of the ^{1}D-effluent during transfer. This approach has been very popular in recent years, but its added value compared to empty loops has never really been demonstrated in on-line LC x LC. Therefore, it could be interesting to conduct such a study.

(iii) Finally, despite good results in terms of separation, the on-line CEX x RPLC-UV-HRMS method developed for the analysis of antibody-drug conjugates in Chapter VI suffered from limited detection sensitivity in MS, which impacted the characterization of the separated species. Possible areas of developments to improve our results were extensively discussed in Chapter VI. They mostly include the use of more MS-compatible ingredients in the mobile phases on one hand, and the exploration of other chromatographic combinations, among which HILIC and RPLC, on the other hand.

SUPPLEMENTARY INFORMATION

A. Supplementary Information for Article 4:

Pushing the limits of resolving power and analysis time in on-line comprehensive hydrophilic interaction x reversed phase liquid chromatography for the analysis of complex peptide samples

Soraya Chapel, Florent Rouvière, and Sabine Heinisch
Journal of Chromatography A, **2019**, 1615, 460753
DOI: 10.1016/j.chroma.2019.460753

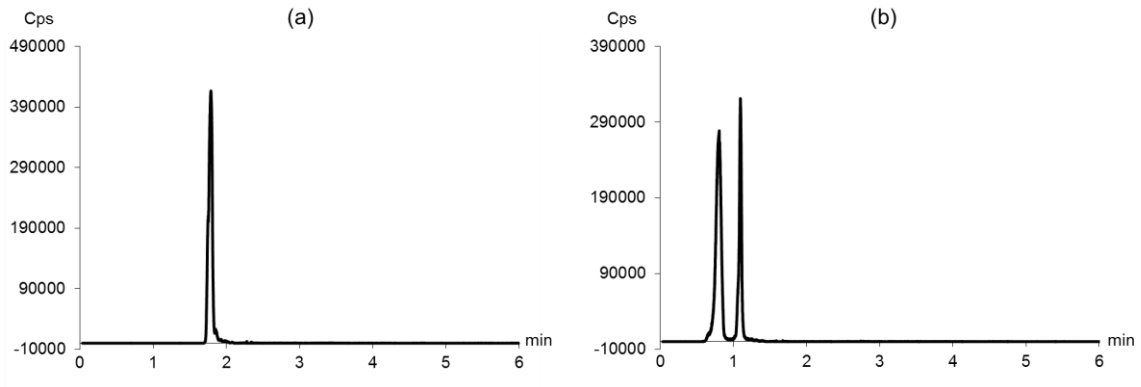

Fig. S1: Extracted ion chromatograms of the same peptide (EIC 1000.5722) in HILIC with different initial composition (a) 2% B, and (b) 13% B. A: Acetonitrile and B: water + 10 mM ammonium acetate. HRMS detection ESI-. Injection volume: 4 µL. Sample: Tryptic digest of 6 proteins in 50:50 ACN/water. Other conditions as in Fig.3.

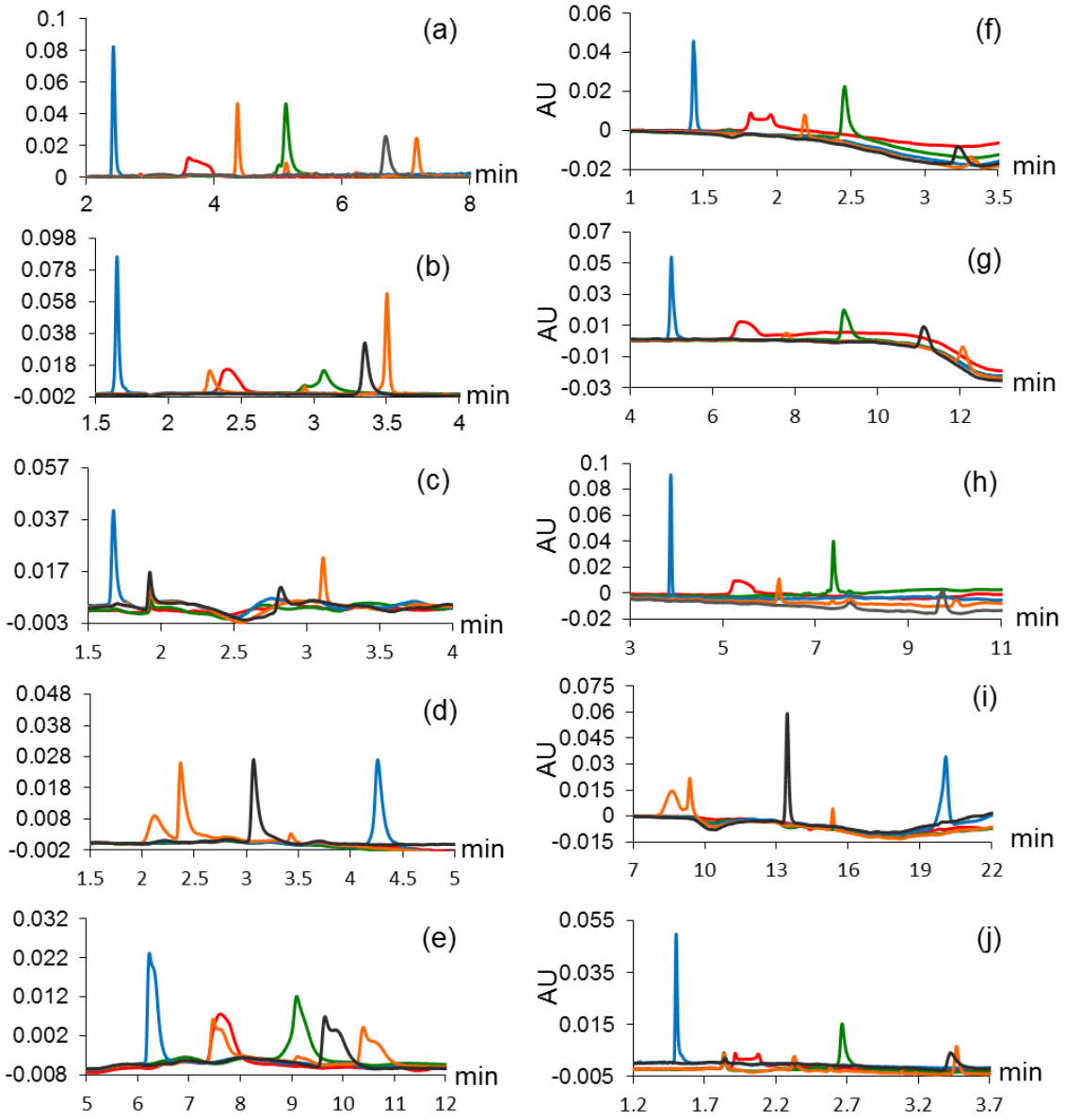

Fig. S2: Separations of standards of peptides (#1 (red), #3 (green), #4 (blue), #5 (orange), and #7 (grey), 42 mg/L) in HILIC-UV with 10 different stationary phases: (a) Hypersil HILIC, (b) Acquity BEH HILIC, (c) Acquity amide, (d) Hypersil Gold HILIC, (e) Nucleodur HILIC, (f) Kinetex HILIC, (g) Nucleoshell HILIC, (h) Accucore HILIC, (i) Luna NH2, and (j) Cortecs HILIC. 0.5% V_0 injected in 75:25 ACN/water (v/v) Column characteristics, flow rates, and gradient times are listed in Table 2. Other conditions are given in the experimental section.

Table S1: Experimental and theoretical peak capacity values obtained for the ten studied stationary phases in HILIC.

#	**Column name** (column dimensions)	n_{exp}	n_{th}	n_{exp}/n_{th}
1	**Hypersil HILIC** (50 mm x 4.6 mm x 3.0 µm)	43	57	0.75
2	**Acquity BEH HILIC** (50 mm x 2.1 mm x 1.7 µm)	59	95	0.62
3	**Acquity BEH Amide** (50 mm x 2.1 mm x 1.7 µm)	27	71	0.38
4	**Hypersil gold HILIC** (50 mm x 2.1 mm x 1.9 µm)	39	105	0.37
5	**Nucleodur HILIC** (60 mm x 1.0 mm x 3.0 µm)	9	47	0.19
6	**Kinetex HILIC** (50 mm x 2.1 mm x 1.7 µm)	31	84	0.37
7	**Nucleoshell HILIC** (100 mm x 2.0 mm x 2.7 µm)	26	82	0.32
8	**Accucore HILIC** (100 mm x 2.1 mm x 2.6 µm)	36	96	0.38
9	**Luna NH_2** (150 mm x 2.0 mm x 3.0 µm)	26	64	0.41
10	**Cortecs HILIC** (50 mm x 2.1 mm x 1.6 µm)	35	84	0.42

Table S2: Desirability function results in HILIC. f_1, f_2, f_3, and f_4 being the values associated to each quality descriptors (n_{exp}/n_{th}, peak asymmetry, number of observed peaks, and elution window, respectively) with the chosen response function varying from 0 to 1 represented in Fig. S3.

Column #	n_{exp}/n_{th}	f_1	Peak asymmetry	f_2	Number of peaks	f_3	Elution window (% A)	f_4	F
1	0.75	1.00	1.40	0.84	33	0.50	37.8	0.89	0.78
2	0.62	0.81	1.38	0.85	46	1.00	42.0	1.10	0.93
3	0.38	0.46	1.74	0.70	40	0.77	38.5	0.93	0.69
4	0.37	0.44	2.15	0.54	26	0.23	35.8	0.79	0.46
5	0.19	0.17	3.49	0.00	25	0.19	30.2	0.51	0.00
6	0.37	0.44	1.29	0.88	38	0.69	30.3	0.52	0.61
7	0.32	0.36	1.24	0.90	34	0.54	33.8	0.69	0.59
8	0.38	0.45	1.13	0.95	40	0.77	30.2	0.51	0.64
9	0.41	0.49	1.22	0.91	29	0.35	32.7	0.64	0.56
10	0.42	0.51	2.01	0.59	42	0.85	32.4	0.62	0.63

Fig. S3: Graphs representing the functions varying from 0 to 1 describing the four quality descriptors used for the column comparison in HILIC: (a) n_{exp}/n_{th}, (b) peak asymmetry, (c) number of observed peaks, and (d) elution window (%B). Other conditions as in Table 2 and Fig.4

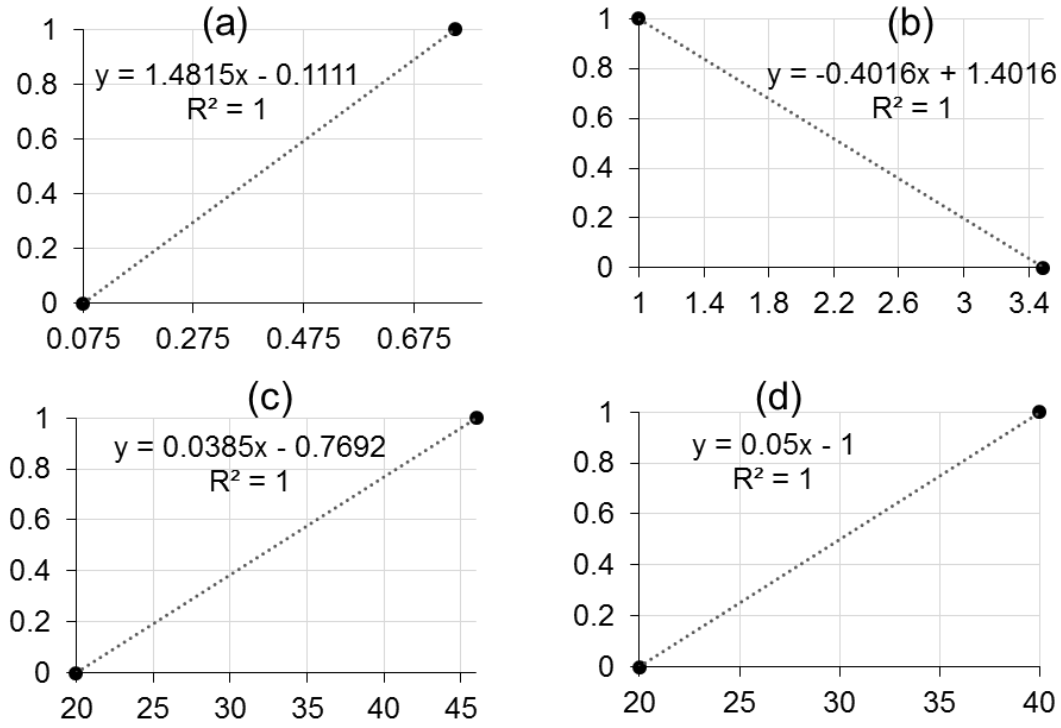

Fig. S4: Overlaid peaks of peptide #4 (161 mg/L in 30:70 water/ACN (v/v)) obtained in RPLC with different injection volumes (1%, 2%, 6%, and 18% V0) emphasizing the impact of the nature of the stationary phase: (a) Kinetex C18 (30 mm x 2.1 mm, 1.3 µm), and (b) Acquity CSH C18 (30 mm x 2.1 mm, 1.7 µm), 1-45% B in 44 t_0. Other conditions as in Fig. 5.

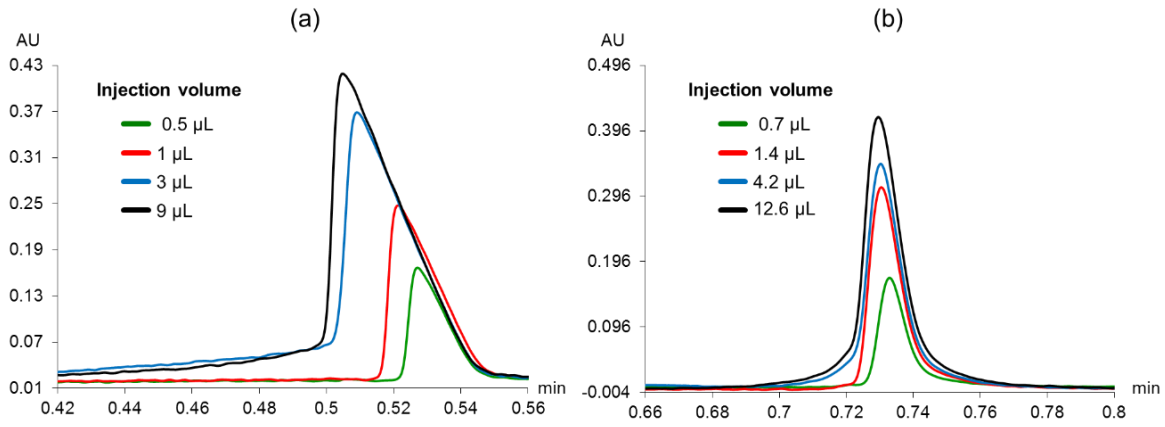

Fig. S5: Evolution of the peak shapes of peptide #6 (50 mg/L) in (a, b, c, d) 50:50 water/ACN (v/v) and (e) 10:90 water/ACN (v/v) with increasing injection volumes: (a, e) 0.35 µL (0.5% V_0), (b) 0.4 µL (0.55% V_0), (c) 0.5 µL (0.68% V_0), and (d) 0.6 µL (0.83% V_0). MS detection ESI+ (EIC 542.6). Other conditions as in Fig.7. The asterisk indicates the breakthrough peak.

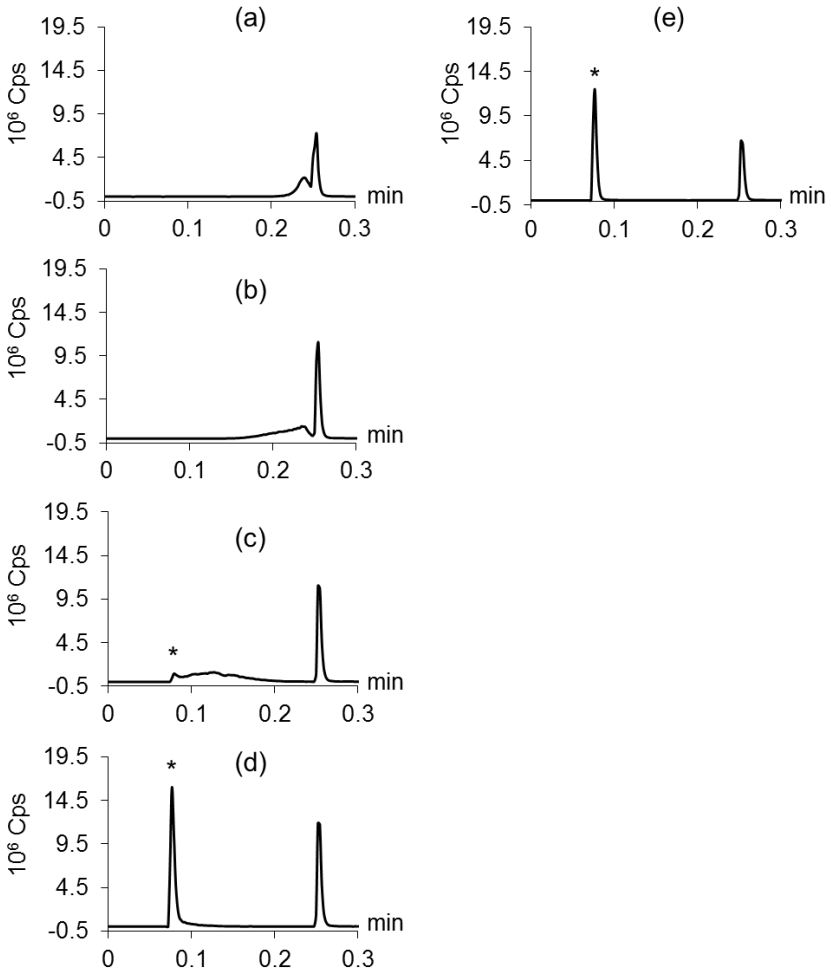

Fig. S6: Entire 2D-chromatograms obtained for the separation of a tryptic digest of 6 proteins in on-line HILIC x RPLC (without split). UV detection at 210 nm. Conditions are given in Table 3.

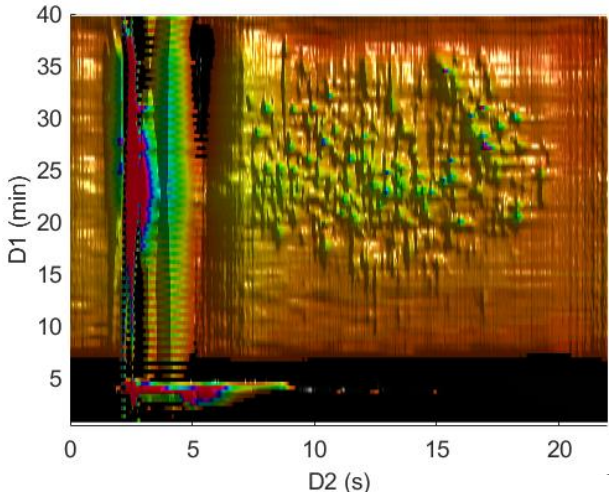

B. Supplementary Information for Article 5:

A comprehensive study on the phenomenon of Total Breakthrough in liquid chromatography

Soraya Chapel, Florent Rouvière, Vincent Peppermans, Gert Desmet, and Sabine Heinisch

Journal of Chromatography A, **2021**, under review

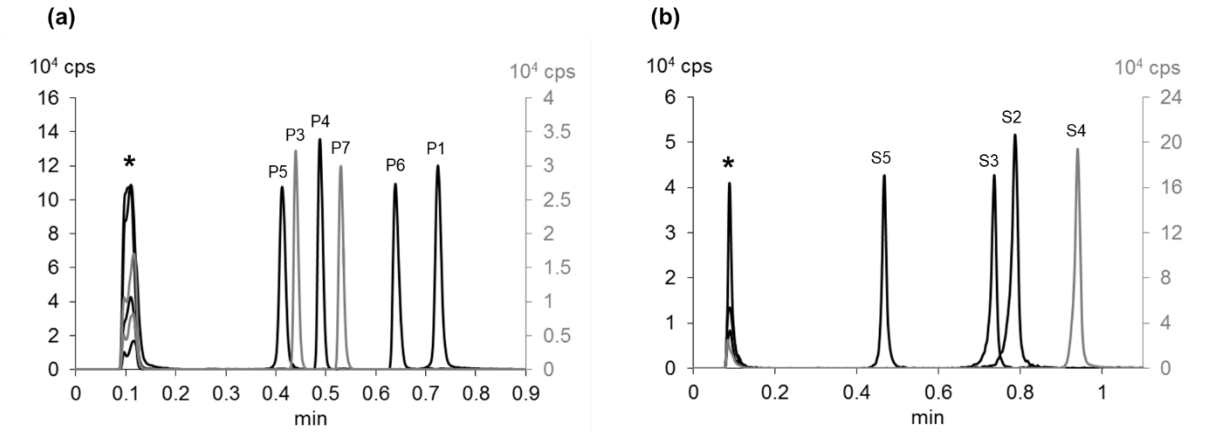

Fig. S1: Overlay of extracted ion chromatograms (EICs) for (a) six peptides (P1 to P6, see Table 1 of main paper) and (b) four small basic compounds (S1 to S4, see Table 1 of main paper) showing the occurrence of Total Breakthrough regardless of the retention of the analyte. Injection volume: 14 µL (19.3% V_0), flow rate: 0.75 mL/min, gradient elution : 1-45-1-1% B in 0-1.08-1.18-2 min (s = 4%). ESI-HRMS detection. Same other conditions as in Fig. 1 of main paper. The asterisk indicates the non-retained breakthrough peak.

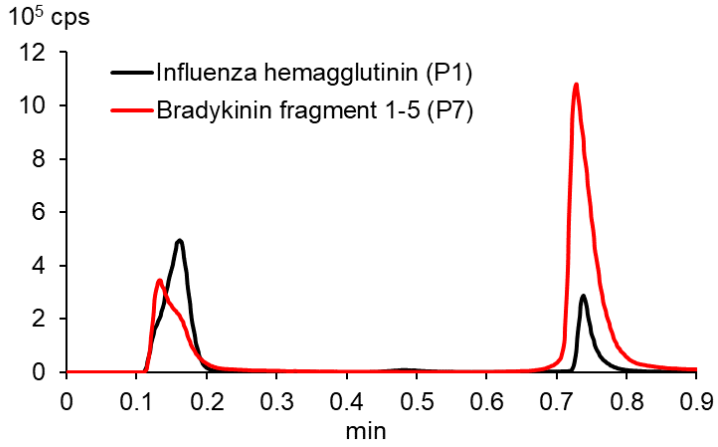

Fig. S2: Overlay of extracted ion chromatograms (EICs) of influenza hemagglutinin (5 mg/L) and bradykinin fragment 1-5 (2 mg/L) showing the occurrence of Total Breakthrough at neutral pH. Injection volume: 14 µL (19.3% V_0). ESI-HRMS detection. Same other conditions as in Figs. 3a and 3b of main paper. The asterisk indicates the non-retained breakthrough peak.

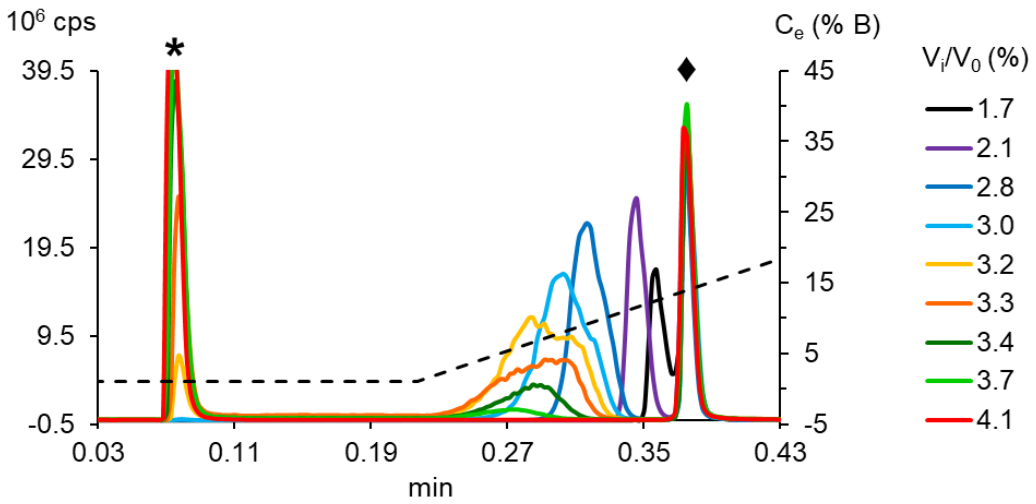

Fig. S3: Evolution of the separation of the middle peak with the injection volume. Sample solvent: 30:70 H_2O/ACN. Solute: Leucine enkephalin. Injected volumes (V_i/V_0) indicated on the right of the graph. Same other conditions as in Fig. 1 of main paper. The asterisk indicates the non-retained breakthrough peak and the diamond indicates the retained peak. The gradient profile at the column outlet is given in dotted line with the composition scale on the right.

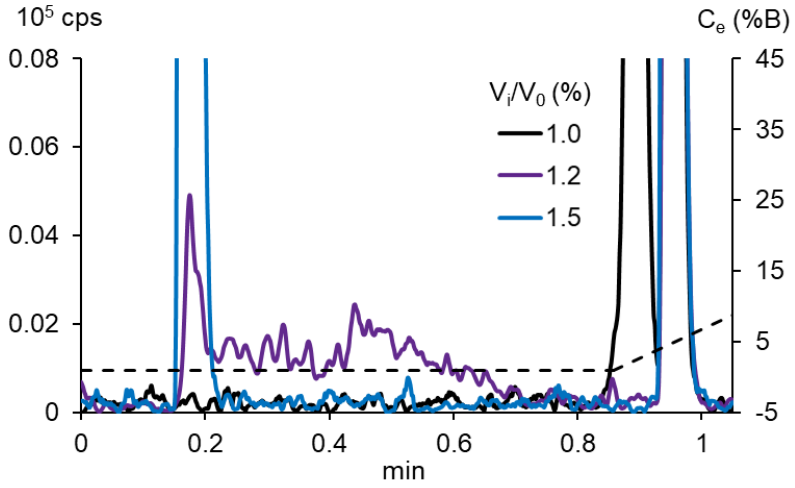

Fig. S4: Zoomed view of Fig. 8c of main paper highlighting the presence of molecules between the breakthrough and retained peaks with 1.2% V_0 injected for [ile]-angiotensin (100 mg/L). Same conditions as in Fig. 8c of main paper.

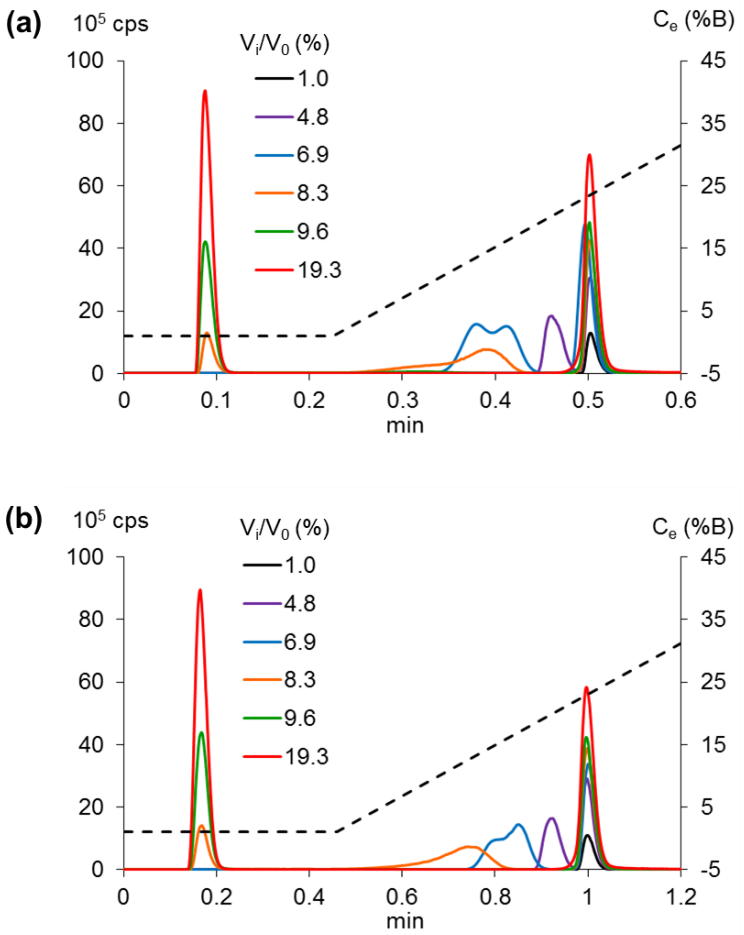

Fig. S5: Effect of the flow rate on the separation of amitriptyline (0.5 mg/L): (a) 1.5 mL/min and (b) 0.75 mL/min. Injected volumes (V_i/V_0) indicated on the graphs. Same other conditions as in Fig. 9 of main paper.

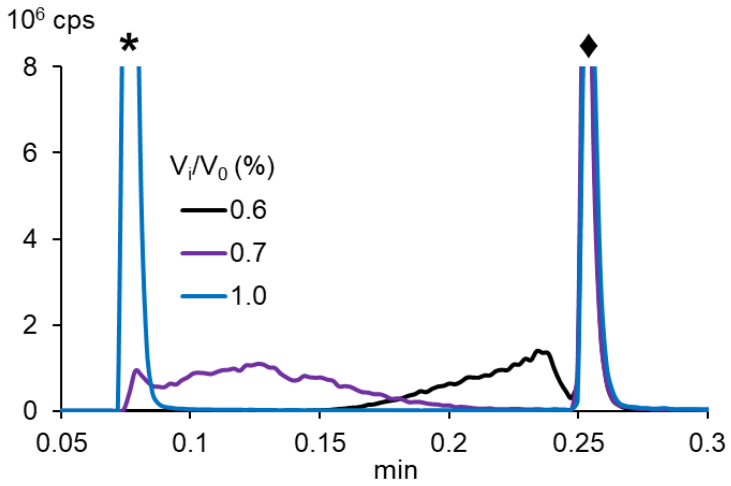

Fig. S6: Evolution of the peak shapes of [arg8]-vasopressin (50 mg/L) with increasing injection volumes (V_i/V_0) from 0.6% to 1.0%. Same other conditions as in Fig. 1 of main paper. The asterisk indicates the non-retained breakthrough peak and the diamond indicates the retained peak.

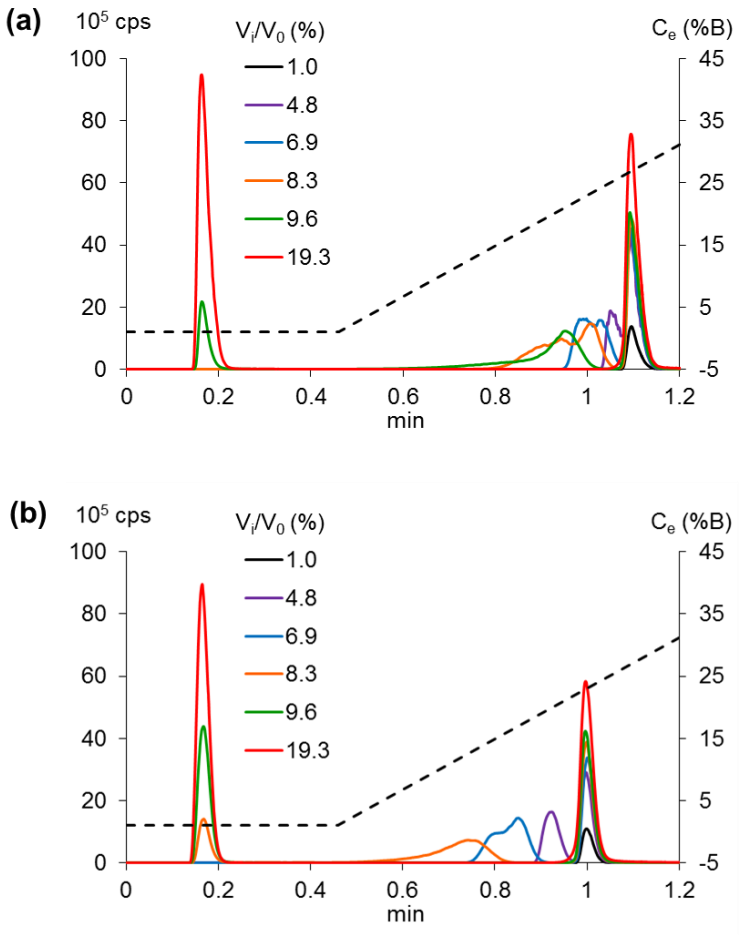

Fig. S7: Effect of the temperature on the separation of amitriptyline (0.5 mg/L): (a) 30°C and (b) 80°C. Injected volumes (V_i/V_0) indicated on the graphs. Same other conditions as in Fig. 9c and 9d of main paper.

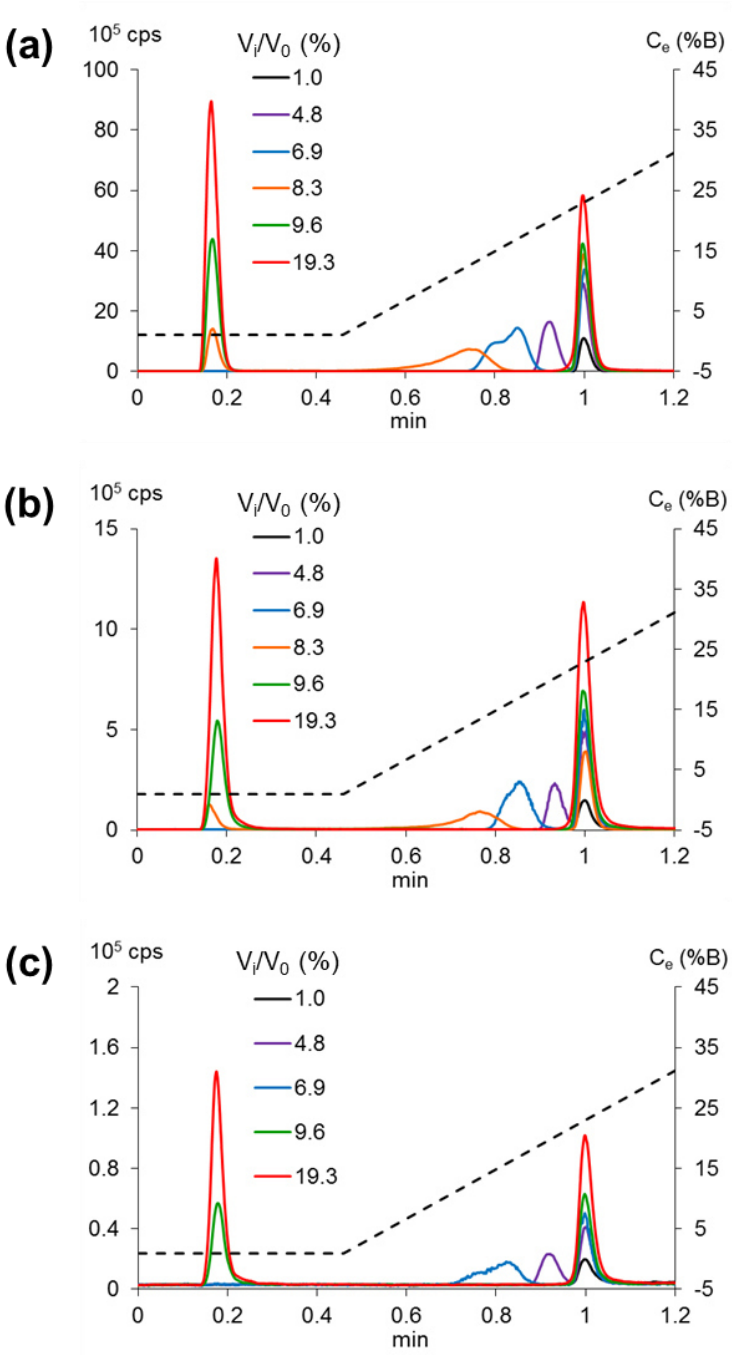

Fig. S8: Effect of the sample concentration on the separation of amitriptyline: (a) 0.5 mg/L, (b) 0.05 mg/L, and (c) 0.005 mg/L. Injection volume (V_i/V_0) indicated on the graphs. Same other conditions as in Fig. 9c and 9d of main paper.

C. Copy of Article 6:

Journal of Chromatography A 1643 (2021) 462078

Contents lists available at ScienceDirect

Journal of Chromatography A

journal homepage: www.elsevier.com/locate/chroma

Detailed numerical study of the peak shapes of neutral analytes injected at high solvent strength in short reversed-phase liquid chromatography columns and comparison with experimental observations

Vincent Pepermans[a], Soraya Chapel[b], Sabine Heinisch[b], Gert Desmet[a,*]

[a] Department of Chemical Engineering, Vrije Universiteit Brussel, Brussels, Belgium
[b] Université de Lyon, Institut des Sciences Analytiques, UMR 5280, CNRS, 5 rue de la Doua, 69100, Villeurbanne, France

ARTICLE INFO

Article history:
Received 17 December 2020
Revised 10 March 2021
Accepted 13 March 2021
Available online 18 March 2021

Keywords:
Numerical simulations
Band broadening
Injection profile
Peak breakthrough

ABSTRACT

We report on a numerical investigation of the different steps in the development of the spatial concentration profiles developing along the axis of a liquid chromatography column when injecting large relative volumes (>10 to 20% of column volume) of analytes dissolved in a high solvent strength solvent band as can be encountered in the second dimension (^{2}D) column of a two-dimensional liquid chromatography (2D-LC) system. More specifically, we made a detailed study of the different retention and the axial band broadening effects leading to the double-headed peak shapes or strongly fronting peaks that can be experimentally observed under certain conditions in 2D-LC. The establishment of these intricate peak profiles is discussed in all its fine, mechanistic details. The effect of the volume of the column, the volume and the shape of the sample band, the retention properties of the analyte and the band broadening experienced by the analytes and the sample solvent are investigated. A good agreement between the simulations and the experimental observations with caffeine and methylparaben injected in acetonitrile/water (ACN/H_2O) mobile phase with different injection volumes is obtained. Save the difference in dwell volume, key features of experimental and simulated chromatograms agree within a few %. The simulations are also validated against a number of simple mathematical rules of thumb that can be established to predict the occurrence of a breakthrough fraction and estimate the amount of breakthrough.

1. Introduction

As chromatography keeps being pushed by a demand for ever faster and more refined separations, more and more research efforts are devoted to two-dimensional LC (2D-LC), as this technique has the potential to produce peak capacities of several thousand in a practically affordable time [1–9] making the separation of difficult-to-resolve or complex mixtures easier and faster. During the transition of the sample from the first dimension (^{1}D) to the second dimension (^{2}D) column, some important problems such as dilution and solvent incompatibility effects arise when using a passive modulation method. In this approach, the ^{1}D effluent is fractionated and directly injected into the ^{2}D, in most cases using a valve with multiple loops [10,11]. This often results in a loss of detector sensitivity and peak deformation in the ^{2}D [12–15]. To circumvent these problems, a lot of research efforts have been devoted to the active modulation between the two dimensions. One example is the use of trap columns [16–18] where the fractions of the effluent of the ^{1}D first get refocused, most often on a short column with a similar stationary phase as the ^{2}D column and are subsequently eluted using a solvent that is more compatible with the mobile phase used in the ^{2}D, potentially leading to an increase in sensitivity and solvent compatibility, and a lower injection volume. Active solvent modulation is another method that has been developed and investigated lately [19–21]. Here, by storing the ^{1}D effluent in a loop and splitting the ^{2}D mobile phase solvent, where one part goes through the loop and the other bypasses it, the fraction gets diluted before entering the ^{2}D column, which improves the solvent compatibility between the two dimensions. The idea to dilute the effluent of the ^{1}D column with a low elution strength liquid to induce appropriate focusing on the column's head has been first introduced by Oda et al. [22]. Other modulation methods are membrane assisted evaporation modulation [23], longitudinal thermal modulation [24], pulsed elution [18] and fractionated sampling and stacking [25].

* Corresponding author.
E-mail address: gedesmet@vub.be (G. Desmet).

https://doi.org/10.1016/j.chroma.2021.462078
0021-9673/

To use these techniques more effectively and search for more universal methods of modulation, it is important to understand in detail what happens to an injected band inside the ^{2}D column when the ^{1}D fractions are injected in this column. One of those factors is the solvent and injection solvent mismatch mentioned earlier, due to the fact that the injected species are dissolved in a solvent that is the effluent from the ^{1}D, which often has a higher solvent strength than the starting mobile phase in the ^{2}D. Another problem is that, given the column diameter ratio between the ^{2}D and ^{1}D (usually 1 to 2), the injection volumes in ^{2}D are often too large to maintain the maximal efficiency of the ^{2}D column. Generally, a 10% loss in efficiency is endured as soon as the variance of the injected band ($\sigma^2_{V,inj}$) makes up more than 10% of the expected column variance ($\sigma^2_{V,col}$), which is proportional to $(1+k)^2$, where k is the retention factor, and hence smallest for high elution strength mobile phases. The effect of the above phenomena on the shape of the peaks eluting off the ^{2}D column has already been thoroughly investigated theoretically and experimentally [15, 26–28]. Gritti [28] and Stoll et al. [15] also already demonstrated that the shape of the injection plug has a large effect on the eventual separation.

In the present study, we dig deeper into the processes leading to the obtained peak shapes by making a fully detailed (numerical) study of how an injected band is transformed inside the column as (part of) the analytes are first lagging behind the injection solvent band (because they are (slightly) retained by the stationary phase) and are subsequently accelerated again when they are picked up by the mobile phase gradient. To gain an insight in the axial, on-column evolution of the band, we use computer simulations [29,30] based on the numerical solution of the generally accepted advection-dispersion mass balance for chromatography [31]:

$$\frac{\partial C_t}{\partial t} = -u_0 \cdot \frac{\partial C_m}{\partial x} + D_{ax} \cdot \frac{\partial^2 C_m}{\partial x^2} \tag{1}$$

$$\text{with } C_t = (1+k) \cdot C_m \tag{2}$$

$$\text{and with } k = K \cdot \frac{V_s}{V_m} \text{ and } K = \frac{C_s}{C_m} \tag{3}$$

wherein C_m and C_s are the analyte species concentration in resp. the mobile and stationary phase, u_0 is the velocity of the mobile phase, D_{ax} is the axial dispersion coefficient, K is the partitioning coefficient, t is the time, x is the position in the column and V_m and V_s are the volumes of the mobile and the stationary phase respectively ($V_s/V_m = (1-\varepsilon_T)/\varepsilon_T$), with $\varepsilon_T = 0.7$ the total porosity, in all simulations). The expression in Eq. (1) is mathematically equivalent to the Craig-model approach developed by Rutan et al. [32], the only difference is that, whereas in the Craig-model the spatial discretization scheme is fixed and 1st order in nature, the more general approach in Eq. (1) allows for higher order accuracy schemes having a higher numerical accuracy.

The D_{ax} describing the degree of band broadening in Eq. (1) is related to the u_0 and plate height (H) via:

$$D_{ax} = \frac{u_0 H}{2} \tag{4}$$

Together with Eq. (1), we simultaneously also solve the advection-dispersion mass balance for the fraction of organic modifier (ϕ). In analogy with Eq. (1), this can be written as:

$$\frac{\partial \phi}{\partial t} = -u_0 \frac{\partial \phi}{\partial x} + D_{ax} \frac{\partial^2 \phi}{\partial x^2} \tag{5}$$

Eqs. (1) and (5) were solved simultaneously using a 4th-order Runge-Kutta numerical integration scheme to compute the evolution with time. During each step, the local ϕ-values are used to compute and update the local value of the retention factor (k(x)), using either the LSS-model [33]:

$$k(x) = k_w \cdot e^{-S\cdot\phi(x)} \tag{6a}$$

Where k_w is the retention factor in 100% water, S is the solvent strength parameter and ϕ(x) is the local value of the fraction of organic modifier, or the more elaborate Neue-Kuss model [34]:

$$k(x) = k_w(1 + S_2 \cdot \phi(x))^2 \cdot e^{-\frac{S_1\phi(x)}{1+S_2\phi(x)}} \tag{6b}$$

Where S_1 is the slope for non-linear models and S_2 is the curvature coefficient.

As discussed previously, the program not only shows the peak profile as a function of time (chromatogram) at the end of the column, but also provides a direct view on the evolution of the concentration © with x, the axial location of the solute along the column. The effect of the retention parameters (k_w, S or k_w, S_1 and S_2)) is thoroughly investigated, as well as the effect of the volume and the shape of the injection plug and the effect of the column efficiency (via H and D_{ax}). Finally, the program has been tested by comparing it with the experimentally observed breakthrough-curves at the end of a short reverse phase liquid chromatography (RPLC) column under conditions mimicking the ^{2}D of an on-line LC x LC separation. Upon simple email request, the authors offer access to the code to Matlab® users.

Experimentally, the effect has been investigated for two different compounds, methylparaben and caffeine, dissolved in a 50/50% (v/v) ACN/H_2O and subjected to a mobile phase gradient going from 1%ε to 45% ACN. Characteristic for the elution of these compounds is that, under the selected experimental injection conditions, they do not elute as a single peak but have a part eluting near the t_0-time of the column (so-called breakthrough fraction), followed by a long tail connecting to a second peak eluting near the expected retention time of the analyte (retained part of the peak). Similar peak shapes have very recently also been reported by Weatherbee et al. [35], who found the exact peak shape to be strongly depending on the shape of the injection profile.

2. Materials and methods

2.1. Experimental set-up

The experiments were performed on an ACQUITY UPLC I-Class instrument from Waters Corporation (Milford, MA, USA) consisting of a binary solvent delivering pump (BSM), a sample manager with a flow-through needle (SM-FTN) injector equipped with a 15 µL loop, a thermostated column oven, a photodiode-array detector (PDA) with a 0.5 µL flow cell. An extension loop of 100 µL was added to the injector. The measured dwell volume (V_D) and extra-column volume (V_{ext}) for this system were 210 μL and 12 μL, respectively. The ACQUITY UPLC CSH C18 column (30 × 2.1 mm, 1.7 µm) was purchased at Waters Corporation (Milford, MA, USA). Instrument control, data acquisition, and data handling were performed by MassLynx v4.1 software (Waters Corporation).

2.2. Solvents and samples

Deionized water was produced using an Elga Purelab Classic UV purification system from Veolia water STI (Décines-Charpieu, France). LC-MS grade acetonitrile (ACN), methylparaben and caffeine were purchased from Sigma-Aldrich (Steinheim, Germany). LC-MS grade formic acid (FA) was purchased from Fischer scientific (Illkirch, France).

2.3. Chromatographic conditions

The column temperature was set at 80°C, the flow rate was 1.5 mL/min, and gradient elution was used with 0.1% formic acid in

water as solvent A (pH = 2.7) and 0.1% formic acid in ACN as solvent B. The gradient profile went from 1-45% B in 0.54 min (normalized gradient slope (s) of 4%). The caffeine and the methylparaben were dissolved in a 50/50% (v/v) ACN/H2O mixture. The chromatograms were recorded at 254 nm for methylparaben and 270 nm for caffeine with an acquisition rate of 40 Hz.

2.4. Numerical methods

Eqs. (1) and (5) were solved with a 4th-order Runge-Kutta integration scheme [36] implemented in Matlab®. Before implementing the Runge-Kutta scheme, the spatial derivatives appearing on the right-hand side of Eqs. (1) and (5) were first discretized using the following scheme (with y either C or ϕ):

$$\frac{\partial y_i}{\partial x} = \frac{1}{\Delta x} \cdot \frac{1}{6}(y_{i-2} - 6y_{i-1} + 3y_i + 2y_{i+1}) \tag{7a}$$

$$\frac{\partial^2 y_i}{\partial x^2} = \frac{1}{\Delta x^2} \cdot \frac{1}{12}(-y_{i-2} + 16y_{i-1} - 30y_i + 16y_{i+1} - y_{i+2}) \tag{7b}$$

where Δx is the discretization step and i is the number of the cell in the column. Before and after the column (i.e., for x<0 and x>L=3 cm), resp. 1800 and 9200 extra computational cells were added. In these cells, the retention factor k was kept at k=0 to represent that the packed region only extended between x=0 and x=L=3 cm.

Zero-flux conditions (∂C/∂x=0 and $\partial\phi/\partial$x=0) were applied as the boundary condition at the first and last computational cells (resp. situated at x=-1.4 cm and x=10 cm). In addition, it was always verified the species concentration never became significant near the first and last computational cells, such that all possible end effects were avoided.

To implement the mobile phase gradient program, the ϕ-value at x=0 (ϕ_0) was subjected to the following condition:

$$\phi(x = 0, t) = \phi_0 \qquad \text{for } t \le t_D \tag{8a}$$

$$\phi(x = 0, t) = \phi_0 + \frac{\Delta\phi}{t_G}(t - t_0) \quad \text{for } t > t_D \tag{8b}$$

where t_G is the gradient time and t_0 is the void time. As the initial condition for ϕ and C_t, an injection band containing the strong sample solvent (with ϕ=ϕ_S=0.5) and the analyte species (with C_m=1) was defined in the region x<0 with the downstream part of the band just touching x=0, i.e. the simulations started when the downstream end of the sample band just reached the column inlet.

To test the numerical accuracy of the model, a number of pure isocratic runs were made (see Fig. S-1 of the SM). These showed that the numerical procedure produces peak variances and hence plate heights that are within 0.0000078% accuracy of the plate heights imposed in the model via the D_{ax}-coefficient (see Fig. S-1a in the Supplementary material, SM). Retention times were found to be within 10^{-10} % accuracy of the theoretically expected value.

In case of the simplified rectangular injections (used in the first part of the study to obtain the purest possible insight in the peak shapes without the complication of the effect of the complex shape of the injection band), the injection band was defined as a rectangle with given width, flanked by two semi-Gauss curves with a standard deviation (σ_x) = 0.012 cm. These two Gaussian flanks were added to make the injection profile more realistic, but especially also to avoid the numerical instabilities one can expect from a perfectly vertical side-walls of a rectangle (concentration gradient= infinite). Given the strong sensitivity of the profiles on the exact shape of the injection band, more realistic injection band shapes were considered in the second part of the study. These were shaped using an expression developed by Gritti [28]:

$$C(0,t) = \frac{C_0}{1 + \exp\left(-\frac{t - t_{dwell} + \frac{V_p}{2F_v}}{\alpha_1}\right)} \cdot \left(1 - \frac{1}{1 + \exp\left(-\frac{t - t_{dwell} + \frac{V_p}{2F_v}}{\alpha_2}\right)}\right) \tag{9}$$

Wherein C_0 is the concentration of the initial peak (can also be the fraction of organic solvent), t is the time the measurement is running, t_{dwell} is the dwell time in front of the column, V_p is the injected volume, F_v is the flow rate, and α_1 and α_2 are two fitting parameters.

This equation was first implemented in MS Excel® and subsequently incorporated into the Matlab© program.

3. Results

Before proceeding, it is important to note that the injected species band and the profile of the fraction ϕ of organic modifier in the sample solvent always have the same shape when they enter the column (see e.g., profile 1 in Figs. 1b,e) in any considered case. In the regions before and after the injection band, ϕ is equal to the fraction of modifier (ϕ_0) in the dwell volume of the gradient (equal to ϕ_0=0.01 in all cases). The fraction of modifier is highest (ϕ=ϕ_S) in the parts of the injected band that enter the column undiluted. In all considered cases, ϕ_S=0.5. Another important remark is that, while the conservation of mass is expressed via the total peak concentration (C_t) (cf. Eq. (2)), the response as measured by the detector is exclusively determined by the concentration in the mobile phase (C_m), given the absence of a stationary phase in the detector.

Fig. 1 describes in full detail how the simulation of the evolution of the concentration in time and space can be used to understand how a given injected peak shape and volume can lead to a given chromatogram recorded at the end of the column. For the sake of simplicity, a simple rectangular injection profile with smoothened flanks (cf. Section 2.4) has been considered. In later figures, notably in Figs. 6-8, more realistic injection profiles are considered by applying Eq. (9). Fig. 1a is the response in time as observed at x=L, i.e., at the end of a 3 cm long column (L). Figs. 1b-c represent how the same injected band is distributed in space at different time intervals (note that the left hand side of the peak in the time domain corresponds to the right hand side of the peak in the space domain and vice versa). The numbers used to identify the timing of the different profiles in Figs. 1b-c are also copied onto Fig. 1a, allowing to reconstruct the observed concentration response at the detector line (cf. dashed vertical line) from the temporal evolution of the band profiles in space shown in Figs. 1b-c. Profile (1) shows the shape of the modeled analyte band peak just prior to arriving at the column's head.

Essential to understand the profiles in Figs. 1b-c is that, when a broad analyte band moves through the column, the species that are initially contained in the high-solvent strength solvent band can leave this band by means of two processes: 1) by means of their retention, which makes them move with a lower velocity than the u_0-velocity with which the injection solvent band moves through the column and 2) by means of dispersion across the band flanks.

Considering the first process, which is by far much more important than the second, the slower migration velocity of the analytes obviously implies the analytes stay behind with respect to the sample band and hence "leave" the band through the upstream flank of the injection solvent band (Fig. 2a). The magnitude of this effect obviously depends strongly on the retention experienced by the analytes when dissolved in the injection solvent (k_s=0.1685 in

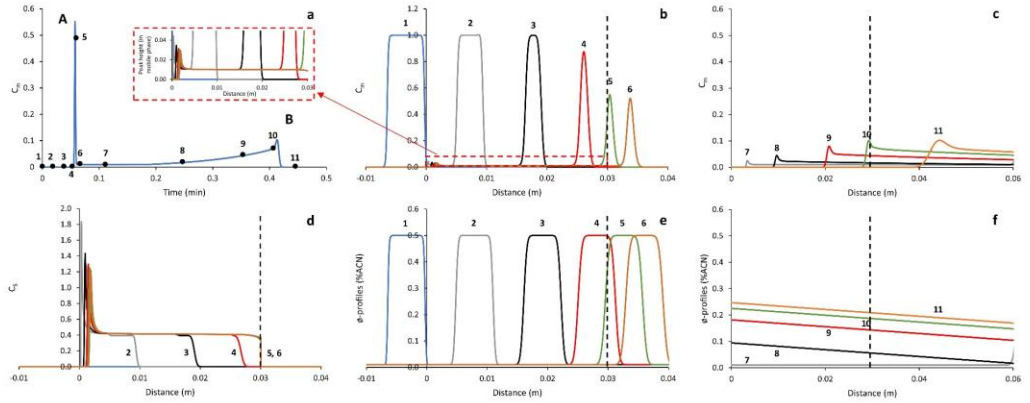

Fig. 1. Simulated mobile phase concentration (C_m) profiles plotted **(a)** as a function of time as recorded at x=L and **(b-c)** as a function of the distance recorded at different subsequent times (resp. at t = 0.018 min, 0.036 min, 0.051 min, 0.058 min, 0.064 min, 0.109 min, 0.245 min, 0.354 min, 0.409 min, 0.445 min for profiles 1-11). Each number i added to (a) represents the C_m-level recorded at the detector line at the moment when profile i is observed in (b-c). **(d)** C_s-profiles corresponding to profiles nr. 1-6 in (b). **(e-f)** ϕ-profiles corresponding to the profiles 1-12 in (b-c). Dashed vertical line=detector line. Simulation parameters: S_1=12.5, S_2=0.5, k_w=20, D_{ax}=3.86·10^{-8} m^2/s, u_0=0.0103 m/s, H=7.5 µm and $V_{p,inj}$=15 µL. The stationary phase is only present between the x=0 and the x=0.03 m-point. Gradient profile reaches head of column at t=0.14 min.

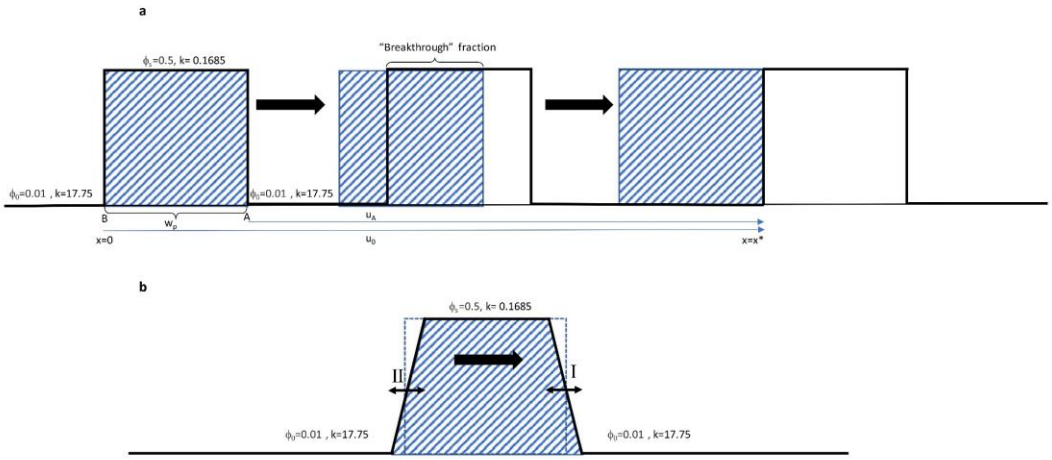

Fig. 2. Conceptual drawing of migration process of sample solvent (bold line shape) and analyte species band (stripe pattern) through column, showing **(a)** difference in migration speed between analyte moving at $u=u_0/(1+k_s)$ and sample solvent band moving at $u=u_0$ and **(b)** dispersion process to explain difference in retention behavior between species dispersing out of the injection solvent band at the upstream (I) and the downstream flank of the band (see text for explanation). Double-headed arrows represent dispersion process. Single-headed arrows represent u_0-velocity.

the present example). Once out of the injection solvent band, the species inevitably enter a low-solvent strength zone where they concentrate in the stationary phase. Considering the 2nd process, Fig. 2b shows that, whereas the dispersion process itself is substantially symmetrical (i.e., has an equal strength in the upstream and downstream direction), the effect on the peak profile can be expected to be asymmetric. Species leaving the band through its downstream flank by means of dispersion (double-headed dispersion arrow I) are suddenly strongly retained and drastically slow down. However, they are immediately caught up again by the high-solvent band following behind and moving with the u_0-velocity (cf. large single-headed arrow). This creates a self-sharpening effect, which helps maintaining a steep species profile at the upstream flank of the band. On the other hand, species leaving the band through its upstream flank (dispersion arrow II), and thus entering a high retention zone, cannot benefit from a similar self-sharpening effect as there is no front of strong solvent following. As a consequence, these analytes stay behind permanently. In summary, both processes hence lead to situation where the band can be expected to "leak" species through its upstream flank and thus deposits a trail of retained species along the column axis.

Returning now to the spatial C_m-concentration profiles in Fig. 1b, it can be readily observed the species band continuously narrows in width as the analyte species gradually leave the sample solvent band through its upstream flank because of the slower migration velocity of the analytes (migrating with velocity $u_0/(1+k_s)$ with k_s=0.1685 in the sample solvent) compared to that of the sample solvent (migrating with velocity u_0). The latter basically retains its original shape (save for the gradual broadening of its side fronts because of the column band broadening) throughout its entire passage through the column (see Fig. 1e which has been put just underneath Fig. 1b for an easy comparison of the corresponding profiles). Comparing the C_m-profiles in Fig. 1b with the ϕ-profiles in Fig. 1e in more detail, we see that the upstream flank of the analyte band and that of the sample solvent band coincide, while the downstream flank of the analyte band stays behind with

respect of that of the sample solvent band, as a reflection of the lower migration velocity of the former. When the analyte band has become sufficiently narrow to have its upstream and downstream flank meeting, the further loss of analyte species not only leads to a further narrowing of the band, but also to a decrease in peak height (cf. profiles 4,5,6 in Fig. 1b). Note that the fact that the decrease in height between profiles 5 and 6 is smaller than that between profiles 4 and 5 is due to the absence of a stationary phase beyond the x=0.03 m-point.

Zooming-in on the bottom part of Fig. 1b (see expanded view added to Fig. 1a), it can be noted that the analytes that left the sample band form a trail of analyte species running from the column's head all the way up to the upstream flank of the sample solvent band.

Making now the link between the spatial profiles in Fig. 1b with the temporal response curve in Fig. 1a by linking the profile numbers, we see that the fraction of analytes that remained into the sample solvent band till the end of the column is recorded at the detector as the breakthrough part of the peak (indicated with letter A in Fig. 1a), with the rise and fall of this part of the breakthrough curve essentially occurring during the moments between profiles 4 (just before onset of breakthrough peak) and 6 (end of breakthrough peak). The breakthrough reaches its maximum close the moment relating to profile nr. 5, corresponding to the t_0-time of the column. After the passage of this breakthrough part, the concentration of eluting analytes does not return to zero but stays at a small, yet clearly non-zero value because of the continuous (albeit slow) elution of the analytes species that dropped out of the sample solvent band.

While the peak profiles in Fig. 1 b appear to lose mass (cf. reducing peak area), it is very important to note these profiles only represent the concentration C_m in the mobile phase, while the concentration C_s in the stationary phase is in fact K times (K=phase equilibrium constant) higher. Fig. 1d shows the stationary phase concentration C_s corresponding to the profiles shown in Fig. 1b. Near their upstream end, these profiles display a very sharp peak, rapidly transiting into a substantially flat part. As the sample band progresses through the column, this flat part gradually expands in width until the end of the column at x=3 cm is reached. The C_s-value in this flat part is dictated by the fact that the analytes in the sample solvent band have a concentration C_m=1. Since the retention factor k_s in the sample solvent (ϕ_S=0.50) in the present example is equal to k_s=0.1685, the corresponding particle-zone equilibrium constant K is equal to $K=k_0V_m/V_s= k(1-\varepsilon_T)/\varepsilon_T = 0.3932$ (assuming ε_T=0.7). We can hence expect a C_s-concentration $C_s=K\cdot C_m=0.3932\cdot 1=0.3932$ wherever C_m=1 concentration in the injection band and this is indeed the level at which the flat part of the C_s-profiles is situated. Upstream of the sample solvent band, the C_s-concentration remains at this level, as there is no driving force to deplete the stationary phase. What does change is the C_m-concentration, which, given the retention factor k_0 in the weak solvent (ϕ_0=0.01) preceding and proceeding the sample solvent band is equal to k_0=17.75, can be expected to be $K=k_0V_m/V_s= k(1-\varepsilon_T)/\varepsilon_T = 41.42$ times lower than the C_s-concentration. And as can be noted from the inset of Fig. 1b this is indeed the case. Turning now to the sharp peak at the upstream end of the C_s-profile, a detailed analysis of the profiles (data not shown) shows this is created when the upstream tail of the band enters the column. As ϕ rapidly drops from ϕ=0.5 to 0.01 in this tail part, the analyte species entering the column in this tail end slow down much more abruptly than their counterparts that entered the column earlier. This leads to a local accumulation of species, which is further enhanced by the fact that the analytes following behind do not experience this deceleration effect and keep on entering the column with an unretained velocity (no stationary phase before x=0). The subsequent profiles 2-6 in Fig. 1b and 1d show how this accumulated sharp peak slowly moves (in fact it does so with a velocity $u_0/(1+17.55)$ given the fact that k=17.75 in the ϕ=0.01 mobile phase in the present example.

At later stages of the elution process (cf. Figs. 1c and 1f), i.e., when the gradient program has increased the fraction of organic modifier to a sufficiently high level at the inlet of the column, the increase in solvent strength gradually releases the retained species that are distributed over the entire column length. As these species gradually dissolve again into the mobile phase, their velocity increases. And as the fraction ϕ of organic modifier is higher on the left-hand side than on the right-hand side, the upstream situated species migrate faster than the downstream moving species, and a self-sharpening effect again establishes. As a consequence, the upstream side of the species band rapidly grows in height ('scooping-up effect"). Obviously, this self-sharpening effect is highest at the upstream end of the band, as this is where species pick up their highest velocity, but the effect nevertheless occurs over the entire length of the column, thus giving rise to an increase of the C_m-concentration over the entire extent of the species profile.

Subsequently focusing on the value of C_m along the vertical dashed line at x = 0.03 cm (detector line) in Fig. 1c, it can be understood how the species concentration gradually increases at the detector when the spatial profiles 7-11 subsequently hit the detector line. The response at the detector obviously reaches its maximum shortly after the moment at which profile nr. 10 is established. Subsequently, the concentration at the detector rapidly drops to zero (cf. profile 11). This second peak top (cf. "B" in Fig. 1a) is further referred to as the retained peak, as it elutes near the time of elution expected based on the gradient program and the retention parameters of the analyte.

In summary, the entire process described above leads to a double headed-peak shape, with one maximum near the breakthrough peak and one maximum near the retained peak position (=position where analytes are expected to elute when the volume is sufficiently small). In between, the signal does not return to the baseline, as a continuous stream of analyte species that "leaked" out of the sample solvent band close to the end of the column keeps on eluting off the column, albeit at a low concentration and a low velocity ($u=u_0/(1+17.75)$). For the sake of comparison, Fig. S-2 in the SM shows that when the sample is dissolved in the solvent marking the onset of the gradient a single neat peak is obtained is in this case the analytes are so strongly retained they immediately leave the sample band when entering the column.

Fig. 3 shows how strongly the profile recorded at the detector response depends on the retention parameters of the solute. Adopting the Neue-Kuss model, where the retention is described by k_w (=retention factor in 100% water), S_1 (=solvent strength parameter) and S_2 (describes the curvature of the model) via $k=k_w(1+S_2\phi)^2\cdot e^{-S1\phi/(1+S2\phi)}$, Fig. 3a shows that the broad, double-headed response profile similar to the one encountered in Fig. 1 is typically observed when k_w is sufficiently low. For larger k_w, the chromatogram narrows and ultimately, when k_w is sufficiently large, displays the shape and elution time of a normally retained peak. This can be understood from the fact that, the lower k_w, the lower the actual retention factor k_s experienced by the species in the solvent sample band, and hence the further they can travel without leaving this band. If k_w is sufficiently low and when the volume of the band is large enough, some of the sample species will still reside in the injection solvent band when this reaches the detector and are hence detected as a "breakthrough" part. In the extreme limit (k_w=0), all species reach the detector together with the injection solvent band and there is only a breakthrough peak. In the other limit (k_w=+ ∞), all species are so strongly retained at the inlet of the column that they immediately leave the injection solvent band, in which case there is no breakthrough part of the peak, and all species now elute within the retained part, reaching

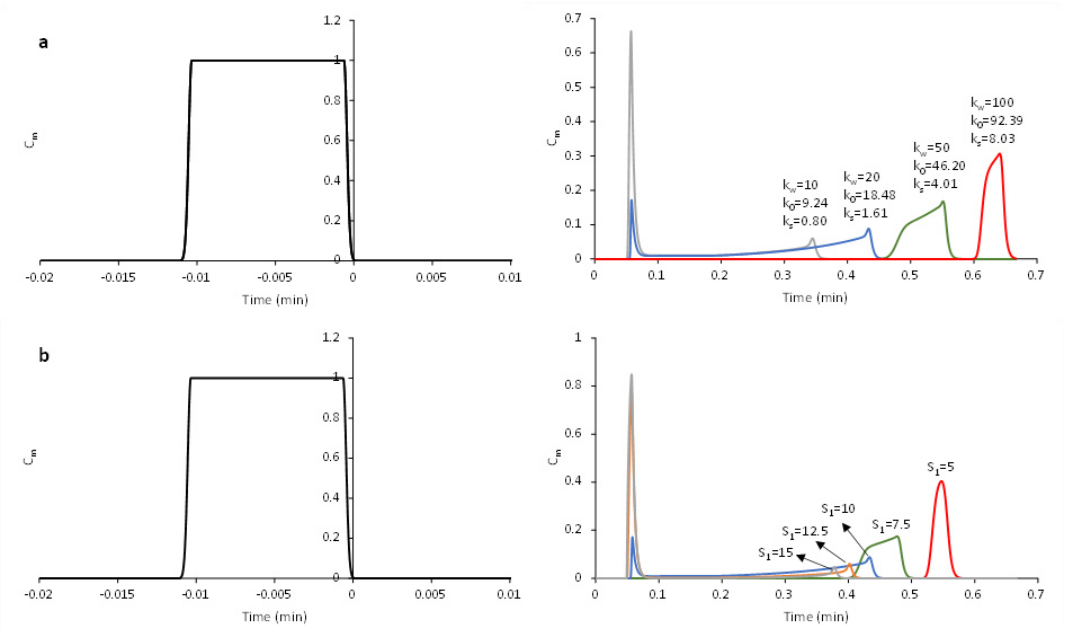

Fig. 3. Simulated mobile phase concentration (C_m) profiles as a function of time as recorded at x=L in response to a rectangular injection band ($V_{p,inj}$=25 µL) for **(a)** a series of analytes with different k_w-value (k_w=10 (grey), 20 (blue), 50 (green), 100 (red)) and same S_1=10 and S_2=1, and **(b)** a series of analytes with different S_1-value (S_1=5 (red), 7.5 (green), 10 (blue), 12.5 (orange), 15 (grey)) and same k_w=20 and S_2=1. Other conditions same as in Fig. 1.

the detector by means of the gradient. The profile for the highest k_w in Fig. 3a approaches this situation. For the intermediate k_w-values, it is obvious to observe some mixed-mode behavior. The effect of S_1 (Fig. 3b) can be rationalized following the same reasoning as above. Since all cases have the same k_w, the highest S_1-values now correspond to the case producing the lowest retention factor k_s experienced in the sample solvent, thus transporting the largest fraction of species along with the sample band through the column and creating the largest breakthrough curve (grey curve). The lowest S_1-values obviously leads to the highest k_s, such that the analyte species already leave the sample band at the column's head, and will therefore reach the detector by virtue of the mobile phase gradient as a normal chromatographic peak at the retention time predicted by the Neue-Kuss model (red curve).

Fig. 4 investigates the effect of the column's band broadening on the concentration profiles recorded by the detector (only zoom-ins of the breakthrough-fraction and the retained peak fraction are shown for the sake of compactness). All represented cases relate to the same rectangular injection band shape, and are compared to a base case (grey curve) where the band broadening (axial dispersion) for both the sample solvent and the analyte is the same and represented by a value D_{ax}= $3.86{\cdot}10^{-8}$ m^2/s in Eq. (1). Keeping the axial dispersion coefficient of the analyte ($D_{ax,an}$) constant and gradually increasing that of the solvent ($D_{ax,solv}$), which corresponds to the practically most relevant case, Figs. 4a shows that a larger $D_{ax,solv}$ tends to lower the breakthrough fraction while increasing (albeit it more moderately) the retained peak fraction. This can be understood as follows. The higher $D_{ax,solv}$, the faster the sample solvent will mix with the surrounding low ϕ-mobile phase. This leads to a reduction of the overall ϕ in the band (especially near its ends), giving rise to larger fractions of the sample band that are subjected to a retention factor > k_s, such that more species tend to leave the sample solvent and hence no longer reach the detector together with the breakthrough fraction in the sample solvent band. As more analyte species drop out, it is also physically straightforward that more species only pick up speed again when they are caught up by the gradient and hence reach the detector with the retained peak fraction. Increasing $D_{ax,an}$, while keeping $D_{ax,solv}$ constant, the effect is smaller (Fig. 4b), basically boiling down to the regular effect an increased band broadening can be expected to have on a chromatographic peak: the higher the axial dispersion, the broader the peak. The increasing asymmetry and shift of the peak apex to earlier elution times of the breakthrough peak that can be observed with increasing $D_{ax,an}$ in Fig. 4b can be understood as follows (see also Fig. S-3 in the Supplementary material (SM) for a detailed study of the on-column C_m- and the ϕ-profiles in case of the lowest and the highest $D_{ax,an}$): while the downstream flank (=fronting end) of the analyte band can display its normal, unrestricted band broadening behavior as it is immersed in the high $\phi = \phi_S$-sample solvent prevailing to its right, the upstream flank C_m-profile of the analyte band inevitably (because of the thermodynamic phase equilibrium that needs to be respected) coincides with the (steep) upstream flank of the sample solvent (see dashed vertical lines added to Fig. S-3). As a consequence, the drop in C_m observed at the upstream flank is not due to the band broadening but is dictated by the drop in ϕ along the upstream flank of the sample solvent band. This drop chases the analytes out of the mobile phase into the stationary phase. Since $D_{ax,solv}$ is kept constant in all elution profiles shown in Fig. 4b (and equal to the smallest considered $D_{ax,an}$), the discrepancy between the unrestricted band broadening at the downstream flank of the analyte band and the drop in concentration along the steep ϕ-curve at its upstream flank increases with increasing $D_{ax,an}$, hence the increasing asymmetry of the breakthrough peaks in the profiles obtained with increasing $D_{ax,an}$.

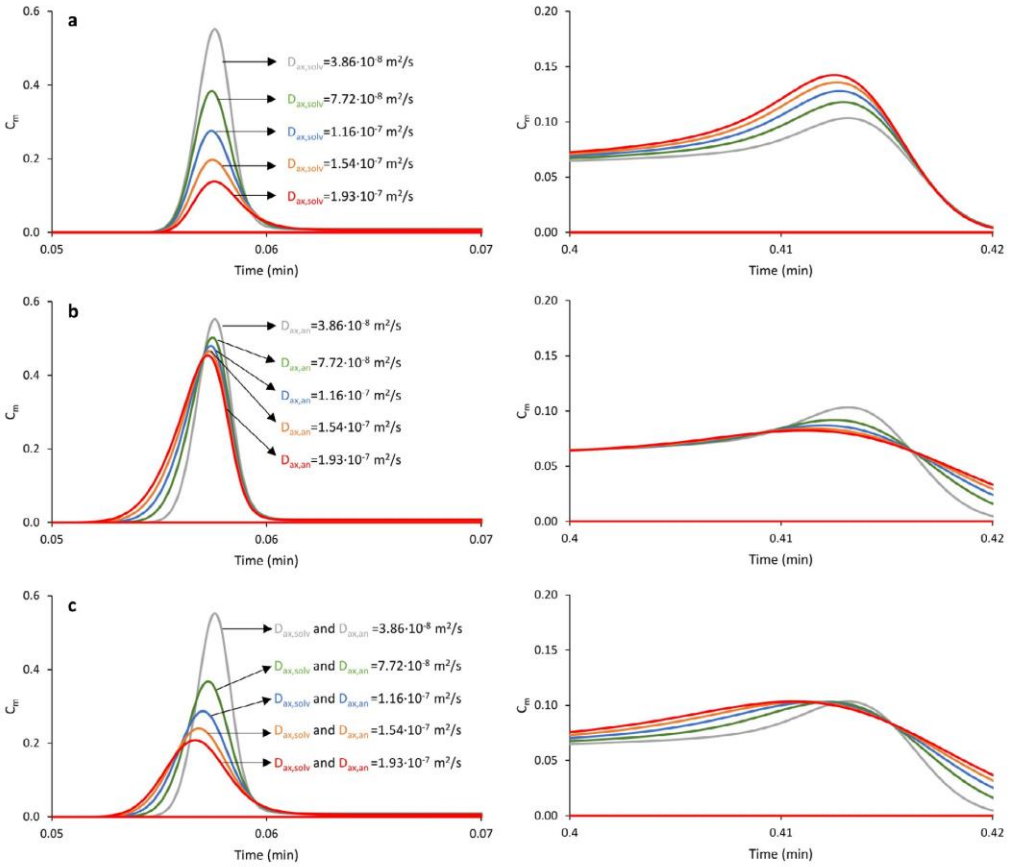

Fig. 4. Zoom-ins on the effect of the axial dispersion of the analyte ($D_{ax,anal}$) and the solvent ($D_{ax,solv}$) on the breakthrough-fraction and the retained peak fraction of the response profiles recorded as a function of time at x=L (rectangular injection band with V_{inj}=15 µL). **(a)** constant $D_{ax,an}$= 3.86·10⁻⁸ m²/s and varying $D_{ax,solv}$=3.86·10⁻⁸ m²/s (grey), 7.72·10⁻⁸ m²/s (green), 1.16·10⁻⁷ m²/s (blue), 1.54·10⁻⁷ m²/s (orange), 1.93·10⁻⁷ m²/s (red). **(b)** constant $D_{ax,solv}$ = 3.86·10⁻⁸ m²/s and varying $D_{ax,an}$ 3.86·10⁻⁸ m²/s (grey), 7.72·10⁻⁸ m²/s (green), 1.16·10⁻⁷ m²/s (blue), 1.54·10⁻⁷ m²/s (orange), 1.93·10⁻⁷ m²/s (red). **(c)** case with $D_{ax,solv}$ = $D_{ax,an}$ =3.86·10⁻⁸ m²/s (grey), 7.72·10⁻⁸ m²/s (green), 1.16·10⁻⁷ m²/s (blue), 1.54·10⁻⁷ m²/s (orange), 1.93·10⁻⁷ m²/s (red). Other conditions: S_1=12.5, S_2=0.7, k_w=20, u_0=0.0103 m/s and H=7.5 µm.

Increasing $D_{ax,an}$ and $D_{ax,solv}$ simultaneously (Fig. 4c), clearly a combination of both aforementioned effects is obtained, in agreement with one's physical expectations.

Obviously, the shape of the recorded elution profiles also depends strongly upon the injection volume (Fig. 5). The larger the volume of the sample solvent band, the larger the relative fraction of species in the breakthrough peak. This is due to the fact that, the wider the injection solvent band, the longer it takes the analyte to escape from the injection solvent, as it takes ever longer for the analytes entering the column near the downstream flank of the sample band (point A in Fig. 2a) to be overtaken by the upstream front of the sample band (point B in Fig. 2a). Under the conditions assumed in Fig. 5, the 50, 25, 15 and 12 μL injections are apparently wide enough to transport a fraction of the analytes through the column without having "leaked out" of the injection solvent band, thus displaying a breakthrough part. For the 50 μL injection, the breakthrough fraction is very large, while this fraction is only minimal for the 12 μL injection (cf. small bump around t=0.065 min in Fig. 5c). When the injection solvent band is small enough, all injected species leave the sample band before this reaches the end of the column, hence the absence of a breakthrough part in the elution profile for injection volumes 1, 5 and 10 μL. While the injection volumes $\geq$ 15 μL are large enough to spread the retained analyte species more or less uniformly across the entire column length during the passage of the injection solvent band (cf. situation for profiles 4, 5, 6 in Figs. 1b and 1e), the injection solvent bands with volumes $<$ 12 μL "lose" all the analyte species they initially contained before reaching the end of the column. The latter can be noted from the fact that the profiles corresponding to these volumes only start to rise well after the t_0-time of the column, i.e., well after the injection solvent band has left the column. This can be understood from the fact that, the smaller the sample band, the earlier on in the column all analytes will have left the injection solvent band. As a consequence, these species will not have travelled very far into the column at the moment at which they are caught up by the gradient and will hence reach the detector later. This explains why the rise in concentration observed in Figs. 5b and d (=zoom-in of b) starts ever later when the injection volume decreases (a detailed analysis of the establishment of the black-coloured profile in Fig. 5d is shown in Fig. S-4 of the SM wherein profile 1 is the axial C_m-profile at the moment of elution of the sample solvent band). Eventually, the 1 µL injection is so small that all species already dropped out of the injection solvent band in the very first fractions of the column. Consequently, they all basically start at the same starting point when they are picked up by the gradient and

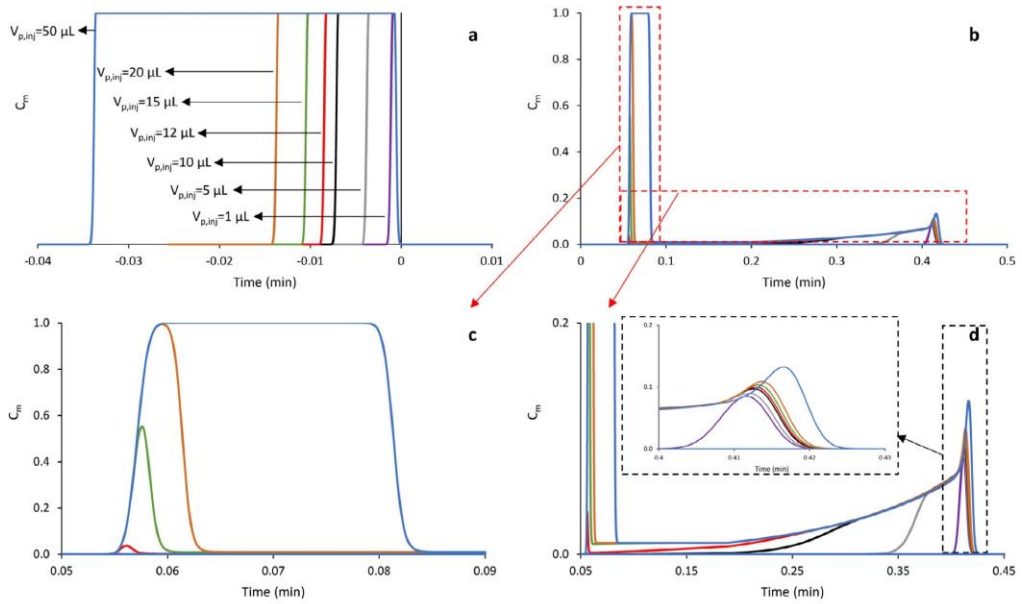

Fig. 5. **(a)** Rectangular injection bands with varying volume (V_{inj} = 1 µL(purple), 5 µL(grey), 10 µL(black), 12 µL(red), 15 µL(green), 25 µL(orange), 50 µL(blue)) leading to **(b)** a different mobile phase concentration (C_m) profile recorded as a function of time at x=L. **(c)** Zoom-in at bottom-part of y-axis of (b). **(d)** Zoom-in of (c) near the elution time of the retained peak fraction. Other conditions same as in Fig. 1.

hence reach the detector as a "normal" Gaussian peak without any fronting.

In fact, the conditions for the occurrence of a breakthrough peak can, with reference to Fig. 2a, easily be determined as follows, at least when neglecting the secondary effects originating from the band broadening process (most prominent for small injection volumes). Consider an analyte entering the column at the most downstream end of the sample band (point A). This will move with a velocity $u_A=u_0/(1+k_s)$ and will, since $u_A<u_0$, therefore eventually be caught up by the upstream flank of the injection solvent band which travels at a velocity u_0. Denoting the time at which point B catches up with point A is time t^*, we can now express that this is the moment at which both points have reached the same position $x=x^*$ in the column:

$$x^* = u_0 \cdot t^* = w_{p,col} + u_A \cdot t^* \tag{10}$$

wherein $w_{p,col}$ is the width of the band when present in the column and in contact with a stationary phase with retention factor k_s.

Replacing u_A by its relation to u_0 in Eq. (10), it is found that:

$$t^* = \frac{w_{p,col}}{u_0} \cdot \frac{1+k_s}{k_s} \tag{11}$$

Since the analytes at position A will be the last species leaving the injection solvent band (cf. Fig. 2a), we can express that there will always be a fraction of the analytes traveling through the column with the injection solvent band as long as the time t^* is not reached within the residence time of the sample solvent band. Translating this into distance, we can state that the response at the detector will display a breakthrough fraction when the catching up point x^* is situated after the detector, or $x^*>L$. Hence combining Eqs. (10) and (11), we find:

$$x^* = u_0 \cdot t^* = w_{p,col} \frac{1+k_s}{k_s} > L \tag{12}$$

Translating the on-column peak width into the on-column peak volume ($V_{p,col}$, assuming for simplicity a rectangular band shape) and comparing it to the injected peak volume ($V_{p,inj}$) measured before entering the column, considering that $V_{p,col}=A\cdot\varepsilon_T\cdot w_{p,col}=V_{p,inj}/(1+k_s)$, while the column void volume ($V_{0,col}$) can be written as $V_{0,col}=A\cdot\varepsilon_T\cdot L$, the condition to have a detector response with a breakthrough part expressed by Eq. (12) can simply be rewritten as:

$$V_{p,inj} > V_{0,col} \cdot k_s \tag{13}$$

In case of a Gaussian-shaped band with $w_{p,col}=4\sigma$, the right-hand-side of Eq. (13) needs to be multiplied with a factor 0.63 (i.e., $\sqrt{2}/4$).

Eq. (13) implies that, for example, for a column with volume 100 μL and an analyte displaying a retention factor of $k_s=0.5$ in the injection solvent, a breakthrough will occur for injection volumes exceeding 50 μL. When $k_s=0.1$, breakthrough will already occur for injection volumes in excess of $V_{p,inj}=10$ μL. The simulations in Fig. 5 have been carried out for a column volume of 72.7 μL, and with $k_s=0.1685$. Applying Eq. (13) then predicts the critical injection volume lies around 12 μL (12.25 μL to be precise). The fact that the 12 μL-case in Fig. 5 leads to a breakthrough that is barely significant (small bump around t_0-time in Fig. 5c) hence shows the simulations and the simple model developed above are in excellent agreement.

Using a similar calculation, it can be shown that the condition for which all sample species leave the sample band "early", defined here as having left the band within a distance not exceeding the initial width of the sample solvent band w_{solv} (with $w_{solv}=V_{inj}/\varepsilon_T.A=w_p^*(1+k_s)$ wherein w_p^* is the initial width of the species band), is simply given by:

$$k_s \geq 1 \tag{14}$$

To prove Eq. (14) it suffices to replace L by w_p on the right-hand side of Eq. (12).

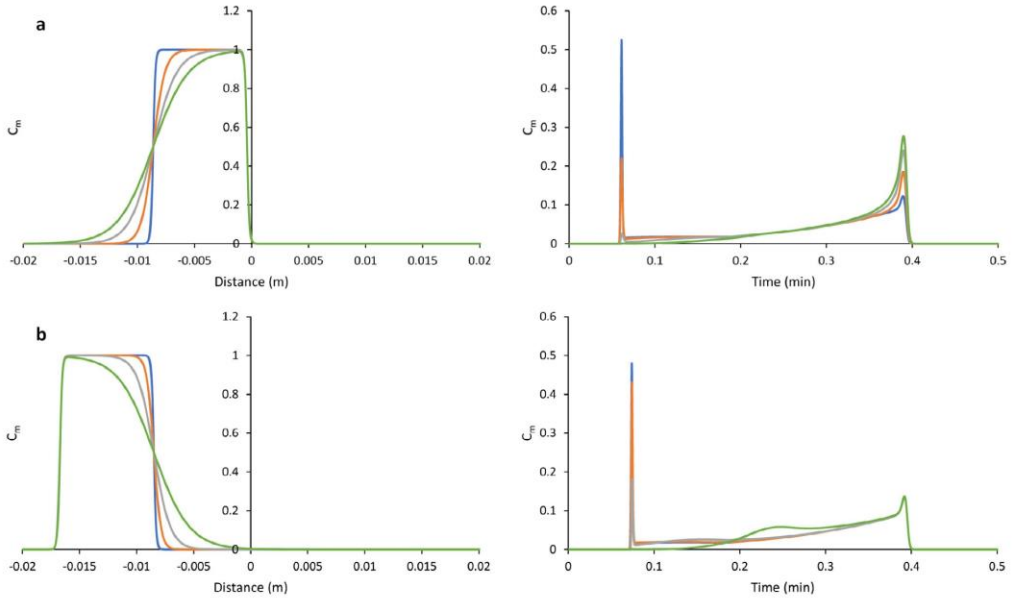

Fig. 6. Simulated mobile phase concentration (C_m) profiles as a function of time as recorded at x=L in response to an injection band with **(a)** profiles with various degrees of tailing in space: α_2=0.01 (blue), α_2=0.05 (orange), α_1=0.10 (grey), α_1=0.15 (green), and **(b)** profiles with various degrees of fronting in space= α_2=0.01 (blue), α_2=0.03 (orange), α_1=0.07 (grey), α_1=0.15 (green). When one α was varied the other one was put on 0.01. Other conditions: S_1=12.5, S_2=0.7, k_w=15, V_{inj}=20 µL, u_0=0.0103 m/s and H=7.5 µm.

Similarly, it can be demonstrated (replacing L by 2L on the right-hand side of Eq. (12)) that the condition leading to a breakthrough peak bringing half of the species to the detector while the other half of the band then reaches the detector at the expected retention time is given by:

$$V_{p,inj} = 2.V_{0,col} \cdot k_s \tag{15}$$

Eq. (15) predicts this condition corresponds, for the presently considered case with $V_{0,col}$=72.7 μL and with k_s=0.1685 to an injection volume of $V_{p,inj}$=24.5 μL. It has been verified by calculating the area under the breakthrough part of the 25 μL injection (orange-coloured curve) in Fig. 5 that this part of the curve indeed carries about 50% of the total injected mass (53% to be precise in represented case).

An important remark to be made concerning Fig. 5 is that, while this figure illustrates the effect of the injection volume $V_{p,inj}$ on the peak shape, the ultimate parameter controlling the detector response is in fact the relative peak volume, i.e. $V_{p,inj}/V_{0,col}$. This is shown in Fig. S-5 of the SM where the response to a 15 μL injection in a column with a 72.7 μL void volume overlaps fairly well with the response to a 30 μL injection in a column with a 145.4 μL void volume (at least provided the t_G and dwell time is doubled as well). The importance of the relative parameter $V_{p,inj}/V_{0,col}$ can also be inferred from the fact that, when dividing both sides of Eqs. (13) and (15) by $V_{0,col}$, expressions depending only on $V_{p,inj}/V_{0,col}$ and k_s are obtained. The small deviation between the two profiles in Fig. S-5 is due to secondary effects of band broadening which are not included in the simplified analysis in Eqs. (10)-(15).

Fig. 6 shows that not only the volume but also the actual shape of the injected band has an important effect on the resulting elution profile, with the shape of the tail (Fig. 6a) being significantly more important than the shape of the front (Fig. 6b). The explanation for this asymmetric behavior is the same as for the asymmetry discussed in Fig. 2b. Considering that the shape of the band flanks determines the amount of species that are present in a low ϕ-mobile phase and are hence much more strongly retained than the species in the center of the band where $\phi = \phi_S$, it is physically straightforward to expect that the initial shape of the downstream flank will always be largely wiped out by the fact that the retained species in this flank are always caught up and thus accelerated again by the high ϕ-region in the center of the sample band, while this self-sharpening catching-up effect does not occur at the upstream flank of the sample band. This implies the initial shape of the upstream flank is not rectified (even more, it will only spread out further by the column's dispersion) and hence directly determines the amount of analyte species staying behind the sample solvent band at each position along the entire column length. Obviously, this has a strong effect on the recorded elution profile for the short column (typical for 2D-LC) considered here. For example, Fig. 6a shows that, whereas a steep upstream flank leads to a narrow and high breakthrough peak, this breakthrough part no longer appears in case of a strongly tailed injection band (which is in fact a shape that is very relevant in practice [27]). This can be understood as follows: the more rectangular in shape, the larger the fraction of injected species that remain dissolved in the mobile phase with the highest ϕ at any time during the band's migration, and hence also the higher the fraction that can be transported through the column with the injection solvent peak. The wider the tail, the lower the average ϕ-value experienced by the migrating analytes and hence the more easily they leave the sample solvent band. When this average ϕ falls below a certain threshold, all analytes leave the injection solvent band by retention before the sample band reaches the end of the column, as happens in case of the orange curve. In this case, all analytes have to wait for the gradient to pick up speed and hence reach the detector all around the normal elution time. This explains the order of the retained peak apexes just before t=0.4 min.

As explained above, the effect of the shape of the downstream flank is much smaller (Fig. 6b). The retained peak part of the elu-

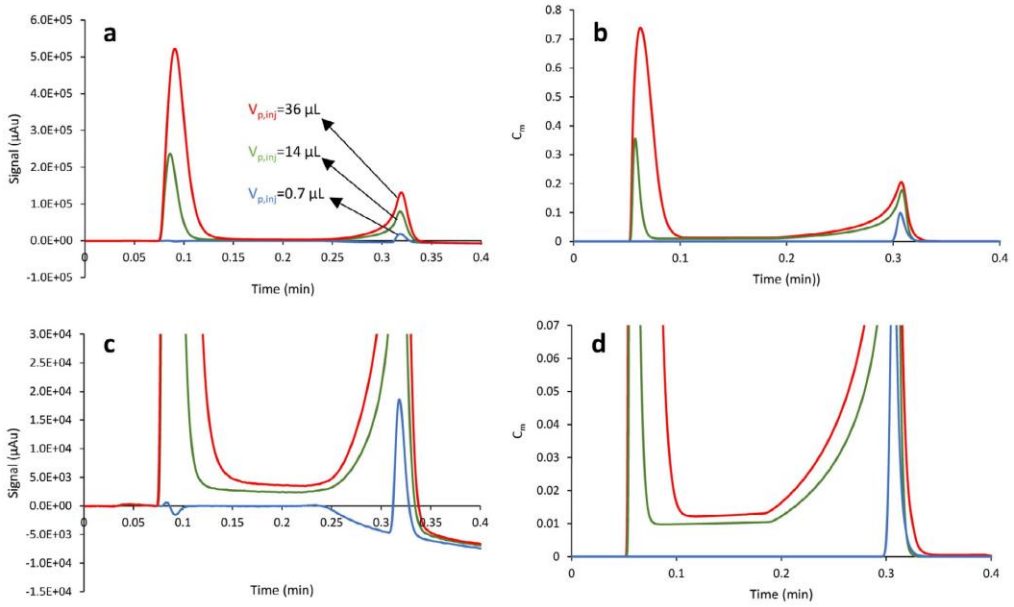

Fig. 7. Experimental **(a)** and simulated **(b)** breakthrough profiles for caffeine for three different peak volumes (36 µL (red), 14 µL (green) and 0.7 μL (blue)). **(c,d)** zoom-in on lower part of y-axis of (a,b) respectively. Adopted retention parameters: k_w=11, S_1=24, S_2=2, u_0=0.0103 m/s and H=7.5 µm. Gradient conditions: 1-45% B in 0.54 min (normalized gradient slope s of 4%). Injection profile (see Fig. S-7a of the SM) with α_1=0.03, α_2=0.2, t_{dwell}=8.4 s and F_v=1.5 ml/min in Eq. (9).

tion profile is even completely insensitive to this shape. The only difference is notable for the breakthrough peak, which seems to be engaged in a "communicating vessel" exchange with a small bump eluting shortly after the breakthrough peak. The fact that it is precisely the initial parts of the elution profile which are affected by the initial band shape is physically expected, as the species present in these early eluting fractions must have reached the detector while residing in the injected sample band, and are therefore most affected by the shape of the latter. The establishment of the small bump just before t=0.25 min can be best understood from the subsequent axial distribution profiles recorded during the simulation (Fig. S-6). These show that, in this particular case, the last fraction of analytes leaves the sample solvent band just before the end of the column. In addition, the rate with which the analytes leave this band strongly increases just when the last fraction of analytes leaves the sample solvent band, as the average ϕ-value experienced by the remaining analytes rapidly drops in these last moments (cf. average ϕ-value for situation in Figs. S-6c-d in the SM). This accelerated drop-out rate gives rise to a local maximum in the species concentration in the stationary phase (C_s), where the majority of the species are stored once they entered the low solvent-strength solvent (ϕ_0). The magnitude of this local maximum depends on the exact shape of the concentration gradients, such that it is more pronounced in some cases than in others. When this local maximum in the C_s-profile is formed far away from the column end, i.e., when all analytes leave the sample band sufficiently far away from the column's end, the presence of this local maximum is already eroded by the ongoing dispersion processes by the time this fraction of the analytes reaches the detector. However, when the local maximum is formed close to the column's end, as is the case for the situation in Fig. 6b, the local maximum is maintained in the C_m-concentration reaching the detector.

Figs. 7 and 8 investigate how well the simulations can represent the experimental data, taking caffeine (Fig. 7) and methylparaben (Fig. 8) as the test analytes and using the retention parameters (cf. k_w and S_i-values in Eq. 6) as measured via independent experiments. Important to note here is that the exact shape of the injected bands in the experimental part of this study is unknown to us and that the shape used here has been obtained by trying different variants of the peak shape represented by Eq. (9) and selecting the one providing the best agreement (see Fig. S-7a in SM for exact shape and degree of tailing and fronting of the considered injection profile). Whereas this profile has been obtained using Eq. (9), it should be remarked it is very similar to the profiles observed in [35] (appears backwards, because Figure S-7 is shown on the distance axis, and the profiles shown in [35] are shown on a time axis).

As can be noted, the qualitative agreement is very good, especially in terms of the effect of the injection volume. The small deviations can be attributed to differences in extra-column band broadening (only simulated here by adding a perfect mixer with volume= 6 µL= volume detector + post-column capillary), small uncertainties on the adopted relation between k and ϕ as well as the aforementioned uncertainty on the exact injection band shape. The slightly larger breakthrough times in the experiments compared to the simulations are probably due to the fact that the acetonitrile in the sample solvent band is also slightly retained as well [37]. The largest deviation between theory and experiment is observed in the initial part of the 25 μL-volume injection for methylparaben (blue curve in Fig. 8d). The deviation observed in this initial part is most probably due to the uncertainty on the exact shape of the injection band shape and the value of the retention parameters of the analyte, as the initial part of the response is most sensitive to the band shape and the retention parameters and we don't have an exact knowledge of them. The peculiar shape displayed by the blue curve in Fig. 8d between 0.2 and 0.3 min is caused by the same phenomena as already described via Fig. S-4 and S-6 of the SM. A detailed analysis of the present case is shown in Fig. S-7 of the SM.

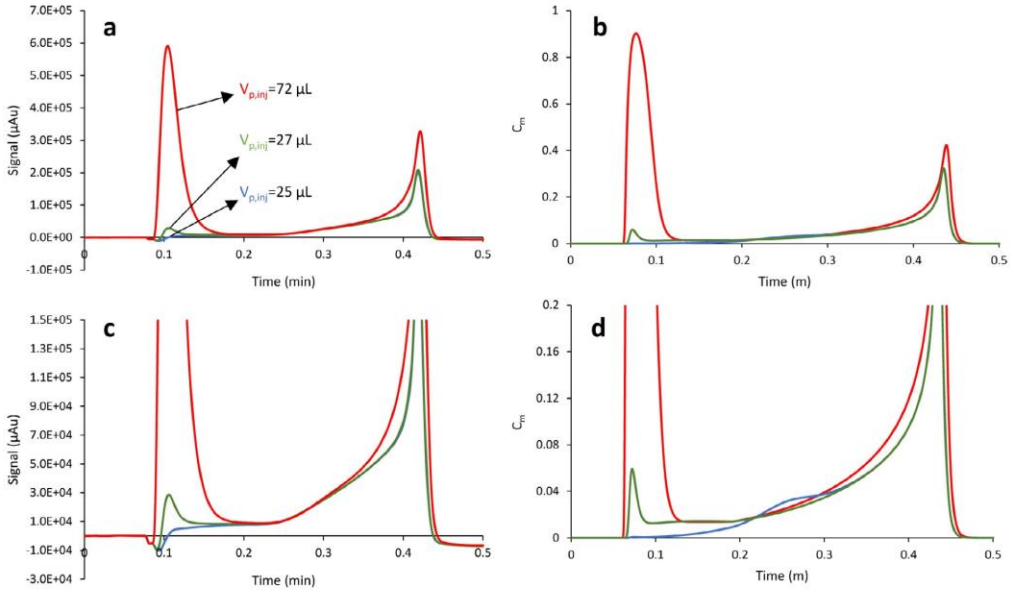

Fig. 8. Experimental **(a)** and simulated **(b)** breakthrough profiles for methylparaben for three different peak volumes (72 µL (red), 27 µL (green) and 25 μL (blue)). **(c,d)** zoom-in on lower part of y-axis of (a,b) respectively. Adopted retention parameters: k_w=23, S_1=13, S_2=0.7, u_0=0.0103 m/s and H=7.5 µm. Gradient conditions: 1-45% B in 0.54 min (normalized gradient slope s of 4%). Same injection profile as in Fig. 7.

4. Conclusions

Numerical simulations of the in-column axial distribution and migration of analyte species obtained by solving the general advection-dispersion mass balance for the analytes and the organic modifier used in the mobile phase and the sample solvent allow to understand the complex peak shapes that can be obtained when injecting large peak volumes (i.e., large with respect to the column volume) dissolved in a strong solvent, as can be the case in the ^{2}D in contemporary 2D-LC.

The axial concentration profiles produced by the simulations show how the elution under this condition basically occurs in two steps. In the first step, analyte species are transported along (part of) the column with the sample solvent band (unretained and hence moving at $u=u_0$) leading to two fractions: 1) a fraction that reaches the detector together with the sample solvent (fraction only if Eq. (13) is satisfied) and 2) a fraction leaving the sample solvent band through its upstream flank and thus being spread out along (part of) the column length. In a second step, the species from fraction 2), being concentrated in the stationary phase and hence moving very slowly as soon as they dropped out of the sample band and entered the low modifier mobile phase following behind the sample solvent band, are eventually "scooped up" by the gradient which accelerates them towards the detector where they are recorded as a retained peak. The latter originates from the self-sharpening effect (band compression) of the gradient profile on the spread-out species that left the sample solvent band. Depending across what fraction of the column length the analyte species are spread out (in turn depending on the injection volume and the retention factor in the sample solvent k_s), this retained peak can be very broad and fronted (large part of column length covered with analyte species when the onset of the gradient reaches the column) or have a "normal" retained peak shape (analytes already left the sample band shortly after entering the column). When the analyte species are distributed along the entire column length (i.e., when Eq. (13) is satisfied), the peak signal does not return to zero between the breakthrough and the retained peak part, thus forming an uninterrupted, double-headed peak.

Given the short length of the investigated column, the eventually recorded peak shape not only depends strongly on the volume but also on the exact shape of the injected sample band, as was also observed by Weatherbee et al. [35]. The degree of band broadening experienced by the analytes and the sample solvent (which are in general different from each other) contributes significantly to the eventual peak shape as well.

Whereas the simulation model is based on first-principles physical relations, with all its parameters fixed by taking the values measured in independent experiments and whereas the use of an idealized injection (rectangular) profile was already sufficient to predict the main characteristics of the observed breakthrough (% of breakthrough, general shape of the profile, elution times of breakthrough and retained fraction), a one-on-one agreement with all the fine details of the experimental response curve requires a close representation of the injection profile. As the latter information was experimentally inaccessible in the present study (see ref. [38] for a possible way to measure the injection profile), this had to be done by tuning the α_1- and α_2-parameters in the literature expression in Eq. (9). As all the other model parameters were obtained from independent experiments, the good agreement between the simulation results and the experiments can hence be used to conclude there is a sound theoretical explanation for the experimental observations.

Finally, it is important to remark that the observed effects of prak splitting are difficult to avoid in the context of 2D-LC given the many constraints that need to be satisfied when optimizing 2D-LC separations. The most effective way to avoid them would be to use on-line dilution, flow splitting or trap columns. Most of these solutions however lead to a loss of sensitivity and require a change in set-up.

Declaration of Competing Interest

The authors declare that they have no known competing financial interests or personal relationships that could have appeared to influence the work reported in this paper.

CRediT authorship contribution statement

Vincent Pepermans: Investigation, Software, Methodology, Writing – original draft. **Soraya Chapel:** Investigation, Formal analysis, Writing – review & editing. **Sabine Heinisch:** Conceptualization, Funding acquisition, Supervision, Writing – review & editing. **Gert Desmet:** Conceptualization, Funding acquisition, Supervision, Writing – original draft.

Acknoweldgments

VP and GD kindly acknowledge the financial support from from FWO-FNRS Belgium (Excellence Of Science grant nr. 30897864) .

Supplementary materials

Supplementary material associated with this article can be found, in the online version, at doi:10.1016/j.chroma.2021.462078.

References

[1] D.R. Stoll, X. Li, X. Wang, P.W. Carr, S.E.G. Porter, S.C. Rutan, Fast, comprehensive two-dimensional liquid chromatography, J. Chromatogr. A 1168 (1-2) (2007) 3–43, doi:10.1016/j.chroma.2007.08.054.
[2] M. Sarrut, A. D'Attoma, S. Heinisch, Optimization of conditions in on-line comprehensive two-dimensional reversed phase liquid chromatography. Experimental comparison with one-dimensional reversed phase liquid chromatography for the separation of peptides, J. Chromatogr. A 1421 (2015) 48–59, doi:10.1016/j.chroma.2015.08.052.
[3] A.F.G. Gargano, M. Duffin, P. Navarro, P.J. Schoenmakers, Reducing dilution and analysis time in online comprehensive two-dimensional liquid chromatography by active modulation, Anal. Chem. 88 (2016) 1785–1793, doi:10.1021/acs.analchem.5b04051.
[4] E. Sommella, O.H. Ismail, F. Pagano, G. Pepe, C. Ostacolo, G. Mazzoccanti, M. Russo, E. Novellino, F. Gasparrini, P. Campiglia, Development of an improved online comprehensive hydrophilic interaction chromatography × reversed-phase ultra-high-pressure liquid chromatography platform for complex multiclass polyphenolic sample analysis, J. Sep. Sci. 40 (10) (2017) 2188–2197, doi:10.1002/jssc.201700134.
[5] D.R. Stoll, P.W. Carr, Two-dimensional liquid chromatography: a state of the art tutorial, Anal. Chem. 89 (1) (2017) 519–531, doi:10.1021/acs.analchem.6b03506.
[6] M. Muller, A.G.J. Tredoux, A. de Villiers, Predictive kinetic optimisation of hydrophilic interaction chromatography × reversed phase liquid chromatography separations: Experimental verification and application to phenolic analysis, J.of Chromatogr.A 1571 (2018) 107–120, doi:10.1016/j.chroma.2018.08.004.
[7] D.R. Stoll, H.R. Lhotka, D.C. Harmes, B. Madigan, J.J. Hsiao, G.O. Staples, High resolution two-dimensional liquid chromatography coupled with mass spectrometry for robust and sensitive characterization of therapeutic antibodies at the peptide level, J. Chromatogr. B 1134-1135 (2019) 121832, doi:10.1016/j.jchromb.2019.121832.
[8] A.A. Alya, M. Muller, A. de Villiers, B.W.J. Pirok, T. Górecki, Parallel gradients in comprehensive multidimensional liquid chromatography enhance utilization of the separation space and the degree of orthogonality when the separation mechanisms are correlated, J. Chromatogr. A 1628 (2020) 461452, doi:10.1016/j.chroma.2020.461452.
[9] S. Chapel, F. Rouvière, S. Heinisch, A theoretical and practical approach to manage high peak capacity and low dilution in on-line comprehensive reversed-phase LC × reversed-phase LC: a comparison with 1D-reversed-phase LC, LCGC Eur. 33 (5) (2020) 17–26.
[10] P. Dugo, F. Cacciola, T. Kumm, G. Dugo, L. Mondello, Comprehensive multidimensional liquid chromatography: theory and applications, J. Chromatogr. A 1184 (1-2) (2008) 353–368, doi:10.1016/j.chroma.2007.06.074.
[11] G. Vanhoenacker, P. Sandra, K. Sandra, F. David, C. Brunelli, R. Szucs, M. Steenbeke, On-line two-dimensional liquid chromatography (2D-LC) for the analysis of pharmaceuticals, LCGC Eur. 29 (11) (2016) 610–617.
[12] K.J. Mayfield, R.A. Shalliker, H.J. Catchpoole, A.P. Sweeney, V. Wong, G.J. Guiochon, Viscous fingering induced flow instability in multidimensional liquid chromatography, J. Chromatogr. A 1080 (2) (2005) 124–131, doi:10.1016/j.chroma.2005.04.093.
[13] P. Jandera, T. Hájek, P. Česla, Effects of the gradient profile, sample volume and solvent on the separation in very fast gradients, with special attention to the second-dimension gradient in comprehensive two-dimensional liquid chromatography, J. Chromatogr. A. 1218 (2011) 1995–2006, doi:10.1016/j.chroma.2010.10.095.
[14] J. De Vos, G. Desmet, S. Eeltink, A generic approach to post-column refocusing in liquid chromatography, J. of Chromatogr. A 1360 (2014) 164–171, doi:10.1016/j.chroma.2014.07.072.
[15] D.R. Stoll, R.W. Sajulga, B.N. Voigt, E.J. Larson, L.N. Jeong, S.C. Rutan, Simulation of elution profiles in liquid chromatography – II: investigation of injection volume overload under gradient elution conditions applied to second dimension separations in two-dimensional liquid chromatography, J. Chromatogr. A 1523 (2017) 162–172, doi:10.1016/j.chroma.2017.07.041.
[16] R.J. Vonk, A.F.G. Gargano. E. Davydova, H.L. Dekker, S. Eeltink, L.J. de Koning, P.J. Schoenmakers, Reducing dilution and analysis time in online comprehensive two-dimensional liquid chromatography by active modulation, Anal. Chem. 87 (10) (2015) 5387–5394, doi:10.1021/acs.analchem.5b00708.
[17] J. De Vos, G. Desmet, S. Eeltink, Enhancing detection sensitivity in gradient liquid chromatography via post-column refocusing and strong-solvent remobilization, J Chromatogr A 1455 (2016) 86–92, doi:10.1016/j.chroma.2016.05.046.
[18] S.S. Jakobsen, J.H. Christensen, S. Verdier, C.R. Mallet, N.J. Nielsen, Increasing flexibility in two-dimensional liquid chromatography by pulsed elution of the first dimension: A proof of concept, Anal. Chem. 89 (17) (2017) 8723–8730, doi:10.1021/acs.analchem.7b00758.
[19] D.R. Stoll, K. Shoykhet, P. Petersson, S. Buckenmaier, Active solvent modulation: a valve-based approach to improve separation compatibility in two-dimensional liquid chromatography, Anal. Chem. 89 (17) (2017) 9260–9267, doi:10.1021/acs.analchem.7b02046.
[20] M. Pursch, A. Wegener, S. Buckenmaier, Evaluation of active solvent modulation to enhance two-dimensional liquid chromatography for target analysis in polymeric matrices, J. Chromatogr. A 1562 (2018) 78–86, doi:10.1016/j.chroma.2018.05.059.
[21] P. Yang, W. Gao, T. Zhang, M. Pursch, J. Luong, W. Sattler, A. Singh, S. Backer, Two-dimensional liquid chromatography with active solvent modulation for studying monomer incorporation in copolymer dispersants, J. Sep. Sci. 42 (17) (2019) 2805–2815, doi:10.1002/jssc.201900283.
[22] Y. Oda, N. Asakawa, T. Kajima, Y. Yoshida, T. Sato, On-line determination and resolution of verapamil enantiomers by high-performance liquid chromatography with column switching, J. Chromatogr. 541 (1991) 411–418, doi:10.1016/S0021-9673(01)96013-3.
[23] E. Fornells, B. Barnett, M. Bailey, R.A. Shellie, E.F. Hilder, M.C. Breadmore, Membrane assisted and temperature controlled on-line evaporative concentration for microfluidics, J. Chromatogr. A 1486 (2017) 110–116, doi:10.1016/j.chroma.2016.12.003.
[24] M.E. Creese, M.J. Creese, J.P. Foley, H.J. Cortes, E.F. Hilder, R.A. Shellie, M.C. Breadmore, Longitudinal on-column thermal modulation for comprehensive two-dimensional liquid chromatography, Anal. Chem. 89 (2017) 1123–1130, doi:10.1021/acs.analchem.6b03279.
[25] B. Ji, B. Xia, J. Liu, Y. Gao, L. Ding, Y. Zhou, Application of fractionized sampling and stacking for construction of an interface for online heart-cutting two-dimensional liquid chromatography, J. Chromatogr. A 1466 (2016) 199–204, doi:10.1016/j.chroma.2016.09.014.
[26] M. Enmark, D. Asberg, A. Shalliker, J. Samuelsson, T. Fornstedt, A closer study of peak distortions in supercritical fluid chromatography as generated by the injection, J. Chromatogr. A 1400 (2015) 131–139 http://dx.doi.org/10.1016/j.chroma.2015.04.059.
[27] L.N. Jeong, R. Sajulga, S.G. Forte, D.R. Stoll, S.C. Rutan, Simulation of elution profiles in liquid chromatography–I: gradient elution conditions, and with mismatched injection and mobile phase solvents, J. Chromatogr. A. 1457 (2016) 41–49 http://dx.doi.org/10.1016/j.chroma.2016.06.016.
[28] F. Gritti, M. Gilar, J. Hill, Mismatch between sample diluent and eluent: maintaining integrity of gradient peaks using in silico approaches, J. Chromatogr. A 1608 (2019) 460414, doi:10.1016/j.chroma.2019.460414.
[29] S.R. Groskreutz, S.G. Weber, Temperature-assisted solute focusing with sequential trap/release zones in isocratic and gradient capillary liquid chromatography: simulation and experiment, J. Chromatogr. A 1474 (2016) 95–108, doi:10.1016/j.chroma.2016.10.062.
[30] L.N. Jeong, S.C. Rutan, Simulation of elution profiles in liquid chromatography – III. Stationary phase gradients, J. Chromatogr. A 1564 (2018) 128–136, doi:10.1016/j.chroma.2018.06.007.
[31] H. Poppe, J. Paanakker, M. Bronckhorst, Peak width in solvent-programmed chromatography: I. general description of peak broadening in solvent-programmed elution, J. Chromatogr. A 204 (1981) 77–84, doi:10.1016/S0021-9673(00)81641-6.
[32] L.N. Jeong, R. Sajulga, S.G. Forte, D.R. Stoll, S.C. Rutan, Simulation of elution profiles in liquid chromatography–I: gradient elution conditions, and with mismatched injection and mobile phase solvents, J. Chromatogr. 1457 (2016) 41–49, doi:10.1016/j.chroma.2016.06.016.
[33] R. Kaliszan, T. Bączek, A. Bucinski, B. Buszewski, M. Sztupecka, Prediction of gradient retention from the linear solvent strength (LSS) model, quantitative structure-retention relationships (QSRR), and artificial neural networks (ANN), J. Sep. Sci. 26 (2003) 271–282, doi:10.1002/jssc.200390033.
[34] U.D. Neue, Nonlinear retention relationships in reversed-phase chromatography, Chromatogr 63 (2006) S45–S53.

[35] S.L. Weatherbee, T. Brau, D.R. Stoll, S.C. Rutan, M.M. Collinson, Simulation of elution profiles in liquid chromatography – IV: experimental characterization and modeling of solute injection profiles from a modulation valve used in two-dimensional liquid chromatography, J. Chromatogr. A 1626 (2020) 461373, doi:10.1016/j.chroma.2020.461373.
[36] W.H. Press, S.A. Teukolsky, W.T. Vetterling, B.P. Flannery, in: Numerical Recipes: The art of Scientific Computing, 3rd ed., Cambridge University Press, New York, USA, 2007, p. 1245.
[37] F. Gritti, G. Guiochon, Separations by gradient elution: Why are steep gradient profiles distorted and what is their impact on resolution in reversed-phase liquid chromatography, J. Chromatogr. A 1344 (2014) 66–75, doi:10.1016/j.chroma.2014.04.010.
[38] A. Moussa, T. Lauer, D. Stoll, G. Desmet, K. Broeckhoven, Numerical and experimental investigation of analyte breakthrough from sampling loops used for multi-dimensional liquid chromatography, J. Chromatogr. A 1626 (2020) 461283, doi:10.1016/j.chroma.2020.461283.

D.Supplementary Information for Article 7:

Comparison of existing strategies for keeping symmetrical peaks in on-line Hydrophilic Interaction Liquid Chromatography x Reversed-Phase Liquid Chromatography despite solvent strength mismatch

Soraya Chapel, Florent Rouvière, and Sabine Heinisch
Journal of Chromatography A, **2021**, 1642, 462001
DOI: 10.1016/j.chroma.2021.462001

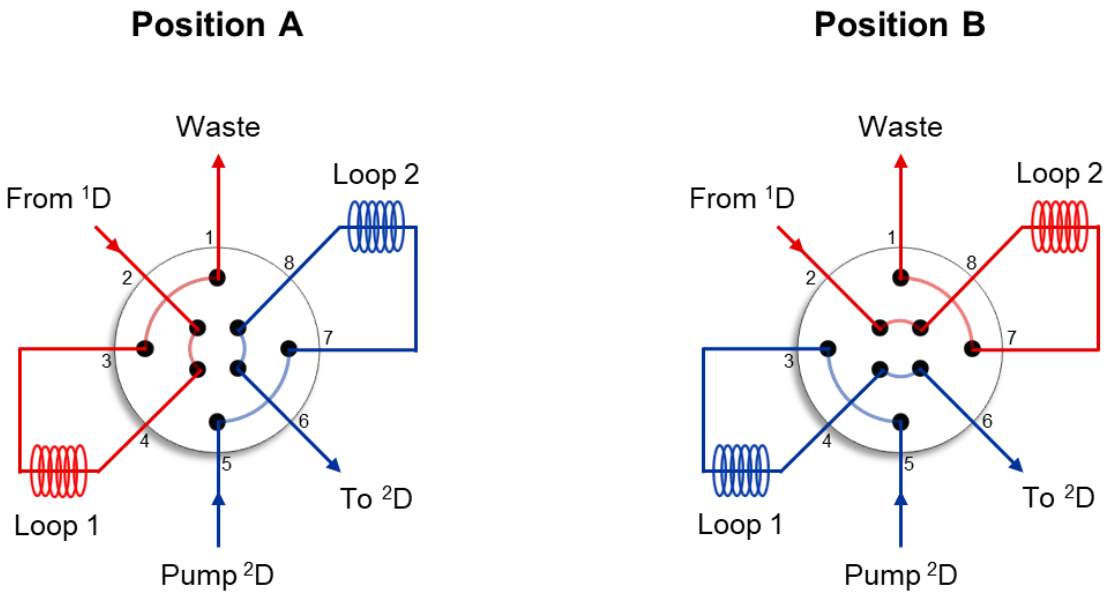

Fig. S1: Schematic representation of the 2-position/4-port duo-valve operation.

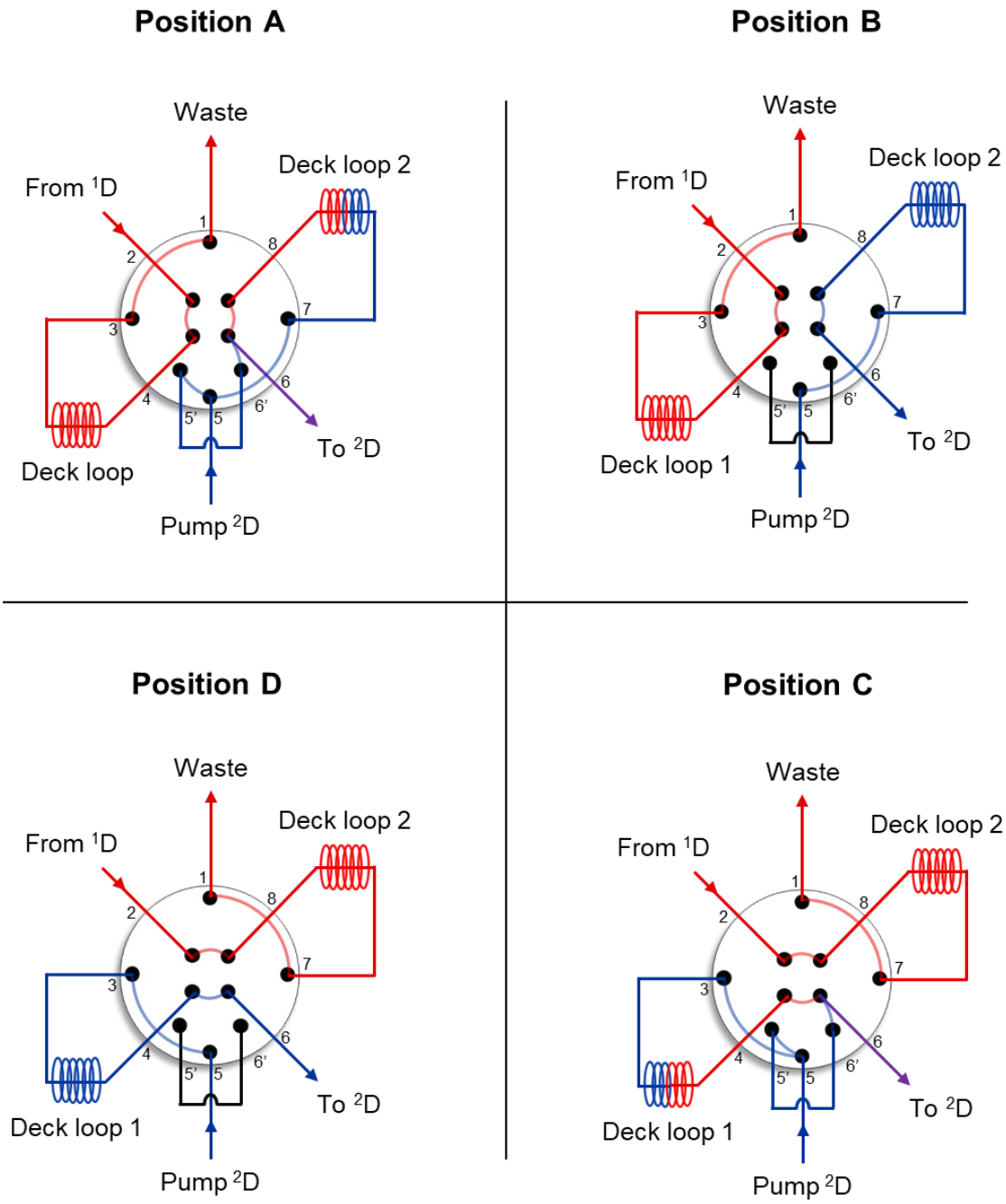

Fig. S2: Schematic representation of the ASM valve operation.

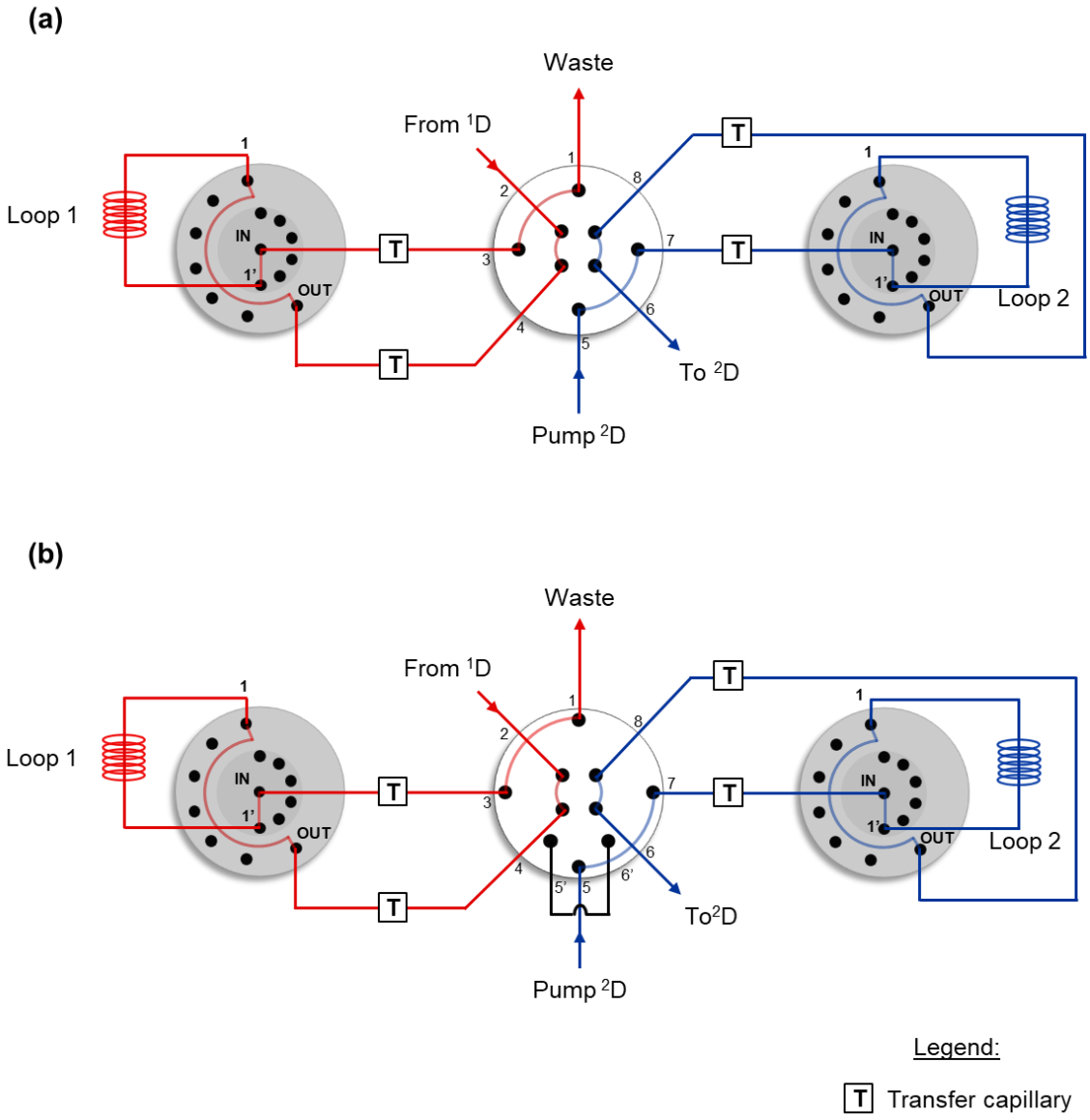

Fig. S3: Schematic representation of the two setups with the two parking decks valves. (a) Setup used for on-line dilution with make-up flow and (b) setup used for on-line dilution with ASM. The main valve is connected to two deck valves (one for each loop) using four 1.9-µL transfer capillaries. The two loops (180 µL for (A) and 40 µL for (B) are mounted to the two deck valves (one on each deck).

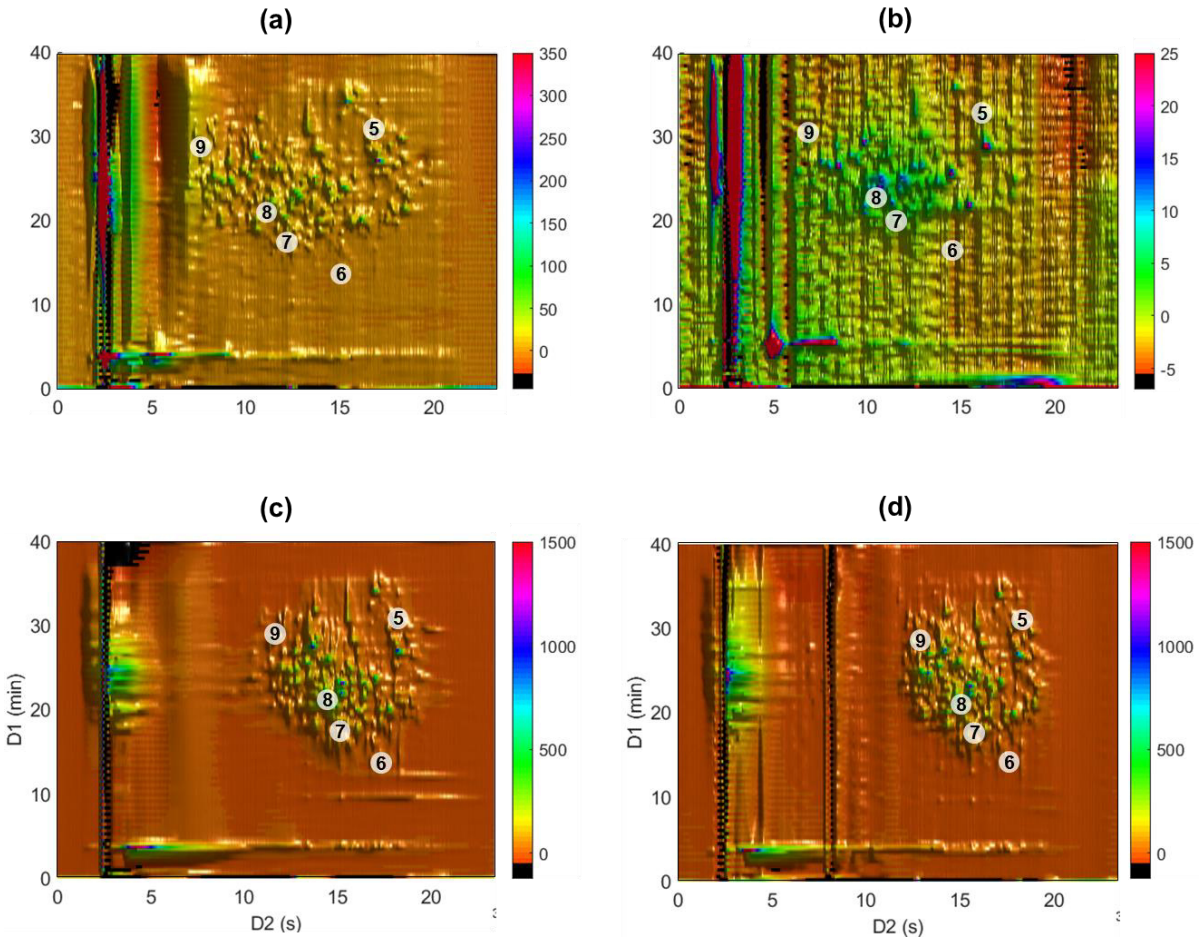

Fig. S4: Entire 2D-chromatograms obtained for the separation of a tryptic digest of six proteins in on-line HILIC x RPLC using (a) Total Breakthrough strategy, (b) Flow splitting strategy (split 1:9), (c) On-line dilution with make-up flow strategy, and (d) On-line dilution with ASM strategy. The numbers on each map indicate the location of the five EICs shown in Figs. 4-8 in the main paper (each number corresponding to the associated figure). UV detection at 210 nm. Conditions are given in the experimental section and Table 1.

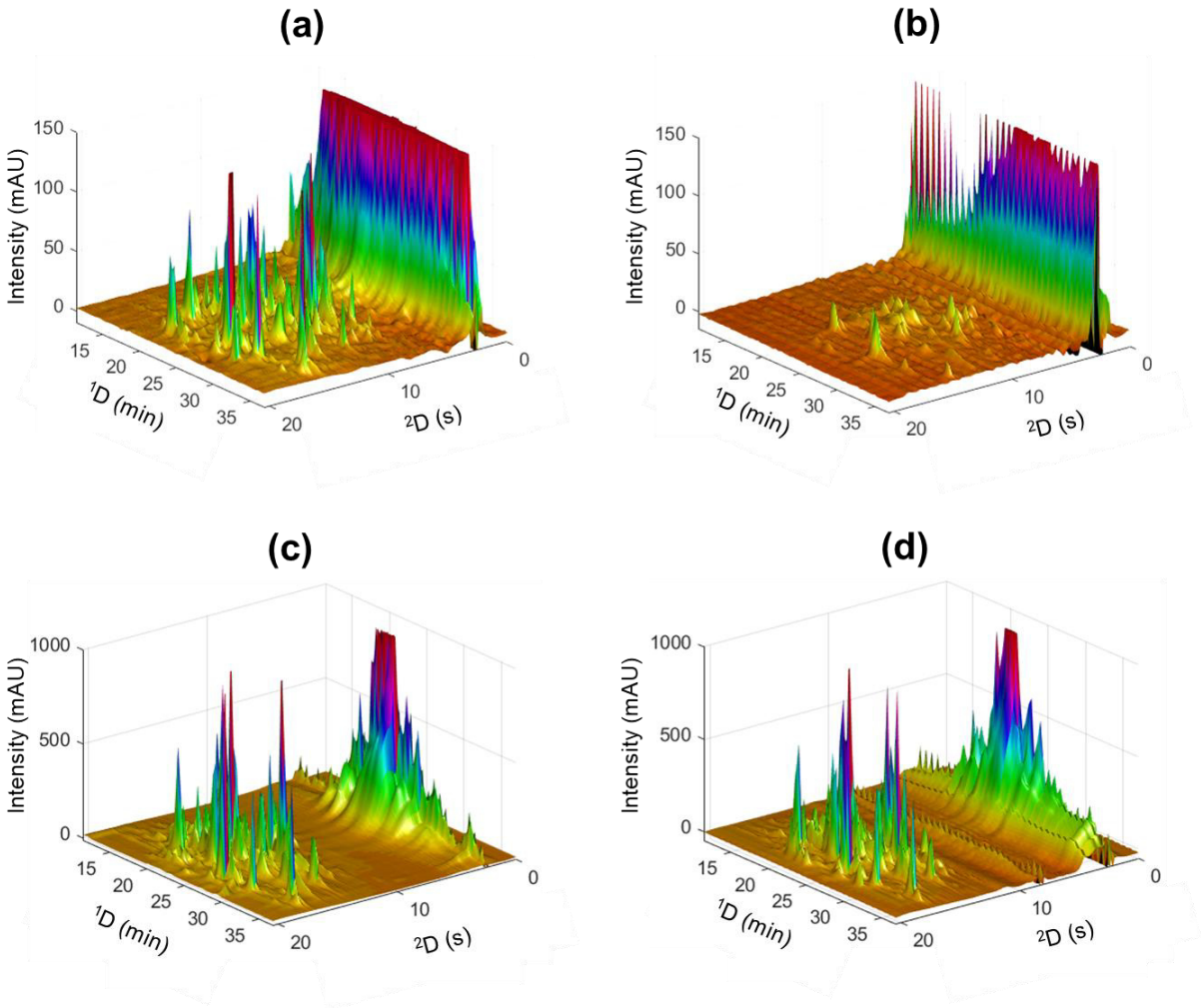

Fig. S5: On-line HILIC x RPLC separations (3D-chromatograms) of a tryptic digest of six proteins with (a) Total Breakthrough strategy, (b) flow splitting strategy (split 1:9), (c) On-line dilution with make-up flow strategy, and (d) On-line dilution with ASM strategy. UV detection at 210 nm. Other conditions given in the experimental section and Table 1.

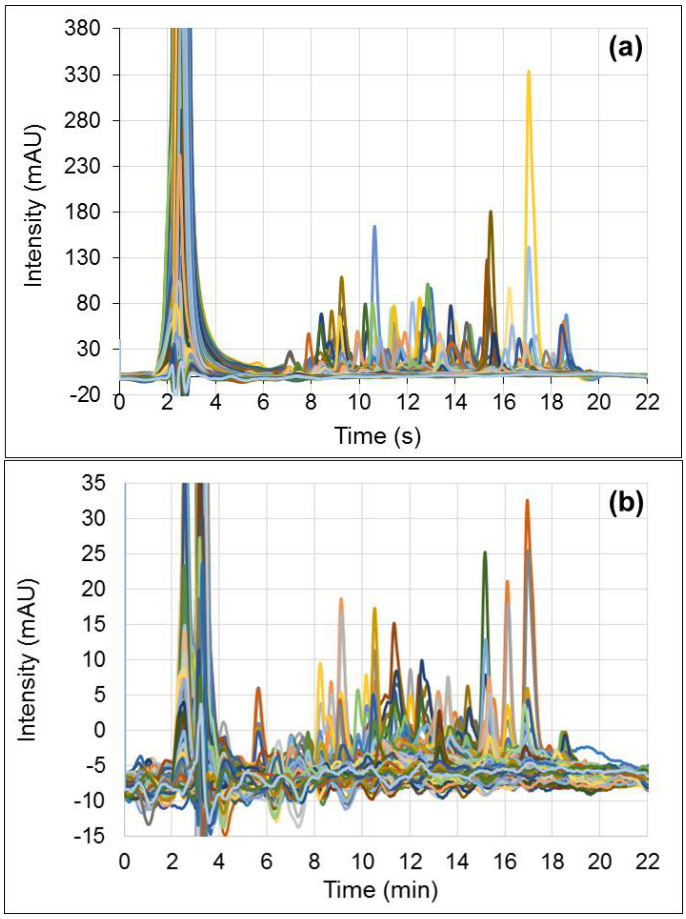

Fig. S6: ^{2}D-chromatograms overlay for (a) Total Breakthrough strategy and (b) flow splitting strategy highlighting the difference in peak intensity between the two strategies. Conditions are given in the experimental section and Table 1.

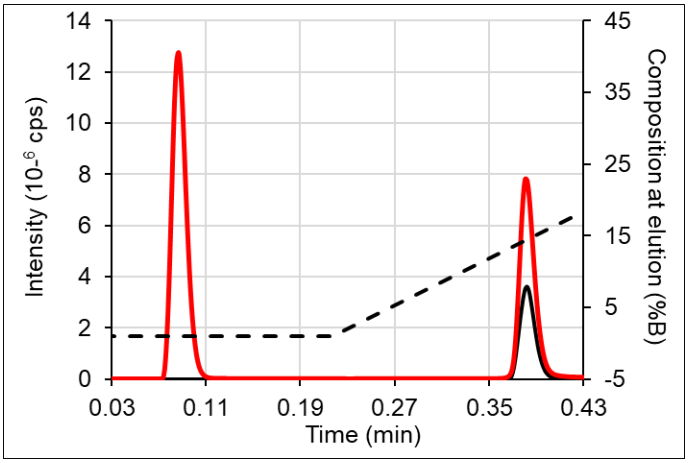

Fig. S7: Superposition of chromatograms highlighting the occurrence of Total Breakthrough for a small monocharged analyte (Propranolol). Sample solvent: 50:50 H2O/ACN. Injection volumes: 0.7 µL (black line) and 4.5 µL (red line) corresponding to 1% and 6.2% of the column void volume (V_0), respectively. Conditions: Acquity CSH C18 column (30 x 2.1 mm, 1.7 µm), flow rate: 1.5 mL/min, temperature: 80°C, mobile phase A: H2O + 0.1% FA and B: ACN + 0.1% FA (pH = 2.7), gradient elution: 1-45-1-1% B in 0-0.54-0.59-1 min (s = 4%). ESI-MS detection in positive mode with single ion recording (SIR) of m/z = 260.2.

E. Supplementary Information for Chapter VI:

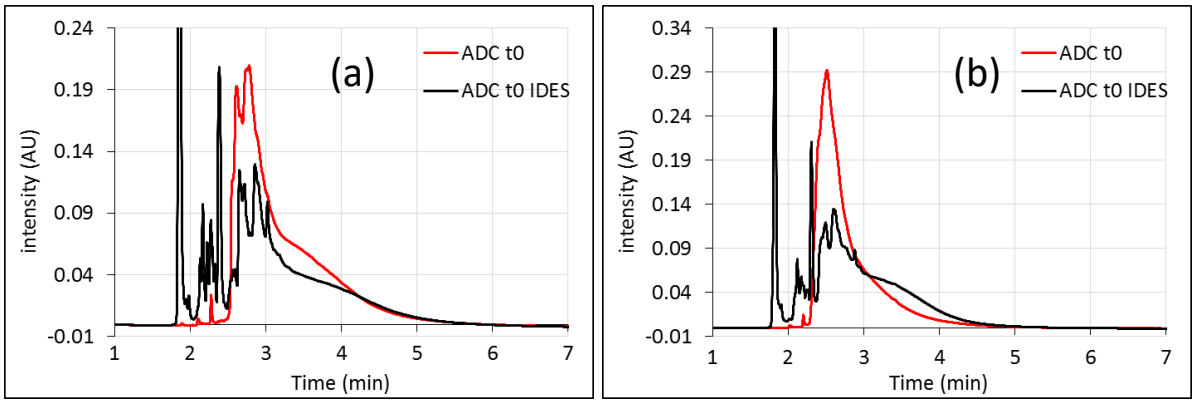

Fig. VI-S1: 1D-RPLC-UV (280 nm) analyses of intact (red) and IdeS treated ADC-S01 (black) using (a) Bioresolve RPmAb (50 x 2.1 mm, 2.7 µm) or (b) Acquity BEH C4 (50 x 2.1 mm, 1.7 µm) columns. Same other conditions as in Fig. VI-4b.

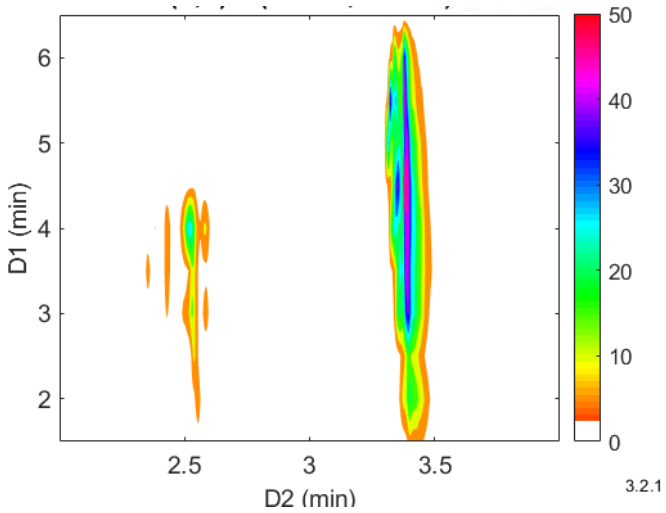

Fig. VI-S2: Contour plot (UV, 280nm) of optimized on-line sCEX x RPLC separation of IdeS-treated ADC-S01 sample. See conditions in Table VI-1.

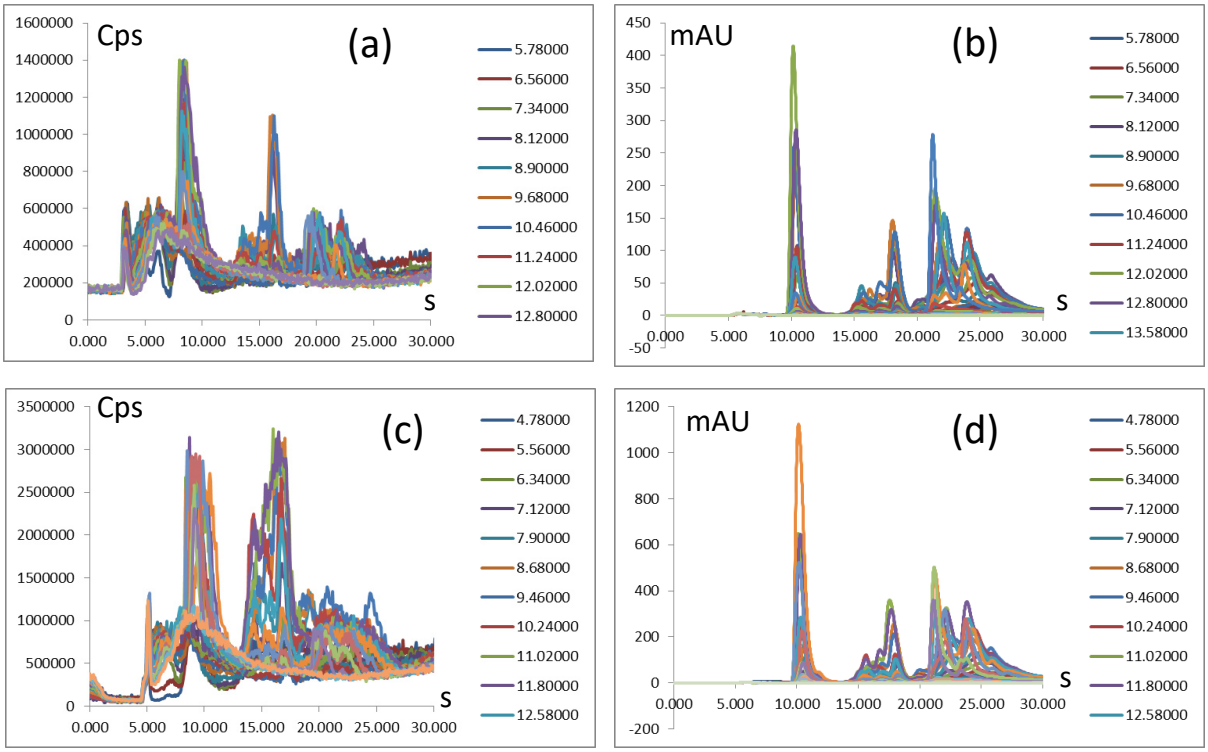

Fig. VI-S3: Overlaid ^{2}D-chromatograms of on-line CEX x RPLC analysis of IdeS treated ADC-S01 sample with (a, b) 40 µL or (c, d) 80 µL injected in ^{1}D. (a, c) MS detection (TIC, ESI+) and (b, d) UV detection 280 nm. See conditions in Table VI-1.

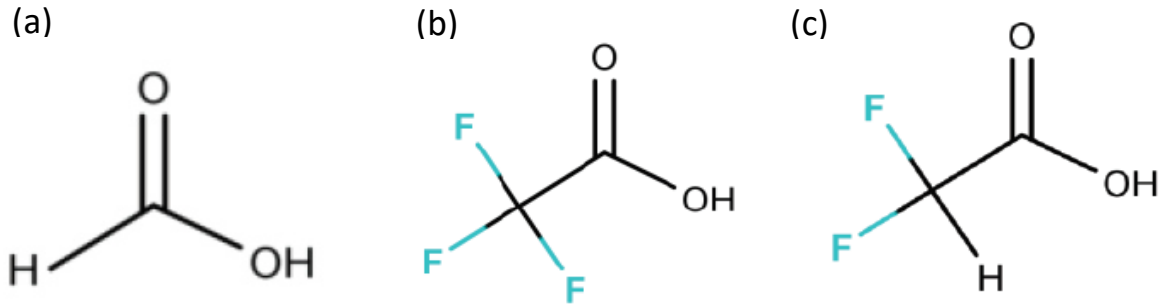

Fig. VI-S4: Structures of (a) formic acid (FA), (b) trifluoroacetic acid (TFA), and (c) difluoroacetic acid (DFA).

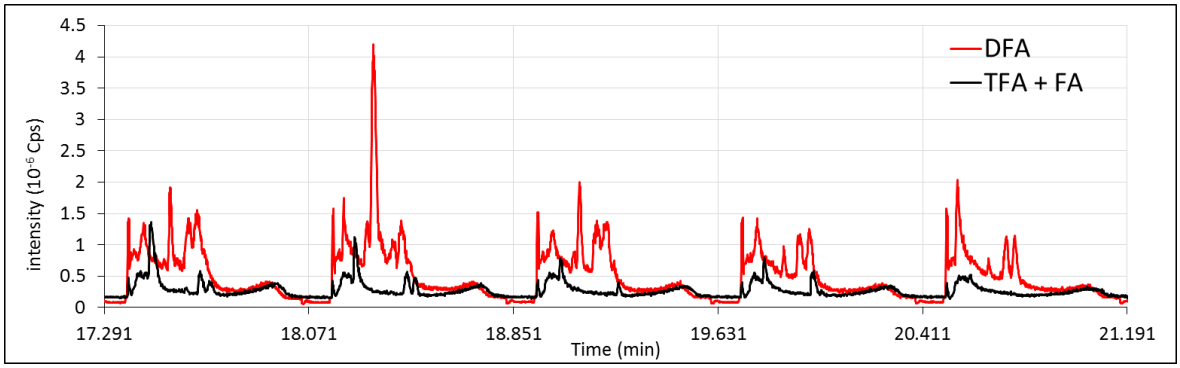

Fig. VI-S5: Overlaid ^{2}D-RPLC-MS (TIC, ESI^{+}) separations of five fractions in on-line CEX x RPLC using either DFA (red line) or TFA + FA (black line) in the mobile phase for the analyses of IdeS-treated ADC-S01 sample. Same other conditions as in Table VI-1.